THE JOURNAL OF

CHEMICAL PHYSICS

VOLUME 22 NUMBER 6

JUNE 1954

published by the

AMERICAN INSTITUTE OF PHYSICS

New York, N. Y.

JOURNAL OF CHEMICAL PHYSICS

EDITORS

WALTER A. [illegible], JR., *Editor*

Associate Editors

Term ending December 31, 1952	Term ending December 31, 1953	Term ending December 31, 1954
[illegible]	RICHARD M. BADGER	BRYCE L. CRAWFORD, JR.
B. S. DAILEY	DAVID M. DENNISON	H. S. GUTOWSKY
HAROLD [illegible]	JOHN G. KIRKWOOD	WILLIAM N. LIPSCOMB
[illegible]	G. B. KISTIAKOWSKY	ELLIOTT W. MONTROLL
[illegible]	A. W. LAWSON	GEORGE SCATCHARD
[illegible]	S. S. PENNER	J. W. STOUT
[illegible]	ROBERT L. SCOTT	GREGORY H. WANNIER

THE JOURNAL OF CHEMICAL PHYSICS is published monthly by the American Institute of Physics. Its purpose is to bridge the gap between journals of physics and journals of chemistry. The artificial boundary between physics and chemistry has now been in actual fact removed, and a large and active group is engaged in research which is as much the one as the other. It is to this group that the Journal is rendering its principal service and makes its greatest appeal, both as a prompt and efficient medium for publication of research and as a convenient and compact collected assemblage of pertinent information.

Information for Contributors

Send manuscripts to Clyde A. Hutchison, Jr., Editor, *The Journal of Chemical Physics*, Institute for Nuclear Studies, University of Chicago, Chicago 37, Illinois. Unless otherwise stated submission of a manuscript is a representation that it has been neither copyrighted, published, nor submitted for publication elsewhere. Textual material (abstract, body of the paper, tabular material, references, and figure captions) must be in English, typewritten (except mathematical expressions) double spaced with wide margins on good bond white paper, preferably letter size. The original copy, not the carbon, should be submitted. For general style, spellings, abbreviations, and forms, consult recent issues of this journal. The authors' institutions are requested to pay a publication charge of $15.00 per page which, if honored, entitles them to 100 free reprints. Instructions will be sent with galley proofs.

An abstract must accompany each article. It should be adequate as an index and as a summary.

All text, tabular, and graphical mathematical expressions should be carefully printed by hand. Be sure to distinguish between capital and small letters. Indicate clearly superscripts and subscripts by inverted carets and carets; superscripts, avoid complicated superscripts and subscripts. Avoid repetition of a complicated expression by representing it by a symbol. Identify in the margin Greek letters and unusual symbols. Use fractional exponents instead of radicals. Use the solidus (/) for fractions wherever its use will save vertical space.

References should appear as footnotes, numbered consecutively. Literature citations of technical journals should be in the form indicated in the Style Manual of the American Institute of Physics and Chemical Abstracts (Chem. Abstracts 45, I-CCLV (1951)).

Tables may be typewritten on sheets separate from the running text. Each table must have a caption which will make the data in the table intelligible without reference to the text. Avoid complicated column headings.

Wherever possible figures should be planned for the width of a column (3 in.). A convenient reduction ratio is about 2:1 or 3:1. Lettering should be large enough on the original that when reduced it shall not be less than about $\frac{1}{16}$ in. (~1.5 mm). Line drawings must be in *india ink* on white paper or tracing cloth. Coordinate paper is not desirable but if used must be blue lined and the coordinate lines which are to show must be inked over. Photographs should have maximum black and white contrast. Identify each original drawing or photograph on the back with the author's name and the figure number. Figures should be numbered consecutively. Captions should be typed on a separate sheet of paper.

A limited number of alterations in proof are unavoidable, but the cost of making extensive alterations after the article has been set in type will be charged to the author.

Proof and all correspondence concerning papers in the process of publication should be addressed to the Publication Manager, American Institute of Physics, 57 East 55 Street, New York 22, New York.

Subscription Price

	U. S. and Canada	Elsewhere
To members of the American Institute of Physics and Affiliated Societies	$12.00	$13.00
To all others	15.00	16.00

Back Number Prices

Yearly rate when complete year is available: $17.00.
Single copies: $1.50 each.

Subscriptions, renewals, and orders for single copies should be addressed to the American Institute of Physics, 57 East 55 Street, New York 22, New York.

Changes of address should be sent to the American Institute of Physics.

This Journal of Chemical Physics is published monthly at Prince and Lemon Streets, Lancaster, Pennsylvania.

Entered as second-class matter December 23, 1932, at the Post Office at Lancaster, Pa., under the Act of August 24, 1912.

Acceptance for mailing at special rate of postage provided for in paragraph (d-2), section 34.40, P. L. & R. of 1948, authorized February 3, 1933.

THE JOURNAL
OF
CHEMICAL PHYSICS

VOLUME 22, NUMBER 6 JUNE, 1954

Effect of Pressure on Diffusion in Polymer Solutions*

A. H. EMERY, JR., L. H. TUNG, AND H. G. DRICKAMER
Department of Chemistry and Chemical Engineering, University of Illinois, Urbana, Illinois
(Received November 6, 1953)

Diffusion measurements have been made using two molecular weights of polysulfide polymer at 25°C and 59°C in toluene solution. One isotherm for the low molecular weight was obtained in chloroform solution. The results indicate that there are two mechanisms of motion in solution. At low pressure the dominant mode involves the expulsion of a solvent molecule from the coiled polymer. At high pressure the motion is segmental.

PREVIOUS work in this laboratory[1–5] on diffusion in liquids under pressure has indicated that high pressure is a very useful tool in the study of the structure of the liquid state and the nature of molecular motion. In particular the concept of the activation volume has proven useful for the elucidation of the mechanism of diffusion.

This paper presents some measurements of diffusion of high polymer in solution. The polymer used was polysulfide of the forms $[S-(CH_2)_6-S]_n$. Two molecular weight fractions were made (5500 and 42 000). Four isotherms were obtained using the low molecular weight polymer [1 percent (by weight) solution in toluene at 25° and 50 percent C, 5 percent solution in toluene at 25°C, and 2 percent solution in chloroform at 25 percent C]. The upper limit of the pressure range, 3000–6000 atmospheres, was determined by the point at which the viscosity of the solution interferred with the operation of the cell.

EXPERIMENTAL PROCEDURE

A. Synthesis of the Polymer

The synthesis of the polymer was made in three steps. The methods used were those described in the literature[6–9] modified slightly to insure maximum yield on sulfur. The radioactive sulfur was obtained as BaS from Oak Ridge National Laboratory. H_2S was generated and bubbled through an aqueous cyanamide solution to form thiourea. This was reacted with hexamethylene dibromide to form the dimercaptan. This was polymerized in an emulsion with KOH and lauric acid. The length of time determined the average molecular weight. Larger batches of nonradioactive polymer were prepared by exactly the same procedure. These were carefully fractionated and molecular weights were determined by light scattering.† The results from light scattering were correlated against intrinsic viscosity measurements on the same fractions. The molecular weights of the fractions used in diffusion measurements were obtained from these correlations.

B. Measurement of Diffusion

The apparatus and method of operation was substantially identical with that used in previous diffusion measurements.[1–5] Because of the slow diffusion it was necessary to shorten the cell length substantially. The upper part consisted of a slice of medium porosity fritted glass 0.088 cm thick. The lower layer consisted of two pieces of Whitman No. 1 filter paper. The effective path length was established by runs with 0.1-N

* This work was supported in part by the U. S. Atomic Energy Commission.

[1] R. C. Koeller and H. G. Drickamer, J. Chem. Phys. **21**, 267 (1953).

[2] R. C. Koeller, and H. G. Drickamer, J. Chem. Phys. **21**, 575 (1953).

[3] Koeller, Cuddeback, and Drickamer, J. Chem. Phys. **21**, 589 (1953).

[4] R. B. Cuddeback and H. G. Drickamer, J. Chem. Phys. **21**, 597 (1953).

[5] E. P. Doane and H. G. Drickamer, J. Chem. Phys. **21**, 1359 (1953).

[6] L. F. Audrieth, *Inorganic Syntheses* (McGraw-Hill Book Company, Inc., New York 1950), Vol. III.

[7] R. L. Frank and P. V. Smith, J. Am. Chem. Soc. **68**, 2103 (1946).

[8] R. R. Renshaw, and D. E. Searle, J. Am. Chem. Soc. **59**, 2056 (1937).

[9] L. E. Olson, Ph.D. thesis, University of Illinois, 1953.

† We are indebted to F. T. Wall and H. Terayama for the use of the light scattering apparatus.

Na_2SO_4 solution. It was found possible to duplicate almost exactly the curve previously obtained at 25° to 5000 atmospheres.[3] Although the two parts of cell were no longer the same length, one of the methods of calculation used previously[1,10] still applied. Very numerous preliminary runs indicated a reproducibility at least within 10 percent.

In each case the lower part of the cell (filter paper) was filled with a solution of nonradioactive polymer, and the upper sleeve was filled with radioactive polymer solution of the same concentration and molecular weight.

RESULTS

The results are listed in Tables I–III and are plotted in Figs. 1–4. Figures 5–7 show the calculated quantities

TABLE I. Low molecular weight polymer.

Temperature °C	1% in toluene Pressure atmos	Diffusion coefficient D cm²/sec ×10⁶
25	80	1.59
25	200	2.36
25	360	2.18
25	360	2.99
25	640	3.24
25	970	2.63
25	1180	2.55
25	1600	1.83
25	1970	1.37
25	2000	1.24
25	3500	0.64
25	3500	0.83
25	3850	0.91
25	6000	0.68
25	6400	0.47
50	250	2.15
50	600	4.0
50	1050	6.8
50	1470	5.9
50	1870	3.29
50	3600	1.57
50	4550	1.20

TABLE II. High molecular weight polymer.

Temperature °C	1% in toluene Pressure atmos	Diffusion coefficient D cm²/sec ×10⁶
25	200	0.276
25	370	0.75
25	610	1.74
25	1220	1.50
25	1970	0.88
25	3650	0.45
50	200	0.73
50	350	1.24
50	600	1.19
50	1200	0.73
50	2000	0.71
50	2000	0.82
50	3500	1.12
50	3600	1.20
50	4500	1.21
50	4500	1.43
50	5650	0.45

[10] K. D. Timmerhaus and H. G. Drickamer, J. Chem. Phys. **19**, 1242 (1951).

TABLE III. Low molecular weight polymer.

Temperature °C	5% in toluene Pressure atmos	Diffusion coefficient D cm²/sec ×10⁶
25	220	1.22
25	400	2.71
25	630	2.34
25	1280	2.16
25	1980	1.23
25	2850	0.80
	Low molecular weight polymer 2% in chloroform	
25	190	1.94
25	220	1.39
25	600	2.20
25	1200	2.22
25	2020	1.79
25	3000	1.84
25	3600	1.65

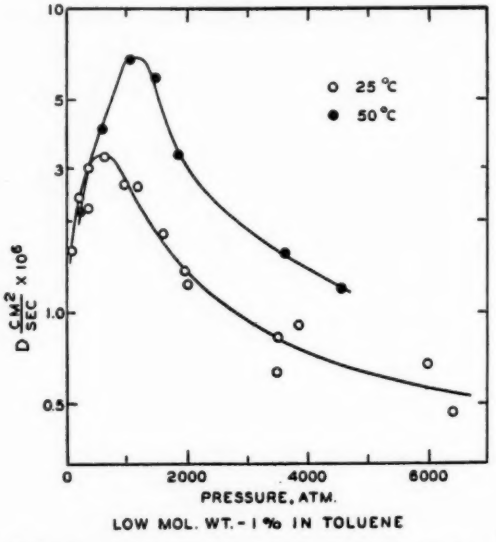

FIG. 1. Diffusion coefficient *versus* pressure low molecular weight 1 percent in toluene 25° and 50° isotherms.

(activation volumes, enthalpies, entropies, and free energies) for 1 percent toluene solutions of both molecular weights. Figure 7 shows activation volumes for the 5 percent toluene solution and 2 percent chloroform solution (both low molecular weight).

All the diffusion curves *versus* pressure (except the 50° isotherm for high molecular weight) show qualitatively the same features. In each case there is a rapid rise in D with pressure to 500 or 1000 atmospheres, followed by a slower decrease with increasing pressure. The low pressure part of the curve corresponds to a large negative activation volume in the low pressure region, and above 1000 atmospheres a positive activation volume decreasing with further increase in pressure.

Figure 3 indicates that there is only a minor effect of increasing the concentration from 1 percent to 5 percent by weight. The chloroform isotherm (Fig. 4) is qualitatively similar in shape to the corresponding toluene

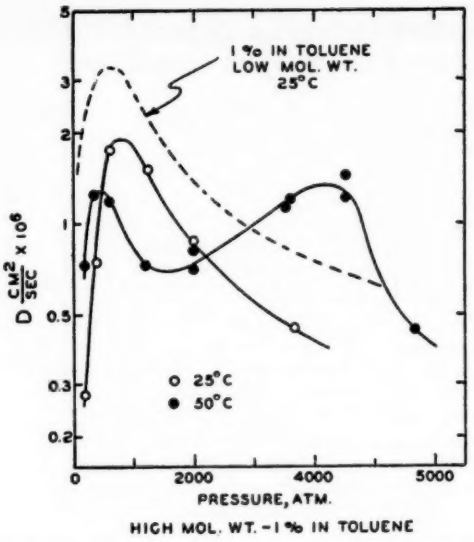

FIG. 2. Diffusion coefficient *versus* pressure high molecular weight 1 percent in toluene 25° and 50° isotherms.

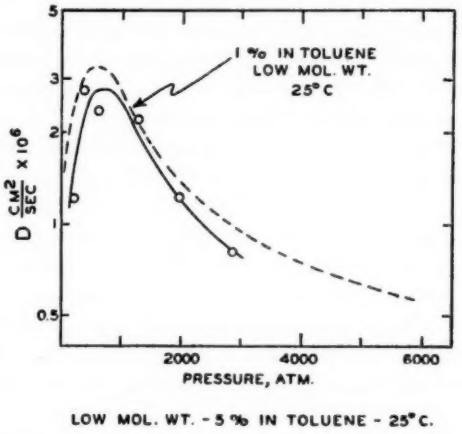

FIG. 3. Diffusion coefficient *versus* pressure low molecular weight 5 percent in toluene 25° isotherms.

curve although chloroform is a considerably better solvent for this polymer. The chloroform solutions proved to be very difficult to handle, which made further work along these lines impractical.

Evidently there are two mechanisms of molecular motion, one controlling at low pressure, and the second at high pressure.

The two mechanisms described below are consistent with our results and with other evidence of structure of polymers in solution, although they are certainly not the only possible descriptions of our results.

One possible mode of motion is segmental. This would result in a positive activation volume, and would therefore describe the controlling mechanism of motion in the high pressure region. The decrease in activation volume (per molal volume of solvent) and of activation enthalpy with pressure in this region would indicate a decrease in the size of the moving segment with pressure.

The second mode of motion depends on the picture of a polymer molecule as loosely coiled in solution with large numbers of solvent molecules trapped in the coils. If a solvent molecule were expelled from one part of the coil, with or without trapping another solvent molecule in a different part of the coil, this would constitute molecular motion which might easily be characterized by a negative activation volume. Further, this mode of motion would become more difficult with increasing pressure, as the solvent molecules become squeezed out and the solvent structure more rigid. It is reasonable to believe that the segmental motion is controlling at the higher pressure.

The high molecular weight isotherm at 50°C is more difficult to explain. If the other curves are the result of two competing modes of motion it would seem that there are at least three competing modes in this case. The indicated reproducibility of the results shows that the shape of the curve is definitely radically different from the others. If the portions of the curve below 400 atmospheres and above 4500 atmospheres are extended to meet, the resulting curve is qualitatively similar to the other curves obtained. It is then the premature drop, at 500 atmospheres, which makes diffusion at

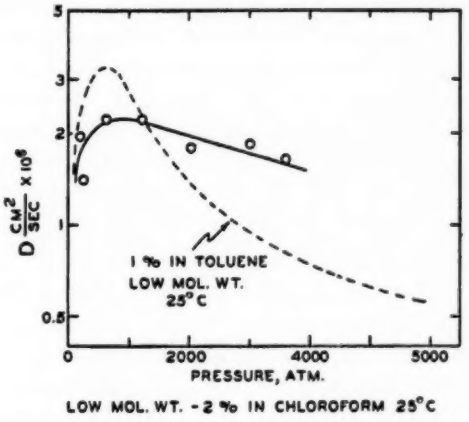

FIG. 4. Diffusion coefficient *versus* pressure low molecular weight 2 percent in chloroform.

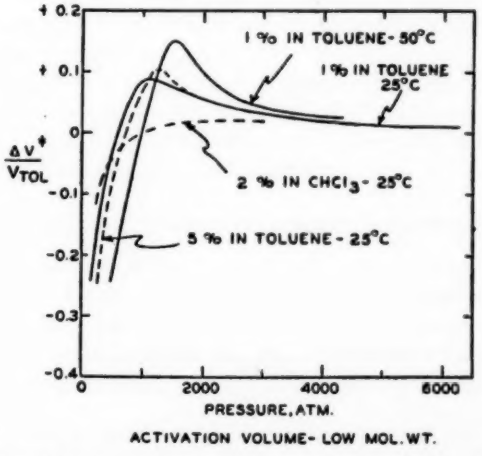

FIG. 5. $\Delta V^{\ddagger}/V_s$ *versus* pressure—low molecular weight polymer.

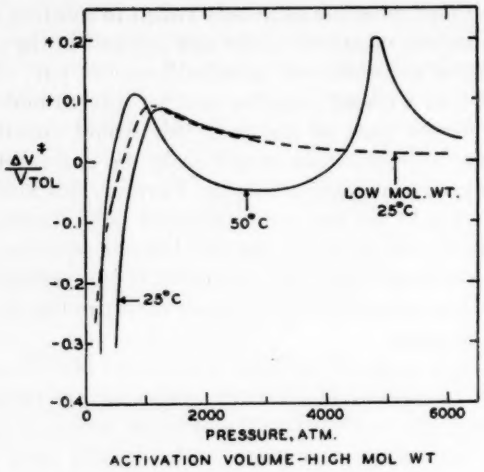

FIG. 6. $\Delta V^{\ddagger}/V_s$ *versus* pressure—high molecular weight *versus* pressure.

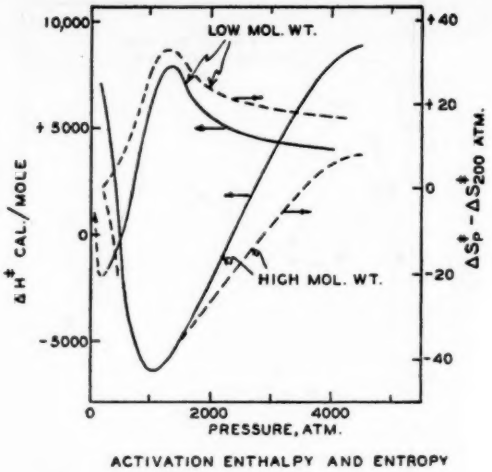

FIG. 7. Enthalpy and entropy of activation.

50°C slower than at 25°C in the region (500–2000 atmospheres) which is to be explained, rather than the rise beginning at 1500 atmospheres.

It is possible that the molecular weight distribution of the high molecular weight polymer is bimodal, and that the "average" rate of diffusion is controlled by different molecular weights at different pressures. Unfortunately, because of the microsynthesis methods used, not enough of a cut was made to determine molecular weight distribution, but the fractionation was not sharp. Various other possible explanations can be put forward, but they are not particularly convincing. The high molecular weight polymer may be coiled in such manner at high temperature and low pressure that expulsion of solvent is not a particularly easy mode of motion. The increase of pressure may increase the coiling and increase the likelihood of this mechanism of motion.

Light scattering experiments over this range of pressure are planned for the near future. It is hoped that these will throw some light on the structure of the polymer molecules in these solutions.

The authors would like to acknowledge the assistance of C. S. Marvel and F. T. Wall of the Department of Chemistry and Chemical Engineering with selection of an appropriate polymer. C. S. Marvel further outlined the method of synthesis. F. T. Wall gave many helpful suggestions on the interpretation of results.

L. H. Tung was supported by a grant from the Guggenheim Foundation. A. H. Emery, Jr., received financial aid from the Shell Fellowship Committee.

Infrared Absorption Studies of Aqueous Complex Ions: I. Cyanide Complexes of Ag(I) and Au(I) in Aqueous Solution and Adsorbed on Anion Resin*

LLEWELLYN H. JONES AND ROBERT A. PENNEMAN
Los Alamos Scientific Laboratory, University of California, Los Alamos, New Mexico

(Received January 13, 1954)

Techniques are described for obtaining infrared absorption spectra of complex cyanide anions in aqueous solution and adsorbed on anion resin. In the system $AuCN-KCN-H_2O$, only the soluble complex ion $Au(CN)_2^-$ is observed; the molar extinction coefficient (ϵ) is 477 ± 25 mole^{-1} liter cm^{-1} at 2147 ± 1 cm^{-1}. When $Au(CN)_2^-$ is adsorbed to the extent of 47 weight percent on Dowex-A-1 resin, its absorption maximum appears at 2138 cm^{-1}. Three distinct silver cyanide complex ions were observed in aqueous solution: $Ag(CN)_2^-$, $\epsilon=264\pm12$ at 2135 ± 1 cm^{-1}; $Ag(CN)_3^{-2}$, $\epsilon=397\pm23$ at 2105 ± 1 cm^{-1}; $Ag(CN)_4^{-3}$, $\epsilon=556\pm83$ at 2092 ± 1 cm^{-1}. Approximate values (calculated in terms of activities) of the dissociation constants for the tri- and tetra-cyanide complexes into the next lower complex are $K_{3,2}=0.20\pm0.05$ mole liter^{-1}, and $K_{4,3}=13{,}4\pm4$ mole liter^{-1}, respectively. Over ranges of silver concentrations from 0.1–1.0 formal and of *free* CN^- *ion* concentrations from 0.05–1.5 molar, the concentrations of $Ag(CN)_2^-$, $Ag(CN)_3^{-2}$ and $Ag(CN)_4^{-3}$ can be calculated to within 5 percent (absolute) using values of the constants adjusted to best overall fit; in terms of concentrations, $K_{3,2}^c=0.108$ and $K_{4,3}^c=2.85$ mole liter^{-1}.

INTRODUCTION

ALTHOUGH Raman work on complex ions is being done extensively, as far as we can tell this study represents the first application of infrared absorption to the study of equilibria among complex anions in aqueous solution or to the adsorbed species on anion resins. The infrared absorption of UO_2^{++}, plus the transuranic XO_2^+ and XO_2^{++} ions, and HF_2^- in aqueous solution, has been reported recently[1,2] by this laboratory. A very general application of the term complex ion might include these species as examples of the type $[XY_2]^n$. We have qualitatively examined most known cyanide complexes in aqueous solution through the types $X(CN)_6$ and $X(CN)_8$. Quantitative aspects of this latter study are still in progress. This paper is concerned with $Au(CN)_2^-$, $Ag(CN)_2^-$, $Ag(CN)_3^{-2}$, and $Ag(CN)_4^{-3}$.

The gold and silver cyanide complexes have been the subject of considerable study. Bassett and Corbet[3] reported the single compound $KAu(CN)_2$ in the system $AuCN-KCN-H_2O$, while the $AgCN-KCN-H_2O$ system yielded three compounds: $KAg_2(CN)_3\cdot H_2O$, $KAg(CN)_2$, and $K_3Ag(CN)_4\cdot H_2O$. [However, unpublished work by E. Staritzky of this laboratory shows $K_3Ag(CN)_4$ is *not* hydrated.] There are ions in aqueous solution corresponding to the solids $KAg(CN)_2$ and $K_3Ag(CN)_4$, but no solid is known containing the $Ag(CN)_3^{-2}$ group, which we find is an important species in aqueous solution. As late as 1942, Brigando[4] stated that $Ag(CN)_4^{-3}$ yielded $Ag(CN)_2^-$ in dissociation, but he did not mention $Ag(CN)_3^{-2}$. The early work of Bodländer and Eberline[5] in 1904 was correct regarding the species $Ag(CN)_2^-$, $Ag(CN)_3^{-2}$, and $Au(CN)_2^-$. Very recently, in a study of an analogous system by a solubility method, Cave and Hume[6] report $Ag(SCN)_2^-$, $Ag(SCN)_3^{-2}$, and $Ag(SCN)_4^{-3}$ ions in aqueous solution.

EXPERIMENTAL

Reagents

Silver cyanide was discarded as a primary standard, since it gave variable results. Potassium silver cyanide, $KAg(CN)_2$, proved to be satisfactory. It was dried over anhydrous magnesium perchlorate and was analyzed crystallographically for homogeneity, and analytically prior to use [the CN/Ag ratio was within 0.1 percent of theory for $KAg(CN)_2$]. Reagent grade KCN was analyzed for cyanide and usually ran >99 percent KCN.

For the quantitative work with the silver cyanide complexes, $KAg(CN)_2$ was weighed into tared 25 ml volumetric flasks, and the calculated weight of KCN (adjusted for cyanide analysis) was added to achieve CN/Ag ratios over the range 2.02/1 to 14/1. Distilled water was added until dissolution was complete; final volume adjustment was made in the constant temperature instrument room at 70°F.

Since only a single gold cyanide complex was observed, independent of the free CN^- concentration, reagent AuCN was satisfactory for use and was dissolved directly in KCN solution.

Adsorption of Cyanide Complexes on Dowex-A-1

This resin is a strong base (quaternary amine) anion exchanger. Spheres of 200–400 mesh in the citrate form were equilibrated 24 hrs with a ten-fold excess of the silver or gold cyanide anions (assuming a capacity of 3 milliequivalents/gram of air-dried resin). The resin

* This work was sponsored by the U. S. Atomic Energy Commission.

[1] L. H. Jones and R. A. Penneman, J. Chem. Phys. **21**, 542 (1953).

[2] L. H. Jones and R. A. Penneman, submitted for publication to J. Chem. Phys.

[3] H. Bassett and A. S. Corbet, J. Chem. Soc. **125**, 1660 (1924).

[4] Jeanne Brigando and M. Paul Lebeau, Compt. rend. **214**, 908 (1942).

[5] G. Bodländer and W. Eberline, Z. anorg. Chem. **39**, 197 (1904).

[6] G. C. B. Cave and D. N. Hume, J. Am. Chem. Soc. **75**, 2893 (1953).

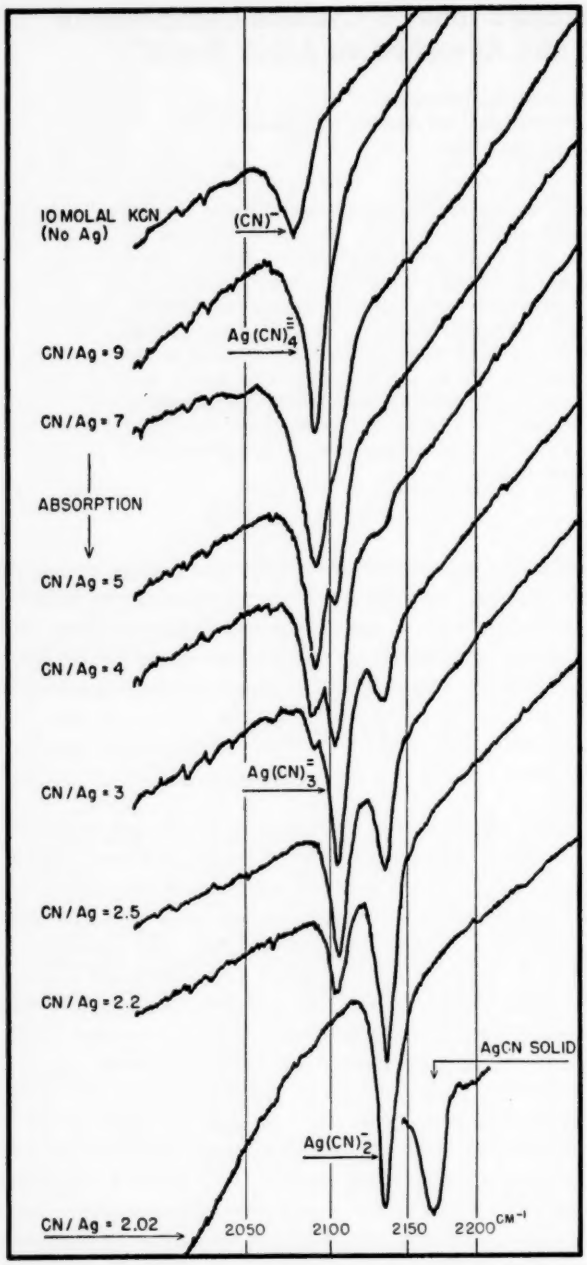

FIG. 1. Infrared absorption of aqueous silver cyanide complexes at 1.5 molal Ag(I), of aqueous KCN, and of solid AgCN. Molal solutions were made up initially to determine the positions of the maxima. For the quantitative measurements, molar solutions were used.

slurry was then centrifuged and the supernatant liquid removed. Washing and centrifugation were repeated until less than 1/1000th of the original concentration of mother liquor remained with the resin.

Preparation of Solid Cyanides for Observation of Infrared Spectra

The solid compounds $KAu(CN)_2$, $KAg(CN)_2$, and $K_3Ag(CN)_4$ were prepared by recrystallizing from aqueous solution or aqueous KCN solution using the phase diagrams of Bassett and Corbet.[3] The dried crystals (crystallographically homogeneous) were ground up with mineral oil for observation of the infrared spectrum.

It was not possible to grind up the AgCN and AuCN to form suitable mineral oil mulls. Therefore, a thin layer of AgCN was formed by spreading dilute aqueous KCN over the surface of a silver chloride window and washing with water. A thin layer of AuCN was precipitated on the surface of a CaF_2 window by acidification of an aqueous solution of $KAu(CN)_2$ using HCl. The dried preparation was coated with mineral oil to reduce light scattering.

INSTRUMENT AND TECHNIQUE

The instrument was the single-beam Perkin-Elmer Model 12-C recording infrared spectrograph converted to double pass. A LiF prism was used, calibrated against gaseous NH_3, CO_2, CO, HBr, HCl, and H_2O. Part of the H_2O and CO_2 spectra were run on each graph as check points.

For the resin studies, a thin smear of the resin containing the adsorbed complex ion was air-dried on a calcium fluoride plate and then wet with a drop of mineral oil to cut down light scattering.

The spectra of aqueous solutions were determined between CaF_2 flats using measured tantalum spacers 12.4 and 26.4 microns thick. However, it was found that a thin film of liquid amounting to 2.55 microns was pulled by capillary attraction on each side of the spacer, making the actual path 31.5 microns using the 26.4 micron spacer. This extra thickness was determined by observation of the optical density of the $Ag(CN)_2^-$ peak for a given solution using each thickness of spacer. The assumption was made that the capillary layer between spacer and window was the same for each spacer. Solutions of various concentrations containing only the $Ag(CN)_2^-$ complex were used to check Beer's law and to determine the extinction coefficient of this species. Known amounts of cyanide ion were added to change the ratio of concentration of $Ag(CN)_2^-$ species to that of $Ag(CN)_3^{-2}$. Simultaneous equations were set up and solved for extinction coefficients of the two species. Additional cyanide was added to get the species, $Ag(CN)_4^{-3}$. The concentration of this latter species was determined by difference, knowing the concentrations of the other two species. In all cases the concentration of free Ag^+ was neglected, which is

TABLE I. Asymmetric cyanide stretching frequencies of $Ag(CN)_2^-$, $Ag(CN)_3^{-2}$, $Ag(CN)_4^{-3}$, and the CN^- frequency, and their extinction coefficients.

Aqueous species	ν, cm^{-1}	ϵ, $moles^{-1}$ liters cm^{-1}
$Ag(CN)_2^-$	2135±1	264±12
$Ag(CN)_3^{-2}$	2105±1	397±23
$Ag(CN)_4^{-3}$	2092±1	556±83
CN^-	2080±1	29±1

TABLE II.

C_{CN^-}	$C_{Ag(CN)_2^-}$	$C_{Ag(CN)_3^{-2}}$	$C_{Ag(CN)_4^{-3}}$	$K_{3,2}^c$	$K_{4,3}^c$	μ^a	$F_{2,3}$	$F_{4,3}$	$K_{3,2}^f$	$K_{4,3}^f$
0.050	0.620	0.370	...	0.084	...	1.78	1.81	...	0.152	...
0.110	0.135	0.115	...	0.129	...	0.59	1.71	...	0.221	...
0.134	0.380	0.620	...	0.082	...	2.37	1.83	...	0.150	...
0.156	0.206	0.294	...	0.109	...	1.24	1.78	...	0.194	...
0.328	0.017	0.046	...	0.121	...	0.48	1.69	...	0.204	...
0.550	0.076	0.370	0.048	0.113	4.24	2.02	1.82	4.07	0.206	17.26
0.622	0.015	0.095	0.016	0.098	3.69	5.52[a]	1.86	4.54	0.182	16.75
0.628	0.020	0.087	0.018	0.144	3.04	1.02	1.77	3.68	0.255	11.19
0.720	0.059	0.369	0.075	0.115	3.54	2.34	1.83	4.15	0.210	14.69
0.960	0.050	0.363	0.087	0.132	4.00	2.62	1.83	4.21	0.242	16.84
1.197	0.017	0.163	0.070	0.125	2.79	5.13[a]	1.86	4.51	0.232	12.58
1.206	0.016	0.166	0.068	0.116	2.94	2.13	1.82	4.10	0.211	12.05
1.74	0.011	0.212	0.152	0.090	2.43	4.05[a]	1.85	4.41	0.166	10.72
2.247	0.012	0.225	0.263	0.120	1.92	4.51	1.86	4.46	0.223	8.56
				Av. 0.113	3.18				Av. 0.203	13.40

[a] Ionic strength increased by the addition of $NaNO_3$.

certainly justified by the small dissociation constant of $Ag(CN)_2^-$.[5,7-9]

RESULTS AND DISCUSSION

Complex Ions, $Ag(CN)_2^-$, $Ag(CN)_3^{-2}$, and $Ag(CN)_4^{-3}$

As demonstrated in Fig. 1, there are absorption peaks for three distinct silver cyanide complex anions. The frequencies of maximum absorption and molar extinction coefficients are given in Table I. All of these frequencies arise from asymmetric cyanide stretching vibrations. In the case of the dicyanide complex, the asymmetric cyanide stretching vibration is a motion approximately as shown in Fig. 2. In the tri- and tetracyanide complexes, the CN groups are probably arranged tetrahedrally about the silver atom, with one water molecule of hydration for the tri-cyanide ion. For these latter two ions, this asymmetric cyanide stretching vibration is no doubt similar to the asymmetric CO stretching vibration of $Ni(CO)_4$ as discussed by Crawford and Cross.[10]

The main source of error in determination of di- and tri-cyanide concentrations is believed to be the uncertainty in actual path length, since the two peaks are completely resolved. In the case of the tetracyanide complex, there is another source of error in that the tetracyanide peak is overlapped by both the tricyanide and free cyanide absorption peaks. Although the extinction coefficient of free cyanide ion is small, a large excess over the tetracyanide is necessary because of its comparatively small association constant, thus leading to an appreciable CN^- contribution to optical density at the tetracyanide position. The di-, tricyanide complexes and free cyanide ions were found to obey Beer's law quite well. The extinction coefficients of the tricyanide complex and free cyanide at the position of the tetracyanide absorption maximum were determined so that their contribution to the apparent optical density of the $Ag(CN)_4^{-3}$ could be compensated for.

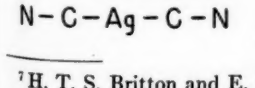

FIG. 2. Asymmetric cyanide stretching vibration of the $Ag(CN)_2^-$ ion.

DISSOCIATION CONSTANTS FOR $Ag(CN)_3^{-2}$ AND $Ag(CN)_4^{-3}$

Once the extinction coefficients of the various species were determined, it was possible to measure the concentration of each ion. The CN^- concentration was determined by stoichiometry as its absorption coefficient is small. The hydrolysis of CN^- is negligible in the solutions studied. "Concentration" equilibrium constants (see Table II) were then calculated from these data.

$$K_{3,2}^c = (C_{Ag(CN)_2^-})(C_{CN^-})/(C_{Ag(CN)_3^{-2}}) = 0.113,$$

and

$$K_{4,3}^c = (C_{Ag(CN)_3^{-2}})(C_{CN^-})/(C_{Ag(CN)_4^{-3}}) = 3.18.$$

These average values for concentration equilibrium constants give equal weight to all the values listed in Table II. Over ranges of silver concentration 0.1–1.0 formal, and of free cyanide ion from 0.05–1.5 molar, the concentrations of $Ag(CN)_2^-$, $Ag(CN)_3^{-2}$, and $Ag(CN)_4^{-3}$ can be calculated to within 5 percent (absolute) using compromise values of dissociation constants adjusted for best overall fit, in terms of concentrations: $K_{3,2}^c = 0.108$ and $K_{4,3}^c = 2.85$ mole liter^{-1}.

In order to estimate thermodynamic equilibrium constants, molar activity coefficients were calculated using the formula

$$\log f_i = -0.51\, Z_i^2(\mu_c)^{\frac{1}{2}}/1 + 0.33 a_0(\mu_c)^{\frac{1}{2}}; \quad \text{(Equation 1)}$$

f_i = molar activity coefficient of ion (i),
Z_i = charge on ion (i),
μ_c = molar ionic strength of solution, and
a_0 = distance (in angstrom units) of closest approach of negative ion (i) to K^+.

[7] H. T. S. Britton and E. N. Dodd, J. Chem. Soc. **1932**, 1940.
[8] R. Gaugin, J. Chim. Phys. **42**, 28 (1945).
[9] M. Randall and J. O. Halford, J. Am. Chem. Soc. **52**, 178 (1930).
[10] B. L. Crawford and P. C. Cross, J. Chem. Phys. **6**, 525 (1938).

Equation (1) is actually for mole fraction activity coefficient. Solution densities were measured and it was found that the molar activity coefficient of each species is less than 2 percent greater than the mole fraction activity coefficient. This difference is negligible compared to experimental error.

From x-ray studies on solid KCN and NaCN at room temperature, the $C-N^-$ ions appear to rotate and have spherical symmetry with an ionic radius of 1.8A.[11] For aqueous $Ag(CN)_2^-$ we have assumed an Ag—C distance of 2.13A,[12] C—N distance of 1.15A,[12] and a van der Waals' radius of 1.5A[13] giving an ionic radius of 4.8A. Also, we have assumed spherical symmetry due to rotation, as with CN^-. The ions $Ag(CN)_3^{-2}\cdot H_2O$ and $Ag(CN)_4^{-3}$ will thus also have radii of ~4.8A. The a_0 for the various ions are then obtained by adding the approximate ionic radius of K^+ (hydrated) = 1.9A.[14] These assumptions yield an a_0 of 3.7A for CN^- with K^+, and an a_0 of 6.7A for the three silver cyanide complexes with K^+.

Using these values of a_0 and known ionic strengths, the activity coefficient quotients were calculated and are listed in Table II where

$$F_{3,2}=\frac{(f_{Ag(CN)_2^-})(f_{CN^-})}{f_{Ag(CN)_3^{-2}}} \quad \text{and} \quad F_{4,3}=\frac{(f_{Ag(CN)_3^{-2}})(f_{CN^-})}{f_{Ag(CN)_4^{-3}}}.$$

A thermodynamic equilibrium constant K^t was then calculated, from

$$K_{3,2}{}^t = K_{3,2}{}^c F_{3,2},$$

and

$$K_{4,3}{}^t = K_{4,3}{}^c F_{4,3}.$$

Over the range of ionic strength of the solutions studied, the concentration equilibrium constants and the calculated activity coefficient quotients were fairly constant. Even though the individual activity coefficients vary markedly, the activity quotient is a rather slowly varying function from $\mu=1$ to 5. Therefore, the values of the thermodynamic equilibrium constants are satisfactorily constant. The data are reported in Table II. From the results of Table II, the average values are

$$(a_{Ag(CN)_2^-})(a_{CN^-})/(a_{Ag(CN)_3^{-2}}) = 0.20\pm0.05 \text{ mole liter}^{-1},$$

and

$$(a_{Ag(CN)_3^{-2}})(a_{CN^-})/(a_{Ag(CN)_4^{-3}}) = 13.4\pm4 \text{ mole liter}^{-1}.$$

These two equilibrium constants were taken as the averages of all the values given in Table II. Equation 1 is generally found to apply quite well at ionic strengths less than 1.0, but to require added terms at higher concentration. Perhaps the best single value for $K_{3,2}{}^t$ is 0.221, obtained from a solution having a molar ionic strength of 0.59, and concentration of $Ag(CN)_2^-$ and $Ag(CN)_3^{-2}$, 0.135 and 0.115 molar respectively. However, this value is well within the estimated uncertainty of the average value. The lowest ionic strength at which we could determine a value for $K_{4,3}{}^t$ was 1.02. This gave a value of 11.19 for $K_{4,3}{}^t$, again well within the limits assigned to the average value. There appears to be no regular trend in equilibrium constants with ionic strength. However, the value for $K_{4,3}{}^t$ becomes smaller rapidly with increasing cyanide above ~1.5 molar free CN^-. In fact at 5 molar free CN^-, $Ag(CN)_3^{-2}$ is barely detectable, leading to an approximate value for $K_{4,3}{}^t \sim 1$.

From the various values for the dissociation constant of $Ag(CN)_2^-$: $5\times10^{-22(7)}$, $8\times10^{-22(8)}$, $8.8\times10^{-22(5)}$, and $3.8\times10^{-19(9)}$, we will use 8×10^{-22}. We can now calculate the complete dissociation constants of $Ag(CN)_3^{-2}$ and $Ag(CN)_4^{-3}$.

$$K_{III}=\frac{(a_{Ag^+})(a_{CN^-})^3}{a_{Ag(CN)_3^{-2}}}=(1.6\pm0.4)\times10^{-22},$$

and

$$K_{IV}=\frac{(a_{Ag^+})(a_{CN^-})^4}{a_{Ag(CN)_4^{-3}}}=(2.3\pm1.2)\times10^{-21}.$$

Bodländer and Eberline[5] give a value for K_{III} of 1.13×10^{-22}, determined in 1904, which should be increased to 1.47×10^{-22} after allowing properly for $Ag(CN)_2^-$ and $Ag(CN)_4^{-3}$ (they assumed only $Ag(CN)_3^{-2}$).

We are confident of the assignment of frequencies to the three silver cyanide complex ions for several reasons:

1. The equilibrium constants for various ratios of the species are constant.

2. The species we have assigned as $Ag(CN)_2^-$ can hardly be anything else, as it is the predominant species in a solution having a CN/Ag ratio of 2.02; and no solution of appreciable Ag(I) concentration could be prepared having a ratio of CN/Ag = 2.00 or less.

TABLE III. Asymmetric cyanide stretching frequencies of solid and aqueous cyanide complexes of Ag(I), and the species adsorbed on Dowex-A-1 resin.

Species	ν_{solid} cm^{-1}	$\nu_{on\ resin}$ cm^{-1}	$\nu_{aqueous}$ cm^{-1}
AgCN	2164[a]±2	···	not observed
$KAg(CN)_2$	2139±1	2131±5	2135±1
$K_2Ag(CN)_3$	not observed	2097[b]±5?	2105±1
$K_3Ag(CN)_4$	2097±1 (strong) 2091±1 (medium)	2097[b]±5?	2092±1

[a] This value of 2164 cm^{-1} does not quite agree with a value of 2178 cm^{-1} obtained by W. D. Stallcup and D. Williams [J. Chem. Phys. 10, 199 (1942)] using a rock salt prism, which has much poorer resolution in this region than our LiF prism.

[b] The peak at 2097 cm^{-1} arises from either $Ag(CN)_3^{-2}$ or $Ag(CN)_4^{-3}$ on the resin.

[11] Ralph W. B. Wyckoff, *Crystal Structure* (Interscience Publishers, Inc., New York, 1951), Vol. I, chap. III, p. 12 (text).

[12] A. F. Wells, *Structural Inorganic Chemistry* (Clarendon Press, Oxford, 1945), p. 448.

[13] L. Pauling, *Nature of the Chemical Bond* (Cornell University Press, Ithaca, 1945), p. 189.

[14] H. S. Harned and B. B. Owen, *The Physical Chemistry of Electrolytic Solutions* (Reinhold Publishing Corporation, New York, 1943), p. 381.

3. The solid compounds $KAg(CN)_2$ and $K_3Ag(CN)_4$ have been prepared and positively identified. Their asymmetric cyanide stretching vibrations are similar to those assigned to $Ag(CN)_2^-$ and $Ag(CN)_4^{-3}$ in solution, as shown in Table III.

4. Where $Ag(CN)_2^-$ and $Ag(CN)_3^{-2}$ are present without much excess $CN^-(CN/Ag<3)$, there is not enough cyanide ion to assume the $Ag(CN)_3^{-2}$ is $Ag(CN)_4^{-3}$.

5. Similar reasoning from stoichiometry requires that the $Ag(CN)_4^{-3}$ assignment is correct.

Study of Adsorbed Species of Silver Cyanide Anions on Dowex-A-1

Examination of the species of silver cyanide anions which were adsorbed on the dried resin spheres, and silver analysis, showed that $Ag(CN)_2^-$ was adsorbed strongly, yielding an average molecular weight of 270 for the resin per unit positive charge. In addition, with solutions having excess cyanide so that $Ag(CN)_4^{-3}$ was predominant, and no $Ag(CN)_2^-$ was detectable by infrared absorption, there was always $Ag(CN)_2^-$ found on the resin. It appears that only $Ag(CN)_2^-$ and one other complex are adsorbed. We have not been able to determine whether the other peak arises from $Ag(CN)_3^{-2}$ or $Ag(CN)_4^{-3}$ on the resin, or whether it is from both (unresolved); see Fig. 3. In each case, the upper curve in Fig. 3 is that of the solution species, and the lower curve of each pair is the resin after equilibration with the particular solution. Analyses for the silver on the resins show that with increasing excess free cyanide, there is less silver adsorbed. Table III gives a comparison of frequencies of the complex silver cyanide ions in the solid, aqueous solutions, and adsorbed on anion resins.

STUDIES OF $Au(CN)_2^-$ IN AQUEOUS SOLUTION AND ADSORBED ON DOWEX-A-1

Aqueous potassium cyanide solutions containing gold cyanide were examined qualitatively over a range of CN/Au ratios of 2 to 10. Only a single absorption peak was observed. Quantitative work at 0.504 f Au(I), 1.054 f CN^- (CN/Au = 2.09) established the extinction coefficient of $Au(CN)_2^-$ as 477 mole^{-1} liter cm^{-1}. Repetition of this work in a solution 0.250 f Au(I), 1.25 f CN^- (CN/Au = 5.0) gave the same value for the extinction coefficient and did not shift the absorption maximum of the $Au(CN)_2^-$. From this we conclude that there is only a single gold cyanide complex, $Au(CN)_2^-$.

TABLE IV. Absorption maxima of $Au(CN)_2^-$.

Condition	Max, cm^{-1}	Remarks
Aqueous soln. 0.25 f $KAu(CN)_2$	2147±1	Extinction coefficient = 477±25
Dowex-A-1+$Au(CN)_2^-$	2138±5	47 percent $Au(CN)_2^-$
Solid[a] $KAu(CN)_2$	2141±1	
AuCN solid	2261±2	

[a] L. H. Jones, J. Chem. Phys. 21, 1891 (1953).

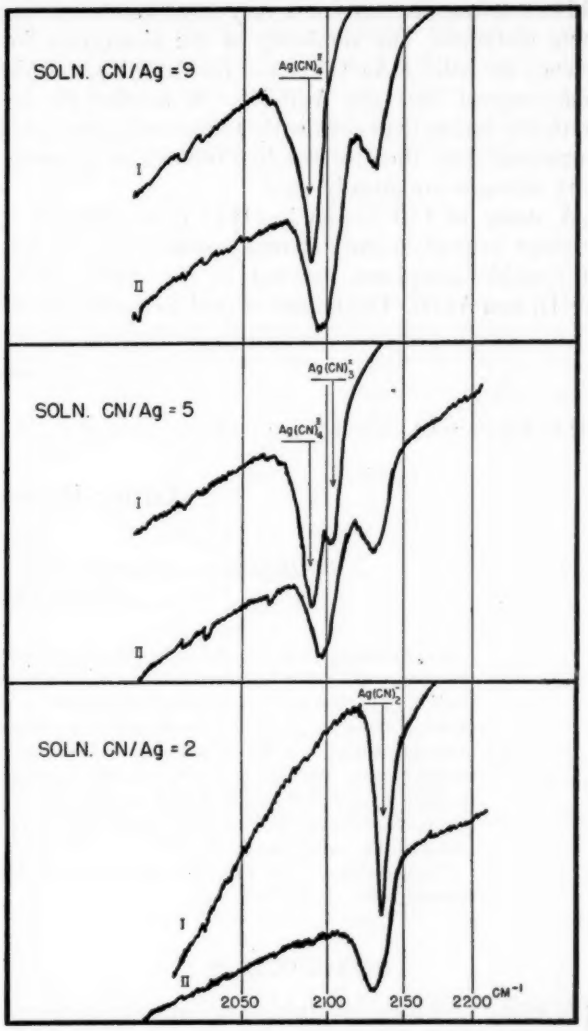

FIG. 3. Infrared absorption of silver cyanide complexes in aqueous solution and adsorbed on Dowex-A-1 anion resin. Curves labeled I are of aqueous solution at 1.5 molal Ag. Curves labeled II are of A-1 resin thoroughly washed after equilibration with each solution.

A gram of gold [as $Au(CN_2)^-$] was adsorbed on Dowex-A-1 resin, well washed and air dried as already described. Gold analysis gave 37.2 percent Au or 47.015 percent $Au(CN)_2^-$, from which the average molecular weight of the N^+ unit [assuming $N^+-Au(CN)_2^-$] of 281 was calculated. Since the molecular weights are so similar and the tendency of the $Au(CN)_2^-$ to be adsorbed on the resin is so great, it was thought that the structure of the material might resemble that of a salt such as a quaternary ammonium halide. A sample of the same material which had been analyzed and used for infrared absorption spectra reported in Table IV was sent to F. H. Ellinger and W. H. Zachariasen for x-ray analysis; they used both powder techniques and "single crystal" examination of a resin sphere. They reported that there was no average gold-gold distance, from which Zachariasen concluded that there were

either random distances or a very large number of discrete distances. The similarity of the absorption frequency for solid $KAu(CN)_2$ and for $Au(CN)_2^-$ on the resin suggest that the $Au(CN)_2^-$ is bonded electrostatically rather than covalently to the resin; this is not surprising since the four bonding orbitals of a quaternary nitrogen are already used.

A study of $CuCN-KCN-H_2O$ is in progress to attempt to explain the different number and stability of cyanide complexes existing in the series Cu(I), Ag(I), and Au(I). The failure of gold to assume its sp^3 configuration with four cyanide anions needs explanation.

ACKNOWLEDGMENT

It is a pleasure to acknowledge our appreciation to Dale E. Armstrong for preparation of the figures and some of the solutions; to A. L. Henicksman for quantitative analytical work; to E. Staritzky for crystallographic analysis; to F. H. Ellinger and W. H. Zachariasen for the x-ray work; and to E. McLaren for some measurements.

THE JOURNAL OF CHEMICAL PHYSICS VOLUME 22, NUMBER 6 JUNE, 1954

Order-Disorder Phenomena

BRUNO LINDER
The Department of Chemistry, University of California, Los Angeles, California
(Received September 16, 1953)

The thermodynamics of the order-disorder transition in β brass is explored by making the assumption that the energy difference between the disordered and ordered state has the form E_0-BT^2. Such a law suggests itself if the coupling of the thermal expansion to the order-disorder transformation is emphasized and the effect of short range order is neglected. The constant B is shown to be related to the lattice vibrations of both the ordered and disordered phases. A very rough estimate of B was obtained from electrical resistivity measurements, the assumption being made that the connection between the resistivity and the vibrational frequency, $\rho \propto T/M\theta^2$, holds. A heat capacity *versus* temperature curve, which was calculated on the basis of a nonconstant energy of disordering and which also includes the effect of lattice vibrations, is shown to agree well with the experimental one.

The usefulness of the form E_0-BT^2 is not confined to β brass and the same expression may be applied to systems other than solid-solid.

INTRODUCTION

IN many problems involving heat of mixing the assumption is often made that the excess potential energy between a pair of unlike molecules over the average of a pair of like molecules is independent of temperature. While such an assumption greatly simplifies the problem in question, it is nevertheless conceivable that some of the difficulties connected with the theory of solutions may stem from a neglect of the temperature dependent part of the energy of mixing. In the present paper the potential energy between a pair of molecules is examined and the conclusion is reached that to a first approximation the energy of transition should depend on the square of the temperature. In view of the often reported anomalous behavior of the heat capacity in second order transitions,[1,2,3] it would seem appropriate to redetermine the heat capacity curve for β brass by considering a nonconstant energy of disordering and by taking into account lattice vibrations, with which the former is intimately connected, in the hope of obtaining better agreement between the theoretical and experimental curves. Although specific calculations were carried out for β brass, the procedure is general and should apply to other 1–1 binary alloys.

PROCEDURE

The energy of interaction between a pair of molecules can, in general, be represented by a formula of the type

$$\mathcal{E}=-k/r^m+j/r^n, \tag{1}$$

or more conveniently as

$$\mathcal{E}=\mathcal{E}_0\left[\frac{n}{n-m}\left(\frac{r_0}{r}\right)^m-\frac{m}{n-m}\left(\frac{r_0}{r}\right)^n\right], \tag{2}$$

where r_0 is the equilibrium distance and $\mathcal{E}_0$ the minimum energy at 0°K.[4] Expanding $\mathcal{E}$ about $\mathcal{E}_0$ by means of a Taylor series, we obtain

$$\mathcal{E}=\mathcal{E}_0+(r-r_0)\left(\frac{d\mathcal{E}}{dr}\right)_{r=r_0}+\tfrac{1}{2}(r-r_0)^2\left(\frac{d^2\mathcal{E}}{dr^2}\right)_{r=r_0}+\cdots. \tag{3}$$

[1] E. A. Guggenheim, *Mixtures* (The Clarendon Press, Oxford, 1952), pp. 128 and 143.
[2] C. Sykes and H. Wilkinson, J. Inst. Metals, **61**, 223 (1937).
[3] R. H. Fowler and E. A. Guggenheim, *Statistical Thermodynamics* (Cambridge University Press, Cambridge, 1952), pp. 576–581.
[4] See for example, reference 3, pp. 280–289.

$(d\mathcal{E}/dr)_{r=r_0}$ is, of course, equal to zero and

$$\left(\frac{d^2\mathcal{E}}{dr^2}\right)_{r=r_0}=\frac{\mathcal{E}_0}{r_0^2}[-mn]=-mn\frac{\mathcal{E}_0}{r_0^2}. \tag{4}$$

Equation (3), therefore, reduces to

$$\mathcal{E}=\mathcal{E}_0[1-(mn/2)(r-r_0)^2/r_0^2]. \tag{5}$$

At constant pressure, $(r-r_0)^2/r_0^2$ is roughly equal to, or proportional to, α^2T^2, where α is the coefficient of linear expansion. Consequently, we may write for $\mathcal{E}$,

$$\mathcal{E}=\mathcal{E}_0[1-(mn/2)\alpha^2T^2]. \tag{6}$$

For 1-1 Cu−Zn, the coefficient of linear expansion is approximately constant up to the temperature where considerable disordering sets in. Measurements on the Cu−Au system by Nix and MacNair[5] also reveal a remarkable constancy of α over a wide range of temperatures before disordering sets in and after disordering is complete. It is therefore not unreasonable to assume that, were it not for the effect of disorder, $\mathcal{E}$ could be represented by an equation of the type

$$\mathcal{E}=\mathcal{E}_0(1-AT^2),$$

where A is a constant equal to $mn\alpha^2/2$. Similarly, for a completely disordered alloy we may write

$$\mathcal{E}'=\mathcal{E}_0'(1-A'T^2).$$

Consequently, we may represent the difference in energy per mole between a completely disordered ($s=0$) and a completely ordered ($s=1$) system, at a given temperature T, by the following expression:

$$E(0)-E(1)=E_0-BT^2. \tag{7}$$

When dealing with a state of order other than zero the energy is a complicated function of s. However, if we make the assumption of complete random distribution, an assumption which characterizes the theory of regular solutions and the Bragg and Williams approximation, the change in energy takes the simple form[3]:

$$E(s)-E(1)=(1-s^2)[E(0)-E(1)]. \tag{8}$$

Although order-disorder transformations are often treated as involving no change in vibration frequencies,[6] omission of the latter is no longer permissible if one assumes the energy to be temperature dependent. Consider a crystal (of order s) which has no other degrees of freedom than the vibrational ones. At sufficiently high temperatures the Helmholtz free energy will take the form[7]:

$$A=E+3RT\ln(\theta/T). \tag{9}$$

[5] F. C. Nix and D. MacNair, Phys. Rev. **60**, 320 (1941).

[6] For a discussion of second order transitions see for example F. C. Nix and W. Shockley, Revs. Modern Phys. **10**, 1 (1938); and references (1) and (3).

[7] R. H. Fowler and E. A. Guggenheim, see reference 3, loc. cit. p. 327.

In this expression E stands for the potential energy and $\theta=h\nu/k$, ν being the Einstein vibration frequency. The equilibrium volume is determined by the condition that $(\partial A/\partial v)_T$, and consequently $(\partial A/\partial r)_T$ vanish. (The small contribution of the external pressure is here neglected). Upon differentiation, Eq. (9) reduces to

$$\left(\frac{\partial E}{\partial r}\right)_T=-3RT\frac{d\ln\theta}{dr}. \tag{10}$$

If we substitute into Eq. (10) the result of our approximation obtained in expression (5), the left-hand side member of Eq. (10) becomes $-mn(r-r_0)/r_0^2E_0$. Furthermore, by our previous approximation the equilibrium r varies with T so that Eq. (10) further reduces to

$$mnE_0\frac{r-r_0}{r_0^2}=3RT\frac{d\ln\theta}{dT}\frac{dT}{dr}. \tag{11}$$

For $(r-r_0)/r_0$ we now write αT, and dT/dr is equal to $1/r_0\alpha$. Expression (11), therefore, becomes

$$mnE_0\alpha^2=3R\frac{d\ln\theta}{dT}. \tag{12}$$

It should be emphasized that s is kept constant throughout, and that E_0, α, and θ are all functions of s. If we write Eq. (12) as the difference between a state of order s and one of order $s=1$, we get

$$mn[E_0\alpha^2(s)-E_0\alpha^2(1)]=3R\frac{d\ln[\theta(s)/\theta(1)]}{dT}. \tag{13}$$

By Eq. (8), the left-hand side member of Eq. (13) now reduces to $(1-s^2)[mn(E_0\alpha^2(0)-E_0\alpha^2(1))]$. But the term within brackets is precisely what was previously called $2B$, so that Eq. (13) now becomes

$$(1-s^2)2B=3R\frac{d\ln[\theta(s)/\theta(1)]}{dT}. \tag{14}$$

Equation (14) does not depend in any way upon the choice of s and should hold for all s. A necessary condition that Eq. (14) be satisfied for all s is that $\ln[\theta(s)/\theta(1)]$ be equal to $(1-s^2)\ln[\theta(0)/\theta(1)]$. From Eq. (14), we, therefore, get the result

$$2B=3R\frac{d\ln[\theta(0)/\theta(1)]}{dT}. \tag{15}$$

In order to obtain a more useful approximation for B we integrate Eq. (15) between the limits $T=0$ and T and the corresponding frequencies of the disordered and ordered states. This gives us

$$2BT=3R\left[\ln\frac{\theta(0)}{\theta(1)}-\ln\frac{\theta_0(0)}{\theta_0(1)}\right]. \tag{16}$$

Assuming random distribution, the change in free energy, for a 1–1 binary alloy is given by[6]:

$$A(s)-A(1)$$
$$=\frac{RT}{2}\{(1+s)\ln(1+s)+(1-s)\ln(1-s)-2\ln 2\}$$
$$+\{E(s)-E(1)\}+3RT\ln\frac{\theta(s)}{\theta(1)}. \quad (17)$$

The last terms of Eq. (17) may be written as

$$(1-s^2)\{E_0-BT^2+3RT\ln[\theta(0)/\theta(1)]\}.$$

If we add and subtract $(1-s^2)\{3RT\ln[\theta_0(0)/\theta_0(1)]\}$, and make use of Eq. (16), the former becomes $(1-s^2)[E_0+BT^2+CT]$ where $C=3R\ln[\theta_0(0)/\theta_0(1)]$. Substituting this expression into (17) and changing the reference state to one of complete disorder, we get

$$A(s)-A(0)$$
$$=\frac{RT}{2}\{(1+s)\ln(1+s)+(1-s)\ln(1-s)\}$$
$$-s^2\{E_0+BT^2+CT\}. \quad (18)$$

The heat capacity can now be calculated in a conventional manner. In order to obtain the equilibrium value of s at a given temperature T, we set the first derivative of (18) with respect to s equal to zero. We get

$$\tanh^{-1}s=\frac{2[E_0+BT^2+CT]s}{RT}$$
$$=\frac{2[E_0^*+B^*T^2+C^*T]s}{T}, \quad (19)$$

where $E_0+B+C=(E_0^*+B^*+C^*)R$. The change in energy between a state of order s and one of complete order is given by

$$E(s)-E(1)=(1-s^2)[E_0^*-B^*T^2]R, \quad (20)$$

from which we obtain the molar heat capacity

$$\frac{C_P(s)-C_P(1)}{R}=-2B^*T-2s[E_0^*-B^*T^2]\frac{ds}{dT}$$
$$+s^2(2B^*T). \quad (21)$$

ds/dT can easily be determined if we differentiate (19) implicitly. For this we get

$$\frac{ds}{dT}=\frac{s[(2E_0^*/T^2)-2B^*]}{[(2E_0^*/T)+2B^*T+2C^*-1/(1-s^2)]}. \quad (22)$$

This expression substituted in (21) gives the final result:

$$\frac{C_P(s)-C_P(1)}{R}=\frac{-s^2[(2E_0^*/T)-2B^*T]^2}{[(2E_0^*/T)+2B^*T+2C^*-1/(1-s^2)]}$$
$$+(1-s^2)(-2B^*T). \quad (23)$$

RESULTS AND DISCUSSION

We shall now apply Eq. (23) in calculating the heat capacity for β brass. But first we must find an estimate of the parameters B and C. Equation (15) shows how B is related to the characteristic vibration frequencies. The latter are, in turn, related to the specific resistances by the following approximation, $\rho\propto(T/M\theta^2)$.[8,9] Thus, if we substitute $(T/\rho)^{\frac{1}{2}}$ for θ into Eq. (15) we obtain

$$2B=-\tfrac{3}{2}R\left\{\frac{d\ln[\rho(0)/T]}{dT}-\frac{d\ln[\rho(1)/T]}{dT}\right\}. \quad (24)$$

It is here implied that the electrical resistance has different values for different states of order only because the characteristic temperatures differ. The resistance of the disordered phase can, of course, be measured only at high temperatures while the resistance of the ordered phase can be measured at low temperatures only. It is therefore best to determine the quantity

$$-\tfrac{3}{2}R\frac{d\ln[\rho(0)/T]}{dT}=2A'$$

at some high temperature (T'), and

$$-\tfrac{3}{2}R\frac{d\ln[\rho(1)/T]}{dT}=2A$$

at some low temperature (T). In this manner extrapolations over a wide temperature range are avoided. For convenience, we shall choose the temperatures $T'=400$°C and $T=200$°C. From the $\rho-T$ curves measured by W. Webb[10] we find that

$$2A'=-\tfrac{3}{2}R\left[\frac{1}{13}\,\frac{9}{400}-\frac{1}{673}\right]=-\tfrac{3}{2}R(2.449\times10^{-4})$$
$$2A=-\tfrac{3}{2}R\left[\frac{1}{7}\,\frac{3}{200}-\frac{1}{473}\right]=-\tfrac{3}{2}R(0.286\times10^{-4}), \quad (25)$$

giving $B=A'-A=-1.62\times10^{-4}R$.[11] The constant C can now easily be determined if we integrate $2A'$ be-

[8] N. F. Mott and H. Jones, *The Theory of the Properties of Metals and Alloys* (Oxford University Press, New York, 1936), p. 268.

[9] F. Seitz, *The Modern Theory of Solids* (McGraw-Hill Book Company, Inc., New York, 1940), p. 529.

[10] W. Webb, Phys. Rev. **55**, 297 (1939).

[11] The resistivity curve from which (25) is determined is actually given for β brass which contains 51.25 percent Cu but it is felt that the difference between this alloy and the ideal 50–50 Cu–Zn cannot be too great.

tween the limits $T_0'=0°K$ and T', and $2A$ between $T_0=0°K$ and T, and then take the difference. This gives us

$$2A'T'-2AT=-\tfrac{3}{2}R\left[\ln\frac{\rho'(0)}{\rho(1)}-\ln\frac{\rho_0(0)}{\rho_0(1)}-\ln\frac{T'}{T}\right]. \quad (26)$$

With $\rho(0)/\rho(1)=13/7$, A', A, T' and T as quoted above, we find that $-\frac{3}{2}R\ln[\rho_0(0)/\rho_0(1)]$, which is equal to C, is $-0.172R$. In our calculations, the actual values used for B and C were respectively $-1.725\times10^{-4}R$ and $-0.15R$.

E_0 can now also be determined. We observe that Eq. (18) goes through a point of inflection at $s=0$. Setting the second derivative of (18) with respect to s equal to zero we obtain

$$E_0+BT_c^2+CT_c=RT_c/2. \quad (27)$$

With $B=-1.725\times10^{-4}R$, $C=-0.15R$, and $T_c=742°K$, we find that $E_0=577.27R$ cal/mole. Substituting these values into (23) gives the heat capacity curve for β brass. The calculated heat capacity curve is compared with the experimental data as determined by Moser[12] in Fig. 1. The heat capacity curve of the completely ordered phase is assumed to be the mean of experimental curves for pure Cu and pure Zn. In view of the crudeness of method employed, the agreement must be considered good. It is expected that a better choice of the constants B and C and the use of a more refined theory, such as the "quasi-chemical method," would give further improvement.

It might, at first, seem surprising that a small correction term in the energy of disordering should bring about such large differences in the heat capacity. (In fact, the limiting value of $(3/2)R$ in the Bragg and Williams theory is being more than tripled.) That the heat capacity is indeed quite sensitive to the B term can be seen from the following considerations. If we expand $\tanh^{-1}s$ of Eq. (19) into a power series we get

$$1+\tfrac{1}{3}s^2+\tfrac{1}{5}s^4+\cdots=\frac{2[E^*+B^*T^2+C^*T]}{T}. \quad (28)$$

Near the critical temperature $s\to0$. If we neglect powers of s higher than two, expression (28) reduces to

$$1+\tfrac{1}{3}s^2=\frac{2E_0^*}{T}+2B^*T+2C^*, \quad (29)$$

from which

$$-s^2=3\left\{1-\left(\frac{2E_0^*}{T}+2B^*T+2C^*\right)\right\} \quad (30)$$

[12] H. Moser, Physik. Z. 37, 737 (1936).

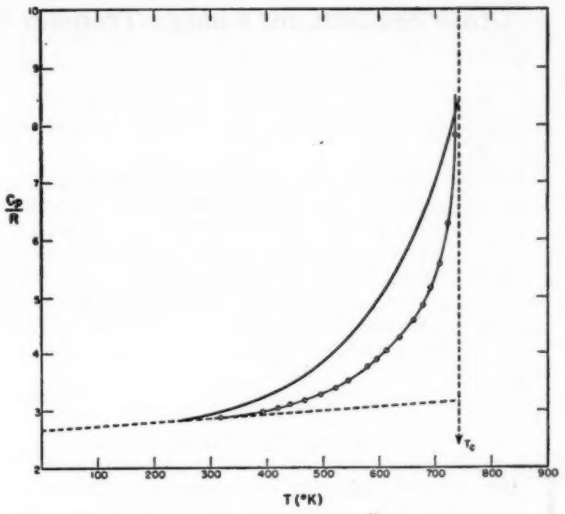

FIG. 1. The heat capacity of β brass. The drawn curve is calculated; the circles are experimental points as determined by Moser (see reference 11); the dashed curve is the mean of the curves for pure Cu and pure Zn ($C_P(1)$].

is obtained. To the order of this approximation

$$-2s\frac{ds}{dT}=+\frac{6[E_0^*-B^*T^2]}{T^2}. \quad (31)$$

Substituting Eqs. (30) and (31) into (21) yields

$$\frac{C_P(s\to0)-C_P(1)}{R}=\left\{4-3\left(\frac{2E_0^*}{T}+2B^*T+2C^*\right)\right\}\times(-2BT)+\frac{6(E^*-B^*T^2)^2}{T^2}. \quad (32)$$

We observe that $2E_0^*/T_c+2B^*T_c+2C^*=1$, so that

$$C_P(s\to0)-C_P(1)=-2B^*T_cR+\tfrac{3}{2}R\left[\frac{E_0^*-B^*T_c^2}{T_c/2}\right]^2. \quad (33)$$

In the case of Bragg and Williams $B=0$, $E_0^*=T_c/2$ so that $\Delta C_P(s\to0)=\frac{3}{2}R$. The presence of the B term in $E_0^*-B^*T^2$ not only makes $E_0^*-B^*T_c^2>T_c/2$ (B is negative) but $E_0^*>T_c/2$ as well (Eq. 27). The effect is even more pronounced in the heat capacity where $(E_0^*-B^*T_c^2)/\,T_c/2$ has to be squared thus making the limiting ΔC_P value quite sensitive to B.

In conclusion we wish to remark that since the considerations which led to Eq. (6) are general, it would seem profitable to investigate systems other than β brass. In particular, expression (6) may find some useful application in liquid-liquid and liquid-vapor equilibria.

ACKNOWLEDGMENT

The author wishes to express his appreciation to Dr. Robert L. Scott for his valuable comments and criticisms, and his constant encouragement.

Cross Sections for Charge Transfer Collisions of Low-Energy Ions in N_2 and O_2

ROY F. POTTER
National Bureau of Standards, Washington, D. C.
(Received January 29, 1954)

Measurements have been made of the cross sections for charge transfer collisions between the low-energy (9–250 ev) ions, N_2^+, O_2^+, O^+ and N^+, and the molecules N_2 and O_2. Two reactions (N^+, N_2; O^+, N_2) have been reported by other workers and are compared with present work.

The experimental method utilizes a radio-frequency mass spectrometer as an ion source. The ions are collimated and enter a weak radial electric field of cylindrical symmetry. The secondary ions are separated from the primary beam and the ratio of the two currents is measured as a function of pressure.

Results are discussed in terms of the adiabatic collision condition and possible internal energy states of the ions and molecules.

INTRODUCTION

THE charge transfer phenomenon, that is, the transfer of an electron from a neutral gas molecule to an ion, has been studied by many observers since the 1920's. Massey and Burhop[1] have given a comprehensive list of such experiments up to 1950. Renewed interest in this effect has been stimulated by recent theories of production mechanisms of the various layers of the ionosphere.[2]

The reaction between ions of type A atoms and type B atoms may be written

$$A^+ + B \rightarrow A + B^+.$$

At the present time, this reaction, which results from an inelastic collision, is only imperfectly understood. The earliest experiments[3,4] showed, however, that the closer the ionization potential of particle A approximated that of B, the greater was the chance that the reaction would occur. In all such reactions the net energy, potential and kinetic, cannot be negative.

If the collision approximates adiabatic conditions, i.e., the perturbation allows sufficient time for the electronic states to adjust themselves internally, transitions have little probability of occurring. These adiabatic conditions prevail when

$$a\Delta E/hv \gg 1,$$

where a is the interaction distance, v is the relative velocity of the particles, and ΔE is net difference in the initial and the final energy states of the particles.* For the case of an ion beam moving through a gas where the neutral particles are at thermal energies, the velocity is proportional to $(V/M)^{\frac{1}{2}}$, where V is beam voltage and M is mass of the ion in amu. When $a \sim 4 \times 10^{-8}$ cm, the adiabatic condition can be written as

$$6.8\Delta E(M/V)^{\frac{1}{2}} \gg 1.$$

Hasted[5,6] has studied a number of atomic cases for various ΔE's as a function of $\sqrt{V}$. His results did corroborate the fact that as the conditions were made less and less adiabatic the cross section for the reaction increased.

The present experiment was initiated to study the charge transfer reactions of some of the ions and gases of the upper atmosphere. Cross-section measurements were made for energies between 9 and 250 volts for the following reactions:

$$N_2^+ + N_2 \rightarrow N_2 + N_2^+$$
$$O_2^+ + O_2 \rightarrow O_2 + O_2^+$$
$$N^+ + N_2 \rightarrow N + N_2^+$$
$$O^+ + O_2 \rightarrow O + O_2^+$$
$$O^+ + N_2 \rightarrow O + N_2^+$$
$$N^+ + O_2 \rightarrow N + O_2^+$$
$$N_2^+ + O_2 \rightarrow N_2 + O_2^+$$
$$O_2^+ + N_2 \rightarrow O_2 + N_2^+.$$

EXPERIMENTAL APPARATUS AND METHOD

A schematic sketch of the apparatus is shown in Fig. 1. Section A is a radio-frequency mass spectrometer as developed by W. H. Bennett[7] with additional grids for suppression of secondary emission. In a previous experiment[8] a spectrometer similar to A was used with a cylinder enclosed on the ends with knitted tungsten mesh. The primary ions were accelerated to a selected voltage in the cylinder; the ions extracted from the cylinder were subjected to a stopping potential analysis. The energy distribution for three cases of rare gas ions in their parent gases are shown in Fig. 2. The larger peak at the higher energy is that due to the primary beam at the potential of the source, while the smaller peak is that due to secondary ions formed at the potential of the cylinder (zero volts in this instance). This confirms previous work on the state of the secondary

[1] H. S. W. Massey and E. H. S. Burhop, *Electronic and Ionic Impact Phenomena* (Clarendon Press, Oxford, 1952).
[2] Proceedings of the Conference on Ionospheric Physics, Pennsylvania State College (1950).
[3] G. P. Harnwell, Phys. Rev. **29**, 683 (1927).
[4] T. R. Hogness, and E. G. Lunn, Phys. Rev. **30**, 26 (1927).
* See reference 1, p. 441.
[5] J. B. Hasted, Proc. Roy. Soc. (London) **A205**, 421 (1951).
[6] J. B. Hasted, Proc. Roy. Soc. (London) **A212**, 235 (1952).
[7] W. H. Bennett, J. Appl. Phys. **21**, 143 (1950).
[8] R. F. Potter, Phys. Rev. **87**, 232(A) (1952).

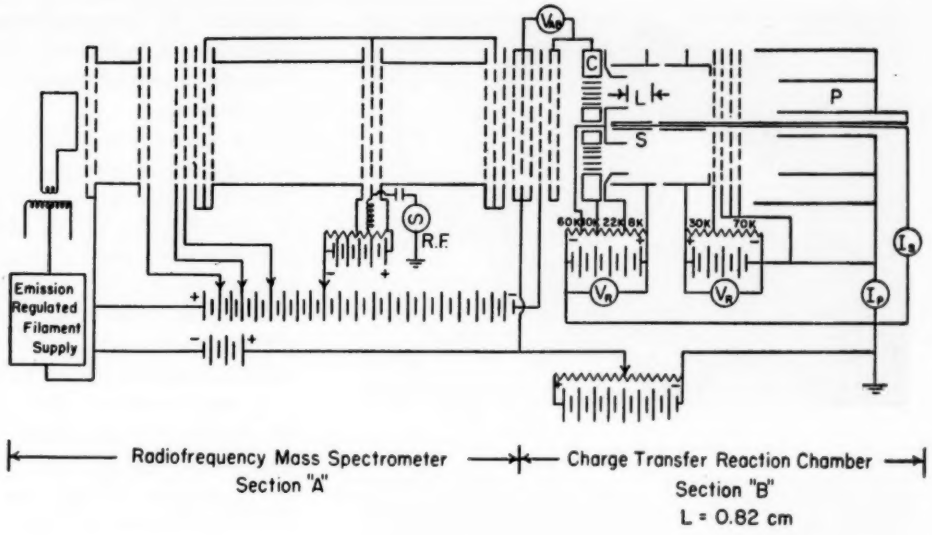

FIG. 1. Schematic sketch of experimental apparatus. C is the ion collimator, S the secondary ion collector, and P is the primary ion collector.

ions formed as a result of charge transfer, i.e., the ions are formed with little or no velocity component in the forward direction.[1]

Although cross sections for the three rare gas cases were reported from this experiment, the method was unfeasible for charge transfer collisions of small cross sections. Consequently a method was devised similar in principle to that used by Hasted, Rostagni, and others[1] in that the secondary ions formed at rest are swept to a second collector by small electric and/or magnetic fields which are too small to effectively perturb the primary beam. In the present experiment, the wide ion beam from the spectrometer made it possible to use electric fields with cylindrical symmetry.

Section B in Fig. 1 shows the reaction chamber. "C" is a collimator formed of parallel nichrome sleeves 0.050 in. in diameter, 0.255 in. in length. A photograph of one such collimator used is shown in Fig. 3(a).

An arrangement of conducting cylinders with suitable electric potentials was worked out on a resistance network analog computer constructed by the Electron Physics Section of the National Bureau of Standards.[9] This arrangement approximated a radial electric field of cylindrical symmetry. A sketch of the equipotential lines is shown in Fig. 4. The central cylinder has the advantage of providing a small target for elastically scattered primary ions while being a very efficient collector for the secondary ions. The secondary collector was divided in two, and the exposed part of that marked S defined the path length for the reaction. The grids just in front of the collector plate in Fig. 1 were provided for further stopping potential analyses of the ion beam. "P" indicates the collector for the primary current, although the current to all electrodes to the right of S is collected as I_p in the cross-section measurements. All exposed metal surfaces used in Sec. B were made of nichrome V. Figure 3(b) is an end view of the reaction chamber with the collimator removed.

A study of the action of the radial field for the ions N^+, N_2^+ in N_2 is shown in Fig. 5. As V_R, the voltage supplying the radial field of the cylindrical reaction chamber, is varied from 0 volts to $+V_R$, the ratio (R) of I_s (the current to S) to I_p (the remaining primary current) increases linearly until a plateau is reached, indicating a saturation of secondary ions collected. At higher values of V_R, the increase in R indicates elas-

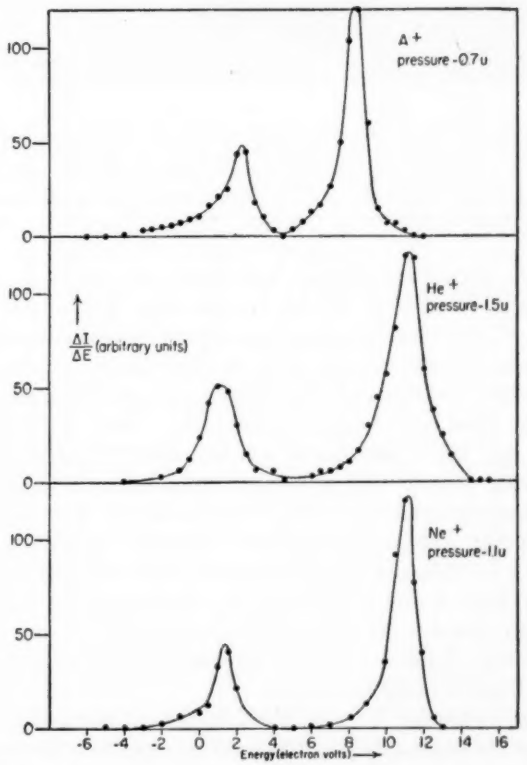

FIG. 2. Three energy spectra of ions leaving the reaction chamber. The indicated ion is reacting with its own gas.

[9] Natl. Bur. Standards Tech. News Bull. **37**, 19 (1953).

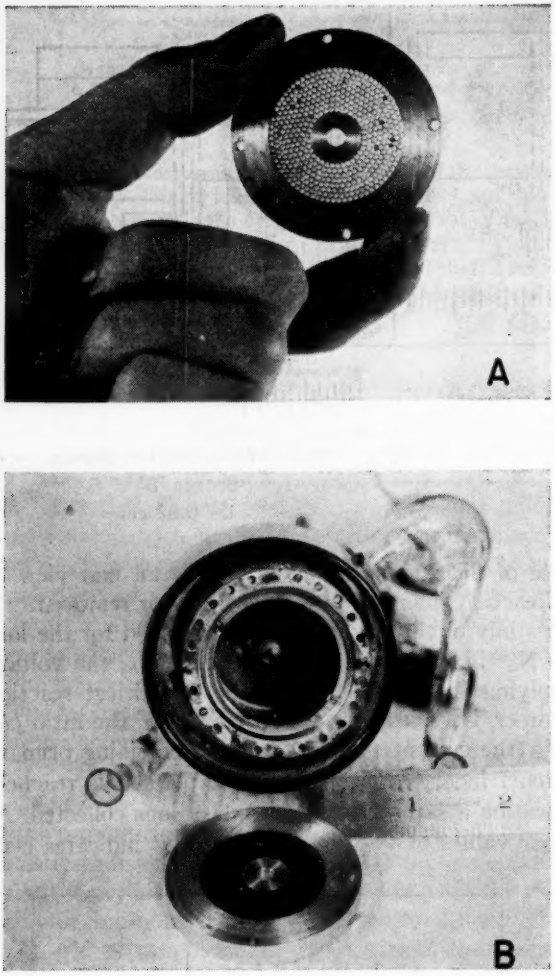

FIG. 3. (a) The collimator C is made up of *ca* 400 nichrome V cathode sleeves 0.050 in. diameter by 0.255 in. length. (b) End view of the collision reaction chamber. The secondary ion collector S, a nichrome V cathode sleeve 0.050 in. diameter, is in the center. The collimator is shown in the foreground.

tically scattered primary ions begin to arrive at the secondary collector. It can be seen that in the case of N_2^+, N_2, the elastic scattering does not have appreciable wide angle components down to 8 ev, while the ion N^+ with half the mass of the N_2 molecule undergoes relatively wide angle scattering at 25 ev. Thus 25 ev and 8 ev are the lower limits for the kinetic energies of primary atomic and molecular ions, respectively, for the measurement of charge transfer cross sections in molecular gases. The positive intercept for the case of N^+, N_2 indicates a small degree of lack of collimation. Both Figs. 2 and 5 indicate the characteristics of the charge transfer reaction which is essential for the experiment, namely that the secondary ion is produced with little or no kinetic energy.

The voltmeter V_{AB} of Fig. 1 indicated the potential of the ion beam entering the reaction chamber. Because the spectrometer grids were constructed of knitted tungsten and the parts of the reaction chamber were nichrome V, there was present a contact potential difference. A correction for this was obtained from stopping potential curves for the ion beam in the reaction chamber.

The vacuum system consisted of a Princeton type mercury jet pump backed by a Duoseal forepump. Pressure measurements were made with a DPI McLeod gauge calibrated by the author, and a VG-1A type ion gauge which was regularly calibrated against the McLeod gauge.

All gases used were commercial grade from tank cylinders and were passed through liquid nitrogen traps before admission to the sample system.

I_p was measured with a Millivac voltmeter model No. 17XB with the shunt box to give an ultimate full scale sensitivity of 2.5×10^{-10} amperes. I_s was measured by either the Millivac meter or a GL-5674 General Electric electrometer tube circuit[10] which was calibrated against the Millivac.

All measurements of Q were made with $V_R=6.0$ volts. The electron energy in the primary ionization chamber of the spectrometer was 75 ev.

The current strength of a beam of ions passing a distance L cm through a gas at pressure P mm Hg is given by

$$I=I_0e^{-QLP},$$

where I_0 is the current at $L=0$, and Q is the cross section, in units of cm^{-1} at 1 mm pressure, for all processes which remove ions. In the case of charge transfer, the

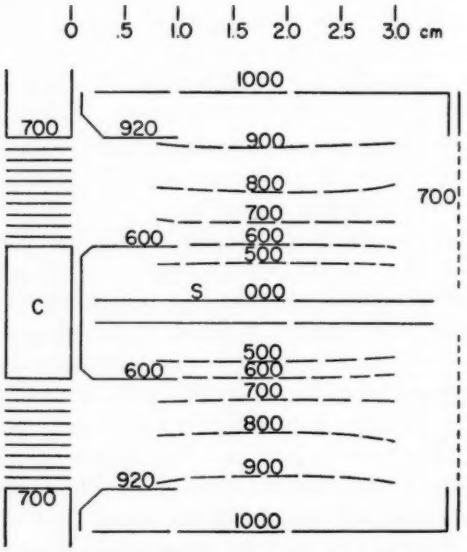

FIG. 4. Schematic sketch of the cylindrical reaction chamber. Solid lines represent solid nichrome V metal surfaces, and short dashed lines represent a nichrome fine mesh grid. The longer dashed lines represent the equipotential resulting when the relative potentials shown are placed on the metal surfaces. The scale is indicated at the top.

[10] J. M. Lafferty and K. H. Kingdon, J. Appl. Phys. **17**, 894 (1946).

current of secondary ions is given by

$$I_s = I_0(1-e^{-QLP}) = I_p(e^{QLP}-1),$$

where I_p is the current of primary ions at L.

$$I_s/I_p = R = (e^{QLP}-1), \quad \ln(R+1) = QLP.$$

If the exponent is small, $R \approx QLP$.

With measurements of R as a function of the gas pressure P and a knowledge of L, the cross section Q can be determined. The plots of R *vs* P for various energies for the case requiring the greatest sensitivity is shown in Fig. 6. This was the reaction

$$N^+ + N_2 \rightarrow N + N_2^+.$$

To study the reactions of the ion of one gas in another gas, a mixture had to be used. A small amount

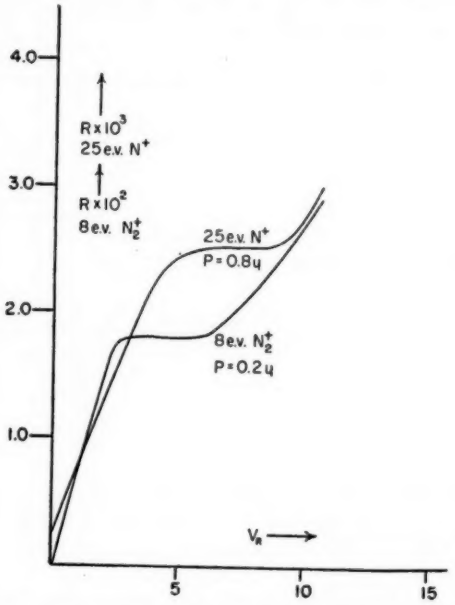

FIG. 5. The ratio R for the primary ions indicated in N_2 is shown as a function of the potential, V_R, across the reaction cylinder. The plateau indicates all charge transfer secondary ions are being collected. It would appear that the gas scattering of N^+ in N_2 is appreciably greater than that of N_2^+.

of gas to form the desired ions was introduced and held at a constant partial pressure while the reacting gas pressure was varied over the desired range. In this case we may write

$$I_s/I_p = R = \exp\{(Q_1P + [Q_2-Q_1]P_2)L\} - 1,$$

where Q_1 is desired cross section, Q_2 is cross section of ion in its own gas, P_2 is the partial pressure of the primary ion's gas, and P is the total pressure in the system. A plot of $\ln(R+1)$ *vs* P gives a straight line with a slope Q_1L and intercept $(Q_2-Q_1)P_2L$. The intercepts found were consistent with the cross sections measured.

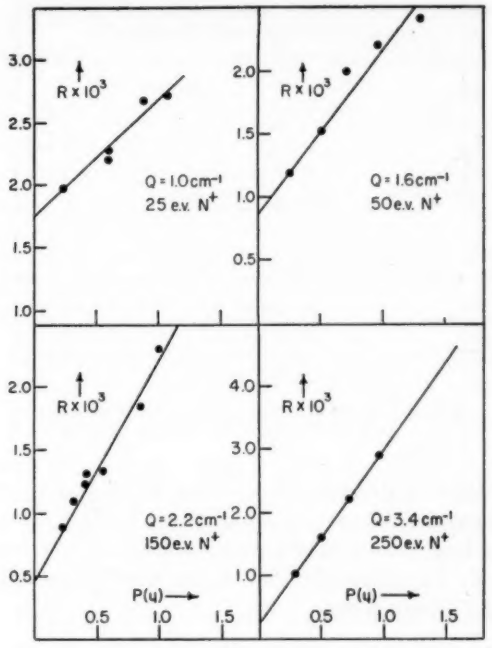

FIG. 6. The ratio R of secondary ion current to primary ion current as a function of pressure is shown for several energies of N^+ ions in N_2. The positive intercept, which decreases for higher energies, indicates some degree of imperfect collimation.

RESULTS AND DISCUSSION

The cross sections as a function of primary ion energy for the reactions studied are shown in Figs. 7 through 10. The helium and argon studies of Fig. 9 were made to compare with those of Hasted.[6] Hasted's data for 0^+, N_2 and Wolf's data[11] for N^+, N_2 are compared in Fig. 10 with the present data.

The accuracy of the determinations of pressure, path length, and ion currents limits the reliability of the cross sections calculated from these quantities to about ± 15 percent. Figures 7 and 8 show that the reproducibility of the data is much better than this. Hasted estimates his absolute accuracy as ± 10 percent.

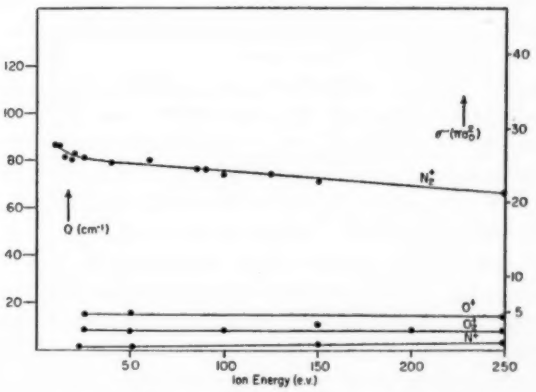

FIG. 7. Charge transfer collision cross sections for N_2^+, N^+, O_2^+, O^+ ions in N_2.

[11] F. Wolf, Ann. Physik **30**, 313 (1937).

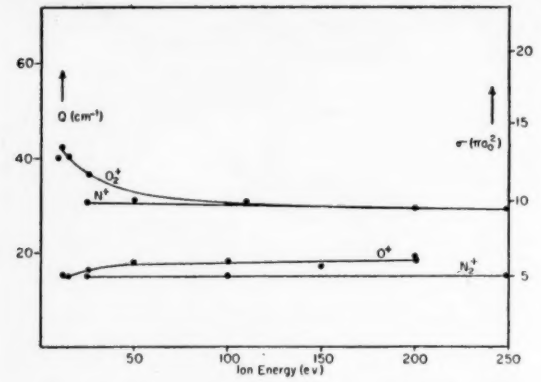

FIG. 8. Charge transfer collision cross sections for O_2^+, O^+, N_2^+, N^+ ions in O_2.

The range of disagreement varies from *ca* 25 percent in the case of A^+, A to virtually zero for He^+, He.

The large value of the cross section in the case of N_2^+, N_2 indicates the ion beam consists wholly of $N_2^+(^2\Sigma_g^+)$ ions. Thus,

$$N_2^+(^2\Sigma_g^+)+N_2(X^1\Sigma)\rightarrow N_2(X^1\Sigma)+N_2^+(^2\Sigma_g^+).$$

The low value cross sections for O_2^+ in O_2 (low compared to the nitrogen case) indicates that exact resonance is not always available to the reaction. An examination of the potential diagrams of the O_2 ion and molecule shows appreciable difference of the minima (see Table I). Thus, the reaction

$$O_2^+(^2\pi_g)+O_2(^3\Sigma_g^-)\rightarrow O_2(^3\Sigma_g^-)+O_2^+(^2\pi_g),$$

has zero energy defect between the lowest ground state vibrational levels of the reactants and should be a resonance reaction with a high cross section. However, by the Franck-Condon principle and because of considerable overlap of the higher vibrational levels in each state, the resulting products could be formed in vibrational levels where both v and v' are greater than zero. Thus some of the reactions could be endothermic by as much as 1.0 ev, and a mixture of such non-resonant and resonant reactions would result in a reduced value of the cross section.

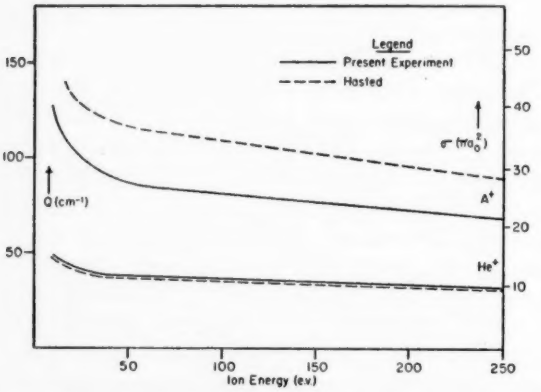

FIG. 9. Charge transfer collision cross sections for He^+ in He and A^+ in A are shown for comparison with the reported results of Hasted.

The asymmetrical case of N^+ ion in O_2 is quite striking. To avoid adiabatic conditions at the low energies, the reaction would have to be the following, in which the neutral N atom is left in the metastable $N(^2D)$ state:

$$N^+(^3P)+O_2(^3\Sigma)\rightarrow N(^2D)+O_2^+(^2\pi_g)+0.1 \text{ ev}.$$

The extra 0.1 ev could easily be taken up in the vibrational levels of the O_2^+, allowing the reaction to approach the conditions of symmetry. If the reaction were

$$N^+(^3P)+O_2(^3\Sigma)\rightarrow N(^4S)+O_2^+(^2\pi_g)+2.3 \text{ ev},$$

the adiabatic restrictions would preclude such a large cross section. The Franck-Condon rule prohibits the excitation of the $O_2^+(^2\pi_g)$ ion into vibrational levels higher than one ev by a direct excitation from the ground state of the molecule.

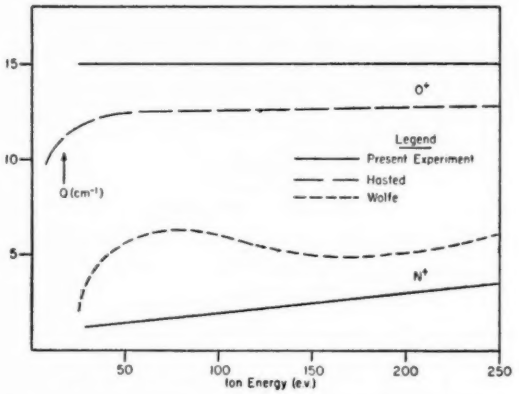

FIG. 10. Charge transfer collision cross sections for O^+ and N^+ ions in N_2 are compared with the reported results of Hasted (O^+, N_2) and Wolf (N^+, N_2).

Because the endothermic reaction

$$N^+(^3P)+O_2(^3\Sigma)\rightarrow N(^4S)+O_2^+(^4\pi_u)-1.0 \text{ ev}$$

will always have an energy defect greater than 1.0 ev, it will be adiabatic and have small cross section at low ion energies.

Except for the symmetric case of (N_2^+, N_2), all of the reactions in O_2 occur much more readily than those in N_2. In nitrogen the endothermic nature of the reactions plays a decided part in keeping the cross sections to small values. The relatively large cross section for O^+ in N_2 at low energies indicates that some of the beam might consist of some metastable $O^+(^2D)$ as well as the ground state $O^+(^4S)$ ion.

$$O^+(^2D)+N_2(^1\Sigma)\rightarrow O(^3P)+N_2^+(^2\Sigma)+1.3 \text{ ev}.$$

Table II shows the suggested reactions.

In conclusion, charge transfer reaction cross sections have been measured for the ions of N_2 and O_2 in those

TABLE I. Values of r_e (nuclear separation at the potential minimum) for the ground states of N_2 and O_2 (ions and molecules).

Molecule	State	r_e(A)[a]
O_2	$X^3\Sigma_g^-$	1.207
O_2^+	$X^2\pi_g$	1.123
N_2	$X^1\Sigma_g^+$	1.094
N_2^+	$X^2\Sigma_g^+$	1.116

[a] G. Herzberg, *Spectra of Diatomic Molecules* (D. Van Nostrand Company, Inc., New York, 1950).

TABLE II. Reactions that are likely to be dominant in giving the cross section observed.

Reaction	ΔE(ev)
$O_2^+(^2\pi_g)+O_2(^3\Sigma)\rightarrow O_2(^3\Sigma)+O_2^+(^2\pi_g)$	0.0
$O^+(^4S)+O_2(^3\Sigma)\rightarrow O(^3P)+O_2^+(^2\pi_g)$	+1.4
$N^+(^3P)+O_2(^3\Sigma)\rightarrow N(^2D)+O_2^+(^2\pi_g)$	+0.1
$N_2^+(^2\Sigma)+O_2(^3\Sigma)\rightarrow N_2(^1\Sigma)+O_2^+(^4\pi_u)$	+0.1
$N_2^+(^2\Sigma)+O_2(^3\Sigma)\rightarrow N_2(^1\Sigma)+O_2^+(^2\pi_g)$	+3.4
$N_2^+(^2\Sigma)+N_2(^1\Sigma)\rightarrow N_2(^1\Sigma)+N_2^+(^2\Sigma)$	0.0
$N^+(^3P)+N_2(^1\Sigma)\rightarrow N(^4S)+N_2^+(^2\Sigma)$	−1.1
$O^+(^4S)+N_2(^1\Sigma)\rightarrow O(^3P)+N_2^+(^2\Sigma)$	−2.0
$O^+(^2D)+N_2(^1\Sigma)\rightarrow O(^3P)+N_2^+(^2\Sigma)$	+1.3
$O_2^+(^2\pi_g)+N_2(^1\Sigma)\rightarrow O_2(^3\Sigma)+N_2^+(^2\Sigma)$	−3.4
$O_2^+(^4\pi_u)+N_2(^1\Sigma)\rightarrow O_2(^3\Sigma)+N_2^+(^2\Sigma)$	−0.1

gases. With the aid of spin considerations, Franck-Condon principle, and the adiabatic condition of interaction, the possible reactions have been discussed in terms of the initial and final states of the reactants.

The author wishes to express his appreciation of the support of the Central Radio Propagation Laboratory for this project. His thanks go to Dr. R. G. Breckenridge and Dr. L. M. Branscomb for encouragement and suggestions in carrying out the experiments. Many fruitful discussions were had with Mr. F. L. McCrackin during the course of the experiment. The author also wishes to thank the Electron Physics Section of the National Bureau of Standards for the use of the resistance network analog computer. Finally, acknowledgment must be made for the fine craftsmanship contributed to the construction of the apparatus by Mr. W. J. McKean, Mr. J. M. Smith, and Mr. R. D. Lantzer.

THE JOURNAL OF CHEMICAL PHYSICS VOLUME 22, NUMBER 6 JUNE, 1954

The Interaction of Rare Gas Atoms with Surfaces*†

W. A. STEELE‡ AND G. D. HALSEY, JR.
Department of Chemistry, University of Washington, Seattle, Washington

(Received September 9, 1953)

The apparent volumes of vessels containing high surface area powders have been measured with rare gases and analyzed. The interaction energies and distances of closest approach have been evaluated. A new method for the estimation of surface area is presented.

I. INTRODUCTION

THE interaction of rare gas atoms with solid surfaces has been considered by numerous authors.[1–6] In a number of cases, experimental data have been interpreted in the light of these calculations.[7–10] However, the data have in general been taken below the critical temperature of the adsorbate, usually in the region of the boiling point. In this region lateral interaction, multilayer formation, and possible capillary condensation must be considered. Since the theory of these phenomena is at least as difficult as the theory of liquids, it seemed attractive to investigate behavior at higher temperatures. If the temperature is sufficiently high and the gas pressure low, interaction between the rare gas atoms can be ignored and the problem of the interaction of a single atom with the surface investigated.

For this purpose a sample of solid with a total B.E.T. area of at least 3000 square meters was introduced into a bulb and the "dead space" volume measured at different temperatures with various rare gases. This volume V depends on the temperature and the gas used. In principle, it should be measured at a number of pressures and then extrapolated to zero pressure. In every case reported here, that extrapolation was unnecessary, because the temperature was always high enough to make V sensibly independent of pressure over the pressure range used. This independence is the

* This research was supported by Contract AF19(604)-247 with the Air Force Cambridge Research Center.

† Presented at the 124th national meeting of the American Chemical Society, Chicago, Illinois, September 6–11, 1953.

‡ Presented in partial fulfillment of the requirements for the Ph.D. degree.

[1] R. H. Fowler, *Statistical Mechanics* (Cambridge University Press, Cambridge, 1939), p. 335.
[2] W. J. C. Orr, Trans. Faraday Soc. **35**, 1247 (1939).
[3] D. M. Young, Trans. Faraday Soc. **47**, 1228 (1951).
[4] J. E. Lennard-Jones, Trans. Faraday Soc. **28**, 333 (1932).
[5] J. E. Lennard-Jones and A. F. Devonshire, Proc. Roy. Soc. (London) **A156**, 6 (1936).
[6] J. E. Lennard-Jones and A. F. Devonshire, Proc. Roy. Soc. (London) **A158**, 242 (1937).
[7] D. M. Young, Trans. Faraday Soc. **47**, 77 (1951).
[8] D. M. Young, Trans. Faraday. Soc. **48**, 548 (1952).
[9] R. M. Barrer, Proc. Roy. Soc. (London) **A161**, 476 (1937).
[10] W. J. C. Orr, Proc. Roy. Soc. (London) **A173**, 349 (1939).

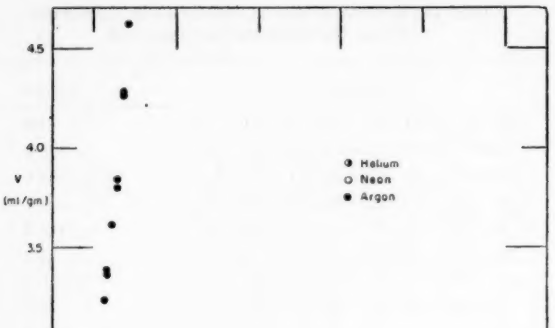

FIG. 1. Experimental values of apparent gas space volume for a sample of carbon black plotted against reciprocal temperature in degrees absolute.

criterion for the effective absence of interaction between two or more gas atoms, and it allows relatively simple theoretical calculations to be applied.

An equivalent method of expressing the experimental results would be in terms of gas adsorbed in excess of that in the true dead space. This adsorption would be proportional to pressure. However, the theoretical treatment which follows can be developed much more simply in terms of apparent volume, because of the kinship with the theory of imperfect gases which emerges.

The effect of temperature on apparent volume turned out to be quite large and easily measurable. In Fig. 1 the values of V are shown for a sample of carbon black. Even the helium volumes are strikingly dependent on temperature.

II. EXPERIMENTAL

A conventional gas transfer apparatus was used. The temperature was regulated by means of vapor baths. To accomplish this, the sample bulb was placed in a glass jacket, with a thermocouple well and a reflux condenser at the top, and a ground glass joint at the bottom. The liquids used for the vapor baths were contained in a number of glass bulbs fitted with ground glass joints so they could be attached to the bottom of the glass jacket. The reflux condenser was connected to a manostat operated by a magnetic switch capable of holding the pressure of the vapor bath constant to within 2 mm Hg (0.05°C variation in boiling temperature for most liquids). The jacket was wound with nichrome wire and covered with asbestos. This served a double purpose: to act as an oven when the samples were being outgassed, and to minimize heat losses from the vapor baths. The liquids were boiled at about one-half atmosphere and at atmospheric pressure, and were chosen such that readings were taken at intervals of about 20° between room temperature and 220°C. When temperatures below room temperature were required, the glass jacket was removed and the sample bulb immersed in suitable freezing baths.

The temperature measurements were made with a copper-constantan thermocouple. The electromotive force was measured on a Leeds and Northrup Type K-2 potentiometer in conjunction with a galvanometer such that temperature differences of 0.02°C were detectable. The thermocouple was calibrated at dry ice, ice, steam, and the melting point of tin, the readings at the calibration points being reproducible to 0.05°C. For each sample, isotherms were run at low temperatures to determine the temperature below which V became a function of pressure, and, once this was done, isosteres were run over the available range of higher temperatures. The pressures (about 300 mm at room temperature) were indicated by a constant volume manometer, and could be read with a cathetometer to 0.005 cm. The volume of the system remaining at room temperature was determined before the bulb was attached, and usually amounted to about 10 percent of the total volume of the gas space. Because of this fact, the correction for the amount of gas in the system outside of the sample bulb was quite important, and, therefore, room temperature was determined to within 0.5°C and its variation taken into account.

A blank run, using the system as a gas thermometer, with argon in an otherwise empty sample bulb, showed that the over-all accuracy of the pressure-temperature measurements was ±0.05 percent.

The helium used was tank helium from Western Oxygen, Inc. The other gases were reagent grade gases from Air Reduction Sales Company. All gases were mass spectrometrically analyzed and were shown to be better than 99.9 percent pure.

The samples used were as follows: porous glass from Corning Glass Company (obtained from Professor P. H. Emmett); alumina (obtained from Dr. T. D. Oulton of the Filtrol Corporation) (calcined before using for two hours at 800°C); carbon black designated "Black Pearls No. 71", heated to 1000°C in air before using (from Dr. W. R. Smith and W. Schaeffer, Godfrey L. Cabot, Inc.); a sample of "Saran 1100H" prepared for us by Professor Conway Pierce and Professor Nelson Smith of Pomona College by carbonizing Saran at 400°C, heating in vacuum to 1100°C, treating with hydrogen at that temperature, and then cooling in vacuum.

The B.E.T. area was determined for each sample at liquid nitrogen temperatures. Each sample was outgassed for 36 hours at 400°C before using, and outgassed overnight at 400°C between runs.

The values calculated for V from the experimental data were reproducible to ±0.1 percent, and no appreciable drift over a series of runs could be detected.

III. THEORETICAL

The geometrical volume V_{geo} of the system gas-solid is defined here as the total volume of the sample bulb minus the volume of the enclosed solid. The surface of division is defined as passing through the centers of the atoms that make up the surface of the solid. The area of the surface is A and the distance of closest approach of the centers of the gas atoms is D. For the hard sphere repulsion used here, D is independent of temperature. (At present no account will be taken of the periodic structure of the surface of the crystal; for that reason D can be compared only roughly with the sum of the atomic radii of the atoms of the gas and of the crystal.) A portion of V_{geo} equal to AD is thus unavailable to the centers of the gas atoms. Up to a point, the density of packing of the solid should not affect the interaction volume, and so a useful excess volume is defined as

$$V_{ex}=V-V_{geo}+AD. \tag{1}$$

This volume approaches zero at high temperature when

$$V=V_{geo}-AD. \tag{2}$$

In other words, the true dead space volume equals the geometric volume minus the volume that the centers of the measuring gas cannot reach.

The apparent volume V of the system at any temperature is equal to the integral over each volume element weighted by $\exp(-\epsilon/kT)$ where ϵ is the energy of interaction in that volume element.[11] Thus,

$$V=\int^{V_{geo}} \exp(-\epsilon/kT)dV. \tag{3}$$

In terms of V_{ex} [Eq. (1)],

$$V_{ex}=\int^{V_{geo}} [\exp(-\epsilon/kT)-1]dV+AD. \tag{4}$$

In this form the limit of integration can be removed as in the usual virial coefficient integral:

$$V_{ex}-AD=\int_0^{\infty} [\exp(-\epsilon/kT)-1]dV. \tag{5}$$

This integral corresponds formally to twice the second virial coefficient for a pair of atoms (with the sign reversed).[12] One must now specify the form of ϵ, the van der Waals energy between a single gas atom and an array of atoms in the solid.

If one assumes that the attractive energy is due to London forces,

$$\epsilon=\sum C/x^6, \tag{6}$$

where C is a constant and x the interatomic distances. This summation has been made for a variety of crystal structures.[2–4] It will be replaced here by the simpler assumption of a semi-infinite structureless solid bounded by a plane. The summation is replaced by integration and one finds[13]

$$\epsilon=\pi CN_0/6r^3, \tag{7}$$

where N_0 is the number of particles per cubic centimeter of solid and r is the distance from the plane of the solid to the gas atom. Thus the final form of the interaction energy is

$$\epsilon=+\infty \qquad r<D, \tag{8}$$
$$\epsilon=-\epsilon^*D^3/r^3 \quad r>D.$$

The quantity

$$\epsilon^*=\pi CN_0/6D^3 \tag{9}$$

is the energy of interaction at the hard-sphere distance D. If this interaction energy is inserted in Eq. (5), it emerges that

$$V_{ex}=AD\sum_{\tau=1}^{\infty}\{1/\tau!(3\tau-1)\}(\epsilon^*/kT)^{\tau}, \tag{10}$$

analogous to Keesom's expression for the second virial coefficient.[14] This series has been summed for appropriate values of ϵ^*/kT. Upon combining Eq. 10 with Eq. 1, the final expression for the apparent volume becomes

$$V=V_{geo}-AD+AD\sum_{\tau=1}^{\infty}\{1/\tau!(3\tau-1)\}(\epsilon^*/kT)^{\tau}. \tag{11}$$

It is possible to relate the parameters D and ϵ^* using an expression for the London constant C due to Kirkwood and Müller:[15]

$$C=6\,mc^2\alpha_1\alpha_2/(\alpha_1/\chi_1)+(\alpha_2/\chi_2). \tag{12}$$

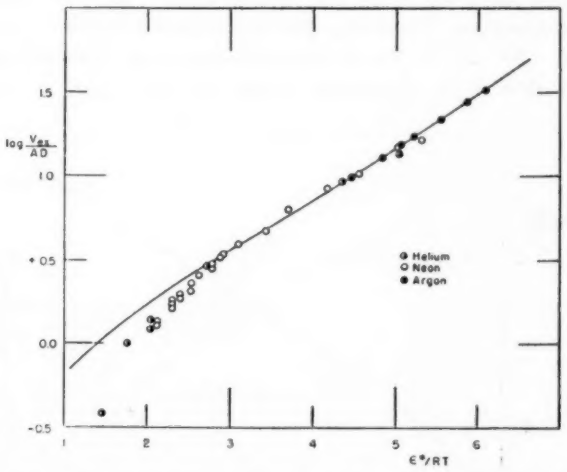

FIG. 2. Values of excess volume for carbon black plotted against reciprocal temperature (in reduced units); preliminary fit.

[11] R. H. Fowler and E. A. Guggenheim, *Statistical Thermodynamics* (Cambridge University Press, Cambridge, 1939), p. 300.
[12] See reference 11, p. 265.
[13] T. L. Hill, J. Chem. Phys. **16**, 181 (1948).
[14] See reference 11, p. 273.
[15] A. Müller, Proc. Roy. Soc. (London) **A154**, 624 (1936).

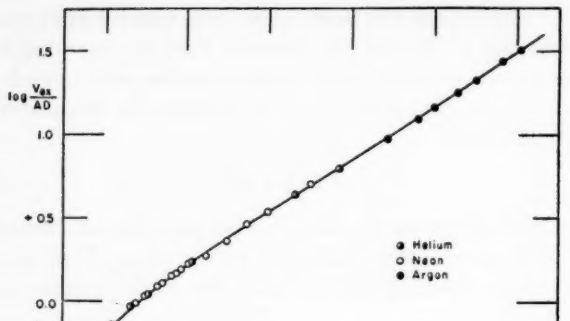

FIG. 3. Fitted values of excess volume for carbon black plotted against reciprocal temperature (in reduced units). Curve is calculated from Eq. (10).

Here mc^2 is the mass of the electron times the velocity of light squared and α and χ are the polarizabilities and diamagnetic susceptibilities of the two interacting atoms. When inserted in Eq. 9, this expression yields the value

$$\epsilon^* = (N_0\, mc^2\pi/D^3)\{\alpha_1\alpha_2/(\alpha_1/\chi_1)+(\alpha_2/\chi_2)\}. \qquad (13)$$

With this expression, one can calculate D in terms of the observed ϵ^*, and with the observed value of AD calculate A. The procedure constitutes a new method of determining surface area that is independent of any theory of multilayer adsorption or any estimate of molecular cross section.

IV. EXPERIMENTAL RESULTS

The apparent volumes measured at various temperatures (see appendix) were fitted to Eq. (11) by a process of trial and error. First a trial value of $V_{geo}-AD$ was estimated from the helium dead space at high temperature. Then V_{ex} was calculated using Eq. (1). Eq. (10) can be put in dimensionless form by dividing by AD. The theoretical value of $\log(V_{ex}/AD)$ was

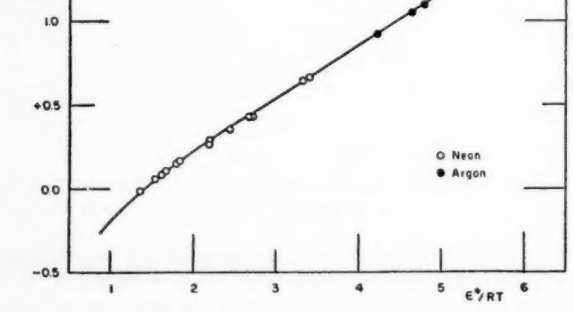

FIG. 4. Fitted values of excess volume for Saran charcoal plotted against reciprocal temperature (in reduced units). Curve is calculated from Eq. (10).

then plotted against ϵ^*/RT, shown as a continuous line in Figs. 2–6. The experimental data were then made to lie on this line by adjusting the scale. The experimental value of V_{ex} where $V_{ex}/AD=1$ yields AD. Similarly, the value of $1/T$ where $\epsilon^*/RT=1$ yields ϵ^*/R.

The preliminary choice of $V_{geo}-AD$ did not always give a good fit for helium and neon. For example, a preliminary fit for the carbon black data is shown in Fig. 2. The data for helium and neon deviate at high temperature, although the low temperature slope is adjusted correctly. Therefore, V_{geo} was adjusted for these two gases to perfect the fit. The choice of V_{geo} for the argon and krypton data was not critical, so the original estimate was retained.

TABLE I. Experimental values of parameters determined from Eq. 11.

Adsorben	Gas	Helium dead space (ml/g)	V_{geo} (ml/g)	AD (ml/g)	ϵ^* (kcal)
Carbon black	Helium		2.371	0.114	0.60
	Neon		2.352	0.0993	1.36
	Argon	2.317	2.389	0.0719	4.34
Saran charcoal	Neon		5.12	0.211	1.33
	Argon	4.91	5.09	0.172	4.14
Porous glass	Neon		0.823	0.0194	1.56
	Argon	0.819	0.835	0.0156	3.79
Alumina	Argon	0.923	0.949	0.0245	2.80
	Krypton	0.919	0.949	0.0282	3.46

TABLE II.

	Atomic susceptibility· 10^{29}	Atomic polarizability· 10^{24}
Alumina	1.66[a]	4.52[c]
Porous glass	4.91[a]	3.96[c]
Saran charcoal	3.79[a]	1.02[c]
Carbon black	3.79[a]	1.02[c]
Helium	0.292[b]	0.205[d]
Neon	1.12[b]	0.393[d]
Argon	3.24[b]	1.623[d]
Krypton	4.65[b]	2.46[d]

[a] *International Critical Tables* (McGraw-Hill Book Company, Inc., New York, 1928), Vol. VI, pp. 354–364.
[b] K. F. Mann, Z. Physik **98**, 548 (1936).
[c] Calculated from refractive indices in *International Critical Tables* (McGraw-Hill Book Company, Inc., New York, 1926), Vol. I, pp. 102–174.
[d] H. Margenau, J. Chem. Phys. **6**, 896 (1938).

It is interesting to note that Barrer and Barrie's[16] measurements of the adsorption of argon on porous glass fall almost in the range of the present investigation. Four of these points recalculated from the authors' data are shown in Fig. 5. These points are somewhat below the theoretical curve, which indicates that the region of argon-argon interaction is just being reached. The samples were, of course, not identical.

The values of the parameters ϵ^*, AD, and V_{geo} are tabulated in Table I. The fitted results are shown in Figs. 3–6. For argon and krypton, the original estimates of $V_{geo}-AD$ used to obtain the fit are tabulated as helium dead space.

[16] R. M. Barrer and J. A. Barrie, Proc. Roy. Soc. (London) **A213**, 250 (1952).

The value of $V_{geo}-AD$ for helium with carbon black is slightly smaller than the helium dead space, extrapolated to high temperature. This discrepancy reflects a slight deviation of the helium data from the theory at high temperatures. This may indicate that at high temperature more surface is available to the helium than at low temperature. Note also that the values of V_{geo} needed to fit neon and helium are different; this is an indication that part of the surface available to the helium is blocked to the neon. These indications are confirmed more directly in what follows.

The values of D were calculated from ϵ^*, with the use of Eq. 13. The polarizabilities and susceptibilities used are given in Table II. It was not possible to make a very critical choice for the parameters in the case of the finely divided solids. For the glass, values for amorphous silica were used; for alumina, values for anhydrous bulk alumina were used; in both cases the susceptibility and polarizability are per formula weight; N_0 is then the number of formula weights per cubic centimeter. For carbon black and Saran charcoal the values for gas carbon were used. In general, these figures seem as accurate as the crude theory presented warrants.

TABLE III. Distances of closest approach (D) in angstroms calculated from Eq. (13).

Adsorbent	Helium	Neon	Argon	Krypton
Carbon black	2.47	2.70	2.75	
Saran charcoal		2.72	2.79	
Porous glass		1.93	2.21	
Alumina			1.87	1.99

TABLE IV. Surface areas in square meters per gram.

Adsorbent	Helium	Neon	Argon	Krypton	B.E.T.
Carbon black	462	367	262		337
Saran charcoal		774	786		800
Porous glass		101	71		117
Alumina			131	141	181

The calculated values of D are presented in Table III.

Values of A calculated from the value of AD (Table I) and D (Table III) are given in Table IV. The B.E.T. area is given for comparison. The indication of a difference in accessibility for the various rare gases shown by V_{geo} is strikingly confirmed by the areas shown for the carbon black. A similar difference is encountered with porous glass. The areas for Saran charcoal agree nicely with the B.E.T. areas. The other areas are remarkably close when one considers the difference in method.

V. CONCLUSIONS

The large value of the interaction energy (Table I) indicates that the light rare gas atoms interact strongly with surfaces. The surface concentration and "stickiness" of more complex molecules must be similarly affected, even at the high temperatures of ordinary surface reactions. For example, Becker[17] has postulated such an interaction to explain the high values of the accommodation coefficient for the chemisorbtion of nitrogen on tungsten.

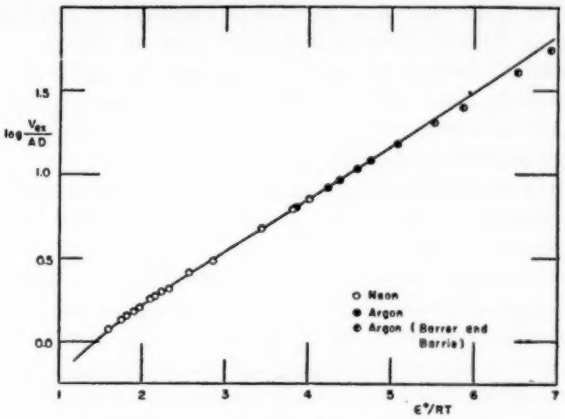

FIG. 5. Fitted values of excess volume for porous glass plotted against reciprocal temperature (in reduced units). Curve is calculated from Eq. (10).

The use of the Kirkwood-Müller formula to calculate the hard sphere D is an oversimplification; indeed, if a well-characterized surface had been investigated, a more detailed calculation and summation of forces would be justified as a test of the expression. However, the value of D depends upon the cube root of ϵ^*; the error in the formula would have to be large to cause a smaller change in D. The somewhat small values of D calculated using this formula may be the consequence of the periodic force field parallel to the surface. The optimum energy of interaction results when the gas atom is nestled in the center of a lattice cell. In this position the perpendicular distance to the surface layer of atoms is smallest, and indeed, the model used here becomes most unrealistic.

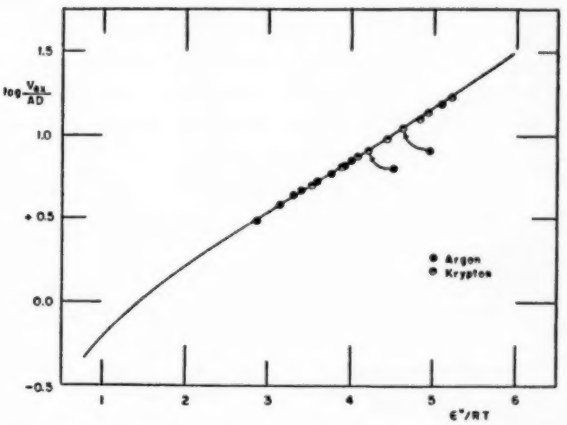

FIG. 6. Fitted values of excess volume for alumina plotted against reciprocal temperature (in reduced units). Curve is calculated from Eq. (10).

[17] J. A. Becker and C. D. Hartman, Phys. Rev. 83, 877 (1952).

The large value of ϵ^* for helium supports the hypothesis of Mastrangelo and Aston[18] that at the B.E.T. "point B" helium is absorbed to a depth of two or more layers. At a few degrees absolute, more than one layer would be held very tightly by an interaction energy so large relative to the energy of vaporization.

It is unwarranted to attach too much significance to the absolute magnitudes of the areas calculated here; however, it seems impossible to force all the rare gas areas to equal the B.E.T. area, even if the argon values were normalized to the B.E.T. areas. It is not suggested here that the difference in accessibility is due to size alone; it is highly probable that diffusion into inner voids is involved. For example, the electron microscope area of the carbon black is about 130 m^2/g[19] although the B.E.T. area is 337 m^2/g, which suggests surface roughness at least. The lighter gases, which interact less strongly, may penetrate to small interior voids left by the random packing of the crystallites that make up the carbon black particle.[20,21]

Preliminary calculations show that if two surfaces are near each other (as in a small void) the treatment of this paper underestimated the surface area; one concludes that the "area" of amorphous solids is a function of the gas used. It is anticipated that (necessarily very precise) measurements on well-defined low surface area crystalline solids will not show this discrepancy.

VI. ACKNOWLEDGMENT

The authors wish to thank Dr. Ahlborn Wheeler and Professor P. H. Emmett for many valuable discussions.

APPENDIX

The numerical values of the apparent volume (V) as a function of the temperature for the various systems considered are shown below. The units of V are milliliters per gram of solid, and the temperatures are in degrees absolute.

Alumina

Krypton		Argon	
T	V	T	V
332.6	0.4793	302.9	0.2739
350.4	0.3929	332.4	0.2066
358.0	0.3605	350.3	0.1792
373.3	0.3152	358.1	0.1655
392.0	0.2691	373.6	0.1496
412.7	0.2316	392.1	0.1323
425.6	0.2112	412.5	0.1175
448.1	0.1840	425.8	0.1071
491.5	0.1428	447.6	0.0951
		491.8	0.0760

Porous glass

Neon		Argon	
T	V	T	V
153.3	1.074	373.0	1.056
194.6	0.942	397.9	1.009
205.1	0.924	411.8	0.989
226.9	0.896	431.9	0.964
247.2	0.882	447.1	0.949
273.2	0.863	490.7	0.918
302.9	0.854		
336.5	0.845		
349.5	0.843		
361.8	0.841		
373.2	0.839		
396.8	0.836		
411.9	0.834		
431.1	0.832		
447.2	0.830		
491.2	0.828		

Carbon black

Helium		Neon	
T	V	T	V
78.0	2.976	194.7	2.751
78.1	2.960	205.1	2.721
90.4	2.771	227.2	2.593
90.4	2.761	248.6	2.539
145.1	2.454	273.2	2.481
194.6	2.383	303.2	2.439
227.2	2.364	335.7	2.424
273.1	2.335	349.5	2.412
303.3	2.327	372.9	2.394
		395.9	2.383
Argon		411.7	2.377
		435.8	2.368
359.3	4.634	453.1	2.364
373.1	4.264	490.7	2.352
396.0	3.798		
411.7	3.612		
434.9	3.361		
452.5	3.224		
489.7	3.013		

Saran charcoal

Neon		Argon	
T	V	T	V
195.7	5.882	348.3	9.916
200.3	5.844	361.5	9.295
224.4	5.519	372.9	8.760
249.1	5.480	396.8	7.883
273.2	5.386	411.3	7.500
303.2	5.315	430.6	7.118
349.2	5.231	446.5	6.847
361.5	5.223	490.5	6.353
372.7	5.209		
397.3	5.180		
412.3	5.163		
431.4	5.151		
491.6	5.117		

[18] S. V. R. Mastrangelo and J. G. Aston, J. Chem. Phys. **19**, 1370 (1951).
[19] W. R. Smith, private communication.
[20] J. Biscoe and B. E. Warren, J. Appl. Phys. **13**, 364 (1942).
[21] R. D. Rossman and W. R. Smith, Ind. Eng. Chem. **35**, 972 (1943).

THE JOURNAL OF CHEMICAL PHYSICS VOLUME 22, NUMBER 6 JUNE, 1954

Structures of the Boron Hydrides*

WILLIAM N. LIPSCOMB
School of Chemistry, University of Minnesota, Minneapolis, Minnesota
(Received November 16, 1953)

Evidence for the structures of B_2H_6, B_4H_{10}, B_5H_9, B_5H_{11}, and $B_{10}H_{14}$ is reviewed. Correlations of the boron arrangements with known structures have been pointed out, and a systematic discussion of the boron-hydrogen distances is given.

INTRODUCTION

THE relations of the formulas of the well-established boron hydrides, B_2H_6, B_4H_{10}, B_5H_{11}, B_5H_9, B_6H_{10}, and $B_{10}H_{14}$, to their structures have long been subjects of interest and speculation. Several attempts have been made, without success, to derive the correct molecular structures from the general concepts available at various times. The importance of the structural principles of these compounds is certainly greater than merely an explanation of these and even other compounds of boron, for it is generally recognized that these compounds represent small molecules on the border-line between metals and nonmetals. Further, the electronic levels here are uncomplicated by interactions of *d* levels, being restricted to relatively simple *s* and *p* levels. Hence, it may be expected that these structural principles will contribute to an understanding of the simplest possible bonding concepts in intermetallic compounds and metals.

With the exception of B_6H_{10}, the structure of which is still undetermined, the molecular geometries of the known boron hydrides are established. As expected, there are remarkably close similarities among these structures. The experimental results of the investigations leading to these structures are collected here, and somewhat critically examined. Certain features, such as the B—H distances, are not well known, and methods for estimating these parameters from structural principles are described. On the other hand, the general molecular geometry and the B—B distances are now established with a high degree of certainty.

As will be described, the structure of B_2H_6 was first established chiefly by spectroscopic techniques. With this exception, the certainty with which the structures are known is due to the x-ray diffraction studies. The results of all of these x-ray studies are completely independent of one another and independent of chemical or structural assumptions. This includes even the positions of the hydrogen atoms, which were located by each of the x-ray diffraction studies, because of the fortunately low atomic number of boron. The electron diffraction studies, however, are not easily described, for it matters when and by whom they were made. As further complication these studies have partly derived the structural principles and have partly been derived from these principles. Although, unlike the x-ray studies, not one of the recent electron diffraction studies yields unambiguously the correct structure, they have provided sufficient experimental data for the recognition of most of the structural principles of this group of compounds. Again, no one of these studies is complete in its investigation of the possible ambiguous models. On the other hand, these recent electron diffraction studies are much more precise than the earlier ones which are proved to be incorrect, and, taken together, the results of these recent studies are comparatively convincing.

* In order to distinguish experimental results from their interpretation in terms of valence theory, this paper is separated from the following one, and is primarily an introduction and a critique of the experimental studies.

STRUCTURES

B_2H_6

That the bridge-type of structure is the correct one for diborane is generally recognized to have been established by Price[1] on the basis of the infrared spectrum. Prior to this study, however, there did exist a general realization[2–5] that the physical evidence was overwhelmingly in favor of this structure. The failure of general acceptance of, for example, the high barrier to internal rotation and the earlier infrared evidence[2] as indicative of the bridge structure must be attributed to the insistence[6] that the early electron diffraction evidence favored the ethane-type of structure. A recent electron diffraction study,[7] however, confirmed the bridge structure and was in disagreement with the ethane type of structure. The molecular parameters (Fig. 1) are B—B=1.77, B—H=1.19, B—H_b(bridge) =1.33A, and $\angle$HBH=121.5°.

The correct molecular geometry was first proposed by Dilthey.[8] However, interpretations in terms of molecular orbitals were made only comparatively recently.[4,5,9] Whether one thinks in terms of a "protonated double bond" (four-atom bridge bond) in an ethylenic type of structure or in terms of the interaction of two BH_3 groups is, in any complete analysis, merely a

[1] W. C. Price, J. Chem. Phys. **15**, 614 (1947); **16**, 894 (1948).
[2] F. Stitt, J. Chem. Phys. **8**, 981 (1940); **9**, 780 (1941).
[3] H. C. Longuet-Higgins and R. P. Bell, J. Chem. Soc. **1943**, 250.
[4] K. S. Pitzer, J. Am. Chem. Soc. **67**, 1126 (1946).
[5] R. S. Mulliken, Chem. Revs. **41**, 207 (1947).
[6] S. H. Bauer, J. Am. Chem. Soc. **59**, 1896 (1937); Chem. Revs. **31**, 46 (1942).
[7] K. Hedberg and V. Schomaker, J. Am. Chem. Soc. **73**, 1482 (1951).
[8] W. Dilthey, Z. angew. Chem. **34**, 596 (1921).
[9] A. D. Walsh, J. Chem. Soc. **1947**, 89.

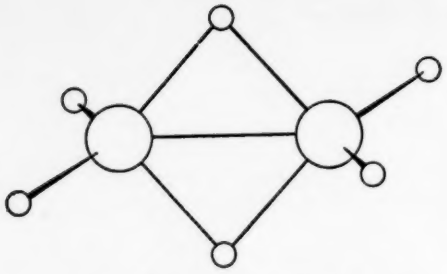

FIG. 1. The structure of B_2H_6.

matter of taste, but the analogy of bonding geometry and electronic structure with these properties of ethylene is very striking.

$B_{10}H_{14}$

In an extensive x-ray diffraction study[10] of the molecular structure of decaborane the molecular geometry, including both boron and hydrogen positions, has been uniquely established (Fig. 2). The probable, but not unique, structure assigned in an electron diffraction study,[11] is incorrect, but these electron diffraction data have since been shown[12] to be consistent with the correct structure.

The boron arrangement is closely related to the icosahedron found earlier[13] in $B_{12}C_3$ and subsequently in elementary boron.[14] If two adjacent boron atoms are removed the B_{10} skeleton remains, on which one "stitches up" the open face with bridge hydrogens and attaches one hydrogen atom to each boron atom. The close B—B distances range from 1.73 to 1.81A, with an average value of 1.76A; the ten regular B—H distances are in the range of 1.20 to 1.30A. Each bridge bond is unsymmetrical with a short leg of 1.34A and a long leg of 1.42. The longer leg is attached to the outer boron atom of the structure. This structure was not predicted before its discovery.

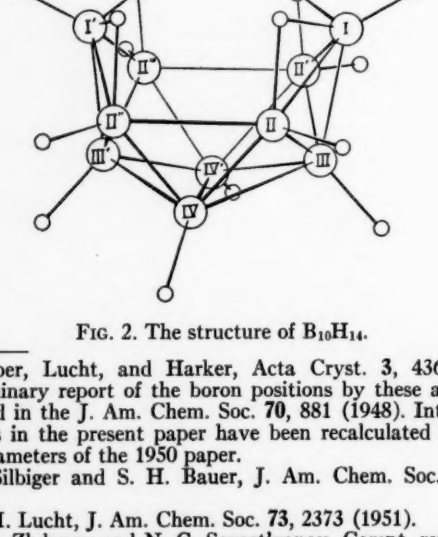

FIG. 2. The structure of $B_{10}H_{14}$.

B_5H_9

The certainty with which this structure (Fig. 3) is established is based upon the crystal structure study,[15] in which, at the outset, molecules of C_{4v} symmetry were required. Hydrogen atoms were located by subtraction of boron contributions and, in addition, are also uniquely placed by the packing in the crystal. This structure was arrived at previously and independently in a recent electron diffraction study.[16] Because these electron diffraction data were also consistent with at least three other structures,[17] the indications of a molecule of high symmetry from the infrared spectrum and entropy were included in the argument which led to the structure in the electron diffraction study. The molecular parameters of these studies are in reasonably good agreement, and in view of the confirmation of this structure by the microwave study,[18] the most probable molecular parameters are B—B(base) = 1.80 and B—B(slant) = 1.69A. Parameters involving hydrogen atoms are discussed in Table I.

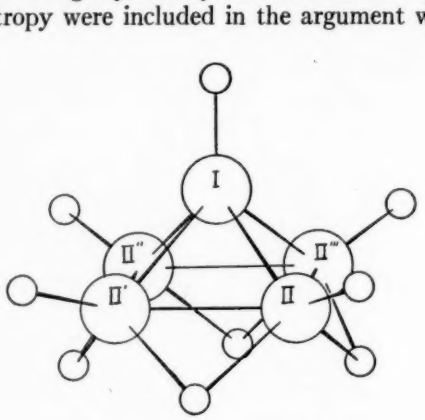

FIG. 3. The structure of B_5H_9.

The boron arrangement is closely related to the octahedron found in the cubic borides.[19] If one removes one boron atom from the octahedron, stitches up the open face with bridge hydrogens, and attaches one hydrogen to each boron atom, the B_5H_9 structure can be expected.[20] This boron arrangement was advocated by Pauling[21] during both the early electron diffraction study,[22] which discarded it in favor of an incorrect

[10] Kasper, Lucht, and Harker, Acta Cryst. **3**, 436 (1950). A preliminary report of the boron positions by these authors is published in the J. Am. Chem. Soc. **70**, 881 (1948). Interatomic distances in the present paper have been recalculated from the final parameters of the 1950 paper.

[11] G. Silbiger and S. H. Bauer, J. Am. Chem. Soc. **70**, 115 (1948).

[12] C. M. Lucht, J. Am. Chem. Soc. **73**, 2373 (1951).

[13] G. S. Zhdanov and N. G. Sevast'yanov, Compt. rend. acad. sci. U.R.S.S. **32**, 432 (1941); H. K. Clark and J. L. Hoard, J. Am. Chem. Soc. **65**, 2115 (1943).

[14] Hoard, Geller, and Hughes, J. Am. Chem. Soc. **73**, 1892 (1951).

[15] W. J. Dulmage and W. N. Lipscomb, J. Am. Chem. Soc. **73**, 3539 (1951); Acta Cryst. **5**, 260 (1952).

[16] Hedberg, Jones, and Schomaker, J. Am. Chem. Soc. **73**, 3538 (1951); Proc. Natl. Acad. Sci. U.S. **38**, 679 (1952).

[17] Hedberg, Schomaker, and Jones, Abstracts, Chicago Meeting, A.C.S. (1950).

[18] Hrostowski, Myers, and Pimentel, J. Chem. Phys. **20**, 518 (1952).

[19] L. Pauling and S. Weinbaum, Z. Krist. **87**, 181 (1934).

[20] M. V. King and W. N. Lipscomb (to be unpublished).

[21] L. Pauling (private communication).

[22] S. H. Bauer and L. Pauling, J. Am. Chem. Soc. **58**, 2403 (1936).

TABLE I. Bond distances in the boron hydrides.

	B_2H_6	B_4H_{10}	B_5H_{11}	B_6H_9	$B_{10}H_{14}$
Ratio H/B	3	2.5	2.2	1.8	1.4
(B−B)[a]*XR*	...	1.75(1) 1.84$_5$(4)	1.74(5) 1.86$_5$(2)	1.66[c](4) 1.77[c](4)	1.76[b](19) 2.01(2)
(B−B)*ED*	1.77	1.76(1) 1.85(4)	...	1.70[c](4) 1.80[c](4)	...
(B−H)*XR*		1.11	1.07	1.20	1.25[b]
(B−H)*ED*	1.19	1.19	...	1.23	...
(B−H_b)*XR*	...	1.21(4) 1.37(4)	1.24	1.35	1.34(4) 1.42[b](4)
(B−H_b)*ED*	1.33	1.33[d](4) 1.43[d](4)	...	1.36	...
B−B bond order[e]	0.50	0.54 0.37	0.56 0.35	0.68[c] 0.45[c]	0.52 0.20
Bond order/H atom	0.92	0.90	0.86	0.83_1	0.83_7
Probable B−H[f]	1.19	1.20	1.21	1.22	1.22
Probable av. B−H_b	1.37	1.38	1.39	1.40	1.40
B−H_b distances for equal B valence[g]	1.37	1.32(4) 1.44(4)[h]	1.33(2) 1.47(2)[h]	1.40	1.36(4)[h] 1.44(4)
H_u in B_5H_{11}			1.30(1) 1.72(2)		

[a] The number of distances is indicated in parentheses.
[b] Recalculated from the final results given in the $B_{10}H_{14}$ study.
[c] The more reliable microwave values of 1.69 and 1.80A are used in the calculations.
[d] The x-ray study establishes that the asymmetry is the reverse of that given in the electron diffraction study.
[e] Calculated from Pauling's equation $d = 1.59 - 0.6 \log n$, from the x-ray or microwave values, except for B_2H_6.
[f] The value of 1.19A for B_2H_6 and its bond order of 0.92 are assumed, and Pauling's equation is then employed. A bridge hydrogen is assumed to have the same total bond order as a normal hydrogen, an assumption which seems questionable for B_6H_9.
[g] This assumption results in the correct prediction of the direction of the asymmetry of the hydrogen bridges.
[h] To B_{11} in figures.

model, and the recent electron diffraction study,[16] which initially erroneously eliminated this model.[23]

B_4H_{10}

Both hydrogen and boron positions (Fig. 4) were established unambiguously by the x-ray diffraction study[24] in which there were 616 observed reflections to determine 14 parameters counting the boron, scale, and temperature parameters. Hydrogen atoms, not included in the counting of parameters, appeared both in the presence of the boron atoms and when the boron atoms were subtracted out in the electron density maps. A pseudoambiguity in the interpretation of the Patterson function produced a remarkably good false model,[25] which, however, gave very much poorer agreement between observed and calculated intensities than did the correct model.[24] The recent electron-diffraction study[26] independently and previously suggested this model on the bases of its plausible relation to the other boron hydrides and of its consistency with the electron-diffraction data. Again the results are not unambiguous, for a slight modification of the model decided upon in the earlier diffraction study[27] is equally consistent with the data though chemically less reasonable. Tests of other possible models were not made in the present electron diffraction study, but the results of the earlier study were shown to be incorrect.

Comparison of the results of the x-ray and electron-diffraction study results in the molecular parameters, $B_1-B_2=1.85$A, $B_1-B_1=1.75$A, $\angle B_2B_1B_2=98°$, B−H $=1.19$A, $B_1-H_b=1.33$A, and $B_2-H_b=1.43$A. This is a model obtained from the x-ray values of boron-boron distances and bond angles (including hydrogen angles) and from the electron diffraction values of the B−H distances, but with the asymmetry of the hydrogen bridges reversed to agree with the x-ray results. This combination avoids the systematic errors introduced by the lack of complete convergence of the Fourier series in the hydrogen distances of the x-ray study and the very large uncertainties in the bond angles in the electron diffraction study.

The boron arrangement can be considered a fragment of either the icosahedron or the octahedron because the $B_2-B_1-B_2$ bond angle is between 105° and 90°.

B_5H_{11}

Although the x-ray diffraction data[28] were less complete than for B_4H_{10}, the use of 299 observed reflections to determine the 17 parameters (x,y,z for each boron atom plus scale and temperature factors) yielded the boron positions with certainty. Subtraction of these boron atoms from the electron density map yielded the

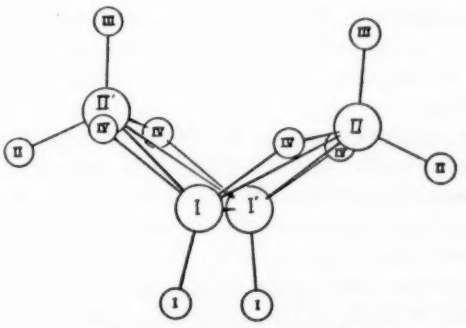

FIG. 4. The structure of B_4H_{10}.

[23] V. Schomaker, J. chim. phys. **46**, 252 (1949).
[24] C. E. Nordman and W. N. Lipscomb, J. Am. Chem. Soc. **75**, 4116 (1953); J. Chem. Phys. **21**, 1856 (1953).
[25] M. Atoji and W. N. Lipscomb, J. Chem. Phys. **21**, 172 (1953).
[26] Jones, Hedberg, and Schomaker, J. Am. Chem. Soc. **75**, 4116 (1953).
[27] S. H. Bauer, J. Am. Chem. Soc. **60**, 805 (1938).
[28] L. Lavine and W. N. Lipscomb, J. Chem. Phys. (to be published).

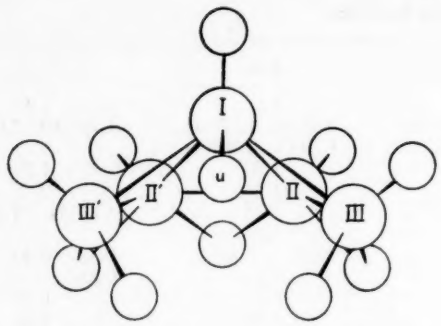

FIG. 5. The structure of B_5H_{11}.

hydrogen positions as the eleven highest remaining peaks. Unlike the B_4H_{10} study, where the remaining background was low, there were false peaks nearly as high as these hydrogen peaks, but they were too far from the boron atoms to correspond to bonded atoms. Hence the probability is very high indeed that the structure shown in Fig. 5 is correct, independently of any chemical assumptions. A recent electron diffraction study[29] is consistent with the boron arrangement but yields no direct information concerning the hydrogen positions. Certainly the previous electron diffraction results[30] are incorrect.

Except for the two B—B distances of 1.86_5A from the apex to the outer two boron atoms, the B—B distances have an average value of 1.74A. The B—H distances are probably all in the normal range even though they appear to be systematically about 0.1A short because of the lack of convergence of the Fourier series. The case of B_5H_{11} was unlike the cases of B_4H_{10}, B_5H_9, and $B_{10}H_{14}$, where the x-ray studies proved that the hydrogen bridges were, respectively, unsymmetrical, symmetrical, and unsymmetrical, in that no definite conclusion about the symmetry of the bridge hydrogens in B_5H_{11} could be drawn from the experimental data.

DISCUSSION

The various structural data and some further calculations are summarized in Table I. The B—B distances observed by various methods are in very good agreement. The most accurate values are the electron diffraction results for B_2H_6, the microwave values for B_5H_9, and the x-ray values for the remaining compounds. These values were employed in the remainder of the discussion.

It is apparent that the B—H distances obtained in the x-ray studies are not sufficiently reliable for any theoretical discussion. There appear to be effects due to lack of convergence of the Fourier series which have shortened abnormally these B—H distances by amounts almost proportional to the fraction of complete *hkl* data observed in B_5H_9, B_4H_{10}, and B_5H_{11}, and it is possible that there is a similar effect causing a slight lengthening of B—H in $B_{10}H_{14}$. Hence a discussion based upon Pauling's bond order equation, $d=d_1-0.6\log n$, is employed to infer the probable B—H distances from the much more reliable B—B distances. Finally, the assumption of equal total valence of all borons within a given molecule is employed to decide the direction and magnitude of the asymmetry of the unsymmetrical hydrogen bridges. It must be recognized that this method is largely one of convenience in obtaining quantitative relations between valence and bond distances and that similar results will be expected from a more thorough treatment. However, it is quite probable that the B—H and B—H_b distances obtained by this argument are considerably more reliable than the experimental values in the x-ray diffraction studies.

The relations of these boron arrangements as fragments of the octahedron or icosahedron, the presence of bridge hydrogens in the open parts of the molecule, the ligancy of five or six for boron, and the strong tendency for the formation of boron triangles are the most obvious structural principles. It is most interesting to build models of these structures and to superimpose them upon one another, for then some further significant relations become obvious. The boron triangle and the triangle formed by the bridge hydrogen and its two boron congeners are interchangeable as one passes from one member of the series to another. Moreover the diborane geometry is present or very nearly present throughout the structures, particularly in the open faces where bridge hydrogens occur, but also elsewhere to a lesser extent. Often there is merely a substitution of two "almost half bonds" for the "almost full bond" between boron and one of the normally bonded hydrogen atoms, as one goes to higher members of the series. The angle between these "almost half bonds" is usually small.

These ideas suggest that to a considerable degree the hybridization about boron in many of these higher hydrides is not greatly different from the hybridization in diborane. In addition the probable reason for the predominance of boron triangles is the concentration of the bonding electron density more or less towards the center of the triangle so that the bridge orbitals (π orbitals in B_2H_6) of the three boron atoms in the triangle overlap.[31] It does seem very likely from these structural comparisons that the outer orbitals of an atom are not always exactly directed toward the atoms to which it is bonded. This property is to be expected for atoms which are just starting to fill new levels and therefore may be a general property of metals and intermetallic compounds.

[29] Jones, Hedberg, and Schomaker (private communication).
[30] S. H. Bauer, J. Am. Chem. Soc. 60, 805 (1938).
[31] Somewhat similar ideas have been proposed, with different hybridization, for the bond shortening in cyclopropane [A. D. Walsh, Seminar Notes, University of California, Berkeley (1950)] and for the bonding in B_4Cl_4 [G. H. Duffey, J. Chem. Phys. 21, 761 (1953)].

THE JOURNAL OF CHEMICAL PHYSICS VOLUME 22, NUMBER 6 JUNE, 1954

The Valence Structure of the Boron Hydrides

W. H. EBERHARDT,* *School of Chemistry, Georgia Institute of Technology, Atlanta, Georgia*

AND

BRYCE CRAWFORD, JR., AND WILLIAM N. LIPSCOMB, *School of Chemistry, University of Minnesota, Minneapolis, Minnesota*

(Received November 16, 1953)

A set of extended valence postulates is presented including the concept of the localized three-center bond. These postulates are applied systematically to the boron hydrides and account for their unusual geometry, their unexpected dipole moments, and the fact that they are not "electron-deficient."

I. INTRODUCTION

THE boron hydrides have long served as a stimulating test for the chemist's understanding of valence structures. Recently sufficient data on their geometrical structures[1] have been collected to suggest that a search for a pattern might be worthwhile. We have studied these data and have indeed been led to a systematic approach which makes comprehensible the structures of the known hydrides and their dipole moments. We have even ventured a few predictions, knowing that if we must join the ranks of boron-hydride predictors later proved wrong, we shall be in the best of company.

In our approach, the only new, or rather, unfamiliar concept is that which we call the "three-center bond" (not to be confused with the three-electron bond). The normal covalent bond may be called a two-center bond; 2 atoms supply 2 orbitals, one centered on each atom, and these interact to form one bonding orbital and one antibonding orbital; if 2 electrons are available, they will just fill the bonding orbital and constitute a covalent bond. Similarly, 3 atoms may supply 3 orbitals, one on each atom, and these will interact as discussed below to form one bonding and 2 antibonding orbitals; 2 electrons may just fill the bonding orbital to constitute a three-center bond. Both of these bond types are indeed special cases of the more general multicenter molecular orbital represented as a linear combination of atomic orbitals. The special value which attends their use lies in the intuitive feeling for the chemical bonding which results from localizing the bonding electrons in particular regions of the molecule and which frequently makes possible the extension of understanding from simple structures to more complicated ones. The multicenter molecular orbital can of course be described in terms of resonating single bonds, but we find the explicit recognition of the three-center bond concept to be most perspicuous in the treatment of the boron hydrides.

It is at once clear that the three-center bond will be used only by "electron-deficient" molecules, i.e., only where there are more usable atomic orbitals than electrons. The normal two-center bond provides a comfortable home for as many electrons as it uses atomic orbitals: 2 atomic orbitals are used, one bonding orbital is formed, and 2 electrons can be housed. If n atomic orbitals are used to form two-center bonds, they can form $n/2$ bonding orbitals and accommodate n electrons; any more would have to go into the antibonding orbitals which are energetically unfavorable. If these n atomic orbitals are combined into three-center bonds, they form only $n/3$ bonding orbitals which can accommodate only $2n/3$ electrons; any more electrons would have to go into undesirable antibonding orbitals. Of course, if n atomic orbitals remain unshared they can be filled with $2n$ electrons as "lone pairs," which are neither bonding nor antibonding to a first approximation. We see that if the atoms forming a molecule provide altogether n orbitals and m electrons, then when $m=n$, as in hydrocarbons, normal bonds will be favored; three-center bonds would be unfavorable because some electrons would be forced into antibonding orbitals. When $m>n$ as in NH_3 and H_2O, "lone pairs" will be used as far as possible to take off the excess. When $m<n$ as in the boron hydrides, three-center bonds will be used insofar as they are energetically favorable.

Moreover, if we specify that all bonding orbitals be filled and no antibonding orbitals be used, then the valence pattern for a given set of atoms is restricted to a few well-defined possibilities. This principle, with some empirical additions, provides the basis of our approach.

There are clearly other cases, such as Al_2Cl_6, where the same approach may be useful. The three-center bond is very useful in considering bent triatomic structures, such as nitrosyl halides or the carboxylate ion. Likewise there are many boron compounds other than hydrides whose valence structure is clarified by this approach; thus our picture of B_2H_6 is readily modified to account for $B_2H_5N(CH_3)_2$, where the extra electrons from the N permit "normal" B—N bonds to be formed. But in this paper we shall consider only the hydrides.

II. PRINCIPLES

A. Basic Assumptions

The fundamental assumptions underlying the approach suggested here may be enumerated as follows:

* Honorary Fellow at the University of Minnesota, on sabbatical leave from Georgia Institute of Technology, 1953.

[1] All structural data are summarized in the preceding paper by W. N. Lipscomb, J. Chem. Phys. **22**, 985 (1954), to which reference should be made for the nomenclature of particular compounds, numbering of the atoms, etc.

1. Only the $1s$ orbital of hydrogen and the four $2sp^3$ orbitals of boron are used. The boron orbitals are hybridized as suggested by the environment of each boron.

2. Each external B—H bond is regarded as a "normal," localized, single bond requiring the hydrogen orbital, one hybridized boron orbital, and one electron each from the hydrogen and the boron. Because of the very small difference in electronegativity of hydrogen and boron these bonds are assumed to be nonpolar. It is a structural fact that every boron forms at least one but never more than two such external bonds in the compounds to be considered here.

3. Each B—H—B bridge bond is regarded as a filled, three-center, localized bonding orbital requiring the hydrogen orbital and one hybrid orbital from each boron. For purposes of accounting, the hydrogen is assumed to contribute one electron, and each boron one-half electron to this orbital. These bonds are also assumed to be essentially nonpolar.

4. The orbitals and electrons of any particular boron are allotted so as to satisfy first the requirements of the external B—H single bonds and the bridge B—H—B bonds. The remaining orbitals and electrons are contributed to framework molecular orbitals.

5. The framework molecular orbitals are constructed from hybridized boron orbitals directed as suggested by the immediate environment of each atom or, where alternatives exist, in directions convenient for forming linear combinations transforming properly according to the irreducible representations of the symmetry group associated with the molecular geometry. The relative energies of these molecular orbitals may be estimated through the usual LCAO secular equations in terms of exchange integrals related qualitatively to the degree of overlap between orbitals. In fitting electrons into the resultant energy scheme only the bonding orbitals are used for any given stable molecule, and these are completely filled with the available framework electrons.

6. The framework dipole moment is calculated to a first approximation by assigning electrons to an atom as dictated by the squares of the coefficients of the corresponding atomic orbital in the simple LCAO wave functions for the filled molecular orbitals. As a somewhat better approximation the Coulomb integrals appearing in this simple approach are modified as suggested by the self-consistent LCAO treatment of Moffitt.[2]

B. Three-Center Orbitals

Although the three-center problem has been discussed in detail several times in the literature, its importance in the structures of the boron hydrides makes it advisable to summarize here the essential results of the LCAO treatment. Three atomic orbitals ϕ_A, ϕ_B, and ϕ_C are involved, each on a separate atom, with single-electron Coulomb integrals H_{AA}, H_{BB}, and H_{CC} and single-electron, two-center exchange integrals H_{AB}, H_{BC}, and H_{AC}. The usual LCAO variation functions are expressed as

$$\psi_i=\sum_j a_j{}^i\phi_j,$$

and lead to the equations[2]

$$\sum_j a_j{}^i(H_{jk}{}^i-E^iS_{jk})=0; \quad j,k=A,B,C.$$

For the applications envisaged here, nonorthogonality effects may be ignored, i.e., $S_{jk}=\delta_{jk}$, and the exchange integrals may be evaluated symmetrically such that $H_{AB}=H_{BC}=\beta$ and $H_{AC}=\gamma$. To a first approximation, all the coulomb integrals $H_{jk}{}^i$ may be set equal to a constant H_0; to a somewhat better approximation these integrals may be evaluated as suggested by the self-consistent treatment of Moffitt in terms of the coefficients $a_j{}^i$, to be considered different for each molecular orbital. The exchange integrals are considered to be the same for all the molecular orbitals.

In the approximation of constant H_0, the variation equations lead immediately to values of the energy given by the expressions.

$$E_+=H_0+\frac{\gamma}{2}+\left[\left(\frac{\gamma}{2}\right)^2+2\beta^2\right]^{\frac{1}{2}}$$

$$E_0=H_0-\gamma$$

$$E_-=H_0+\frac{\gamma}{2}-\left[\left(\frac{\gamma}{2}\right)^2+2\beta^2\right]^{\frac{1}{2}}.$$

These three levels are sketched in Fig. 1 as a function of γ/β. It will be noticed that for all values of this parameter, only one bonding orbital is available E_+ and the other orbitals are either nonbonding or antibonding. For the special case $\gamma/\beta=1$, the equilateral triangular configuration, the two excited levels are degenerate.

The forms of the wave functions corresponding to these levels may be written down readily. In the limit of $\gamma/\beta=0$, the bonding three-center orbital is given

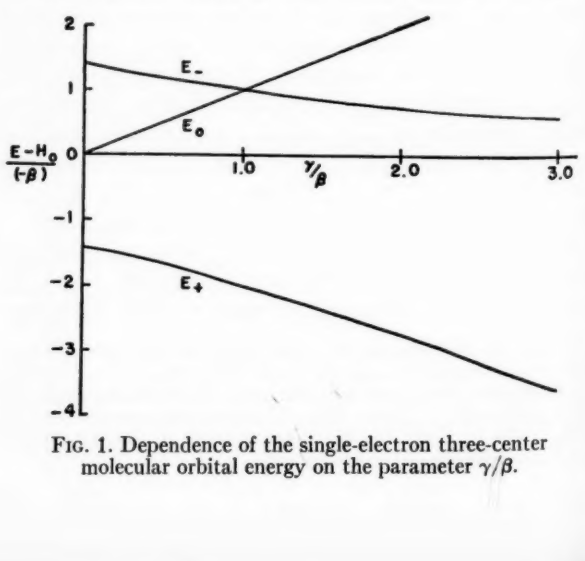

FIG. 1. Dependence of the single-electron three-center molecular orbital energy on the parameter γ/β.

[2] W. Moffitt, Proc. Roy. Soc. (London) **A196**, 510 (1949).

explicitly by the expression $\psi_+=\frac{1}{2}(\phi_A+\sqrt{2}\phi_B+\phi_C)$ and lies entirely along the (bent) line joining the three atoms. In the limit $\gamma/\beta=1$ the bonding orbital takes the form $\psi_+=(1/\sqrt{3})(\phi_A+\phi_B+\phi_C)$ and is distributed evenly among the three atoms. In the limit $\gamma/\beta=\infty$, the bonding orbital represents a single bond between atoms A and C, and B is not bonded to the system. In the applications to follow we shall find three general types to be of special interest: The B—H—B bridge bonds are all considered as examples of the "open" type with $\gamma/\beta=0$ and the electron density concentrated along the line joining the atoms. The coefficients of this type of orbital place $\frac{1}{2}$ electron on each of the two boron atoms and 1 electron on the hydrogen; consequently the hydrogens are electrically neutral. The boron framework orbitals are of two types: an "open" bond with $\gamma/\beta=0$ using a π orbital of the central boron and two nearly σ AO's from the end borons, and a "central" type with $\gamma/\beta=1$ using σ AO's from all three borons. In the "central" type the electron density is concentrated near the center of the triangle joining the atoms.

Deviations of the Coulomb integrals from equality will, of course, change the energy levels and coefficients. In particular, an increase in the absolute magnitude of a Coulomb integral will result in an increase in the coefficient of the corresponding atomic orbital in the LCAO form at the expense of the other atomic orbitals. The effect of such distortions is to introduce an asymmetry into an otherwise symmetric three-center bond.

III. STUDY OF KNOWN STRUCTURES

A. B_2H_6

The structure of diborane has been discussed previously in terms of a protonated double bond[1] and also from the standpoint of two three-center orbitals for the bridge hydrogen bonds.[3] In this molecule each boron forms two normal B—H bonds at an angle of 121.5±7° as shown in reference 1 (Table I and Fig. 1). Assuming the angle between these bonds to be identical with that between the maxima of the two sp^3 hybrid orbitals used for their formation, it is possible to construct two other *equivalent* boron orbitals as indicated by Torkington.[4] These two orbitals lie in a plane normal to the plane of the external B—H bonds and make an angle of 103° with each other. As indicated in the figure referred to, the two bridge-hydrogens are found by experiment to lie in this plane and make an H—B—H angle of 97±3°. Thus, it is evident that the hybrid boron orbitals can be regarded as pointed almost directly towards the bridge hydrogens and the conditions for the formation of two localized, three-center bridge bonds are very favorable. On the basis of our assumptions, each boron contributes one-half an electron to each of these two orbitals, and together with the hydrogen electrons, these electrons just suffice to fill the bonding orbitals. Since the orbitals formed correspond closely to the "open" limit $\gamma/\beta=0$, the coefficient of the boron atomic orbital in each three-center orbital is $\frac{1}{2}$ and each filled three-center orbital then puts $2\times(\frac{1}{2})^2=\frac{1}{2}$ electron on each boron. The resultant charge distribution is then such that each atom is electrically neutral insofar as the assumption of equal coulomb integrals is acceptable. A more refined treatment taking into account small changes in the Coulomb integrals and also possibly finite values for γ would lead to some polarity in these bonds, but such a treatment is not within the scope of the present work.

B. B_4H_{10}

The structural data for this molecule are presented in reference 1 (Table I, Fig. 4). Each boron of type II in this structure forms two external B—H bonds and two B—H—B three-center bridge bonds. These four bonds account completely for the four $2sp^3$ hybrids of the boron atom and the three boron electrons. It is to be noted, however, that the angle between the bridge hydrogen bonds is considerably greater in this structure than in B_2H_6 because of the triangular configuration of the borons. Hence the overlapping of the boron hybrids and the hydrogen orbital is not as favorable and the bonds may well be somewhat weaker than in B_2H_6. Each boron of type I forms only one external B—H bond and two three-center bonds. These bonds account for three of the boron orbitals and two electrons and hence leave a single orbital and one electron which may be used to form essentially a normal single bond between the two borons of type I. It is also of interest that the configuration of the three hydrogens surrounding borons of type I is approximately trigonal and suggests approximately tetrahedral hybridization for these borons. Such hybridization would predict a 120° angle between the two boron-triangle planes (experimentally determined as 118.1°) and would lend further support to the assignment of the bond between the two borons of type I as a "normal" single bond. Although the observed length of this bond (1.75A) is considerably less than the bridge boron lengths (1.845A), it does not appear anomalously short and suggests a deviation from strictly tetrahedral hybridization in a direction which may be anticipated as weakening the B—B single bond but strengthening the B—H—B bonds. Such an effect would result in asymmetry of the B—H—B bridge so as to reduce the B_I—H distance at the expense of the B_{II}—H distance. This is indeed the direction of asymmetry observed (1.21 and 1.37A, respectively). Such asymmetry may also be influenced by other factors, notably the unfavorable H—B_{II}—H angle as compared with B_2H_6 and the change in Coulomb integrals consequent to the over-all charge distribution. In the case

[3] H. C. Longuet-Higgins, J. chim. phys. **46**, 275 (1949); discussion; G. H. Duffey, J. Chem. Phys. **19**, 963 (1951), footnote page 964.

[4] P. Torkington, J. Chem. Phys. **19**, 528 (1951).

of B_4H_{10} all borons are electrically neutral to a first approximation, and the change in Coulomb integrals is expected to be of secondary importance. The reduced overlap resulting from the unfavorable $H-B_{II}-H$ angle should also lead to asymmetry in the direction observed.

Many of the more detailed features of the structure may be ascribed to H—H repulsion. Thus, the angle $B_I-B_I-H_I$ is observed to be 118°, and the corresponding H_I-H_I distance is 2.80A. Similarly, repulsion between the two hydrogens of type III at the experimentally determined distance of 2.81A probably accounts for the slight twist of the boron tetrahedra which makes the plane of $H_{IV}-B_{II}-H_{IV}$ incline at a slight angle to the plane of $B_I-B_I-B_{II}$. No attempt is made to include such fine details within the general approach suggested here.

As pointed out above, all the borons are electrically neutral and the dipole moment due to framework electrons is expected to be very small; in fact, zero to a first approximation. Such negligible dipole moment as may actually be found for the molecule is then to be ascribed to second-order effects and the B—H bond moments. No experimental determinations of this moment have been published.

C. B_5H_9 [5]

The structural data for this molecule are given in reference 1, (Table I, and Fig. 3). In this molecule each of the base boron atoms, type II in the figure, forms one external B—H bond and two B—H—B bridge bonds. These bonds consume three of the boron orbitals and two electrons leaving a single orbital and one electron for the framework molecular orbitals. It is evident on inspection that the three hydrogens surrounding borons of type II exhibit very nearly trigonal symmetry and suggest strongly that this framework orbital is directed almost along the edge of the pyramid towards the apex boron, type I. The apex boron forms only one external B—H bond which uses one orbital and one boron electron. Thus, this atom contributes three other orbitals and two electrons to the framework. For convenience in forming molecular orbitals, one of these orbitals I_z is considered as an sp hybrid pointing directly away from the external B—H bond and lying along the C_4 symmetry axis. The other two orbitals, I_x and I_y, are chosen as pure p bonds normal to the C_4 axis, one lying in the II—I—II″ plane and pointing towards boron II, the second lying in the II′—I—II‴ plane and pointing towards boron II′. These seven orbitals may be combined into symmetry orbitals as follows:

$$\psi_1(a_1)=\frac{1}{\sqrt{2}}\phi_{I_z}+\frac{1}{2\sqrt{2}}[\phi_{II}+\phi_{II'}+\phi_{II''}+\phi_{II'''}] \qquad E_1=H_0+2\alpha$$

$$\left.\begin{aligned}\psi_2(e)&=\frac{1}{\sqrt{2}}\phi_{I_x}+\tfrac{1}{2}[\phi_{II}-\phi_{II''}]\\ \psi_{2'}(e)&=\frac{1}{\sqrt{2}}\phi_{I_y}+\tfrac{1}{2}[\phi_{II'}-\phi_{II'''}]\end{aligned}\right\} \qquad E_2=H_0+\sqrt{2}\beta$$

$$\psi_3(b_1)=\tfrac{1}{2}[\phi_{II}-\phi_{II'}+\phi_{II''}-\phi_{II'''}] \qquad E_3=H_0$$

$$\left.\begin{aligned}\psi_4(e)&=\frac{1}{\sqrt{2}}\phi_{I_x}-\tfrac{1}{2}[\phi_{II}-\phi_{II''}]\\ \psi_{4'}(e)&=\frac{1}{\sqrt{2}}\phi_{I_y}-\tfrac{1}{2}[\phi_{II'}-\phi_{II'''}]\end{aligned}\right\} \qquad E_4=H_0-\sqrt{2}\beta$$

$$\psi_5(a_1)=\frac{1}{\sqrt{2}}\phi_{I_z}-\frac{1}{2\sqrt{2}}[\phi_{II}+\phi_{II'}+\phi_{II''}+\phi_{II'''}] \qquad E_5=H_0-2\alpha.$$

The energy levels have been evaluated on the basis of the exchange integrals $H_{I_z,II}=\alpha$, $H_{I_x,II}=\beta$, and $H_{II,II'}=0$. It is not unreasonable to choose $-\alpha>-\beta$ under which circumstances the orbitals $\psi_1(a_1)$ and $\psi_2(e)$ are bonding, $\psi_4(e)$ and $\psi_5(a_1)$ are antibonding, and $\psi_3(b_1)$ is nonbonding. Since there are six electrons to be placed into this framework, the bonding orbitals are just filled as required in our basic principles. The electronic configuration for the nonlocalized framework orbitals may then be represented as $(a_1)^2(e)^4\,{}^1A_1$ in which the highest filled molecular orbital is the doubly degenerate $\psi_2(e)$.

The charge distribution may be computed immediately on the basis of these filled molecular orbitals and leads to a net charge of -1 electronic charge on atom I and $+\frac{1}{4}$ electronic charge on each atom of type II. Since the altitude of the pyramid is known experimentally to be 1.09A, this charge distribution gives the molecule a dipole moment of $1\times4.80\times1.09=5.23$ Debye. This value is obviously an upper limit since the simple LCAO approach neglects the repulsion of electrons accumulated on the same atom. The approach suggested by Moffitt[2] may be applied to this type of problem with considerable ease if the nondegenerate bonding electrons are assumed unpolarized and the entire correction is taken up in the highest filled, doubly degenerate orbital. In this calculation, given in detail in Appendix I, the coefficients appearing in the expressions for $\psi_2(e)$ and $\psi_2'(e)$ are determined by an algebraic equation involving the parameter $\beta/(I-E)$, where I and E are the ionization potential and electron affinity appropriate to the valence state of the atoms. Although

[5] A brief preliminary discussion of this molecule was given by G. H. Duffey, J. Chem. Phys. **20**, 195 (1952). A treatment essentially equivalent to ours has been carried out independently by H. C. Longuet-Higgins, as reported in J. Roy. Inst. Chem. **77**, 197 (1953).

there is no unambiguous way of estimating these quantities, it is perhaps sufficient to use the valence state values suggested by Mulliken[6] for $B^-(V_2)$, $B(V_3)$, and $B^+(V_2)$: $I=8.63$ ev, and $E=-0.21$ ev. The exchange integral may be estimated to be of the order of -2 to -3 ev. These choices lead to net charges on the apex atom of -0.32 to -0.39 electronic charges and a dipole moment of 1.7 to 2 Debye, respectively, in delightfully good agreement with the reported value 2.13 ± 0.04 D determined from microwave spectra.[7] It should be pointed out, however, that the very great simplifications and approximations inherent in this calculation lead us to regard the numerical value of this dipole moment as indicating only qualitatively the magnitude of the redistribution of charge resulting from electronic repulsion. In fact, Moffitt's technique applied to other molecules seems to overestimate the magnitude of this repulsion and results in abnormally low moments.

It is interesting to note that on the basis of the crude LCAO model, the first allowed electronic transition of the molecule would be $(a_1)^2(e)^4\,{}^1A_1\rightarrow(a_1)^2(e)^3(b_1)^1E$ at an energy of $-\sqrt{2}\beta$. With the values suggested for β such a transition would appear around 4400–2900A. The absorption spectrum of this substance reported by Platt[7a] shows strong absorption commencing in the neighborhood of 2200A and increasing in intensity to shorter wavelengths. Therefore one is led to favor the higher value for $-\beta$ and, correspondingly, the higher dipole moment.

D. B_5H_{11}

The structural data for this compound are given in Table I and Fig. 5 of reference 1. In this molecule, the unique boron, type I, forms two external B–H bonds which use up two of the boron orbitals and two electrons. This atom then contributes two orbitals and a single electron to the framework. There is no unambiguous way of choosing these orbitals on the basis of the molecular geometry, but, for convenience, one may be chosen as the third member of an sp^2 set lying in the plane of symmetry and designated I_d, and the other may be chosen as essentially a pure p orbital normal to this plane and designated I_p. The sp^2-type orbital of this pair then points almost directly at the center of the line joining the two borons of type II. Each of these borons forms a single external B–H bond and two bridge bonds utilizing a total of three orbitals and two electrons. Because of the nearly trigonal symmetry of the hydrogens about these atoms, it seems reasonable to take the remaining orbital as pointing towards the unique atom I. The two orbitals from atoms II and the orbital of atom I lying in the symmetry plane may then be considered as forming a localized three-center orbital characterized by a parameter $\gamma/\beta\sim1$ and concentrated in the triangular face I–II–II′. Each atom of type III forms two external B–H bonds and a single bridge bond. These bonds require the use of three orbitals and two and a half electrons and leave one orbital and one-half an electron for the framework. Again the nearly trigonal symmetry of the hydrogens about the boron atoms suggests strongly that the remaining orbital is pointed almost directly toward the unique atom I. Hence, the pair of orbitals from III and III′ along with the single p orbital contributed by atom I may be considered as forming a localized "open" three-center orbital lying essentially along the line joining the three atoms. Out of the six framework orbitals contributed by all the atoms, there are expected only two strongly bonding three-center orbitals, one nonbonding, and three antibonding three-center orbitals given essentially by the expressions

$$\psi_1(a')=\frac{1}{\sqrt{3}}[\phi_{I_d}+\phi_{II}+\phi_{II'}] \quad \text{bonding}$$

$$\psi_2(a'')=\frac{1}{\sqrt{2}}[\phi_{II}-\phi_{II'}] \quad \text{antibonding}$$

$$\psi_3(a')=\frac{1}{\sqrt{6}}[2\phi_{I_d}-\phi_{II}-\phi_{II'}] \quad \text{antibonding}$$

$$\psi_4(a'')=\tfrac{1}{2}[\phi_{III}+\sqrt{2}\phi_{I_p}-\phi_{III'}] \quad \text{bonding}$$

$$\psi_5(a')=\frac{1}{\sqrt{2}}[\phi_{III}+\phi_{III'}] \quad \text{nonbonding}$$

$$\psi_6(a'')=\tfrac{1}{2}[\phi_{III}-\sqrt{2}\phi_{I_p}-\phi_{III'}] \quad \text{antibonding.}$$

Since there is a total of four electrons contributed to this framework, the two bonding orbitals are just filled and the resultant electronic configuration may be represented as $(a')^2(a'')^2={}^1A'$. Of course, as pointed out above, the choice of the forms for the two orbitals contributed by atom I is entirely a matter of convenience, and hence the form of the wave functions is a matter of convenience. In essence, any linear combination of the three orbitals of symmetry a' and the three orbitals of symmetry a'' will provide acceptable substitutes, but the general pattern of energy levels should not be greatly altered by such symmetrizing procedures since the forms chosen are such as to give qualitatively the largest exchange integrals and the least interaction integrals between localized orbitals.

The coefficients given in the foregoing expressions for the bonding orbitals now allow a rapid first approximation to the charge distribution and dipole moment. Thus, the resultant net charge on atom I becomes $-\frac{2}{3}$ of an electronic charge and that on atoms of type II becomes $+\frac{1}{3}$ of an electronic charge; atoms of type III are electrically neutral. This charge distribution together with the experimental dimensions of the molecule

[6] R. S. Mulliken, J. Chem. Phys. **2**, 792 (1934).
[7] Hrostowski, Myers, and Pimentel, J. Chem. Phys. **20**, 518 (1952).
[7a] J. R. Platt, J. Chem. Phys. **15**, 600 (1947).

lead to a dipole moment of $(2/3)\times 4.80\times 1.48 = 4.75$ Debye with the negative end on atom I. Again this value is an upper limit since electron repulsion will reduce the tendency for charge to pile up on atom I.

Self-consistent variation of the Coulomb integrals similar to that utilized in discussing the dipole moment of B_5H_9 may be employed to estimate the reduction. In this case, both filled three-center orbitals must be polarized since the charge will certainly tend to spread over the entire molecule insofar as possible. These calculations are outlined in Appendix I and lead to dipole moments of 1.1 and 1.9 D corresponding to exchange integrals of -2 and -3 ev, respectively. The general features of the charge distribution are as expected intuitively from the simple treatment: the large negative charge of atom I is reduced by spreading to atoms II and III. Thus atoms of type III which were originally neutral become slightly negative, atoms of type II become less positive.

It is interesting to note that the charge distribution suggested for this molecule should lead to asymmetry of the bridge hydrogens with the hydrogens closer to boron II and farther from boron III. The crystal structure studies do not give sufficient detail to confirm this effect.

E. $B_{10}H_{14}$

The structural data for this molecule are summarized in reference 1 (Table I, and Fig. 2). The molecule exhibits C_{2v} symmetry and has four different types of boron atoms, all of which form only a single normal B—H external bond. The end atom, type I, forms in addition two B—H—B bridge bonds which, together with the external B—H bond, consume three orbitals and two electrons. The remaining orbital probably points directly towards a type-III boron atom as suggested by the essentially trigonal symmetry of the hydrogens about the boron of type I. The type-III borons form only the one normal B—H bond and hence contribute three other orbitals and two electrons to the framework. Again there is no unambiguous way of choosing these three orbitals but consistent with the symmetry of the molecule, it is convenient to regard two as forming an sp^2 hybrid with the normal B—H bond orbital, all three lying in the vertical plane containing the C_2 axis and atoms I and III. The fourth orbital is then a pure p orbital normal to this plane. It is evident from inspection that this form of hybridization directs one orbital towards atom I and the second towards the center of the line joining the atoms IV and IV′. It seems reasonable then to regard the two orbitals directed along the line between atoms I and III as forming a localized single B—B bond of the same sort as formed between the atoms of type I in B_4H_{10}. The other sp^2 hybrid may be treated as forming a localized three-center orbital with atoms IV and IV′ and the pure p orbital may be considered as forming a three-center orbital with atoms II and II′. The part of the structure comprising the atoms II, II′, III, IV, and IV′ is then almost identical in electronic structure with the simple molecule B_5H_{11}; that comprising the atoms I, II, II′, and III is comparable to B_4H_{10}. That such an arrangement is possible results from the environment of atoms IV and IV′. These atoms use one orbital for the external B—H bond and the other three are hybridized in essentially tetrahedral symmetry so as to form three sets of three-center orbitals: one involving the atoms II, II″, and IV, or, equivalently, II′, II‴, and IV′; the second involving IV, IV′, and III; the third involving IV, IV′, and III′. Of these, the kind involving the atoms III is probably characterized by a parameter $\gamma/\beta\sim 1$ whereas those involving the atoms II may well be characterized by a smaller magnitude for this parameter. For ease in computing charge distribution, however, it will be assumed as a first approximation that these orbitals are all of similar character and that each atomic orbital contributes equally in the bonding molecular orbital. Atoms of type II form, in addition to the external B—H bond, one B—H—B bridge bond. These two bonds use two boron orbitals and one and a half electrons leaving two orbitals and one and a half electrons for the framework. These orbitals point in the general direction of atoms III and the center of the triangle formed by the neighboring type II and IV atoms. This orientation is again consistent with the localized three-center bond formulation previously outlined.

In summary, there are available twenty-two hybrid boron orbitals and sixteen electrons from which to construct the framework. Normal single bonds are formed between atoms I and III using a total of four boron orbitals and giving two strongly bonding localized orbitals requiring four electrons. Four three-center orbitals are formed requiring twelve boron atomic orbitals and giving rise to four strongly bonding localized three-center orbitals concentrated in the triangles formed by atoms of the types III, IV, IV′ and IV, II, II″. These four bonding orbitals require eight electrons. The remaining orbitals form weaker three center orbitals lying along the line of atoms II, III, II′ and the corresponding trio II″, III′, II‴. Each of these gives rise to one bonding orbital, one nonbonding orbital, and one antibonding orbital and hence require the remaining four electrons for filling the bonding orbitals. There are thus a total of eight bonding orbitals which are just filled by the available sixteen electrons. The highest filled one of these orbitals is probably the weak three-center orbital between atoms II, III, II′ and excitation of an electron from this orbital to the first excited, nonbonding level is perhaps responsible for the absorption spectrum in the near ultraviolet. Since this orbital is characterized by the parameter $\gamma/\beta\sim 0$, the energy of the transition should be approximately $-\sqrt{2}\beta$ on the crude LCAO model and by comparison with the absorp-

tion spectrum reported by Pimentel and Pitzer[8] allows an estimate of -2.5 ev for the exchange integral β.

The molecular orbitals are given above in terms of simple prototype, localized three-center orbitals. Naturally, delocalization can be obtained by combining these according to the appropriate symmetry properties of the molecule, but the choice of orbitals indicated above is such as to minimize serious interaction between them, and hence little change in the energy level pattern or coefficients of individual atomic orbitals is to be expected in this process. The coefficients may be determined immediately from the corresponding three-center prototypes and lead to the following charge distribution: atoms of type I: neutral; type II: $+\frac{1}{3}$ electronic charge; type III: $-\frac{2}{3}$ electronic charge; type IV: neutral. Thus, the charge displacement appears between atoms II and III and gives rise to a dipole moment of $2\times(2/3)\times4.80\times0.92=6.2$ Debye, where the altitude of the triangle formed by II, III, and II′ is estimated as 0.92A. Again this value is to be taken as an upper limit which will be reduced by a redistribution of the coefficients of the weak three-center orbitals. Such a redistribution, given in Appendix I, leads to a resultant dipole moment of 1.6 to 2.2 Debye corresponding to exchange integrals of -2 to -3 ev, respectively. This value is to be compared with the experimental moment 3.52 ± 0.02 Debye determined by Laubengayer and Bottei[9] from dielectric-constant studies on solutions. While the experimental value may be too high because of underestimation of atomic polarization, we shall be the first to point out that our calculation of the redistribution of charge is subject to significant improvement.

Although it is not within the province of the present study to discuss the finer details of the structure, some of the gross features are of interest. Thus, the charge distribution suggested by the above argument puts positive charges on atoms of type II. Since these are adjacent in the molecular structure, the repulsion between them is expected to increase the boron-boron distance significantly. It is notable that this distance, 2.01A, is indeed longer than the average of the other distances, 1.76A. The displacement of the bridge hydrogens in the B—H—B bonds between atoms I and II is also indicative of this net positive charge on the II atoms since, as suggested in the discussion on the three-center bond, an increase in the Coulomb integral such as would attend the net positive charge on the boron II atoms will distort the bridge structure to favor a stronger bond between the II atom and the bridge hydrogen at the expense of that between the I boron and the bridge hydrogen. This is also the direction of asymmetry determined experimentally and indicated by the distances 1.36 and 1.44A, respectively. It is also notable that the bond between atoms I and III is suggested to be essentially a single bond, and hence the boron-boron distance might be expected to be somewhat shorter than the other boron-boron distances. This effect is indeed indicated by the experimental data but there may be some doubt as to the magnitude, 1.73A, as compared to the average B—B distance of 1.76A (neglecting the long bonds).

IV. DISCUSSION

A. B_4H_4, B_6H_6, $B_{12}H_{12}$

None of these pseudospherical hydrides has been reported, but related structures lead us to consider them to find what predictions, if any, arise from our approach. The tetrahedral B_4H_4, symmetry T_d, is suggested by the known B_4Cl_4; octahedral B_6H_6, symmetry O_h, by B_5H_9 and by the B_6 octahedra in CaB_6 and other metal borides; icosahedral $B_{12}H_{12}$, symmetry group P_h,[10] by $B_{10}H_{14}$ and by the B_{12} icosahedra in C_2B_{12} and in elemental boron.

Each boron is taken as forming one "normal" B—H bond, and thus contributing 3 orbitals and 2 electrons to the highly symmetrical framework. The 3 orbitals may be chosen as 3 equivalent hybrids, or as 1 centrally directed and 2 tangentially directed hybrids, in setting up the LCAO calculation. Symmetry is, of course, of great utility.

In B_4H_4, we may conveniently choose the AO's as 3 hybrids directed approximately along the edges of the tetrahedron, i.e., roughly toward the neighboring borons. (This of course carries no implication that the final bonding orbitals will lie along the edges: in fact, they turn out to lie in the faces of the tetrahedron.) Standard group-theory methods then yield the LCAO representation $A_1+E+2F_1+F_2$; a simplified calculation yields the MO energies:

A_1:	$H_0+\beta+2\gamma+4\delta$	Bonding
F_2:	$H_0-\beta-\gamma-2\delta$	Antibonding
E:	$H_0+\beta-\gamma-2\delta$	Nonbonding?
F_1:	$H_0+\beta-\gamma$	Bonding
	$H_0-\beta+2\gamma-2\delta$	Antibonding?

In this calculation an algebraic approximation has slightly *under*estimated the splitting of the F_1 levels; β, γ, and δ are the exchange integrals between atomic orbitals directed as indicated by the vectors in Fig. 2. It seems probable that we may take $|\beta|>|\gamma|>|\delta|$, so that the A_1 and lower F_1 levels indicated are bonding, thus providing a home for the 8 electrons available, 2 in the A_1 and 6 in the triply degenerate F_1 level. We may note that if we transform these 4 filled MO's into localized "equivalent orbitals" in Lennard-Jones's

[8] G. C. Pimentel and K. S. Pitzer, J. Chem. Phys. 17, 882 (1949).
[9] A. W. Laubengayer and R. Bottei, J. Am. Chem. Soc. 74, 1618 (1952).

[10] This is the group of order 120 generated by the rotations of the icosahedron and a center of symmetry, somewhat unfamiliar to chemists since Nature considerately avoids its use. The representations (symmetry species) Γ_1, Γ_2, Γ_3, Γ_4, Γ_5 have degeneracies 1, 3, 3, 4, 5, respectively; g and u refer as usual to symmetric and antisymmetric behavior on reflection in the origin.

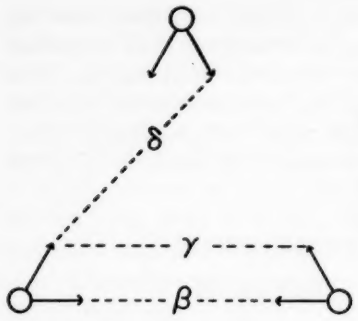

FIG. 2. Designation of certain exchange integrals on boron A.O.'s, oriented as indicated by the vectors, in a symmetric triangle of boron atoms in the B_4 tetrahedron.

sense,[11] these would lie in the four faces of the tetrahedron, as Duffey[12] suggested.

The actual stability of such a molecule would depend on the magnitudes of β, γ, and δ, and so on the hybrids available; this would be strongly influenced by the nature of the 4 external single bonds. Hence it might well be that, although B_4Cl_4 is quite stable, B_4H_4 would be at best metastable. Deeper calculation might clarify this point. Here we shall conclude our discussion by noting that our results indicate the regular tetrahedral form of B_4Cl_4 to be stable; presumably the slight irregularity found in the crystal is the result of the intermolecular forces.

Passing to B_6H_6, octahedral, we find a more interesting result. We choose our 3 AO's on each B to consist of one centrally directed, ϕ_c, and 2 tangentially directed. Then the representation works out as $A_{1g}+E_g+F_{1g}+F_{2g}+2F_{1u}+F_{2g}$; of these the A_{1g}, E_g, and one of the F_{1u} triplets may be formed from the six ϕ_c. If we define certain integrals in terms of atomic orbitals as indicated in Fig. 3, we find the following levels:

A_{1g}:	$H_0+4\beta+\eta$	Bonding
E_g:	$H_0-2\beta+\eta$	Antibonding
F_{1g}:	$H_0-2\epsilon$	Antibonding
F_{2g}:	$H_0+2\epsilon$	Bonding
F_{1u}:	$H_0+2\delta+\Delta$	Bonding
	$H_0-\eta-\Delta$	Antibonding
F_{2u}:	$H_0-2\delta$	Antibonding

Here the quantity $\Delta=[\frac{1}{4}(\eta+2\delta)^2+8\gamma^2]^{\frac{1}{2}}-\frac{1}{2}(\eta+2\delta)$. But the exact distribution of the F_{2g} and F_{1u} levels is not important: the significant point is the strongly anti-

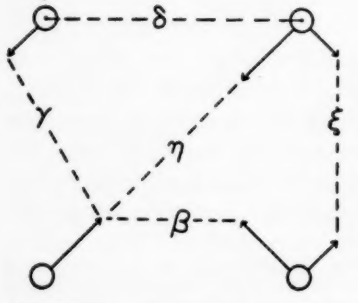

FIG. 3. Diametrical section of B_6 octahedron, showing designation of certain exchange integrals on boron A.O.'s indicated by the vectors. The integral δ is on the two parallel tangential A.O.'s which point straight up from the plane of the paper.

bonding character of the E_g level. Since this level is up beyond reach, we must make up the ground state by packing our 12 electrons into the bonding orbitals A_{1g}, F_{1u}, and F_{2g}. The lowest is beyond doubt the A_{1g}, which absorbs 2 electrons; the triplet F_{1u}(say) is next and absorbs 6; and now we find a triplet F_{2g}, with only 4 electrons left!

Since we cannot fill the bonding MO's, we cannot satisfy our rules, and are forced to conclude that octahedral B_6H_6 should not exist. It seems likely that the lowest state would exhibit orbital degeneracy; and this, according to an elegant theorem of Jahn and Teller[13] which Nature seems to avoid testing, would cause the equilibrium nuclear configuration to have lower symmetry than O_h. But this question is one for deeper calculation. It is interesting to note that we may fill the bonding MO's by adding 2 electrons to form $B_6H_6^=$, a "stable ion."

We have not carried the $B_{12}H_{12}$ icosahedral model so far, because the LCAO calculations are moderately complex and seem to belong to the next stage of investigation. Again using 1 radial and 2 tangential AO's from each boron, we find that the group representation[10] is $\Gamma_{1g}+\Gamma_{2g}+\Gamma_{4g}+\Gamma_{5g}+2\Gamma_{2u}+\Gamma_{3u}+\Gamma_{4u}+2\Gamma_{5u}$. In the absence of LCAO calculation, we may speculate on the order of these levels by counting nodes—correlating with the levels of a sphere,[8] or better a spherical shell. If we examine the representations given by spherical harmonics, we find

$$s\sim\Gamma_{1g};\ p\sim\Gamma_{2u};\ d\sim\Gamma_{5g};\ f\sim\Gamma_{3u}+\Gamma_{4u};\ g\sim\Gamma_{4g}+\Gamma_{5g};\ \text{etc.}$$

If we make the obvious correlation and arrange the order of energy levels as $\Gamma_{1g}<\Gamma_{2u}<\Gamma_{5g}$, etc., with the higher Γ_{2u} level well up, we may put 18 of our 24 electrons in the singlet A_{1g}("s"), the triplet Γ_{2u}("p"), and the quintuplet Γ_{5g}("d"). If the Γ_{3u} triplet is lower than the Γ_{4u} quartet (both are "f"), then the remaining 6 electrons will just pack in nicely to satisfy our rules; if the converse is true, the ground state will exhibit orbital degeneracy as in the B_6H_6 case, and hence the molecule will not exist with such high symmetry.[13a]

B. B_3H_9 and B_6H_{10}

Plausible structures for the reaction intermediate,[14] B_3H_9, and for the hydrogen arrangement in B_6H_{10}[14a] can be suggested. For B_3H_9 our scheme leads uniquely

[11] J. E. Lennard-Jones, Proc. Roy. Soc. (London) **A198**, 1, 14 (1949).

[12] G. H. Duffey, J. Chem. Phys. **21**, 761 (1953).

[13] H. A. Jahn and E. Teller, Proc. Roy. Soc. (London) **A161**, 220 (1937).

[13a] *Note added in proof.*—Professor H. C. Longuet-Higgins has carried out a very thorough study of the levels in B_6 octahedra and B_{12} icosahedra in connection with the structures of the crystalline borides. His results agree with ours in so far as ours go; he finds that the quartet level of the B_{12} icosahedron is bonding. This result enables us to say, according to our argument, that $B_{12}H_{12}$ should not exist with icosahedral symmetry. We should like to express our thanks to Professor Longuet-Higgins for a helpful and stimulating discussion.

[14] A. T. Whatley and R. N. Pease, J. Am. Chem. Soc. **76**, 835 (1954).

[14a] K. Eriks, W. N. Lipscomb, and R. Schaeffer, J. Chem. Phys. (to be published).

to $3BH_2$ units joined by 3 bridge hydrogen atoms, and hence we suggest a ring structure analogous to cyclopropane. For B_6H_{10} we form a pentagonal pyramid, the cap of the icosahedron, by adding one B atom to the B_5 arrangement of B_5H_{11} (see Fig. 5 of reference 1). The three nearest hydrogen atoms to this newly added boron atom are removed, and two are attached by single bonds to this boron atom. This newly added BH_2 group lies in the symmetry plane of the molecule and the new B is joined to the apex B by a normal covalent bond and to the two next nearest B atoms by an open three-center bond. Bonding in the remainder of the molecule is very similar to that in B_5H_{11}.

C. B_8H_{16}

Although no molecule of this formula has yet been studied, there seems to be some chemical evidence for the existence of a B_8 hydride;[15] and since a reasonable model can be constructed based on the known structure of $B_{10}H_{14}$, it is of interest to determine whether such a model would satisfy the conditions of stability required by our postulates. Thus, considering the structure of $B_{10}H_{14}$ as presented in Fig. 5 of reference 1, the two atoms of type I are removed and B−H−B bridges are used to join atoms II and III. In addition, a second external hydrogen is added to atom II. The topological structure of this molecule is then representable as in Fig. 4.[16]

It is evident from this figure that the four three-center bonding orbitals are maintained essentially unaltered and are just filled with the eight available framework electrons. The resultant charge distribution is obtained by the same arguments as before and leads to neutrality for borons IV and a net charge of $+\frac{1}{3}$ electronic charge on the atoms III and $-\frac{1}{6}$ electronic charge on atoms II. The resultant dipole moment should then be about half that of $B_{10}H_{14}$ or 3.1 Debye to a first approximation and of the order of 0.8 to 1.2 Debye to a slightly better approximation.

D. Consolidation

Looking back at the known structures and our interpretation of their valence structure, we note the following:

(1) The hybridized orbitals actually used by the borons correspond closely to one or the other of the usual modish hybridized sets, either (a) the tetrahedral sp^3 set of 4, or (b) the plane-trigonal sp^2 set of 3 plus a 4th perpendicular pure p. The directional properties of both sets are familiar.

(2) The framework orbitals among the borons can be reduced to localized orbitals of 3 types, (a) normal

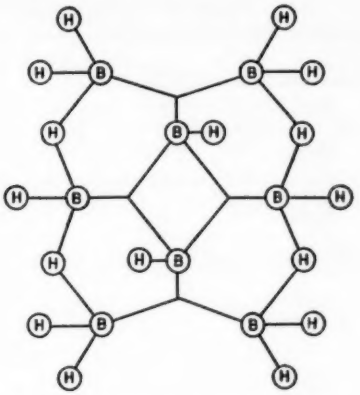

FIG. 4. Topological configuration suggested for B_8H_{16}.

2-center covalent bonds, (b) "open" 3-center bonds with $\gamma/\beta=0$, and (c) "equilateral" 3-center bonds with $\gamma/\beta\sim1$.

The case of B_5H_9 fits this pattern only with a touch of the shoehorn; *viz.*, in the same sense that the benzene structure involves only single and double bonds. Namely, we can set up *two* sets of bonds satisfying our simplified pattern: each involves 2 covalent bonds from the apex boron to base borons, and one open 3-center bond on the apex and the remaining base borons. Allowing resonance between these two structures, as we do between Kekule structures in benzene, we obtain precisely the bonding framework orbitals previously found; details are in Appendix II.

If we accept this simplified pattern, the "building blocks" of possible boron hydrides are few in number:

(1) BH units using tetrahedral sp^3 orbitals
(2) BH units using trigonal sp^2 plus p orbitals
(3) BH_2 units using trigonal sp^2 plus p orbitals
(4) BH_2 units using tetrahedral sp^3 orbitals.

The links are of 4 kinds only (the 3 boron-framework bonds listed above plus the B−H−B 3-center bond), and the approximate geometry of both the units and the links is established.

Moreover, for a given empirical formula, our assumptions severely limit the range of possible units and links. Consider the hydride B_pH_q: let x be the number of BH_2 units, s the number of BHB links, t the number of 3-center framework links, and y the number of covalent framework links. Then an "orbital balance" requires

$$4p=(q-s)+2s+3t+2y;$$

an "electron accounting" requires

$$3p=(q-s)+s+2(t+y);$$

and if we add a "hydrogen balance" and the requirement that t and y be non-negative, we find the useful limits:

$$t+y=(3p-q)/2,$$
$$s\leq q-p;\quad s\geq(q-p)/2;\quad s\leq p,$$
$$t=p-s,$$
$$x=q-p-s.$$

[15] A. B. Burg and H. I. Schlesinger, J. Am. Chem. Soc. **55**, 4009 (1933); F. J. Norton, J. Am. Chem. Soc. **72**, 1849 (1950); Professor R. Schaeffer, Iowa State College (private communication, 1953).

[16] An obvious intermediate is B_9H_{15}, obtained by modifying only one end of $B_{10}H_{14}$.

TABLE I. Examination of boron hydrides.

	p	q	$(t+y)$	s	t	y	x
B_2H_6	2	6	0	[a] 2	0	0	2
B_4H_{10}	4	10	1	3	1	0	3
				[a] 4	0	1	2
B_5H_9	5	9	3	2	3	0	2
				3	2	1	1
				[b] 4	1	2	0
B_5H_{11}	5	11	2	[a] 3	2	0	3
				4	1	1	2
				5	0	2	1
$B_{10}H_{14}$	10	14	8	2	8	0	2
				3	7	1	1
				[a] 4	6	2	0
B_6H_{10}	6	10	4	2	4	0	2
				[c] 3	3	1	1
				4	2	2	0
B_8H_{16}	8	16	4	[c] 4	4	0	4
				5	3	1	3
				6	2	2	2
				7	1	3	1
				8	0	4	0

[a] Possibility utilized by Nature.
[b] Used in B_5H_9; but see text and Appendix II.
[c] Possibility preferred by us.

Table I shows this orbital-electron balance applied to certain known and unknown hydrides to limit their possible valence topologies; the possibilities must still pass the geometrical test imposed by the geometries of the units and links. We have not by any means considered all of the isomeric boron hydrides listed; no doubt a systematic examination would be interesting. Indeed, the systematic application of the orbital-electron balance to "electron-deficient" compounds in general might well prove rewarding.

ACKNOWLEDGMENT

We wish to express our appreciation to Professor R. S. Mulliken for helpful comments.

APPENDIX I. SELF-CONSISTENT LCAO APPROXIMATION TO THE CHARGE DISTRIBUTION

B_5H_9

The simple LCAO approximation with constant single-electron Coulomb integrals, H_0, places net charges of $+\frac{1}{4}$ e on atoms of type II and -1 e on the apex atom I. It is intuitively evident that the modification of the Coulomb integrals attending this charge distribution will cause a redistribution of charge which is probably best taken up in the highest filled framework orbitals ψ_2(e) and ψ_2'(e). However, as written in the text, these degenerate orbitals individually do not adequately reflect the symmetry of the molecule, and a simpler calculation in which cross terms between the two orbitals are minimized may be obtained in terms of the linear combinations

$$\psi=\frac{1}{\sqrt{2}}(\psi_2+\psi_2')=\frac{\sin\theta}{\sqrt{2}}(\phi_{I_x}+\phi_{I_y})+\frac{\cos\theta}{2}(\phi_{II}+\phi_{II'}-\phi_{II''}-\phi_{II'''}),$$

and

$$\psi'=\frac{1}{\sqrt{2}}(\psi_2-\psi_2')=\frac{\sin\theta}{\sqrt{2}}(\phi_{I_x}-\phi_{I_y})+\frac{\cos\theta}{2}(\phi_{II}-\phi_{II'}-\phi_{II''}+\phi_{II'''}).$$

The variation equations for the ψ orbital may then be written as follows: for ϕ_{I_x}:

$$(\sin\theta)(\xi_I-E_2)+2\frac{\cos\theta}{\sqrt{2}}\beta=0,$$

and for ϕ_{II}:

$$(\sin\theta)\beta+\frac{\cos\theta}{\sqrt{2}}(\xi_{II}-E_2)=0.$$

When the energy E_2 is eliminated, these equations give

$$(\xi_I-\xi_{II})+2\sqrt{2}\beta\cot 2\theta=0.$$

In this equation, the coulomb integrals may be approximated as suggested by Moffitt[2] as

$$\xi_j{}^i=-I+(I-E)(W_j{}^i-2),$$

where $W_j{}^i$ represents the total electron density on atom j, less one electron in the molecular orbital ψ_i for which the calculation is being made, and I and E are the valence-state ionization potential and electron affinity. For the orbital in question

$$W_I=2+3\sin^2\theta,$$
$$W_{II}=(9/4)+(3/4)\cos^2\theta,$$

and the variation equation becomes

$$\frac{7}{8}-\frac{15}{8}\cos 2\theta=-\frac{2\sqrt{2}\beta}{I-E}\cot 2\theta.$$

This equation is solved numerically for assumed values of β and $I-E$ as discussed in the text and leads to the coefficients, net charges q, and dipole moment μ shown in Table II.

TABLE II. Charge distribution for B_5H_9.

β	$\sin\theta$	q_I	q_{II}	μ
-2 ev	0.574	-0.318 e	$+0.079$ e	1.7 D
-3	0.590	-0.392	$+0.098$	2.1
$-\infty$ [a]	0.707	-1.000	$+0.250$	5.2

[a] Simple LCAO approximation, i.e., exchange effects overwhelm modifications in Coulomb integrals.

B_5H_{11}

In the simple LCAO treatment a charge of $-\frac{2}{3}$ e appears on atom I and charges of $+\frac{1}{2}$ e appear on atoms of type II. Qualitatively, the negative charge on atom I is expected to spread to neutralize partially the charge on atoms II and also to put a small negative charge on atoms III. In order to accomplish this redistribution, it is necessary to consider simultaneous variation in the two framework orbitals. Thus, writing

$$\psi_1=\frac{\sin\theta_1}{\sqrt{2}}\phi_{\mathrm{III}}+(\cos\theta_1)\phi_{\mathrm{I},\pi}-\frac{\sin\theta_1}{\sqrt{2}}\phi_{\mathrm{III}'},$$

and

$$\psi_2=\frac{\sin\theta_2}{\sqrt{2}}\phi_{\mathrm{II}}+(\cos\theta_2)\phi_{\mathrm{I},\sigma}+\frac{\sin\theta_2}{\sqrt{2}}\phi_{\mathrm{II}'},$$

in which $\phi_{\mathrm{I},\sigma}$ and $\phi_{\mathrm{I},\pi}$ are the hybrid sp^2 and π orbitals forming the three-center bonds as described in the text, the variation equations become, for ψ_1,

$$\frac{\sin\theta_1}{\sqrt{2}}(\xi_{\mathrm{III}}{}^1-E_1)+\cos\theta_1\gamma=0,$$

$$2\frac{\sin\theta_1}{\sqrt{2}}\gamma+\cos\theta_1(\xi_{\mathrm{III}}{}^1-E_1)=0,$$

and for ψ_2,

$$\frac{\sin\theta_2}{\sqrt{2}}(\xi_{\mathrm{II}}{}^2-E_2)+\left(\cos\theta_2+\frac{\sin\theta_2}{\sqrt{2}}\right)\beta=0,$$

$$2\frac{\sin\theta_2}{\sqrt{2}}\beta+\cos\theta_2(\xi_{\mathrm{I}}{}^2-E_2)=0.$$

Eliminating E_1 and E_2 from these pairs of equations gives two equations in θ_1 and θ_2,

$$(\xi_{\mathrm{III}}{}^1-\xi_{\mathrm{I}}{}^1)+2\sqrt{2}\gamma\cot2\theta_1=0$$

and

$$(\xi_{\mathrm{II}}{}^2-\xi_{\mathrm{I}}{}^2)+2\sqrt{2}\beta\cot2\theta_2=0.$$

The Coulomb integrals are to be evaluated as before

$$W_{\mathrm{I}}{}^1=2+\cos^2\theta_1+2\cos^2\theta_2,$$

$$W_{\mathrm{I}}{}^2=2+2\cos^2\theta_1+\cos^2\theta_2,$$

$$W_{\mathrm{II}}{}^1=2+\sin^2\theta_2,$$

$$W_{\mathrm{II}}{}^2=2+\frac{\sin^2\theta_2}{2},$$

$$W_{\mathrm{III}}{}^1=\frac{5}{2}+\frac{\sin^2\theta_1}{2},$$

$$W_{\mathrm{III}}{}^2=\frac{5}{2}+\sin^2\theta_1.$$

TABLE III. Charge distribution for B_5H_{11}.

$\gamma=\beta$	$\cos\theta_1$	$\cos\theta_2$	q_{I}	q_{II}	q_{III}	μ
-2	0.682	0.276	-0.082	$+0.076$	-0.035	1.1
-3	0.703	0.367	-0.258	$+0.135$	-0.006	1.9
$-\infty$ [a]	0.707	0.577	-0.667	$+0.373$	0	4.7

[a] Simple LCAO approximation.

By use of these expressions for $W_j{}^i$, the two equations become

$$1+\cos2\theta_1+\frac{4}{3}\cos2\theta_2=-\frac{4}{3}\left(-\frac{2\sqrt{2}\gamma}{I-E}\right)\cot2\theta_1,$$

and

$$\frac{5}{4}+\cos2\theta_1+\frac{3}{4}\cos2\theta_2=-\left(-\frac{2\sqrt{2}\beta}{I-E}\right)\left(\cot2\theta_2+\frac{1}{2\sqrt{2}}\right).$$

These equations are solved numerically for assumed values of $\gamma=\beta$ and $I-E$ as discussed in the text and lead to the results in Table III for the coefficients, net charges q and dipole moments μ.

$B_{10}H_{14}$

In the simple LCAO treatment, net charges of $+\frac{1}{3}$ e, $-\frac{2}{3}$ e, and 0 appear on atoms II, III, and IV, respectively. Although II and IV are connected by the highest filled framework orbitals, it seems desirable to include in the variation treatment other orbitals which will allow the charge to spread to atom IV. Thus, the variation orbitals are chosen as

$$\psi_1(\mathrm{II,IV,II''})=\frac{\sin\theta_1}{\sqrt{2}}\phi_{\mathrm{II},a}+\cos\theta_1\phi_{\mathrm{IV},a}-\frac{\sin\theta_1}{\sqrt{2}}\phi_{\mathrm{II}'',a},$$

$$\psi_2(\mathrm{III,IV,IV'})=\frac{\sin\theta_2}{\sqrt{2}}\phi_{\mathrm{IV},b}+\cos\theta_2\phi_{\mathrm{III},\sigma}+\frac{\sin\theta_2}{\sqrt{2}}\phi_{\mathrm{IV}',b},$$

$$\psi_3(\mathrm{III',IV,IV'})=\frac{\sin\theta_2}{\sqrt{2}}\phi_{\mathrm{IV},c}+\cos\theta_2\phi_{\mathrm{III}',\sigma}+\frac{\sin\theta_2}{\sqrt{2}}\phi_{\mathrm{IV}',c},$$

$$\psi_4(\mathrm{II,III,II'})=\frac{\sin\theta_4}{\sqrt{2}}\phi_{\mathrm{II},b}+\cos\theta_4\phi_{\mathrm{III},\pi}-\frac{\sin\theta_4}{\sqrt{2}}\phi_{\mathrm{II}',b},$$

where the atomic orbitals are differentiated according to the three-center bond to which they contribute. The variation equations lead to the following three pairs for ψ_1:

$$\frac{\sin\theta_1}{\sqrt{2}}(\xi_{\mathrm{II}}{}^1-E_1)+\beta\left(\frac{\sin\theta_1}{\sqrt{2}}+\cos\theta_1\right)=0,$$

$$2\beta\frac{\sin\theta_1}{\sqrt{2}}+\cos\theta_1(\xi_{\mathrm{IV}}{}^1-E_1)=0,$$

for ψ_2 and ψ_3:

$$\frac{\sin\theta_2}{\sqrt{2}}(\xi_{\mathrm{IV}}{}^2-E_2)+\beta\left(\frac{\sin\theta_2}{\sqrt{2}}+\cos\theta_2\right)=0,$$

$$2\beta\frac{\sin\theta_2}{\sqrt{2}}+\cos\theta_2(\xi_{\mathrm{III}}{}^2-E_2)=0,$$

for ψ_4:

$$\frac{\sin\theta_4}{\sqrt{2}}(\xi_{\mathrm{II}}{}^4-E_4)+\gamma\cos\theta_4=0,$$

$$2\gamma\frac{\sin\theta_4}{\sqrt{2}}+\cos\theta_4(\xi_{\mathrm{III}}{}^4-E_4)=0.$$

By eliminating the energies from these equations, there results

$$(\xi_{\mathrm{II}}{}^1-\xi_{\mathrm{IV}}{}^1)+\frac{2\sqrt{2}\beta}{I-E}\left(\cot2\theta_1+\frac{1}{2\sqrt{2}}\right)=0,$$

$$(\xi_{\mathrm{IV}}{}^2-\xi_{\mathrm{III}}{}^2)+\frac{2\sqrt{2}\beta}{I-E}\left(\cot2\theta_2+\frac{1}{2\sqrt{2}}\right)=0,$$

$$(\xi_{\mathrm{II}}{}^4-\xi_{\mathrm{III}}{}^4)+\frac{2\sqrt{2}\gamma}{I-E}\cot2\theta_4=0.$$

Again the Coulomb integrals are evaluated in terms of $W_j{}^i$ which are as follows:

$$W_{\mathrm{II}}{}^1=\tfrac{3}{2}+\frac{\sin^2\theta_1}{2}+\sin^2\theta_4,$$

$$W_{\mathrm{II}}{}^4=\tfrac{3}{2}+\sin^2\theta_1+\frac{\sin^2\theta_4}{2},$$

$$W_{\mathrm{III}}{}^2=2+\cos^2\theta_2+2\cos^2\theta_4,$$

$$W_{\mathrm{III}}{}^4=2+2\cos^2\theta_2+\cos^2\theta_4,$$

$$W_{\mathrm{IV}}{}^1=1+\cos^2\theta_1+2\sin^2\theta_2,$$

$$W_{\mathrm{IV}}{}^2=1+2\cos^2\theta_1+\tfrac{3}{2}\sin^2\theta_2.$$

In terms of the angles only, the variation equations become

$$\frac{1}{4}\frac{3}{4}\cos2\theta_1-\frac{1}{2}\cos2\theta_4+\cos2\theta_2=-\frac{2\sqrt{2}\beta}{I-E}\left(\cot2\theta_1+\frac{1}{2\sqrt{2}}\right)$$

$$-\frac{3}{4}+\cos2\theta_1-\frac{5}{4}\cos2\theta_2-\cos2\theta_4=-\frac{2\sqrt{2}\beta}{I-E}\left(\cot2\theta_2+\frac{1}{2\sqrt{2}}\right)$$

$$\frac{5}{4}\frac{1}{2}\cos2\theta_1-\frac{3}{4}\cos2\theta_4-\cos2\theta_2=-\frac{2\sqrt{2}\gamma}{I-E}\cot2\theta_4.$$

TABLE IV. Charge distribution for $B_{10}H_{14}$.

$\beta=\gamma$	$\cos\theta_1$	$\cos\theta_2$	$\cos\theta_4$	q_{II}	q_{III}	q_{IV}	μ, D
−2 ev	0.401	0.387	0.652	+0.085	−0.148	−0.022	1.6
−3	0.471	0.456	0.623	+0.110	−0.190	−0.030	2.2
$-\infty$	0.577	0.577	0.707	+0.333	−0.667	0.000	6.2

These equations are solved numerically and give the coefficients, net charges, and dipole moments shown in Table IV.

APPENDIX II. "RESONANCE" IN B_5H_9

For the framework valence structure on the simplified pattern, we may use for the apex boron two atomic orbitals of an sp^2 type approximately and a third pure p. In terms of the set of atomic orbitals described in Sec. IIIC, we may prescribe two equivalent sets:

Set A: ϕ_{I_x},

$$\phi_{+y}=\frac{1}{\sqrt{2}}(\phi_{\mathrm{I}_z}+\phi_{\mathrm{I}_y}),$$

$$\phi_{-y}=\frac{1}{\sqrt{2}}(\phi_{\mathrm{I}_z}-\phi_{\mathrm{I}_y}).$$

Set B: ϕ_{I_y},

$$\phi_{+x}=\frac{1}{\sqrt{2}}(\phi_{\mathrm{I}_z}+\phi_{\mathrm{I}_x}),$$

$$\phi_{-x}=\frac{1}{\sqrt{2}}(\phi_{\mathrm{I}_z}-\phi_{\mathrm{I}_x}).$$

Then the two corresponding sets of framework bonds would be

Set A: $\phi_{A'}=\frac{1}{\sqrt{2}}(\phi_{+y}+\phi_{\mathrm{II}'})$
covalent bond on I and II′,

$\phi_{A'''}=\frac{1}{\sqrt{2}}(\phi_{-y}+\phi_{\mathrm{II}'''})$
covalent bond on I and II‴,

$\phi_{A_x}=\frac{1}{\sqrt{2}}\phi_{\mathrm{I}_x}+\frac{1}{2}(\phi_{\mathrm{II}}-\phi_{\mathrm{II}''})$
open 3-c bond on I, II, and II″.

Set B: $\phi_B=\frac{1}{\sqrt{2}}(\phi_{+x}+\phi_{\mathrm{II}})$
covalent bond on I and II,

$\phi_{B''}=\frac{1}{\sqrt{2}}(\phi_{-x}+\phi_{\mathrm{II}''})$
covalent bond on I and II″,

$\phi_{B_y}=\frac{1}{\sqrt{2}}\phi_{\mathrm{I}_y}+\frac{1}{2}(\phi_{\mathrm{II}'}-\phi_{\mathrm{II}'''})$
open 3-c bond on II, II′, III‴.

The easiest way to show that a resonance hybrid of structures A and B is equivalent to the structure given in Sec. IIIC is to reduce *both* descriptions to the valence-bond picture.

Consider Set A. If we put two electrons in $\phi_{A'}$, multiply out, and throw away ionic terms, we get

$$\phi_{A'}(1)\phi_{A'}(2)\rightarrow\tfrac{1}{2}[\phi_{+\nu}(1)\phi_{\mathrm{II}'}(2)+\phi_{+\nu}(2)\phi_{\mathrm{II}'}(1)]$$

$$\sim\phi_{+\nu}\phi_{\mathrm{II}'},$$

a bond function between I and II′. Similarly $\phi_{A'''}$ filled with two electrons, corresponds to a bond function on I and II‴. The three-center orbital ϕ_{Ax} gives us

$$\phi_{Ax}(1)\phi_{Ax}(2)\rightarrow\frac{1}{\sqrt{2}}[\phi_{\mathrm{I}x}\phi_{\mathrm{II}}-\phi_{\mathrm{I}x}\phi_{\mathrm{II}''}]-\tfrac{1}{2}\phi_{\mathrm{II}}\phi_{\mathrm{II}''}.$$

The last term corresponds to a bond between borons II and II″ and can be thrown out since, to our approximation, the exchange integral on these two is neglected. Hence, ϕ_{Ax} corresponds to resonance between a bond on I and II and a bond on I and II″. In terms of the VB structures listed in Table V, Set A corresponds to a resonance hybrid of structures a and b.

TABLE V. Designation of valence-bond structures.

VB Structure	Boron I bonded to: II	II′	II″	II‴
a	x	x		x
b		x	x	x
c	x	x	x	
d	x		x	x

Similarly, set B corresponds to a hybrid of c and d.

Turning to the orbitals of Sec. IIIC, the degenerate pair are, of course, identical with ϕ_{Ax} and ϕ_{By} which we have already examined; together they correspond to a hybrid in which I is bonded to each of II, II′, II″, II‴ in half the structures. The a_1 orbital multiplies out to give

$$\psi(a_1)\psi(a_1)\rightarrow\tfrac{1}{2}[\phi_{\mathrm{I}x}\phi_{\mathrm{II}}+\phi_{\mathrm{I}x}\phi_{\mathrm{II}'}+\phi_{\mathrm{I}x}\phi_{\mathrm{II}''}+\phi_{\mathrm{I}x}\phi_{\mathrm{II}'''}],$$

plus terms of the type $\phi_{\mathrm{II}}\phi_{\mathrm{II}'}$ which we reject for the reason mentioned above. This orbital therefore corresponds to a hybrid of four structures, involving a bond of type $\phi_{\mathrm{I}}\phi_{\mathrm{II}}$ resonating in its four equivalent positions.

Thus we see that the three orbitals together correspond to a resonance hybrid of all four structures of Table V, precisely as does a hybrid of Sets A and B.

THE JOURNAL OF CHEMICAL PHYSICS VOLUME 22, NUMBER 6 JUNE, 1954

The Bipyramidal XY_3Z_2 Molecular Model. Part I. Classical Vibration Problem

JOSEPH S. ZIOMEK
De Paul University, Chicago 14, Illinois
(Received November 30, 1953)

Symmetry coordinates are set up from the standpoint of group theory for describing the normal modes of oscillation of the XY_3Z_2 molecular model in such a manner that maximum factorization of the secular determinant is accomplished. The cubic and quartic portions of the anharmonic potential function are derived, and the components of vibrational angular momentum are set down. The complete valence-type potential function is discussed. Explicit relations are derived between the force constants occurring in the secular determinant and the physical valence force constants.

I. INTRODUCTION

THE bipyramidal XY_3Z_2 molecular model has the symmetry D_{3h} and includes, as examples, the mixed halides of phosphorous and others. The normal vibrations of this molecular model and the quantum-mechanical evaluation of its allowed rotation-vibration energies have not been treated in the literature. This paper is intended to form the classical part of the basis for the interpretation of both the gross vibrational and fine rotational structure of the Raman and infrared spectra of bipyramidal XY_3Z_2 molecule. Furthermore, this paper deals with the purely vibrational aspects of the problem and includes discussions of the molecular symmetry, characteristic modes of vibrations, and potential functions.

II. GEOMETRY AND SYMMETRY

The equilibrium configuration of the model assumed for the bipyramidal XY_3Z_2 is shown in Fig. 1, along with a right-handed rectangular coordinate system, xyz, whose origin coincides with the center of mass and whose axes are principal axes of inertia. The respective atoms are indicated by an arbitrary index i ($i=1,2\cdots6$) for reference. The three Y atoms (1,2,3) and the X atom (4) lie in the xy plane, the two Z atoms (5,6) lie in the xz plane, while Z atoms 5 and 6, and X atom lie on the z axis. The masses (m_i) and equilibrium coordinates (x_{0i},y_{0i},z_{0i}) of the respective atoms are listed in Table I.

The twelve covering operations of symmetry point group D_{3h} form six classes as follows: E, the identity

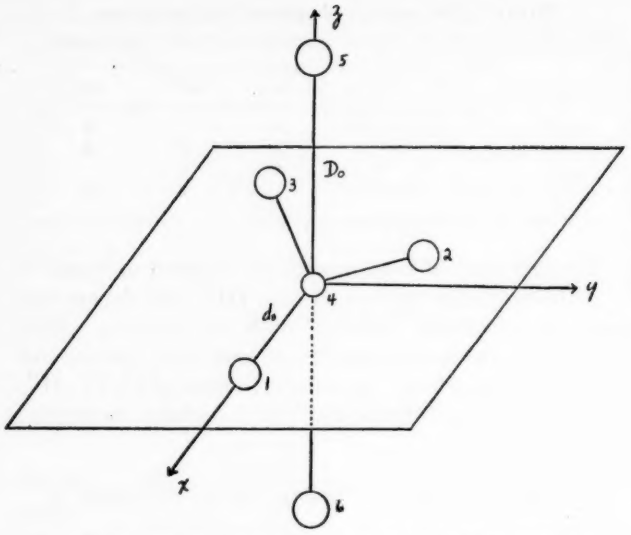

FIG. 1. The equilibrium configuration of the XY_3Z_2 molecule.

operation; $2C_3$, rotations by $\pm 2\pi/3$ around the z axis; $2S_3$, rotations by $\pm 2\pi/3$ around the z axis plus reflection in the xy plane; $3C_2'$, rotation by π around the axes passing through atoms Y (1,2,3) and X, respectively; $3\sigma_v$ reflection in the xz plane, in the plane containing z axis and atom $Y2$, and in the plane containing z axis and atom $Y3$; and σ_h, a reflection in the xy plane. Table II contains the characters of the various classes of covering operations performed on the six possible types (A_1',A_2',A_1'',A_2'',E',E'') of physical quantities. The types A are nondegenerate and E are twofold degenerate. Quantities associated with the vibrations and rotations of the XY_3Z_2 model have the following species assignments: (a) of the components of linear displacement, x and y form an E' pair and z is A_2''; (b) of the components of angular momentum, P_x and P_y form an E'' pair and P_z is A_2'; (c) of the components of the electric dipole moment, M_x and M_y form an E' pair and M_z is A_2''; and (d) the polarizability tensor has components of species A_1', E', and E''.

III. COORDINATES FOR INFINITESIMAL VIBRATIONS

The body-fixed rectangular coordinate system, which was introduced in Sec. II for the description of the equilibrium configuration, is suitable for analytical discussion of the rotations and modes of vibration of the molecular model if it moves with the molecular framework subject to the following two conditions:[1,2] (a) the coordinate origin remains at the center of mass, and (b) none of the modes of vibration results in angular momentum of rotation of the molecular framework as a whole inside the coordinate system. The instantaneous coordinates of the ith atoms during infinitesimal vibrations will be given by $x_i=x_{0i}+x_i'$, etc., where x_{0i}, y_{0i}, and z_{0i} denote the equilibrium values of the coordinates, and x_i', y_i', z_i' denote components of displacement from the equilibrium position. The conditions (a) and (b) are satisfied by the following relations which are given in terms of the displacement coordinates:

$$\sum_i m_i x_i'=\sum_i m_i y_i=\sum_i m_i z_i'=0 \tag{1}$$

$$p_{0x}=\sum_i m_i(y_{0i}\dot{z}_i'-z_{0i}\dot{y}_i')=0, \tag{2a}$$

$$p_{0y}=\sum_i m_i(z_{0i}\dot{x}_i'-x_{0i}\dot{z}_i')=0, \tag{2b}$$

$$p_{0z}=\sum_i m_i(x_{0i}\dot{y}_i'-y_{0i}\dot{x}_i')=0. \tag{2c}$$

For the XY_3Z_2 model these conditions are satisfied by the following equations:

$$m_1(x_1'+x_2'+x_3')+m_3(x_5'+x_6')+m_2x_4'=0, \quad \text{etc.}, \tag{1'}$$

and

$$[(3)^{\frac{1}{2}}/2]m_1d_0(z_2'-z_3')+m_3D_0(y_6'-y_5')=0, \tag{2'a}$$

$$(1/2)m_1d_0(-2z_1'+z_2'+z_3')+m_3D_0(x_5'-x_6')=0, \tag{2'b}$$

$$(m_1/2)d_0[(2y_1'-y_2'-y_3'+(3)^{\frac{1}{2}}(x_3'-x_2')]=0. \tag{2'c}$$

The methods of group theory show that the twelve normal modes of vibration of the XY_3Z_2 molecule of symmetry D_{3h} have the following species classification: two of A_1', none of A_2', none of A_1'', two of A_2'', three pairs of E', and one pair of E''. The complete vibrational secular determinant can accordingly be broken up at once, if one uses generalized coordinates with proper symmetry properties, into steps as follows: two twofold, two identical threefold, and two identical onefold steps. It can be shown with the aid of group theory methods that the following twelve linear combinations of dis-

TABLE I. Masses and equilibrium coordinates.

Atom	i	m_i	x_{0i}	y_{0i}	z_{0i}
Y	1	m_1	d_0	0	0
Y	2	m_1	$-d_0/2$	$(3)^{\frac{1}{2}}d_0/2$	0
Y	3	m_1	$-d_0/2$	$-(3)^{\frac{1}{2}}d_0/2$	0
X	4	m_2	0	0	0
Z	5	m_3	0	0	D_0
Z	6	m_3	0	0	$-D_0$

TABLE II. Characters of point group D_{3h}.

	E	σ_h	$2C_3$	$2S_3$	$3C_2$	$3\sigma_v$
A_1'	1	1	1	1	1	1
A_2'	1	1	1	1	−1	−1
A_1''	1	−1	1	−1	1	−1
A_2''	1	−1	1	−1	−1	1
E'	2	2	−1	−1	0	0
E''	2	−2	−1	1	0	0

[1] C. Eckart, Phys. Rev. 47, 552 (1932).
[2] E. B. Wilson, Jr. and J. B. Howard, J. Chem. Phys. 4, 260 (1936).

placement coordinates form a set of orthonormal generalized coordinates of appropriate symmetries for setting up the normal vibration problem: (see appendix)

A_1':

$$S_1=\frac{1}{2\sqrt{3}}[2\xi_1-\xi_2-\xi_3+\sqrt{3}(\eta_2-\eta_3)]$$

$$S_2=\frac{1}{\sqrt{2}}(\zeta_5-\zeta_6);$$

A_2'':

$$S_3=\left(\frac{c}{6}\right)^{\frac{1}{2}}[-2m_3^{\frac{1}{2}}(\zeta_1+\zeta_2+\zeta_3)+3m_1^{\frac{1}{2}}(\zeta_5+\zeta_6)]$$

$$S_4=(ac)^{\frac{1}{2}}[(m_1m_2)^{\frac{1}{2}}(\zeta_1+\zeta_2+\zeta_3)+(m_2m_3)^{\frac{1}{2}}(\zeta_5+\zeta_6)-(3m_1+2m_3)\zeta_4];$$

E':

$$S_{5a}=(ac)^{\frac{1}{2}}[(m_1m_2)^{\frac{1}{2}}(\xi_1+\xi_2+\xi_3)+(m_2m_3)^{\frac{1}{2}}(\xi_5+\xi_6)-(3m_1+2m_3)\xi_4]$$

$$S_{5b}=(ac)^{\frac{1}{2}}[(m_1m_2)^{\frac{1}{2}}(\eta_1+\eta_2+\eta_3)+(m_2m_3)^{\frac{1}{2}}(\eta_5+\eta_6)-(3m_1+2m_3)\eta_4]$$

$$S_{6a}=\left(\frac{c}{6}\right)^{\frac{1}{2}}[-2m_3^{\frac{1}{2}}(\xi_1+\xi_2+\xi_3)+3m_1^{\frac{1}{2}}(\xi_5+\xi_6)]$$

$$S_{6b}=\left(\frac{c}{6}\right)^{\frac{1}{2}}[-2m_3^{\frac{1}{2}}(\eta_1+\eta_2+\eta_3)+3m_1^{\frac{1}{2}}(\eta_5+\eta_6)]$$

$$S_{7a}=\frac{1}{2(3)^{\frac{1}{2}}}[-2\xi_1+\xi_2+\xi_3+(3)^{\frac{1}{2}}(\eta_2-\eta_3)]$$

$$S_{7b}=\frac{1}{2(3)^{\frac{1}{2}}}[2\eta_1-\eta_2-\eta_3+(3)^{\frac{1}{2}}(\xi_2-\xi_3)];$$

E'':

$$S_{8a}=\frac{1}{2}\left(\frac{1}{I_{ex}}\right)^{\frac{1}{2}}[2m_3^{\frac{1}{2}}D_0(\zeta_2-\zeta_3)+(3m_1)^{\frac{1}{2}}d_0(\eta_5-\eta_6)]$$

$$S_{8b}=\frac{1}{2(3I_{ex})^{\frac{1}{2}}}[2m_3^{\frac{1}{2}}D_0(-2\zeta_1+\zeta_2+\zeta_3)-3m_1^{\frac{1}{2}}d_0(\xi_5-\xi_6)];$$

where

$$\xi_i=m_i^{\frac{1}{2}}x_i';\quad \eta_i=m_i^{\frac{1}{2}}y_i';\quad \zeta_i=m_i^{\frac{1}{2}}z_i';$$

$m_1=m_i$ for $i=1,2,3$; $m_2=m_4$; $m_3=m_i$ for $i=5,6$;

$$c=\frac{1}{3m_1+2m_3};\quad a=\frac{1}{3m_1+m_2+2m_3},\quad \text{and}\quad I_{ey}=I_{ex},$$

$$I_{ex}=\tfrac{3}{2}m_1d_0^2+2m_3D_0^2,\quad \text{and}\quad I_{ez}=3m_1d_0^2.$$

The vibrational kinetic energy T_v must be of symmetry species A_1', and is given by the expression

$$2T_V=\sum_{i=1}^{12}m_i(\dot{x}_i^2+\dot{y}_i^2+\dot{z}_i^2). \tag{3}$$

In terms of the symmetry coordinates this becomes

$$2T_V=\sum_{i=1}^{4}\dot{S}_i^2+\sum_{j=5}^{8}(\dot{S}_{ja}^2+\dot{S}_{jb}^2). \tag{4}$$

The harmonic or zero-order potential energy U_0 must be of the symmetry species A_1', and is given by the following expression

$$2U_0=\sum_{ii'}k_{ii'}\frac{S_iS_{i'}}{(\mu_i\mu_{i'})^{\frac{1}{2}}}+\sum k_{jj'}\frac{S_jS_{j'}}{(\mu_j\mu_{j'})^{\frac{1}{2}}}+\sum_{k,k'}k_{kk'}\frac{S_{ka}S_{k'a}+S_{kb}S_{k'b}}{(\mu_k\mu_{k'})^{\frac{1}{2}}}+k_8\frac{S_{8a}^2+S_{8b}^2}{\mu_8}, \tag{5}$$

where

$$\mu_1=\mu_7=m_1;\quad \mu_3=\mu_6=\mu_{13}=\frac{6m_1m_3}{3m_1+2m_3},$$

$$\mu_4=\mu_5=\frac{m_2(3m_1+2m_3)}{3m_1+2m_3+m_2},\quad \text{and}\quad \mu_8=\mu_{13}.$$

Since there are thirteen force constants and only eight fundamental frequencies, an approximation must be made in the evaluation of the five force constants or these five must be evaluated from data on isotopic molecules.

IV. THE NORMAL MODES OF VIBRATION

The frequencies ω_n of the normal or characteristic modes of vibration of the molecular model are obtained from the solution of Lagrange's determinantal equation, $|\lambda T_v-U_0|=0$, where $\lambda_n=4\pi^2c^2\omega_n^2$, if c is the velocity of light in cm/sec, and ω_n is the frequency in cm^{-1}. The steps of the secular determinant associated with the various symmetry species have the following forms:

A_1':

$$\begin{vmatrix}\lambda-\dfrac{k_{11}}{m_1} & -\dfrac{k_{12}}{m_1}\\ -\dfrac{k_{12}}{m_1} & \lambda-\dfrac{k_{22}}{m_1}\end{vmatrix}=0 \tag{5a}$$

A_2': none.
A_1'': none.

A_2'':

$$\begin{vmatrix}\lambda-\dfrac{k_{33}}{\mu_{13}} & -\dfrac{k_{34}}{(\mu_{13}\mu_4)^{\frac{1}{2}}}\\ -\dfrac{k_{34}}{(\mu_{13}\mu_4)^{\frac{1}{2}}} & \lambda-\dfrac{k_{44}}{\mu_4}\end{vmatrix}=0 \tag{5b}$$

$$\begin{vmatrix} \lambda-\frac{k_{55}}{\mu_4} & -\frac{k_{56}}{(\mu_5\mu_{13})^{\frac{1}{2}}} & -\frac{k_{57}}{(\mu_4 m_1)^{\frac{1}{2}}} \\ -\frac{k_{56}}{(\mu_5\mu_{13})^{\frac{1}{2}}} & \lambda-\frac{k_{66}}{\mu_{13}} & -\frac{k_{67}}{(m_1\mu_{13})^{\frac{1}{2}}} \\ -\frac{k_{57}}{(\mu_4 m_1)^{\frac{1}{2}}} & -\frac{k_{67}}{(m_1\mu_{13})^{\frac{1}{2}}} & \lambda-\frac{k_{77}}{m_1} \end{vmatrix}=0 \quad (5c)$$

E'':

$$\lambda-\frac{k_8}{\mu_8}=0. \quad (5d)$$

The following relations among the frequencies of various symmetry species can be obtained from the expansion of the steps of the secular determinant:

A_1':

$$\lambda_1+\lambda_2=\frac{k_{11}+k_{22}}{m_1}, \qquad \lambda_1\lambda_2=\frac{k_{11}k_{22}-k_{12}^2}{m_1^2}; \quad (6a)$$

A_2'':

$$\lambda_3+\lambda_4=\frac{k_{33}}{\mu_{13}}+\frac{k_{44}}{\mu_4}, \qquad \lambda_3\lambda_4=\frac{k_{33}k_{44}-k_{34}^2}{\mu_{13}\mu_4}; \quad (6b)$$

E':

$$\lambda_5+\lambda_6+\lambda_7=\frac{k_{55}}{\mu_4}+\frac{k_{66}}{\mu_{13}}+\frac{k_{77}}{m_1},$$

$$\lambda_5\lambda_6+\lambda_5\lambda_7+\lambda_6\lambda_7=\frac{k_{55}k_{66}-k_{56}^2}{\mu_5\mu_{13}}+\frac{k_{55}k_{77}-k_{57}^2}{\mu_4 m_1}+\frac{k_{66}k_{77}-k_{67}^2}{\mu_{13}m_1}, \quad (6c)$$

$$\lambda_5\lambda_6\lambda_7=\begin{vmatrix} \frac{k_{55}}{\mu_4} & \frac{k_{56}}{(\mu_5\mu_{13})^{\frac{1}{2}}} & \frac{k_{57}}{(\mu_4 m_1)^{\frac{1}{2}}} \\ \frac{k_{56}}{(\mu_5\mu_{13})^{\frac{1}{2}}} & \frac{k_{66}}{\mu_{13}} & \frac{k_{67}}{(m_1\mu_{13})^{\frac{1}{2}}} \\ \frac{k_{57}}{(\mu_4 m_1)^{\frac{1}{2}}} & \frac{k_{67}}{(\mu_{13}m_1)^{\frac{1}{2}}} & \frac{k_{77}}{m_1} \end{vmatrix}$$

E'':

$$\lambda_8=\frac{k_{88}}{\mu_8}. \quad (6d)$$

The following equations give the transformation from the symmetry coordinates of Eq. (3) to the normal coordinates Q_n: for the species A_1',

$$S_i=\sum_{k=1}^{2} n_{ik}Q_k, \quad i=1,2, \quad (7)$$

where n_{ik} is the normalized cofactor of the ki element of the secular determinant in Eq. (5a) with $\lambda=\lambda_k$; for species A_2'',

$$S_l=\sum_{m=3}^{4} n_{lm}Q_m, \quad l=3,4, \quad (8)$$

where n_{lm} is the normalized cofactor of the ml element of the secular determinant in Eq. (5b) with $\lambda=\lambda_m$; for species E',

$$S_{ja}=\sum_{l=5}^{7} n_{jl}Q_{la},$$

$$S_{jb}=\sum_{l=5}^{7} n_{jl}Q_{lb}, \quad j=5,6,7, \quad (9)$$

where n_{jl} is the normalized cofactor of the lj element of the secular determinant in Eq. (5c) with $\lambda=\lambda_l$. Finally, S_{8a} and S_{8b} are already normal coordinates. In terms of the normal coordinates, the kinetic and harmonic potential energies of vibration become

$$T_v=\tfrac{1}{2}[\sum_{i=1}^{4}\dot{Q}_i^2+\sum_{l=5}^{7}(\dot{Q}_{la}^2+\dot{Q}_{lb}^2)], \quad (10)$$

and

$$U_0=\tfrac{1}{2}\{\sum_{i=1}^{4}\lambda_i Q_i^2+\sum_{l=5}^{8}\lambda_l(Q_{la}^2+Q_{lb}^2)\}. \quad (11)$$

It is convenient to introduce dimensionless coordinates q_n, which are given by the transformation,

$$Q_n(h/2\pi c\omega_n)^{\frac{1}{2}}q_n$$

and in terms of which the zero-order vibrational energy is given in the Hamiltonian form as

$$H_{0v}=\left(\frac{hc}{2}\right)\left\{\sum_{i=1}^{4}\left[\left(\frac{p_i^2}{\hbar^2}\right)+q_i^2\right]+\sum_{k=5}^{8}\omega_k\left\{\left(\frac{p_{ka}^2+p_{kb}^2}{\hbar^2}\right)+(q_{ka}^2+q_{kb}^2)\right\}\right\}. \quad (12)$$

V. ANHARMONIC POTENTIAL FUNCTION

Since each term in the expression for the total energy must belong to the symmetry type A_1', it can be shown by direct multiplication of the characters in Table II that the cubic combinations of normal coordinates occurring in the anharmonic potential function of a molecule belonging to symmetry group D_{3h} are: $A_1'^3$, $A_1'^2A_1'$, $[A_2'^2A_1']$, $[A_1''^2A_1']$, $A_2''^2A_1'$, $A_1'^{(2)}A_1'$,

$[A_2'^{(2)}A_2']$, $[A_1''^{(2)}A_1'']$, $A_2''^{(2)}A_2''$, and $A_1'^{(3)}$. Likewise, the quartic combinations occurring are: $A_1'^4$, $A_1'^3A_1'$, $A_1'^2A_1'^2$, $[A_1'^2A_1''^2]$, $[A_1'^2A_2'^2]$, $A_1'^2A_2''^2$, $[A_2'^4]$, $[A_2'^2A_1''^2]$, $[A_2'^2A_2''^2]$, $[A_1''^4]$, $[A_1''^2A_2''^2]$, $A_2''^4$, $(A_1'^{(2)})^2$, $A_1'^{(2)}A_1'^2$, $[A_1'^{(2)}A_1''^2]$, $[A_1'^{(2)}A_2'^2]$, $A_1'^{(2)}A_2''^2$, $(A_2'^{(2)})^2$, $(A_1''^{(2)})^2$, $(A_2''^{(2)})^2$, $A_1'^{(3)}A_1'$, $[A_2'^{(3)}A_2']$, $[A_1''^{(3)}A_1'']$, and $A_2''^{(3)}A_2''$. The terms in square brackets, such as $[A_2'^2A_1''^2]$ do not occur in the case of the XY_3Z_2 because there is no normal coordinate of the first degree of the type A_2' and A_1'', respectively. The designations $X^{(n)}$ are used to refer to the quadratic or cubic combinations of degenerate normal coordinates of the various symmetry types.[3] The most general cubic portion U_1 of the anharmonic potential function of the XY_3Z_2 molecular model is given by:[4]

$$\begin{aligned}\frac{U_1}{hc}=&\sum_{i=1}^{2}\{\beta_{iii}q_i^3+\sum_{i'}\beta_{iii'}q_i^2q_{i'}+\sum_j\beta_{ijj}q_iq_j^2\\&+\sum_{j,j'}\beta_{ijj'}q_iq_jq_{j'}+\sum_k\beta_{ikk}q_i(q_{ka}^2+q_{kb}^2)\\&+\sum_{k'}\sum_{(k'>k)}\beta_{ikk'}(q_{ka}q_{k'a}+q_{kb}q_{k'b})q_i\\&+\beta_{i88}q_i(q_{8a}^2+q_{8b}^2)\}+\sum_j\sum_k\beta_{jk8}q_j(q_{ka}q_{8b}+q_{kb}q_{8a})\\&+\sum_k\beta_{k88}[2q_{8a}q_{8b}q_{ka}+(q_{8a}^2-q_{8b}^2)q_{kb}]\\&+\sum_{k''}\sum_{k'}\sum_k\beta_{kk'k''}\{(q_{ka}q_{k'b}+q_{kb}q_{k'a})q_{k''b}\\&-(q_{ka}q_{k'a}-q_{kb}q_{k'b})q_{k''a}\}.\end{aligned}\tag{13}$$

To second-order approximation[5] the quartic portion U_2, of the anharmonic potential function is given by:

$$\begin{aligned}\frac{U_2}{hc}=&\sum_{i=1}\{\gamma_{iiii}q_i^4+\sum_{i'}\gamma_{iii'i'}q_i^2q_{i'}^2\}\\&+\sum_j\{\gamma_{jjjj}q_j^4+\sum_{j'}\gamma_{jjj'j'}q_j^2q_{j'}^2\}\\&+\sum_k\{\gamma_{kkkk}(q_{ka}^2+q_{kb}^2)^2\\&+\sum_{k'>k}\gamma_{kkk'k'}(q_{ka}q_{k'a}+q_{kb}q_{k'b})^2\\&+\sum_{k'>k}\gamma_{kkk'k'}(q_{ka}^2+q_{kb}^2)(q_{k'a}^2+q_{k'b}^2)\\&+\sum_{k'>k}\gamma_{kkk'k'}(q_{ka}q_{k'b}-q_{kb}q_{k'a})^2\}\\&+\sum_j\{\sum_k\gamma_{jjkk}q_j^2(q_{ka}^2+q_{kb}^2)+\gamma_{jj88}q_j^2(q_{8a}^2+q_{8b}^2)\}\\&+\sum_i\{\sum_j\gamma_{iijj}q_i^2q_j^2+\sum_k\gamma_{iikk}q_i^2(q_{ka}^2+q_{kb}^2)\\&+\gamma_{ii88}q_i^2(q_{8a}^2+q_{8b}^2)\}+\sum_k\{\gamma_{kk88}(q_{ka}^2+q_{kb}^2)\\&\times(q_{8a}^2+q_{8b}^2)+\gamma_{k8k8}(q_{ka}q_{8a}-q_{kb}q_{8b})^2\\&+\gamma_{k8k8}(q_{ka}q_{8b}+q_{kb}q_{8a})^2\}+\gamma_{8888}(q_{8a}^2+q_{8b}^2)^2.\end{aligned}\tag{14}$$

VI. VIBRATIONAL ANGULAR MOMENTUM

The components of internal angular momentum of vibration p_x, p_y, and p_z have importance in connection with the Coriolis interaction between the total and internal angular momenta and are of the same symmetry type as the components of total angular momentum. An E'' pair is formed between p_x and p_y and while p_z is of the type A_2'. These components are defined as:

$$p_x=\sum_{i=1}^{6}m_i(y_i'\dot{z}_i'-z_i'\dot{y}_i'),$$

$$p_y=\sum_{i=1}^{6}m_i(z_i'\dot{x}_i'-x_i'\dot{z}_i'),$$

$$p_z=\sum_{i=1}^{6}m_i(x_i'\dot{y}_i'-y_i'\dot{x}_i'),$$

and are expressed in terms of the dimensionless normal coordinates q_i and conjugate moments p_i as follows:

$$\begin{aligned}p_x=&\sum_{i=1}^{2}\xi_i\left[\left(\frac{\omega_{8a}}{\omega_i}\right)^{\frac{1}{2}}p_{8a}q_i-\left(\frac{\omega_i}{\omega_{8a}}\right)^{\frac{1}{2}}q_{8a}p_i\right]\\&+\sum_{k,j}\xi_{kj}\left[\left(\frac{\omega_j}{\omega_{kb}}\right)^{\frac{1}{2}}q_{kb}p_j-\left(\frac{\omega_{kb}}{\omega_j}\right)^{\frac{1}{2}}q_jp_{kb}\right]\\&+\sum_k\xi_k\left[\left(\frac{\omega_{8a}}{\omega_{ka}}\right)^{\frac{1}{2}}q_{ka}p_{8a}-\left(\frac{\omega_{ka}}{\omega_{8a}}\right)^{\frac{1}{2}}q_{8a}p_{ka}\right]\\&+\sum_k\xi_k\left[\left(\frac{\omega_{kb}}{\omega_{8b}}\right)^{\frac{1}{2}}q_{8b}p_{kb}-\left(\frac{\omega_{8b}}{\omega_{kb}}\right)^{\frac{1}{2}}p_{8b}q_{kb}\right],\end{aligned}$$

---

[3] The quadratic combinations are as follows: $(q_{ka}^2+q_{kb}^2)$ and $q_{ka}q_{k'a}+q_{kb}q_{k'b})$ of type $A_1'^{(2)}$; $q_{ka}q_{k'b}-q_{kb}q_{k'a}$ of type $A_2'^{(2)}$; $q_{ka}q_{8a}-q_{kb}q_{8b}$ of type $A_1''^{(2)}$; and $q_{ka}q_{8b}+q_{kb}q_{8a}$ of type $A_2''^{(2)}$. The cubic combinations are as follows: $(q_{ka}q_{k'b}+q_{kb}q_{k'a})q_{k''b}-(q_{ka}q_{k'a}-q_{kb}q_{k'b})q_{k''a}$ of type $A_1'^{(3)}$; $(q_{ka}q_{k'b}+q_{kb}q_{k'a})q_{k''a}+(q_{ka}q_{k'a}-q_{kb}q_{k'b})q_{k''b}$ of type $A_2'^{(3)}$; $(q_{ka}q_{8b}-q_{kb}q_{8a})q_{k'a}-(q_{ka}q_{8a}+q_{kb}q_{8b})q_{k'b}$ of type $A_2''^{(3)}$; $(q_{ka}q_{8b}-q_{kb}q_{8a})q_{k'b}+(q_{ka}q_{8a}+q_{kb}q_{8b})q_{k'a}$ of type $A_1''^{(3)}$; and $2q_{8a}q_{8b}q_{ka}+(q_{8a}^2-q_{8b}^2)q_{kb}$ of type $A_1'^{(3)}$.

[4] In the remainder of this paper, coordinates of type A_1' will be denoted by subscripts $i=1,2$; A_2'' by $j=3,4$; E' by $k=5,6,7$; and E'' by $1=8$. Primed and unprimed subscripts in a given summation refer to different coordinates of the same symmetry type. Each combination of subscripts may occur only once, i.e. permutations are not allowed.

[5] The most general quartic portion of the anharmonic potential function contains the following additional terms which are of odd degree in at least one coordinate and do not ordinarily contribute to the allowed energies: $q_i^3q_i'$, $q_j^3q_j'$, $(q_{ka}^2+q_{kb}^2)(q_{ka}q_{k'a}+q_{kb}q_{k'b})$, $(q_{ka}^2+q_{kb}^2)(q_{k'a}q_{k''a}+q_{k'b}q_{k''b})$, $(q_{ka}q_{k'a}+q_{kb}q_{k'b})(q_{ka}q_{k''a}+q_{kb}q_{k''b})$, $q_iq_i'(q_{ka}q_{k'a}+q_{kb}q_{k'b})$, $q_i^2(q_{ka}q_{k'a}+q_{kb}q_{k'b})$, $q_j^2(q_{ka}q_{k'a}+q_{kb}q_{k'b})$, $q_jq_{j'}(q_{ka}q_{k'a}+q_{kb}q_{k'b})$, $q_iq_{i'}(q_{8a}^2+q_{8b}^2)$, $q_iq_j(q_{ka}q_{8b}+q_{kb}q_{8a})$, $(q_{kb}q_{k'b}-q_{kb}q_{k'a})(q_{ka}q_{k''b}-q_{kb}q_{k''a})$, $(q_{8a}^2+q_{8b}^2)(q_{ka}q_{k'a}+q_{kb}q_{k'b})$, $(q_{ka}q_{8a}-q_{kb}q_{8b})(q_{k'a}q_{8a}-q_{k'b}q_{8b})$, $(q_{ka}q_{8b}+q_{kb}q_{8a})(q_{k'a}q_{8b}+q_{k'b}q_{8a})$, $(q_{ka}q_{k'b}+q_{kb}q_{k'a})q_{k''b}-(q_{ka}q_{k'a}-q_{kb}q_{k'b})q_{k''a}q_i$, $2q_{8a}q_{8b}q_{ka}+(q_{8a}^2-q_{8b}^2)q_{kb}q_i$, and $(q_{ka}q_{8b}-q_{kb}q_{8a})q_{ka}-(q_{ka}q_{8a}+q_{ka}q_{8b})q_{k'b}q_j$.

$$p_v=\sum_{i=1}^{2}\eta_i\left[\left(\frac{\omega_{8b}}{\omega_i}\right)^{\frac{1}{2}}q_ip_{8b}-\left(\frac{\omega_i}{\omega_{8b}}\right)^{\frac{1}{2}}p_iq_{8b}\right]$$

$$+\sum_{k,j}\eta_{kj}\left[\left(\frac{\omega_{ka}}{\omega_j}\right)^{\frac{1}{2}}q_jp_{ka}-\left(\frac{\omega_j}{\omega_{ka}}\right)^{\frac{1}{2}}q_{ka}p_j\right]$$

$$+\sum_{k}\eta_k\left[\left(\frac{\omega_{kb}}{\omega_{8a}}\right)^{\frac{1}{2}}q_{8a}p_{kb}-\left(\frac{\omega_{8a}}{\omega_{kb}}\right)^{\frac{1}{2}}q_{kb}p_{8a}\right]$$

$$+\sum_{k}\eta_k\left[\left(\frac{\omega_{ka}}{\omega_{8b}}\right)^{\frac{1}{2}}q_{8b}p_{ka}-\left(\frac{\omega_{8b}}{\omega_{ka}}\right)^{\frac{1}{2}}q_{ka}p_{8b}\right],$$

and

$$p_z=\sum_{k,k'}\zeta_{kk'}\left[\left(\frac{\omega_{k'b}}{\omega_{ka}}\right)^{\frac{1}{2}}q_{ka}p_{k'b}-\left(\frac{\omega_{ka}}{\omega_{k'b}}\right)^{\frac{1}{2}}q_{k'b}p_{ka}\right]$$

$$+\zeta_8\left[\left(\frac{\omega_{8b}}{\omega_{8a}}\right)^{\frac{1}{2}}q_{8a}p_{8b}-\left(\frac{\omega_{8a}}{\omega_{8b}}\right)^{\frac{1}{2}}q_{8b}p_{8a}\right], \quad (15)$$

where

$$\xi_i\equiv\left(\frac{m_3}{I_{ez}}\right)^{\frac{1}{2}}D_0n_{1i}-\left(\frac{I_{ez}}{2I_{ez}}\right)^{\frac{1}{2}}n_{2i}=\eta_i$$

$$\xi_k\equiv\left(\frac{m_3}{I_{ez}}\right)^{\frac{1}{2}}D_0n_{7k}=\eta_k$$

$$\xi_{kj}\equiv(n_{6k}n_{3j}+n_{5k}n_{4j})=\eta_{kj} \text{ for } j=3,4;\ k=5,6,7$$

$$\zeta_{kk'}\equiv n_{5k}n_{5k'}+n_{6k}n_{6k'}-n_{7k}n_{7k'}$$

$$\zeta_8\equiv\frac{I_{ez}}{2I_{ez}}.$$

VII. VALENCE SYMMETRY COORDINATES

The generalized symmetry coordinates defined in Eqs. (3) were used in setting up the general quadratic potential function given in Eq. (5). The generalized force constants occurring in Eq. (5) do not have obvious physical significance and are not appropriate for use in the analysis of experimental data. It has been found in many cases that a suitable potential function for analysis of data is based on so-called valence coordinates which are changes in the length of valence bonds and changes in the included valence angles. For infinitesimal displacements there are linear relationships between the valence coordinates and the generalized symmetry coordinates defined in Eqs. (3). One can obtain linear relations between the generalized force constants in Eq. (5) and those in a valence-type quadratic potential function.

The valence coordinates can best be described in terms of changes in distances between pairs of atoms. The infinitesimal change in distance p_{mn} between the mth and nth atoms is given in terms of the original rectangular coordinates and displacements as follows:

$$\delta p_{mn}=[(x_{0m}-x_{0n})(x_m'-x_n')+(y_{0m}-y_{0n})(y_m'-y_n')+(z_{0m}-z_{0n})(z_m'-z_n')]/p_{0mn}. \quad (16)$$

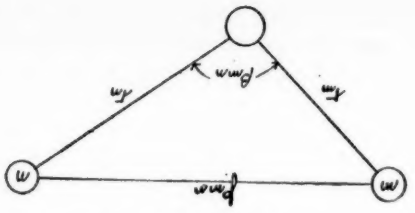

FIG. 2. Valence coordinates.

The valence coordinates suitable for description of infinitesimal vibrations of a group of three atoms (m, n, and a central atom) are illustrated in Fig. 2, where $r_m=r_{0m}+\delta r_m$, $r_n=r_{0n}+\delta r_n$, and $\beta_{mn}=\beta_{0mn}+\delta\beta_{mn}$; r_m, r_n, and β_{mn} denote, respectively, the instantaneous values of the two valence bond lengths and the included bond angle, while r_{0m}, r_{0n}, and β_{0mn} denote their equilibrium values, and δr_m, δr_n, and $\delta\beta_{mn}$ denote changes occurring during vibrations. The quantity $\delta\beta_{mn}$ is given for infinitesimal vibrations by

$$\delta\beta_{mn}=[p_{0mn}\delta p_{mn}-(r_{0m}-r_{0n}\cos\beta_{0mn})\delta r_m-(r_{0n}-r_{0m}\cos\beta_{0mn})\delta r_n]/r_{0m}r_{0n}\sin\beta_{0mn}, \quad (17)$$

where p_{mn} is the distance between atoms m and n.

Following a procedure similar to that outlined by Shaffer and Herman[6] it is possible to obtain the combination of valence coordinates (orthonormal) listed below for the XY_3Z_2-molecular model which belong to the various symmetry types.

Type A_1':

$$\Delta_1=1/(3)^{\frac{1}{2}}(\delta r_1+\delta r_2+\delta r_3)=a_1S_1,$$

$$\Delta_2=1/(2)^{\frac{1}{2}}(\delta r_5+\delta r_6)=a_2S_2,$$

$$\Delta_{01}=1/(3)^{\frac{1}{2}}(\delta\alpha_{12}+\delta\alpha_{13}+\delta\alpha_{23})\equiv0,$$

$$\text{(redundant coordinate)}=a_0S_1,$$

$$\Delta_{02}=1/(6)^{\frac{1}{2}}(\delta\beta_{15}+\delta\beta_{16}+\delta\beta_{25}+\delta\beta_{26}+\delta\beta_{35}+\delta\beta_{36})\equiv0,$$

$$\text{(redundant coordinate)}=\sum_{i=1}^{2}a_{0i}S_i,$$

Type A_2': none.

Type A_1'': none.

Type A_2'':

$$\Delta_3=1/(2)^{\frac{1}{2}}(\delta r_5-\delta r_6)=\sum_{j=3}^{4}a_{3j}S_j,$$

$$\Delta_4=1/(6)^{\frac{1}{2}}(\delta\beta_{15}-\delta\beta_{16}+\delta\beta_{25}-\delta\beta_{26}+\delta\beta_{35}-\delta\beta_{36})=\sum_{j=3}^{4}a_{4j}S_j. \quad (18)$$

[6] W. H. Shaffer and R. C. Herman, J. Chem. Phys. 12, 494 (1944); R. C. Herman and W. H. Shaffer, J. Chem. Phys. 17, 30 (1949).

Type E':

$$\Delta_{5a}=1/(6)^{\frac{1}{2}}(2\delta r_1-\delta r_2-\delta r_3)=\sum_{k=5}^{7} a_{5k}S_{ka}$$

$$\Delta_{5b}=1/(2)^{\frac{1}{2}}(\delta r_2-\delta r_3)=\sum_{k=5}^{7} a_{5k}S_{kb},$$

$$\Delta_{6a}=1/(6)^{\frac{1}{2}}(\delta\alpha_{12}+\delta\alpha_{23}-2\delta\alpha_{13})=\sum_{k=5}^{7} a_{6k}S_{ka},$$

$$\Delta_{6b}=1/(2)^{\frac{1}{2}}(\delta\alpha_{23}-\delta\alpha_{12})=\sum_{k=5}^{7} a_{6k}S_{kb},$$

$$\Delta_{7a}=1/(12)^{\frac{1}{2}}(2\delta\beta_{15}-\delta\beta_{25}-\delta\beta_{35}+2\delta\beta_{16}-\delta\beta_{26}-\delta\beta_{36})=\sum_{k=5}^{7} a_{7k}S_{ka}$$

$$\Delta_{7b}=1/2(\delta\beta_{25}-\delta\beta_{35}+\delta\beta_{26}-\delta\beta_{36})=\sum_{k=5}^{7} a_{7k}S_{kb}.$$

Type E'':

$$\Delta_{8b}=(1/12)^{\frac{1}{2}}(2\delta\beta_{15}-\delta\beta_{25}-\delta\beta_{35}-2\delta\beta_{16}+\delta\beta_{26}+\delta\beta_{36})=a_8S_{8b},$$

$$\Delta_{8b}=1/2(\delta\beta_{25}-\delta\beta_{35}-\delta\beta_{26}+\delta\beta_{36})=-a_8S_{8a},$$

where

$$a_1=\left(\frac{1}{m_1}\right)^{\frac{1}{2}};\quad a_2=\left(\frac{1}{m_3}\right)^{\frac{1}{2}};\quad a_0\equiv\frac{1+2\cos\alpha_{012}}{m_1^{\frac{1}{2}}d_0\sin\alpha_{012}};$$

$$a_{01}=\frac{\cot\beta_{015}}{d_0}\left(\frac{2}{m_1}\right)^{\frac{1}{2}};\quad a_{02}=\frac{\cot\beta_{015}}{D_0}\left(\frac{3}{m_3}\right)^{\frac{1}{2}};$$

$$a_{33}=\left(\frac{3m_1c}{m_3}\right)^{\frac{1}{2}};\qquad a_{34}=\left(\frac{2}{\mu_4}\right)^{\frac{1}{2}};$$

$$a_{43}=2c^{\frac{1}{2}}\delta_0';\qquad a_{44}=-\gamma_0\left(\frac{6}{\mu_4}\right)^{\frac{1}{2}};$$

$$a_{55}=\left(\frac{3}{2\mu_4}\right)^{\frac{1}{2}};\quad a_{56}=-\left(\frac{m_3c}{m_1}\right)^{\frac{1}{2}};\quad a_{57}=-\left(\frac{1}{2m_1}\right)^{\frac{1}{2}};$$

$$a_{65}=\frac{\alpha_0}{2}\left(\frac{3}{2\mu_4}\right)^{\frac{1}{2}};\quad a_{66}=-\frac{\alpha_0}{2}\left(\frac{m_3c}{m_1}\right)^{\frac{1}{2}};\quad a_{67}=\frac{\beta_0}{2}\left(\frac{1}{2m_1}\right)^{\frac{1}{2}};$$

$$a_{75}=\gamma_1\left(\frac{3}{\mu_4}\right)^{\frac{1}{2}};\quad a_{76}=-(2c)^{\frac{1}{2}}\delta_1';\quad a_{77}=-\epsilon_0\left(\frac{1}{m_1}\right)^{\frac{1}{2}};$$

$$a_8=\left(\frac{I_{ez}}{m_1m_3}\right)^{\frac{1}{2}}\frac{1}{d_0D_0\sin\beta_{015}}=-a_9 \qquad (19)$$

$$\alpha_0\equiv\frac{1-\cos\alpha_{012}}{d_0\sin\alpha_{012}};\quad \beta_0\equiv\frac{2+\cos\alpha_{012}}{d_0\sin\alpha_{012}};\quad \epsilon_0=\frac{\cot\beta_{015}}{d_0};$$

$$\delta_1'\equiv\left(\frac{1}{m_1m_3}\right)^{\frac{1}{2}}\left(\frac{3m_1}{2D_0}+\frac{m_3\cos\beta_{015}}{d_0}\right)\frac{1}{\sin\beta_{015}};$$

$$\gamma_0\equiv\left(\frac{1}{d_0}-\frac{\cos\beta_{015}}{D_0}\right)\frac{1}{\sin\beta_{015}};$$

$$\gamma_1\equiv\left(\frac{1}{D_0}-\frac{\cos\beta_{015}}{d_0}\right)\frac{1}{\sin\beta_{015}};$$

$$\delta_0'\equiv\left(\frac{1}{m_1m_3}\right)^{\frac{1}{2}}\left[\frac{m_3}{d_0}+\frac{3m_1\cos\beta_{015}}{2D_0}\right]\frac{1}{\sin\beta_{015}}.$$

One needs the inverse transformation giving the intermediate symmetry coordinates, S_i's defined in Eqs. (3) in terms of the valence symmetry coordinates defined above, in order to set up the kinetic and potential energy expressions in terms of the valence coordinates. These relations are given below.

$$S_1=(m_1)^{\frac{1}{2}}\Delta_1;$$

$$S_2=(m_3)^{\frac{1}{2}}\Delta_2$$

$$S_j=\sum_{j'=3}^{4} b_{jj'}\Delta_{j'} \quad \text{for} \quad j=3,4$$

$$S_{ka}=\sum_{k'=5}^{7} b_{kk'}\Delta_{k'a} \quad \text{for} \quad k=5,6,7 \qquad (20)$$

$$S_{kb}=\sum_{k'=5}^{7} b_{kk'}\Delta_{k'b} \quad \text{for} \quad k=5,6,7$$

$$S_{8a}=b_8\Delta_{8b},$$

$$S_{8b}=b_9\Delta_{8a},$$

where

$$b_{33}=\frac{\gamma_0}{\sigma_0}\left(\frac{6}{\mu_4}\right)^{\frac{1}{2}};\quad b_{34}=\frac{1}{\sigma_0}\left(\frac{2}{\mu_4}\right)^{\frac{1}{2}}$$

$$b_{43}=\frac{2c^{\frac{1}{2}}\delta_0'}{\sigma_0};\qquad b_{44}=-\frac{1}{\sigma_0}\left(\frac{3m_1c}{m_3}\right)^{\frac{1}{2}};$$

$$b_{55}=\frac{1}{2D}\left(\frac{c}{m_1}\right)\left[\alpha_0\epsilon_0\left(\frac{m_3}{m_1}\right)^{\frac{1}{2}}+\beta_0\delta_1'\right];$$

$$b_{56}=\frac{1}{D}\left(\frac{c}{m_1}\right)^{\frac{1}{2}}\left[\delta_1'-\epsilon_0\left(\frac{m_3}{m_1}\right)^{\frac{1}{2}}\right];$$

$$b_{57}=-\frac{1}{2D}\left(\frac{m_3c}{2m_1^2}\right)^{\frac{1}{2}}(\alpha_0+\beta_0);$$

$$b_{65}=\frac{1}{2D}\left(\frac{3}{2\mu_4m_1}\right)^{\frac{1}{2}}(\alpha_0\epsilon_0-\beta_0\gamma_1);$$

$$b_{66}=-\frac{1}{D}\left(\frac{3}{2\mu_4m_1}\right)^{\frac{1}{2}}(\epsilon_0+\gamma_1);$$

$$b_{67}=-\frac{1}{4D}\left(\frac{3}{\mu_4 m_1}\right)^{\frac{1}{2}}(\alpha_0+\beta_0);$$

$$b_{75}=-\frac{\alpha_0}{2D}\left(\frac{3c}{\mu_4}\right)^{\frac{1}{2}}\left[\delta_1'+\gamma_1\left(\frac{m_3}{m_1}\right)^{\frac{1}{2}}\right];$$

$$b_{76}=\frac{1}{D}\left(\frac{3c}{\mu_4}\right)^{\frac{1}{2}}\left[\delta_1'+\gamma_1\left(\frac{m_3}{m_1}\right)^{\frac{1}{2}}\right];$$

$$b_{77}=0;\quad b_8=-\left(\frac{m_1m_3}{I_{ex}}\right)d_0D_0\sin\beta_{015}=-b_9,$$

where

$$\sigma_0\equiv\left[3\left(\frac{2m_1c}{\mu_4m_3}\right)^{\frac{1}{2}}\gamma_0+2\left(\frac{2c}{\mu_4}\right)^{\frac{1}{2}}\delta_0'\right],$$

and

$$D\equiv\frac{1}{2}\left(\frac{3c}{2\mu_4m_1}\right)^{\frac{1}{2}}\left[(\alpha_0+\beta_0)\left\{\delta_1'+\gamma_1\left(\frac{m_3}{m_1}\right)^{\frac{1}{2}}\right\}\right].$$

The vibrational kinetic energy, T_v, can be written in terms of the valence symmetry coordinates with the aid of Eqs. (20) and (4) and is given by the following expression:

$$2T_v=\sum_{i=1}^{2}M_i\dot{\Delta}_i^2+\sum_{j=3}^{4}\{M_j\dot{\Delta}_j^2+2\sum_{j'>j}M_{jj'}\dot{\Delta}_j\dot{\Delta}_{j'}\}$$
$$+\sum_k\{M_k(\dot{\Delta}_{ka}^2+\dot{\Delta}_{kb}^2)$$
$$+2\sum_{k'>k}M_{kk'}(\dot{\Delta}_{ka}\dot{\Delta}_{k'a}+\dot{\Delta}_{kb}\dot{\Delta}_{k'b})\}$$
$$+M_8(\dot{\Delta}_{8a}^2+\dot{\Delta}_{8b}^2); \tag{23}$$

$$M_1=m_1;\quad M_2=m_3;\quad M_3=b_{33}^2+b_{43}^2;$$

$$M_4=b_{34}^2+b_{44}^2;\quad M_{34}=b_{33}b_{34}+b_{43}b_{44};$$

$$M_k=2\sum_{k=5}^{7}b_{kk'}b_{kk'};$$

$$M_{kk'}=2\sum_{k''=5}^{7}(b_{k''k}b_{k''k'}+b_{k''k'}b_{k''k})$$

for $k'>k$, and

$$M_8=\left(\frac{m_1m_3}{I_{ex}}\right)(d_0D_0\sin\beta_{015})^2.$$

VIII. VALENCE POTENTIAL FUNCTION

The most general quadratic potential function U_0 satisfying the symmetry conditions is given in terms of the valence symmetry coordinated by:

$$2U_0=\sum_{i\pm1}\{K_i\Delta_i^2+2\sum_{i'>i}K_{ii'}\Delta_i\Delta_{i'}\}$$
$$+\sum_j\{K_j\Delta_j^2+2\sum_{j'>j}K_{jj'}\Delta_j\Delta_{j'}\}$$
$$+\sum_k\{K_k(\Delta_{ka}^2+\Delta_{kb}^2)$$
$$+2\sum_{k'>k}K_{kk'}(\Delta_{ka}\Delta_{k'a}+\Delta_{kb}\Delta_{k'b})\}$$
$$+K_8(\Delta_{8a}^2+\Delta_{8b}^2),$$

in which the cross products occur only among symmetry coordinates of the same type. The complete valence-type potential function U_0 for the XY_3Z_2 molecular model can be written in terms of the valence coordinates as

$$2U_0=c_1(\delta r_1^2+\delta r_2^2+\delta r_3^2)+c_2(\delta r_5^2+\delta r_6^2)+c_3d_0^2(\delta\alpha_{12}^2+\delta\alpha_{13}^2+\delta\alpha_{23}^2)+c_4(d_0D_0)\sum_{i=1}^{3}(\delta\beta_{i5}^2+\delta\beta_{i6}^2)$$
$$+2c_1'\sum_{j>i=1}^{3}\delta r_i\delta r_j+2c_2'\delta r_5\delta r_6+2c_3'd_0^2(\delta\alpha_{12}\delta\alpha_{13}+\delta\alpha_{12}\delta\alpha_{23}+\delta\alpha_{13}\delta\alpha_{23})+2d_0D_0[\delta\beta_{15}\{c_4'(\delta\beta_{25}+\delta\beta_{35})+c_4''\delta\beta_{16}$$
$$+c_4'''(\delta\beta_{26}+\delta\beta_{36})\}+\delta\beta_{25}\{c_4'\delta\beta_{35}+c_4'''(\delta\beta_{16}+\delta\beta_{36})+c_4''\delta\beta_{26}\}+\delta\beta_{35}\{c_4''\delta\beta_{36}+c_4'''(\delta\beta_{16}+\delta\beta_{26})\}$$
$$+c_4'\delta\beta_{16}(\delta\beta_{26}+\delta\beta_{36})+c_4'\delta\beta_{26}\delta\beta_{36}]+2d_0[\delta r_1\{c_{13}'\delta\alpha_{23}+c_{13}(\delta\alpha_{12}+\delta\alpha_{13})\}+\delta r_2\{c_{13}'\delta\alpha_{13}+c_{13}(\delta\alpha_{12}+\delta\alpha_{23})\}$$
$$+\delta r_3\{c_{13}'\delta\alpha_{12}+c_{13}(\delta\alpha_{13}+\delta\alpha_{23})\}]+2(d_0D_0)^{\frac{1}{2}}\{(\delta\beta_{15}+\delta\beta_{16})[c_{14}\delta r_1+c_{14}'(\delta r_2+\delta r_3)+d_0\{c_{34}'\delta\alpha_{23}$$
$$+c_{34}(\delta\alpha_{12}+\delta\alpha_{13})\}+(\delta\beta_{25}+\delta\beta_{26})[c_{14}\delta r_2+c_{14}'(\delta r_1+\delta r_3)+d_0\{c_{34}'\delta\alpha_{13}+c_{34}(\delta\alpha_{12}+\delta\alpha_{23})\}]$$
$$+(\delta\beta_{35}+\delta\beta_{36})[c_{14}\delta r_3+c_{14}'(\delta r_1+\delta r_2)+d_0\{c_{34}'\delta\alpha_{12}+c_{34}(\delta\alpha_{13}+\delta\alpha_{23})\}]\}+2c_{23}d_0(\delta r_5+\delta r_6)(\delta\alpha_{12}+\delta\alpha_{13}+\delta\alpha_{23})$$
$$+2(d_0D_0)^{\frac{1}{2}}[(\delta\beta_{15}+\delta\beta_{25}+\delta\beta_{35})(c_{24}\delta r_5+c_{24}'\delta r_6)+(\delta\beta_{16}+\delta\beta_{26}+\delta\beta_{36})(c_{24}\delta r_6+c_{24}'\delta r_5)$$
$$+2c_{12}(\delta r_1+\delta r_2+\delta r_3)(\delta r_5+\delta r_6) \tag{25}$$

$$K_1=c_1+2c_1';\quad K_{12}=6^{\frac{1}{2}}c_{12};\quad K_{1,01}=2c_{13}+c_{13}';$$
$$K_2=c_2+c_2';\quad K_{1,02}=2^{\frac{1}{2}}(c_{14}+2c_{14}');$$
$$K_{2,01}=6^{\frac{1}{2}}c_{23};\quad K_{2,02}=3^{\frac{1}{2}}(c_{24}+c_{24}');$$
$$K_{01,01}=c_3+2c_3';\quad K_{01,02}=2^{\frac{1}{2}}(2c_{34}+c_{34}');$$
$$K_3=c_2-c_2';\quad K_{34}=3^{\frac{1}{2}}(c_{24}-c_{24}');\quad K_4=c_4-c_4''+2(c_4'-c_4''');$$
$$K_5=c_1-c_1';\quad K_{56}=\tfrac{1}{2}(c_{13}'-c_{13});\quad K_{57}=2^{\frac{1}{2}}(c_{14}-c_{14}');$$
$$K_6=c_3-c_3';\quad K_{67}=\frac{\sqrt{2}}{2}(c_{34}'-c_{34});$$
$$K_7=c_4-c_4'+c_4''-c_4''';$$
$$K_8=c_4-c_4'-c_4''+c_4'''. \tag{26}$$

Substitutions of Eqs. (18) into Eq. (24) and comparison of the resulting expression with Eqs. (5), lead to the relations between the K's of Eqs. (18) and the generalized force constants of Eqs. (5). Substitution of Eq. (26) into the latter relations yields the expressions for the generalized force constants of Eqs. (5) in terms of the valence force constants.

In the analysis of experimental data it is necessary to assume that some force constants are negligible as a first approximation since sufficient data are not available. In this respect it is necessary to examine similar molecules so that it is possible to make a judgment as to which constants to neglect.

ACKNOWLEDGMENT

This work was supported by a contract (DA-11-022-ORD-1281) with the Office of Ordnance Research, U. S. Army.

APPENDIX

In addition to the twelve linear combinations of displacement coordinates for the vibrational problem there are six linear combinations for the rotations and translations. Together, these eighteen combinations form a complete orthonormal set. Moreover, these six linear combinations are so chosen that they appear as Eckart conditions multiplied by a factor:

They are as follows.

$A_2'(R_z)$

$$S_9=\frac{1}{2}\left(\frac{m_1}{I_{ez}}\right)^{\frac{1}{2}}d_0[(2\eta_1-\eta_2-\eta_3)+3^{\frac{1}{2}}(\xi_3-\xi_2)]=0$$

$A_2''(T_z)$

$$S_{10}=a^{\frac{1}{2}}[m_1^{\frac{1}{2}}(\zeta_1+\zeta_2+\zeta_3)+m_2^{\frac{1}{2}}\zeta_4+m_3^{\frac{1}{2}}(\zeta_5+\zeta_6)]=0$$

$E'(T_x,T_y)$

$$S_{11a}=a^{\frac{1}{2}}[m_1^{\frac{1}{2}}(\xi_1+\xi_2+\xi_3)+m_2^{\frac{1}{2}}\xi_4+m_3^{\frac{1}{2}}(\xi_5+\xi_6)]=0$$

$$S_{11b}=a^{\frac{1}{2}}[m_1^{\frac{1}{2}}(\eta_1+\eta_2+\eta_3)+m_2^{\frac{1}{2}}\eta_4+m_3^{\frac{1}{2}}(\eta_5+\eta_6)]=0$$

$E''(R_x,R_y)$

$$S_{12a}=\frac{1}{2I_{ex}^{\frac{1}{2}}}[(3m_1)^{\frac{1}{2}}d_0(\zeta_2-\zeta_3)+2m_3^{\frac{1}{2}}D_0(\eta_6-\eta_5)]=0$$

$$S_{12b}=\frac{1}{2I_{ex}^{\frac{1}{2}}}[m_1^{\frac{1}{2}}d_0(-2\zeta_1+\zeta_2+\zeta_3)+2m_3^{\frac{1}{2}}D_0(\xi_5-\xi_6)]=0,$$

where R_x, R_y, and R_z are the rotations, and T_x, T_y, and T_z are the translations.

The Frequency of the Irradiating Light as a Determinant of the Joshi Effect in Oxygen under Silent Electric Discharge

S. R. MOHANTY
Chemical Laboratories, Banaras Hindu University, India
(Received November 24, 1953)

Ceteris paribus, the negative Joshi effect $-\Delta i$ in oxygen under electrical excitation increases linearly with the frequency ν of the irradiating light:

$$-\Delta i/i_D = A(\nu - \nu_m),$$

where i_D is the rms current in dark, ν_m the minimum threshold frequency, and A a constant dependent upon the nature of the electrode surface, gas pressure, applied potential V, etc. ν_m decreases with increase in V because of the occurrence of the photoelectric analog of the Schottky effect. The increase in $-\Delta i$ with $\nu(>\nu_m)$ is the consequence of a similar variation in the photoelectric yield. Superimposed on this are factors which tend to reduce $-\Delta i$: (1) the increase in photoelectron energy with ν, which diminishes the probability of attachment, and (2) reduction in emission because of the negative space charge and the image force.

INTRODUCTION

THE marked dependence of the Joshi effect, the instantaneous and reversible photovariation (enhancement $+\Delta i$ and diminution $-\Delta i$) of the current i under silent electrical discharge, in oxygen, on the nature of the irradiating light was suggested by the earlier results of the author and Kamath.[1] It was of interest, therefore, to determine the quantitative relationship between $\pm\Delta i$ and the light frequency. This has now been done using narrow monochromatic bands of identical intensity.

EXPERIMENTAL

A transformer discharge of 50-cycles (input) frequency was produced in the annular space of a glass Siemens' tube[2] filled with pure oxygen at 349 mm Hg (23°C) pressure. The tube was irradiated, perpendicular to its axis, through Kodak Wratten monochromats 71A–76, with a 500-w, 200-v incandescent tungsten-filament (in glass) lamp. The ultraviolet and the heat radiations from this last were cut off with appropriate filters. At a given exciting potential V the discharge current was observed, with a Cambridge vacuum thermocouple ("Vacuo-junction") connected to a sensitive d'Arsonval galvanometer, when the discharge tube was in dark (i_D) and when it was irradiated with the various filtered bands (i_L).

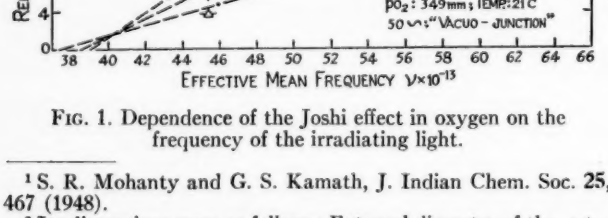

FIG. 1. Dependence of the Joshi effect in oxygen on the frequency of the irradiating light.

The effective mean frequency ν of the light bands was determined by standard optical methods. The intensity of the bands at the ozonizer axis, as observed with a Kipp and Zonen surface thermopile and a sensitive galvanometer, was kept constant by varying the distance between the light source and the ozonizer. The response of the thermopile-galvanometer system was sensibly linear with respect to the absolute amount of radiant energy, and was very nearly nonselective with respect to wavelength.

Table I contains a typical set of results at 5.34, 6.41, and 7.48 kv (rms). Figure 1 relates ν of the various bands with the corresponding relative *effect* $-\%\Delta i(=-\Delta i\times 100/i_D;\ -\Delta i=i_D-i_L)$.

DISCUSSION

In the earlier preliminary results of the author and Kamath,[1] values for $-\Delta i$ in oxygen were in the order: unfiltered white>blue>green-red. That $-\Delta i$ in green was not larger than that in red, despite the large frequency difference, was attributed to the very small intensity of the former compared with that of the latter. It is seen from the present results (Table I) that, intensity of the light bands remaining the same, $-\Delta i$ varies frequencywise. Thus, e.g., at 5.34 kv, $-\Delta i$ is 0.83, with light of $\nu=45.44\times10^{13}$, and increases progressively to 3.44 at $\nu=65.55\times10^{13}$; the corresponding values of $-\%\Delta i$ are respectively 8.3 and 34.4. Further, the $-\%\Delta i-\nu$ plots (Fig. 1) are linear over the ν range investigated. On extrapolation, each curve, corresponding to a given V, gives a different value for ν_m, the threshold frequency at which $-\%\Delta i$ (and $-\Delta i$)=0.

[1] S. R. Mohanty and G. S. Kamath, J. Indian Chem. Soc. **25**, 467 (1948).

[2] Its dimensions were as follows: External diameter of the outer tube, 10.8 mm; internal diameter of the outer tube, 9.0 mm; external diameter of the inner tube, 5.5 mm; internal diameter of the inner tube, 3.7 mm; thickness of the glass walls, 0.9 mm; interelectrode distance, 2.65 mm; length of the electrode column, 3.0 cm.

TABLE I. Variation of the Joshi effect in oxygen with the frequency of the irradiating light.
pO_2: 349 mm (23°C) Temperature: 21°C Frequency of the ac supply: 50 cps
Detector: "Vacuo-junction" Source of light: One 500-w, 200-v tungsten-filament (glass) lamp.

Effective mean frequency $\times 10^{-13}$	5.34 kv; $i_D=10.00$			6.41 kv; $i_D=11.92$			7.48 kv; $i_D=14.10$		
	i_L	$-\Delta i$	$-\%\Delta i$	i_L	$-\Delta i$	$-\%\Delta i$	i_L	$-\Delta i$	$-\%\Delta i$
65.55	6.56	3.44	34.4	9.17	2.75	23.1	11.87	2.23	15.8
60.89	7.35	2.65	26.5	9.33	2.59	21.7	12.37	1.73	12.3
55.29	7.93	2.07	20.7	10.1	1.82	15.3	12.53	1.57	11.1
51.71	8.31	1.69	16.9	10.44	1.48	12.4	13.04	1.06	7.5
48.76	8.72	1.28	12.8	10.77	1.15	9.6	13.23	0.87	6.2
45.44	9.17	0.83	8.3	11.22	0.70	5.9	13.56	0.54	3.8

Therefore,

$$-\Delta i/i_D=A(\nu-\nu_m),$$

where A is a constant dependent upon the nature of the electrode surface, gas pressure, applied V, etc. A linearity similar to that in Fig. 1 has also been observed by B. N. Prasad[3] in mercury vapor, and in chlorine by Deo,[4] and Tawde and Gopalkrishnan.[5] The decrease in ν_m (Fig. 1) with V is due to the occurrence of the photoelectric analog of the Schottky effect.[6] That, however, the $\sqrt{V}-\nu_m$ plots (inset, Fig. 1) show considerable variation from anticipated linearity is the result of the distortion of the applied field by the negative space charge responsible for $-\Delta i$ (*vide infra*).

The extent and the intensity of the (weak) absorption in the visible of oxygen, as also of ozone (which is formed to a small extent under conditions productive of the *effect*), is greater in the red-green than in the blue.[1] That, despite this fact, $-\Delta i$ should vary frequencywise shows, as suggested by Joshi,[7] that it is extremely unlikely that $\pm\Delta i$ is entirely a consequence of selective gas bulk light absorption.[1]

Joshi's theory[8–10] of the phenomenon contemplates emission of electrons, under light, from an activated adsorptionlike ionic+molecular layer on the electrodes, as primary to $\pm\Delta i$. Capture of these photoelectrons by the electronegative gas particles in the discharge, conditioned by high probability of electron attachment P, forms slow-moving negative ions leading to a negative space charge and the *effect* $-\Delta i$. Generally, P is an inverse function of the electron energy, i.e., E_a/p, where E_a is the applied field and p the gas pressure.[11] At low P, the electrons escape capture and cause an increase in i_D, the positive *effect* $+\Delta i$.

On the above theory, an increase in $-\Delta i$ would result from a similar variation in (1) the number of photoelectrons emitted, and (2) the attachment probability P. The photoelectrons[12] possess velocities ranging from zero to a maximum v_{max} obtainable from the Einstein equation

$$h\nu=\phi+\tfrac{1}{2}mv_{max}^2=h\nu_0+\tfrac{1}{2}mv_{max}^2;$$

the symbols have their usual significance. Further, dn, the total number of electrons of all velocities ejected in unit time by unit intensity of absorbed light of frequency range between ν and $\nu+d\nu$, is given by

$$dn=F(\nu)d\nu,$$

where $F(\nu)$ is the spectral distribution function. The emission is zero at and below ν_0, and increases with $\nu(>\nu_0)$. The observed increase in $\pm\Delta i$ therefore, follows. Superimposed on this is a reduction in $-\Delta i$ due to the simultaneous increase in the electron energy, and the consequent reduction in P. Further, two factors tend to limit the photoelectron emission under conditions productive of the *effect* $-\Delta i$: (1) the image force and (2) the negative space charge in the immediate neighborhood of the photoactive layer. The author[13] has already shown that (2) leads to saturation in $-\Delta i$ with respect to the light intensity.

[3] B. N. Prasad (unpublished results).
[4] P. G. Deo, Proc. Indian Acad. Sci. **A29**, 28, (1949).
[5] N. R. Tawde and K. Gopalkrishnan, Proc. Indian Acad. Sci. **A29**, 171 (1949).
[6] W. Schottky, Z. Physik, **14**, 63 (1923); I. Langmuir and K. T. Compton, Revs. Mod. Phys. **2**, 124 (1930).
[7] S. S. Joshi, Proc. Indian Sci. Congr., Part II, 70–75 (1943).
[8] S. S. Joshi, Proc. Indian Sci. Congr., Part III, Physics Sec., Abst. 26 (1946).
[9] S. S. Joshi, Proc. Indian Sci. Congr., Part III, Physics Sec., Abst. 25 (1947).
[10] S. S. Joshi, Current Sci. (India) **16**, 19 (1947).
[11] L. B. Loeb, *Fundamental Processes of Electrical Discharge in Gases* (John Wiley and Sons, Inc., New York, 1939).
[12] A. L. Hughes and L. A. DuBridge, *Photoelectric Phenomena* (McGraw-Hill Book Company, Inc., New York, 1932).
[13] S. R. Mohanty, J. Phys. Chem. (to be published).

Temperature Dependence of the Ultraviolet Absorption Spectrum of Naphthalene in Solution

RICCARDO PASSERINI,* *William Ramsay and Ralph Forster Laboratories, University College, London, England*

AND

IAN G. ROSS,† *University College, London, England, and Department of Chemistry, Florida State University, Tallahassee, Florida*

(Received December 14, 1953)

The absorption spectrum of naphthalene solutions has been measured, in the region 3300–2400A, at temperatures between +60°C and −185°C. Particular attention was given to the long-wavelength vibrational bands of the first electronic transition (3200–2900A), in order to locate and establish the identity of the band origin. The band acquires most of its intensity through the participation of an active vibration, whose ground-state frequency measured from two observed vibrational bands, is 525±20 cm^{-1}, in adequate agreement with the value 544±60 cm^{-1} found from the temperature dependence of intensity of the 0←1 band in this frequency. This is probably the Raman a_g frequency 512 cm^{-1}, which identification, in conjunction with previous polarization measurements, assigns the transition as $B_{2u}\leftarrow A_g$. Frequency and intensity data are given for 26 bands of this and the next transition (2900–2400A); the latter appears, vibrationally, to be allowed.

THE ultraviolet absorption spectrum of naphthalene records transitions from the ground state, which is undoubtedly described by a totally symmetric (A_g) wave function, to excited states whose symmetries remain uncertain despite numerous experimental and theoretical investigations.[1] Most interest at present attaches to the first two singlet transitions, which occur in the regions 3200–2900A and 2900–2400A, respectively, and the present work is a further contribution to the study of these absorption bands. The spectra have been measured in solution, over a wide range of temperature. Advantage was taken of the enhanced resolution of vibrational structure obtained at low temperatures, and also of the information yielded by the temperature variation of the intensity of a key band which originates from an excited vibrational level of the ground state.

The spectra were measured with a transmission-recording Cary spectrophotometer (Model 10), using the double absorption cell described elsewhere.[2] The locations of sharp peaks (see Tables I and II) are accurate to ±10 cm^{-1} and agree well with those reported by Clar,[3] who measured the spectrum in the same solvent at room temperature and −170°C. Extinction coefficients (corrected for solvent contraction[2]) are accurate to 3 percent, except probably at the lowest temperatures; here the half-widths of many bands were comparable with the spectral widths of the spectrophotometer slits (about 10A throughout), and greater errors are possible.

TABLE I. Characteristic points of the spectrum of naphthalene in absolute ethanol (first singlet transition).

Band	$\nu/10$ (cm^{-1}) All temps	ϵ +60°	+20°	−80°	−180°C[a]
B′	3123	22	17	6.5	0.4
A	3175.5	*S*[b]	65*S*	59	52
B	3218	226	249	330	385
C	3249	···	···	112*S*	119
D	3270	*S*	200S	208	222
E	3293		218	235	265
F	3321	290	294	327	333
G	3336	···	*S*	282	298
H	3366	321	326	357	400
I	3391	···	···	···	*S*
J	3415	···	···	*S*	*S*

[a] In EtOH:MeOH (4:1). The change of solvent did not sensibly affect the spectrum.
[b] *S* denotes an unresolved shoulder.

FIRST SINGLET TRANSITION (3200–2900A)

Our measurements of this portion of the spectrum are shown in Fig. 1 and Table I. The problems associated with the analysis of this spectrum have been reviewed by Sponer[4] and McClure,[5] so that only those considerations which bear directly on the present work need be outlined here. The absorption in this region is of very low intensity (f value approximately 0.002),[6] and thus the transition could be either symmetry forbidden or else allowed but intrinsically weak. The transition is polarized in the plane of the molecule and along the shorter molecular axis; the upper state accordingly has *vibronic* symmetry B_{2u}. This could be the symmetry of the nonvibrating molecule as well, but it could equally be obtained from any other symmetry through the superposition of a suitable, nontotally symmetric vibration. The most likely alternative assignment[4,5,7] is $A_g\times b_{2u}$, A_g being the electronic symmetry of the upper state and b_{2u} the symmetry of the active vibration. These two possibilities will be discussed here.

* Present address: Istituto di Chimica Industriale, Viale Risorgimento 4, Bologna, Italy.
† Present address: Chemistry Department, University of Sydney, Sydney, Australia.

[1] Comprehensive bibliographies are given in references 4 and 5 of this paper.

[2] R. Passerini and I. G. Ross, J. Sci. Instr. **30**, 274 (1953).
[3] E. Clar, Acta Spectrochim. **4**, 116 (1950).
[4] H. Sponer and G. P. Nordheim, Discussions Faraday Soc. **9**, 19 (1950).
[5] O. Schnepp and D. S. McClure, J. Chem. Phys. **20**, 1375 (1952).
[6] M. Kasha and R. V. Nauman, J. Chem. Phys. **17**, 516 (1949).
[7] D. P. Craig, Proc. XIth Intern. Congr. Chem. (London, July, 1947).

(1) If the transition is indeed $A_g \leftarrow A_g$, then the vibrational structure should resemble that of the known forbidden transition ($B_{2u} \leftarrow A_{1g}$) at 2600A in benzene. Here the band origin is completely missing in the vapor absorption and fluorescence, and the first strong vibrational bands in each involve one quantum of an active (e_{2g}) vibration. In absorption, the 1←0 band is naturally stronger than the 0←1 band, whose intensity is strongly temperature-dependent. These intensity relationships are reversed in the fluorescence. From each of the bands there originate extended progressions in a frequency corresponding to the totally symmetric molecular breathing vibration, and in these series of bands resides most of the intensity of the transition.

(2) If the naphthalene transition is instead allowed but weak, it could gain intensity by interaction with a higher state of the same symmetry, through the intervention of some totally symmetric vibrational mode *or modes*. In this case, however, the band origin *should* be detectable, though perhaps very weakly, in the vapor absorption and fluorescence, and the vibrational structure could involve a somewhat intricate set of combinations of, almost entirely, totally symmetric vibrations.

A cursory reading of the recent literature leaves the impression that (1) would be a closer description of the naphthalene transition than (2); and there is indeed the pattern of an indefinite band origin, spanned by distinct 0←1 and 1←0 bands. But beyond this the situation is in fact rather unclear. The only detailed measurements of the vapor spectrum so far published are those of Henri and de Laszlo,[8] who list some hundreds of vibration-rotational bands. Subsequent workers have reported being able to analyze these or their own results in terms of several upper-state frequencies,[4,5,9] but no details of the combinations so invoked have been given. Since the analysis is undoubtedly not simple, and not a single upper state vibrational frequency is securely known, these analyses must be taken with some reserve. The fluorescence spectrum of the vapor has recently been measured by Schnepp and McClure,[5] who concluded that the transition was $A_g \leftarrow A_g$, but as a result of later studies of the crystal spectrum,[10] these authors have changed their assignment, which now stands as $B_{2u} \leftarrow A_g$. The analysis which they earlier gave of this fluorescence is much more reliable than any analysis of the absorption could be, since it largely involves the known ground-state frequencies, but as they point out in their later note,[10] the analysis can be made just as consistent with the second as with the first assignment.

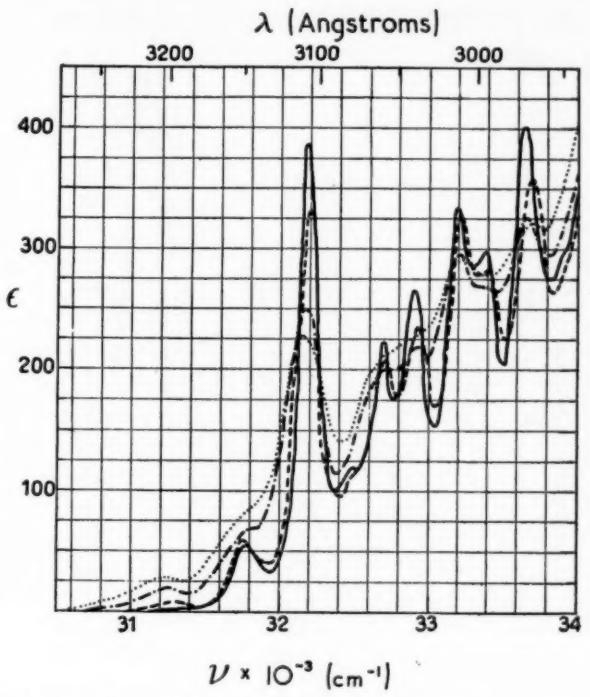

FIG. 1. Spectrum of naphthalene (first transition). ..... +60°C; -·-·-·-·- +20°C; - - - - - -80°C (all in EtOH); ——— −180°C (in EtOH:MeOH 4:1).

TABLE II. Characteristic points of the spectrum of naphthalene in absolute ethanol (second transition).

Band	ν/10 (cm⁻¹) +50°	+20°	−80°	−180°C[a]	ε/10 +50°	+20°	−80°	−180°C[a]
a			3477	3468			415	525
K[b]	3506	3503	3496	3496	385	385	385	300
b	3534	3531	3529	3523	385	385	400	405
c	...	...	...	3560	...	...	...	*S*[c]
d	3640	3634	3621	3611	550	575	620	705
e	...	...	3668	3663	*S*	*S*	525	505
f	...	...	...	3710	...	...	...	*S*
g	3768	3763	3759	3754	495	515	525	550
h	...	...	...	3805	...	...	*S*	385
i	...	...	...	3865	...	...	...	*S*
j	...	...	3882	3891	*S*	*S*	360	355
k	...	...	...	3960	...	...	...	*S*
l	...	...	...	4055	*S*	*S*	*S*	*S*

[a] In EtOH:MeOH (4:1). The change of solvent did not materially affect the spectrum.
[b] Assigned to the first transition (see text).
[c] *S* denotes an unresolved shoulder.

[8] V. Henri and H. de Laszlo, Proc. Roy. Soc. (London) **A105**, 662 (1924); H. de Laszlo, Z. Physik. Chem. **118**, 369 (1925).
[9] A. F. Prikhotjko, Izvest. Akad. Nauk U. S. S. R, Ser. Fiz. **12**, 499 (1948).

The bands denoted by B' and B in Table I correspond to bands at 32 511 and 32 455 cm^{-1} in the vapor spectrum[8]; the intensity of B' is temperature dependent

[10] O. Schnepp and D. S. McClure, J. Chem. Phys. **21**, 959 (1953).
[11] J. R. Platt, J. Chem. Phys. **19**, 1418 (1951); H. McConnell and D. S. McClure, J. Chem. Phys. **21**, 1296 (1953).

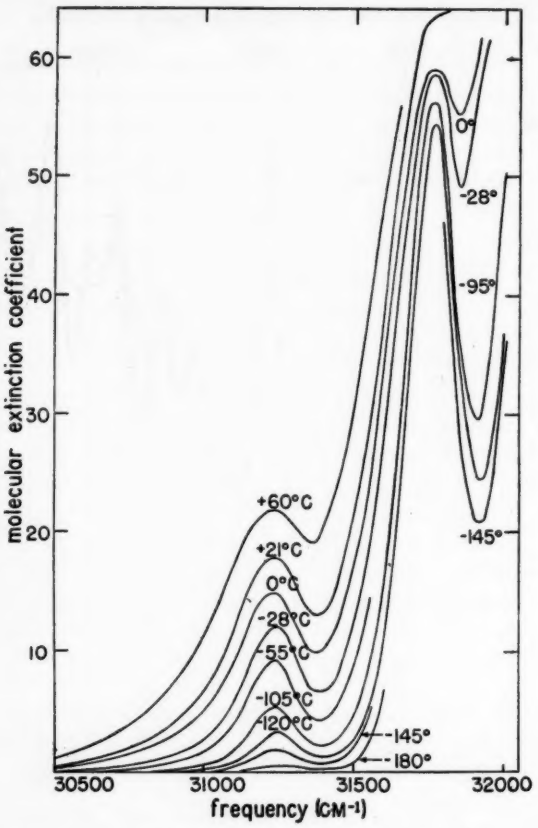

FIG. 2. Temperature dependence of the long-wavelength vibrational bands (B' and A) in the first transition of naphthalene (in EtOH:MeOH 4:1).

(see Fig. 2), and there is little doubt that they are 0←1 and 1←0 bands, respectively. There is also evidence,[12] further supported here (see below), that they do involve a quantum of the same vibrational mode. Their spacing (950 cm^{-1} here, 944 cm^{-1} in the vapor[13]) is the sum of the ground and excited state frequencies of this mode but until the band origin is located unequivocally, it cannot be known how this 944 cm^{-1} interval should be divided, and thus what the active frequency is. The vapor spectrum shows at least three bands between these two, none of which is an obvious 0←0 band. In the solution spectra there is a band A, which is intensified as the solution rigidifies and which has for some time been regarded as the band origin, but its position was known only approximately. From this the ground state frequency of the active vibration was known to be about 500 cm^{-1}. Barrow and McClellan[14] list two ground-state fundamentals in this vicinity: 512 cm^{-1}(a_g) and 476 cm^{-1}(b_{3u} or b_{2u}[15]), and identification of the $B'-A$ interval with the latter frequency has been made by Sponer[4,16] and others. However, in the present work the spacing was measured from spectra obtained at −100°C, at which temperature band A is well resolved, and band B' still intense enough for its maximum to be determined accurately, and the spacing was found to be 525±25 cm^{-1}. This figure appears incompatible with the 476 cm^{-1} assignment and strongly supports the 512 cm^{-1} choice; the upper-state frequency of the active mode is then 432 cm^{-1}. The drop in frequency is fairly large but not unreasonably so.

It still remains to demonstrate that band A is indeed the band origin and to confirm that B' and B involve one and the same vibrational mode. To this end the long-wavelength tail of the absorption was examined particularly closely, using solutions of concentrations between 0.008M and 0.06M, which, in the 1-cm cells used, were sufficient for the intensity and peak wavelength of band B' to be measured accurately. Nine such solutions were examined, each at several temperatures; a representative set of the absorption curves so obtained is shown in Fig. 2. This figure shows in a particularly striking fashion the temperature dependence of the first two vibrational bands. Band B' is clearly enhanced by increase of temperature, while band A, at 60°C obtained only as a weak shoulder, becomes stronger and sharper as the solutions contract, presumably because of the increased perturbation of solute by solvent.

We have applied to these measurements the same approach as was recently and independently essayed by Knipe, Sponer, and Cooper;[16] namely, the use of the temperature dependence of the B' band intensity to calculate the energy, which we shall call ν_1, of the vibrational level from which it originates. Denote by f', f the apparent oscillator strengths, i.e., those calculated from the measured absorption curves, of bands B' and B. Also, denote by f_0', f_0 the true oscillator strengths of the 0←1, 1←0 transitions which we consider to be the nature of these bands. Then, if N_t is the total number of molecules in the solution, and N_0, N_1 are, respectively, the number of these in the ground state and in the vibrational level ν_1, we can write

$$f'=f_0'N_1/N_t;\quad f=f_0N_1/N_t;\quad N_1/N_0=e^{-\nu_1/kT},\quad \text{(1a,b,c)}$$

whence

$$\log(f'/f)=\log(f_0'/f_0)-\nu_1/2.303\ kT. \qquad (2)$$

If B' and B have been correctly interpreted, then f_0'/f_0 should be of the order of unity, as has already

[12] See reference 5, p. 1380.

[13] H. Sponer and G. P. Nordheim (reference 4) and O. Schnepp and D. S. McClure (reference 5), respectively, quote 941 and 949 cm^{-1} as the values for this spacing, both giving Henri and de Laszlo's study as reference. Here and elsewhere in this paper we have adopted as the frequencies of vibrational levels the Q-branch origins as assigned by Henri and de Laszlo; it cannot be said, however, that the rotational analyses in this early work have been confirmed.

[14] G. M. Barrow and A. L. McClellan, J. Am. Chem. Soc. **73**, 573 (1951).

[15] Although given as b_{2u} by G. C. Pimentel and A. L. McClellan, J. Chem. Phys. **20**, 270 (1952), the assignment of this frequency (private communication from Dr. G. C. Pimentel) is now regarded as more likely to be b_{3u}. If this is confirmed, the case for the assignment A_g←A_g for the first electronic band is demolished entirely.

[16] Knipe, Sponer, and Cooper, J. Chem. Phys. **21**, 376 (1953).

been pointed out.[16] If this ratio is independent of temperature and we make this assumption, then experimental measurement of the left-hand side of Eq. (2) should give access to ν_1.

Before applying the equation, however, we should examine its derivation more closely. In solution measurements, the width of the vibrational bands is such that many weak vibrational transitions may be covered by strong ones. In particular, the intensity of the 1←0 transition (which we will now write as $\nu_1'\leftarrow 0$, as measured by the intensity of band B, will include contributions from transitions $\nu_{1,i}'\leftarrow\nu_i''$. Here ν_i'' is any ground-state vibrational level (not necessarily a fundamental frequency) and $\nu_{1,i}'$ is that upper-state level which has the same vibrational quanta as ν_i'', plus one quantum of ν_1. We now make the assumption, drastic, but made more plausible by the circumstance that there are no degenerate vibrations to complicate the selection rules, and mitigated moreover by a like assumption we shall make concerning band B', that the true oscillator strengths of all such transitions are equal to f_0. Then Eq. (1a) is to be replaced by

$$f=f_0(N_0+\Sigma_i N_i)/N_i=f_0. \qquad (3a)$$

Here N_i is the number of molecules in vibrational state ν_i'', and the summation is over all such states.

Likewise, with band B', we must consider transitions of type $\nu_i''\leftarrow\nu_{1,i}'$, whose frequencies are close to the 0←1 (that is, $0\leftarrow\nu_1''$) frequency. Proceeding as before, we replace Eq. (1b) by

$$f'=f_0'(N_1+\textstyle\sum_i N_{1,i})N_i$$
$$=f_0'N_1(1+\textstyle\sum_i N_i)/N_i=f_0e^{-\nu_1/kT}. \qquad (3b)$$

If we combine Eqs. (3a), (3b) we again obtain Eq. (2). This derivation indicates the tenuousness of the assumption that f_0'/f_0 is a constant. However, we may test the general validity of the equation by observing the temperature dependence of bands B and B' individually. Naphthalene has vibrations of frequency as low as 191 cm^{-1}, or even 80 cm^{-1},[14] and even at 0°C the ground state is heavily depopulated in consequence. Equation (1a) thus predicts that f, the measured intensity of B, should decrease appreciably with rising temperature; while Eq. (3a), on the other hand, predicts no temperature variation. In fact (see following) almost no temperature dependence is observed, and though this conceivably could be due to an increase with temperature of the true oscillator strength of the 1←0 band, due to increasing solvent perturbation, it does strongly point to the necessity of justifying Eq. (2) via Eqs. (3), when working with solution spectra.

Again, Eqs. (1b) and (3b), respectively, predict that $\log f'$ should not, and should, vary linearly with $1/T$; a very nearly linear dependence is, in fact, observed.

Since, then, there are strong indications of significant contributions to the intensities of bands B and B' by transitions other than 1←0 and 0←1, and since we have taken them into account so crudely in deriving Eq. (2), it is expected that there will be an extra error in the value of ν_1, derived through the use of Eq. (2), over and above normal experimental errors. This additional error we cannot estimate. The largest experimental uncertainty arises from the difficulty of estimating areas under absorption curves which overlap other curves. Fortunately, however, a highly accurate value of ν_1 is not necessary merely in order to discriminate between possible observed band origins.

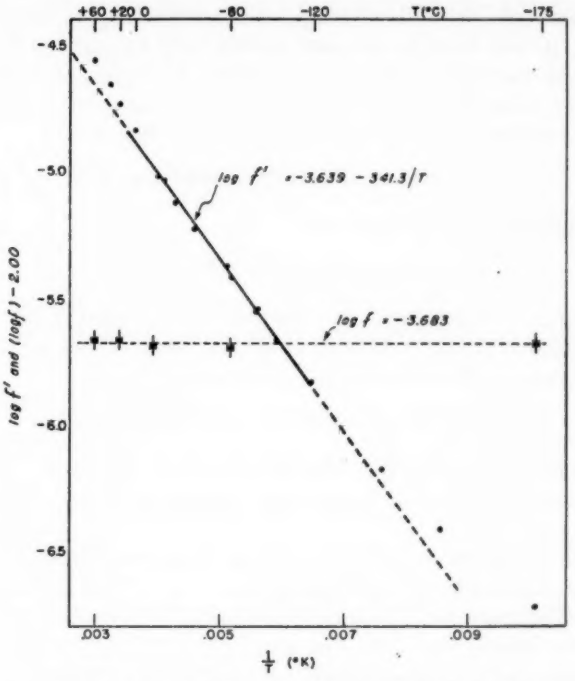

FIG. 3. Oscillator strengths of bands B' and B as a function of reciprocal absolute temperature.

The oscillator strengths of band B' were calculated using the expression $f=4.31\times10^{-9}\times2\int_0^{\nu_{max}}\epsilon d\nu$, the integral here being the area under the absorption curve, as far as the frequency of maximum absorption. The values obtained have an accuracy of about 5 percent, although they are less reliable above 20°C, because of overlapping by band A, and below −120°C, where the band becomes very weak (solutions of concentration greater than $0.05M$ crystallized on rigidification, preventing more accurate measurements at the lowest temperatures). The measured values of $\log f'$ are plotted in Fig. 3.

The areas under the envelope of band B—compare with Fig. 1—are much more difficult to measure accurately, since there are overlapping bands on both sides. Five measurements at temperatures between +60° and −180° gave results which showed no significant variation, having in mind an estimated error of 10 percent. The corresponding values of $\log f$ are also shown in Fig. 3.

Since the dependence of $\log f'$ upon $1/T$ is almost linear over the range in which the measurements are

most reliable, and since $\log f$ is sensibly independent of T, it was considered most satisfactory to express the data for each quantity separately in terms of $1/T$. The least-squares equation for $\log f'$, calculated using the points traversed by the solid line in Fig. 3, is

$$\log f' = (-3.64 \pm 0.03) - (340 \pm 20)/T,$$

while for $\log f$ we shall use

$$\log f = (-3.68 \pm 0.04) - (0 \pm 20)/T,$$

roughly estimated but plausible values having been assigned to the probable limits of error in this latter equation. Hence,

$$\log(f'/f) = (0.04 \pm 0.07) - (340 \pm 40)/T.$$

Comparison with Eq. (1) yields the final values:

$$f_0'/f_0 = 1.1 \pm 0.2; \quad \nu_1 = 544 \pm 60 \text{ cm}^{-1},$$

the probable errors here being those based on the assumption that Eq. (2) is exact.

The value of f_0'/f_0 confirms our expectation that the true intensities of the two bands should be almost the same and is excellent evidence for taking both bands to involve the same active vibrational mode. The value found for ν_1 is sufficiently close to the value, 525 cm^{-1}, found from the B' to A spacing, to make it impossible that any other of the bands observed in solution should be the origin, and is entirely consistent with band A being so identified.

These findings are in accord with the results, if not the conclusions, of Sponer *et al.*[16] These authors measured the optical densities of the B' and B band maxima in the vapor spectra, at three temperatures only, and found that their three points favored a value of f_0'/f_0 of about unity, and a value of ν_1 in the region of 500 cm^{-1}, a result which they took, however, to indicate that 476 cm^{-1} was the frequency of the active vibration.

ANALYSIS

Granted the identification of the 512 cm^{-1} a_g vibration as the active vibration of the transition, the origin of the vapor spectrum should be located at 31 511+512 = 32 023 cm^{-1}. It is most significant that de Laszlo does indeed record a comparatively weak band (Band VI in his notation), with Q-branch origin at 32 022 cm^{-1}. The existence of such a band is almost essential to our interpretation of the spectrum. A similar $0 \leftarrow 0$ band would be expected, from the data of Schnepp and McClure,[5] to appear in the fluorescence at about 32 013 cm^{-1}; however, no such band could have been detected in their measurements because of interference by mercury lines at 31 990 and 31 926 cm^{-1} deriving from the arcs used to excite the fluorescence.

It is plausible, then, that the origin of the electronic transition is at 32 022 cm^{-1}. Previous attempts at the vibrational analysis of the absorption spectrum have all taken the $0 \leftarrow 1$ band (32 455 cm^{-1} vapor) as effective origin and have sought to find progressions and combinations originating from this frequency. This would parallel the fluorescence analysis of Schnepp and McClure. However, just as about one-quarter of the fluorescence bands admit of alternative assignments which do not involve the principal active frequencies 512 and 432 cm^{-1}, so one would look for vibrational bands in the absorption spectrum which also do not involve these frequencies. Yet we have been unable to find a sufficient number of separations from the $0 \leftarrow 0$ band, which coincide with other separations (or combinations of separations) from the $1 \leftarrow 0$ band, to justify claiming that our $0 \leftarrow 0$ band assignment materially simplifies the analysis. On the other hand, the absorption spectrum has no unequivocal progressions in any frequency, and even assuming, with Prikhotjko,[9] that seven (out of a total of nine) totally symmetric vibrations appear in the spectrum, all originating from the $0 \leftarrow 1$ band, there are more bands unassigned than are accounted for. As a result, further speculation at this stage on the analysis of this transition in absorption, whether in the vapor or in solution, seems unjustified.

SECOND SINGLET TRANSITION (2900–2400A)

The absorption curves relating to this part of the spectrum have been published by us elsewhere,[2] but without comment. The numerical data are given in Table II. The bands of the transition move towards the red with decreasing temperature; since the bands of the first transition do not shift at all with change of temperature, we have a further demonstration that there are actually two transitions involved, and a ready criterion for assigning vibrational bands to one or other transition. This criterion was used in the case of band K, which at room temperature is superimposed on band a (compare with Table II). On cooling, the two peaks are resolved, the former remaining stationary, the latter moving away from it towards lower frequencies.

On the basis of polarization studies,[10] the transition has been assigned as allowed, $B_{3u} \leftarrow A_g$. The vibrational structure appears to be comparatively simple, and at $-180°$C the bands of Table II are completely described by an analysis which takes band a as origin, and expresses the rest of the system by the formula 34 680 $+550p+920q+1430r$, where $(p,q) = (0,0), (0,1)$, or $(1,0)$, and $r = 0, \cdots, 4$. Such an analysis is in no way inconsistent with the assignment quoted. In particular there is no obvious sign of a weak band origin of the kind found in the first transition.

The authors are indebted to Professor D. P. Craig for helpful discussion, and especially wish to thank Dr. G. E. W. Wolstenholme of the Ciba Foundation, London, for hospitality extended to R. P. This work was supported by a grant from the Italian Consiglio Nazionale delle Ricerche (to R. P.) and by an Australian National University Scholarship (to I. G. R.).

THE JOURNAL OF CHEMICAL PHYSICS VOLUME 22, NUMBER 6 JUNE, 1954

Semiempirical Potential Energy Functions. I. The H_2 and H_2^+ Diatomic Molecules

ARTHUR A. FROST AND BORIS MUSULIN
Department of Chemistry, Northwestern University, Evanston, Illinois
(Received February 1, 1954)

After setting up certain theoretical criteria for a semiempirical potential energy function, two such functions for H_2^+ and H_2 are constructed, the simplest of which has the form

$$V=e^{-aR}\left(\frac{e^2}{R}-b\right),$$

where V is the potential energy with its zero corresponding to infinite separation. R is the internuclear distance, e the electronic charge, and a and b parameters. This function is used to correlate the experimental quantities: dissociation energy, equilibrium internuclear distance, force constant, third and fourth derivatives of V with respect to R, united atom energy, and critical distance.

A more complicated function is also presented which with one molecular parameter fixed by the dissociation energy is capable of then predicting internuclear distance and force constant.

GENERAL INTRODUCTION

THE potential energy of a set of atoms as a function of their relative positions is fundamental to all of chemistry. Potential energy minima determine possible structures and are thus related to bond strength and valence. The curvatures of the potential energy surface, the second derivatives of the potential energy with respect to distance in certain specified directions, are the force constants for the various modes of vibration and determine the vibrational energy levels. These vibrational energy levels, together with rotational levels determined by the moments of inertia, which are calculable from the configuration of minimum potential energy, correlate the infrared and microwave spectra, as well as determine the thermodynamic properties of the substance. Gas imperfections are due to potential energy changes in molecular collisions while reaction rates are determined by the potential energy surface of the activated complex of reacting molecules. It is therefore of the greatest importance to have a suitable representation of the potential energy as a function of the relative positions of the nuclei.

Potential energy functions used in the past have been either primarily empirical or primarily theoretical. Examples of the former are the Morse,[1] the Hulburt-Hirschfelder,[2,3] and the Lippincott[4] functions for diatomic molecules and the various potential energy functions, or force fields, used to interpret fundamental vibration frequencies of polyatomic molecules.[5] Theoretical potential energy curves or functions are of great interest because of their fundamental nature. However, the difficulty of their accurate calculation from quantum mechanics is well known, satisfying results being available only for simple molecules such as H_2^+,[6] H_2,[7] and O_2.[8]

It is proposed here to emphasize *semiempirical* methods as a means of by-passing the difficulties of accurate theoretical calculation, but at the same time having a system with some theoretical significance. It can be expected that if the form of a potential energy function is chosen to meet certain theoretical requirements then there very well may be fewer unknown parameters than data available, so that it would be possible to make certain verifiable predictions which would not be possible with a purely empirical function, such as the Hulburt-Hirschfelder function.[2]

Semiempirical quantum-mechanical calculations of electronic energies of molecules or complexes is an old technique. As examples may be cited: the resonance energy calculations of Pauling, Wheland,[9] and others; activation energy calculations of Eyring[10] and co-workers; more recently the "magic formula" of Mulliken,[11] and calculations by Moffitt[12] and by Parr[13] and co-workers, and by Hall.[14] In nearly all of this work the energies are estimated for only the equilibrium configuration of a molecule or for a very limited range of internuclear distances in that neighborhood. The principal exceptions to this are the activation energy calculations where the potential energy surfaces are mapped out over a range of configurations of the nuclei. In this work semiempirical functions will be set up to cover essentially the whole range from the "united atom" to the completely separated atoms, the known properties of these extreme cases being used to aid in determining an appropriate form of the functions.

[1] P. M. Morse, Phys. Rev. **34**, 57 (1929).
[2] H. M. Hulburt and J. O. Hirschfelder, J. Chem. Phys. **9**, 61 (1941).
[3] See also review in G. Herzberg, *Spectra of Diatomic Molecules* (D. Van Nostrand Company, Inc., New York, 1950), second edition, pp. 101–103.
[4] E. R. Lippincott, J. Chem. Phys. **21**, 2070 (1953).
[5] See review in G. Herzberg, *Infrared and Raman Spectra of Polyatomic Molecules* (D. Van Nostrand Company, Inc., New York, 1945), pp. 159–238.
[6] E. Teller, Z. Physik **61**, 458 (1930), and previous references quoted there.
[7] H. M. James and A. S. Coolidge, J. Chem. Phys. **1**, 825 (1933).
[8] A. Meckler, J. Chem. Phys. **21**, 1750 (1953).
[9] G. W. Wheland, J. Am. Chem. Soc. **63**, 2025 (1941).
[10] Glasstone, Laidler, and Eyring, *The Theory of Rate Processes* (McGraw-Hill Book Company, Inc., New York, 1941), Chap. III.
[11] R. S. Mulliken, J. Phys. Chem. **56**, 295 (1952).
[12] W. Moffitt, Proc. Roy. Soc. (London) **A210**, 224, 245 (1951).
[13] For example, F. G. Fumi and R. G. Parr, J. Chem. Phys. **21**, 1864 (1953).
[14] G. G. Hall, Proc. Roy. Soc. (London) **A205**, 541 (1951).

In this paper only the simplest cases H_2 and H_2^+ will be examined. A succeeding paper is in preparation dealing with diatomic molecules in general. It is hoped that the same techniques can usefully be also applied to polyatomic molecules as well as to activated complexes.

THEORETICAL CRITERIA FOR A POTENTIAL ENERGY FUNCTION FOR DIATOMIC MOLECULES

1. The Potential Energy (for Nuclear Motion), V, is the Algebraic Sum of Two Parts

(a) The nuclear repulsive potential corresponding to merely a Coulomb force $Z_1Z_2e^2/R$, with e the electronic charge, Z_1 and Z_2 the atomic numbers, and R the internuclear distance; and (b) the purely electronic energy defined as V_e, which is also a function of R. The existence of the potential energy function as well as this separation in the first is not theoretically precise, but is based on the adiabatic approximation where the nuclear motion is considered negligible as compared with the electronic motion.[15] The greatest error of this approximation would be expected in H_2 and H_2^+, but the theoretical calculations of Burrau, Teller, and James and Coolidge,[6,7] have nevertheless shown excellent agreement, within 0.01 ev in the energy, or about 0.1 percent of the dissociation energy. This is certainly adequate for all ordinary chemical considerations. Therefore we shall write for H_2 and H_2^+

$$V=\frac{e^2}{R}+V_e.$$

2. V Becomes Infinite as R Approaches Zero

This is because of the nuclear repulsion term e^2/R, assuming V_e does not become infinite in an equal and opposite sense. Of course if nuclear structure and forces are taken into account this statement is not precisely correct. However, since the object of this criterion is to aid in the search for a suitable form for the molecular potential energy function a change in this form at internuclear distances of 10^{-12} cm is of no consequence. The fact that the Morse and most other functions give finite V at $R=0$ is usually disregarded as unimportant in its effect at normal molecular internuclear distances. Evidence will be given below that this is not the case.

3 a. V_e is Finite at $R=0$
3 b. $V_e=V_e^0$ at $R=0$

where V_e^0 is the known "united" atom energy. 3 b is a slightly more stringent condition than 3 a and may or may not be satisfied by a useful function.

4. $V_e \propto -e^2/R$ for Large R

This is based upon the choice of $V=0$ at infinite R and is a required condition to cancel the nuclear repulsion potential since the total V goes to zero faster than inversely as the first power of R. The exception to this will be ionic states, in which case the $1/R$ term will still be present but with a negative coefficient of larger magnitude.

5. $dV_e/dR=0$ at $R=0$

This condition is known to exist for H_2^+ as its electronic energy approaches the united atom He^+.[16] This is believed to be correct also for other diatomic molecules, but the proof has apparently not been given.

6. V Must be Capable of Going through a Minimum as R Varies

Other criteria for a good function could be stated but will not be used in this paper. In particular, the van der Waals' forces should introduce in addition to the inverse first power term in 4, inverse fourth and higher powers for H_2^+ [17] and inverse sixth and higher powers for H_2.[18]

A SIMPLE TWO-PARAMETER FUNCTION FOR H_2 AND H_2^+

In the following atomic units will be used to simplify the expressions: unit of length a_0, radius of the first Bohr orbit of hydrogen; unit of energy e^2/a_0, twice the ionization energy of the hydrogen atom; unit of mass m, the mass of the electron. From these it follows that the charge on the electron is unity and the internuclear repulsion in H_2 and H_2^+ becomes simply $1/R$.

A simple function that satisfies criteria 1, 2, 3a, 4, and 6 is the following:

$$V=e^{-aR}\left(\frac{1}{R}-b\right), \tag{1}$$

where a and b are parameters to be adjusted. The corresponding electronic energy is

$$V_e=-\frac{1}{R}(1-e^{-aR})-be^{-aR} \tag{2}$$

with the limiting value as $R\to 0$

$$V_e^0=-(a+b). \tag{3}$$

The particular form (2), and therefore (1) by addition of $1/R$, was arrived at by considering possible products of an exponential with powers of R. This is an expected form because the overlap, Coulomb, and exchange integrals of quantum-mechanical theory are all of this type. The first term on the right of (2) gives the $-1/R$ dependence at large R as in criterion 4 but also provides the finite V_e^0 of $3a$ after evaluation of the indeterminate form at $R=0$. The first term alone is insufficient since the corresponding V has no minimum and criterion 6 is not satisfied. Therefore the second term of (2) is included as the simplest additional term which would

[15] M. Born and J. R. Oppenheimer, Ann. Physik **84**, 457 (1927).

[16] This is inherent in the formulas found in F. A. Matsen, J. Chem. Phys. **21**, 928 (1953), and in previous work referred to there.

[17] C. A. Coulson, Proc. Roy. Soc. (Edinburgh) **61**, 20 (1941).

[18] L. Pauling and J. Y. Beach, Phys. Rev. **47**, 686 (1935).

satisfy all criteria except possibly 3b and 5. A choice of $a+b$ can be made to satisfy 3b, but there is some doubt that 3b should be satisfied without 5. To satisfy 5 would require more complicated expressions which will be considered below.

The testing of function (1) can be done in several ways. In principle the two parameters, a and b can be fixed by requiring the function to agree with any two of the known experimental quantities such as R_e, equilibrium internuclear distance; D_e, dissociation energy from the minimum of the curve; k_e, force constant for infinitesimal amplitudes, which is equal to (d^2V/dR^2) at $R=R_e$; (d^3V/dR^3) at R_e, which is related to the spectroscopic constant α_e; (d^4V/dR^4) at R_e, which is related to both α_e and the constant $x_e\omega_e$[19]; and finally V_e^0, the united atom energy which is known from atomic spectroscopy. If the V_e^0 value could be used as in (3) there would then be only one parameter to be fixed by purely *molecular* information and predictions could be made of the other four listed above as well as possibly others.

Tables I and II show experimental values and calculated results for the ground states of H_2^+ and H_2. Table I contains in addition to the previously defined quantities, R_c, the critical distance, a quantity obtained indirectly from mass spectrometry appearance potentials. R_c is the value of R, less than R_e, at which $V=0$, or the same as at infinite separation. Stevenson[20] has shown how R_c may be obtained for certain molecules and that it is in serious disagreement with the Morse function since the latter does not represent the repulsive potential energy at all well. The Morse function predicts for H_2^+ $R_c=0.50$A or 0.94 at .un., or 16 percent low as compared with Stevenson's experimental value of 0.595A or 1.12 at .un. The table shows how much better the present function makes this prediction.

TABLE I. Data and calculated results for ground state of H_2^+ (atomic units used).

	Experimental values	Calculation 1	2	3	4	5	6
R_e	2.00	...	...	2.07 +4%	...	2.05 +3%	2.06 +3%
D_e	0.102	...	0.082 −20%	...	0.184 +82%	...	0.095 −7%
k_e	0.101	0.111 +10%	...	...	0.138 +37%	0.105 +4%	...
$-\left(\frac{d^3V}{dR^3}\right)_{R_e}$	0.241	0.289 +20%	0.275 +14%	0.254 +5%	0.322 +34%	0.264 +10%	0.257 +7%
$\left(\frac{d^4V}{dR^4}\right)_{R_e}$	0.549	0.694 +26%	0.685 +25%	0.586 +7%	0.724 +32%	0.616 +12%	0.598 +9%
$-V_e^0$	1.500	1.54 +3%	1.58 +5%	1.48 −1%	...	...	...
R_e	1.12	1.136 +1%	1.17 +4%	1.17 +4%	1.00 −11%	1.16 +4%	1.18 +5%
a	...	0.658	0.726	0.627	0.500	0.637	0.650
b	...	0.881	0.853	0.856	1.000	0.863	0.850

[19] See discussion in A. A. Frost and B. Musulin, J. Am. Chem. Soc. (to be published).

[20] D. P. Stevenson, Vortex 12, 198 (May, 1951). Also private communication.

TABLE II. Data and calculated results for ground state of H_2 (atomic units used).

	Experimental values	Calculation 1	2	3
R_e	1.405	...	...	1.382 −2%
D_e	0.175	...	0.211 +20%	...
k_e	0.369	0.340 −8%	...	...
$-\left(\frac{d^3V}{dR^3}\right)_{R_e}$	1.255	0.972 −23%	1.240 −1%	1.304 −4%
$\left(\frac{d^4V}{dR^4}\right)_{R_e}$	4.22	4.12 −2%	4.13 −2%	4.43 +5%
$-V_e^0$	1.904	2.17 +14%	2.14 +12%	2.20 +16%
a	...	0.865	0.790	0.886
b	...	1.304	1.350	1.315

The various calculations in the tables are defined by the corresponding blank entries, e.g., calculation 1 uses experimental R_e and D_e values to fix a and b. Calculations 4, 5, and 6 for H_2^+ in Table I make use of the experimental V_e^0 value and therefore only one *molecular* quantity. These calculations are seen to be less satisfactory than calculations 1, 2, and 3. Calculations like 4, 5, and 6 were also attempted for H_2 but are not included in Table II inasmuch as either no solution was possible or the results were extremely poor.

These calculations are greatly aided by the introduction of a dimensionless parameter x, defined as aR_e. Various combinations of experimental quantities can then be expressed as follows:

$$D_eR_e=\frac{e^{-x}}{x}, \tag{4}$$

$$k_eR_e^3=e^{-x}(2+x), \tag{5}$$

$$-\left(\frac{d^3V}{dR^3}\right)_{R_e}\cdot R_e^4=e^{-x}(6+6x+2x^2), \tag{6}$$

$$\left(\frac{d^4V}{dR^4}\right)_{R_e}\cdot R_e^5=e^{-x}(24+24x+12x^2+3x^3), \tag{7}$$

$$-V_e^0R_e=\frac{x^2+x+1}{x}. \tag{8}$$

The parameters can be expressed as

$$a=\frac{x}{R_e}, \tag{9}$$

$$b=\frac{x+1}{R_ex}. \tag{10}$$

TABLE III. Application of Eq. (14) to H_2^+ and H_2.

	D_e used to determine κ H_2^+		Atomic units used H_2	
	Calc.	Exper.	Calc.	Exper.
κ	0.266	...	0.115	...
R_e	2.00	2.00	1.405	1.405
k_e	0.102	0.101	0.39	0.369
R_e	1.12	1.12	...	...

These equations were solved graphically to get the results in Tables I and II.

A MORE COMPLEX TWO-PARAMETER FUNCTION

The simple function (1) of the previous section as used in calculations 1, 2, and 3 satisfied all of the listed theoretical criteria except 3b and 5. To satisfy 5, i.e., to make V_e approach the united atom value with zero slope, it is convenient to make each term of Eq. (2) have this property. This is easily accomplished by multiplying the exponentials by appropriate binomials in R. Also to simplify the calculations replace R by α/a so that

$$\alpha = aR. \tag{11}$$

Equation (2) for V_e would then be modified to

$$V_e = -\frac{a}{\alpha}\left\{1-e^{-\alpha}\left(1+\frac{\alpha}{2}\right)\right\}-be^{-\alpha}(1+\alpha). \tag{12}$$

If now $1/R$ is added and $(a+b)$ set equal to $-V_e^0$, the resulting potential function satisfies all listed criteria and has a single parameter remaining,

$$V = e^{-\alpha}\left\{\frac{a}{\alpha}\left(1+\frac{\alpha}{2}\right)+(a+V_e^0)(1+\alpha)\right\}. \tag{13}$$

Unfortunately, no choice of the parameter a will provide a satisfactory value of R_e, this quantity being too small by 20–30 percent and very insensitive to the value a while the D_e varies considerably.

There is a striking coincidence between the two terms of V_e in (12) and the results of a simple theoretical calculation of H_2^+ using $1s$ orbitals of H. The first and second terms are precisely of the same form as the Coulomb and exchange integrals, respectively.[21] This then opens up possibilities of further modifying the V_e in a semiempirical manner by introducing overlap integrals and effective atomic numbers. The final potential energy function obtained in this way is

$$V = a\left[\frac{1}{\alpha}-\tfrac{1}{2}(A-B)\right]+V_e^0 B, \tag{14}$$

where A and B are functions of α,

$$A(\alpha) = \frac{\frac{2}{\alpha}\{1-e^{-2\alpha}(1+\alpha)\}}{1+e^{-\alpha}\left(1+\alpha+\frac{\alpha^2}{3}\right)}, \tag{15}$$

$$B(\alpha) = \frac{2e^{-\alpha}(1+\alpha)}{1+e^{-\alpha}\left(1+\alpha+\frac{\alpha^2}{3}\right)} \tag{16}$$

and where a, which can be considered analogous to an effective atomic number, is allowed to vary with α (and therefore with distance) according to

$$a = 1+e^{-\kappa\alpha}. \tag{17}$$

Equation (17) is chosen to cause a to vary from a value 2 for the united atom to a value 1 for the separated atoms. There is now only one parameter left, κ.

Table III shows the application of the function in (14) to the ground states of H_2^+ and H_2. The parameter κ has been determined by a graphical method so that $V=-D_e$ at $R=R_e$. The fact that this point is actually a minimum is found by graphing the function. All of the quantities so far determined agree with the experimental values well within the error of reading the graphs except possibly the value of the force constant for H_2.

DISCUSSION

The simple function (1) has the advantage of ease of manipulation for predicting certain quantities analytically or by simple graphical methods. It is gratifying that with its use several experimental quantities can be approximately predicted using only two of these quantities as known to fix the two parameters. However, it does not accomplish satisfactorily the one task that would be most desirable from a practical standpoint, i.e., to predict dissociation energy from other properties.

The more complicated function (14) is remarkable in that by using only one molecular quantity several other properties can be accurately predicted. This is not too surprising for H_2^+ inasmuch as the function has the familiar form of Coulomb and exchange integrals. However for H_2 it is surprising because in this case the corresponding Coulomb and exchange integrals are much more complicated and the interelectronic repulsion which is present is not explicitly recognized in this semiempirical treatment. This function is of course more difficult for computation.

ACKNOWLEDGMENT

This work has been supported by a research grant from the National Science Foundation.

[21] L. Pauling, Chem. Revs. **5**, 173 (1928); L. Pauling and E. B. Wilson, Jr., *Introduction to Quantum Mechanics* (McGraw-Hill Book Company, Inc., New York, 1935), p. 329.

The Photoconductivity of Anthracene. I.*

A. G. CHYNOWETH† AND W. G. SCHNEIDER
National Research Laboratories, Ottawa, Canada

(Received November 30, 1953)

Pure crystals of anthracene became photoconducting when illuminated with wavelengths lying within their fundamental absorption band. The majority carriers were positive holes, which, as they drifted through the crystal, took part in trapping processes. From the variation of the photocurrent with temperature it was concluded that the number of positive hole traps fell off exponentially as their height above the valence band increased. From the behavior of the photocurrent at various applied fields and light intensities, it was concluded that the conventional energy band diagram as used for inorganic substances could be applied to organic compounds also. Evidence was found, however, indicating that there were large potential irregularities in the energy levels throughout the crystal.

INTRODUCTION

THE phenomenon of photoconductivity has been studied extensively for a variety of inorganic substances. Comparatively little is known about the photoconductive properties of organic compounds. Of the latter, the so-called conjugated compounds are of particular interest because of the nature of their electronic structures, and, in fact, photoconductivity in certain organic dyes has been known for some time.[1–4] It appears likely that this property may occur in a wide variety of conjugated compounds. However, it was felt that for an initial investigation of the fundamental mechanism of photoconductivity in organic substances, it was desirable to choose a substance with the following properties: (i) it should present a relatively simple molecule; (ii) it should be obtainable in a high degree of purity; (iii) it should be obtainable in a convenient crystal form. These conditions were fulfilled by the anthracene crystals that were commercially obtainable for use in scintillation counters. Four such crystals were available to us; they were all about one inch square and between one and two-tenths of an inch in thickness. When irradiated with ultraviolet light they emitted the blue fluorescence characteristic of pure anthracene. (The principal impurity of anthracene is usually naphthacene, which, if present in minute amounts, will quench the blue fluorescence and instead will cause the crystal to give out the greenish fluorescence characteristic of the naphthacene molecule.[5]) On visual examination the crystals showed a few flaws (including completely internal cracks) but by suitable placing of the electrodes, the experiments could be performed on parts of the crystals that were free from such obvious flaws.

Anthracene is one of the few organic compounds in which the internal photoelectric effect has been studied previously. Byk and Borck first noted that anthracene placed between two charged plates became conducting when illuminated.[6] Volmer[7] studied the internal photoelectric effect and found that a photocurrent was produced if the anthracene was illuminated in its fundamental absorption band, i.e., with wavelengths shorter than 4000A. More recently, Bayliss and Riviere[8] have attempted to measure the photoelectric effect, but their results were criticized by Vartanyan,[9] who pointed out that the method employed by them would lead to quite erroneous results. Vartanyan stated that he had detected an internal effect in anthracene, that the photocurrent took about a minute to reach an equilibrium value after the illumination was commenced, and that the photocurrent obeyed Ohm's law.

EXPERIMENTAL ARRANGEMENT

All the experiments to be described concerned the measurement of the direct current produced when the crystal was illuminated between two electrodes across which there was connected a high voltage. The photocell is shown in Fig. 1. The crystal was mounted on a hollow metal table through which could be circulated a suitable fluid to control the temperature of the crystal. The crystal was electrically insulated from the table by a thin disk of fused quartz. Two different electrode assemblies were used: (i) the sandwich cell, in which the crystal was placed between the electrodes; the lower electrode was a disk of platinum and the upper electrode was a very fine platinum gauze; (ii) the surface cell, in which the two electrodes were both placed on the upper surface of the crystal and separated by a gap of one or two millimeters. The whole crystal-electrode assembly was held rigid by another polished quartz disk on top of the assembly, the disk being pressed down by means of spring clips. The photocell was mounted in a chamber that could be evacuated. The light source was a Hanovia mercury vapor lamp, and a

* National Research Council Report No. 3253.

† National Research Laboratories postdoctorate fellow. Present address: Bell Telephone Laboratories, Murray Hill, New Jersey.

[1] Z. Petrikaln, Z. physik. Chem. **B10**, 9 (1930).

[2] A. T. Vartanyan, J. Phys. Chem. (U.S.S.R.) **20**, 1065 (1946).

[3] A. T. Vartanyan, Acta Physicochim. (U.S.S.R.) **22**, 201 (1947).

[4] A. T. Vartanyan, Zhur. Fiz. Khim. **24**, 1361 (1950).

[5] E. J. Bowen, *Chemical Aspects of Light* (Oxford University Press, London, 1946), second edition, p. 180.

[6] A. Byk and H. Borck, Ber. deut. physik. Ges. **8**, 621 (1910).

[7] M. Volmer, Ann. Physik. **40**, 775 (1913).

[8] N. L. Bayliss and J. C. Riviere, Nature **163**, 765 (1949).

[9] A. T. Vartanyan, Doklady Akad. Nauk. (U.S.S.R.) **71**, 641 (1950).

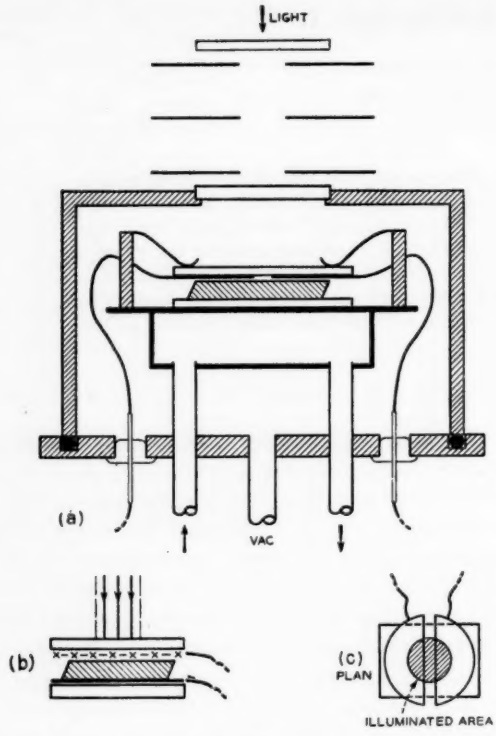

FIG. 1. The experimental photocell. The electrode arrangements are shown: (b) for the sandwich cell; (c) for the surface cell.

beam of light was directed on to the crystal by means of an external slit system. Suitable filters were placed in the light beam when required and for all these experiments, unless otherwise stated, a filter was used that cut off all radiation of wavelength shorter than about 2800A. The external photoelectric effect for anthracene has been studied by Hughes[10] who found that the threshold wavelength was about 2200A. Furthermore, the magnitude of the photocurrent was unaltered when the crystal was placed in an atmosphere of nitrogen or argon. It could therefore be assumed that all the currents measured originated as the internal photoelectric effect. The light intensity could be varied over a range of about 20:1 by placing previously calibrated wire gauze screens in the beam.

A regulated high-voltage supply enabled fields of up to several thousand volts per cm to be obtained. The other crystal electrode fed into a dc amplifier. The time constant of the input circuit was of the order of 10^{-1} sec; this was somewhat less than that of the Speedomax paper recorder that was connected to the output of the amplifier.

It was soon found that when the crystal was irradiated in the presence of a field, a space charge was set up very rapidly. This space charge reduced the effective field inside the crystal, thereby causing some reduction in the current. On removing the field, a current could be obtained in the opposite direction when the crystal was kept illuminated though very little space charge current occurred in the dark. The space charge current decayed to zero when an equal and opposite space charge had built up, and the net result was that the crystal would behave immediately afterwards as if "space-charge-free."

In order to attain the space-charge-free condition before each measurement it was convenient to provide for automatic switching on and off of (i), the electric field, (ii) the light beam, and (iii), the amplifier. To do this a commutator was built similar to that described by one of the authors elsewhere.[11] By means of this commutator the following cycle of operations was performed: (1) The field was switched on, followed quickly by (2), the switching on of the amplifier. After a suitable pause the light was switched on (3). After the photocurrent had attained its peak or equilibrium, the light was switched off (4), followed by (5), the switching off of the amplifier and (6), the field. The amplifier was then switched on again (7), followed by the light (8). As there was no field during this illumination, the space charge was gradually neutralized, and when the photocurrent had reached zero the light was switched off (9), followed by the amplifier (10). The whole cycle was then repeated and the steady cycle could be carried on indefinitely. With the commutator the timing of the various makes and breaks could be varied between wide limits, and the contacts were therefore adjusted so that the condition of zero space charge current was always reached before applying the field. The field was controlled by an electromagnetic relay, the light beam was controlled by an electromagnetic shutter, and the amplifier input could be grounded by a Raytheon thermal delay relay. It was necessary to switch off the amplifier when the voltage surge took place so as to prevent it from overloading.

The behavior of the current throughout the cycles, as recorded on the paper recorder, is shown in Fig. 2. It will be seen that by adopting the cycle technique, a measurement of the dark current could be made before each photocurrent measurement. In all experiments it was found that the dark current was never more than 10^{-13} amp, usually considerably less. These

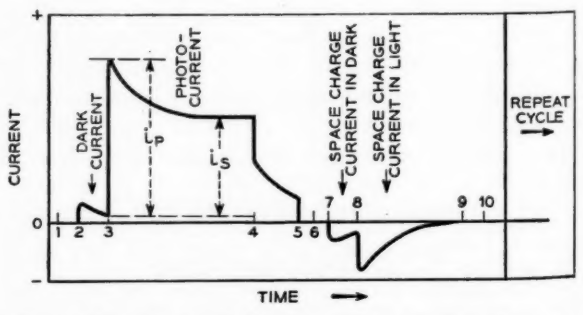

FIG. 2. The variation of the current with time throughout the field-light cycle controlled by the commutator.

[10] A. L. Hughes, Phil. Mag. **24**, 380 (1912).

[11] A. G. Chynoweth, Phys. Rev. **83**, 254 (1951).

currents were generally negligible compared with the photocurrent.

INTERPRETATION OF CURRENT CYCLE

The significance of the behavior of the current during the cycle will now be considered. It was found that in general both the sandwich cell and the surface cell showed similar behavior as regards this cycle.

Referring to Fig. 2, it will be noted that there was some space charge current in the dark. This, presumably, was due to the thermal release of charge carriers from shallow traps, the current decaying to a negligible value when the emptying of the shallow traps had been completed. However, carriers lying in deep traps were unaffected in the dark, and there remained a residual space charge which was observed to be undiminished even after several days. To neutralize this residual field it was found necessary to illuminate the crystal for a period with light of wavelength shorter than 4000A, i.e., in the fundamental absorption band. After this illumination, the net space charge field was zero as demonstrated by the criterion described above. The light had either: (i) liberated the deeply trapped carriers, or (ii), liberated lattice electrons and holes. The space charge was neutralized, therefore, by either of two possible processes: (i) the carriers liberated from traps could recombine, or (ii) liberated electrons and holes could become trapped or retrapped so as to set up a space charge opposing and neutralizing the former space charge. Thus, after a period of field-free illumination the net space charge field was zero, though there may still have been many trapped carriers in traps of different depths. Wavelengths longer than those necessary for exciting the crystal were found to be ineffective for detrapping the carriers. Similar behavior has been observed by Garlick and Mason[12] in some inorganic phosphors, even though they possess large numbers of traps.

When a field was applied in the dark a small current flowed, though it decayed to a negligible value after a few seconds. The rate of decay of the dark current was unaffected by illumination with yellow or red light. Further, the transient dark current could be observed whatever the period that had elapsed since the previous field-free illumination, i.e., up to several days. It was most unlikely that the field could modify the depth of the deep traps to such an extent as to make thermal release of these carriers so much easier, and it was therefore concluded that the current surge was not caused primarily by the release of trapped carriers. An alternative explanation of the transient dark current will be proposed below.

Immediately on illuminating the crystal, the current rose by an amount i_p and then quickly started to decay to a steady value i_s, which it reached in about half a minute. It was observed that i_p was independent of whether or not the dark current had fully decayed. When the light was cut off, the current immediately fell to a much lower value and thereafter decayed away to zero. In general, the only noticeable difference in the behavior of the surface and sandwich cells during the cycle was that the ratio i_s/i_p was much smaller in the latter type.

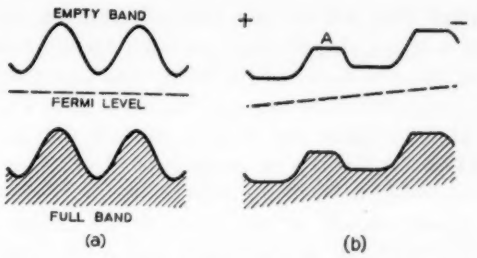

FIG. 3. The energy band diagrams for the crystal when (a) undisturbed, (b) under the influence of an applied field and illumination.

Thus, the field-light cycle allowed measurements to be made of (i), the dark current, (ii), the photocurrent in a space-charge-neutralized crystal, (iii), the eventual steady photocurrent, and (iv), the manner in which the current varied with time. Further consideration of the current behavior will be left until after a discussion of the possible energy band configuration.

ENERGY BAND DIAGRAMS

It has been customary in solid-state theory to regard the energy bands as level throughout the crystal. However, Wannier[13] has pointed out that in practice the bands will present undulations, as shown diagrammatically in Fig. 3(a). These irregularities are brought about by inhomogeneities in the trap distribution so that certain regions become negatively or positively charged according to whether the traps are mainly for electrons or holes. The effect that these irregularities have on the photocurrent will now be discussed; the discussion applies equally well whatever the sign of the majority carriers.

When left in the dark, the energy bands adjust themselves with respect to the Fermi level so as to reach an equilibrium state, as in Fig. 3(a). When a field is applied, still in the dark, this equilibrium is disturbed because of the changes in barrier widths and heights brought about both inside the crystal and at the crystal-electrode boundaries. Thus, there will be a net flow of charge until a new equilibrium distribution is obtained, this flow constituting the transient dark current.

When the crystal is illuminated, many electrons and holes are created, and these will drift through the crystal under the influence of the applied field, thus giving rise to the photocurrent. The motion of the carriers, however, will be particularly restricted in the neighborhood of the potential barriers and if they cannot surmount

[12] G. F. J. Garlick and D. E. Mason, Trans. Electrochem. Soc. 96, 90 (1949).

[13] G. H. Wannier, Phys. Rev. 76, 438 (1949).

the latter, they will become trapped in such a way as to set up a space charge field opposing the applied field. In this way the floors of the wells (and also the barrier peaks) will gradually become flattened as in Fig. 3(b), so that eventually the regions around the gross imperfections will carry no more current. In the normal lattice, devoid of such imperfections, the photocurrent will remain steady all the time. Space charge effects here will be small in the case of the surface cell if the mean free path of the carriers is small compared to the crystal dimensions, as then the charges will neutralize one another over the bulk of the crystal.

Thus, we regard the crystal as a normal lattice containing randomly scattered, grossly perturbed regions. The normal lattice contributes a time invariant component to the photocurrent, while the large irregularities contribute a current that decays smoothly to zero. The total current will then behave as in Fig. 2.

FIELD DISTRIBUTION IN THE CRYSTAL

In the preceding section it was tacitly assumed that there is a more or less uniform potential drop across the crystal when an external field is applied. In view of the possible complications at the crystal-electrode boundaries and large flaws, it was safer first to justify this assumption by some experiment. To do this a surface cell was set up in which the electrodes were separated by a gap of several millimeters. A slit of light one millimeter in width was then collimated on to the crystal so that the illuminated strip lay parallel to the electrodes. Keeping the field and light intensity constant, the photocurrent was measured as the slit was moved, one millimeter at a time, from one electrode to the other. To within experimental error the photocurrent remained constant for the whole distance between the electrodes. On the conventional picture of the behavior of a photoconductor this would suggest that the field was uniform across the crystal. There is another possibility, however: it is known that anthracene can transmit energy through its lattice by the process of quantum-mechanical resonance. Thus, the absorbed energy could migrate out of the illuminated zone to find elsewhere a suitable center for the liberation of carriers. If this is the explanation of constant photocurrent, then the field distribution need not be uniform. In this case suppose that, as would be most likely, most of the drop in field took place near one of the electrodes; then the energy would of necessity have to travel a mean free path of several centimeters if carriers were to be excited in the region of one boundary when illumination was taking place at the other. Moreover, it seems more likely that most of the energy would end up at other boundaries rather than reach the active boundary and again one would expect a gradual drop in photocurrent as the slit moved away from the hypothetical active layer. It was concluded, therefore, that the field was, in general, uniform throughout the crystal (that is, apart from local variations).

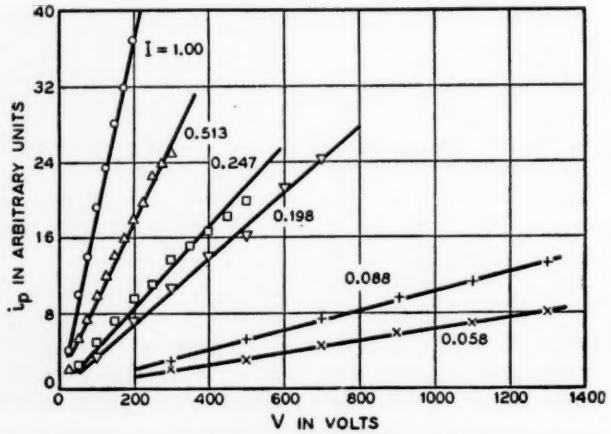

FIG. 4. The variation of the peak current i_p with applied voltage for various light intensities using the surface cell.

CURRENT-FIELD RELATIONS

In Fig. 4 the measured current i_p (taken to correspond to space-charge-neutralized conditions) is plotted against the applied voltage for various light intensities. It is seen that, to within experimental error, a series of straight lines resulted and that there was no suggestion of the current approaching a saturation value at the highest fields used (up to 10 000 v/cm). It was concluded that the mean free path of the carriers was small compared to the distance between the electrodes.

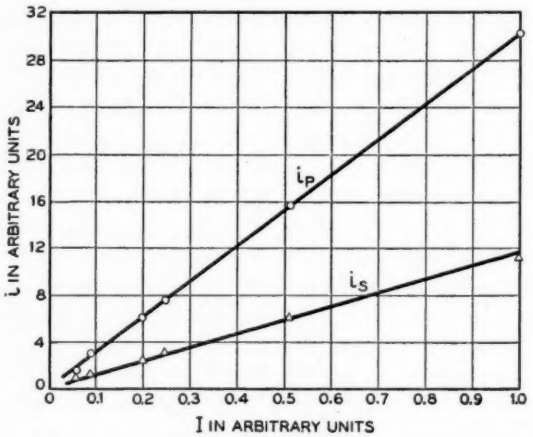

FIG. 5. The dependence of the peak and steady currents on the light intensity for the surface cell.

The currents i_s were also found to increase linearly with the applied field.

In terms of the above picture, when the carriers in a potential well had redistributed themselves, no further current flowed in the region of the well. In effect, this region of the crystal had been eliminated from taking part in the photocurrent, and similarly, when all other such regions had been eliminated, the effective volume of the crystal was reduced by a certain fraction, f. Consequently, the total photocurrent was likewise re-

duced by the same fraction f, irrespective of the actual light intensity or the applied field. The steady photocurrent i_s was drawn through the crystal in those regions unaffected by such large potential fluctuations and space charge effects. Hence, this current was proportional to the applied field.

CURRENT-LIGHT INTENSITY RELATIONS

From plots like those of Fig. 4 the currents i_p and i_s could be plotted against the light intensity. This is done for a given field in Fig. 5, and it is seen that both i_p and i_s were proportional to the light intensity to within experimental error. These results were interpreted as further support of the above picture. For instance, suppose instead that the diminution in current from i_p to i_s was due entirely to the building up of a corresponding space charge field. Then, from Fig. 5, the magnitude of the space charge field should be proportional to the light intensity, or, to a fair approximation, the number of trapped charges in the steady

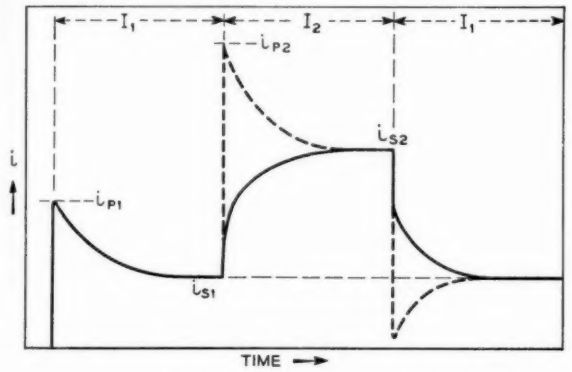

FIG. 6. The time variation of the current when the light intensity is suddenly altered. (Surface cell.)

state should be proportional to the light intensity. Now in the steady state the rate of creation of carriers equals the rate of recombination, and, also, the rate of trapping of carriers equals the rate of detrapping. Such conditions of equilibrium normally do not lead to a space charge field proportional to the light intensity.

In another experiment the current was allowed to reach its steady value i_{s1} at a given light intensity I_1. Then the intensity was raised suddenly from I_1 to I_2. The current followed the curve shown in Fig. 6. If a formation of space charge were solely responsible for the decay from i_{p1} to i_{s1}, it would be expected that when the intensity was increased, the space charge would have to grow to a new equilibrium value. Thus, the current would be expected to show a peak i_{p2} followed by a decay to a steady value i_{s2}. Instead, the current was observed to grow steadily to the value i_{s2}. Likewise, the current decayed continuously to the value i_{s2} again when the intensity was reduced suddenly to I_1. This behavior was also in conformity with the aforementioned ideas. The redistribution of electrons in

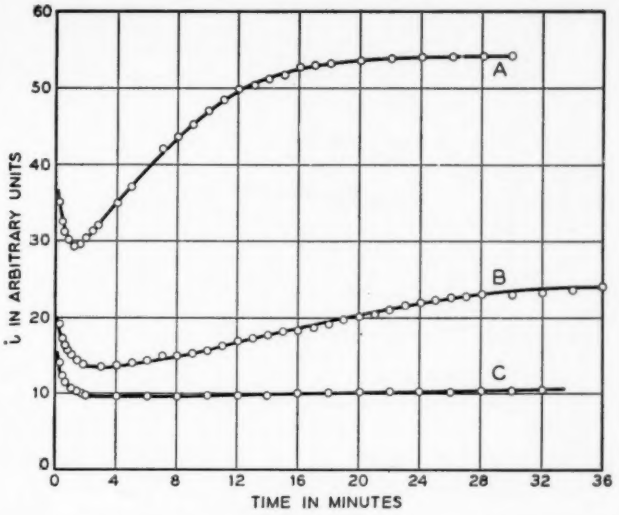

FIG. 7. The variation of the current in the surface cell with time. (A) At high field and high light intensity; (B) at high field and moderate light intensity; (C) at moderate field and high light intensity.

the potential wells was complete when the current reached i_{s1}. Thereafter, there was negligible time dependent current from these regions no matter how the light intensity was varied; thus, the peak i_{p2} was not observed.

EFFECT OF PROLONGED IRRADIATION AT HIGH FIELDS

Referring again to Fig. 3, it might be expected that if the potential irregularities were smoothed out by some means, the mean free path of the carriers would be increased. Now there must always be a slow leak of carriers over the potential barriers, and thus, after a sufficient time has elapsed, the current should have increased. The rate of leakage of the carriers will increase steadily with light intensity (owing to the greater rate of creation of free carriers). It will also rise rapidly with the applied field since the rate of flow over the potential barrier is a sensitive function of the field. Thus, the smoothing out of the barriers and walls will take place more quickly the greater the light intensity and the greater the field.

A. Results with the Surface Cell

In Fig. 7 are plotted curves showing the variation of the current with time under prolonged illumination of the whole of the crystal between the electrodes. Curve A was taken at a high field and high light intensity and shows well the later increase of the current towards a steady value. When the steady state had been reached, then according to the ideas expressed in the preceding paragraph, all the possible smoothing out of the energy bands had taken place. Curve B shows the changes that occurred when the light intensity was halved from that of Curve A, the field being kept the same. The curve shows the same form as A but, as expected, it took

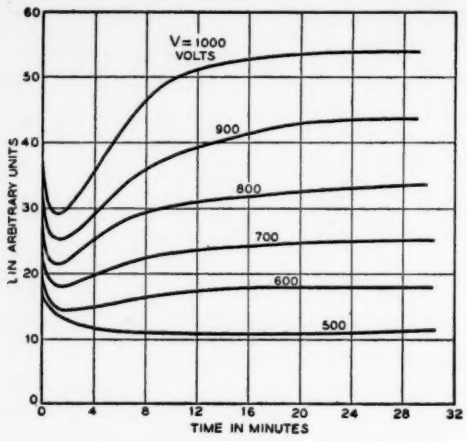

FIG. 8. The variation with time of the current in the surface cell for a high light intensity and various fields.

roughly twice as long to reach the steady state. The eventual steady current was approximately half that of Curve *A*.

Curve *C* shows the effect of halving the field from that of Curve *A* but keeping the light intensity the same. It will be noted that after the initial decay there was a very slight rise in the current which took several hours to reach a steady state. Thus, as predicted, the effect of reducing the field was to lengthen considerably the time required for the smoothing out process to be completed.

A series of curves taken at different voltages is shown in Fig. 8, where the effect of gradually increasing the applied field is brought out more clearly.

B. Sandwich Cell

An effort was made to determine whether the aforementioned types of curves could be obtained with the sandwich cell under similar conditions. It was found that when the crystal was subjected to simultaneous application of a high light intensity and high field there was no evidence of a later rise towards a steady current. That is, the current showed the initial peak followed by a decay towards a steady value i_s. (In these experiments the illuminated electrode was positive.) The indications were that, owing to the thickness of the crystal, the applied field was not sufficiently great to reproduce the effect observed with the surface cell where the electrodes were much closer to each other.

DECAY OF SPACE CHARGE IN THE DARK

It was noted above that there was some space charge current in the dark and that this was due, presumably, to the thermal release of trapped carriers. By modification of the experimental technique the rate of decay of the space charge field could be investigated. To do this, the crystal was first subjected to a period of intense illumination in the presence of a high electric field. This treatment created a space charge field in the crystal and the period of illumination required for the space charge field to reach its maximum value was found by a separate experiment. Having reached this condition, the light and field were removed simultaneously and the crystal left in the dark for a measured time interval. At the end of the interval the light was again switched on (in the absence of the field) and the initial value of the space charge current was recorded. This procedure was repeated for a large number of different intervals and by assuming that the initial current was proportional to the space charge field (by analogy with the linearity between the space charge free current and the applied field), the variation of the space charge field with time could be obtained. This is shown in Fig. 9, where it is seen that the field decayed to a steady value in about twenty minutes. No further decay took place even after the crystal had been kept in the dark for three days. The rapidly decaying component of the space charge field was found to have a half-life of about 250 sec.

In order to make a rough estimate of the trap depth, two further assumptions were made: (i) that the space charge field was approximately proportional to the

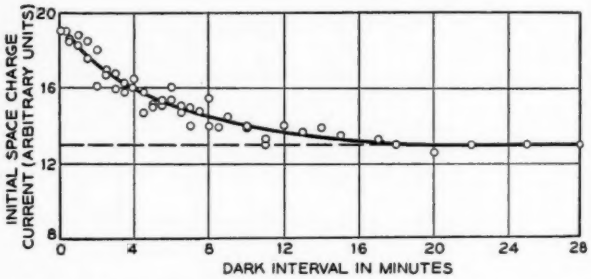

FIG. 9. The decay of the space charge field with time when the crystal is left in the dark and without an external field. (Surface cell.)

number of trapped charges, and (ii) that the decay during the first twenty minutes was caused by carriers being released from one mean trap depth only and with no retrapping. Then, if n is the number of "insecurely" trapped carriers at a given instant,

$$(dn/dt) = -ns \exp(-E/kT),$$

where s is a constant, E is the thermal trap depth, and T is the absolute temperature.[14] From this equation the half-life for the trapped carriers is

$$\tau = \ln 2/s \exp(-E/kT).$$

Assuming s to be of the order of 10^8 sec^{-1},[14] $\tau = 250$ sec, then the thermal trap depth was approximately 0.6 ev. The significance of this particular trap depth has not been investigated.

EFFECT OF TEMPERATURE ON THE PHOTOCURRENT

In Fig. 10 is shown the dependence of the space-charge-neutralized photocurrent on the temperature,

[14] J. T. Randall and M. H. F. Wilkins, Proc. Roy. Soc. (London) **A184**, 366 (1945).

over a rather limited range. Several plausible models for the energy band diagram were analyzed to see whether their predicted current-temperature behavior would fit the experimental results. For each model the analysis depended upon the attainment of equilibrium between: (i), trapping and detrapping of carriers, and (ii), creation and recombination of free carriers. Several conventional trapping mechanisms were considered, and also dealt with was the case of the light energy exciting existing carriers to a metastable level with their subsequent release by thermal energy. The current-temperature relation yielded by each of these models was operated on so as to give a straight line plot and this was compared with the experimental results. Only one model gave good agreement; the other models gave results completely at variance with the experiment.

The agreement was obtained using a model based on an exponential distribution of trap levels, as discussed recently by Rose.[15] Rose obtains the following current-

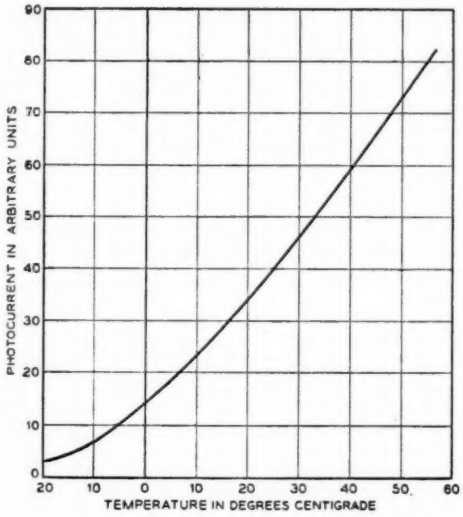

FIG. 10. The variation of the space-charge-neutralized photocurrent with temperature.

temperature dependence:

$$i_p=\alpha\left[\left(\frac{\beta I}{v\sigma T_1}\right)^{T_1/(T+T_1)}\right]\cdot N_c^{T/(T+T_1)}.$$

Where α, β are constants; v is the thermal velocity of the carrier; σ is the cross section for recombination of a hole and an electron; N_c is the number of accessible states at the bottom of the conduction band; T is the absolute temperature; and T_1 is some characteristic temperature. The following relation can be obtained easily:

$$[d(\log i)/dT]^{-\frac{1}{2}}=T/cT_1^{\frac{1}{2}}+T_1^{\frac{1}{2}}/c,$$

where c is a constant if the temperature variation is not too great. Thus, a plot of $[d(\log i)/dT]^{-\frac{1}{2}}$ against T

[15] A. Rose, R.C.A. Rev. **12**, 362 (1951).

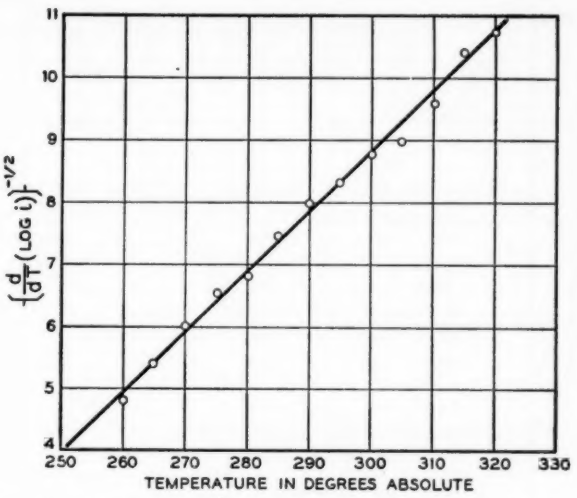

FIG. 11. A temperature plot based on the assumption that there is an exponential distribution of trap depths.

should be a straight line. In Fig. 11 it is seen that the experimental points conform to a straight line remarkably well. From this fact, together with the observation that all other models failed completely to conform to the experiment, it was tentatively concluded that the number of carrier traps decreased approximately exponentially as their depth increased.

CURRENT-FIELD RELATIONS FOR THE SANDWICH CELL

The photocurrent was measured as a function of the voltage applied across the sandwich cell for both directions of the field in turn. The results are shown in Fig. 12. The curve denoted by circles was taken with the illuminated electrode positive and the curve shown by triangles with it negative. It is seen that the current in the latter curve approaches a steady value while that in the former increases steadily.

After striking the crystal the light energy in the fundamental absorption band is absorbed in a small fraction of a centimeter. Assuming that the creation of free carriers takes place fairly uniformly, then, on the average, the carriers can be regarded as being created at a depth α below the crystal surface where $1/\alpha$ is of the order of the absorption coefficient; i.e., $\alpha\sim10^{-4}$ cm.[16] If only one sign of carrier is free to move, the other being rapidly and firmly trapped, the current will show a saturation when the mean free path of the carriers is of the order of 10^{-4} cm and they are proceeding towards the illuminated electrode. Thus, from the above results it would appear that positive holes were mainly responsible for carrying the photocurrent. This agrees with Putseiko,[17] who determined the sign of the carriers of the photocurrent in a large number of substances. Thus, at fields of the order of 2000 v/cm

[16] Reference 5, p. 127.

[17] E. K. Putseiko, Doklady Akad. Nauk. (U.S.S.R.) **67**, 1009 (1949).

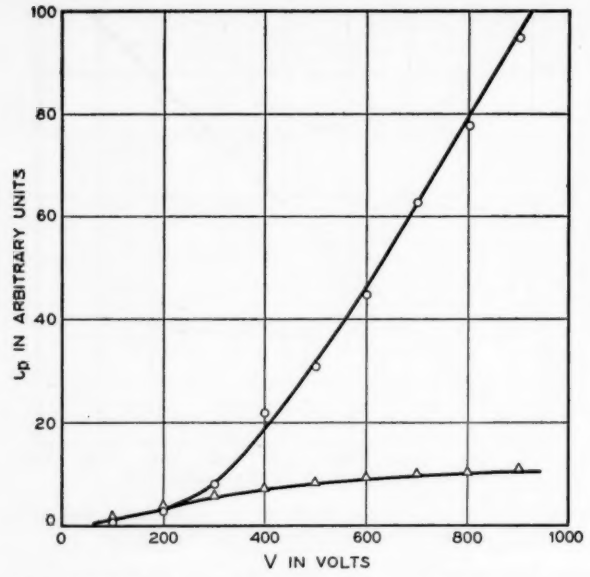

FIG. 12. The dependence on the applied field of the peak current in the sandwich cell when the illuminated electrode is (a) positive (circles), (b) negative (triangles).

the mean free path of the holes, λ, was of the order of 10^{-4} cm. Since $\lambda=\mu F\tau_0$ where τ_0 is the mean free time of the carrier, F is the field strength, and μ is the mobility, $\mu T\simeq 5\times 10^{-8}$. If $\tau_0\sim 5\times 10^{-8}$ sec,[18] this gives $\mu\sim 1$ cm^2/sec/v, a figure comparable to the values obtained in photoconductivity experiments with some inorganic substances possessing high trap densities.[15]

CONCLUSIONS

Crystalline anthracene has been found to photoconduct when illuminated with wavelengths lying within its fundamental absorption spectrum. These wavelengths are not sufficiently energetic to liberate electrons completely[19] and from this fact, together with the observation that the majority of the charge carriers are positive holes, we suggest the following mechanism: When light is absorbed by the crystal, electrons are excited either directly, or through the intermediate process of exciton formation, into a metastable level. From this level they can either recombine with the hole (fluorescence) or make a transition to a relatively stable trapping level. The holes drift through the crystal under the action of the field, but their rate of drift is influenced by hole traps of various depths. The number of these traps appears to decrease exponentially with their height above the valence band. Many hole traps seem to be very high and at room temperature can be emptied only by optical energy. Further, under steady-state conditions, recombination must be occurring between positive holes in the full band and the trapped electrons. It is easy to show that, if the optical release of trapped holes is dominant over thermal detrapping, the mode of action postulated can give rise to a current that varies linearly with the light intensity, as observed.

The experiments have been considered on the basis of the energy band picture usually associated with inorganic crystals. The picture seems to serve sufficiently well for organic crystals also, as far as the above experiments are concerned. To explain particular results, Wannier's hypothesis of undulating energy bands was used with some success. It seems probable that undulating energy bands are a property of insulating crystals in general.[20]

The study of the photoconductivity of conjugated compounds may prove to be of considerable interest, particularly in view of their occurrence in nature. In this connection, chlorophyll, the carotenoids, and carcinogenic molecules are of some interest, the former because of its obvious relation to photosynthesis. Carotenoid compounds, which contain long conjugated chains, are found in the retina of the eye where the existence of electric fields has often been demonstrated. Perhaps photoconductivity plays a part in the primary process of vision?

[18] Estimates of τ_0 have been made for a number of inorganic crystals, especially those used for conduction counters. The figures used above are a reasonable mean of the published results.

[19] E. J. Bowen, Nucleonics **10**, 14 (1952).

[20] Results similar to the current-time variations described above have been observed by various authors in diamond crystal counters: A. G. Chynoweth, Phys. Rev. **76**, 310 (1949); R. K. Willardson and G. C. Danielson, Phys. Rev. **77**, 300 (1950); G. P. Freeman and H. A. van der Velden, Physica **16**, 493 (1950); S. Kojima and S. Kono, J. Phys. Soc. Japan **7**, 84 (1952).

The Effect of Oxygen on the Photoconductivity of Anthracene. II*

A. G. CHYNOWETH†‡
National Research Laboratories, Ottawa, Canada
(Received November 30, 1953)

The photoconductivity in the surface layers of crystalline anthracene has been found to increase considerably over its vacuum level when it is measured in the presence of oxygen or air. Replacing the oxygen by nitrogen or argon causes no such increase. The increased photoconductivity is attributed to the photo-oxidation of the surface, both the light and the oxygen being necessary to produce the effect. No reaction takes place in the dark. The oxide formed is fairly unstable and dissociates in the dark. Its rate of dissociation is considerably increased when the crystal is illuminated in the absence of oxygen. The experiments indicate that the peroxide is formed by a two-stage process, the highly unstable intermediate product being formed very rapidly while the final peroxide is formed much more slowly. The nature of the intermediate product is not known for certain. The end product is very likely the oxide formed by an oxygen bridge across the 9, 10 carbon atoms of the anthracene molecule. Apparently, both the oxidation products modulate the photocurrent solely by their effect on the mean free path of the carriers; the intermediate product producing a relatively large increase while the end product produces a smaller decrease in the mean free path.

It is suggested that the technique of photoconductivity measurements might prove to be useful in the study of the kinetics of certain photochemical reactions.

INTRODUCTION

IN the preceding paper[1] experiments were described which established some of the photoconductive processes in pure crystalline anthracene in vacuum. During the course of some experiments with compressed samples of powdered anthracene it was noticed that when the photocell was opened to the air, there followed a large increase in the photoconductive sensitivity over its value as measured in vacuum. This effect was found to be reversible; the vacuum level of photocurrent was again obtained after the cell had been pumped continuously for a sufficient period. This paper describes preliminary investigations of this effect and some speculations based on the observations.

Vartanyan[2] has observed that admitting oxygen to a photoconducting deposited film of anthracene increases the photoconductivity, in contrast to the results of Bayliss and Riviere;[3] there is reason to believe that the latter's experiments were confused with the external photoelectric effect. However, Vartanyan does not enlarge upon his observation and the author does not know of any subsequent publications by him on the photoconductivity of anthracene.

EXPERIMENTAL OBSERVATIONS

(a) Steady Conditions

In some preliminary experiments on the photoconductivity of compressed samples of powdered commercial anthracene, using a sandwich cell and the space-charge-neutralization technique described in paper I,[1] photocurrents of the order of 10^{-10} to 10^{-11} amp were obtained in vacuum. However, when the photocurrent was measured in the presence of air it was found to have increased by a factor of approximately five. After two or three days of continuous pumping (at a dynamic pressure of the order of 10^{-6} cm of mercury) the photocurrent regained its original vacuum value and the whole cycle could then be repeated, apparently indefinitely. In order to obtain more meaningful results, experiments were then made on single crystals of pure anthracene.

The first experiments with the single crystal were made using the surface cell arrangement. The illumination was afforded by a mercury vapor lamp with a filter preventing radiations of wavelengths shorter than 2800A from reaching the crystal. The procedure was to measure the current-voltage characteristics, at a standard light intensity, after various treatments.

The photocell was first pumped in the dark for several days after which measurements were made at daily intervals in order to establish that the photoconductivity had reached its equilibrium value. The points denoted as "Run 1" in Fig. 1 show the current-voltage characteristic under vacuum conditions. Next, dry oxygen was admitted to the cell in the dark and allowed to remain there at atmospheric pressure for nineteen hours. Measurements were again taken after the photocell had been pumped out for two hours in the dark. No significant change in the photocurrent had taken place (Run 2 of Fig. 1).

On completion of the above tests, one atmosphere of dry oxygen was again admitted to the cell which was then kept illuminated for nineteen hours. The light was then shut off, the cell was pumped for two hours, and the current-voltage characteristic obtained (Run 3). Again there was no significant change in the conduc-

* National Research Council Report No. 3287.
† National Research Laboratories Postdoctorate Fellow.
‡ Present address of author: A. G. Chynoweth, Bell Telephone Laboratories, Inc., Murray Hill, New Jersey.
[1] A. G. Chynoweth and W. G. Schneider, J. Chem. Phys. **23**, 1021 (1954).
[2] A. T. Vartanyan, Doklady Akad. Nauk. U.S.S.R. **71**, 641 (1950).
[3] N. L. Bayliss and J. C. Riviere, Nature, **163**, 765 (1949).

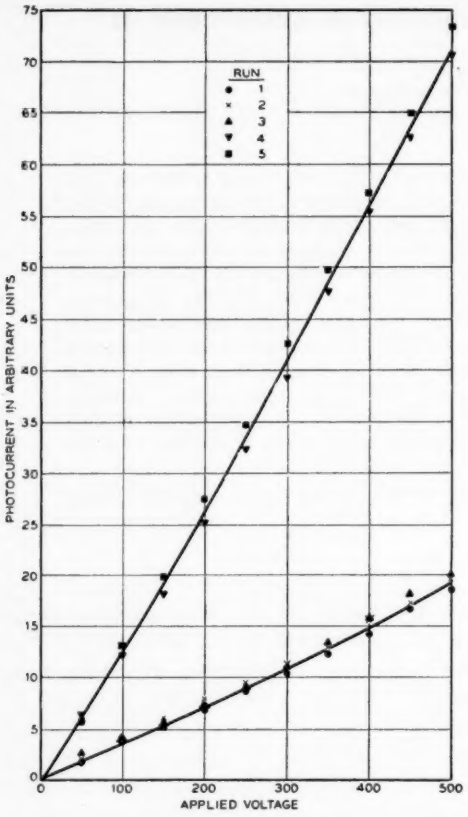

FIG. 1. The photocurrent plotted against the applied voltage after various treatments: (1) After being kept in the dark and in vacuum for several days. (2) After being left in oxygen in the dark for several hours, the measurements being made in vacuum. (3) After being left in oxygen for several hours while illuminated, the measurements being made in vacuum. (4) After being left in oxygen for several hours while illuminated, the measurements being made with the oxygen still present. (5) After being left in air for several hours while illuminated, the measurements being made with the air still present.

tivity from that of Run 1. This behavior was very different to that of the experiment with the powdered sample, where, after photo-oxygen treatment, an increased photoconductive sensitivity remained appreciable over a period of days.

Next, the oxygen was admitted to the cell for sixteen hours while the crystal was kept illuminated. Current measurements were then made with the oxygen still present. This time the currents were about three times as large as those measured previously, as shown by Run 4. After a subsequent two hours of pumping the photocurrents again reproduced the vacuum readings. (It should be noted that the current readings in all these experiments were reproducible, whatever the order of voltage settings.)

In order to be sure that the increased conductivity was not associated with a gas discharge the experiments were repeated using atmospheres of nitrogen, and argon. These gases produced no observable change in the photoconductive sensitivity. When, however, air was allowed into the cell, the experiments repeated those made with oxygen. Thus it was concluded that oxygen was necessary for the increase in conductivity to take place. Further, to within the limits of experimental error, the partial pressure of oxygen in air was sufficient for the chemical effect to saturate (Run 5, Fig. 1). No other investigation was made of the effect of oxygen pressure.

By taking measurements immediately after the crystal had been kept in oxygen in the dark for several hours, it was established that such treatment did not produce any increased conductivity. Thus, in order to increase the conductivity it was necessary to illuminate the crystal while in the presence of oxygen. This conclusion was verified by a large number of experiments in which variations were made in the oxygen and light treatments and the time intervals.

All the foregoing experiments were concerned with the surface cell. The experiments were repeated using the sandwich cell for both directions of the applied field, as the current-voltage characteristic differs between the two directions.[1] After an intensive study it was established that the photo-oxygen treatment increased the photoconductivity for both directions of the field, but by only 10 to 20 percent as compared with about 200 percent for the surface cell. This result is at variance with that obtained using the powdered sample though this can be taken as further evidence for the deeper penetration of the air around the powder grains.

(b) Nonequilibrium Behavior

The photochemical reactions taking place lead to an unstable product as evidenced by the fact that pumping the crystal for two hours in the dark after photo-oxygen treatment returned the crystal to its vacuum state of conductivity. Most probably, the photochemical reaction was confined to the surface of the crystal. This could explain why the enhanced conductivity disappeared more rapidly in the case of the single crystal than in the powdered sample. In the latter, the gas would penetrate between the grains and would be more difficult to remove.

Some idea of the rate of dissociation of the unstable product was obtained from the following experiment. The crystal was brought to its state of high conductivity by photo-oxygen treatment, and the photocurrent was measured at a high applied field in the presence of the oxygen. The light was then shut off and the oxygen pumped out. As soon as the pressure was low enough to withstand the high field (after 10 minutes of pumping) photocurrent readings were obtained as a function of time, always at the same field and light intensity. The results are shown in Fig. 2 where it is seen that the photoconductivity decayed slightly during the ten-minute dark period. Of course, in order to take the readings, the crystal had to be illuminated both during the actual measurements, and the period

for space-charge-neutralization between measurements. From Fig. 2 it is evident that the unstable state decayed much more rapidly when illuminated than when left in the dark.

We summarize the basic experimental observations: (i) The simultaneous action of light and oxygen produced a photochemical change on the surface of the crystal which increased greatly the photoconductive sensitivity along the surface layers, but only slightly increased it in a direction perpendicular to the surface, for both directions of the applied field. (ii) The photochemical change produced was unstable and the crystal reverted to its original condition in two hours or less in the dark, at room temperature. The rate of return to its original condition was greatly accelerated if the crystal was illuminated in vacuum.

(c) Effect of Varying the Light Intensity

In the foregoing experiments the same light intensity was used throughout, both for performing the photochemical reaction and for determining the photoconductive sensitivity. It was of interest to determine how this sensitivity depended on the light intensity.

The crystal was first illuminated in oxygen at maximum light intensity for seventeen hours. Readings were then taken of the photocurrent at a fixed field for different light intensities, the oxygen being present always. It was noticed that when the light intensity was altered the photocurrent took some time (20 to 30 minutes) to reach equilibrium. When the steady state was reached the current was noted. To within experimental error, and over the range of light intensities used (20:1), the equilibrium photocurrent was directly proportional to the light intensity. These current readings, it must be emphasized, refer to the crystal in the space-charge-neutralized condition and the time effects are not to be confused with those associated with the formation of a space charge in the crystal. The latter, from the experiments reported in paper I, were known to exhibit much faster rates of decay to equilibrium values.

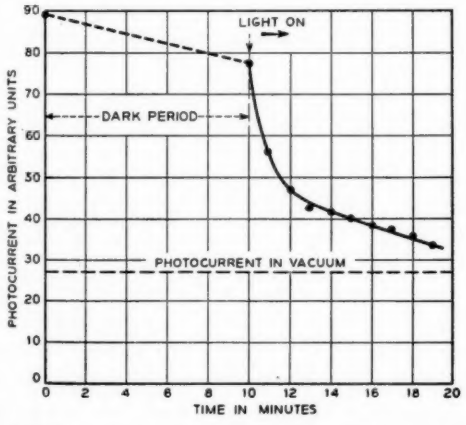

FIG. 2. The decay of the space-charge-neutralized photocurrent on pumping the oxygen out of the cell. The first ten minutes shows the decay that took place in the dark; the remainder of the curve shows the accelerated decay when the crystal was illuminated.

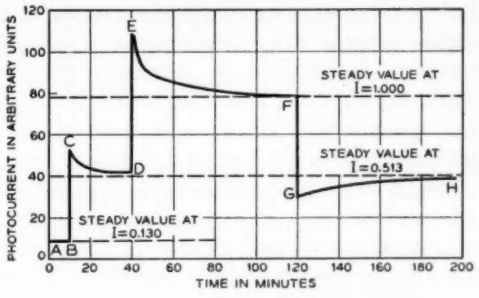

FIG. 3. The behavior of the space-charge-neutralized photocurrent when the light intensity was suddenly altered. At *B*, *D*, the intensity was suddenly raised while at *F*, it was suddenly lowered.

The manner in which the photocurrent approached a new equilibrium value after a change in light intensity was of significant interest. This is shown in Fig. 3. Portion *AB* represents the steady photocurrent measured with a light intensity I_1. At *B* the intensity was suddenly raised from I_1 to I_2 and it is seen that the current rose rapidly, *BD* (instantaneously compared to the response time of the apparatus), followed by a gradual decay over a considerable time to a new equilibrium level, higher than *AB*. Increasing the light intensity further, from I_2 to I_3, caused a similar initial peak followed by a decay (*EF*) to a new higher level. At *F*, the light intensity was suddenly returned to I_2, and it is seen that the current initially dipped well below its eventual equilibrium level. Along *GH*, the current gradually rose to the same equilibrium value as previously at *D*.

DISCUSSION

It is reasonable to conclude that the increased photoconductivity in oxygen is caused by photo-oxidation of the anthracene. This process has been studied extensively by Dufraisse and co-workers[4] and by Bowen,[5] who conclude that: (a) The photo-oxidation of anthracene occurs in solution when irradiated with wavelengths lying within the fundamental absorption range of anthracene. (b) Probably, the final peroxide is formed by oxygen reacting with a highly unstable anthracene dimer to form first a weakly-bound complex, the latter then proceeding to further reaction to reach the more stable peroxide molecule. (c) The final peroxide can be dissociated readily by slight heating.

Several workers[6–8] have reported that oxygen

[4] C. Dufraisse, Bull. soc. chim. France, **6**, 422 (1939). A review article which gives many references to the photo-oxidation of organic compounds.

[5] E. J. Bowen, *Chemical Aspects of Light* (Oxford University Press, London, 1946), second edition.

[6] J. Weiss and H. Weil-Malherbe, J. Chem. Soc. **1944**, 541.

[7] J. Weiss, Nature **152**, 176 (1943).

[8] J. A. Miller and C. A. Baumann, J. Am. Chem. Soc. **65**, 1540 (1943).

quenches the fluorescence of anthracene but that the fluorescence returns when the oxygen is pumped out of the system or replaced by nitrogen. They believe that photo-oxidation of the anthracene is responsible for the quenching. These experiments obviously compare with the results reported in this paper.

The reason why photo-oxidation of some or all of the surface of the crystal should lead to an increased photoconductivity is not clear. In some inorganic photoconductors the presence of oxygen on the surface has been observed to increase the *p*-type conductivity in the surface layers. Two mechanisms for this increase have been postulated: (i) The oxygen atoms create additional electron traps which, when filled, are able to maintain a hole current through the crystal. This cannot be the explanation for the effects with anthracene as the mean free path of the carriers is very small compared with the crystal dimensions. (ii) Oxidation may create potential barriers whose height can be modulated by the photorelease of carriers nearby, this modulation resulting in the release of relatively large numbers of additional carriers. It was found difficult to accept this as an explanation of the anthracene results in view of the fact that the oxygen increased the photoconductivity (though only slightly) in the sandwich cell for both directions and all available magnitudes of the applied field.

It is now suggested that the photoconductivity results can be explained by assuming that the photo-oxidation reduces the rate of recombination of carriers in the surface layers. That is, the carrier lifetime (and hence the photocurrent) is larger in the peroxide than in the unoxidized anthracene. Thus, in the sandwich cell where the carriers spend most of their free time in the unoxidized part of the crystal, the photocurrent is increased only slightly, but it will be increased for both directions of the field. In the surface cell, the carriers find relatively much more oxidized anthracene in their path and consequently, there is a much larger increase in the photocurrent.

In view of the above hypothesis and the results depicted in Fig. 3, it is necessary to postulate a two-stage process for the formation of the oxide. Let the intermediate product be X_1 and the final product be X_2. Then, from Fig. 3, X_1 grows and decays very rapidly when the light is switched on or off while X_2 grows and decays more slowly. X_1 produces a large increase in the mean free path but as the concentration of X_2 grows, the effective free path decreases somewhat in order to account for the decay of the photocurrent along *CD*, *EF*, and also the growth along *GH*. (Removing the light at *F* leaves the crystal abnormally rich in X_2.)

It is tempting to associate X_1 with the highly unstable intermediate stages of photo-oxidation, as previously mentioned. If X_1 is a form of dimer it could conceivably account for the increase in the mean free path of the carriers though it is difficult to accept a picture of dimerization in the surface layers of a crystal. Alternatively, if X_1 is an intermediate form of oxide, as discussed by Dufraisse and Bowen, the joining up of loose bonds along the surface by oxygen molecules might also increase the mean free path of the positive holes.

It seems reasonable to regard X_2 as the more stable form of peroxide discussed in detail by Dufraisse, where the oxygen molecule forms a bridge between the 9, 10 carbon atoms. However, this structure results in a kinking of the anthracene molecule[4,9] and if this is occurring in the looser surface layers of the crystal one would expect some distortion of the lattice and the introduction of fresh carrier traps. In this way X_2 would serve to decrease the mean free path. Further, the ensuing destruction of the conjugated double bond system would be expected to reduce the mobility of the carriers.

The foregoing discussion suggests several possible lines of investigation and the technique of photoconductivity measurements might prove to be of some use in the study of the kinetics of certain photochemical reactions.

[9] I. Gillet, Bull. soc. chim. France **1950**, 1135.

Symbolic Structural Formulas for Boron Hydrides

JOHN R. PLATT
Department of Physics, University of Chicago, Chicago 37, Illinois
(Received January 5, 1954)

A structural convention is proposed, intended to serve the same function for boron hydrides that the standard valence bond convention serves for organic compounds. It involves the auxiliary concept of the "valence cone," which is the cone swept out by three tetrahedral orbitals rotating about the fourth as an axis. The known open boron hydrides B_nH_{n+p} then appear to be even-electron molecules with the boron atoms approximately in a close-packed equilateral-triangular network on the convex surface formed by their overlapping valence cones; with n single B—H bonds normal to this surface; and with p (even) added peripheral hydrogen in the surface located so that every boron atom has neighbors in all three sectors of its valence cone. As long as this network does not form a complete polyhedron, we may represent it on paper by a flat triangular network having the same topology.

This prescription gives uniquely and correctly the structures and formulas for the known B_2, B_4, B_5, B_6, and B_{10} hydrides and predicts other possible open compounds up to B_{11}. It would be consistent with the existence of closed inert polyhedral hydrides B_nH_n up to $B_{12}H_{12}$ and with chains and lattices of such polyhedra.

THE structures of organic compounds is represented on paper by the standard valence-bond convention with four lines connecting every carbon to its neighbors, and so on. This symbolism encompasses the practical empirical rules of chemical and physical behavior, such as the number and kinds of isomers; the primary, secondary, and tertiary differences; the topology of the system; and, with proper interpretation, the possible spatial geometries; although it ignores the finer details of bond angles and lengths, electron distribution, and dipole moments.

The boron hydrides and other boron compounds are in need of a similar structural convention. But here the valence bond convention is unsuccessful; and the representation of the higher hydrides by structures with conjugated bridge bonds has proved incompatible with the x-ray evidence. However, Lipscomb has recently summarized the known geometrical structures of these compounds,[1] and Eberhardt, Crawford, and Lipscomb (ECL) have interpreted their electronic structures.[2] I wish to show that their results may now be reduced to a form suitable for a more hopeful symbolic representation of the boron hydrides.

BASIS OF THE SYMBOLISM

1. Normal BH Bond and Valence Cone

Each boron and one of the hydrogens bonded to it with a normal single bond, called the "external BH bond" by ECL,[1] we shall represent by the usual symbol BH in our structural formula. The other orbitals of a tetrahedral sp^3 boron atom lie on what we may call the "valence cone." This is the cone, of half-angle 70.5°, swept out in space by three tetrahedral bonds rotating about our normal single B-H bond as an axis. For maximum binding, the other neighbors of the boron atom should lie in or near this cone.

The essential property of the valence cone for the present discussion is that it is a surface of positive curvature convex toward the normal single B-H bond; and it retains this property even when it is distorted, as it would be, for example, in representing trigonal orbitals.

2. Triangular Close-Packing on the Valence Surface

Electron-deficient hydrides like the boron compounds seem not to form singly connected open chains with strongly directed valence like the electron-balanced or electron-excess hydrides—that is, the paraffins, amines, and ethers. Instead, their heavy-atom bonds tend to form a close-packed network of almost equilateral triangles, the triangle sides being equal within about 10 percent in the boron compounds.[2] This network is a multiply connected system in which the available electrons spread themselves so as to connect as many atoms as possible. If the neighbor borons of any given boron are near its valence cone, the triangular network is then a two-dimensional network—a two-dimensional metal—in the convex surface or "valence surface" formed by the overlapping valence cones. The normal B-H bonds project out from this surface approximately at right angles.

When the number of boron atoms is large enough, the triangular network on the convex surface may be completed, forming a closed polyhedron, or "pseudo-spherical" compound (ECL). Such polyhedral boron structures are known for other boron compounds but have not yet been identified in the hydrides. We will call these hypothetical structures "the closed hydrides" and will devote a separate paragraph to them later.

The Flat Representation

But the known hydrides are "open": the polyhedra are incomplete, and consequently the two-dimensional network may be mapped on the flat two-dimensional

[1] W. N. Lipscomb, J. Chem. Phys. **22**, 985 (1954).
[2] Eberhardt, Crawford, and Lipscomb, J. Chem. Phys. **22**, 989 (1954).

surface of a piece of paper, as shown in the structural formulas below. Of course they may be mapped more accurately on the proper space polyhedron, but this is usually less convenient. The flat representation does not show the bond lengths and angles correctly, and need not do so, since its correspondence to the spatial representation is easily remembered.

Number of Boron Neighbors

No boron can have 6 boron neighbors, since six equilateral triangles would lie in a plane and not on the valence cone. (In orbital terms, the orbitals toward the neighbors would not have the necessary components extending in the direction opposite to the normal B-H bond). With 5 boron neighbors, the bond directions are those of the intersecting edges of an icosahedral network, and give a fairly good fit to the valence cone. The directions on an octahedral network, where a central boron would have 4 neighbors, and on a tetrahedral network, where it would have 3, give progressively worse fits. In the open hydrides, the octahedral network occurs only for B_5H_9; and no tetrahedral network has been found as yet in the hydrides, although such a structure is known for B_4Cl_4.

3. Peripheral Packing of Excess Hydrogens

Turning now to the excess hydrogens, we see that their number must be even if we are to have a filled-shell electronic ground state, since both boron and hydrogen have odd numbers of electrons. This requirement is of course satisfied by the two known hydride classes, B_nH_{n+4} and B_nH_{n+6}. These other hydrogens should be distributed in our convex surface around the perimeter of the boron network—that is, on the valence cones of those peripheral boron atoms which have the fewest boron neighbors, since these have the most orbitals to fill.

The Sector Rule

In fact, if we divide each boron valence cone into three equal 120° sectors, one for each of its orbitals, then we find the following rule satisfied, that each boron has at least one neighbor, hydrogen or boron, in each of its sectors. The excess hydrogens may form ordinary B-H bonds approximately perpendicular to the perimeter but lying in the valence surface; or they may form bridge bonds lying in this surface, symbolized by

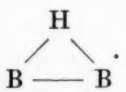

Number of Excess Hydrogens

The number p of excess hydrogens needed in the open hydrides is related to the maximum number q of empty 120° sectors on the boron perimeter, which is easily found to be given by

$$q=2b_{1p}+2b_{2p}+b_{3p}+b_{4p}, \quad (1)$$

where b_{1p} is the number of peripheral borons connected to 1 other boron; b_{2p} is the number connected to 2; and so on. In general, as p must be even,

$$p=q \quad \text{for } q \text{ even} \quad (2a)$$

and

$$p=q-1 \quad \text{for } q \text{ odd}, \quad (2b)$$

since some bridge hydrogens may fill simultaneously the sectors on adjacent boron atoms. In rare cases, we may satisfy the sector rule with even fewer hydrogens, as in the B_{10} hydride, where several adjacent peripheral borons with four boron neighbors permit

$$p=q-2 \quad (\text{for special } b_{4p} \text{ arrangements}), \quad (2c)$$

as is easily seen on examination of an icosahedral B_{10} fragment.

Table I gives p for the open hydrides B_nH_{n+p}, as determined by the sector rule and Eqs. (1) and (2). It can be seen by trial that smaller even numbers than those given for p cannot satisfy the sector rule without either introducing great strain or forcing some hydrogen to be shared by more than two borons. The known hydrides are given in boldface. Only for $n=5$ should the internal structure of the network affect p. Smaller networks may be regarded indifferently as octahedral icosahedral fragments; and larger ones seem unlikely to be stable if any central borons have four neighbors (octahedral) since this is accompanied by steric hindrance or by large departures from some valence cone.

Table I implies a set of possible formulas and structures. Predicting relative stability or instability within this set is beyond the scope of our simple symbolic representation, just as such predictions are beyond the scope of the simple valence-bond representation of organic compounds; and some of the possible hydrides listed may prove nonexistent even if it should happen that the structures of the others are given correctly.

The predictions of Table I disagree with the prediction of ECL on the structure of the tentative B_8 hydride, which has not yet been determined. Their proposed formula B_8H_{16} has two more hydrogens than

TABLE I. Predicted excess hydrogens p for different numbers of borons in open hydrides B_nH_{n+p} from the sector rule.

n	p	
2	4	
3	6	
4	6	
5	4	(octahedral)
5	6	(icosahedral)
6	4	(pentapyramid)
7	6	
8	6	
9	6	
10	4	
11	4	

are required by the sector rule for close-packed B_8. Evidently the present rules, although originally invented to symbolize the ECL rules for the known structures, diverge for the unknown compounds; a decision between the two sets may be possible in the future.

Positions of Excess Hydrogens

The excess hydrogens tend to be triangular close-packed to the boron network, although the triangles are not equilateral because the B-H bond is shorter than the B-B bond. This means that the hydrogens tend to go when possible toward the peripheral unfilled icosahedral sites; except in B_2H_6, where the peripheral borons can have only four neighbors by the sector rule, and so cannot be icosahedral.

APPLICATION OF THE SYMBOLISM TO STRUCTURAL FORMULAS OF OPEN HYDRIDES

In sum, the open boron hydrides B_nH_{n+p} appear to be even-electron molecules with the boron atoms approximately in a close-packed equilateral-triangular network on the convex surface formed by their overlapping valence cones; with n single B-H bonds normal to this surface; and with p (even) added peripheral hydrogens in the surface located so that every boron atom has neighbors in all three sectors of its valence cone. And as long as this network does not form a complete polyhedron, we may represent it on paper by a flat triangular network having the same topology.

This prescription leads to the following flat representations of the open boron hydrides, including the presently proposed B_6 and B_8 structures.

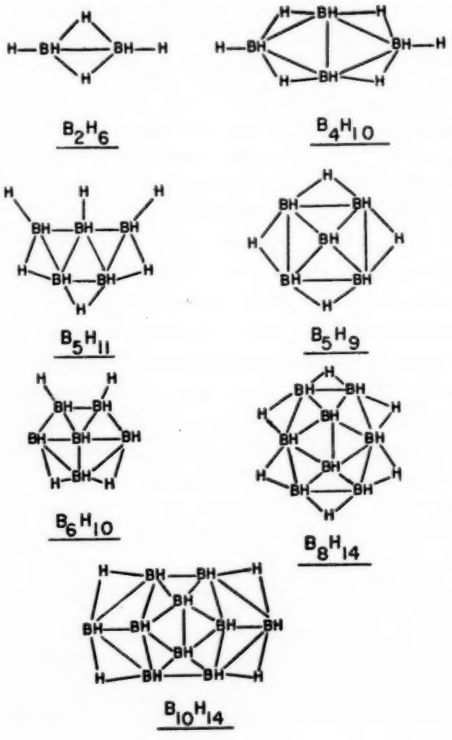

THE CLOSED HYDRIDES

The foregoing assumptions 1 and 2 lead also to convex closed polyhedral hydrides, not necessarily regular, $(BH)_n$, with $n=4$, 5, 6, 7, 8, 9, 10, and 12. We cannot map these closed structures on a flat surface without misrepresenting some of the borons as being in preferred edge positions, so the best flat representation is probably the structureless formula, $(BH)_n$, which may be taken to imply a closed triangular polyhedral structure with n corners.

The smaller closed hydrides should be highly strained, as remarked already. There may also be group- theoretical reasons more sophisticated than the present symbolism, why some should not be filled-shell compounds, as ECL found to be the case with $(BH)_6$. But as a class these closed hydrides might be expected to be more inert chemically and more paraffin-like than the open hydrides, since their hydrogens are all tightly bound to the strongly directed normal external bonds, and the possibility and advantage of rearrangement of either hydrogens or borons is much reduced.

We may even imagine that two such polyhedral closed units might be joined together by strong normal boron-boron bonds, and perhaps strong chains and lattices might be formed of such units. We could represent the dimers by $(BH)_{n-1}B\text{-}B(BH)_{n-1}$, and so on. (Such polymerization, with normal B-B bonds replacing the normal B-H bonds, is also conceivable with the open hydrides, but may be more difficult to achieve chemically because of the reactivity of the excess hydrogens and the ease of rearrangement of the networks with open perimeters.) Perhaps the insoluable white residues of approximate formula $(BH)_n$ found in boron hydride reactions may consist of one or more of these closed hydrides, either in separate units or in chains and lattices. If there is such a paraffin-like stability and multiplicity of arrangement, size, and cross linkage, it would make their chemistry considerably different from the chemistry of the open hydrides.

The stability of some of the closed hydrides may be inferred by comparing them with open hydrides which have an isoelectronic valence surface. Thus, the stability of octahedral B_5H_9 with 14 electrons in the valence surface speaks for the stability both of the octahedral ion, $(BH)_6^{=}$, which ECL inferred on other grounds, and of the octahedral unit $(B)_6^{=}$, with 6 normal external bonds, which occurs in CaB_6. Parenthetically, we may note that B_4H_{10} also has 14 electrons in its valence surface.

In the same way the great stability of icosahedral $B_{10}H_{14}$ with 24 valence-surface electrons suggests even greater stability in the more symmetrical $(BH)_{12}$ with 24 surface electrons. (ECL's postulated B_9H_{15}, like ours, would also have 24 surface electrons; as would their B_8H_{16}, but not our B_8H_{14}.) If such an icosahedral $(BH)_{12}$ exists, it would be both the largest and the most stable of the single-unit boron hydrides, either

open or closed. The first strong electronic absorption band of such a compound might be expected to be near the same energy as that of $B_{10}H_{14}$, perhaps shifted to shorter wavelengths because the surface electrons would be more tightly bound by the added boron nuclei; but additional weak forbidden transitions may turn up at long wavelengths in $(BH)_{12}$, as in certain symmetrical conjugated hydrocarbons, as a result of the degeneracies in the orbitals involved in the first electron jump.

ON DIRECTED VALENCE

The rules here given represent a modification of the strongly-directed valence rules suitable for organic compounds. They move toward the rules of the electron-deficient metallic binding at the left side of the periodic table, where space packing comes to govern the nuclear positions more strongly than directed valence. The remnants of directed valence here, such as the one normal BH bond on each boron, and the valence cone, are supplemented by close-packing in the cone; no doubt even these remnants would be further reduced in compounds of elements to the left of, and below, boron in the periodic table. As directed valence gets weaker, the atoms have more freedom of movement and do not have to traverse such high potential barriers in passing from one site to another as they would have to traverse, for example, in the isomerization of paraffins. The result is the characteristic interstitial diffusion in metals, and disproportionation in the boron hydrides, giving us protean structures difficult to fix and to analyze chemically.

ACKNOWLEDGMENT

I am much indebted to W. H. Eberhardt, Bryce Crawford, Jr., and William N. Lipscomb for letting me see a preprint of their manuscript, and particularly to Professor Bryce L. Crawford, Jr., for a very stimulating lecture which turned my attention to the problem of symbolic representation of these compounds.

THE JOURNAL OF CHEMICAL PHYSICS VOLUME 22, NUMBER 6 JUNE, 1954

Statistical Computation of Mean Dimensions of Macromolecules. I*

F. T. WALL AND L. A. HILLER, JR., *Noyes Chemical Laboratory, University of Illinois, Urbana, Illinois*

AND

D. J. WHEELER,† *Digital Computer Laboratory, University of Illinois, Urbana, Illinois*

(Received December 28, 1953)

The configurations of flexible coiling type polymer molecules have been investigated statistically with a high-speed electronic digital computer by generation of large numbers of "random walks." These walks were carried out subject to the excluded volume effect in simple cubic and tetrahedral lattices. It was found that the walk attrition obeys an exponential decay law with a half-walk of 6.7 steps in the cubic lattice and 17.3 steps for the tetrahedral. Mean square end-to-end separations, $\langle r_n^2 \rangle_{Av}$, were also obtained, and two distinct kinds of empirical formulas have been fitted to the data. So far, the statistical data are insufficient to establish unequivocally the nature of the functional dependence of $\langle r_n^2 \rangle_{Av}$ for large values of n, the number of steps. A study was also made on the probabilities of ring closures for restricted random walks in the cubic system. It was found that for rings greater than 6 steps, the probability of formation varies inversely as the square of the ring size.

INTRODUCTION

THE theoretical calculation of the mean dimensions of flexible, coiling type molecules has been the subject of numerous publications in recent years. Beginning with the random walk model introduced by Kuhn,[1] various procedures have been employed to approximate mathematically the distributions of the configurations that flexible linear macromolecules might assume.

The early random walk approximations did not take into account the fact that segments of real polymer chains occupy positions in space. Accordingly, a great many of the simple random walk configurations involve superposition of atoms, which would be impossible for real polymer systems. Various mathematical procedures to compute the effect of eliminating these impossible configurations have been given by a number of authors in recent publications.[2–14] This exclusion of disallowed

* The work discussed herein was supported in part by the research project sponsored by the Reconstruction Finance Corporation, Office of Synthetic Rubber, in connection with the Government Synthetic Rubber Program.

† Present Address: Trinity College, Cambridge, England.

[1] W. Kuhn, Kolloid-Z. **68**, 2 (1934); W. Kuhn and F. Grun, Kolloid-Z. **101**, 248 (1942).

[2] J. J. Hermans, Rec. trav. chim. **69**, 220 (1950).

[3] Hermans, Klamkin, and Ullman, J. Chem. Phys. **20**, 1360 (1952).

[4] R. Ullman and J. J. Hermans, J. Polymer Sci. **10**, 559 (1953).

[5] E. Montroll, J. Chem. Phys. **18**, 734 (1950).

[6] H. Hadwiger, Makromol. Chem. **5**, 148 (1951).

[7] Frisch, Collins, and Friedman, J. Chem. Phys. **19**, 1402 (1951).

configurations has been called the "excluded volume effect," and the problem has been characterized as a "restricted" random walk, the term "restricted" referring to the exclusion of configurations involving multiple occupancy of points in space.

Unfortunately, the mathematics involved in an analytical treatment of restricted random walks is rather complex, and to date no general agreement has been reached as to what precisely is the effect of the excluded volume.

The dimensions of a random-coiling polymer are most conveniently characterized in terms of the mean square end-to-end separation of the polymer chain $\langle r_n^2 \rangle_{Av}$, where n is the number of steps. The dependence of this distance on molecular weight or chain length of the polymer is one of the principal points of disagreement. Certain authors referred to above, for example, Hermans *et al.*[2–4] and Wall,[14] have given arguments in favor of the idea that the mean square length becomes proportional to molecular weight as the molecular weight increases, or in other words, that the quotient, $\langle r_n^2 \rangle_{Av}/n$, approaches a limit as n becomes infinite. Other authors, for example, Flory[9] and James,[12] do not favor this idea of convergence, but rather suggest that $\langle r_n^2 \rangle_{Av}/n$ continues to increase as $n \rightarrow \infty$. Because of the great mathematical difficulties that stand in the way of obtaining the still unrealized exact solution of this problem, all of the treatments employed so far have involved certain assumptions and approximations.

A second difficulty facing investigators of this problem is that it is not easy to check theoretical results against experimental data. This has been attempted by Flory and collaborators[15–17] and by Kunst[18] but the interpretations of the experimental data have led to diverse conclusions as to the behavior of $\langle r_n^2 \rangle_{Av}/n$, and hence to no positive clarification of this problem.

One way out of these difficulties is to investigate restricted random walks by strictly numerical procedures. King[19], has already described a program for obtaining such data by means of IBM punch card machines. It is more practical, however, to generate random walks in various lattice systems by means of electronic digital computers and thus accumulate statistical data describing the average molecular behavior. It is the purpose of the present article to report initial results of an investigation of this kind.

The electronic digital computer in operation at the University of Illinois (the ILLIAC) has been used for carrying on this research. The work reported in the present article deals with "walks" in the simple cubic and in the tetrahedral (diamond type) lattice systems. The cubic lattice system was first selected since it is the simplest geometrical arrangement in three dimensions. The tetrahedral system more closely represents a chain of C—C bonds, so it was chosen as a second example for study. Both models are, of course, highly artificial, so the results must be interpreted from the point of view of trends and functional forms and not with respect to specific details.

It should be pointed out that the work described in the present article does not represent a completed study of restricted random walks by computer techniques. We are continuing work on the problem at the present time and have expanded the scope of the investigation to include a number of additional lattice systems, in two as well as in three dimensions. The primary objective of this work is to characterize the behavior of $\langle r_n^2 \rangle_{Av}/n$ for large values of n by purely numerical procedures, as a quasi-experimental approach to the solution of the problem.

GENERATION OF RESTRICTED RANDOM WALKS

Large numbers of random walks, subject to the excluded volume effect, were generated for the two above mentioned lattice systems, simple cubic and tetrahedral. In both systems the distance between adjacent lattice points was taken to be unity and in the cubic system all bond angles were restricted to 90°.

The procedure for generating the walks in the cubic lattice was as follows. Each walk was represented by a sequence of unit vectors. The first two vectors were arbitrarily taken as $+x$ followed by $+y$, and the third vector was chosen to be one of the four vectors $(\pm z, \pm x)$ perpendicular to the second. A computed pseudo-random number determined the choice of the vector. The procedure of randomly selecting vectors perpendicular to the last added vector was continued indefinitely, subject however to a verification that each temporary terminal point did not coincide with a previous point of the walk. Each vector in any given walk was recorded in the memory of the computer and after each additional vector was added, the following check procedure was employed. The last chosen vector was added to the preceding vector which sum in turn was added to the vector before that and so on until either a zero sum was obtained or the origin was reached without a zero sum. A zero sum of the vectors was indicative, of course, of a closed loop, or double occupancy of a lattice site. Any walk that led to a closed loop was promptly rejected, and a new walk started. When a step was permitted, however, the square of the resulting end-to-end separation was added to an appropriate part of the memory reserved for the correspondlng number of steps. Such a walk was then subjected to another

[8] T. B. Grimley, Proc. Roy. Soc. (London) **A212**, 339 (1952).
[9] P. J. Flory, J. Chem. Phys. **17**, 303 (1949).
[10] R. J. Rubin, J. Chem. Phys. **20**, 1940 (1952).
[11] F. Bueche, J. Chem. Phys. **21**, 205 (1953).
[12] H. M. James, J. Chem. Phys. **21**, 1628 (1953).
[13] Zimm, Stockmayer, and Fixman, J. Chem. Phys. **21**, 1716 (1953).
[14] F. T. Wall, J. Chem. Phys. **21**, 1914 (1953).
[15] P. J. Flory and T. G. Fox, Jr., J. Am. Chem. Soc. **73**, 1904, 1909, 1915 (1951).
[16] P. J. Flory, J. Chem. Phys. **17**, 1347 (1949).
[17] W. R. Krigbaum and P. J. Flory, J. Polymer Sci. **11**, 37 (1953).
[18] E. Kunst, Rec. trav. chim. **69**, 125 (1950).
[19] G. W. King, Natl. Bur. Standards, Appl. Math. Ser. **AMS12**, (June 11, 1951).

random vector addition followed by a verification, etc. Following a failure (closed loop), the vector history of the walk was erased, but the statistics of the successful portions of the walk were, of course, retained in the storage elements of the memory.

In the tetrahedral or diamond type lattice, essentially the same procedure was followed except that one of 3 vectors was chosen each time. In the tetrahedral lattice, there are actually eight different vectors involved, but they fall into two groups which can be represented (without normalization) as follows:

Group A	Group B
α: $+x, +y, +z$	$-\alpha$: $-x, -y, -z$
β: $+x, -y, -z$	$-\beta$: $-x, +y, +z$
γ: $-x, +y, -z$	$-\gamma$: $+x, -y, +z$
δ: $-x, -y, +z$	$-\delta$: $+x, +y, -z$

Any vector from group A must be followed by one of group B excluding the negative of the last added group A vector; a similar restriction applies for a vector of the B type which must be followed by one from A. Thus α could be followed by $-\beta$, $-\gamma$, or $-\delta$ but not $-\alpha$. Likewise $-\beta$ could be followed by α, γ, or δ but not β.

The program of the computer was so arranged that after a large number of walks had been completed, a table was printed giving the mean square distance, $\langle r_n^2\rangle_{Av}$, associated with any given number of steps as well as the actual number of successful walks N_n corresponding to those steps.

Another phase of our work involved the statistical determination of the probabilities of loop closures. To do so the ILLIAC was programmed to generate the aforementioned random walks, except now the number of steps in the loops associated with failures were recorded together with the total number of steps involved. By these means we were able to learn empirically about the probability of ring closures.

NUMBER OF ALLOWED CONFIGURATIONS

One of the significant quantities obtained from the computer studies is the number of successful walks N_n

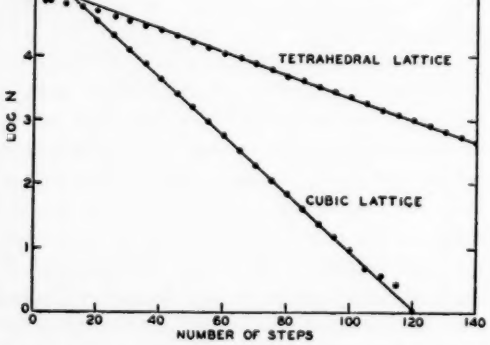

FIG. 1. Number of successful samples *versus* number of steps in random walks.

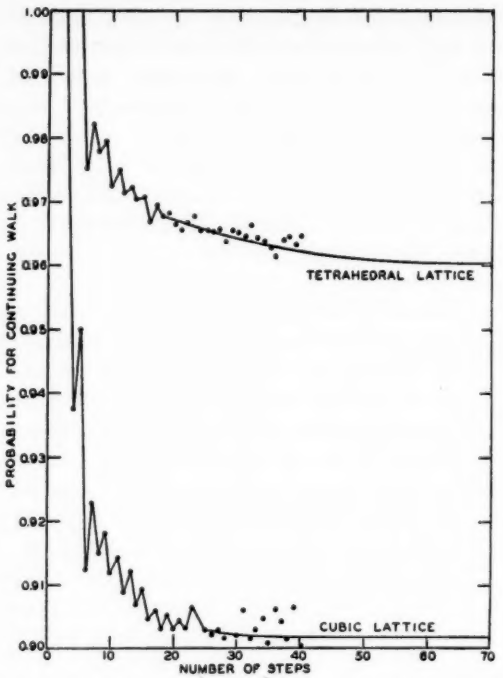

FIG. 2. Probability for continuing restricted random walks for low values of n.

as a function of the number of steps. If there were no failures, the total number of configurations possible after n steps would be 4^{n-2}, recognizing that the first choice of direction starts with the third step. Since the problem was coded in such a way that walks were discontinued as soon as a failure was encountered, it is evident that the values of N_n should be directly proportional to the fraction of all configurations that are allowed after taking n steps.

If $\log N_n$ is plotted against the number of steps, as shown in Fig. 1, a rather interesting result is obtained. For both types of lattices, cubic and tetrahedral, the graphs become quite linear after a relatively few steps have been taken. This means that the probability of failure, $1-N_{n+1}/N_n$, approaches a constant value, a result that is not at all unreasonable. In the case of the cubic lattice, the first failure can occur at step number 4, but it takes about 15 steps before the probability of failure assumes a reasonably constant value. In the tetrahedral lattice the first failure occurs at 6 steps, and the state of uniform attrition does not set in until about 40 steps have been completed. In either lattice we conclude, for large enough n, that an equation of the following type governs the number of allowed configurations:

$$N_n = N_0 \exp(-\lambda n). \tag{1}$$

In this equation N_0 is the extrapolated initial number of trials and not the actual starting number, since the log plot departs from linearity for small n. Utilizing the straight line portions of the graphs, the parameter λ can be computed for each of the two lattices by determining

the slopes of the lines. Using a method of least squares, it turns out for the cubic lattice that λ equals 0.104 and for the tetrahedral lattice 0.040. These figures mean that the fractional decrease in number of samples per step, namely, $\exp(-\lambda)$, will equal 0.10 and 0.04 for the two types of lattices. Since the log plot is linear, it is evident that the walk attrition is subject to the same kind of mathematical considerations that apply to a radioactive decay or to other first order reactions. In the present instance, we can talk about "half-walks," which for the cubic and tetrahedral lattices are, respectively, 6.7 and 17.3 steps. It is not surprising that attrition occurs, but the magnitude, particularly for the simple cubic lattice, seems remarkably high.

The striking linearity exhibited by the graphs in Fig. 1 leaves little doubt that this same behavior can be expected to continue for even longer walks. In the case of the cubic lattice the data are uncertain after 100 steps, simply because the remaining number of samples is not large enough for good statistical averaging. Out of the original 140 000 walks started in the cubic system, the longest one lasted 121 steps. The intermediate region from $n=20$ to 100 gives a line as straight as any that could be expected from experimental measurements. In the case of the tetrahedral lattice, the numbers of samples remained sufficiently large up to 140 steps to maintain a uniform straight line over a wide range of values for n.

The probability of continuing a walk, N_{n+1}/N_n, has been plotted *versus* n in Fig. 2. For low values of n, it is clear that this probability exhibits alternations in magnitude which arise because only even numbered rings can be closed. Whenever a new size of ring can form, the probability of continuing a walk is diminished, but part of that probability is restored in the following step as manifested by the zig-zag nature of the graph. As n increases, the curve tends to become smoother except for uncertainties resulting from the ever decreasing number of samples.

The foregoing results are compatible with the view

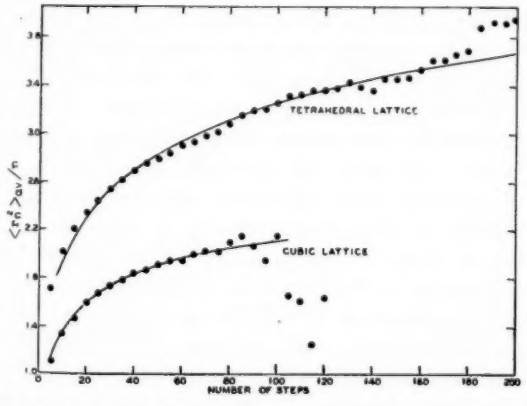

FIG. 3. Plot of the quotient, $\langle r_n^2\rangle_{Av}/n$ *vs* the number of steps in restricted random walk. Solid lines computed according to Eqs. (6) and (7).

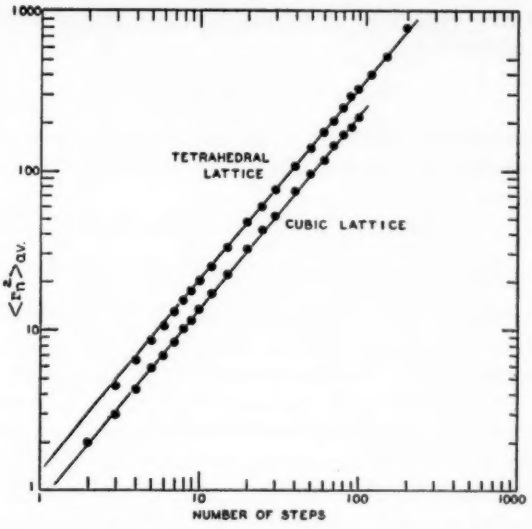

FIG. 4. Log-log plot of mean square length *vs* number of steps.

that the probability of ring closure diminishes with increasing ring size sufficiently rapidly so that the sum of all closure probabilities converges toward a limiting value in a relatively short time. This means that as far as attrition is concerned, the short range interferences are the most important. This does not mean, however, that the long range interferences do not have a significant effect upon the mean square molecular dimensions.

MEAN SQUARE MOLECULAR LENGTHS

The data obtained from the ILLIAC also included mean square molecular lengths for the allowed walks that were discussed in the preceding section. Now a quantity of fundamental significance in connection with the overall problem is the ratio $\langle r_n^2\rangle_{Av}/n$. To see how this quotient depends upon n, we plotted and analyzed the numerical results in different ways with the hope that valid empirical relationships might be found. First of all we plotted $\langle r_n^2\rangle_{Av}/n$ *vs* n as shown in Fig. 3. Examination of the results does not suggest any positive conclusion as to divergence or convergence of the ratio. In addition, the logarithm of the mean square distance was plotted *versus* log$n$ in Fig. 4. It will be observed that for both kinds of lattices, the log-log plot yields straight lines with slopes equal to 1.22. This suggests that the mean square length of a coiling type polymer molecule might be expressed by a formula of the type

$$\langle r_n^2\rangle_{Av} = \text{constant} \cdot n^{1.22}, \qquad (2)$$

a result which can be reconciled with intrinsic viscosity formulas of the type $[\eta]=KM^a$.

As attractive as the above relationship might be, we recognize that it is unwise to extrapolate a log-log plot for any distance, so the results cannot be regarded as proof of divergence of the ratio $\langle r_n^2\rangle_{Av}/n$.

We also took the data and adjusted parameters to fit converging types of functions. The form first assumed

was that suggested by an approximate theory worked out earlier,[14] *viz.*,

$$\langle r_n^2\rangle_{Av}=An+B\sqrt{n}+C. \quad (3)$$

Adjusting the constants A, B, and C to give the best fit to the data we obtained the following results for the two lattices:

$$\text{Cubic } \langle r_n^2\rangle_{Av}=2.34n-3.31\sqrt{n}+0.345; \quad (4)$$

$$\text{Tetrahedral } \langle r_n^2\rangle_{Av}=5.01n-23.0\sqrt{n}+51.1. \quad (5)$$

It should be borne in mind that the above equations are expressed in dimensionless form, since unit distances were assumed for the random steps. A generalization can be worked out for each lattice taking into account size of polymer segments, etc., but that will contribute nothing to the question of functional form with respect to n.

Other empirical forms that predict convergence of $\langle r_n^2\rangle_{Av}/n$ have also been tried with even better agreement. These are for the cubic lattice

$$\frac{\langle r_n^2\rangle_{Av}}{n}=1+1.77\left\{\frac{1-2.2/\sqrt{n}}{1+2.6/\sqrt{n}}\right\} \quad (6)$$

and for the tetrahedral

$$\frac{\langle r_n^2\rangle_{Av}}{n}=2-\frac{1.5}{n}+3.54\left\{\frac{1-3.0/\sqrt{n}}{1+9.6/\sqrt{n}}\right\}. \quad (7)$$

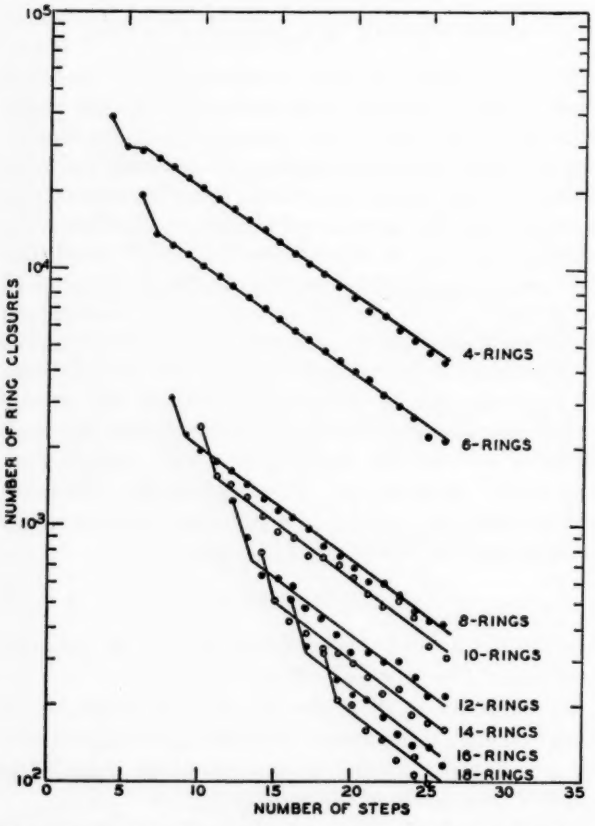

FIG. 5. Logarithm of numbers of ring closures plotted *vs* number of steps. Cubic lattice only.

TABLE I. Probabilities for ring closures in restricted random walk.

Ring size	Probability Initial	Limiting
4	628.9 $\times10^{-4}$	519.3 ±7.2 (1.4%)$\times10^{-4}$
6	351.7	257.4 ±4.3 (1.7%)
8	71.2	46.2 ±4.2 (9.1%)
10	61.7	40.3 ±1.5 (3.7%)
12	38.5	25.1 ±1.7 (6.8%)
14	28.9	19.1 ±1.5 (7.8%)
16	25.5	14.4 ±1.4 (9.7%)
18	17.7	11.2 ±1.1 (9.8%)
20	13.5	8.30±1.06(12.8%)
22	13.2	7.47±0.82(11.0%)
24	10.4	6.19±0.63(10.2%)
26	10.2	5.42±0.68(12.5%)
28	6.62	4.12±0.69(16.7%)
30	6.58	3.85±0.62(16.1%)
32	5.10	3.08±0.70(22.7%)
34	3.56	3.19±0.57(17.9%)
36	2.71	2.96±0.66(22.3%)
38	2.62	2.65±0.54(20.4%)
40	4.00	2.45±0.48(19.6%)
42	2.34	1.84±0.78(42.4%)
44	4.22	1.83±0.73(39.9%)
46	1.66	2.11±0.97(46.0%)
48	2.92	1.35±0.71(52.6%)
50	1.81	1.26±0.79(62.7%)
52	3.57	1.36±0.55(40.4%)

The asymptotic values for the significant ratio as predicted by the empirical equations are 2.34 and 2.77 (cubic) and 5.01 and 5.54 (tetrahedral). Obviously it is difficult to determine accurately the asymptotic value (if it exists) because it involves an extrapolation based on relatively meagre data.

A comparison of calculations based on Eqs. (6) and (7) appears as the solid lines drawn in Fig. 3. As far as the data indicate, Eqs. (6) and (7) are just as good as Eq. (2). This can be demonstrated by replotting the results of Eq. (2) in a graph of the form appearing in Fig. 3, and by similarly plottlng the results expressed by Eqs. (6) and (7) in log-log form (Fig. 4). In both instances, superposition of curves is obtained, so neither convergence nor divergence is favored.

PROBABILITY OF SINGLE RING CLOSURE AT END OF WALK

Another phase of the excluded volume problem investigated by the high-speed electronic digital computer technique was that concerned with the probability of forming a ring or loop at the end of a walk. Such loops are detected by zero vector sums, and their occurrence constitutes the basis for throwing out a walk. Our specific problem was concerned with determining the probability of loop formation as a function of the number of steps in the loop and the total number of steps taken up to the formation of the loop.

In this connection it will be recalled that, for the unrestricted random walk problem, the probability of forming any loop of k steps varies inversely as $k^{\frac{3}{2}}$, at least for large values of k. We would predict that this probability for loop closure is actually too great, since the formation of multiple looped configurations is not

ruled out in the unrestricted problem. For example, if one forms a loop of 10 members, the number of ways of doing so in the unrestricted case will include configurations involving smaller loops formed prior to the closure of 10. When one takes cognizance of the volume restriction, however, the probability of closing a big loop will diminish in a significant way since we now count only the first time a loop appears and are not concerned with the history of a walk thereafter.

To get at this problem statistically, the ILLIAC was programmed to carry out random walks in a simple cubic lattice subject to right angle bonds; the sizes and numbers of loops were then counted for a total of 2 600 000 random walks with values of n ranging up to 100.

In Fig. 5 we have plotted the logarithm of the number of ring closures of size k *versus* the total number of steps n. Except for the initial points, which correspond to closing loops back to the origin ($n=k$), the points all lie on sets of parallel straight lines, with one line for each value of k. We shall accordingly distinguish between the initial probabilities of ring closure (for $k=n$) and the limiting probabilities of such closures, which appear to depend on k only. Both sets of values are given in Table I. By plotting the logarithms of these probabilities *versus* the logarithm of k, we obtain straight lines of slope equal to -2, excluding points corresponding to $k=4$ and $k=6$ (see Fig. 6). From these lines we deduce empirically that for $k \geqslant 8$,

$$p_k^0 = 0.5/k^2$$

and (8)

$$p_k = 0.36/k^2,$$

where p_k^0 is the initial probability of ring closure ($n=k$) and p_k is equal to the limiting probability of ring closure. The formulas expressed by Eqs. (8) are not, of course, valid for $k=4$ or 6.

Although our evidence is somewhat fragmentary, it appears that the probability of ring closure in the restricted random walk varies inversely as the square of k, the number of steps in the loop. This conclusion is by no means certain, but it is certainly not unreasonable to expect that the power would be a simple number like

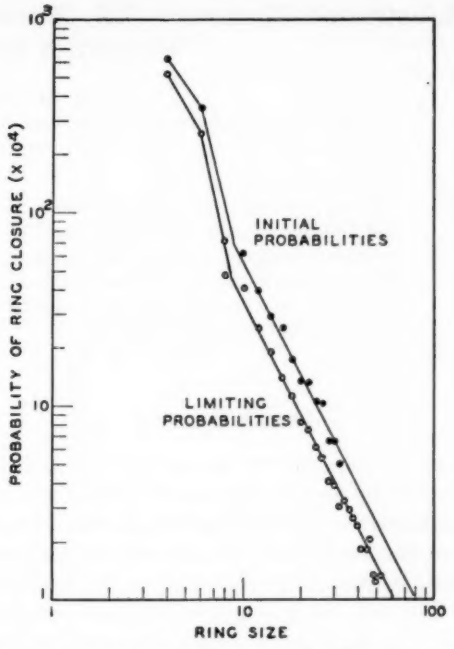

FIG. 6. Log-log plot of probability of ring closure *vs* ring size. Cubic lattice only.

$\frac{3}{2}$, 2, 5/2, etc. The inverse square relationship, as opposed to the inverse $\frac{3}{2}$ rule that holds for the unrestricted problem, presumably comes about because most of the attrition can be attributed to the smaller loops. Hence, the probability of formation of larger loops must diminish more rapidly in the restricted case than for the unrestricted problem where configurations with multiple loops are permitted.

If the inverse square law holds and if we make the assumption, which is only approximately correct, that the mean length of failures resulting from loops of size k after n steps is the same as the mean length of successes at $n-k$ steps, then it can be shown that $\langle r_n^2\rangle_{Av}/n$ diverges as $n\to\infty$. However, if the inverse square law is replaced by one in which the negative exponent is $2+\epsilon$ instead of 2, where ϵ is any positive number, then the quotient can converge. It is evident, therefore, that $\langle r_n^2\rangle_{Av}/n$ is on the threshold of convergence and that an absolute proof one way or another remains to be found.

Substituted Methanes. XX. Potential Constants and Calculated Thermodynamic Properties for Some Dibromomethanes

JEROME M. DOWLING AND ARNOLD G. MEISTER
Spectroscopy Laboratory, Department of Physics, Illinois Institute of Technology, Chicago 16, Illinois*
(Received February 24, 1954)

Using previous infrared and Raman data, a reasonable set of potential constants were obtained for CH_2Br_2 and CD_2Br_2, by means of the Wilson FG matrix method, with a potential energy function containing all possible second degree terms. Fundamental frequencies for $CHDBr_2$ were then calculated using the potential constants found for CH_2Br_2 and CD_2Br_2. Finally the heat content, free energy, entropy, and heat capacity for the ideal gaseous state at 1 atmos pressure were calculated for these three molecules for twelve temperatures from 100°K to 1000°K with a rigid rotator harmonic oscillator approximation.

INTRODUCTION

In previous papers[1–4] of this series, Raman and infrared spectral data, assignments, potential constants, and calculated thermodynamic properties were given for some dihalogenated methanes. A similar treatment has been carried out for CH_2Br_2, CD_2Br_2, and $CHDBr_2$, except that no new spectral data have been obtained. The existing data were collected and subjected to a critical examination in order to decide upon the best values for the fundamental frequencies. The fundamental frequencies have been calculated for $CHDBr_2$ in the present investigation using the potential constants obtained from CH_2Br_2 and CD_2Br_2. In addition, the heat content, free energy, entropy, and heat capacity were calculated for the ideal gaseous state.

SYMMETRY, SELECTION RULES AND ASSIGNMENTS

The CH_2Br_2 and CD_2Br_2 molecules have the symmetry of the C_{2v} point group. $CHDBr_2$ has the symmetry of the C_{1h} point group. CH_2Br_2 and CD_2Br_2 have nine normal vibrations: 4 type a_1; 1 type a_2; 2 type b_1, and 2 type b_2. According to the selection rules all fundamentals, overtones, and combinations are allowed in the Raman spectra, while all fundamentals, except a_2, all overtones except $A_2{}^n$ (n odd), and all combinations except $A_1 \times A_2$ and $B_1 \times B_2$ are allowed in the infrared. In the Raman spectra the a_1 vibrations correspond to polarized lines, the others to depolarized lines.

$CHDBr_2$ has nine normal vibrations; 6 type a' and 3 type a''. All fundamentals, overtones, and combinations are allowed in both the Raman and infrared spectrum. The a' lines should be polarized, while the a'' lines should be depolarized.

PREVIOUS DATA AND ASSIGNMENTS

Dibromomethane CH_2Br_2

There have been a number of papers published on the Raman spectra of CH_2Br_2.[5–12] A summary of fundamentals is given in Table I. The most probable values for the wave numbers of the fundamental frequencies are listed in Table II.

The infrared spectrum has been reported by Plyler[13] *et al.* and also by Emschwiller and Lecomte.[14] These wave numbers for the fundamental frequencies are also given in Table I.

Plyler assigned the band at 1096K as a fundamental corresponding to the a_2 vibration which is forbidden in the infrared. Of course the selection rules may break down in the liquid state due to intermolecular forces, but such behavior has not been observed in this laboratory for any other molecule. This band cannot be assigned as a binary combination, and if selection rules are to be obeyed, it must be assigned as a ternary combination. In Plyler's notation the assignment $2\nu_9 - \nu_4$ or $2(637) - 174 = 1100$K seems to fit the band best. All other bands were assigned satisfactorily with the exception of a band at 729K which was thought to be due to the impurity CH_2BrCl.

Dibromodideuteromethane CD_2Br_2

The CD_2Br_2 molecule has not been investigated as extensively as CH_2Br_2. Trumpy[15] has obtained the Raman spectra of CD_2Br_2. However, he found only 6 fundamentals and this data is summarized in Table II. Halverson[16] calculated the missing frequencies using

* Publication No. 98.

[1] Voelz, Cleveland, Meister, and Bernstein, J. Opt. Soc. Am. **43**, 1061 (1953).

[2] Decker, Meister, Cleveland, and Bernstein, J. Chem. Phys. **21**, 1781 (1953).

[3] Decker, Cleveland, and Bernstein, J. Chem. Phys. **21**, 189 (1953).

[4] Davis, Cleveland, and Meister, J. Chem. Phys. **20**, 454 (1952).

[5] H. Gockel, Z. physik. Chem. **B29**, 79 (1935).

[6] K. W. F. Kohlrausch and G. P. Ypsilanti, Z. physik. Chem. **B29**, 274 (1935).

[7] B. Trumpy, Z. Physik **90**, 133 (1934).

[8] J. Wagner, Z. physik. Chem. **B45**, 69 (1939).

[9] M. L. Delwaulle, Compt. rend. **217**, 172 (1944).

[10] M. L. Delwaulle and F. Francois. J. phys. radium **7**, 15 (1946).

[11] A. Dadieu and K. W. F. Kohlrausch, J. Opt. Soc. Amer. **21**, 286 (1931).

[12] J. R. Nielsen and N. E. Ward, J. Chem. Phys. **10**, 81 (1942).

[13] Plyler, Smith, and Acquista, J. Research Natl. Bur. Standards **44**, 503 (1950).

[14] G. Emschwiller and J. Lecomte, J. phys. radium **8**, 130 (1937).

[15] B. Trumpy, Z. Physik **100**, 250 (1936).

[16] F. Halverson, Revs. Modern Phys. **19**, 87 (1947).

TABLE I. Observed wave numbers of the fundamentals of CH_2Br_2.

Raman												Infrared			
Gockel		K. & Y.		Trumpy			Wagner			Delwaulle		Delwaulle & Francois		D. & K.		Nielsen & Ward				P. S. & A.		E. & L.
$\Delta\nu$	I	$\Delta\nu$	I	$\Delta\nu$	I	ρ	$\Delta\nu$	I	ρ	$\Delta\nu$	ρ	$\Delta\nu$	ρ	$\Delta\nu$	I	$\Delta\nu_g$	I_g	$\Delta\nu_1$	I_1		ν_1	ν_g	ν_1
175	8	175	15	175	16	0.4	174	290	0.35	174	P	174	0.45	178	3	169	10	172	8	ν_4			
578	8	576	20	578	20	0.12	577	380	0.11	576	P	576	0.11	578	2	584	10	578	10	ν_2	579	591	575
645	4	636	10	639	4	0.89	639	91	0.84	639	D	639	0.83	634	½	640	0	640	1	ν_9	639	648	644
809	00	806	0.5							810	D	810	D							ν_7	813	810	810
1100	0	1088	3				1089	8	0.92	1092	D	1092	0.85							ν_5	1096		1078
		1183	1				1183	4	0.82	1191	D	1191	D							ν_8	1190	1195	1176
1392	3	1387	7	1390	1	D	1387	29	0.53	1390	P	1390	0.53			1402	0	1390	2	ν_3	1385		1375
2988	4	2986	10	2986	7	0.10	2988	59	P	2988	P	2988	P	2995	0	3008	1	2990	5	ν_1	2988		
3063	2	3060	···	3050	1	0.85	3061	4	D	3060	D	3060	D							ν_6	3065		

$\Delta\nu$ = Raman displacement in cm^{-1} (K); I = relative intensity; ρ = depolarization factor; P = polarized; D = depolarized; ν = wave number in cm^{-1}; ν_g = wave number for gaseous state; and ν_1 = wave number for liquid state; K. & Y. = Kohlrausch and Ypsilanti; D. & K. = Dadieu and Kohlrausch; P. S. & A. = Plyler, Smith, and Acquista; E. & L. = Emschwiller and Lecomte.

the product rule, and Decius[17] calculated the fundamentals for both CH_2Br_2 and CD_2Br_2. However, he did not use the most general quadratic potential energy function.

Dibromodeuteromethane $CHDBr_2$

No published vibrational spectra were found in the literature for $CHDBr_2$. Using potential constants from CH_2Br_2 and CD_2Br_2 the fundamental frequencies have been calculated. These are listed in Table II.

NORMAL COORDINATE TREATMENT

As a check on the assignments, as well as to obtain reliable values of the potential (force) constants, a normal coordinate treatment (Wilson FG matrix method)[18] using the most general quadratic potential energy function was carried out. The symmetry coordinates and the F and G matrix elements are not given because they are formally the same as those of Decker *et al.*[2] For $CHDBr_2$ they are formally the same as those described by Weber *et al.*[19] The potential constants are expressed in the descriptive notation introduced in paper VIII.[4] Values for the masses, and the bond lengths used to calculate the G matrix elements are listed in Table III. Decius[17] and Stepanov[20] have calculated values for some of the potential constants for CH_2Br_2.

TABLE II. Probable and calculated values of the wave numbers of the fundamentals of CH_2Br_2, CD_2Br_2, and $CHDBr_2$.

Type	Degeneracy	CH_2Br_2 prob. value	Calc.	CD_2Br_2 prob. value	Calc.	Type	Degeneracy	$CHDBr_2$ Calc.[a]
a_1	1	174	177	175	176	a'	1	176.5
a_1	1	576	578	548	545	a'	1	556
a_1	1	1388	1384	1023	1025	a'	1	1236
a_1	1	2988	3005	2195	2180	a'	1	2214
b_1	1	3061	3039	2235	2251	a'	1	3023
b_1	1	810[b]	810		636	a'	1	701
b_2	1	1183	1182		877	a''	1	1145
b_2	1	637	635	609	612	a''	1	621
a_2	1	1091	1091		773	a''	1	821

[a] No experimental data.
[b] Gaseous state.

[17] J. C. Decius, J. Chem. Phys. **16**, 214 (1948).
[18] E. B. Wilson, Jr., J. Chem. Phys. **7**, 1047 (1939); **9**, 76 (1941).
[19] Weber, Meister, and Cleveland, J. Chem. Phys. **21**, 930 (1953).
[20] B. Stepanov, Acta Physicochimica **20**, 174 (1945).

These values are listed in Table IV along with the present results.

Potential constants were transferred from the CBr_3X,[21] CBr_2Cl_2,[4] and $CHBr_2Cl$[22] molecules. After several modifications the resulting potential constants yielded calculated wave numbers within 1.7 percent of the probable values for the liquid. These potential constants were also used to calculate the frequencies for CD_2Br_2 and $CHDBr_2$.

THERMODYNAMIC PROPERTIES

The heat content, free energy, entropy, and heat capacity at constant pressure for CH_2Br_2, CD_2Br_2, and $CHDBr_2$, with a rigid rotator, harmonic oscillator approximation for the ideal gaseous state at 1 atmos pressure, were calculated for twelve temperatures in the 100°K to 1000°K range.

The values used for the bond distances, products of inertia, and symmetry numbers are given in Table III. Since it was sometimes necessary to use liquid state wave numbers the results may be slightly greater in the last significant figure, because an increase of a few K in the wave number usually occurs in going from the liquid to the gaseous state. The thermodynamic func-

TABLE III. Bond distances, products of inertia, symmetry numbers and masses of the carbon, hydrogen, bromine, and deuterium atoms.

	CH_2Br_2	CD_2Br_2	$CHDBr_2$
C−D	···	1.093[a]	1.093
C−H	1.093	···	1.093
C−Br	1.910	1.910	1.910
$I_{xx}I_{yy}I_{zz}$	3.288×10^{6}	4.468×10^{6}	3.875×10^{6}
σ[b]	2	2	1

$M_C = 12.010$
$M_H = 1.008$
$M_D = 2.01418$
$M_{Br} = 79.916$

[a] Bond distances, products of inertia and masses are in A (Awu A^2),[3] and Awu, respectively.
[b] σ = symmetry number.

[21] Meister, Rosser, and Cleveland, J. Chem. Phys. **18**, 346 (1950).
[22] Pontarelli, Meister, Cleveland, Voelz, Bernstein, and Sherman, J. Chem. Phys. **20**, 1949 (1952).

TABLE IV. Potential constants for CH_2Br_2, CD_2Br_2, and $CHDBr_2$

Potential constant	Decius	Stepanov	Present[a]
f_h	5.04	5.023	5.0455[b]
f_b	2.840	2.856	2.8965
$f_h{}^h$	0	0.029	0.06791
$f_b{}^b$	0.186	0.147	0.35568
$f_b{}^h$	0	0.059	0.05890
$f_h{}^{hh}$	0	0.225	0.22645
$f_h{}^{bb}$	0	0	0.05000
$f_b{}^{hh}$	0	0	−0.06250
$f_b{}^{bb}$	0.342	0.568	0.37750
$f_b{}^{bh}$	0.305	0.492	0.25970
$f_b{}^{b'h}$	−0.152	0	−0.15200
$f_h{}^{bh'}$	0	0	0.07750
$f_h{}^{bh}$	0	0.310	0.23249
$f_{bh}{}^{bh'}$	−0.026	0.042	−0.02341
$f_{bh}{}^{b'h'}$	−0.060	0	−0.05303
f_{bb}	1.061	0.937	1.0868
f_{bh}	0.589	0.673	0.59500
$f_{bh}{}^{b'h}$	−0.005	0.084	0.00475
f_{hh}	0.530	0.525	0.61688
$f_{bb}{}^{hh}$	0	0	0.02499
$f_{bh}{}^{hh}$	0	0.042	0.06000
$f_{bb}{}^{bh}$	0	0.056	0.05000

[a] Bond stretching and bond interaction constants are in units of md/A; angle-bond interaction constants are in md/rad; angle, and angle interactions are in md A/rad².

[b] This number of significant figures is not really justified, but is necessary to give best reproduction of the observed wave numbers and to secure internal consistency in the calculations.

TABLE V. Heat content, free energy, entropy, and heat capacity for CH_2Br_2 for ideal gaseous state at 1 atmos pressure.[a]

T	$(H^0-E_0{}^0)/T$	$-(F^0-E_0{}^0)/T$	S^0	$C_p{}^0$
100	8.40	50.02	58.41	9.21
200	9.22	56.08	65.30	10.98
273.16	9.89	59.06	68.96	12.57
298.16	10.14	59.93	70.08	13.11
300	10.16	60.00	70.16	13.15
400	11.16	63.06	74.22	15.11
500	12.12	65.65	77.77	16.68
600	12.98	67.94	80.92	17.92
700	13.76	70.00	83.76	18.92
800	14.46	71.88	86.34	19.75
900	15.09	73.62	88.71	20.45
1000	15.66	75.25	90.90	21.06

[a] In this and subsequent tables T is °K and the other quantities are in cal deg^{-1} mole^{-1}.

tions of CH_2Br_2, CD_2Br_2, and $CHDBr_2$ are listed in Tables V, VI, and VII.

Stevenson and Beach[23] have calculated the thermodynamic functions for CH_2Br_2 for temperatures from 298 to 600°K. However, they choose the 478 K line to be a fundamental. The normal coordinate treatment shows this assumption to be in error. Edgell and Glockler[24] have calculated the heat capacity for temperatures from 298.1 to 600°K and also report a value for the entropy at 298.1°K. They used essentially the same wave numbers given in the present work. Their values range from 0.02 cal deg^{-1} mole^{-1} to 0.05 cal deg^{-1} mole^{-1} higher than the present values. Gelles and Pitzer[25] have recently calculated the thermodynamic functions for a number of substituted methanes, one of which was CH_2Br_2. Their values range from 0.04 cal deg^{-1} mole^{-1} higher to 0.08 cal deg^{-1} mole^{-1} lower than the present values. On the whole, the agreement is very good.

The thermodynamic functions for the molecule CD_2Br_2 are calculated from a hybrid of observed and calculated wave numbers. Three of the fundamentals have not been observed as yet. In these three cases the calculated values of the wave numbers were used.

The thermodynamic functions of the molecule $CHDBr_2$ were based on the calculated wave numbers. The calculated value for the 176.5 K fundamental was replaced by 174.5 K in that the corresponding calculated wave numbers for both CH_2Br_2 and CD_2Br_2 were higher than the observed value. The value 174.5 represents the mean of the observed corresponding wave numbers for CH_2Br_2 and CD_2Br_2.

TABLE VI. Heat content, free energy, entropy, and heat capacity for CD_2Br_2 for ideal gaseous state at 1 atmos pressure.

T	$(H^0-E_0{}^0)/T$	$-(F^0-E_0{}^0)/T$	S^0	$C_p{}^0$
100	8.40	50.35	58.75	9.24
200	9.37	56.45	65.83	11.69
273.16	10.29	59.51	69.80	13.85
298.16	10.62	60.42	71.04	14.53
300	10.64	60.49	71.13	14.57
400	11.91	63.73	75.64	16.79
500	13.06	66.51	79.57	18.40
600	14.12	69.04	83.16	19.69
700	14.92	71.21	86.14	20.60
800	15.68	73.26	88.94	21.38
900	16.35	75.15	91.50	22.02
1000	16.94	76.89	93.84	22.54

TABLE VII. Heat content, free energy, entropy, and heat capacity for $CHDBr_2$ for ideal gaseous state at 1 atmos pressure.

T	$(H^0-E_0{}^0)/T$	$-(F^0-E_0{}^0)/T$	S^0	$C_p{}^0$
100	8.40	51.57	59.97	9.23
200	9.30	57.66	66.95	11.34
273.16	10.10	60.67	70.77	13.21
298.16	10.38	61.57	71.95	13.81
300	10.40	61.63	72.03	13.85
400	11.54	64.78	76.32	15.93
500	12.58	67.47	80.05	17.53
600	13.51	69.85	83.36	18.77
700	14.34	72.00	86.34	19.75
800	15.07	73.96	89.03	20.56
900	15.72	75.77	91.48	21.24
1000	16.30	77.45	93.75	21.80

ACKNOWLEDGMENTS

This work was part of a research program which has been aided by a contract with the Office of Ordnance Research, U. S. Army; and by grants from the American Academy of Arts and Sciences and the Socony-Vacuum Laboratories. The authors are thankful for this assistance.

[23] D. P. Stevenson and J. Y. Beach, J. Chem. Phys. **6**, 25 (1938).
[24] W. F. Edgell and G. Glockler, J. Chem. Phys. **9**, 484 (1941).
[25] E. Gelles and K. Pitzer, J. Am. Chem. Soc. **75**, 5259 (1953).

The Solution of the Boltzmann Equation for a Shock Wave using a Restricted Variational Principle*

PHILIP ROSEN
Applied Physics Laboratory, The Johns Hopkins University, Silver Spring, Maryland
(Received January 18, 1954)

Using a variational method and the Mott-Smith velocity distribution function, the thickness of a plane shock wave is calculated for various Mach numbers. The results compare fairly well with those obtained by Mott-Smith. It is also shown that the Mott-Smith distribution function becomes a better choice as the Mach number increases.

I. INTRODUCTION

IT has been shown by Mott-Smith[1] that the applicability of the Enskog-Chapman method for solving the Boltzmann transport equation for a strong shock wave is doubtful. For strong shocks the thickness of the shock wave is comparable to the mean free path and one must use other approximation methods. Mott-Smith uses the integral form of the transport equation for an arbitrary transport property and assumes a particular form for the distribution function. He then proceeds to calculate the variation of the gas density through the shock.

In this study we will use another method of approximation to attack the problem of calculating the thickness of a shock wave. In a previous study the author developed a variational method for solving the Boltzmann equation.[2] The purpose of this work is to compare our method of approximation with the method of Mott-Smith so that it may be evaluated as a method for solving problems in kinetic theory when the system under study is far from equilibrium.

We shall concern ourselves with a plane shock wave which is stationary in the observer's system, through which a steady flow of gas passes from $x=-\infty$ to $x=+\infty$. We shall assume that no external force is present and that no relaxation effects take place.

II. THE VARIATIONAL METHOD

The Boltzmann equation[3] for our problem reduces to:

$$\frac{u\partial f(x,\mathbf{c})}{\partial x}=\frac{\partial_e f}{\partial t}=\int\int(f'f_1'-ff_1)k_1 d\mathbf{k}d\mathbf{c}_1. \quad (1)$$

The notation used here is that of reference 3. Let us now consider the following restricted variational principle:

$$\lim_{\tilde{f}\to f}\delta\int_{-\infty}^{+\infty}\int_{\mathbf{c}}\left[\tilde{f}u\frac{\partial f}{\partial x}+\frac{\partial_e\tilde{f}}{\partial t}f\right]dxd\mathbf{c}=0 \quad (2)$$

such that f is varied as a function of x and $\mathbf{c}$ and $\tilde{f}$ is held fixed when the variation is carried out. We also take f to be given at the boundaries $x=\pm\infty$, $|\mathbf{c}|=\infty$. The variational principle then leads to

$$\int_{-\infty}^{+\infty}\int_{\mathbf{c}}\left[u\frac{\partial f}{\partial x}-\frac{\partial_e f}{\partial t}\right]\delta f dxd\mathbf{c}=0.$$

If δf is arbitrary, then we obtain Eq. (1).

We can state the variational method in an alternate manner. If in the integral

$$I=\int_{-\infty}^{+\infty}\int_{\mathbf{c}}\left[\tilde{f}u\frac{\partial F}{\partial x}+\frac{\partial_e\tilde{f}}{\partial t}F\right]dxd\mathbf{c},$$

we substitute

$$F=f(x,\mathbf{c})+\epsilon\eta(x,\mathbf{c})$$
$$\tilde{f}=f(x,\mathbf{c})+\epsilon'\eta(x,\mathbf{c}),$$

where $\eta(x,\mathbf{c})$ is an arbitrary function which vanishes at the boundaries, and ϵ, ϵ' are small parameters then

$$\lim_{\epsilon'\to\epsilon\to 0}\frac{\partial I(\epsilon,\epsilon')}{\partial\epsilon}\epsilon'=0$$

is equivalent to having $f(x,c)$ satisfy Eq. (1).

In any actual problem we must use trial solutions and since we must satisfy the equations of conservation of mass, momentum, and energy we shall demand that the trial solution satisfy

$$\int\Phi_i u\frac{\partial f}{\partial x}d\mathbf{c}=0, \quad (3)$$

where Φ_i represents the collision invariants, $\Phi_1=1$, $\Phi_2=u$, $\Phi_3=c^2+(2/m)E_{\text{int}}$. E_{int} is the internal energy of a molecule and m is the mass.

We now assume as Mott-Smith does that the distribution function is of the form

$$f=f_\alpha+f_\beta \quad (4a)$$

with

$$f_\alpha=n_\alpha(x)\left(\frac{A_\alpha}{\pi}\right)^{\frac{3}{2}}\exp\{-A_\alpha(\mathbf{c}-\mathbf{i}u_\alpha)^2\}$$
$$\equiv n_\alpha(x)\left(\frac{A_\alpha}{\pi}\right)^{\frac{3}{2}}h_\alpha(\mathbf{c}) \quad (4b)$$

* Supported by the Bureau of Ordnance, Department of the Navy, under Contract NOrd 7386.

[1] H. M. Mott-Smith, Phys. Rev. **82**, 885 (1951).

[2] P. Rosen, "On the Use of Restricted Variational Principles for the Solution of Differential Equations," J. Appl. Phys. **25**, 336 (1954).

[3] S. Chapman and T. G. Cowling, *The Mathematical Theory of Non-Uniform Gases* (Cambridge University Press, Cambridge, 1939).

$A_\alpha \equiv m/2kT_\alpha$ and similarly for f_β with α replaced by β. T_α and u_α are the gas temperature, and velocity, respectively, at $x=-\infty$. The quantities T_β, u_β refer to conditions in the subsonic stream at $x=+\infty$.

The substitution of the above distribution function into Eq. (3) will yield essentially the same relationships as Eq. (7) of reference 1 which can be reduced to the equations:

$$\frac{u_\beta}{u_\alpha}=\frac{M^2+a-2}{(a-1)M^2}, \tag{5a}$$

$$\frac{A_\alpha}{A_\beta}=\frac{T_\beta}{T_\alpha}=\frac{(M^2+a-2)(aM^2-1)}{(a-1)^2M^2}, \tag{5b}$$

and

$$n_\alpha(x)u_\alpha+n_\beta(x)u_\beta=n_\alpha(-\infty)u_\alpha\equiv n_0u_\alpha \tag{5c}$$

where $a=2\gamma/\gamma-1$ (γ is the ratio of specific heats), and $M^2=[2(a-2)/a]A_\alpha u_\alpha^2$ where M is the Mach number of the supersonic stream.

We are now prepared to use the variational method to determine $n_\alpha(x)$. If we substitute in the integral

$$I=\int_{-\infty}^{+\infty}\int_{\mathbf{c}}\left[\bar{f}u\frac{\partial f}{\partial x}+\frac{\partial_e\bar{f}}{\partial t}f\right]dxd\mathbf{c},$$

the functions

$$f=n_\alpha(x)\left(\frac{A_\alpha}{\pi}\right)^{\frac{3}{2}}h_\alpha(\mathbf{c})+\frac{u_\alpha}{u_\beta}[n_0-n_\alpha(x)]\left(\frac{A_\beta}{\pi}\right)^{\frac{3}{2}}h_\beta(\mathbf{c}),$$

$$\bar{f}=\bar{n}_\alpha(x)\left(\frac{A_\alpha}{\pi}\right)^{\frac{3}{2}}h_\alpha(\mathbf{c})+\frac{u_\alpha}{u_\beta}[n_0-\bar{n}_\alpha(x)]\left(\frac{A_\beta}{\pi}\right)^{\frac{3}{2}}h_\beta(\mathbf{c})$$

and integrate over velocities we find:

$$I=\int_{-\infty}^{+\infty}\left\{\left[\left(\frac{A_\alpha}{\pi}\right)^3L_\alpha+\left(\frac{A_\beta}{\pi}\right)^3L_\beta\left(\frac{u_\alpha}{u_\beta}\right)^2-\frac{2}{\pi^3}(A_\alpha A_\beta)^{\frac{3}{2}}\frac{u_\alpha}{u_\beta}L_{\alpha\beta}\right]\bar{n}_\alpha\frac{dn_\alpha}{dx}+\left[\left(\frac{A_\alpha}{\pi}\right)^3\left(\frac{A_\beta}{\pi}\right)^{\frac{3}{2}}\frac{u_\alpha}{u_\beta}J_1-\left(\frac{A_\beta}{\pi}\right)^3\left(\frac{A_\alpha}{\pi}\right)^{\frac{3}{2}}\left(\frac{u_\alpha}{u_\beta}\right)^2J_2\right]\bar{n}_\alpha(n_0-\bar{n}_\alpha)n_\alpha+\text{terms in }\bar{n}_\alpha\right\}dx. \tag{6}$$

The integrals L_α, L_β, and $L_{\alpha\beta}$ are defined as follows and offer no difficulty in evaluation:

$$L_\alpha\equiv\int_{\mathbf{c}}h_\alpha^2(\mathbf{c})ud\mathbf{c}=\left(\frac{\pi}{2A_\alpha}\right)^{\frac{3}{2}}u_\alpha, \tag{7a}$$

$$L_\beta\equiv\int_{\mathbf{c}}h_\beta^2(\mathbf{c})ud\mathbf{c}=\left(\frac{\pi}{2A_\beta}\right)^{\frac{3}{2}}u_\beta, \tag{7b}$$

$$L_{\alpha\beta}\equiv\int_{\mathbf{c}}h_\alpha(\mathbf{c})h_\beta(\mathbf{c})ud\mathbf{c}=\pi^{\frac{3}{2}}\frac{(A_\alpha u_\alpha+A_\beta u_\beta)}{(A_\alpha+A_\beta)^{5/2}}\times\exp[-(Z_1^2-Z_2^2)], \tag{7c}$$

where the quantities Z_1^2 and Z_2^2 which occur in other integrals to be evaluated are

$$Z_1^2=\left(2A_\alpha\Big/\frac{2A_\alpha}{A_\beta}+1\right)(u_\alpha-u_\beta)^2,$$

$$Z_2^2=\left[A_\alpha\Big/\left(\frac{2A_\alpha}{A_\beta}+1\right)\left(\frac{A_\alpha}{A_\beta}+1\right)\right](u_\alpha-u_\beta)^2.$$

The integrals J_1 and J_2 are defined as follows:

$$J_1=J_{11}+J_{12}-J_{13}-J_{14}$$

where

$$J_{11}\equiv\int_{\mathbf{c}}\int_{\mathbf{c}_1}\int_{\mathbf{k}}h_\alpha(\mathbf{c})h_\alpha(\mathbf{c}')h_\beta(\mathbf{c}_1')k_1d\mathbf{k}d\mathbf{c}_1d\mathbf{c},$$

$$J_{12}\equiv\int_{\mathbf{c}}\int_{\mathbf{c}_1}\int_{\mathbf{k}}h_\alpha(\mathbf{c})h_\alpha(\mathbf{c}_1')h_\beta(\mathbf{c}')\mathbf{k}_1d\mathbf{k}d\mathbf{c}_1d\mathbf{c},$$

$$J_{13}\equiv\int_{\mathbf{c}}\int_{\mathbf{c}_1}\int_{\mathbf{k}}h_\alpha(\mathbf{c})h_\alpha(\mathbf{c})h_\beta(\mathbf{c}_1)k_1d\mathbf{k}d\mathbf{c}_1d\mathbf{c},$$

$$J_{14}\equiv\int_{\mathbf{c}}\int_{\mathbf{c}_1}\int_{\mathbf{k}}h_\alpha(\mathbf{c})h_\alpha(\mathbf{c}_1)h_\beta(\mathbf{c})k_1d\mathbf{k}d\mathbf{c}_1d\mathbf{c},$$

and J_2 is obtained from J_1 by interchanging the subscripts α and β. It is necessary to use a molecular model to evaluate the J integrals. Because of the difficulty of evaluating the J integrals we shall carry out the analysis for elastic spherical molecules. The evaluation of these integrals will be given in part III.

Since the integrand in Eq. (6) is now expressed in terms of n_α and $\bar{n}_\alpha$ we can vary n_α as a function of x (except at the boundaries) keeping n_α fixed and then let $\bar{n}_\alpha$ approach n_α. We then obtain the differential equation:

$$\left[\left(\frac{A_\alpha}{\pi}\right)^3L_\alpha+\left(\frac{A_\beta}{\pi}\right)^3L_\beta\left(\frac{u_\alpha}{u_\beta}\right)^2-\frac{2}{\pi^3}(A_\alpha A_\beta)^{\frac{3}{2}}L_{\alpha\beta}\frac{u_\alpha}{u_\beta}\right]\frac{dn_\alpha}{dx}=\frac{u_\alpha}{u_\beta}\left[\left(\frac{A_\alpha}{\pi}\right)^3\left(\frac{A_\beta}{\pi}\right)^{\frac{3}{2}}J_1-\frac{u_\alpha}{u_\beta}\left(\frac{A_\beta}{\pi}\right)^3\left(\frac{A_\alpha}{\pi}\right)^{\frac{3}{2}}J_2\right](n_0-n_\alpha)n_\alpha \tag{8a}$$

or

$$\frac{dn_\alpha}{dx}+B'(n_0-n_\alpha)n_\alpha=0, \tag{8b}$$

where

$$B'=\frac{2^{\frac{1}{2}}}{\pi^3}\frac{\frac{u_\alpha}{u_\beta}A_\beta^3 J_2-(A_\alpha A_\beta)^{\frac{1}{2}}J_1}{u_\beta+u_\alpha\left(\frac{A_\beta}{A_\alpha}\right)^{\frac{1}{2}}-2^{5/2}A_\beta^{\frac{1}{2}}\frac{L_{\alpha\beta}}{\pi^{\frac{1}{2}}}}. \tag{8c}$$

In Eq. (8c) we have made use of the values of the integrals L_α and L_β as given in Eqs. (7a) and (7b). We shall show later that the collision integrals J_1 and J_2 are proportional to the cross section, $\pi\sigma^2$, for elastic spherical molecules. Consequently, if we define

$$B=\frac{B'}{2^{\frac{1}{2}}\pi\sigma^2},$$

we can write Eq. (8b) as

$$\frac{d(n_\alpha/n_0)}{dx}+\frac{B}{l}n_\alpha/n_0\left(1-\frac{n_\alpha}{n_0}\right)=0 \tag{9}$$

with the solution $n_\alpha/n_0=1/(1+e^{Bx/l})$, where $1/2^{\frac{1}{2}}\pi n_0\sigma^2$ is the mean free path in the supersonic stream. Equation (9) is of the same type as that obtained by Mott-Smith for n_α, except that our values for B will be different. If we define the thickness of the shock wave as Mott-Smith does, then the thickness, $X=4l/B$.*

III. EVALUATION OF J_1 AND J_2 FOR ELASTIC SPHERES

In order to calculate numerical values of B we must first evaluate the integrals J_1 and J_2. For elastic spheres the quantity[3] $k_1 d\mathbf{k}=(\sigma^2/2)g\cos(\chi/2)\sin(\chi/2)d\chi d\epsilon$ where $\mathbf{g}=\mathbf{c}_1-\mathbf{c}$, $\mathbf{g}'=\mathbf{c}_1'-\mathbf{c}'$, $\mathbf{k}=\mathbf{c}'-\mathbf{c}=\mathbf{c}_1-\mathbf{c}_1'=\frac{1}{2}(\mathbf{g}-\mathbf{g}')$, χ is the angle between $\mathbf{g}$ and $\mathbf{g}'$, and ϵ is the angle between the plane of $\mathbf{k}$ and $\mathbf{g}$ with any plane passing through $\mathbf{g}$ and a fixed direction. With the above value of $k_1 d\mathbf{k}$, and making use of the theorem that velocities before and after collision can be exchanged† we have for J_{11}:

$$J_{11}=\frac{\sigma^2}{2}\int_{\mathbf{c}}\int_{\mathbf{c}'}\int_0^{2\pi}\int_0^{\pi}\times\exp\{-A_\alpha(\mathbf{c}'-\mathbf{i}u_\alpha)^2-A_\alpha(\mathbf{c}-\mathbf{i}u_\alpha)^2-A_\beta(\mathbf{c}_1-\mathbf{i}u_\beta)^2\}g\cos\frac{\chi}{2}\sin\frac{\chi}{2}d\chi d\epsilon d\mathbf{c}d\mathbf{c}_1.$$

To simplify the integration we make use of the orthogonal transformation:

$$\mathbf{c}=\mathbf{i}u_\alpha+\mathbf{F}-\mathbf{G}\frac{A_\beta}{A_\beta+2A_\alpha}$$
$$\mathbf{c}_1=\mathbf{i}u_\beta+F+\mathbf{G}\frac{2A_\alpha}{A_\beta+2A_\alpha}. \tag{10}$$

Then

$$\mathbf{c}'=\mathbf{k}+\mathbf{i}u_\alpha+\mathbf{F}-G\frac{A_\beta}{A_\beta+2A_\alpha}$$
$$\mathbf{G}=\mathbf{g}+\mathbf{i}(u_\alpha-u_\beta)$$

and

$$d\mathbf{c}d\mathbf{c}_1=d\mathbf{F}d\mathbf{G}.$$

The transformation (10) causes the argument of the exponential to contain terms in F^2 and $\mathbf{F}\cdot\mathbf{k}$. Using the vector $\mathbf{k}$ as specifying a fixed direction, the integration over $\mathbf{F}$ is readily accomplished and we obtain:

$$J_{11}=\frac{\sigma^2\pi^{5/2}}{(2A_\alpha+A_\beta)^{\frac{1}{2}}}\exp\left(\frac{-2A_\alpha A_\beta(u_\alpha-u_\beta)^2}{2A_\alpha+A_\beta}\right)\times\int_{\mathbf{g}}\int_0^{2\pi}\int_0^{\pi}\exp\{-S(\chi)g^2\}\times\exp\left\{\frac{-A_\alpha A_\beta}{2A_\alpha+A_\beta}(u_\alpha-u_\beta)g[3\cos\theta_g+\cos\theta_{g'}]\right\}\times g^3\cos\frac{\chi}{2}\sin\frac{\chi}{2}\sin\theta_g d\epsilon d\chi d\theta_g dg, \tag{11}$$

where θ_g is the angle between $\mathbf{g}$ and $\mathbf{i}$, and $\theta_{g'}$ is the corresponding angle for $\mathbf{g}'$, and

$$S(\chi)=\frac{2A_\alpha A_\beta}{2A_\alpha+A_\beta}+\frac{A_\alpha(A_\alpha-A_\beta)}{2A_\alpha+A_\beta}\sin^2\frac{\chi}{2}.$$

From spherical trigonometry we have

$$\cos\theta_{g'}=\cos\theta_g\cos\chi+\sin\theta_g\sin\chi\cos\epsilon.$$

In order to proceed we need the integral

$$2\int_0^{\pi}\int_0^{\pi}\exp\left\{\frac{-A_\alpha A_\beta}{2A_\alpha+A_\beta}(u_\alpha-u_\beta)\times g[3\cos\theta_g+\cos\theta_g\cos\chi+\sin\theta_g\sin\chi\cos\epsilon]\right\}\sin\theta_g d\theta_g d\epsilon.$$

This integral is of the form of Gegenbauer's double integral[4] and reduces to:

$$4\pi\frac{\sinh R(\chi)g}{R(\chi)g},$$

where

$$R(\chi)=\frac{\sqrt{2}A_\alpha A_\beta}{2A_\alpha+A_\beta}(5+3\cos\chi)^{\frac{1}{2}}=\frac{2A_\alpha A_\beta}{2A_\alpha+A_\beta}\left(4-3\sin^2\frac{\chi}{2}\right)^{\frac{1}{2}}.$$

* An additional factor of 2 appears in the definition of l given in reference 1 which appears to be a misprint.

† See reference 3, page 67, Eq. (1).

[4] G. N. Watson, *Theory of Bessel Functions* (Cambridge University Press, Cambridge, 1944), p. 51.

Thus the integral in Eq. (11) reduces to:

$$2\pi\int_0^\pi\int_0^\infty \frac{\exp\{-S(\chi)g^2+R(\chi)g\}-\exp\{-S(\chi)g^2-R(\chi)g\}}{R(\chi)} g^2dg\sin\frac{\chi}{2}\cos\frac{\chi}{2}d\chi$$

which in turn integrates to:

$$2\pi\int_0^\pi\left[\frac{1}{S(\chi)R(\chi)}+\frac{R(\chi)}{2S^2(\chi)}\right]\frac{\exp\left[\frac{R^2(\chi)}{4S(\chi)}\right]}{S^{\frac{1}{2}}(\chi)}\operatorname{Erf}\left[\frac{R(\chi)}{2S^{\frac{1}{2}}(\chi)}\right]\sin\frac{\chi}{2}\cos\frac{\chi}{2}d\chi+\pi\int_0^\pi\frac{1}{S^2(\chi)}\sin\frac{\chi}{2}\cos\frac{\chi}{2}d\chi$$

where

$$\operatorname{Erf}[y]=\int_0^y\exp(-t^2)dt.$$

The second of these integrals can easily be evaluated; however, the first requires more labor. If we make use of the alternate expression[5]

$$\operatorname{Erf}[y]=\frac{\sqrt{\pi}}{2}-y\int_1^\infty\exp(-y^2w^2)dw$$

and change variable to Z, where

$$Z^2=\frac{3A_\alpha A_\beta^2}{2A_\alpha+A_\beta}\frac{(u_\alpha-u_\beta)^2}{A_\alpha-A_\beta}\times\left[\frac{4}{3}-\sin^2\chi/2\Big/\left(\frac{2A_\beta}{A_\alpha-A_\beta}\right)+\sin^2\frac{\chi}{2}\right]$$

the first integral can be evaluated. The final value of J_{11} is then found to be:

$$J_{11}=\sqrt{2}\pi\sigma^2\Delta\exp(-Z_1^2)\times\{Z_1\exp(Z_1^2)E_2(Z_1)-Z_2\exp(Z_2^2)E_2(Z_2)\},\quad(12)$$

where

$$\Delta=\frac{\pi^3}{2\sqrt{2}}\frac{(A_\alpha/A_\beta)^2[2+(A_\beta/A_\alpha)]^{\frac{1}{2}}}{A_\alpha^{9/2}(u_\alpha-u_\beta)^2}$$

and

$$E_2(Z)=\frac{2}{\sqrt{\pi}}\operatorname{Erf}[Z].$$

The functions $E_n(Z)$ are tabulated by Jahnke and Emde.[6] The definitions of Z_1 and Z_2 which were given previously are the values of Z for $\chi=0$, π, respectively.

By similar methods J_{12} is evaluated and is found to equal $J_{11}\cdot J_{13}$ can be evaluated by using the transformation (10) which enables one to integrate readily over **F** and **g** or **G**. We find that

$$\frac{J_{13}}{\sqrt{2}\pi\sigma^2}=\frac{A_\alpha+A_\beta}{2A_\beta}(Z_1^2-Z_2^2)\Delta\left[\frac{\exp(-Z_1^2)}{\sqrt{\pi}}+\left(Z_1+\frac{1}{2Z_1}\right)E_2(Z_1)\right].\quad(13)$$

Finally, J_{14} can be reduced to the form of J_{13} and is found to be:

$$\frac{J_{14}}{\sqrt{2}\pi\sigma^2}=\frac{2A_\beta}{A_\alpha+A_\beta}(Z_1^2-Z_2^2)\Delta\left\{\frac{\exp(-Z_1^2)}{\sqrt{\pi}}+\left(Z_2+\frac{1}{2Z_2}\right)\exp[-(Z_1^2-Z_2^2)]E_2(Z_2)\right\}.\quad(14)$$

Adding up all the contributions to J_1 we have:

$$\frac{J_1}{\sqrt{2}\pi\sigma^2}=\Delta\left\{\left[2Z_1-\frac{A_\alpha+A_\beta}{2A_\beta}(Z_1^2-Z_2^2)\left(Z_1+\frac{1}{2Z_1}\right)\right]E_2(Z_1)-\left[2Z_2+\frac{2A_\beta}{A_\alpha+A_\beta}(Z_1^2-Z_2^2)\left(Z_2+\frac{1}{2Z_2}\right)\right]E_2(Z_2)\exp[-(Z_1^2-Z_2^2)]-\left[\frac{2A_\beta}{A_\alpha+A_\beta}+\frac{A_\alpha+A_\beta}{2A_\beta}\right]\frac{(Z_1^2-Z_2^2)}{\sqrt{\pi}}\exp(-Z_1^2)\right\}.\quad(15)$$

[5] E. T. Whittaker and G. N. Watson, *Modern Analysis* (Macmillan Company, New York, 1946), p. 341.
[6] E. Jahnke and F. Emde, *Tables of Functions* (Dover Publications, New York, 1945).

As stated previously, J_2 is found by interchanging the subscripts α and β in the expression for J_1.

IV. NUMERICAL COMPUTATION

It can be seen from the definitions of Z_1, Z_2, and A_α, and Eqs. (5a) and (5b) that Z_1 and Z_2 are functions of the Mach number M and γ. Consequently, from Eq. (12) we see that $A_\alpha^{7/2}J_1$ can be written as a function of M and γ, and similarly for $A_\alpha^{7/2}J_2$. From Eq. (7c) we find that $A_\alpha^2 L_{\alpha\beta}$ can also be written as a function of M and γ. Thus, from Eq. (8c) we see that B' or B is a function of these variables. The choice of elastic spheres as a molecular model causes B to be independent of the temperature of the supersonic stream and the molecular weight of the gas.

As a numerical example we shall take the case of a monatomic gas ($\gamma=5/3$) and calculate the variation of l/X with Mach number. The results are given in Table I for several Mach numbers. Also given in Table I, are the corresponding values obtained by Mott-Smith using u^2 and u^3 as transport properties, for elastic spherical molecules, which are denoted by $(l/X)_{u^2}$ and $(l/X)_{u^3}$, respectively. The results obtained indicate that our values of l/X compare fairly well with those of Mott-Smith.

TABLE I. Values of l/X for several Mach numbers for $\gamma=5/3$ and corresponding values obtained by Mott-Smith.

M	$\frac{l}{X}$	$\left(\frac{l}{X}\right)_{u^2}$	$\left(\frac{l}{X}\right)_{u^3}$
1	0	0	0
1.2	0.075	0.060	0.053
1.4	0.140	0.116	0.105
2	0.278	0.240	0.243
2.5	0.355	0.304	0.332
3	0.414	0.346	0.397
4	0.495	0.397	0.478

Since we have used an approximate distribution function in our calculation, it is desirable to have a measure of the validity of the function used. As a test of the assumed distribution function we shall use the difference:

$$D=\frac{\int_{-\infty}^{+\infty}\int_c fu\frac{\partial f}{\partial x}+f\left(\frac{\partial_e f}{\partial t}\right)d\mathbf{c}dx-2\int_{-\infty}^{+\infty}\int_c f\left(\frac{\partial_e f}{\partial t}\right)d\mathbf{c}dx}{2\int_{-\infty}^{+\infty}\int_c f\left(\frac{\partial_e f}{\partial t}\right)d\mathbf{c}dx}.$$

The quantity D measures the average deviation from zero of the quantity $u(\partial f/\partial x)-(\partial_e f/\partial t)$. Using the distribution function given in Eq. (4) with the solution found previously for $n_\alpha(x)$ we find that

$$D=\frac{1}{2}\left[\frac{B}{B^*}-1\right]$$

where

$$B^*=(\sqrt{2}\pi\sigma^2)^{-1}\frac{2^{\frac{1}{2}}}{\pi^3}\frac{\left[\frac{u_\alpha}{u_\beta}(A_\beta A_\alpha)^{\frac{1}{2}}J_1+A_\beta^3\left(\frac{u_\alpha}{u_\beta}\right)^2 J_2\right]}{\left[\frac{u_\alpha}{u_\beta}\left(\frac{A_\beta}{A_\alpha}\right)^{\frac{1}{2}}-1\right]u_\alpha}.$$

In Table II, values of D are given for several Mach numbers for $\gamma=5/3$. The results show that the distribution function which is a linear superposition of two Maxwellian distributions becomes a better choice as the Mach number increases. Below about $M=2$, the Mott-Smith distribution function leads to values of D which are large. Consequently, for this region of Mach numbers some better choice of distribution function is desirable.

TABLE II. Values of the quantity D at several Mach numbers for $\gamma=5/3$.

M	D
1	−0.500
1.4	−0.350
2	−0.156
3	−0.056
4	−0.030

The Infrared Spectrum of Ketene

BØRGE BAK AND F. ALLAN ANDERSEN
Chemical Laboratory of the University of Copenhagen, Copenhagen, Denmark
(Received March 8, 1954)

The infrared spectrum of gaseous ketene has been reinvestigated in the 500–1200 cm^{-1} region with a recording prism spectrophotometer using KBr and NaCl optics. Because of an experimental procedure which enabled us to subtract the absorption of the impurities, a ketene absorption curve was obtained, probably more correct than that found by previous investigators. An interpretation of the numerous lines in the 500–1000 cm^{-1} interval is given, resulting in a reassignment of some of the fundamental vibrational frequencies. Thermodynamic functions are recalculated.

I. INTRODUCTION

THE infrared spectrum of ketene, $CH_2=CO$ has been the subject of several investigations.[1–3] General agreement exists as to the assignment of fundamentals in the 1100–3200 cm^{-1} frequency interval but considerable dispute has arisen in connection with the interpretation of the complex spectrum in the 500–1000 cm^{-1} region. Lately, Johnson and Strandberg[4] calculated three of the four lowest fundamentals from intensity measurements on "satellite" lines in the microwave spectrum. Their results are not very consistent with earlier accepted data.

Calculated thermodynamic properties were published by Drayton and Thompson in 1948. The microwave results published since then[4,5] made improvements possible. It was felt, however, that a revision of the vibrational data was also desirable. In planning the necessary infrared measurements it was assumed that a main source of the disagreement between the various investigators must be the presence of impurities in the ketene samples used. Efforts were consequently concentrated on preparation of a ketene sample of approximately known composition. Finally, the ketene absorption spectrum was obtained as a difference between the spectrum of the whole sample and the spectrum of the impurities. This "new" ketene spectrum can be given a simple interpretation which is rather complete.

II. EXPERIMENTAL DETAILS

The gases escaping from the cracking apparatus in which acetone was pyrolized in a nitrogen atmosphere were lead through three traps (20°, −10°, −80°C) and condensed in a liquid-air trap. After one hour of pumping with an oil pump which removed most of the methane the trap with ketene was surrounded by an ether-dry ice bath (−80°C) and connected with a vacuum system in which the vapor pressure of the sample could be read. Fractions with $p_{sat} > 10$ mm of Hg were collected in an adjacent liquid-air trap and the rest of the sample was discarded. At a subsequent distillation the fractions with 120 mm $\geqslant p_{sat} \geqslant$ 70 mm were collected. At a second and third distillation the fractions taken had 128 mm $\geqslant p_{sat} \geqslant$ 108 mm and 128 mm $\geqslant p_{sat} \geqslant$ 118 mm, respectively. The yield was 500-ml gas (20°C, 1 atmos) from 25-ml acetone (3–4 percent). The sample (I) was kept at −80°C between experiments but even at that temperature dimerization might sometimes take place.

By means of a stream of dry hydrogen 35 cc of the ketene sample (I) was lead through a gas chromatograph which was filled with silica-gel (length 35 cm, tube diameter 9 mm, temperature 50°C). Fractions of the gases passing the silica column were collected in the time intervals between 3 and 7 minutes (A) and between 7 and 45 minutes (B) as indicated by the Pt wire detector. The infrared spectrum of (A) showed the presence of ethylene (0.4 cc) and carbon dioxide (0.4 cc). In (B) the presence of 2.2 cc acetylene and 4.4 cc propylene was likewise estimated. By refractionation of (B) on the gel, acetylene and propylene were totally separated. Neither ketene nor diketene pass the column since ketene probably polymerizes on the silica and the boiling point of diketene is too high (124°C). No acetone was detected. From this experiment it follows that (I) consists of about 80 percent ketene, 12 percent propylene, 6 percent acetylene, 1 percent carbon dioxide, and 1 percent ethylene.

In another experiment 80.1 cc ketene (I) was condensed in a liquid-air trap containing 40 cc 0.1*n* NaOH saturated with NaCl to depress the solubility of the hydrocarbons. The trap was heated to room temperature and the contents were vigorously shaken in order to decompose ketene fully. After 10 minutes the remaining gases (C) were collected in another trap. Their volume was 7.2 cc. By back-titration of the NaOH with 0.1*n* HCl the amount of acid constituents in (I) was found to correspond to 72 cc gas or about 70 cc ketene if carbon dioxide is subtracted. This gives 87 percent ketene in (I). By taking the infrared spectrum of the gaseous residue (C) the presence of acetylene and pro-

[1] F. Halverson and V. Z. Van Williams, J. Chem. Phys. **15**, 552 (1947).
[2] W. R. Harp, Jr., and R. S. Rasmussen, J. Chem. Phys. **15**, 778 (1947).
[3] L. G. Drayton and H. W. Thompson, J. Chem. Soc. **1948**, 1416 (1948).
[4] H. R. Johnson and M. W. P. Strandberg, J. Chem. Phys. **20**, 687 (1952).
[5] Bak, Knudsen, Madsen, and Rastrup-Andersen, Phys. Rev. **79**, 190 L(1950).

TABLE I. Observed and calculated ketene absorption peak frequencies in the 450–1010 cm^{-1} region. 10-cm gas cell. Numbers for observed optical densities (D) correspond to $p=33$ mm of Hg for frequencies less than 685 cm^{-1} and to $p=400$ mm of Hg for higher frequencies.

Reference 1		Reference 2		Reference 3		This investig.		Calculated frequencies 545 and 916 bands		588 and 942 bands	
ν cm^{-1}	Int	ν cm^{-1}	Int	ν cm^{-1}	Int	ν cm^{-1}	Int (D)	cm^{-1}	K	cm^{-1}	K
458	W	...		...		...		463	−4?		
472	W	...		...		...				467.5	−6?
482	VW	...		...		...		481	−3		
501	S	...		...		498.7	0.23	499	−2		
...		...		505	...	506?	0.18			505.5	−4
520	S	...		...		517.6	0.40	517.5	−1		
...		...		523	...	524?	0.25			524.5	−3
534	M	...		536	...	532.6	0.40	535.5	0		
539?	VW	...		...		...					
546?	VW	...		...		545.9	0.31			542.5	−2
553	S	...		556	...	552.4	0.43	553.5	1		
562	VW	...		563	...	561.2	0.34			561.0	−1
571	W	...		...		571.0	0.33	571.0	2		
580	S	...		581	...	578.2	0.44			579.0	0
596	S	...		595	...	594.5	0.37	589.5	3		
...		...		...		602.4	0.28			597.5	1
...		...		...		612.2	0.24	607.5	4		
620	S	...		621	...	616.3	0.37			616.0	2
...		...		...		627?	0.20	625.5	5		
634	W	...		630	...	631.4	0.21			634.5	3
...		...		...		644.2	0.15	643.5	6		
658	W	...		...		656.8	0.13			652.5	4
...		...		662	...	663.9	0.14	661.5	7		
...		669	2	...		675	0.09			671.0	5
680	W	679	2	678	...	680	0.08	679.5	8		
...		...		...	...	689.8	0.92			689.5	6
698?	?	695	2	...	...	696.0	0.76	697.0	9		
703	S	...		...	...	703.5	0.65			708.0	7
712	S	710	2	708	...	714.5	0.46	715.0	10		
722	S^a	724	2	...		724.5	0.46			726.5	8
728	S^a	731	2	...		730.0	0.52				
731	W	...		734	...	731.6	0.63	733.5	11		
...		740	2	...		742.8	0.40			745.0	9
752	M	751	2	...		751.8	0.29	751.0	12		
760	W	760	2	...		761.8	0.23			763.0	10
...		765	2	...		...					
773	S^b	771	2	...	...	771.2	0.20	768.5	13		
783	S^b	783	1	784	...	783.1	0.25			781.5	11
792	S^b	792	1	790		790.2	0.22	786.5	14		
...		...		...		...				800.0	12
807	?	805	0	...		805.2	0.14	804.5	15		
811	W	...		...	...	812.0	0.12				
819	W	821	3	818	...	820.8	0.10	822.5	16	818.5	13
830	VW	829	3	831	...	829.1	0.10				
...		...		835						837.0	14
841	S	843	3	840	...	841.9	0.17			841.5	−5
851	W	853	3	850	...	852.1	0.15	852.5	−3		
860	M	861	3	858	...	861.2	0.18			860.0	−4
869	M	871	3	869	...	870.7	0.19	870.5	−2		
878	M	880	3	877	...	879.7	0.22			878.5	−3
886	W	...		884	...	886?	0.20	888.5	−1		
891	M	891	3	889	...	892?	0.24				
896	W	...		896	...	897.1	0.24			897.0	−2
907	S	906	3	902	...	905.3	0.30	906.5	0		
912	M	913	3	910	...	910.9	0.28			915.5	−1
...		...		916	...						
918	M	921	3	922	...	921.1	0.28	924.5	1		
927	VW	930	3	927	...	930?	0.26				
932	S	936	3	932	...	934.5	0.32			934.0	0
940	?	...		940	...	...	0.22	942.5	2		
...		...		947	...	...					
948	S	952	3	952	...	951.6	0.27			952.5	1
963	?	...		963	...	...	0.22	961.0	3		
966	S	968	3	968	...	967.3	0.27			971.0	2
...		...		977	...	979?	0.14	979.0	4		
986	S	990	3	989	...	990.3	0.21			989.5	3
...		...		996	...	998?	0.17	997.0	5		
...		...		1002	...	...					
1004	S	1006	3	1007	...	1007.2	0.23			1008.0	4

[a] Definitely due to impurity.
[b] Probably due to impurity.

TABLE II. Symmetry types and characters for ketene normal vibrations. Assignments of frequencies by various and present authors.

Species	A_1				B_1			B_2	
σ_{xz} (plane of ketene)	1				1			−1	
C_2^z	1				−1			−1	
Frequency designation	ν_2	ν_3	ν_4	ν_5	ν_1	ν_6	ν_9	ν_7	ν_8
Reference 1 (infrared)	3066	2153	1386	1122	3162	1011	529	909	588
Reference 2 (infrared)	3066	2155	1391	1124	3162	925	530	731	599
Reference 3 (infrared)	3060	2150	1390	1122	3155	910	540	995	600
Reference 6 (Ramansp.)	2952	2049	1386	1130	3015	998	510	801	599
This invest. (infrared)	3060	2150	1384	1120	···	942	545	916	588
Reference 4 (microwave)	···	···	···	···	···	···	487	674	565

pylene was determined again in approximately the same quantities as before.

Based upon these tests we find it safe to conclude that the ketene sample (I) used for the production of the infrared absorption curves contains about 85 percent ketene, the rest being the hydrocarbons mentioned. Since ketene boils at about −40°C at 1 atmos, ethylene at −104°, acetylene at −84°, and propylene at −47°C, it seems probable that ketene samples prepared by previous authors have not been free of these impurities, especially propylene. Propylene has intense bands with wide-spread fine structure around 912 and 990 cm^{-1}, i.e. in a region of important ketene absorption.

In the final procedure adopted to get the best possible spectrum of ketene itself the amount of (I) necessary to produce the desired pressure was admitted to the gas cell from a container immersed in an ice-water bath. Separate experiments had shown that in this way no harmful quantity of diketene is let in. The recording of the spectrum was started immediately and continued for 5 minutes after which the gas was condensed in a liquid-air trap in direct connection with the gas cell. After 5 minutes of thorough evacuation of the gas cell to make sure that the diketene which may have been formed during the recording of the spectrum was removed, the sample (I) was again admitted to the gas cell from an ice-water bath and the recording of the spectrum was continued for another 5 minutes. In this way the spectrum in the 666–3800 cm^{-1} region was recorded on a Beckmann I.R.II spectrophotometer (NaCl prism; cell length 10 cm) in 20 minutes. Similarly, the spectrum in the 490–700 cm^{-1} interval was recorded in a single run using a Beckmann I.R.III instrument (KBr prism; cell length 10 cm).

When the spectrum of ketene including the impurities had been taken the sample was condensed in a trap with the appropriate amount of 1n NaOH solution saturated with NaCl. The mixture was treated at room temperature as described above. Then the gaseous residue was readmitted to the gas cell from an ice-water bath which retains most of the water. The spectrum was taken and used as the effective background at the drawing of the ketene spectrum proper.

III. OBSERVED INFRARED SPECTRUM

In Table I the absorption peaks in the 450–1010 cm^{-1} interval found by previous investigators and the present authors are given. No serious discrepancies are seen in the line frequencies, but disagreement between the earlier investigators and the present exists as to line number and intensity distribution. It is hard to judge the extent of the improvements obtained but they may form the "missing link" which prevented the assignment of the data (given in the next section) to be made earlier.

IV. ASSIGNMENT OF OBSERVED FREQUENCIES

Table II summarizes the symmetry properties of the normal vibrations of ketene and it reviews the different ways in which the earlier and the present investigators have assigned the observed frequencies to the fundamental vibrations. Serious discrepancies are concerned with the assignments of the normal vibrations ν_6, ν_7, ν_8, and ν_9. Although ketene has only C_{2v} symmetry, it is approximately a symmetric top. From microwave measurements[4] Johnson and Strandberg calculated that the two small rotational constants ($B \sim C$) are 0.343 and 0.330 cm^{-1} (average 0.336). They also concluded that the large rotational constant (A) is 9.47 cm^{-1}. Since ν_6, etc., are perpendicular bands each of them should to a good approximation give rise to a series of equidistant lines ("Q" branches) with the frequency separation $2(A-C)$ or about 18.25 cm^{-1}. Columns 9–12 of Table I show to what extent an assignment based on this has met with success. The formula applied is

$$\nu_Q = \nu \text{ (band center)} - (A-C) + 2K(A-C) \qquad |K| = 0, 1, 2, 3 \cdots.$$

If ν_Q is plotted as a function of K the inclination of the resulting straight line will be $2(A-C)$. The assignment given in Table I corresponds to

$$\nu_9 = 545 - (A-C) + 17.94K \text{ or } 536 + 17.94K$$
$$\nu_8 = 588 - (A-C) + 18.40K \text{ or } 579 + 18.40K$$
$$\nu_7 = 916 - (A-C) + 18.10K \text{ or } 907 + 18.10K$$
$$\nu_6 = 942 - (A-C) + 18.60K \text{ or } 933 + 18.60K.$$

The fixing of the band centers is, of course, based on the intensity distribution. Because of the overlapping of the bands this assignment may be questioned but it cannot be far from correct. In addition it gets support from some of the overtones (to be discussed). In average, therefore, $2(A-C)$ is 18.26 cm^{-1} or $A-C=9.13$. Taking $C=0.36$ we get $A=9.49$ cm^{-1} in good agree-

ment with the microwave result.[4] Arendale and Fletcher[7] have found 9.41 cm^{-1} from studies of the perpendicular bands on a grating spectrometer (details not yet published). At our analysis application of the more complete formula by Nielsen[8] (which takes regard to the possible presence of a Corioli interaction) was attempted but the simple assignment given here was finally found to be the best although clearly some perturbing effect(s) are operating. It is satisfactory to note that the average spacing in the fifth perpendicular band (at 3162 cm^{-1}) was found by Halverson and Williams to be 18.2 cm^{-1}. But here, too, the spacing is pretty irregular.

While the lack of consistency between the assignment made by us and that made by earlier investigators in the infrared may largely be explained by the improved "chemical" power of resolution this does not suffice to explain the assignment in reference 2 of the 731 line as ν_7. Halverson and Williams explain this line as due to an impurity while Harp and Rasmussen definitely exclude this possibility. Both may be right since acetylene, which has a very strong line at 729.1 cm^{-1}, may well have been present in their samples. All our experiments (where the effect of acetylene is eliminated) show, however, that there is a "genuine" line at 730 cm^{-1} which cannot be attributed to any of the perpendicular bands. A possible explanation of the line may be that it is the combination band $2\nu_6-\nu_5$. If ν_6 is assumed to be 2 percent anharmonic, one gets that $1.96\nu_6-\nu_5=1848-1122=726$. This assignment furthermore implies that the band is a $\|$ band fitting well with the fact that it does not seem to give rise to a system of Q branches. If the 730 line is, e.g., the R branch of a $\|$ band the corresponding P branch may fall on top of the line at 703.5.

TABLE III. Observed combination and overtone bands in the 1400–3600 cm^{-1} region and proposed assignments.

Reference 1 ν cm^{-1}	Reference 2 ν cm^{-1}	Reference 3 ν cm^{-1}	Proposed assignments ν cm^{-1}
		1456?	$\nu_6+\nu_9=1487$
		1590, 1604	$2\nu_4-2\nu_8=2768-1176=1592$
	1655	1654	$\nu_5+\nu_9=1665$
		1728	$\nu_5+\nu_8=1708$
		1775	$3\nu_8=1764$
		1833	$2\nu_7=1832$; $\nu_6+\nu_7=1858$
1949, 1974	1940, 1967	1944, 1968	$\nu_2-2\nu_9=1976$; $\nu_2-\nu_5=1940$
	2290	2240, 2265	$2\nu_8+2\nu_9=2266$; $2\nu_5=2240$
2515, 2540	2540	2495, 2520	$2\nu_8+\nu_4=2560$; $\nu_4+\nu_5=2504$
	2605		$\nu_1-\nu_9=2617$
		2873	$\nu_3-\nu_5+2\nu_6=2914$(?)
	2975	2965	$\nu_5+2\nu_6=3004$
3252, 3277	3264	3265	$\nu_3+\nu_5=3270$
3317, 3343		3328	$\nu_3+2\nu_8=3326$
3515, 3538	3510	3532	$\nu_3+\nu_4=3534$

[6] H. Kopper, Z. physik. Chem. **B34**, 396 (1936).
[7] W. F. Arendale and W. F. Fletcher, J. Chem. Phys. **21**, 1898 L(1953).
[8] H. H. Nielsen, Revs. Modern Phys. **23**, 90 (1951).

TABLE IV. $-(F^0-E_0^0)/T$ cal for ketene (rigid rotor-harmonic vibrator approximation).

	Contributions			
T°K	Translational	Rotational	Vibrational	Total
250	31.295	15.069	0.180	46.54
298.16	32.170	15.488	0.325	47.98
300	32.201	15.613	0.331	48.14
400	33.631	16.471	0.750	50.85
500	34.740	17.136	1.277	53.15
600	35.646	17.679	1.863	55.18
700	36.411	18.139	2.490	57.04
800	37.074	18.537	3.126	58.74
900	37.659	18.887	3.765	60.31
1000	38.183	19.202	4.411	61.80

The agreement with the observed Raman frequencies[6] is satisfactory except for ν_7. Kopper discusses the possibility that it may be due to acetone but since the sample used by him was distilled at −80°C this possibility can be excluded. The line at 801 cm^{-1} may be due to $\nu_4-\nu_8=1384-588=796$ cm^{-1}. The "true" ν_7 may not have been observed by Kopper.

From microwave studies of the intensities of *three* satellites Johnson and Strandberg[4] calculated ν_9, ν_8, $\nu_7=487$, 565, 674. Assuming the correctness of our fundamentals one must expect *four* satellites with intensities relative to the "main" line given by 1:0.218:0.177:0.036:0.032. The intensity ratios found by Johnson and Strandberg are 1:0.295:0.205:0.121. Even if it is supposed that one of the satellites represents a coincidence of two, it is impossible to explain the intensity measurements by Johnson and Strandberg.

V. COMBINATION AND OVERTONES

Both previous and the present authors agree in the statement that there are two parallel bands at 1062 and 1190 cm^{-1}, respectively. They are interpreted as $2\nu_9(=1090)$ and $2\nu_8(=1176)$, respectively. Both bands may have been shifted from their unperturbed positions by Fermi resonans with the strong fundamental at 1120 cm^{-1}. Table III gives observed bands and proposed assignments in the frequency region above 1400 cm^{-1} with exception of material concerning the fundamentals ν_1–ν_5.

VI. THERMODYNAMIC PROPERTIES

Since Drayton and Thompson[3] almost picked the correct moments of inertia and fundamental vibrational frequencies no great changes are introduced in the calculated thermodynamic quantities. It suffices to calculate one of the usual functions to see the effect. Table IV gives computed values of $-(F^0-E_0^0)/T$ using $A=9.41$, $B=0.34336$, and $C=0.33045$ cm^{-1} together with the fundamental vibration frequencies 545, 588, 916, 942, 1120, 1384, 2150, 3060, and 3160 cm^{-1}.

Diffusion across an Interface*

P. L. Auer and E. W. Murbach
Research Division, California Research and Development Company, Livermore, California
(Received July 14, 1953)

Ideal diffusion in the sense of Fick's law in a heterogeneous system composed of two liquids is discussed by means of a three-region model where the two bulk liquid regions adjoin a third region which characterizes the liquid-liquid interface. When diffusional resistance terms are defined in the usual manner, three classes of interfacial diffusion may be conveniently described by our model. It is found that extraordinary resistance to diffusion at the interface gives rise to perturbations in the observed concentration profile of the bulk regions; these perturbations diminish with time and disappear in the limit of vanishing resistance.

INTRODUCTION

A NUMBER of recent investigations have been concerned with determining the nature of diffusion across an interface separating two liquid phases.[1–3] Agreement on a schematic mechanism of interfacial diffusion is lacking amongst these investigators. Two main schools of thought are maintained on the subject. The first postulates that the interface offers no extraordinary resistance to the diffusional process and that equilibrium conditions prevail at the interface proper during all times.[4] An alternate view, that the interfacial boundary offers additional resistance to the transport process, has led to a novel solution of the diffusion equation.[5]

In the sections to follow, a model describing diffusion across a two liquid interface will be proposed, and on the basis of this model several classes of interfacial resistance will be discussed. Before proceeding to the description of the model, a brief discussion of diffusion theory will be given.

Whereas formulations for gaseous diffusion in many systems can be derived quite rigorously from kinetic theory, this is not possible, at the present, for diffusion in liquids. In the limit that departures from equilibrium conditions are small, diffusional processes in liquids may be treated by the methods of irreversible thermodynamics.[6] Such a treatment leads to the familiar result that the ordinary mass diffusion current is proportional to the gradient of the chemical potential.

Since diffusion experiments are most often performed with concentration as the observed variable, it is convenient to transform the original diffusion equation in terms of chemical potential to an equation in terms of concentration. The transformation leads to a diffusion coefficient which is predicted to be concentration dependent for all cases;[7,8] and it is only in this sense that Fick's law can be derived. For the purpose of this discussion it will be assumed, nevertheless, that the diffusion system under consideration is ideal enough to obey a simple Fick's law with constant diffusion coefficient. The apparent constant may be an integral diffusion coefficient which adequately describes the transport process throughout its entire course.

The spirit in which the diffusion equation is derived implies that in the absence of sources and sinks the diffusion current as well as the potential function from which it is derived (the chemical potential in this instance) are continuous throughout the system except at boundaries offering infinite resistance, such as the walls of a container. If there is a physical discontinuity in the potential function at a plane boundary, such as the phase interface, there is a strong possibility that the concepts of simple diffusion theory are not applicable in the vicinity of this surface and the true boundary conditions must be derived from more rigorous transport theory. It is useful to keep the above considerations in mind when formulating a consistent model for interfacial diffusion.

A MODEL FOR INTERFACIAL DIFFUSION

A heterogeneous system composed of two liquids is properly described by four distinct phases, two bulk and two surface phases. When only equilibrium bulk properties of the system are of interest, contributions from the surface phases are negligible and are usually disregarded. However, when observing interfacial transport phenomenon, it is to be expected that surface properties will be of importance.

For the sake of simplicity, the model proposed here will consist of three distinct regions only. Two of the regions are the bulk liquid phases, and connecting them is the third region of the interface (Fig. 1). The two surface phases are thus combined into a single interfacial region with the property that the "observed" diffusion coefficient of a given solute species differs in value for this region from its observed values in the

* This work performed under U. S. Atomic Energy Commission Contract Number $AT(11\text{–}1)\text{–}74$.
[1] J. T. Davies, J. Phys. and Colloid. Chem. **54**, 185 (1950).
[2] L. H. Tung and H. G. Drickamer, J. Chem. Phys. **20**, 6, 10 (1952).
[3] A. F. H. Ward and L. H. Brooks, Trans. Faraday Soc. **48**, 1124 (1952).
[4] See, for instance, discussion in W. Jost, *Diffusion in Solids, Liquids, Gases* (Academic Press, New York, 1952), p. 68.
[5] Scott, Tung, and Drickamer, J. Chem. Phys. **19**, 1075 (1951).
[6] S. R. DeGroot, *Irreversible Thermodynamics* (Interscience Publishers, New York, 1952), p. 94.
[7] S. R. DeGroot, *Irreversible Thermodynamics* (Interscience Publishers, New York, 1952), p. 104.
[8] J. G. Kirkwood (unpublished notes), p. 36.

bulk phases. In order to reduce the complexity of mathematical operations, the bulk phases will be considered semi-infinite in extension. This simplification does not affect the problem of evaluating interfacial contributions to the diffusional process. Furthermore, our model accounts specifically for diffusional resistance at the interface only and does not treat other possibilities, a rate determining chemical reaction, for instance.

It is assumed that the simple form of Fick's law adequately describes the diffusion process; therefore, it will be necessary to solve the following equation for the concentration of the species undergoing diffusion.

$$C_t = DC_{xx}. \tag{1}$$

Furthermore, it is assumed that any system ideal enough to obey Fick's law will also obey Henry's law. Three types of interfacial resistance will be studied; the boundary conditions appropriate to each are discussed below.

Case I—General

It is assumed that all three regions contribute effectively to the diffusional resistance in proportion to their D's. Since the chemical potential is continuous through all three regions, Nernst's distributive relation applies at the two boundaries. Thus:

$$\begin{aligned} C^I(t,-a) &= mC^{II}(t,-a), \\ D_1C_x{}^I(t,-a) &= D_2C_x{}^{II}(t,-a), \\ C^{III}(t,a) &= nC^{II}(t,a), \\ D_3C_x{}^{III}(t,a) &= D_2C_x{}^{II}(t,a), \end{aligned}$$

and at start-up

$$\begin{aligned} C(0,x) &= C_0 \quad x \leqslant -a, \\ &= 0. \quad x > -a. \end{aligned} \tag{2}$$

The m and n are the equilibrium distribution coefficients between the bulk and interfacial phases. At equilibrium $C^I/C^{III} = m/n$, and this quantity is the observed distribution coefficient for the bulk phases. The individual m and n may be determined in principle from the Gibbs adsorption equations. While in actual practice the quantities D_2 and $2a$ may not lend themselves to measurement, the quantity $D_2/2a$ (henceforth designated by α) is a permeability parameter which may be used to characterize conveniently the magnitude of interfacial resistance.[5] This subject will be elaborated on in a later section.

Case II—Linear

This is similar to Case I in that all three regions contribute to diffusional resistance, but it is here assumed that the interfacial region is thin enough so that the mass diffusion current throughout the region is effectively a constant for any given time $t>0$. Thus

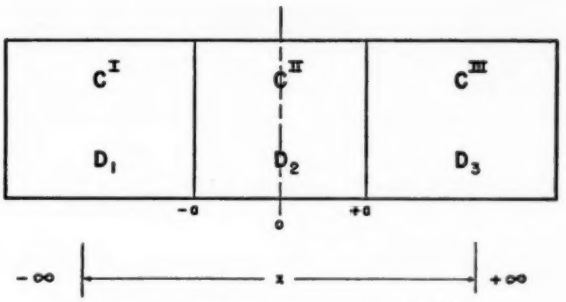

FIG. 1. Three region model for interfacial diffusion.

$$\begin{aligned} C^I(t,-a) &= mC^{II}(t,-a), \\ C^{III}(t,a) &= nC^{II}(t,a), \\ -D_1C_x{}^I(t,-a) &= \alpha[C^{II}(t,-a) - C^{II}(t,a)], \\ &= -D_3C_x{}^{III}; \end{aligned} \tag{3}$$

and the initial conditions are the same as in Case I.

Case III—Plane

If the approximation of linearity introduced in Case II is pursued further, it is found that continuity considerations force the quantity $[C^{II}(t,-a) - C^{II}(t,a)]$ to approach zero as $2a$ approaches zero. Therefore, in the limit that the interfacial region of resistance becomes a plane, the proper boundary conditions become:

$$\begin{aligned} C^I(t,-0) &= m/nC^{III}(t,+0), \\ D_1C_x{}^I(t,-0) &= D_3C_x{}^{III}(t,+0), \\ C(0,x) &= C_0 \quad x \leqslant 0, \\ &= 0. \quad x > 0. \end{aligned} \tag{4}$$

Thus, Case III reduces to the familiar formulation discussed in reference 4. As long as the interface is considered to be a plane region and the continuity argument presented above is adhered to, these boundary conditions appear to be the only valid ones.

Drickamer and his co-workers have proposed in effect[5] that as $2a$ approaches zero the quantity $[C^{II}(t,-a) - C^{II}(t,a)]$ appraches a value different from zero. The validity of such a discontinuous condition may perhaps be questioned on physical grounds.

SOLUTIONS OF THE DIFFUSION EQUATION

Equation (1) subject to the boundary conditions listed in Eqs. (2) and (4) has been solved by the use of Laplace transforms. A brief description of the method used is given in the appendix. The final solutions for the bulk regions I and III will now be listed in order of complexity.

Plane Case

$$C^I/C_0 = 1 - \frac{\Delta_3}{\Delta_1+\Delta_3}\left[1 + Erf\left(\frac{x}{2D_1{}^{\frac{1}{2}}t^{\frac{1}{2}}}\right)\right],$$

$$C^{III}/C_0 = \frac{(n/m)\Delta_1}{\Delta_1+\Delta_3} Erfc\left(\frac{x}{2D_3{}^{\frac{1}{2}}t^{\frac{1}{2}}}\right). \tag{5a}$$

Linear Case

$$C^I/C_0=1-\frac{\Delta_3}{\Delta_1+\Delta_3}\left\{1+Erf\left(\frac{x}{2D_1^{\frac{1}{2}}t^{\frac{1}{2}}}\right)-\exp\left(b^2t-b\frac{x+a}{D_1^{\frac{1}{2}}}\right)Erfc\left(bt^{\frac{1}{2}}-\frac{x+a}{2D_1^{\frac{1}{2}}t^{\frac{1}{2}}}\right)\right\},$$

$$C^{III}/C_0=\frac{(n/m)\Delta_1}{\Delta_1+\Delta_3}\left\{Erfc\left(\frac{x-a}{2D_3^{\frac{1}{2}}t^{\frac{1}{2}}}\right)-\exp\left(b^2t+b\frac{x-a}{D_3^{\frac{1}{2}}}\right)Erfc\left(bt^{\frac{1}{2}}+\frac{x-a}{2D_3^{\frac{1}{2}}t^{\frac{1}{2}}}\right)\right\}. \quad (5b)$$

General Case

$$C^I/C_0=1-\frac{\Delta_2}{\Delta_1+\Delta_2}\left[1+Erf\left(\frac{x+a}{2D_1^{\frac{1}{2}}t^{\frac{1}{2}}}\right)\right]+\frac{2\Delta_1\Delta_2}{\Delta_2^2-\Delta_1^2}\sum_{j=1}^{\infty}\beta^j\left[1+Erf\left(\frac{x+a}{2D_1^{\frac{1}{2}}t^{\frac{1}{2}}}-\frac{j\zeta}{t^{\frac{1}{2}}}\right)\right],$$

$$C^{III}/C_0=2\frac{(n/m)\Delta_1\Delta_2}{(\Delta_1+\Delta_2)(\Delta_2+\Delta_3)}\left\{Erfc\left(\frac{x-a}{2D_3^{\frac{1}{2}}t^{\frac{1}{2}}}+\frac{\zeta}{2t^{\frac{1}{2}}}\right)+\sum_{j=1}^{\infty}\beta^j\left[Erfc\left(\frac{x-a}{2D_3^{\frac{1}{2}}t^{\frac{1}{2}}}+\frac{(2j+1)\zeta}{t^{\frac{1}{2}}}\right)\right]\right\}. \quad (5c)$$

The symbols used in the foregoing have the following meanings:

$$b=\alpha\left(\frac{\Delta_1+\Delta_3}{\Delta_1\Delta_3}\right) \qquad \Delta_1=mD_1^{\frac{1}{2}},$$

$$\zeta=\Delta_2/\alpha \qquad \Delta_2=D_2^{\frac{1}{2}},$$

$$\beta=\left(\frac{\Delta_2-\Delta_1}{\Delta_1+\Delta_2}\right)\left(\frac{\Delta_2-\Delta_3}{\Delta_2+\Delta_3}\right) \qquad \Delta_3=nD_3^{\frac{1}{2}}.$$

The solution for the plane case is essentially the same as the one given by Jost.[9] In the limit that the interfacial resistance is small (both α and b are large), the linear case solution approaches the plane case solution as a approaches zero. The infinite series in the general case solution may be shown to converge, and when α becomes large enough summation of the series yields a solution which approaches the plane case solution as a approaches zero. Therefore, all three cases discussed yield the same solution when the interfacial resistance is inappreciable or the extent of the interface is negligible.

DISCUSSION

According to Eq. (5), extraordinary interfacial resistance gives rise to perturbations in the observed concentration profiles of the bulk liquid regions. Limiting this discussion to one of the bulk regions only, all three classes of resistance may be related to the solution of the plane case, if Eqs. (5) are written in the form

$$\left(\frac{\Delta_1+\Delta_3}{\Delta_3}\right)\left(\frac{C_0-C^I}{C_0}\right)=\Phi(\tau,t), \qquad \textit{Plane Case}$$

$$=\Phi(\tau',t)P_1(\tau',t,b), \qquad \textit{Linear Case} \quad (6)$$

$$=\Phi(\tau',t)P_2(\tau',t,\alpha,\Delta_1,\Delta_2,\Delta_3), \qquad \textit{General Case}$$

where

$$\Phi(\tau,t)=1+Erf(\tau/2t^{\frac{1}{2}}),$$
$$\tau=x/D_1^{\frac{1}{2}}, \qquad -\infty<\tau\leqslant 0,$$
$$\tau'=(x+a)/D_1^{\frac{1}{2}}, \qquad -\infty<\tau'\leqslant 0.$$

The effect of extraordinary interfacial resistance is expressed in the perturbation terms P_1 and P_2

$$P_1=1-\frac{\exp(b^2t-b\tau')Erfc(bt^{\frac{1}{2}}-\tau'/2t^{\frac{1}{2}})}{1+Erf(\tau'/2t^{\frac{1}{2}})},$$

$$P_2=\frac{\Delta_2}{\Delta_3}\left(\frac{\Delta_1+\Delta_3}{\Delta_1+\Delta_2}\right)\left[1+\frac{2\Delta_1}{\Delta_1-\Delta_2}\Psi\right],$$

$$\Psi=\frac{\sum_{j=1}^{\infty}\left(\frac{\Delta_2-\Delta_1}{\Delta_2+\Delta_1}\right)^j\left(\frac{\Delta_2-\Delta_3}{\Delta_2+\Delta_3}\right)^j\left(1+Erf\left[\frac{\tau'-2j\zeta}{2t^{\frac{1}{2}}}\right]\right)}{1+Erf(\tau'/2t^{\frac{1}{2}})},$$

all symbols having their previously given definitions.

It may be shown[10] that $0\leqslant P_1\leqslant 1$. Furthermore, it

TABLE I. Values of the resistance function P_1.

τ^2 (sec) \ t (sec)	10^2	5×10^2	10^3	5×10^3	10^4
			$b=1.4\times10^3$ sec$^{-\frac{1}{2}}$		
0	0.998	0.999	0.999	1.000	1.000
10	0.998	0.999	0.999	1.000	1.000
10^3	0.994	0.998	0.999	1.000	1.000
10^5	0.957	0.990	0.995	0.999	0.999
10^7	0.729	0.928	0.962	0.991	0.995
			$b=2\times10^3$ sec$^{-\frac{1}{2}}$		
0	0.989	0.995	0.996	0.998	0.999
10	0.986	0.994	0.996	0.998	0.999
10^3	0.964	0.990	0.994	0.998	0.999
10^5	0.765	0.938	0.967	0.993	0.996
10^7	0.278	0.649	0.783	0.943	0.969
			$b=1.2\times10^{-1}$ sec$^{-\frac{1}{2}}$		
0	0.317	0.527	0.621	0.802	0.856
10	0.293	0.513	0.611	0.798	0.854
10^3	0.159	0.402	0.526	0.767	0.835
10^5	0.021	0.100	0.183	0.513	0.663
10^7	0.002	0.011	0.021	0.095	0.173

[9] The solution for the plane case given in reference 4 appears to have a slight typographical error. Our solution is the correct one.

[10] See Appendix II.

becomes evident that $\lim_{\substack{b\to\infty \\ t\to\infty}} P_1=1$; while $\lim_{\tau\to\infty} P_1=0$.

Therefore, in the linear case, perturbations arising from interfacial resistance disappear with increasing time and increasing interfacial permeability. The relative magnitude of these perturbations increases with increasing distance from the interface proper.

The behavior of P_1 in terms of τ and t is tabulated in Table I for three values of the parameter b. The quantities D_1 and m are arbitrarily assigned the values 10^{-5} cm^2 sec^{-1} and unity respectively; therefore, given values of b allow α to be specified in terms of Δ_3. Furthermore, it is found that when b is equal to $10^{7/2}$, P_1 remains essentially equal to unity for all times greater than 100 sec and for distances as great as 100 cm. For b equal to $10^{-7/2}$, P_1 is nearly zero for all distances until nearly 100 sec have elapsed, after which it climbs slowly to unity for distances close to the location of the interface.

Since the general case provides a more detailed description of the interfacial resistance zone than does the linear case, it is to be expected that values of P_2 will be determined by the relative values of the resistance parameters in a more complex manner than the values of P_1. When interfacial resistance is small enough so that ζ may be neglected, the error function terms may be cancelled and Ψ summed directly to yield $P_2=1$. When ζ is no longer negligible with respect to τ', the values of P_2 are determined by the relative values of the Δ's.

TABLE II. Behavior of Ψ and P_2 with relative values of Δ's.

Relative magnitude of Δ's	Ψ	Dependence of P_2 on ζ	$\frac{\Delta_3}{\Delta_2}\left(\frac{\Delta_1+\Delta_2}{\Delta_3+\Delta_2}\right)P_2$
$\Delta_1>\Delta_2>\Delta_3$	<0	Increases	$\lesssim 1$
$\Delta_2>\Delta_1>\Delta_3$	>0	Increases	$\lesssim 1$
$\Delta_2>\Delta_3>\Delta_1$	>0	Increases	$\lesssim 1$
$\Delta_3>\Delta_1>\Delta_2$	>0	Decreases	$\gtrsim 1$
$\Delta_1>\Delta_3>\Delta_2$	>0	Decreases	$\gtrsim 1$
$\Delta_3>\Delta_2>\Delta_1$	<0	Decreases	$\gtrsim 1$

The limiting values of P_2 are easily ascertained from the expression given above for the cases Δ_2 approaches Δ_1 or Δ_3 in value. Ψ will disappear in the limit that ζ approaches infinity, and this implies physically that P_2 also approaches zero in this event. Since Ψ is a monotonically decreasing function of ζ, P_2 can either increase or decrease with increasing ζ depending on the sign of the quantity $(2\Delta_1/\Delta_1-\Delta_2)$. Table II summarizes the behavior of P_2 and Ψ for the six permutations in relative values to which the three Δ's admit.

For given values of ζ the function Ψ will have two maximum values

$$\Psi_{max1}=[1+Erf(\tau'/2t^{\frac{1}{2}})]^{-1}\sum_{j=1}^{\infty}\left[1+Erf\left(\frac{\tau'-2j\zeta}{2t^{\frac{1}{2}}}\right)\right],$$

$$\Psi_{max2}=[1+Erf(\tau'/2t^{\frac{1}{2}})]^{-1}\times\sum_{j=1}^{\infty}(-1)^j\left[1+Erf\left(\frac{\tau'-2j\zeta}{2t^{\frac{1}{2}}}\right)\right].$$

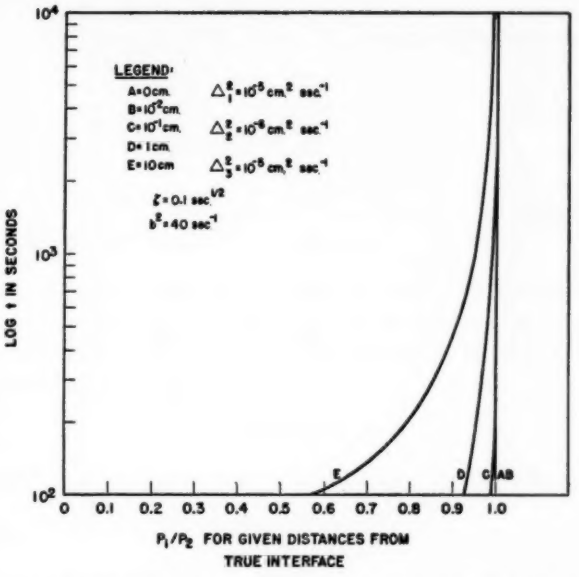

FIG. 2. Comparison of P_1 and P_2 for comparable values of the diffusion resistance parameters.

Direct evaluation of the above sums has not yet been achieved. Examination of Table II indicates two interesting classes of interfacial resistance. Whenever Δ_2 is greater than Δ_3 diffusion from region I to region III is enhanced. In the opposite case, however, the interface offers an effective barrier to diffusion. These two classes of interfacial resistance cannot be predicted on the basis of the simplified linear model. Therefore, it appears that the linear model can approximate the more general description of interfacial diffusion only when the region of the interface offers greater resistance to diffusion than the bulk phases into which diffusion is taking place. Of course, in the event that the interface is readily permeable to the diffusing species all models reduce to the well known equilibrium case.

In the limit that t approaches ∞, P_2 will also approach unity, similar to P_1; and in this respect both Linear and General models predict the same over-all effect. However, the behavior of P_2 with distance resembles its behavior with the resistance term ζ and gives rise to the two categories discussed previously. The behavior of P_2 with time and distance is illustrated in Table III for several values of the resistance parameters. Arbitrary values of 10^{-5} cm^2 sec^{-1} and unity may be assigned again to the values of D_1 and m in order to compare P_1 with P_2.

In Fig. 2 the quantity P_1/P_2 is plotted against time for given values of distance and comparable values of the resistance parameters. It is found that for the particular case chosen, agreement between P_1 and P_2 is quite good for distances close to the true interface, that is, the plane dividing region I from II. However, for distances remote from the interface P_1 consistently predicts greater departures from equilibrium conditions than does P_2. The discrepancy between P_1 and P_2

TABLE III. Values of the resistance function P_2.

Δ_3^2 in. cm^3 sec^{-1}	Δ_2^2 in. cm^3 sec^{-1}	ζ in. sec$^{\frac{1}{2}}$	$t=10^2$ sec $\tau'^2=0$ sec	$t=10^2$ sec $\tau'^2=10^3$ sec	$t=10^2$ sec $\tau'^2=10^7$ sec	$t=10^3$ sec $\tau'^2=0$ sec	$t=10^3$ sec $\tau'^2=10^3$ sec	$t=10^3$ sec $\tau'^2=10^7$ sec	$t=10^4$ sec $\tau'^2=0$ sec	$t=10^4$ sec $\tau'^2=10^3$ sec	$t=10^4$ sec $\tau'^2=10^7$ sec
10^{-3}	10^{-4}	10	0.868	0.838	0.836	0.954	0.932	0.836	0.985	0.983	0.844
		10^{-3}	1.000	1.000	0.996	1.000	1.000	1.000	1.000	1.000	1.000
	10^{-8}	10	0.044	0.034	0.034	0.114	0.088	0.034	0.297	0.274	0.037
		10^{-3}	0.998	0.995	0.688	1.000	0.999	0.957	1.000	1.000	0.996
10^{-5}	10^{-4}	10	1.459	1.516	1.519	1.227	1.297	1.519	1.079	1.091	1.504
		10^{-3}	1.000	1.000	1.022	1.000	1.000	1.002	1.000	1.000	1.000
	10^{-4}	10	7.756	8.318	8.357	5.008	5.897	8.357	2.555	2.774	8.197
		10^{-3}	1.002	1.005	1.434	1.000	1.000	1.045	1.000	1.000	1.005
10^{-7}	10^{-6}	10	2.317	2.621	2.643	1.461	1.679	2.643	1.146	1.171	2.557
		10^{-3}	1.000	1.000	1.041	1.000	1.000	1.004	1.000	1.000	1.000
	10^{-8}	10	0.391	0.341	0.337	0.639	0.559	0.337	0.859	0.840	0.352
		10^{-3}	1.000	1.000	0.961	1.000	1.000	0.996	1.000	1.000	1.000

diminishes with time. It may also be shown that disagreement between the two functions will increase with increasing interfacial resistance. It may be assumed, therefore, that experimental studies on interfacial diffusion should be able to distinguish between our general formulation and the linear approximation to it as long as interfacial resistance differs appreciably in magnitude from the ordinary bulk phase resistance to diffusion.

In general, our three region model of interfacial diffusion predicts that the presence of extraordinary resistance terms at the interface will deform the observed concentration profile in the bulk phases. The extent of these deformations is related to the relative magnitude of interfacial resistance to that encountered in the bulk liquid regions. The effect of interfacial resistance disappears with time and increases in relative magnitude with distance from the interface proper. Although the treatment presented here is based on the validity of Fick's law, it is believed this assumption is correct for certain physical systems. In particular, the equilibrium type of diffusion systems studied by Drickamer and co-workers[2] should obey Fick's law to a very good approximation.

ACKNOWLEDGMENTS

The authors wish to express their thanks to Dr. C. S. Gardner for many helpful discussions concerning mathematical portions of this investigation. The generous aid of this Laboratory's computing group in the preparation of the tables is also gratefully acknowledged.

APPENDIX. I

Letting $L\{C(x,t)\}=\bar{c}(x,p)$, the diffusion equation in the transform of $C(x,t)$ becomes

$$\begin{aligned} &D_1\bar{c}_{xx}-p\bar{c}=C_0 && x\leqslant -a,\\ &D_2\bar{c}_{xx}-p\bar{c}=0 && -a\leqslant x\leqslant a,\\ &D_3\bar{c}_{xx}-p\bar{c}=0 && x\geqslant a; \end{aligned} \tag{i}$$

the solutions of these equations are

$$\begin{aligned} \bar{c}(x,p)&=C_0/p+A\exp(xp^{\frac{1}{2}}/D_1^{\frac{1}{2}}) && x\leqslant -a,\\ &=B\exp(-xp^{\frac{1}{2}}/D_2^{\frac{1}{2}})+E\exp(xp^{\frac{1}{2}}/D_2^{\frac{1}{2}}) && -a\leqslant x\leqslant a,\\ &=G\exp(-xp^{\frac{1}{2}}/D_3^{\frac{1}{2}}) && x\geqslant a. \end{aligned} \tag{ii}$$

The constants in (ii) are evaluated by substitution of the boundary conditions listed in Eqs. (2) to (4) of the text.

Plane case.—With $a=0$

$$\begin{aligned} A&=-C_0/p\left(\frac{\Delta_3}{\Delta_1+\Delta_3}\right)\\ G&=C_0/p\left(\frac{n/m\Delta_1}{\Delta_1+\Delta_3}\right)\\ B&=0=E. \end{aligned} \tag{iii}$$

Substitution of (iii) into (ii) and inversion leads to

Eq. (5a), where

$$Erf(x)=2/\pi^{\frac{1}{2}}\int_0^x \exp(-y^2)dy$$

$$Erfc(x)=1-Erf(x)=2/\pi^{\frac{1}{2}}\int_x^\infty \exp(-y^2)dy.$$

Linear case.—The solutions in (ii) apply to the regions $x\leqslant -a$ and $x\geqslant a$ with

$$A=-C_0/p\left(\frac{\alpha\Delta_3}{\Delta_1\Delta_3 p+\alpha(\Delta_1+\Delta_3)}\right)\exp(ap^{\frac{1}{2}}/D_1^{\frac{1}{2}}),$$
$$G=C_0/p\left(\frac{\alpha\Delta_1 n/m}{\Delta_1\Delta_3 p+\alpha(\Delta_1+\Delta_3)}\right)\exp(ap^{\frac{1}{2}}/D_3^{\frac{1}{2}}). \qquad \text{(iv)}$$

However, the solution for the region $-a\leqslant x\leqslant a$ has to be of the form

$$\bar{c}(x,p)=\alpha[(1/m)\bar{c}(-a,p)-(1/n)\bar{c}(a,p)] \qquad \text{(v)}$$

in order to satisfy the boundary condition in Eq. (4). Substitution of (iv) into (ii) and inversion leads to Eq. (5b).

General case.—Equation (2) provides

$$A=-C_0/p\left(\frac{\Delta_2}{\Delta_1+\Delta_2}\right)\left[\left(\frac{\Delta_3+\Delta_2}{\Delta_2-\Delta_3}\right)\exp(2ap^{\frac{1}{2}}/D_2^{\frac{1}{2}})-\exp(-2ap^{\frac{1}{2}}/D_2^{\frac{1}{2}})\right]\delta^{-1}[\exp(ap^{\frac{1}{2}}/D_1^{\frac{1}{2}})],$$

$$B=C_0/p\left(\frac{n/m\Delta_1}{\Delta_1+\Delta_2}\right)\left(\frac{\Delta_2+\Delta_3}{\Delta_2-\Delta_3}\right)\exp(ap^{\frac{1}{2}}/D_2^{\frac{1}{2}})\delta^{-1},$$

$$E=C_0/p\left(\frac{n/m\Delta_1}{\Delta_1+\Delta_2}\right)\exp(-ap^{\frac{1}{2}}/D_2^{\frac{1}{2}})\delta^{-1},$$

$$G=C_0/p\left(\frac{n/m\Delta_1}{\Delta_1+\Delta_2}\right)\left(\frac{\Delta_2}{\Delta_2-\Delta_3}\right)\exp(ap^{\frac{1}{2}}/D_2^{\frac{1}{2}})\delta^{-1},$$

$$\delta=\left\{\left(\frac{\Delta_2+\Delta_3}{\Delta_2-\Delta_3}\right)\exp(2ap^{\frac{1}{2}}/D_2^{\frac{1}{2}})-\left(\frac{\Delta_2-\Delta_1}{\Delta_1+\Delta_2}\right)\exp(-2ap^{\frac{1}{2}}/D_2^{\frac{1}{2}})\right\}.$$

Expansion of δ^{-1} as an infinite series in powers of $\exp(-4ap^{\frac{1}{2}}/D_2^{\frac{1}{2}})$ and substitution of (v) into (ii) leads to Eq. (5c) after term-by-term inversion of the transform.

APPENDIX II

The quantity P_1 may be written in the form

$$P_1=f(u)/f(v),$$

$$f(z)=2/\pi^{\frac{1}{2}}\int_z^\infty \exp(z^2-\xi^2)d\xi, \qquad \text{(vi)}$$

$$u=(bt^{\frac{1}{2}}+|\tau'|/2t^{\frac{1}{2}}),$$

$$v=|\tau'|/2t^{\frac{1}{2}}.$$

Since $2\xi/2u\geqslant 1$ for $u\leqslant\xi\leqslant\infty$, we may write

$$f(u)\leqslant\int_u^\infty\frac{2\xi}{2u}\exp(u^2-\xi^2)$$
$$\leqslant\tfrac{1}{2}u\int_u^\infty -\frac{d}{d\xi}[\exp(u^2-\xi^2)]d\xi, \qquad \text{(vii)}$$
$$\leqslant\tfrac{1}{2}u.$$

Therefore,

$$f(u)/f(v)\leqslant v/u, \qquad \text{(viii)}$$

and $P_1\leqslant 1$ for positive values of u and v.

PVT Relations of Liquid Carbon Tetrachloride and *n*-Perfluoroheptane and a Test of the Clausius-Mosotti Equation

B. J. Alder, E. W. Haycock,* J. H. Hildebrand, and H. Watts
Department of Chemistry and Chemical Engineering, University of California, Berkeley, California

(Received January 18, 1954)

Values of $(\partial P/\partial T)_v$ for CCl_4 and n-C_7F_{16} have been measured over a range of approximately 20° and 160 atmospheres. The linear relation between P and T found in earlier studies to hold over 20 atmospheres for a number of liquids and solutions is here confirmed over the much larger range. One corollary is that $(\partial c_v/\partial v)_T=0$; another is that the isothermal compressibility of C_7F_{16}, not hitherto known, is 2.38×10^{-4} atmosphere^{-1} at 25° and 1 atmosphere, and could easily be calculated for other temperatures. The terms in the equation $(\partial E/\partial v)_T=T(\partial P/\partial T)_v-P$ are given, also the function $v^2(\partial E/\partial v)_T$, shown in the earlier studies to be constant. Its value for CCl_4 confirms the earlier studies; for n-C_7F_{16} it is 101.5 atmospheres×liters.[2]

The dielectric constant of n-C_7F_{16} has been measured at 16.0° and at 38.4°, and over a pressure range of 115 atmospheres. The values obtained conform closely to the Clausius-Mosotti equation, giving a molar polarization of 49.1 cc.

IN 1928 Westwater, Frantz, and Hildebrand[1] published measurements of $(\partial P/\partial T)_v$ for eight liquids and twelve of their equimolal mixtures, and in 1932 Hildebrand and Carter[2] published a similar study of six tetrahalides and ten of their binary mixtures. The pressure was found to increase linearly with temperature over ranges of from 15 to 20 atmospheres. Carbon tetrachloride was included in both series. In a recent investigation of the temperature coefficient of diffusion of iodine in carbon tetrachloride,[3] we assumed, in order to calculate values at constant volume from values at constant pressure, that the linear relationship holds up to our highest pressures, 200 atmospheres. The present investigation was undertaken primarily to test this assumption.

APPARATUS AND PROCEDURE

The constant volume cell was in principle a thermoregulator. It consisted of a double spiral of glass tubing of 4-mm internal diameter and a volume of 20 cc. This cell was enclosed in a steel bomb in which pressure was applied with helium. In order to hasten thermal equilibrium between the cell and the walls of the bomb, the ratio of the surface of the cell to its volume was large, helium was used instead of nitrogen, and the dead space was filled with copper turnings. The bomb, and the method of loading and pressurizing, have been described in reference 3. The bomb was immersed in an oil thermostat, the temperature of which was regulated by the cell.

The cell was first evacuated and then filled with degassed liquid. A mercury plug prevented access of helium to the liquid. The initial temperature for the 1-atmosphere point was roughly adjusted by warming the cell till the proper amount of liquid was estimated to have been expelled past the mercury plug. A special low-voltage relay circuit was used to avoid fouling the mercury surface on making and breaking the circuit. Because of the thermal lag between the cell and the bath, the temperature of the latter fluctuated over about 0.3°. The heating and cooling periods were made equal so that the temperature of the cell could be taken as the mean of the temperature cycle of the bath. Runs were made with different initial amounts of liquid in the cell.

MATERIALS

CP carbon tetrachloride was shaken with mercury, filtered, and distilled, and this process was repeated until no black material was obtained with mercury. It was next shaken with KOH solution, washed with water, dried over Drierite, and fractionated in a 30-plate column with a reflux rate of 30:1. The fraction used boiled at 76.8° at 764.3 mm.

n-Perfluoroheptane from Union Carbide and Carbon Company was refluxed with chromic acid solution for several hours until a sample of it no longer gave a green color when heated with a fresh solution of chromic acid.

TABLE I. Observed temperatures and pressures (atmospheres).

CCl_4		n-C_7F_{16}	
t°	P	t°	P
19.50	1.0	21.20	1.0
23.35	46.4	28.00	47.1
25.40	70.7	33.85	87.7
28.45	106.4	39.00	121.4
29.20	117.1		
31.40	142.5	23.25	1.0
32.80	160.5	29.65	43.9
34.10	175.0	35.50	77.2
		40.60	119.4
22.00	1.0	43.95	141.9
25.80	45.4		
29.00	83.7	27.85	1.0
32.80	127.9	34.30	43.8
35.35	157.5	39.70	78.9
		45.20	112.9

* Present address, Shell Development Company, Emeryville, California.

[1] Westwater, Frantz, and Hildebrand, Phys. Rev. **31**, 35 (1928).

[2] J. H. Hildebrand and J. M. Carter, J. Am. Chem. Soc. **54**, 3592 (1932).

[3] Haycock, Alder, and Hildebrand, J. Chem. Phys. **21**, 160 (1953).

It was then washed successively with conc. H_2SO_4, water, 10 percent NaOH, and water, dried over Drierite, and fractionated. All of it boiled at 82.0° and 763 mm.

RESULTS

Table I gives the observations. The linear relation previously observed is here confirmed over a much greater range for both liquids. In Table II are shown, in the column headed $\Delta P/\Delta T$, slopes of the straight lines obtained upon plotting the variables in Table I; next, the values for $(\partial P/\partial T)_v$ obtained from $\Delta P/\Delta T$ by correcting for the small volume changes of the glass by the method explained in reference 1. The values of $(\partial E/\partial v)_T$ are calculated by aid of the equation, $(\partial E/\partial v)_T = T(\partial P/\partial T)_v - P$.

In the earlier papers it was shown that over the range studied a van der Waals $a = v^2(\partial E/\partial v)_T$ is remarkably constant, and therefore furnishes an excellent means for correlating the results. The last column gives the constants for these liquids.

TABLE II. Values of the terms in Eqs. (1) and (2).

	t_1	$\Delta P/\Delta T$ atmos/deg	$(\partial P/\partial T)_v$ atmos/deg	$(\partial E/\partial v)_T$ atmos	v cc/mole	a atmos $\times l^2$
CCl_4	19.50	11.95	11.59	3390	96.43	31.50
	22.0	11.72	11.46	3380	96.73	31.60
n-C_7F_{16}	21.20	6.78	6.74	1983	224.5	99.9
	23.25	6.80	6.76	2002	225.2	101.9
	27.85	6.60	6.57	1976	226.9	101.7

For the molal volumes of CCl_4 we use the same values as in the early studies. Oliver, Blumkin, and Cunningham[4] give the expression $d_t = 1.78714 - 0.002765t$ for the density of C_7F_{16}, and we have used this expression to calculate the molal volumes of this liquid given in Table II.

The value for $v^2(\partial E/\partial v)_T$ for CCl_4 is in satisfactory agreement with the values found in the two earlier studies, 31.31 and 31.21, the latter being, within its smaller range, probably the most precise of the three.

We can calculate the differential compressibility, as before,[5] by the relation,

$$\beta = -(\partial \ln V/\partial P)_T = (\partial \ln V/\partial T)_P/(\partial P/\partial T)_v.$$

[4] Oliver Blumkin, and Cunningham, J. Am. Chem. Soc. **73** 5722 (1951).
[5] J. H. Hildebrand, Phys. Rev. **34**, 649 (1929).

TABLE III. Dielectric constant ϵ, and molar polarization P of n-C_7F_{16}.

$t°$	P (atmos)	ϵ	v cc/mole	P cc/mole
16.0	1.0	1.847	222.7	49.1
16.0	60.2	1.859	219.9	49.0
16.0	109.8	1.869	217.9	49.0
38.4	1.0	1.812	231.0	49.2
38.4	64.6	1.827	227.5	49.2
38.4	114.7	1.837	224.7	49.0

The coefficient of expansion of C_7F_{16} at 25° from the foregoing relation for density is 1.607×10^{-3}. Taking $(\partial P/\partial T)_v = 6.75$, we get $\beta = 2.38\times10^{-4}$. This is more than double the compressibility of CCl_4, 1.105×10^{-4}.

It seems worth while, for the sake of its bearing upon theory of the liquid state, to call attention again[6] to a consequence of the linear relation between P and T, which is that $(\partial c_v/\partial v)_T = 0$, indicating that c_v is independent of the size of the molecular "cage."

A Check of the Clausius-Mosotti Equation

Because of the large effects of pressure and temperature upon the fluorocarbon, we thought it interesting to determine its dielectric constant over the considerable range of temperature and pressure available in our apparatus as a test of the Clausius-Mosotti equation, $P = v(\epsilon-1)/(\epsilon+2)$. The method used was that described by Harris, Haycock, and Alder.[7] The results are summarized in Table III. The figures for molar volume were calculated by aid of the expression, $a = v^2[T(P-1)/\Delta t - P]$, obtained from equations given above, and taking 101.5 as the value of a. The constancy of P thus calculated is quite striking considering the range of temperature and pressure covered. It is interesting to note, however, that at 20 kc, the frequency at which ϵ was measured, its value, 1.83 at 25° and 1 atmosphere, is considerably larger than the square of the index of refraction, 1.59. The discrepancy is much greater than in the case of CCl_4, where the values found[7] were 2.23 and 2.13, respectively. It seems evident that in the fluorocarbon a good deal of atomic polarizability still persists at this frequency.

This work has been supported by the U. S. Atomic Energy Commission.

[6] J. H. Hildebrand, Phys. Rev. **34**, 984 (1929).
[7] Harris, Haycock, and Alder, J. Chem. Phys. **21**, 1943 (1953).

Deuterium Effect on Hydrogen Bond Distances in Hafnium Dihydride

S. S. SIDHU
Argonne National Laboratory, Lemont, Illinois
(Received September 21, 1953)

X-ray diffraction data obtained for carefully prepared and annealed samples of HfH_2 and HfD_2 show that as deuterium substitutes for hydrogen atoms the hafnium-hydrogen bond distances decrease. The lattice as a whole contracts, and the density increases. Powder diffraction patterns and the structure data for the two compounds are presented.

INTRODUCTION

THE substitution of deuterium for hydrogen atoms causes contraction in the crystal lattices of some compounds and an expansion in the others, depending upon whether the effect is normal or abnormal.[1] The changes observed in the lattice constants of LiH,[2] UH_3,[3] KH_2AsO_4[4] and KH_2PO_4,[4] when D is substituted for H are:

Compound	Change in lattice constant	Probable error
LiD	0.020	±0.001A
UD_3	0.011	±0.002A
KD_2AsO	0.008	±0.001KX
KD_2PO_4	0.0097	±0.001KX

The first two lattices contract and the latter two expand. The magnitude of such changes in general, however, is very small and in some cases about comparable with experimental error in the determination of the lattice constants. For example, expansions observed in the lattice parameters of hexagonal unit cell of D_2O[5] at 0°C are 0.0030±0.0014A in a_0 and 0.0016 ±0.0012A in C_0. This paper presents changes observed in HfH_2 structure due to substitution of D that appear to be quite marked and readily observable.

EXPERIMENTAL PROCEDURE

The samples of hafnium dihydride and dideuteride were prepared under carefully controlled and identical conditions. The metal was heated and outgassed in an evacuated quartz tube at 1100°C. The temperature was then lowered to 1000°C, and a measured volume of purified gas was admitted into the tube at a known pressure. Most of the absorption of gas took place at 700–800°C. Each sample was cooled from 750°C to 350°C at a rate of about 25° per hour, annealed at 350°C for 48 hours, cooled further to 225°C at the above rate, and then cooled in the furnace in 1½ hours. The gas pressure in the tube during cooling from 350°C to room temperature varied from 170 to 150 mm. The samples were stable in the range of room temperature to 350°C.

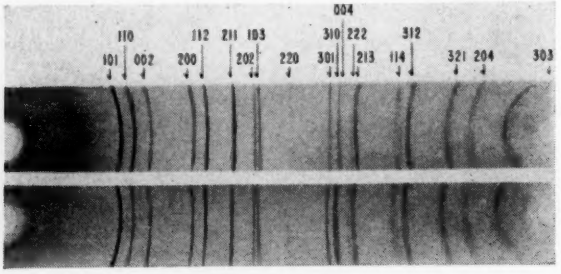

FIG. 1. X-ray diffraction patterns of (a) HfD_2 and (b) HfH_2 (filtered Co Kα-radiation; camera diameter 114.6 mm).

TABLE I. The Miller indices (*hkl*), interplanar spacings (*d*), and the estimated relative intensities (*I/Io*) of HfH_2 and HfD_2.

hkl	HfH_2 *d*(A)	HfH_2 *I/Io*[a]	HfD_2 *d*(A)	HfD_2 *I/Io*[a]
101	2.71	v.s.	2.70	v.s.
110	2.46	s	2.45	s
002	2.181	m	2.173	m
200	1.737	m	1.728	m
112	1.633	s	1.624	m+
211	1.466	s	1.457	s
202	1.359	m	1.354	m
103	1.344	m−	1.336	m
220	1.230	w	1.221	w
301	1.121	m	1.114	m−
310	1.102	m−	1.093	m−
004	1.091	v.w.	1.086	v.w.
222	1.072	w+	1.065	w+
213	1.062	m+	1.058	m+
114	0.997	w+	0.993	m
312	0.982	m+	0.978	m+
321	0.941	m	0.937	m
204	0.924	m+	0.921	m+
303	0.906	s	0.903	s

[a] *v* = very; *s* = strong; *m* = medium; *w* = weak.

TABLE II. Lattice parameters (a_0, c_0), metal-metal and metal-gas atom distances, volume of the unit cell, and calculated density of HfH_2 and HfD_2.

	HfH_2	HfD_2
a_0	3.478±0.004A	3.456±0.003A
c_0	4.363±0.001A	4.345±0.003A
c	1.254	1.257
Metal-metal atom distance	3.287A	3.270A
Metal-gas atom distance	2.053A	2.041A
Volume of unit cell (10^{-24} cc)	52.78	51.90
Calculated density ρ (g/cc)	11.37	11.68

[1] C. E. Nordman and W. N. Lipscomb, J. Chem. Phys. **19**, 1422 (1951).
[2] E. Zintl and A. Harder, Z. physik. Chem. **288**, 478 (1935).
[3] R. E. Rundle, J. Am. Chem. Soc. **69**, 1719 (1947).
[4] D. H. W. Dickson and A. R. Ubbelohde, Acta Cryst. **3**, 6 (1950).
[5] H. D. Megaw, Nature **134**, 900 (1934).

In the preparation of hafnium dideuteride, 99.5 percent pure deuterium gas, obtained from Stuart Oxygen Company, was used.

X-ray diffraction powder patterns were made of annealed specimens at room temperature with Co K$-\alpha$ radiation and a camera of 114.6 mm diameter. At large angles, diffraction lines with well-resolved K$-\alpha$ doublets were obtained.

RESULTS

The powder patterns of HfH_2 and HfD_2 are shown in Fig. 1, and the diffraction data in Table I. The structure is tetragonal,[6] and a body-centered tetragonal unit cell contains $2HfH_2$. The structure constants for each compound are tabulated in Table II.

It is apparent from the results obtained here that as deuterium atoms substitute for those of hydrogen in hafnium dihydride, the hafnium-deuterium bonds shorten, and the structure as a whole contracts.

Thanks are due J. C. McGuire for preparing the samples of HfH_2 and HfD_2 and D. D. Zauberis for making their diffraction patterns.

[6] S. S. Sidhu and J. C. McGuire, J. Appl. Phys. **23**, 1257 (1952).

THE JOURNAL OF CHEMICAL PHYSICS VOLUME 22, NUMBER 6 JUNE, 1954

Theory of Concentration Quenching in Inorganic Phosphors

D. L. DEXTER, *Institute of Optics, University of Rochester, Rochester, New York,* and Solid State Division, Naval Research Laboratory, Washington, D. C.*

AND

JAMES H. SCHULMAN, *Solid State Division, Naval Research Laboratory, Washington, D. C.*

(Received February 8, 1954)

A theory is presented for concentration quenching in solid systems, based on the migration of excitation energy from one activator center to another and eventually to an imperfection which may act as an energy sink. Calculations are made on the dependence of the fluorescence yield on concentration, and to indicate typical activator concentrations at which appreciable quenching may be expected to occur. If the transition in the activator is of the electric dipole or electric quadrupole type, appreciable quenching may arise when the activator concentration is 10^{-3} to 10^{-2}; if it is a magnetic dipole transition, transfer will occur by exchange, rather than by overlapping of magnetic dipole fields, and the critical concentration will be of the order of a few percent. The implications of transfer phenomena upon the observed absence of luminescence in most "pure" inorganic crystals are discussed, and it is concluded that transfer rates are so high in strongly absorbing crystals that the energy can easily migrate to a very few sinks dispersed throughout the lattice.

I. INTRODUCTION

IT is observed experimentally that most pure inorganic crystals do not exhibit appreciable luminescence upon irradiation in their visible or near-ultraviolet absorption bands. Consequently most inorganic luminophors, with which this paper is concerned, consist of a host lattice containing one or more types of impurity atoms or "activators," usually situated substitutionally on normal (cation) sites.[1] In the absence of competing absorptions by lattice defects or nonluminescent centers, and in the absence of interactions of the activators with each other, it is to be expected that the fluorescence yield η defined as the number of photons emitted per photon absorbed by the activators should be independent of the activator concentration x_a. (The concentration x_a will be expressed throughout as the fraction of lattice positions, of the type which can be occupied by an activator, which are so occupied.) Where the true fluorescence yield has been measured, as in the investigations of the concentration dependence of efficiency of organic luminophors in dilute liquid solutions,[2] η is indeed found to be independent of x_a at low concentrations. (In most cases reported in the literature of inorganic phosphors,[3,4] the increase in the so-called "yield" with increasing x_a at low x_a appears to be merely an increase in the fluorescence brightness or in the number of photons emitted per *incident* quantum.) The decrease of η with increasing x_a at high activator concentrations is a well-established fact in both organic[2] and inorganic[5] systems. This decrease in yield is the phenomenon of "concentration quenching," and is the subject of the present paper. We shall briefly review present theories, extend them to more direct applicability to inorganic systems, and

* This research has been supported in part by funds from the U. S. Air Force under Contract No. AF18(600)-688, monitored by Headquarters, A.R.D.C. P.O. Box 1395, Baltimore 3, Maryland.

[1] P. Pringsheim, *Fluorescence and Phosphorescence* (Interscience Publishers, Inc., New York, 1949); H. W. Leverenz, *Introduction to Luminescence of Solids* (John Wiley and Sons, Inc., New York, 1950).

[2] See for example, W. Lewschin, Z. Physik **43**, 230 (1927).

[3] P. D. Johnson and F. E. Williams, J. Chem. Phys. **18**, 1477 (1950).

[4] J. Ewles and N. Lee, J. Electrochem. Soc. **100**, 392 (1953).

[5] F. Kröger, thesis, Amsterdam, 1941.

treat additional processes of importance in the understanding of concentration quenching.

The concentration quenching of organic luminescent systems has been widely investigated,[1,6–10] and many of the concepts that have been employed in comparatively recent attempts to deal with this phenomenon in inorganic phosphors have their origin in the investigation of organic systems. [See reference 10(b) for a summary of the work in organic systems.] As early as 1889, for example, Walter[6] proposed that the concentration quenching of luminescent organic solutes is related to the formation of pairs and higher aggregates of the luminophor molecules as the concentration increases, these aggregates being assumed *ad hoc* to be nonluminescent. This picture of association of monomeric luminescent molecules into nonluminescent polymers derives support in some cases from the observed changes in the absorption spectrum with concentration and from the fact that the quenching is reduced by increasing the temperature.[2] The formation of absorbing but nonluminescent polymers decreases the concentration of luminescent monomer or "isolated" molecules, without affecting the luminescence transition probability of the remaining monomeric species of molecule. It is important to note, then, that when a polymerization mechanism is responsible for concentration quenching, essentially no change in decay time accompanies the decrease in luminescence yield.

This picture has proved inadequate to explain the concentration quenching behavior of many organic luminophor solutions, where it is necessary to assume that diffusion-controlled collisions between excited and unexcited luminophor molecules of the same species lead to a radiationless dissipation of the absorbed energy.[7] An important distinction between this case and the preceding one is the variation (decrease) in decay time that is expected to accompany the concentration-induced decrease in luminescence yield. When the collisional mechanism is the basis for concentration quenching, an alternate (radiationless) process of de-excitation is available to *each* excited molecule. The rate of de-excitation is thus faster than when luminescence emission is the only available de-excitation mechanism. The measured decay times must therefore be shorter in the presence of collisional quenching than in its absence, and the decay time *vs* concentration curve must show a decrease paralleling that in the yield *vs* concentration curve.

Still another mechanism must be invoked to explain the concentration quenching of a third class of organic luminescent solutions. This mechanism, first emphasized by Perrin,[8] involves the radiationless transfer of energy from an excited molecule to another unexcited molecule of the same species separated from the first by comparatively large distances, i.e., several dozens of angstroms. In this way the primarily excited molecule returns to the ground state, and the second molecule is raised to the excited state. By repetition of a resonance process of this sort the absorbed energy may traverse a considerable distance in the solution, jumping from one molecule to the next, until the energy is finally dissipated by jumping to a "quencher" molecule. Here again, as with the preceding mechanism of collisional quenching, the energy absorbed by any one of the luminophor molecules is susceptible to dissipation by a radiationless process, and the observed luminescence decay time decreases with increasing concentration parallel to the decrease in yield.

Although not applicable in detail to most inorganic luminophors, the foregoing considerations are nevertheless of considerable importance in interpreting concentration quenching in inorganic systems. However, these ideas have been largely overlooked in the published research on inorganic phosphors. Workers in this field have confined their efforts to mechanisms similar to the polymerization mechanism discussed above, assuming that the processes of emission and quenching occur on the atom which initially absorbed the energy.[3,4,11,12] The observed quenching is ascribed to a gross modification of the probability of at least one of the internal transitions in the luminescent center as a result of its proximity to another identical center. Insofar as specific processes have been discussed, it is usually suggested that concentration quenching is equivalent to thermal quenching, and that the nearness of another activator results in a substantial decrease in the thermal activation energy for a nonradiative transition to the ground state. Johnson and Williams[3] have extended the assumption implicit in Walter's polmerization model and "recognize" that an activator is unable to luminesce if another activator is within Z nearest suitable lattice sites; they suggest that Z may be as large as 4000 in at least one case. A mathematically similar theory was proposed[12] about 25 years ago by Ewles.[13]

No direct analog to the second type of quenching, by collisions between activator molecules, exists in

[6] B. Walter, Ann. Physik **36**, 502, 518 (1889).
[7] W. Wawilow, Z. Physik **31**, 750 (1925).
[8] F. Perrin, Compt. rend. **192**, 1727 (1931).
[9] F. Duschinsky, Compt. rend. Acad. Sci. U.S.S.R. **14**, 73 (1937).
[10] Th. Förster, (a) Ann. Physik **2**, 55 (1948); (b) *Fluoreszenz Organischer Verbindungen* (Vandenhoeck and Ruprecht, Göttingen, 1951); (c) Z. Naturforsch. **4a**, 32 (1949).
[11] F. Seitz, (a) J. Chem. Phys. **6**, 150 (1938); (b) Revs. Modern Phys. **18**, 384 (1946).
[12] J. Ewles, Proc. Leeds Phil. Lit. Soc., Sci. Sect. **1**, 341 (1929); Proc. Roy. Soc. (London) **A129**, 509 (1930).
[13] As mentioned previously, an increase in decay constant paralleling the concentration quenching is not to be expected on the basis of the foregoing formulations. From the data of Fonda [J. Appl. Phys. **10**, 408 (1939)], Kröger and Hoogenstraaten [Physica, **15**, 557 (1949)], and Larach and Turkevich [Phys. Rev. **89**, 1060 (1953)], it may be seen, however, that such a parallelism is indeed found experimentally in Zn_2SiO_4:Mn, one of the typical inorganic phosphor systems treated by Johnson and Williams (reference 3). No consideration is given to decay rate variations by these authors or by Ewles (references 4 and 12), although the importance of this point was recognized by Larach and Turkevich.

most solids, but of course interactions with lattice vibrations can at all concentrations induce nonradiative transitions to the ground state. This thermal quenching has received a great deal of attention in inorganic luminophors; we shall not be concerned with it here except to include it formally in our development.

We shall be concerned with the third type of concentration quenching, i.e., quenching involving the resonance transfer of electronic excitation energy from the initially absorbing atom or molecule to another identical molecule, and finally to some as yet unspecified quenching site. It should be clearly understood that this process does not require the motion of electrons, and hence does not involve photoconductivity directly. It will be explicitly assumed in the following that there exist in each activator only two electronic states of interest, the ground state and one discrete bound state. It will likewise be assumed, as is customary, that the radiative transition probability, w_r, is unchanged by the weak interaction with nearby activators. This assumption is an excellent one if the separations are more than a few angstroms, as can be seen from the rapid dependence of van der Waals' and exchange forces on distance.

II. RESONANCE TRANSFER OF ELECTRONIC EXCITATION ENERGY

The theory of resonance transfer of electronic excitation energy has been developed by the Perrins,[8] Förster,[10] Dexter,[14] and many others, and need be described here only briefly. Qualitatively, it is found that transfer can occur with high probability (i.e., greater than $w_r \sim 10^8$ sec^{-1}) between centers separated by several dozen angstroms if their absorption bands overlap appreciably their emission bands, and if the transition is an allowed one. The mechanism in this case is an overlapping of the near-zone electric dipole fields of the activators; it does not involve overlapping of the electronic wave functions of the two activators, as does exchange, which can be responsible for transfer over only a relatively short distance, of the order of a few angstroms in many crystals. Explicitly, the transfer probability per unit time by the dipole-dipole (d-d) mechanism is equal to

$$w_{tr}(dd) = \frac{9}{16\pi^2}\frac{\beta^2}{R^6} w_r(d), \tag{1}$$

where

$$\beta = \left[\frac{4\pi\hbar^4 C^4}{3n^4} A \int f_a(E) f_e(E) \frac{dE}{E^4}\right]^{\frac{1}{4}}. \tag{2}$$

In these equations R is the separation of the two activators, β is an effective "volume of influence," n is the index of refraction of the crystalline medium at the wavelength involved, A is proportional to the strength of the optical transition, and is numerically equal to the integrated absorption cross section of the activator, i.e., $A = \int \sigma(E) dE$, and $f_a(E)$ and $f_e(E)$ are normalized shape functions of the absorption and emission spectra, i.e., $\int f(E) dE = 1$. Note that the usual Stokes' shift will reduce the overlap between f_a and f_e, and hence act to decrease the probability of transfer. Evaluating Eq. (2) in a typical case,[15] we may expect $n^4 \sim 6$ and $A \sim 10^{-16}$ cm^2 ev; for order of magnitude purposes we may remove E^{-4} from the integral and replace it by its average, say (3 ev)$^{-4}$. The overlap integral $\int f_a(E) f_e(E) dE$ might then be of the order (1 ev)$^{-1}$ if no Stokes' shift should occur. Since these shifts are in fact sizable in most cases, (10 ev)$^{-1}$ would probably be a better figure. Inserting these values, we find $\beta \sim 1.1 \times 10^{-19}$ cm^3. Thus, from Eq. (1) we see that transfer will probably occur before emission if a neighboring activator is within 30A.

If the probability per unit time for thermal quenching is w_{th}, the transfer yield η_T is given by the average over all possible distributions of the activators of the ratio

$$\eta_T = \langle w_{tr}/(w_{tr}+w_r+w_{th})\rangle_{Av}. \tag{3}$$

If we make use of the rapid R dependence of w_{tr}, we may perform the averaging in a simple way by neglecting transfer to all but the nearest activator, and obtain

$$\eta_T = y_a\{Ci(y_a)\sin y_a - Si(y_a)\cos y_a + (\pi/2)\cos y_a\}. \tag{4}$$

This equation is subject to small corrections for activator concentrations larger than about one percent because in the averaging process we have not taken into account the impossibility of another activator occupying the volume of the initially excited activator. (See reference 14 for a more accurate description of the averaging process.) In this equation the reduced concentration y_a is related to x_a through the relation

$$y_a = x_a C^+ \beta/(1+w_{th}/w_r)^{\frac{1}{4}}. \tag{5}$$

Here C^+ is the concentration (per unit volume) of the lattice sites which may accommodate the activator, usually cation lattice sites. Equation (4) is shown plotted in Fig. 1, as a function of the reduced concentration y_a, and as a function of x_a in a typical case on the upper abscissa scale. To obtain the relation between x_a and y_a we insert $\beta \sim 10^{-19}$ cm^3, $C^+ = 2\times 10^{22}$ cm^{-3}, and assuming the temperature to be sufficiently low that thermal quenching is not very important, we replace $(1+w_{th}/w_r)^{\frac{1}{4}}$ by unity. Thus we find $x_a \sim 5\times 10^{-4}\, y_a$. From Fig. 1 we see that the transfer yield is $\frac{1}{2}$ at $y_a = 0.65$, so that at concentrations greater than 3×10^{-4} most of the excited activators will transfer their energy before emitting a photon.

[14] D. L. Dexter, J. Chem. Phys. **21**, 836 (1953). Additional references are contained therein.

[15] The term "typical case" or "typical system" will be used throughout to designate a system in which transfer effects are rather prominent; transfer can in many cases be much less likely, but will not in most ordinary inorganic systems be a great deal more probable. Thus a typical system is one which might be selected for its transfer properties.

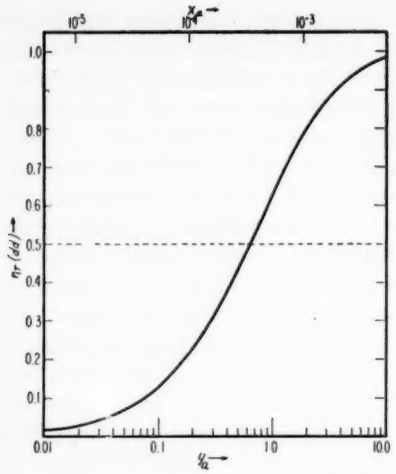

FIG. 1. Quantum yield for transfer between activators, by the mechanism of the overlapping of their electric dipole fields, as a function of the reduced concentration y_a. The upper abscissa scale represents the numerical value of the atomic concentration x_a in a typical case.

At sufficiently low concentrations, the probability that another activator will appear within the sphere of influence of an excited activator is proportional to the concentration, the transfer yield is determined by these chance fluctuations, and η_T varies linearly with concentration, as may be seen by expanding Eq. (4). At concentrations above the critical, on the other hand, the transfer yield is not sensibly dependent on these statistical fluctuations, and the average transfer yield may be obtained by replacing R by its average value in Eq. (1) and inserting in Eq. (3). Making the substitution and the assumption implied, $\langle(4\pi R^3/3)^2\rangle_{Av} = (x_a C^+)^{-2}$, we find for the transfer yield

$$\eta_T = y_a^2/(1+y_a^2) \sim 1-1/y_a^2, \tag{6}$$

at high concentrations. The coefficient of the y_a^{-2} term is only approximate, and depends on the details of the process of averaging over configurations. An exact determination of this quantity in any particular case would be extremely difficult, and we shall not attempt it here. A different averaging process as performed in deriving Eq. (4), leads to the result

$$\eta_T \sim 1-2/y_a^2, \tag{7}$$

as may be seen by expanding Eq. (4) for $y_a > 1$. Still another averaging process has been carried out by Förster[10a] in a slightly different connection, with essentially these same results.

III. CONCENTRATION QUENCHING FOR ACTIVATORS HAVING ALLOWED TRANSITIONS (ELECTRIC DIPOLE TRANSITIONS)

We now have the mechanics for discussing concentration quenching when the radiative transition is an allowed one. Several cases may be distinguished, depending on the type and density of quenching centers and on the probability of transfer to them. Before we proceed with a discussion of the effects of transfer phenomena upon quenching in systems having specific models for the quenching center, it is perhaps worth while to state briefly the qualitative nature of the argument that may be based on transfer effects. We believe, in many systems, that for most of the activators in the crystal the probability of thermal quenching is relatively independent of the presence of the other activators. That is, what additional quenching does take place upon increasing x_a occurs on a small fraction, if any, of the activators. Thus in the absence of transfer effects, only this same fraction of energy quanta can be quenched. However, if the excitation energy on the normal activators has a high probability of transferring to the quenching centers, the quenching yield will be correspondingly increased.

The assumption of the lack of dependence of w_{th} upon x_a restricts us in the following discussion to systems of x_a less than a few percent. For concentrations larger than this, many or most of the activators have other activators as nearest neighbors, the phonon spectrum and lattice constants become changed, and we would expect that w_{th} might be appreciably different than in a dilute solid solution (although not necessarily increased): The change in the thermal activation energy for a nonradiative, quenching process is given by a difference in terms made up of van der Waals' and exchange energies, and a change of 0.1 ev would result in an appreciably different quenching probability. A change of this magnitude seems plausible when the separations are no more than a lattice constant or so, but we believe it to be extremely unlikely, because of the inverse sixth power and exponential dependence on R, that van der Waals' and exchange energies can be significant for R larger than 30A, as suggested by Johnson and Williams for ZnS: Cu.[3] (Since this phosphor is known to be a photoconductor, an interpretation of its quenching based on the motion of charge seems more likely.) In any case, the present discussion is intended to apply only to those systems in which the thermal activation energies of most of the activators are relatively unaffected by interactions with the others.

One case of interest to the investigators of organic luminophors, namely, quenching by associated pairs of molecules in solution, has been treated by Duschinsky.[9] With some changes an analogous treatment may be applied to quenching by pairs of activators in inorganic crystals as follows, on the assumption that such pairs do indeed act as quenching sites. (This assumption may or may not be valid in a given case; it is a possible mechanism, but has not to our knowledge been demonstrated in any inorganic crystal.) The average probability per unit time of transfer from an initially excited activator is equal to approximately $w_r(x_a C^+\beta)^2$. If the probability for transfer to a doublet by an isolated activator is the same as to another

isolated activator at the same distance, and if a fraction f of the centers are doublets, the average probability per unit time of transfer to a quenching center is $fw_r(x_aC^+\beta)^2$. Since the probability per unit time for emission is w_r, the fluorescence yield is given by

$$\eta=\frac{w_r}{w_r+\langle f(\beta x_aC^+)^2w_r\rangle_{Av}+w_{th}}. \tag{8}$$

In writing Eq. (8) we have assumed that if the energy reaches the quenching center, the energy is certainly quenched, that is, emission and transfer from an excited quenching center are relatively improbable. This is the physically interesting case, and we shall make the same assumption throughout. (The assumption could of course be relaxed with a concomitant increase of the fluorescence yield). The yield at low concentration will be denoted by $\eta_0=w_r/(w_r+w_{th})$; so Eq. (8) becomes

$$\eta/\eta_0=1/(1+fy_a^2). \tag{9}$$

In the event that the activators are randomly distributed on the lattice sites, the fraction f is given by αx_a, where $\alpha\sim10$ is the number of nearest like lattice sites in the crystal. Thus the fluorescence yield varies with concentration as

$$\begin{aligned}\eta/\eta_0&=1/(1+\alpha x_a y_a^2)\\&\sim1-\kappa x_a^3,\end{aligned} \tag{10}$$

for x_a sufficiently small. The proportionality constant κ is equal to $\alpha(C^+\beta)^2/(1+w_{th}/w_r)$. In a typical case, where w_{th} is small, κ may be of the order 5×10^7, so that at a concentration $x_a\sim2.7\times10^{-3}$ the fluorescence yield may be reduced to one-half its value in dilute solutions. This result may be viewed in a slightly different way: If η_T is the yield for transfer, then $\eta_T/(1-\eta_T)\sim y_a^2$ is the average ratio of the transfer probability to the sum of the probabilities for the normal radiative and thermal processes, and hence is the average number of jumps N made by the energy quantum before its disappearance by one of these processes. Thus the probability that quenching occurs at one of the quenching sites is given by fN, and we are led to Eq. (10) by making use of Eq. (6). In the typical case just mentioned the number of jumps N is equal to about 30 when $x_a\sim2.7\times10^{-3}$ and $\eta/\eta_0\sim\frac{1}{2}$.

Note that in this case a fraction $\sim\alpha x_a$ of the absorbed energy is directly absorbed at a pair, so that the transfer is roughly $y_a^2\sim30$ times as important in producing quenching as is the initial absorption on quenching centers.

Several assumptions made above for the sake of definiteness are not obviously valid in all systems. For example, it may be that the absorption spectrum of a pair of activators is shifted from that for an isolated activator. If the shift is to the red, the weighted overlap integral in Eq. (2) would generally be increased, and the transfer distance would be correspondingly increased. The Stokes' relaxation would throw the excited pair farther out of resonance with absorption in the unexcited single activators nearby, and thus decrease further the probability for back transfer. Similarly the fluorescence yield would be decreased by the extra oscillator strength which we would expect might be associated with the double quota of electrons on the pair, since in this case again the transfer probability to a pair would be increased.

In the preceding paragraphs we have discussed quenching at sites whose concentration varied as the square of the activator concentration. Another interesting case, which apparently does not arise in organic systems, deals with quenching at lattice imperfections whose concentration may be independent of x_a. A number of possible energy sinks can be readily imagined. For example, Dexter and Heller[16] have considered the energy transfer from excitons to anion vacancies and F centers in the alkali halides, and have showed that low concentrations $x_q<10^{-6}$ of quenching sites are sufficient to quench luminescence in these crystals. (In this case x_a is equal to unity and transfer rates are extremely high, $>10^{13}$ sec^{-1}.) Other possible quenchers might be additional nonluminescent impurity atoms, jogs at dislocations, or normal lattice ions in the immediate vicinity of dislocations.

Let us suppose that the concentration x_q is appreciably less than x_a, so that on the average an energy quantum must make a number of jumps before reaching a quenching site. Then let us define a length R_q such that if an excited activator is within R_q of a quenching site q, it will on the average transfer its energy to q rather than to another unexcited activator. Clearly R_q depends on the activator concentration, since for x_a large, a-a transfer probabilities are large, and R_q must be correspondingly reduced. Denoting $4\pi R_q^3/3$ by V_q, we may state that the fraction of activators within R_q of some quencher is $x_qC^+V_q$, and since the number of jumps made is $N\sim y_a^2$, the fluorescence yield is given by

$$\eta/\eta_0\sim1-x_qC^+V_qy_a^2. \tag{11}$$

One of the most plausible models for q is a nonluminescent impurity atom. If transfer takes place to this atom by resonance transfer through overlapping of the electric dipole fields of q and a, the transfer probability at a separation R_q is given by

$$P_{aq}(dd)=\beta_{aq}^2w_r/V_q^2, \tag{12}$$

where β_{aq} has a value corresponding to Eq. (2) for transfer from an activator to the quenching atom. The quantity which we have previously called β should now be denoted by β_{aa}, and the probability w_r still refers to the activator. R_q and V_q are determined by setting $P_{aq}(dd)$ equal to the average transfer probability from activator to activator, namely $(x_aC^+\beta_{aa})^2w_r$. Solving for V_q, we obtain

$$V_q=\beta_{aq}/(\beta_{aa}C^+x_a), \tag{13}$$

[16] D. L. Dexter and W. R. Heller, Phys. Rev. **84**, 377 (1951).

so that the fluorescence yield is given by

$$\eta/\eta_0 \sim 1-(x_q/x_a)(\beta_{aq}/\beta_{aa})y_a^2. \quad (14)$$

Defining a reduced concentration for the quenching atoms as $y_q=(x_qC^+\beta_{aq})/(1+w_{th}/w_r)^{\frac{1}{2}}$, we obtain

$$\eta/\eta_0 \sim 1-y_ay_q. \quad (15)$$

In a very good quencher, the overlap integral between absorption in q and emission from a, corresponding to that in Eq. (2), might be ten times as large as that between activators, so that β_{aq}/β_{aa} might be as large as 3. In this case, and with the typical system we have so far discussed, Eq. (15) becomes

$$\eta/\eta_0 \sim 1-6x_ax_q(10^6). \quad (16)$$

If the concentration of quenching centers should be ten parts per million, the activator concentration would have to be of the order one percent to give rise to appreciable quenching. Note that if $\beta_{aq}/\beta_{aa}=1$, so that the centers are essentially identical as far as transfer is concerned, V_q in Eq. (13) becomes equal to $(x_aC^+)^{-1}$, and Eq. (14) becomes

$$\eta/\eta_0 \sim 1-(x_q/x_a)y_a^2, \quad (17)$$

which is the same result as given by Eq. (9) upon inserting the ratio $f=x_q/x_a$.

An atom with no allowed transition at or below the resonance energy of the activator might be in an excellent position to quench the excitation energy if the latter were able to get to the quenching site. (This would be expected, of course, since thermal quenching would have a long time in which to operate.) Such transfer can occur in either of two ways if there exist energy states in the quenching atom at the proper energy above the ground state, even though the transition between these states may be forbidden. These mechanisms involve either exchange, or an overlapping of the electric quadrupole or other multipole field of the quencher with the dipole field of the activator. (See reference 14 for a description of these processes.) It turns out, however, that the transfer efficiency is so low by exchange or by the dq method that an extremely high concentration is required for either x_q or x_a or both. Thus we shall not discuss this mechanism further; the inverse process, namely the transfer by the overlapping of the quadrupole field of the activator with the dipole field of the quencher, is of greater importance and will be discussed below.

It should be mentioned that the upward transition in the quenching atom may not be between two discrete states, but may lead to the production of free electrons and perhaps free holes as well. A number of additional effects could occur in this case, such as photoconductivity and slow phosphorescence in either a new or the same emission band.

Another possible quenching site, as mentioned above, might be associated with the presence of dislocations. It is expected that the atoms nearest to a dislocation line would have their optical properties appreciably changed, both as to the energy of the optical transition and as to the extent of the interaction with lattice vibrations. Let us assume that if an excited activator lies within a distance R_q of a dislocation line, it will on the average transfer its energy to a quencher associated with the dislocation before transferring to another activator. Then if the dislocation concentration is given by L line-cm per cm^3, the fractional number of activators lying in one of these quenching regions is πR_q^2L, so that the fluorescence yield is equal to

$$\eta/\eta_0 \sim 1-\pi R_q^2Ly_a^2. \quad (18)$$

In order to determine R_q as a function of the activator concentration, we assume that transfer may occur from an excited activator to any quenching site along the dislocation line by the dipole-dipole method. Thus we find

$$P_{aq}(dd)=\beta_{aq}^2w_r/(4\pi/3)^2\sum_i\frac{1}{R_{ai}^6}$$

$$=(27/128\pi)\beta_{aq}^2w_r/(R_q^5l), \quad (19)$$

where the $\sum_i$ represents a summation over all quenchers along the dislocation, and where l is the spacing of the quenching centers along the dislocation line. Equating this expression to the average transfer probability between activators at concentration x_a, we obtain

$$R_q=\left(\frac{27}{128\pi l}\frac{\beta_{aq}^2}{\beta_{aa}^2x_a^2C^{+2}}\right)^{1/5}, \quad (20)$$

and

$$\eta/\eta_0=1-kLx_a^{6/5}, \quad (21)$$

where

$$k=(9\pi)^{3/5}(C^+\beta_{aa})^{6/5}\beta_{aq}^{4/5}/2^{14/5}l^{2/5}(1+w_{th}/w_r). \quad (22)$$

If there is one site on each atomic plane pierced by a dislocation for which β_{aq} is of the order 10^{-19} cm^3, then k is of the order 0.7×10^{-8} cm^2. Thus if L is of the order 10^{11} line-cm per cm^3, as might be expected in powdered systems, an activator concentration of 2.3×10^{-3} would be sufficient to reduce the fluorescence yield to about half its value in the absence of transfer effects. If L has a value characteristic of well-annealed crystals, less than 10^9/cm^2, say, the activator concentration must be of the order unity, so that the present considerations are not applicable in detail.

The temperature dependence of the fluorescence yield arises from two principal sources; the brief discussion given here is likewise applicable to the various cases treated in the following sections. (1) The transfer probability w_{tr} is a function of temperature primarily through its dependence on the overlapping of $f_a(E)$ and $f_e(E)$. In most cases the broadening of both curves with increasing temperature will result in an increased overlap integral, and hence an increased transfer probability and decreased fluorescence yield. (If absorption in the quenching center is in close

resonance with emission from an activator, on the other hand, the increasing broadening with temperature may result in a decreased overlap integral, thus tending to increase the fluorescence yield.) (2) The second temperature effect arises from the dependence of w_{th} upon temperature, which in most, if not all cases, is a monotonically increasing dependence. Thus an increase in temperature gives rise to the usual thermal quenching whether transfer occurs or not. In all cases we expect η to decrease at sufficiently high temperatures, though a small maximum is possible at lower temperatures. These effects are discussed in greater detail in reference 14.

IV. CONCENTRATION QUENCHING FOR ACTIVATORS HAVING FORBIDDEN TRANSITIONS

Another type of system, of considerable interest in many practical phosphors, is that in which the activator has no allowed transition in the energy range of interest. We shall discuss a typical system in which the activator's transition is an electric quadrupole transition. It might be expected that the weak coupling by the overlapping quadrupole fields of the activators would make transfer by this method unimportant, but this is not the case, as we shall see below.

By an extension of the methods of reference 14, we find that the probability of transfer from one activator to another by the overlapping of their electric quadrupole fields is given by

$$w_{tr}(qq)=\gamma^{10/3}w_r(q)/(4\pi R^3/3)^{10/3}, \tag{23}$$

where $w_r(q)$ is the optical transition probability per unit time for the quadrupole transition, R is the separation of the two activators, and where the "transfer volume" γ is given by

$$\gamma=(4\pi/3)\left[\frac{225\pi\epsilon}{2}\frac{g'}{g}\frac{w_r(q)\hbar^{11}C^{10}}{n^6}\int\frac{f_a(E)f_e(E)dE}{E^{10}}\right]^{3/10}. \tag{24}$$

In this expression ϵ is a numerical constant of the order of unity, g' and g are the degeneracies of the excited and ground states, respectively, and the other symbols have the same meanings as in Eq. (2), to which Eq. (24) is analogous. The transition probability in Eq. (24) could be replaced by an absorption area A as in Eq. (2), but in general A would not be accurately measurable because of the weakness of the absorption band. (The system is supposed in such a case to be excited by electron or x-ray bombardment, or by using a thick sample. If not, only an extremely small fraction of the incident photon flux can be absorbed.)

Several interesting relationships exist between Eqs. (1) and (23). First, it should be noted that a quadrupole transition probability is of the order $(a/\lambda)^2$ times a dipole transition probability, where a is an atomic dimension and λ the wavelength of the photon emitted. Thus, making use of this relation, we compute the ratio of the transfer probabilities,

$$\frac{w_{tr}(qq)}{w_{tr}(dd)}\sim\frac{1}{10}\left(\frac{a}{R}\right)^4. \tag{25}$$

The ratio w_{tr}/w_r expresses the relative probability of transfer and emission at separation R, and determines the critical volume γ or β in Eqs. (23) and (1). The ratio of these two relative probabilities is given by

$$\frac{w_{tr}(qq)/w_r(q)}{w_{tr}(dd)/w_r(d)}\sim\frac{\lambda^2a^2}{10R^4}. \tag{26}$$

Thus, if $\lambda\sim4000$A and $a\sim2$A, transfer is relatively more probable in the quadrupole case when R is less than 90A. This is of course a result of the smallness of quadrupole radiative transition probabilities. The critical volume γ in a typical case may be about 2×10^{-19} cm^3, slightly larger than β. Thus, if the separation of two activators is less than about 35A, transfer will occur on the average before luminescence.

We may define a reduced concentration (analogous to y in the above) by setting z equal to $z=x_aC^+\gamma/[1+w_{th}/w_r(q)]^{3/10}$. Then for x_a large, the average number of jumps made by the energy quantum before emission or thermal quenching occurs is equal to about $z^{10/3}$, and the average jump probability is given by

$$\langle w_{tr}(qq)\rangle_{Av}=(\gamma C^+x_a)^{10/3}w_r(q). \tag{27}$$

The dependence of N and $\langle w_{tr}(qq)\rangle_{Av}$ on x_a is stronger than in the dipole case, as is to be expected from the more rapid R dependence.

Various quenching mechanisms may be investigated as was done above for the dipole case. For example, if a pair of activators represents a quenching site, and if the activators are randomly arranged on the lattice, the fluorescence yield will be of the form

$$\eta/\eta_0=\frac{1}{1+\alpha x_aZ^{10/3}}, \tag{28}$$

where as before $\alpha\sim10$ is the number of nearest like neighbor sites in the crystal. Thus η depends on the 13/3 power of the activator concentration. If thermal quenching is unimportant, η/η_0 is reduced to about one-half in a typical case when x_a is equal to 10^{-3}.

Quenching by other impurities may likewise be estimated in this same way. In this case, though, the wandering quantum of energy can easily be transferred to additional impurities or perturbed ions of the host lattice if they have an allowed transition in resonance with the forbidden transition of the activator. This can be seen from the fact that the q-q transfer is only $\sim(a/R)^2$ as probable as a q-d transfer at the same separation. With reasonable concentrations of quenching centers, say $10^{-4}-10^{-5}$, the activator concentration would have to be about 10^{-3} for appreciable quenching to occur.

The electric quadrupole case contrasts strongly with that for magnetic dipole transitions. If the forbidden transition in the activator is of the magnetic dipole type, the probability for spontaneous emission is of the order $(e^2/\hbar c)^2$ times that for electric dipole transitions, or is of the order 10^3 or 10^4 per second. The ratio of the relative probabilities [as in Eq. (26)] for transfer by the overlapping of magnetic and electric dipole fields is given approximately by

$$\frac{w_{tr}(mm)/w_r(m)}{w_{tr}(dd)/w_r(d)} \sim (e^2/\hbar c)^2, \tag{29}$$

for a given separation R. Thus transfer effects are much less important for systems in which the activator has a magnetic dipole transition than in the other cases we have discussed. The equations describing the magnetic dipole case exhibit the same dependence on R and on x_a as those for the electric dipole case, but the effective volume β must be reduced by a factor of the order $(e^2/\hbar c)$ or 10^{-2}. Magnetic dipole transfer would become important only at concentrations higher than that at which transfer by exchange is already significant. A large variation may be expected in the efficacy of exchange in transfer, depending on the spatial extent of the wave function of the activator, and on the dielectric constant of the host lattice. If the wave functions are well localized, as is to be expected in the alkali halides, for example, we may expect transfer effects to arise when x_a is a few percent. At concentrations as large as this, as mentioned above, it might be possible to explain the observed quenching by a modification of thermal quenching probabilities.

V. QUENCHING IN PURE CRYSTALS

In conclusion, we would like to speculate on the phenomenon referred to in the first sentence of this note, namely, the absence of luminescence in most pure crystals, and to suggest that it be considered an aspect of concentration quenching in strongly absorbing crystals.

Present interpretations of the absence of luminescence are typified by Seitz's suggestion[17] that in the alkali halides the quanta of electronic excitation energy, called excitons in systems where $x_a=1$, become "self-trapped" as a result of lattice relaxation in the vicinity of the excited atom. The relaxation is considered to be induced by the circumstance that the excited state of the halide ions is a repulsive state. Seitz suggests further that the thermal activation energy for a nonradiative transition of the self-trapped exciton to the ground electronic state is zero or at least very small, so that thermal processes occur more rapidly than do radiative transitions. We suggest that this mechanism is applicable to systems of low oscillator strength where transfer rates are small, and that transfer of energy to special quenching sites is the mechanism responsible for quenching in crystals such as the alkali halides with oscillator strengths of the order unity.

For example, as discussed in reference 14, calcium tungstate has a small oscillator strength in the WO_4 ion, and transfer probably occurs by the exchange mechanism. In the absence of relaxation effects, the transfer probability may be of the order of 10^{10} per second, which is small in comparison with relaxation rates of the lattice. Thus an excited WO_4 ion does not have time to transfer its excitation energy before relaxation occurs which produces a Stokes' shift capable of throwing the excited ion out of resonance with surrounding ions. Since the shift may be large (2400A for the absorption band and 4200A for the emission band of $CaWO_4$), the transfer rates are greatly reduced, and the fluorescence yield is determined primarily by the ratio $w_r/(w_r+w_{th})$ in each ion. Further, since radiative transition probabilities are small, the mechanism proposed by Seitz seems reasonable to explain the quenching.

This situation is to be contrasted with that in a system such as NaCl where the Cl ion has an oscillator strength greater than unity in the transitions associated with the excitons. In this case, transfer from one ion to the next will proceed by the overlapping of the near zone dipole fields of the Cl ions, as discussed by Heller and Marcus,[18] with a probability greater than that for lattice relaxation. Thus most of the excitons will not be self-trapped, and will remain free to migrate through the crystal. With transfer rates greater than 10^{13} sec^{-1} and a diffusion length of 10^{-4} cm, the probability is essentially unity that the exciton arrives at a quenching site in crystals of perfection and purity obtainable in practice. Thus we conclude that in ionic crystals in which the exciton concept may properly be applied, that is, in crystals which exhibit rapid transfer, luminescence is expected to be absent, because of the quick transfer of the excitation energy to quenching impurities and imperfections. Crystals in which transfer rates are small may or may not show luminescence depending on the relative quenching rates on the individual ions.

[17] F. Seitz, Trans. Faraday Soc. **35**, 84 (1939).

[18] W. R. Heller and A. Marcus, Phys. Rev. **84**, 809 (1951).

Scattering of High-Velocity Neutral Particles. IV. He−A; A−He

I. AMDUR, E. A. MASON,* AND A. L. HARKNESS
Department of Chemistry, Massachusetts Institute of Technology, Cambridge, Massachusetts
(Received March 8, 1954)

Total collision cross sections have been measured for helium atoms with energies between 500 and 2100 ev, scattered in room temperature argon, and for argon atoms with energies between 600 and 2100 ev, scattered in room temperature helium. In each case, two detectors of different geometric aperature have been used, and potential energy functions have been obtained by procedures previously applied to helium scattered in helium.

The average function for the potential energy between a helium atom and an argon atom derived from the measured cross sections may be represented by

$$V(r)=9.95\times10^{-11}/r^{7.25}\text{ergs},$$

for values of r between 1.64A and 2.27A. Since this potential is in good agreement with the geometric mean of the potential between two helium atoms and that between two argon atoms in the range represented by the arithmetic average of the individual interaction distances, it is suggested that the parameters of a point repelling type potential function may, in general, be combined in this manner.

ADDITIONAL potential energy information at close distances of interaction has recently been obtained from scattering experiments[1,2] involving the systems of like particles, He-He and A-A. The present investigation of the scattering of high velocity He atoms in room temperature A, and of high velocity A atoms in room temperature He, was undertaken for the following reasons:

(a) to obtain potential energy information at close distances of interaction for the system He-A,

(b) to ascertain whether the interaction potential derived from the scattering of He in A is the same, within experimental error, as that derived from the scattering A in He, a necessary condition that must be satisfied if derived potentials are to be independent of specific apparatus characteristics, and

(c) to determine the feasibility of obtaining potential energy information for systems of like particles from suitable scattering experiments involving systems of unlike particles. For example, it is not possible to produce a beam of high-velocity neutral polyatomic molecules free of atomic or molecular fragments produced by electron or ion bombardment of the polyatomic molecules in the source of the beam. It would, therefore, be highly desirable to be able to obtain the interaction potential between like polyatomic molecules by combining the results of experiments in which beams of high velocity rare gas atoms are scattered by polyatomic molecules, with those in which the same rare gas atoms occur in the beam and in the scattering gas.

As in the case of the recent measurements on helium[1] and argon,[2] two detectors, referred to as wide and narrow, were used to obtain total collision cross sections as a function of energy. The method of converting the geometric apertures of these detectors (13.4 and 0.96 min) to effective apertures, as well as the nomenclature and symbolism which will be used in the present paper are discussed in the helium paper, hereafter referred to as Paper II.

The present experimental results are shown in Table I where the experimental cross sections, $\bar{S}_w$ and

TABLE I. Summary of collision cross-section results.

	Wide detector			Narrow detector		
E ev	$\bar{S}_w$ A^2	S_w A^2	Percent deviation	$\bar{S}_n$ A^2	S_n A^2	Percent deviation
			A. He-A system			
500	14.44	14.61	−1.2	16.24	16.23	+0.1
600	13.86	13.90	−0.3	15.51	15.54	−0.2
700	13.24	13.32	−0.6	14.82	14.98	−1.1
800	12.77	12.85	+0.6	14.43	14.51	−0.6
900	12.64	12.44	+1.6	14.08	14.11	−0.2
1000	12.12	12.08	+0.3	13.86	13.76	+0.7
1100	11.84	11.77	+0.6	13.44	13.45	−0.1
1200	11.54	11.49	+0.4	13.28	13.18	+0.8
1300	11.40	11.24	+1.4	13.12	12.93	+1.4
1400	11.05	11.02	+0.3	12.75	12.70	+0.4
1500	10.79	10.81	−0.2	12.56	12.50	+0.5
1600	10.68	10.62	+0.6	12.32	12.31	+0.1
1700	10.52	10.45	+0.7	12.10	12.13	−0.2
1800	10.40	10.28	+1.2	12.15	11.97	+1.5
1900	10.14	10.13	+0.1	11.70	11.81	−0.9
2000	9.85	9.99	−0.4	11.52	11.67	−1.3
2100	9.59	9.86	−2.8	11.43	11.54	−1.0
			B. A-He system			
600	11.97	12.06	−0.8	13.79	13.99	−1.5
700	11.56	11.55	+0.1	13.43	13.33	+0.8
800	11.10	11.12	−0.2	13.09	12.76	+2.5
900	10.64	10.75	−1.0	12.42	12.29	+1.0
1000	10.36	10.43	−0.7	11.98	11.88	+0.9
1100	10.22	10.15	+0.7	11.74	11.52	+1.5
1200	10.05	9.91	+1.4	11.43	11.21	+1.9
1300	9.78	9.68	+1.0	11.17	10.92	+2.2
1400	9.64	9.48	+1.7	11.01	10.67	+3.1
1500	9.32	9.30	+0.2	10.43	10.43	0.0
1600	9.26	9.13	+1.4	10.24	10.22	+0.2
1700	8.94	8.97	−0.3	9.89	10.02	−1.3
1800	8.67	8.83	−1.8	9.76	9.84	−1.1
1900	8.65	8.69	−0.5	9.53	9.67	−1.1
2000	8.56	8.57	−0.1	9.34	9.52	−1.9
2100	8.36	8.45	−1.1	9.11	9.37	−2.9

* Present address: Department of Chemistry, Pennsylvania State University, State College, Pennsylvania.
[1] I. Amdur and A. L. Harkness, J. Chem. Phys. **22**, 664 (1954).
[2] I. Amdur and E. A. Mason, J. Chem. Phys. **22**, 670 (1954).

TABLE II. Potential parameters.

System	Detector	K, ergs-A^s	s	Range, A
He-A	wide	1.40×10^{-10}	7.29	1.77–2.16
He-A	narrow	2.60×10^{-10}	8.42	1.92–2.27
A-He	wide	7.15×10^{-11}	7.03	1.64–1.96
A-He	narrow	3.93×10^{-11}	6.25	1.73–2.11

$\bar{S}_n$, have been computed from Eq. (1) in Paper II, and the smoothed values S_w and S_n, have been calculated from the following equations, obtained by the method of least squares:

He-A system:

$$\log S_w = -0.27432 \log E - 1.33058, \quad (1)$$

$$\log S_n = -0.23768 \log E - 0.95183; \quad (2)$$

A-He system:

$$\log S_w = -0.28434 \log E - 1.48243, \quad (3)$$

$$\log S_n = -0.32002 \log E - 1.73990. \quad (4)$$

In the above equations S_w and S_n are in A^2 and E is in ergs.

If the interaction potential is assumed to be of the form $V(r)=K/r^s$, application of the calculation procedure described in Paper II to Eqs. (1)–(4) leads to the potential parameters shown in Table II.

For the He-A system the ratio of the $V(r)$ values derived from the wide detector results to those derived from the narrow detector results increases from 1.12 to 1.28 as r increases from 1.92A to 2.16A. If the potential functions are extrapolated slightly so that they cover the maximum range, 1.77A to 2.27A, the above ratio ranges from 1.02 to 1.35. The intermediate function

$$V(r)=1.89\times10^{-10}/r^{7.86} \text{ ergs} (1.77\text{A} \leqq r \leqq 2.27\text{A}), \quad (5)$$

is taken as representative of the results obtained for the He-A system from both detectors. Equation (5) leads to calculated values of S_w which average 0.9 percent lower than the corresponding values in Table I, and to calculated values of S_n which are 0.9 percent higher than those in the table. In the case of the A-He system, the ratio of $V(r)$ values from the wide detector results to those from the narrower detector results decreases from 1.19 to 1.08 as r increases from 1.73A to 1.96A. Extension of the functions to cover the maximum common range, 1.64A to 2.11A, causes the ratio to range from 1.24 to 1.02. The intermediate potential function for the A-He system which is taken as

$$V(r)=5.24\times10^{-11}/r^{6.64} \text{ ergs} (1.64\text{A} \leqq r \leqq 2.11\text{A}), \quad (6)$$

leads to calculated values of S_w and S_n which average 2.9 percent lower and 2.9 percent higher, respectively, than the smoothed values in Table I.

The authors are unable to reconcile quantitatively the divergence between the cross sections of He-A and A-He as measured on a given detector. The following factors, however, may contribute in varying degree.

1. Since the chamber which contains scattering gas has openings through which the beam passes on its way from the source to the detector, there must, in principle, be a nonuniform pressure distribution in the column of gas which attenuates the beam. If the degree of nonuniformity were different for helium than for argon, divergent cross sections could result.

2. The pressure in the scattering chamber is measured by a Pirani gauge which must necessarily lie somewhat outside of the path of the beam. If, as is likely, there is nonuniformity of pressure in the plane perpendicular to the beam axis as well as along it, the pressure measured by the gauge may not refer to the region of the scattering chamber where scattering actually occurs.

3. Erroneous pressure readings may also result from an "anemometer effect," namely, loss of heat associated with the slow mass flow of gas past the Pirani gauge wire.

4. In scattering experiments involving unlike systems, there is the possibility that a trace of scattering gas can find its way into the arc and change the composition of the positive ion beam which, after partial neutralization, becomes the neutral beam which is scattered. Although this possibility has been minimized in the present apparatus by essential isolation of the scattering chamber, it is conceivable that the effect may be present in small degree.

5. The high-energy neutral beam may contain metastable atoms, produced by neutralization of positive ions at metal surfaces, as well as normal atoms. A system consisting of a metastable atom and a normal atom would be expected to have an appreciably larger cross section than the corresponding system of two normal atoms. The cross sections of the systems He-A and A-He might differ for this reason. However, in view of the fact that the potential energy information obtained from scattering experiments for He-He and for A-A has been shown to be consistent with that derived from measurements of gaseous compressibility, viscosity, and, in the case of argon, crystal data, the authors are inclined to believe that there are probably relatively few metastable atoms in the beam, and that, in the main, the neutral beam is produced by charge exchange in the gas phase, rather than by neutralization at metal surfaces.

In view of the above considerations, a geometric mean of the functions represented by Eqs. (5) and (6), namely,

$$V(r)=9.95\times10^{-11}/r^{7.25} \text{ ergs} (1.64\text{A} \leqq r \leqq 2.27\text{A}) \quad (7)$$

is taken to represent the interaction potential between a helium atom and an argon atom, in the hope that the mean potential will be closer to the true potential than either Eq. (5) or Eq. (6). Values of S_w calculated from Eq. (7) average 9 percent lower than the S_w

values for He-A and 6 percent higher than the S_w values for A-He given in Table I. In the case of S_n, values calculated from Eq. (7) average 6 percent lower and 10 percent higher than the corresponding tabulated values for He-A and A-He, respectively.

For a potential of the form $V(r)=K/r^s$, it is proposed that the potential function for two dissimilar particles, $V_{12}(r)$, be obtained from the two potential functions for the systems of similar particles, $V_{11}(r)$ and $V_{22}(r)$, in the following way:

Let

$$\ln V_{11}(r)=\ln K_{11}-s_{11}\ln r \quad (a\leqq r\leqq b),$$

and

$$\ln V_{22}(r)=\ln K_{22}-s_{22}\ln r. \quad (c\leqq r\leqq d).$$

Then

$$\ln V_{12}(r)=\ln K_{12}-s_{12}\ln r \quad (e\leqq r\leqq f),$$

where

$$\ln K_{12}=\tfrac{1}{2}(\ln K_{11}+\ln K_{22}), \quad s_{12}=\tfrac{1}{2}(s_{11}+s_{22}),$$
$$e=\tfrac{1}{2}(a+c), \quad \text{and} \quad f=\tfrac{1}{2}(b+d).$$

This method of combining the parameters of a point repelling potential is similar to that suggested[3] for combination of the parameters of a Lennard-Jones type potential for a gas consisting of nonpolar, spherically symmetrical molecules.

Recently, potential functions have been suggested for the interaction of two helium atoms,[1]

$$V(r)=7.55\times10^{-12}/r^{5.94}\ \text{ergs}(1.27\text{A}\leqq r\leqq 1.59\text{A}), \quad (8)$$

and of two argon atoms,[2]

$$V(r)=1.36\times10^{-9}/r^{8.33}\ \text{ergs}(2.18\text{A}\leqq r\leqq 2.69\text{A}). \quad (9)$$

Combination of the parameters of Eqs. (8) and (9) in the manner proposed above leads to the following relation for the potential between a helium atom and an argon atom:

$$V(r)=1.01\times10^{-10}/r^{7.14}\ \text{ergs}(1.72\text{A}\leqq r\leqq 2.14\text{A}). \quad (10)$$

As seen from Fig. 1, values of $V(r)$ from Eq. (7), curve A, agree very well with those from Eq. (10),

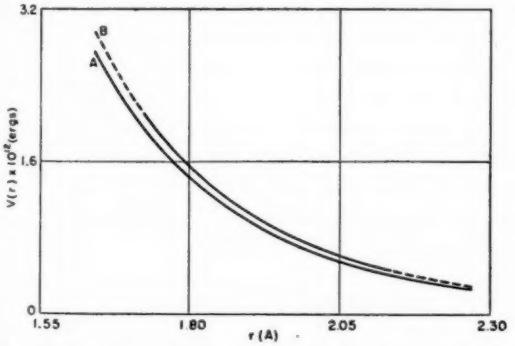

FIG. 1. Potential energy between a helium atom and an argon atom: (A) Results from scattering of He in A, and A in He; (B) results from scattering of He in He, and A in A.

[3] J. A. Beattie and W. H. Stockmayer, *States of Matter* (D. van Nostrand Company, Inc., New York, 1951), H. S. Tayler and S. Glasstone, Editors, pp. 350–352.

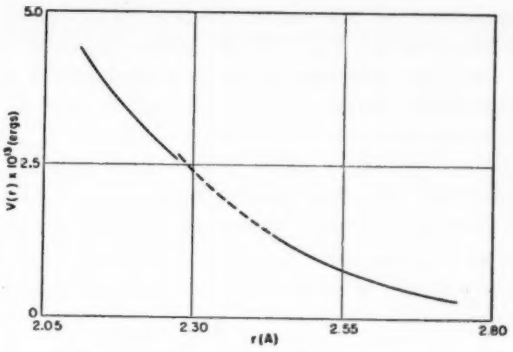

FIG. 2. Comparison of potential energy curves at small and large interaction distances.

curve B, whose range has been extended slightly to equal that covered by Eq. (7). Over the full range of r, 1.64A to 2.27A, curve A averages 8 percent lower than curve B. In terms of cross sections, values of S_w and S_n calculated from Eq. (7) are 2 percent lower, on the average, than corresponding values calculated from Eq. (10).

It is interesting to see if the potential between a helium atom and an argon atom at small separation distances given by Eq. (7) is consistent with that at larger distances obtained from measurements of gaseous compressibility, viscosity, and crystal properties. This latter potential may be obtained from the potential between two helium atoms, which may be written as

$$V(r)=[2.87\exp(-3.96r)-0.0232/r^6]\times10^{-10}\ \text{ergs}(1.90\text{A}\leqq r\leqq 2.30\text{A}), \quad (11)$$

and that between two argon atoms, which may be written as

$$V(r)=[153\exp(-3.62r)-0.994/r^6]\times10^{-10}\ \text{ergs}(2.98\text{A}\leqq r\leqq 4.83\text{A}). \quad (12)$$

Equations (11) and (12) give the following potential between a helium atom and an argon atom:

$$V(r)=[21.0\exp(-3.79r)-0.152/r^6]\times10^{-10}\ \text{ergs}(2.44\text{A}\leqq r\leqq 3.56\text{A}), \quad (13)$$

when combined in the manner suggested by Mason and Rice[4] who also give the potential parameters which lead to Eqs. (11) and (12). Figure 2 shows as solid lines the terminal portion of the potential given by Eq. (7) and the initial portion of the potential given by Eq. (13). When extrapolated from 2.44A to 2.27A, Eq. (13) predicts a value of $V(r)$ which is 3.9 percent greater than that given by Eq. (7). At 2.44A the value of $V(r)$ from Eq. (13) is 15.9 percent lower than the extrapolated value obtained from Eq. (7). Although this represents reasonably good concordance, it should be pointed out that extrapolation of a two-parameter potential such as Eq. (7) may be less justifiable than

[4] E. A. Mason and W. E. Rice, J. Chem. Phys. **22**, 843 (1954).

extrapolation of the more flexible three-parameter potential given by Eq. (13). It seems apparent, however, that the character of the potential in the intermediate range, 2.27A to 2.44A, is well defined by the combination of the two solid curves in Fig. 2.

Although the close agreement between Eq. (7) and Eq. (10) and the consistency of Eqs. (7) and (13) may be in part fortuitous, it seems reasonable to conclude that useful quantitative potential energy information at small distances of separation can be obtained for a system on which no experimental measurements have been made, by suitable combination of two potential energy functions which have been experimentally determined. Specifically, combination according to a geometric mean seems suitable for a function of the general form $V(r)=K/r^s$.

ACKNOWLEDGMENT

The authors wish to thank the Research Corporation for its generous support of the work with grants-in-aid.

THE JOURNAL OF CHEMICAL PHYSICS VOLUME 22, NUMBER 6 JUNE, 1954

The Reaction of Methyl Radicals with Aceto- and Propio-Nitrile

M. H. J. WIJNEN
Division of Pure Chemistry, National Research Council, Ottawa, Canada
(Received February 22, 1954)

The reaction of CD_3 radicals with aceto- and propio-nitrile has been studied over the temperature range 100 to 300°C at various intensities. The CD_3 radicals were produced by photodecomposition of acetone-d_6. As activation energies for the reactions

$$CD_3+CH_3CN\rightarrow CD_3H+CH_2CN \quad (2)$$

and

$$CD_3+C_2H_5CN\rightarrow CD_3H+C_2H_4CN, \quad (3)$$

we obtained $E_2=10\pm0.5$ kcal and $E_3=8.5\pm0.5$ kcal.

INTRODUCTION

THE reactions of methyl radicals with various compounds have been reported in the literature. We have extended these to the reactions of CD_3 radicals with CH_3CN and C_2H_5CN. We were particularly interested in these compounds since in these laboratories investigations are under way to study the photodecomposition of these compounds at 1849A.

The following mechanism of methane and ethane formation is proposed when acetone-d_6 is photolyzed in presence of CH_3CN or of C_2H_5CN.

$$CD_3+CD_3COCD_3\rightarrow CD_4+CD_2COCD_3, \quad (1)$$

$$CD_3+CH_3CN\rightarrow CD_3H+CH_2CN, \quad (2)$$

or

$$CD_3+C_2H_5CN\rightarrow CD_3H+C_2H_4CN, \quad (3)$$

$$2CD_3\rightarrow C_2D_6. \quad (4)$$

From this mechanism it is clear that

$$k_2/k_4^{\frac{1}{2}}=\frac{R_{CD_3H}}{R^{\frac{1}{2}}_{C_2D_6}}\cdot\frac{1}{[CH_3CN]}, \quad \text{I}$$

and

$$k_2/k_1=\frac{R_{CD_3H}}{R_{CD_4}}\cdot\frac{[\text{acetone}]}{[CH_3CN]}. \quad \text{II}$$

Similar equations may be derived for $k_3/k_4^{\frac{1}{2}}$ and k_3/k_1.

EXPERIMENTAL

The apparatus was mainly the same as described elsewhere.[1] The storage vessels containing CD_3COCD_3, CH_3CN, and C_2H_5CN were separated from the reaction cell by mercury cutoffs. Since neither CH_3CN nor C_2H_5CN absorb above 2160A,[2] the light of the S-500 Hannovia lamp was not filtered. Experiments showed that CH_3CN and C_2H_5CN did not decompose when irradiated in absence of acetone. The acetone-d_6 was prepared by Dr. L. C. Leitch of this laboratory, and contained 96 percent C_2D_6CO. Due to the presence of small fractions of not completely deuterated acetone, some CD_3H was found when acetone was photolyzed alone. The amount of CD_3H thus produced was 10 percent of the amount of CD_4 produced. CH_3CN and C_2H_5CN were obtained from the Eastman Kodak Company and were distilled once in vacuo before use.

The light beam was collimated by one stop and two lenses and formed an illuminated volume of 100 cc in the 200 cc quartz cell.

RESULTS AND DISCUSSION

In Table I are given the results of experiments done at various temperatures for various mixtures of CH_3CN

[1] M. H. J. Wijnen and E. W. R. Steacie, J. Chem. Phys. **20**, 205 (1952).
[2] H. Sponer, *Molekul Spektren* (Verlag Julius Springer, Berlin, 1935, 1936), Vol. I (tables), Vol. II (text).

TABLE I. The reaction of CD_3 radicals with CH_3CN.

Exp No.	Temp °C	[Ac]$_i$ mole/cc $\times 10^{-17}$	[CH_3CN]$_i$ mole/cc $\times 10^{-17}$	In mole/cc sec $\times 10^{-12}$ R_{CD_4}	R_{CD_3H}	$R_{C_2D_6}$	$k_1/k_4^{\frac{1}{2}} \cdot 10^{14}$	$k_2/k_4^{\frac{1}{2}} \cdot 10^{12}$	k_2/k_1
1	100	4.05	11.55	0.13	1.43	28.17	6.06	2.31	3.82
2	100	8.35	8.51	0.30	1.27	39.79	5.66	2.32	4.10
3	100	9.66	6.16	0.35	1.01	40.59	5.63	2.51	4.46
4	100	8.33	13.58	0.07	0.66	3.45	4.47	2.57	5.75
5	290	4.88	4.10	11.32	24.24	7.60	842.56	205.00	2.43
6	290	3.83	8.45	4.65	27.00	1.94	873.06	225.79	2.57
7	290	3.04	11.46	2.46	24.76	1.47	667.76	176.64	2.64
8	290	10.25	3.93	33.04	40.91	14.46	831.01	251.28	3.02
10	200	6.71	8.02	3.37	12.93	12.46	142.40	44.51	3.13
11	200	4.94	14.12	1.86	16.94	...	...	...	3.15
12	133	10.04	4.78	0.55	0.55	12.36	15.74	2.98	1.89
13	133	12.38	5.80	0.21	0.41	1.17	16.05	6.18	3.85
14	133	8.29	6.63	0.44	1.37	...	...	...	3.80

and CD_3COCD_3. In the introduction we pointed out that

$$k_2/k_4^{\frac{1}{2}} = \frac{R_{CD_3H}}{R^{\frac{1}{2}}_{C_2D_6}} \cdot \frac{1}{[CH_3CN]}, \qquad \text{I}$$

and

$$k_2/k_1 = \frac{R_{CD_3H}}{R_{CD_4}} \cdot \frac{[\text{acetone-}d_6]}{[CH_3CN]}. \qquad \text{II}$$

These equations represent the ideal case in which the acetone-d_6 would have been completely deuterated. Since in our case CD_3H is also produced in the photolysis of acetone-d_6 alone, and since the amount of CD_3H thus produced is equal to $\frac{1}{10}$ of the amount of CD_4 produced, $k_2/k_4^{\frac{1}{2}}$ and k_2/k_1 are given by

$$k_2/k_4^{\frac{1}{2}} = \frac{R_{CD_3H} - 1/10 R_{CD_4}}{R^{\frac{1}{2}}_{C_2D_6}} \cdot \frac{1}{[CH_3CN]}, \qquad \text{(Ia)}$$

and

$$k_2/k_1 = \frac{R_{CD_3H} - 1/10 R_{CD_4}}{R_{CD_4}} \cdot \frac{[\text{acetone-}d_6]}{[CH_3CN]}. \qquad \text{(IIa)}$$

The data of $k_2/k_4^{\frac{1}{2}}$ and k_2/k_1 thus obtained are given in Table I, columns 9 and 10. In Figs. 1 and 2 we plotted $\log k_2/k_4^{\frac{1}{2}}$ and $\log k_2/k_1$ against $1/T$. From the slopes of these lines we obtain $E_2 - \frac{1}{2}E_4 = 9.9$ kcal and $E_2 - E_1 = -1.2$ kcal. Accepting $E_4 = 0$ kcal, we obtain $E_2 = 9.9$ kcal.

From the equation

$$k_1/k_4^{\frac{1}{2}} = \frac{R_{CD_4}}{R^{\frac{1}{2}}_{C_2D_6}} \cdot \frac{1}{[\text{acetone-}d_6]},$$

it is possible to calculate a value for E_1 from our data. In Fig. 1 we plotted $\log k_1/k_4^{\frac{1}{2}}$ against $1/T$.

Since it is a well-established fact that the Arrhenius plot starts curving below 125°C, less importance should be given to the data obtained at 100°C. Doing so, we obtained $E_1 - \frac{1}{2}E_4 = 11.5$ kcal. An activation energy of $E_1 - \frac{1}{2}E_4 = 10.8$ kcal would be obtained if also the data at 100°C were included. Previous values suggested for E_1 are 11.6 kcal[3,4] and 10.6 kcal.[5] While the lower value is somewhat suspicious because it was based on an Arrhenius plot which tended to curve at lower temperatures, it seems reasonable to accept $E_1 = 11.3 \pm 0.3$ kcal. This value is confirmed by recent work in these laboratories. We obtain $E_2 = 9.9$ kcal (Method I), and $E_2 = 11.3 - 1.2 = 10.1$ kcal (Method II). For the reaction of CD_3 radicals with CH_2CN we therefore suggest an activation energy of 10 ± 0.5 kcal.

In Table II are given the results obtained for mixtures of acetone-d_6 and propio-nitrile. The initial intensity of the light source was cut down by the use of neutral

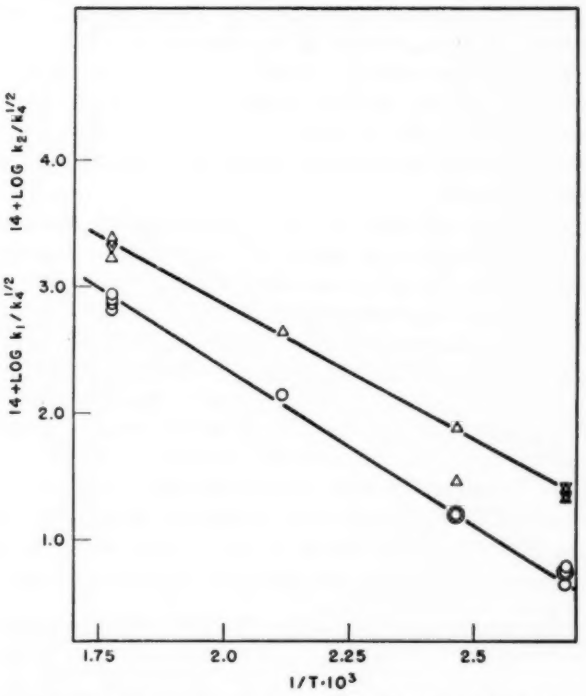

FIG. 1. CD_3+Acetone-d_6 (○) and CD_3+CH_3CN (△).

[3] E. Whittle and E. W. R. Steacie, J. Chem. Phys. **21**, 993 (1953).
[4] McNesby, Davis, and Gordon, (to be published).
[5] T. G. Majury and E. W. R. Steacie, Can. J. Chem. **30**, 800 (1952).

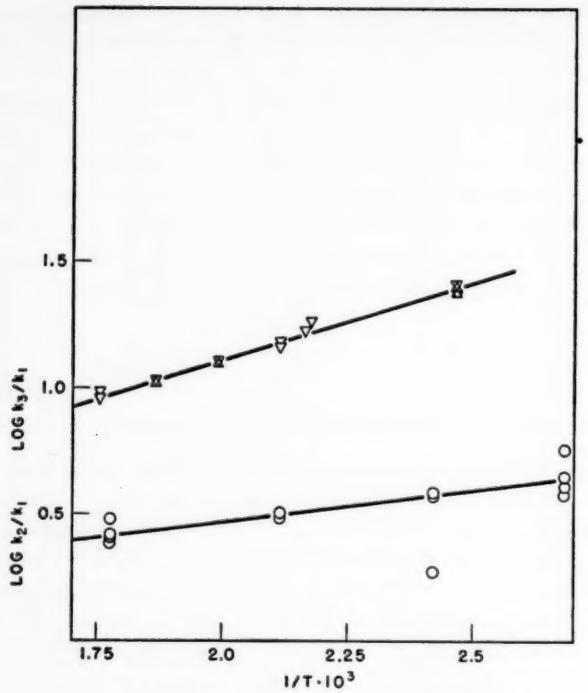

FIG. 2. CD_3+CH_3CN (○) and $CD_3+C_2H_5CN$ (Δ).

density filters in several experiments as indicated in column 3. Owing to the fact that CD_3 radicals react faster with C_2H_5CN than with CH_3CN, the amounts of C_2D_6 produced were very small and were therefore not measured. Only Method II has been used to determine the activation energy of reaction 3. In column 6, Table II, we give the data obtained for k_3/k_2. In Fig. 2 we plotted $\log k_3/k_2$ against $1/T$. Accepting again $E_1=11.3$ kcal, an activation energy of $E_3=8.5\pm0.5$ kcal was obtained.

Recently, Cvetanovic, Raal, and Steacie[6] made an extensive study of the photolysis of acetone in presence of CCl_4 and CCl_3H. They observed an increase in CH_4 formation and corresponding decrease in C_2H_6 formation, with increase in CCl_4 or CCl_3H pressure. This they explained by an acetone photosensitized decomposition of CCl_4 and CCl_3H with a subsequent formation of HCl. In our experiments no test for HCN was made. Tables I and II, however, indicate that increase in pressure of CH_3CN and of C_2H_5CN did have no effect on the values obtained for k_2/k_1 and k_3/k_1. Variations of intensity did not alter the values of k_3/k_1 as may be seen in Table II.

No other data are available concerning the reaction of methyl radicals with CH_3CN and C_2H_5CN. As an approximation, reactions (2) and (3)

$$CD_3+CH_3CN\rightarrow CD_3H+CH_2CN, \quad (2)$$

$$CD_3+C_2H_5CN\rightarrow CD_3H+C_2H_4CN, \quad (3)$$

might perhaps be compared with the reactions

$$CD_3+CH_3CH_3\rightarrow CD_3H+CH_2CH_3, \quad (5)$$

$$CD_3+C_2H_5CH_3\rightarrow CD_3H+C_2H_4CH_3. \quad (6)$$

This approximation seems reasonable if we compare our value of $E_2=10\pm0.5$ kcal with $E_5=10.4$ kcal.[7] No value for E_6 has as yet been published. Realizing the difference in bond strengths between C_2H_5-H and C_3H_7-H we might draw a parallel with the $CNCH_2-H$ and CNC_2H_4-H bonds. This would suggest for E_3 a value smaller than E_2, as has been observed.

TABLE II. The reaction of CD_3 radicals with C_2H_5CN.

Exp. No.	Temp. °C	Intensity, relative	$[Ac]_i/[C_2H_5CN]_i$	$(R_{CD_3H}-1/10R_{CD_4})/R_{CD_4}$	k_2/k_1
2	187	100	1.72	10.40	17.90
3	189	100	2.48	6.75	16.74
5	133	100	2.36	10.71	25.32
6	133	1	4.79	5.12	24.51
7	133	8	2.31	10.53	24.31
8	133	100	1.86	13.71	25.51
9	200	8	2.07	7.13	14.79
10	200	100	2.33	6.24	14.51
11	297	100	2.42	3.91	9.46
12	297	8	4.00	2.22	8.89
13	230	100	3.63	3.46	12.56
14	230	8	2.16	5.81	12.55
15	263	8	2.31	4.55	10.54
16	263	100	2.25	4.72	10.62

Accepting for the collision diameters of acetone-d_6 CH_3CN, C_2H_5CN, and CD_3 5.5, 5, 5.5, and 3.5×10^{-8} cm, respectively, we calculated the following values for the steric factor ratios $P_2/P_1=0.9$ and $P_3/P_1=0.85$. Using Whittle and Steacie's[3] value $P_1/P_4^{\frac{1}{2}}=3.3\ 10^{-3}$, we obtain $P_2/P_4^{\frac{1}{2}}=3.10^{-3}$ and $P_3/P_4^{\frac{1}{2}}=2.8\ 10^{-3}$.

ACKNOWLEDGMENTS

The author wishes to thank Dr. E. W. R. Steacie for his continuing interest and his advice during the progress of this work. He also wishes to thank Miss Frances Gauthier and Miss June Fuller for the mass spectrometer analyses.

[6] Cvetanovic, Raal, and Steacie, Can. J. Chem. **31**, 171 (1953).

[7] Trotman-Dickenson, Birchard, and Steacie, J. Chem. Phys. **19**, 163 (1951).

Solution Spectra and Oscillator Strengths of Electronic Transitions of Pyridine and Some Monosubstituted Derivatives*†

HAROLD P. STEPHENSON‡§
Department of Physics, Duke University, Durham, North Carolina
(Received February 12, 1954)

The near ultraviolet absorption spectra of the following substances have been measured in iso-octane and ethyl alcohol solutions: pyridine, the isomeric picolines, 2- and 3-fluoropyridine, 2- and 3-chloropyridine, and 2- and 3-bromopyridine. Solvent effects were observed and oscillator strengths were measured for the singlet-singlet $\pi-\pi^*$ and $n-\pi^*$ electronic transitions which occur in the spectral region 34 000 cm^{-1} to 48 000 cm^{-1}. It was found that in this spectral region the $n-\pi^*$ transition is missing in the case of 2-fluoro-, 2-chloro- and 2-bromopyridine.

INTRODUCTION

THE fact that in the near ultraviolet absorption spectra of pyridine, the diazines, and many of their derivatives there occur $n-\pi^*$ electronic transitions as well as $\pi-\pi^*$ transitions, makes it essential that criteria be available for distinguishing the two types. Two such criteria, which are proving particularly useful, are a comparison of solvent effects and a comparison of oscillator strengths (f values).[1] In the research reported here solvent effects have been observed and the oscillator strengths measured for the following substances: pyridine, the isomeric picolines, 2- and 3-fluoropyridine, 2- and 3-chloropyridine, and 2- and 3-bromopyridine. The solution spectra of all these compounds are known in the literature. Several of them, however, have been studied in only one solvent and without prior knowledge of the existence of the two types of electronic transitions. In order to make the oscillator strength determinations it was necessary, therefore, to make new measurements for all the substances.

EXPERIMENTAL

The spectrograms reported here in Figs. 1 through 10 were measured with a Beckman spectrophotometer using iso-octane and 95 percent ethyl alcohol solutions. The molar extinction coefficients ϵ were calculated from the equation

$$I=I_0 10^{-\epsilon c l}, \qquad (1)$$

where c is the concentration in moles per liter and l is the path length in cm. Cells one cm long were used throughout this research.

The compounds were obtained from various sources. The pyridine was a commercial Merck product which had been purified by being distilled twice under ordinary pressure and then a third time after standing over potassium hydroxide. Dr. J. J. McGovern of the Mellon Institute supplied the samples of 2-picoline 99.85 percent pure (bp 129.44°) and 3-picoline 99 percent pure (bp 143.0–143.5°). The 4-picoline (bp 144.5–145.0°) was purified by Dr. J. C. Shivers of the Department of Chemistry, Duke University, and was purified further in this laboratory by an additional distillation.

Very pure samples of 2-chloropyridine, 2-bromopyridine, and 3-bromopyridine were obtained from Dr. M. Kasha. A few grams of 3-chloropyridine were synthesized and purified to special order by the Delta Chemical Works. Purity specifications were not available, but experiments with vapor absorption have indicated a high degree of purity. The samples of 2- and 3-fluoropyridine were given to us by Dr. Arthur Roe of the Department of Chemistry, the University of North Carolina. The samples had been very carefully dried and distilled and were supplied in vacuum-tight breakseals.

In the course of the research some difficulty with chemical decomposition arose for 2- and 3-bromopyridine and 2-fluoropyridine. The nature of the decomposition was rather imperfectly understood, but it has appeared reasonably certain that the spectra were inappreciably affected thereby. A comparison with the literature, the major outline of which is given in Table I, shows that there is good agreement between the spectrograms reported in this research and those reported elsewhere. With regard to the difficulties with decomposition, it is significant that our data for the halogenated pyridines agree so well with the data of

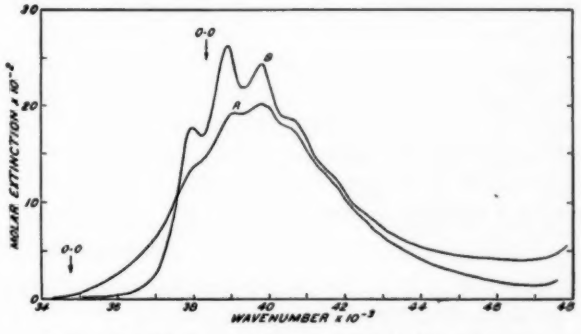

FIG. 1. Pyridine in (A) iso-octane and (B) 95 percent ethyl alcohol.

* Taken from part of a thesis submitted by Harold P. Stephenson in partial fulfillment of the requirements for the degree of Doctor of Philosophy at Duke University, 1952.

† This investigation was assisted by the U. S. Office of Naval Research under Contract N6ori-107, Task Order I, with Duke University.

‡ Shell Oil Company Fellow at Duke University, 1950–1951.

§ Present address: Department of Physics, Illinois Wesleyan University, Bloomington, Illinois.

[1] J. R. Platt, J. Chem. Phys. **19**, 101 (1951).

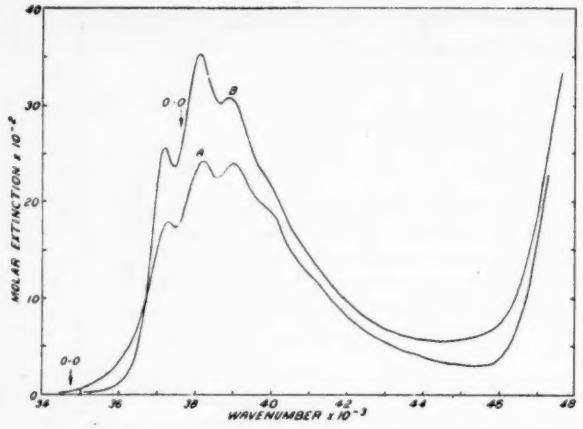

FIG. 2. 2-Picoline in (*A*) iso-octane and (*B*) 95 percent ethyl alcohol.

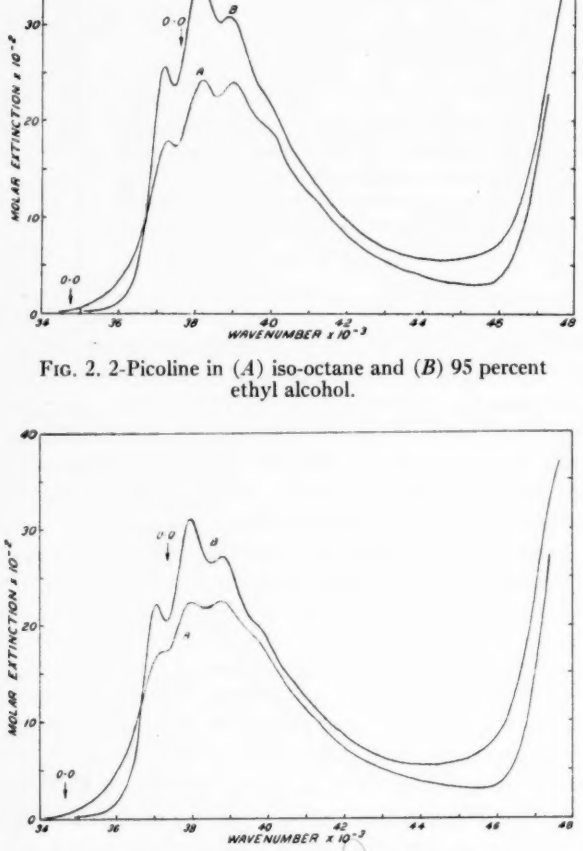

FIG. 3. 3-Picoline in (*A*) iso-octane and (*B*) 95 percent ethyl alcohol.

Wibaut and Spiers[2] published in 1937 and the more recent data of Miller, Knight, and Roe.[3] The largest discrepancy was noted for 3-bromopyridine in nonpolar solvents.

SOLVENT EFFECTS

It has been largely due to the work of Kasha,[4] and Rush and Sponer[5,6] that in pyridine the existence of at least one singlet-singlet $\pi-\pi^*$ electronic transition and at least one singlet-singlet $n-\pi^*$ electronic transition has been established. One of these transitions (referred to as Transition I) has its O—O band at 34 769 cm^{-1} in the vapor and is now recognized[4,5] as an $n-\pi^*$ transition. The second transition (referred to as Transition II) has its O—O band at about 38 350 cm^{-1} in the vapor[6] and long remained undetected as a system independent of Transition I, because its bands are very diffuse and overlap Transition I around 38 500 cm^{-1}.

Kasha first advanced the idea that in the diffuse region beginning at about 38 500 cm^{-1} there is a strong $\pi-\pi^*$ transition (here called Transition II) and a somewhat weaker transition due to excitation of one of the nitrogen nonbonding (sp^2) electrons ($n-\pi^*$ transition). He also came to the conclusion that Transition I is likewise an $n-\pi^*$ transition and not a $\pi-\pi^*$ transition as formerly supposed. According to this view there would be three singlet-singlet transitions in the region 33 000 cm^{-1} to 48 000 cm^{-1} (see Fig. 1). Rush and Sponer definitely identified two of these transitions (Transitions I and II) in the vapor spectra of the isomeric picolines. The existence of the second $n-\pi^*$ system could not be definitely established from the vapor spectra studies.

It was upon interpretations of solvent effects that Kasha chiefly based his ideas. In this research the solvent effects which may be observed for Transition I have been investigated in considerable detail for pyridine and several derivatives. The essential features of the effects may be understood from Fig. 1 for pyridine. The O—O band positions as determined from vapor measurements are indicated with arrows. That the spectrogram taken in alcohol should be so much more discrete than that taken in iso-octane solution has been the evidence given by Kasha for the existence of two transitions in the region of Transition II. Because of the

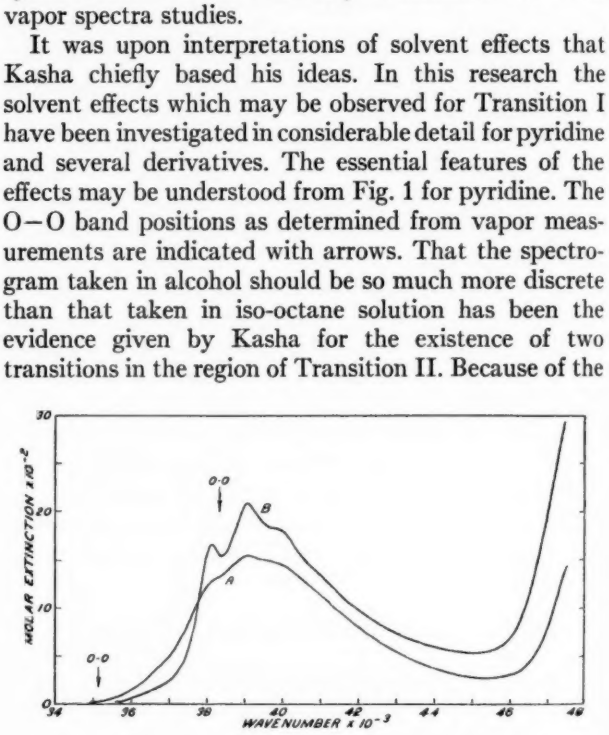

FIG. 4. 4-Picoline in (*A*) iso-octane and (*B*) 95 percent ethyl alcohol.

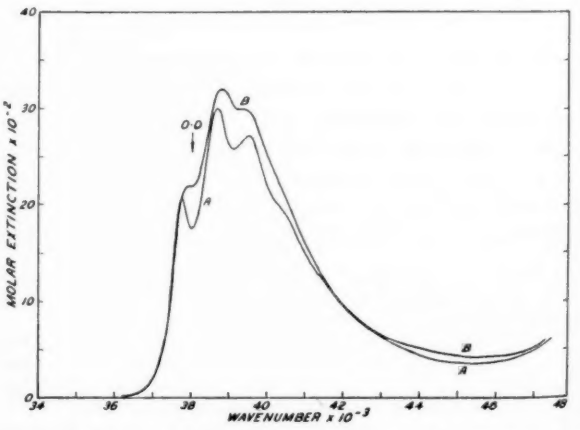

FIG. 5. 2-Fluoropyridine in (*A*) iso-octane and (*B*) 95 percent ethyl alcohol.

[2] J. P. Wibaut and C. W. F. Spiers, Rec. trav. chim. **56**, 573 (1937).
[3] Miller, Knight, and Roe, J. Am. Chem. Soc. **72**, 1629 (1950).
[4] M. Kasha, Disc. Faraday. Soc. **9**, 14 (1950).
[5] J. H. Rush and H. Sponer, J. Chem. Phys. **20**, 1847 (1952). See this paper for many earlier references.
[6] H. Sponer and J. H. Rush, J. Chem. Phys. **17**, 587 (1949).

lack of supporting data from vapor spectra, the evidence must be considered to be inconclusive at the present time. The situation is much more satisfactory with regard to Transition I.

From the spectrogram one can see that in the region of Transition I (about 34 000 cm^{-1} to 37 500 cm^{-1}) the intensity of pyridine absorption decreases in alcohol solution as compared to that in iso-octane solution. The intensity decrease may be interpreted by the assumption that in alcohol the nitrogen nonbonding (sp^2) electrons become involved in the formation of a hydrogen bond, and that consequently their excitation requires more energy and thus the $n-\pi^*$ transition moves towards the violet. An assumed hydrogen bond strength of about 6 kcal/mole might be expected to correspond to a shift of about 2000 cm^{-1}. Such a shift would be sufficient to cause Transition I to move well into the region of Transition II, and hence to be obscured by the latter transition.

In accordance with the results of Rush and Sponer that all three of the picolines possess a Transition I and a Transition II, one sees from Figs. 2, 3, and 4 that the effect of the two solvents upon the spectrograms of the picolines is the same as for pyridine, that is, the region of Transition I decreases in intensity when the change is made from iso-octane to alcohol, while the region of Transition II increases in intensity. The spectrograms of 3-fluoropyridine, 3-chloropyridine, and 3-bromopyridine shown in Figs. 6, 8, and 10 reveal that these substances also react to a solvent change in exactly the same way as pyridine. The vapor spectra of these substances have also been measured in this laboratory, and the existence of the two transitions for these compounds has been definitely established.

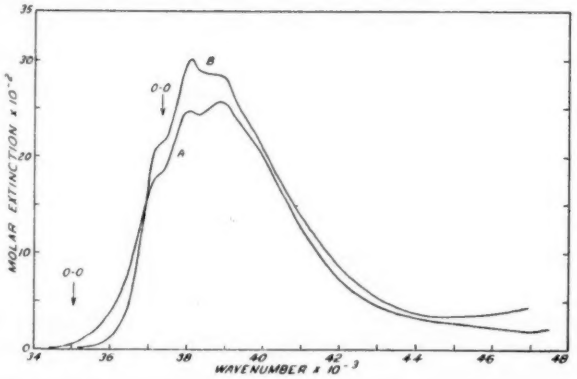

FIG. 6. 3-Fluoropyridine in (*A*) iso-octane and (*B*) 95 percent ethyl alcohol.

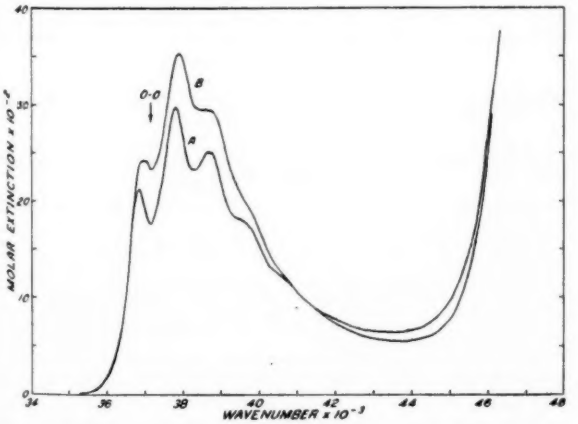

FIG. 7. 2-Chloropyridine in (*A*) iso-octane and (*B*) 95 percent ethyl alcohol.

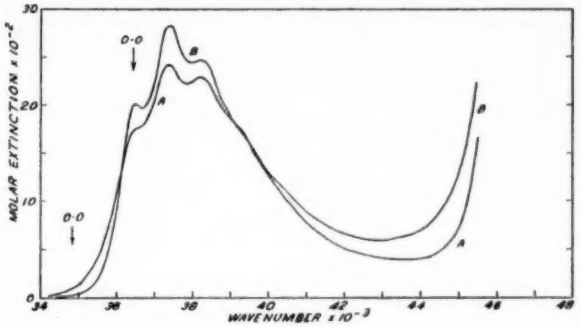

FIG. 8. 3-Chloropyridine in (*A*) iso-octane and (*B*) 95 percent ethyl alcohol.

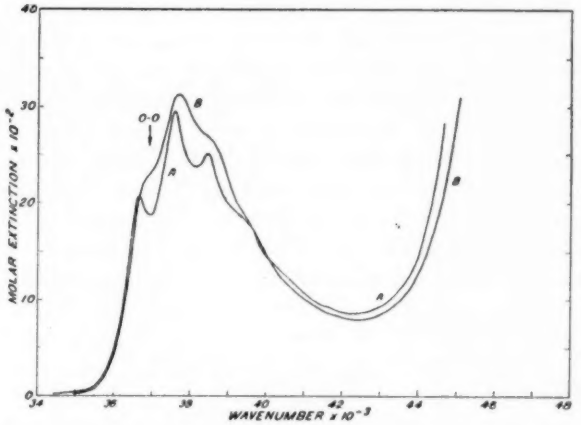

FIG. 9. 2-Bromopyridine in (*A*) iso-octane and (*B*) 95 percent ethyl alcohol.

The situation is very different, however, for 2-fluoropyridine, 2-chloropyridine, and 2-bromopyridine. Figures 5, 7, and 9 show that these substances do not react to a solvent change in the same way as does pyridine. In the low-energy regions of the spectrograms the strength of absorption is practically the same in alcohol solution as in iso-octane solution. It appears as though the solvent effect criterion for assigning Transition I as a nonbonding electron transition has no validity for these *ortho*-substituted compounds. Vapor spectra studies made in this laboratory have shown, however, that these substances actually do not have a singlet-singlet $n-\pi^*$ transition in the spectral regions explored by these experiments. It will be made clear later how this fact may be interpreted so as to add weight to the argument that Transition I is an $n-\pi^*$ transition.

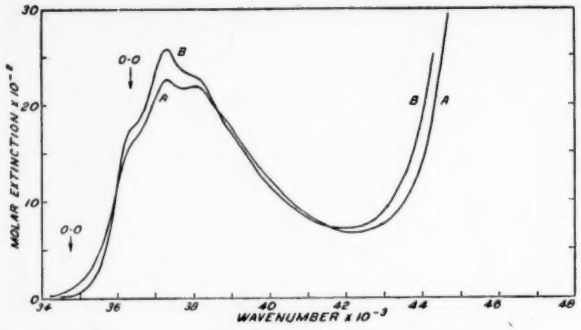

FIG. 10. 3-Bromopyridine in (*A*) iso-octane and (*B*) 95 percent ethyl alcohol.

DETERMINATION OF OSCILLATOR STRENGTHS

From Figs. 1 through 10 it can be seen that Transitions I and II are very close together in the spectrograms in which they appear as identifiable transitions and are furthermore not separated by a minimum. However, from the following considerations it is possible to arrive at a separation of the two absorbing regions. For all the spectrograms, even if there is no Transition I, the absorption intensity in the region of Transition II increases when the solution change from iso-octane to alcohol is made. If we assume the extreme case that it is mainly Transition II whose intensity is increased in alcohol and that Transition I is negligibly weak when it is shifted into the second region, we may construct separated curves for iso-octane solution in the following way:

Let the first principal maximum at 38 000 cm^{-1} (Fig. 1) be chosen to represent a measure of the relative intensity increase of Transition II in alcohol. The increase is 20 percent (from 1370 to 1765). If now the entire portion of the curve in alcohol solution from this maximum toward smaller wave numbers is diminished by 20 percent and the derived curve portion is joined at 38 000 cm^{-1} with the experimental curve in iso-octane, a spectrogram for Transition II in iso-octane is obtained which might be measured if Transition I were entirely missing. This empirical spectrogram is shown in Fig. 11. When the ordinates, from the connecting point to lower wave numbers, of the experimental and the derived iso-octane spectrograms are subtracted from one another, absolute ordinate values for Transition I are obtained, and these have been plotted in Fig. 11 in dashed outline.

On the other hand, if it is assumed that the increase in absorption of the alcohol solution spectrogram in the region from 38 000 cm^{-1} to larger wave numbers is entirely due to the shifted Transition I, then the oblong area between the iso-octane curve (curve *A*) and the alcohol curve (curve *B*) from 34 000 cm^{-1} to 37 500 cm^{-1} in Fig. 1 should be equal in magnitude to the portion of the curve *B* over curve *A* between 37 500 cm^{-1} and 41 000 cm^{-1}. It may be seen that the two areas are approximately in the ratio 2:3. This would mean that only $\frac{1}{3}$ of the intensity increase must stem from a solution effect on Transition II. Consequently, the low energy part of curve *B* should be corrected by only $\frac{1}{3}$ of 20 percent, that is by 7 percent, and the dashed area of Transition I would be correspondingly smaller. The best approximate values would lie between these two extreme cases. Since the whole variation is small and since not more than the correct order of magnitude may be expected, the *f* values given in Table II have been obtained by using the method giving the maximum correction. Although the procedure is probably good enough for an approximate separation of the transitions, it should not be forgotten that what here has been called

TABLE I. Comparison of experimental results with literature.

Compound	Band maximum cm^{-1}	Maximum molar extinction	Solvent	Reference
Pyridine	39 750	2020	Iso-octane	This research
	39 750	2040	Cyclohexane	a
	39 750	1630	Hexane	b
	39 750	2300	Heptane	c
	39 750	1970	Iso-octane	d
	39 750	1770	Iso-octane	e
	39 750	2070	Cyclohexane	f
	38 900	2630	Alcohol	This research
	38 900	2240	Alcohol	g
	38 900	2600	Alcohol	h
2-Picoline	38 230	2420		
	39 000	2385	Iso-octane	This research
	38 160	2430		
	38 900	2450	Iso-octane	i
	38 160	2420		
	38 900	2530	Cyclohexane	j
	38 160	2700		
	38 900	2700	Cyclohexane	f
3-Picoline	38 750	2260	Iso-octane	This research
	38 750	2250	Cyclohexane	f
4-Picoline	39 050	1550	Iso-octane	This research
	39 050	1600	Cyclohexane	f
2-Fluoropyridine	38 750	3200	Alcohol	This research
	38 750	3250	Alcohol	h
3-Fluoropyridine	38 160	2990	Alcohol	This research
	38 160	3050	Alcohol	h
2-Chloropyridine	37 800	2920	Iso-octane	This research
	37 200	2750	Heptane	c
3-Chloropyridine	37 370	2400	Iso-octane	This research
	37 900	2450	Heptane	c
2-Bromopyridine	37 580	2950	Iso-octane	This research
	37 000	3000	Heptane	c
3-Bromopyridine	37 300	2270	Iso-octane	This research
	37 500	2000	Heptane	c

[a] See reference 11.
[b] H. Fischer and P. Steiner, Compt. rend. **175**, 882 (1922).
[c] See reference 2.
[d] American Petroleum Institute Research Project 44 at the National Bureau of Standards. Catalog of Ultraviolet Spectrograms. Serial No. 34, Pyridine, contributed by the Union Oil Company of California.
[e] API Research Project 44. Serial No. 108, Pyridine, contributed by the California Research Corporation.
[f] E. F. G. Herington, Disc. Faraday Soc. **9**, 26 (1950).
[g] Landolt-Börnstein, *Physikalisch-Chemische Tabellen* (Verlag Julius Springer, Berlin, 1935), 5th edition, 3rd supplement, p. 1416.
[h] See reference 3.
[i] API Research Project 44. Serial No. 35, 2-Picoline, contributed by the Union Oil Company of California.
[j] API Research Project 44. Serial No. 213, 2-Picoline, contributed by the Mellon Institute.

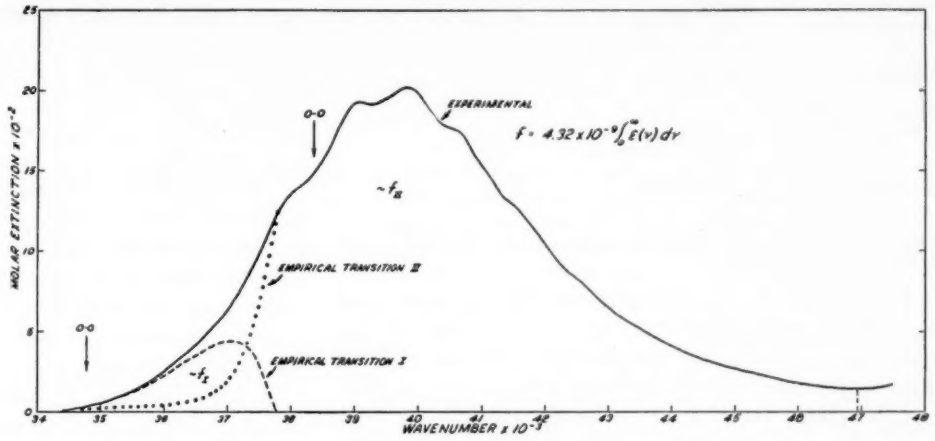

FIG. 11. Diagram for pyridine of empirical construction of spectrograms.

Transition II might consist of a $\pi-\pi^*$ and an $n-\pi^*$ transition as mentioned before. This fact would introduce a complication into the treatment of this region.

According to the well-known equation

$$f=4.32\times10^{-9}\int_0^\infty \epsilon d\nu, \qquad (2)$$

the oscillator strength of an electronic transition is proportional to the area under the absorption curve. In the case of pyridine, therefore, the oscillator strengths of Transitions I and II may be immediately determined from the areas enclosed by the curves of Fig. 11. In this research the actual measurements were made with a polar planimeter from drawing-board size graph paper, the constructions for all the substances being similar to that for pyridine. For Transition II a special element of arbitrariness arises in the area measurement, because at no place on the high wave number side of the spectrograms does the value of ϵ drop to zero. It was assumed that in the region around 46 000–48 000 cm^{-1} Transition II and the next strong transition further to the violet overlap one another symmetrically about the point of minimum absorption. At this point (see Fig. 11) a vertical line was used to define the edge of the measured area. The results of all the f value determinations are given in Table II, where all the numbers have been rounded off to two significant figures.

DISCUSSION

Sklar,[7] in his study of the intensities of π-electron transitions in substituted benzenes, has shown that when two substituents are both either *ortho-para*-directing or *meta*-directing, first-order addition of "migrational moments" may be made according to the following theorem: the transition (migrational) moment due to a second radical in the position ξ is rotated from that of a radical in position ζ by an angle $\tau=(\xi 0\zeta)$ and multiplied by $(-1)(3\tau/\pi)$. The separate vector moments need not be of the same magnitude. When the substituents are dissimilar in their ring-directing property, the vector addition is governed by the theorem that the migration moment due to a *meta*-directing group is 180° out of phase from that which would be produced by an *ortho-para*-directing group in the same ring position. Sklar presented empirical evidence which justified the omission of induction and vibration effects in the calculations and assumed the intensity of the electronic transitions to be proportional to the square of the migrational moments alone.

Sklar's theoretical predictions checked very well with data on the near ultraviolet absorption spectra of benzene derivatives for which it could be assumed that the ring perturbations were not too strong and no new transitions were introduced by the substituents (methyl benzenes, for example). It is interesting, therefore, under the assumption that the nitrogen in pyridine acts as a *meta*-directing substituent, that the f values reported here for pyridine and the picolines check rather well with the Sklar theory in the case of Transition II. Disregarding factors of proportionality, the transition moment diagrams for pyridine and the picolines would be as shown in Fig. 12. The phases for the diagrams have been chosen so that the transition moment of the first substituent (*meta*-directing N atom) points along the negative x-axis. One sees immediately that 2- and 3-picoline should have the same f values. Using pyridine and 4-picoline as the "standards," the calculated f value for 2- and 3-picoline is 0.046. This result is in excellent

TABLE II. Oscillator strengths (f values).

Compound	Solution in iso-octane Transition I $n-\pi^*$	Solution in iso-octane Transition II $\pi-\pi^*$	Solution in ethyl alcohol Transition II $\pi-\pi^*$
Pyridine	0.0030	0.041	0.049
2-Picoline	19	47	59
3-Picoline	22	45	53
4-Picoline	23	32	40
2-Fluoropyridine	...	49	54
3-Fluoropyridine	22	49	55
2-Chloropyridine	...	48	55
3-Chloropyridine	14	44	48
2-Bromopyridine	...	47	50
3-Bromopyridine	095	42	43

[7] A. L. Sklar, J. Chem. Phys. **10**, 135 (1942); and Revs. Modern Phys. **14**, 232 (1942).

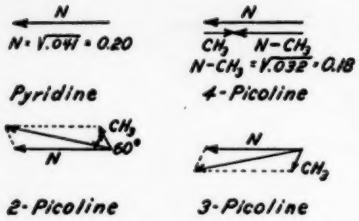

FIG. 12. Diagram of transition moments for pyridine and the picolines.

agreement with the experimental values of 0.047 and 0.045 (see Table II).

From Table II one can conjecture that the same good agreement with Sklar's theory would exist for the halogenated pyridines if measurements on the unstable *para*-derivatives could be made. It is important to point out, however, that for the picolines and all the halogenated pyridines, except the fluorine compounds, the *ortho*-substituted substances possess a slightly higher f value than the *meta*-substituted ones. This systematic difference is not taken care of by the Sklar theory. That the fluorinated pyridines have the largest f values is in accord with corresponding results for fluorinated benzenes.[8]

In contrast to Transition II, the intensity distribution of Transition I in pyridine and the picolines cannot be adapted to the predictions of the Sklar theory. This failure of agreement is in accord with the view that the transition is not due to π electrons but rather to the nitrogen nonbonding electrons. The fact that the various Transitions I have oscillator strengths of the same order of magnitude as the forbidden 2600A transition in benzene ($f \sim 10^{-3}$) was the reason for a suggestion by Kasha that these transitions are forbidden ones. However, the analysis of the vapor spectra[5] has shown that the Transitions I are not forbidden by symmetry as is the case for benzene where a weak transition occurs due to the interaction of an antisymmetric vibration of particular symmetry. From symmetry arguments it follows that the polarization vector is perpendicular to the plane of the ring and is rather small since the excited orbital has a node where the ground-state orbital has a maximum. An additional reason for the weakness is that the excited electron must move from an orbital localized on the nitrogen atom into a nonlocalized orbital distributed over the entire molecule ("spatial" forbiddenness, Platt).[1]

SPECIAL BEHAVIOR OF ORTHO-HALOGENATED PYRIDINES

It is significant that the disappearance of Transition I in the *ortho*-halogenated pyridines is not an isolated phenomenon. A number of years ago Uber[9] and Uber and Winters[10] studied the near ultraviolet absorption spectra of pyrimidine (1,3-diazine) and several chloropyrimidines both in the vapor state and in solution, and they found that some 125 sharp, line-like bands which appear with pyrimidine in the 2700–3300A region disappear entirely with dichloropyrimidine. Halverson and Hirt[11] have extended the work of Uber and Winters to include a study of the chlorinated pyrazines (1,4-diazine) and rather less completely a study of the corresponding pyridazines (1,2-diazine). In pyrazine, they identified an $n-\pi^*$ transition at 31 000 cm^{-1}, and found that the O—O band shifted towards the violet by 1700 cm^{-1} with 2-chloropyrazine, by 3200 cm^{-1} with 2,3-chloropyrazine, and by comparable amounts for several other chloropyrazines. Thus, with this series of compounds the violet shift could be followed step by step.

Since the excited π^* orbital in the pyrazines probably decreases in energy upon the chlorine substitution, the localized orbital of the nitrogen nonbonding electrons must then correspond in energy to a firmer binding in order to account for the violet shift of the $n-\pi^*$ transition. A general lack of ionization potential and dissociation constant data does not permit one to check independently that in these halogenated heterocyclics the nonbonding electrons are more firmly bound than in the parent molecule, but the strongly inductive character of halogen atoms makes the assumption of increased binding energy very plausible, particularly if the halogen atom is located very near the nitrogen atom. With respect to the results of this research, it can be conjectured, therefore, that Transition I is "missing" for 2-fluoro-, 2-chloro-, and 2-bromopyridine, simply because the inductive attraction of the halogen atoms attached to the carbon atom adjacent to the nitrogen atom increases the binding energy of the nonbonding electrons over that existing in pyridine. It is assumed that the increase in energy is such that the $n-\pi^*$ transition shifts into the spectral region of the $\pi-\pi^*$ transition or further.

With regard to 3-fluoro-, 3-chloro-, and 3-bromopyridine, data secured in this laboratory from vapor-state measurements indicate, if one assumes a constant variation for the energy of the excited state, that the term value of the nonbonding orbital progressively increases as the electronegativity of the halogen atom increases. The increase in binding energy is, however, in these cases never large enough to cause Transition I to shift completely into the region of Transition II (see Figs. 6, 8, and 10). This situation is undoubtedly due to the meta-location of the halogen atoms.

ACKNOWLEDGMENTS

In conclusion, the author wishes to express his sincere appreciation to Dr. H. Sponer, under whose direction this research project was carried out. He is grateful for many helpful suggestions during the writing of this paper. To Dr. M. Kasha, Dr. J. J. McGovern, Dr. J. C. Shivers, and particularly to Dr. A. Roe, the author owes a great debt of gratitude for assistance in obtaining the compounds used in this research. Lastly, a very helpful discussion with Dr. J. R. Platt is gratefully acknowledged.

[8] H. Sponer, J. Chem. Phys. **22**, 234 (1954).
[9] F. M. Uber, J. Chem. Phys. **9**, 777 (1941).
[10] F. M. Uber and R. Winters, J. Am. Chem. Soc. **63**, 137 (1941).
[11] F. Halverson and H. C. Hirt, J. Chem. Phys. **19**, 711 (1951).

Szilard-Chalmers Reaction in Crystalline Compounds of Chromium*

GARMAN HARBOTTLE
Chemistry Department, Brookhaven National Laboratory, Upton, Long Island, New York
(Received Februrary 24, 1954)

The Szilard-Chalmers reaction has been observed in a number of crystalline compounds of tri- and hexavalent chromium. The effect of neutron and external gamma irradiation has also been investigated. It was found that in a series of alkali chromates and dichromates the retention varied from 50 to 90 percent, while ammonium chromate and dichromate were much lower. The results are interpreted in terms of hot-atom reactions of the recoil fragments in the crystal, and hydrolysis and reduction reactions taking place on dissolution of the crystals.

INTRODUCTION

SOON after the discovery of the Szilard-Chalmers effect in liquid ethyl iodide[1] the Roman group of Amaldi *et al.*[2] studied the irradiation of crystalline compounds such as sodium chlorate, bromate and iodate, and potassium permanganate with slow neutrons. The Szilard-Chalmers effect permitted them to separate the respective radioisotopes in far higher specific activities than could otherwise have been attained.

Since that time a number of crystalline salts have been employed for the production of high specific activities,[3] but very few studies have been made in which a single system was investigated to elucidate the mechanism of the recoil separation or the identity of the primary recoil fragments. Potassium permanganate and sodium phosphate have been investigated in this way by Libby,[4] and several permanganates, potassium chloriridate, and triphenylarsine by Maddock and co-workers[5]; potassium bromate has been extensively studied by Boyd *et al.*,[6] cobaltic trisethylenediamine nitrate by Zuber,[7] and a series of iodates by Cleary *et al.*[8]

The present paper is concerned with a number of crystalline compounds of chromium, and is a continuation of studies previously reported by Green, Maddock, and the author.[9]

MATERIALS

With a few exceptions all reagents were of the purest commercially available grade and were used without further treatment. Lithium chromate and dichromate were synthesized, recrystallized from water, and analyzed in this laboratory. The analyses for lithium, chromium, and water of hydration gave results within a few tenths of a percent of the theoretical for Li_2CrO_4 and $Li_2Cr_2O_7 \cdot 2H_2O$. Anhydrous sodium chromate, sodium dichromate, and lithium dichromate were prepared by dehydration of the corresponding hydrated salts in vacuo.

NEUTRON IRRADIATION

Unless otherwise noted, all bombardments were made with thermal neutrons in the thermal column of the Brookhaven Reactor. The neutron flux at the bombardment site was 6×10^8 neutrons/cm^2 sec, the gamma-ray flux approximately 50 roentgens/hour and the temperature that of the building, 20–25°C. In some cases, as noted, bombardments were made in other positions within the pile.

RADIOCHEMICAL ANALYSIS AND COUNTING

The bombarded crystals were dissolved in aqueous solutions, previously adjusted to *p*H 2, which contained trivalent chromium carrier in the case of hexavalent chromium compounds, or hexavalent carrier when trivalent salts had been bombarded. Two aliquot portions were then removed: to the first was added an excess of lead nitrate; lead chromate was filtered off, and the filtrate, which contained trivalent chromium, was collected in a volumetric flask. The lead chromate was dissolved in concentrated nitric acid and collected in a second volumetric flask. The second aliquot portion was made basic with sodium hydroxide, oxidized with sodium peroxide, heated to destroy excess peroxide, adjusted to *p*H 2.5 ± 0.5, and lead chromate precipitated, filtered off, washed, and dissolved as before. Three solutions were then counted, representing trivalent and hexavalent fractions, and total chromium. The agreement between the sum of the first two and the third was usually better than two percent, and constituted a check on the absence

* Research carried out under the auspices of the U. S. Atomic Energy Commission.

[1] L. Szilard and T. A. Chalmers, Nature **134**, 462 (1934).

[2] Amaldi, D'Agastino, Fermi, Pontecarvo, Rasetti, and Segre, Proc. Roy. Soc. (London) **A149**, 522 (1935).

[3] A. C. Wahl and N. A. Bonner, *Radioactivity Applied to Chemistry* (John Wiley and Sons, Inc., New York, 1951), Table 8A.

[4] W. Libby, J. Am. Chem. Soc. **62**, 1930 (1940).

[5] (a) K. J. McCallum and A. G. Maddock, Trans. Faraday Soc. **49**, 1150 (1953); (b) Croatto, Giacomello, and Maddock, Ricerca sci. **22**, 265 (1952); (c) N. Sutin and A. G. Maddock, Research **6**, 75 (1953).

[6] (a) Boyd, Cobble, and Wexler, J. Am. Chem. Soc. **74**, 237 (1952). (b) J. Cobble and G. E. Boyd, J. Am. Chem. Soc. **74**, 1282 (1952).

[7] A. Zuber, unpublished research.

[8] Cleary, Hamill, and Williams, J. Am. Chem. Soc. **74**, 4675 (1952).

[9] Green, Harbottle, and Maddock, Trans. Faraday Soc. **49**, 1413 (1953).

TABLE I. Retention as hexavalent chromium in various chromates and dichromates.

Crystal	Retention, percent
Li_2CrO_4	66.0±0.5
$Li_2Cr_2O_7$	54.5±0.6
Na_2CrO_4	73.6±1.4
$Na_2Cr_2O_7$	79.9±0.6
K_2CrO_4	60.8±0.3
$K_2Cr_2O_7$	89.9±0.9
$(NH_4)_2CrO_4$	17.5±1.0
$(NH_4)_2Cr_2O_7$	31.9±1.2
$Na_2CrO_4 \cdot 4H_2O$	87.8±1.1
$Na_2Cr_2O_7 \cdot 2H_2O$	72.7±0.4
$MgCrO_4$	55.3±0.6
$ZnCrO_4$	34.6±1.0

of foreign activities. This procedure had been previously tested and found to give a clean separation, not subject to serious errors due to coprecipitation or induced exchange.[9]

Radioactive chromium-51 (half-life 27 days), whose decay scheme has been described previously,[9] was counted in solution in glass cells by observation of its 325 kilovolt gamma ray. The cells were reproducibly oriented beneath a sodium iodide (thallium-activated) scintillation crystal. The gamma-ray scintillations were recorded by a photomultiplier whose pulses were amplified and fed into a dual-discriminator anti-coincidence pulse-height analyzer.[10] The channel of the analyzer was set to accept only pulses resulting from photoelectric absorption of the chromium-51 gamma ray in the counter. This discrimination had several beneficial effects: (a) the ratio of sample count to background was increased by a factor of four; and (b) possible contamination activities were recorded with only a very low efficiency.

EXPERIMENTAL RESULTS

Compounds of Hexavalent Chromium

The "retention," defined as the probability that a radioactive chromium will appear after dissolution of the crystal in the same oxidation state as the parent compound, was determined for a number of crystals. All crystals were bombarded in the thermal column for one week and were permitted to stand for another week before analysis. All samples were dissolved at *p*H 2 in solutions containing trivalent carrier. The results, presented in Table I, in all cases represent averages of two or more determinations. The errors given are root-mean-square deviations from the average where more than two determinations were made, or the spread of results of duplicate determinations.

It was thought that oxygen present in the solutions in which crystals were dissolved might influence the distribution of chromium oxidation states. To test this hypothesis, a sample of irradiated sodium dichromate dihydrate was dissolved in a solution actively swept out with argon. The retention was unchanged. Since ammonium chromate and dichromate gave such low retentions it was thought that recoil fragments might be reacting with ammonium ions upon dissolution. Again, irradiated sodium dichromate dihydrate was dissolved in solutions 0.2 and 2.0 m in ammonium ion (at *p*H 2) and the retention was unaltered.

In another experiment, a sample of irradiated sodium dichromate dihydrate ($R=72.7\pm0.4$ percent) was dehydrated at room temperature in vacuo. The retention was then determined on the dehydrated salt as 73.3±0.9 percent. This value is within experimental error of the original retention but significantly different from the value for neutron-bombarded, anhydrous sodium dichromate ($R=79.9$ percent).

TABLE II. Retention in various compounds of trivalent chromium.

Crystal	Retention as Cr^{+++}, percent
$Cr_2(SO_4)_3 \cdot K_2SO_4 \cdot 24H_2O$	91.6±0.4
$Cr_2(SO_4)_3 \cdot (NH_4)_2SO_4 \cdot 24H_2O$	90.2±1
$Cr_2(SO_4)_3 \cdot 18H_2O$	96.3±0.2
$Cr(NO_3)_3 \cdot 9H_2O$	92.4±0.3

[10] This instrument was constructed by the Electronics Department of the Brookhaven National Laboratory; Designation EHI-493.

TABLE III. Chromate retention in mixed crystals.

Mixed crystal	Mole percent K_2CrO_4	Retention as Cr VI, percent	Irradiation conditions
$K_2CrO_4-K_2SO_4$	2.77	68.6±1	1 week thermal column
$K_2CrO_4-K_2SO_4$	0.485	69.8±3	4 weeks thermal column
$K_2CrO_4-K_2BeF_4$	1.56	22.3±3	2 weeks thermal column
$K_2CrO_4-K_2BeF_4$	1.56	25.5±1	2 weeks thermal column
$K_2CrO_4-K_2BeF_4$	1.56	25 ±3	7 min, water-cooled hole[a]
K_2CrO_4 (control)	100	60.8±0.4	1 week thermal column or 10 min, water-cooled hole

[a] In the water-cooled hole the flux was 1.3×10^{12} neutrons/cm²/sec and the temperature about 25°C.

Compounds of Trivalent Chromium

Several hydrated salts of trivalent chromium were bombarded for two days in the thermal column. Samples were dissolved in aqueous solutions (*p*H 2) containing hexavalent chromium carrier and analyzed as above. In the case of the chromic alums and sulfate, lead sulfate coprecipitated with lead chromate, but it was found possible to dissolve the crystalline mixture in concentrated nitric acid. The results (averages of two or more determinations) are presented in Table II. As above, the errors cited are root-mean-square deviations, or spread in duplicate determinations.

Mixed Crystals

Potassium chromate is isomorphous with potassium sulfate and fluoberyllate (K_2BeF_4) and forms mixed crystals with either. Mixed crystals of potassium sulfate-chromate and potassium fluoberyllate-chromate were grown from solution and carefully washed free of excess chromate. The crystals, which were visibly homogeneous, were grown under such conditions that the concentrations of the various components of the

TABLE IV. Retention of neutron-irradiated potassium chromate dissolved in solutions containing various added reagents.

Description of solvent	Retention percent
Water, *p*H 2, carrier Cr III, 10 percent ethanol	63.9±1.5
Water, *p*H 2, carrier Cr III, 15 percent ethanol	67.5±1.5
Control, no ethanol	63.8±0.6
Water, *p*H 2, carrier Cr VI, 10 percent ethanol	62.6±1.5
Water, *p*H 2, carrier Cr VI, 10 percent isopropanol	61.8±1.5
Control, no alcohol	60.8±0.4
Water, unbuffered solution, carrier Cr VI, 10 percent ethanol	69.3±1.0
Control, no ethanol	67.2±1.0
Water, no carrier, 15 percent ethanol (final *p*H 8.6)	67.0±1.0
Same, 15 percent isopropanol	67.9±1.0
Control, no alcohol	65.8±1.0
Glacial acetic acid, carrier Cr III	59.0±1.3[a]
Same, no carrier Cr III	59.4±1.3[a]
Control, aqueous solution *p*H 2, carrier Cr III	60.8±0
Water 1 *f* Cr III carrier *p*H 2	59.0±1
Water 1 *f* Cr VI carrier *p*H 2	64.3±1[b]
Control, *p*H2	60.8±0.4

[a] Corrected for solubility of lead chromate in glacial acetic acid.
[b] Solution diluted before precipitation of lead chromate to avoid co-precipitation of Cr III.

solutions did not change appreciably during the crystallization. For analysis, weighed portions of the crystals were dissolved in water and the chromate determined spectrophotometrically. The crystals were bombarded with neutrons and the oxidation states of chromium separated in the usual way. The results, expressed as retention of hexavalent chromium, are presented in Table III. In this table, a separate entry is made for each irradiation of crystals. The errors are root-mean-square deviations, or spread of duplicate determinations.

Experiments with Solutions Containing Added Reagents

It was thought possible that intermediate oxidation states of chromium (Cr V or IV), if present in the recoil fragment, could be made to react with reagents added to the solution in which the crystals were dissolved. It had been shown by Westheimer[11] that the kinetics of certain chromic acid oxidation reactions strongly suggested the existence of Cr V and IV as transitory species participating in the stepwise reduction of Cr VI to Cr III. Experiments were carried out in which ethanol and isopropanol were added to the solvent before dissolution of the irradiated potassium chromate crystals. It had been shown that reduction of hexavalent chromium is negligible under the conditions of this experiment (ice-bath temperature, *p*H 2.0). The effect of the addition of these alcohols is shown in Table IV.

Additional experiments were made in which neutron-irradiated crystals of potassium chromate were dissolved in 1 formal solutions of hexavalent and trivalent chromium adjusted to *p*H 2. Finally, a few experiments were carried out in which irradiated potassium chromate crystals were dissolved in glacial acetic acid and the entire procedure of lead chromate precipitation and filtration carried out in the absence of water. The results of these experiments are also presented in Table IV. All errors given are root-mean-square deviations, or spread in duplicate determinations.

The Effect of Radiation on Retention in Potassium Chromate

It has been reported by Green, Harbottle, and Maddock[9] that the retention in potassium chromate increased with increasing exposure to neutrons in the nuclear reactor. They also reported that gamma-ray irradiation of previously neutron-bombarded potassium chromate caused an increase in the retention. The same phenomenon has now been observed in a number of other systems.[6,7,8]

In the experiments reported in Table V both effects (neutron and gamma-ray induced recombination) have been further studied. The results (with some previously reported data) are plotted in Figs. 1 and 2.

TABLE V. Effect of various radiations on retention in neutron-activated potassium chromate.

Radiation	Flux neutrons/cm²/sec or roentgens/hr	Time	Temp °C	Radiation dose	Retention, percent
Pile neutrons	10^{12}/cm²/sec	3 sec	room	3×10^{12} *n*/cm²	59.7±1
Same		30 sec		3×10^{13}	60 ±0.5
Thermal column neutrons	6×10^{8}	1 week		4×10^{14}	60.8±0.3
Pile, water-cooled hole	1.3×10^{12}	10 min		8×10^{14}	60.8±0.4
Thermal column neutrons	6×10^{8}	4 weeks		1.6×10^{15}	63.8±1
Pile, water-cooled hole	1.3×10^{12}	2 hr		9×10^{15}	66.5±0.5
Same		24 hr		1.1×10^{17}	72.3±0.5
Co-60 gammas	2.5×10^{5} r/hr	80 hr	−28°C	20×10^{6} r	67.8±0.4
		280 hr		70×10^{6}	78.5±1.5
		480 hr		120×10^{6}	83.5±1
	7.8×10^{5} r/hr	66.7 hr	room	52×10^{6}	79.9±1.5
		109 hr		85×10^{6}	86.3±0.5
Ta-182 gammas	5.8×10^{4} r/hr	293 hr		17×10^{6}	78.2±1
		690 hr		40×10^{6}	87 ±1
Control		0		0	60.8±0.3
Sunlight		4 hr	20°C		60.7±0.8
Control		0		0	59.8±0.8

[11] F. Westheimer, Chem. Revs. **45**, 429 (1949).

FIG. 1. Retention in potassium chromate *versus* neutron dose. Open circles, this work, Brookhaven National Laboratory reactor; closed circles, Green, Harbottle, and Maddock (see reference 9) Harwell (England) reactor.

Since it had been thought that the temperature during neutron irradiation might be a significant factor, several experiments were made in which potassium chromate was maintained at liquid air and dry-ice temperatures during neutron bombardment. The samples were then permitted to stand (at room temperature) for the usual period of one week before analysis and counting. The results of these experiments are compared with others, at room and elevated temperature, in Table VI. The very high retention for a bombardment at 180°C may, of course, be attributed to rapid thermal annealing or recombination of recoil fragments, which begins to be important at around 100°C.[9]

Finally, in a single experiment, the effect of optical radiation in the wavelengths of sunlight was examined. An optically clear crystal of potassium chromate about 0.5 mm thick was exposed to thermal neutrons. After a week of storage the crystal was broken in half: one half was exposed to bright sunlight on a clear day for four hours. Both halves of the crystal were then analyzed as usual. The (negative) result of this experiment is also given in Table V.

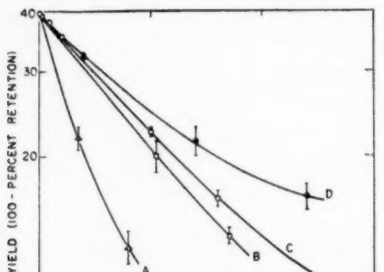

FIG. 2. Decrease in yield resulting from bombardment of neutron-activated potassium chromate with gamma radiation. (Yield = 100 − percent retention). Curve A: Tantalum-182, room temperature, 5.8×10^4 r/hr; Curve B: Cobalt-60, room temperature, 7.8×10^5 r/hr; Curve C: Cobalt-60, room temperature, 2.5×10^5 r/hr; [data of Green, Harbottle, and Maddock (see reference 9)]; Curve D: Cobalt-60, −28°C, 2.5×10^5 r/hr.

SUMMARY AND DISCUSSION

We may summarize the experimental observations on recoil processes in crystalline chromium compounds as follows:

1. Retention in alkali chromates and dichromates is high (50-90 percent) while in ammonium chromate and dichromate it is much lower (18–32 percent).

2. In mixed crystals, when potassium chromate is diluted with potassium sulfate, the retention is slightly higher than in chromate alone (69 percent *versus* 61 percent), while in mixed crystals containing potassium fluoberyllate as diluent the retention is very much lower (25 percent).

3. The *p*H and temperature of the solution in which irradiated potassium chromate is dissolved have little effect on the retention.[9] Neither do the presence of alcohol, large concentrations of chromic or chromate ions or plumbous ions[9] (which immediately react with chromate on dissolution of the crystals) have any large effect. The retention does not change when a neutron-irradiated hydrated crystal is dehydrated.

TABLE VI. Effect of temperature of bombardment on retention in potassium chromate.

Temperature of crystals during bombardment	Retention, percent
−180°C	58.6±0.5
−80	59.7±0.5
+20	60.0±0.5
+180	99.1±0.2

4. Both heat[9] and ionizing radiation cause an increase in retention in potassium chromate. The rate of recombination in either case increases with increasing temperature. Irradiation with gamma rays or heating the crystal in vacuo before exposure to neutrons does not affect the retention.[9] Neutron irradiation of potassium chromate held at 180°C results in virtually 100 percent retention.

In an earlier paper by Green, Maddock, and the author[9] two hypotheses were proposed to explain the data then available on the recoil processes in compounds of hexavalent chromium. These may be summarized as follows:

(A) As a consequence of the nuclear process oxide ions may be ejected or lost from the original molecular ion $CrO_4^=$. In principle the number of oxide ions so lost may run from zero to four and in analogy with Libby's theory of permanganate retention,[4] the chromium fragments may be considered to be initially distributed among the species $CrO_4^=$, CrO_3, CrO_2^{++}, CrO^{++++}, Cr^{6+}. No statement is made as to the actual process of oxide loss but one might assume that the oxide ions are "brushed off" during passage of the recoil fragment through the intense electrostatic fields in the crystalline matrix. The relative numbers of the species $CrO_4^=$, CrO_3, etc., would depend on the crystal structure, the nature of the electrostatic

crystalline fields, the energy of recoil, and the other components of the crystal. It seems unlikely that the bare sextuply-charged ion Cr^{6+} could persist in the crystal: its large electrostatic potential would allow it to acquire electrons and so be reduced.

We know from the ordinary chemistry of chromium that the species CrO_3 and CrO_2^{++} (chromyl ion) are hydrolyzed to chromate on contact with water at all *p*H's and are not reduced. Since we imagine, however, that the species $CrO_4^{=}$, CrO_3, $\cdots Cr^{6+}$ form a series of increasing oxidation potential, and since many of the chromium recoils in chromates do appear as reduced chromium on dissolution, we conclude that CrO^{4+} and/or Cr^{6+} are the species responsible for the production of trivalent chromium. It should be mentioned that we see no need to postulate, as did Libby,[4] a competition between reduction and hydration (hydrolysis) reactions when the fragments come in contact with water.

On the basis of this theory we can partially account for the relatively high retention observed in chromates. With $CrO_4^{=}$ at least three oxide ions must be lost before a species is reached which can oxidize water. The inference is made that the (net) loss of at least three oxides is not so probable as the sum of the probabilities for the loss of none, one, and two oxides. It is possible that even in an isolated chromate ion recoil might still produce rupture in no more than two Cr-O bonds because of what McCallum and Maddock term "nuclear inefficiency,"[5a] i.e., partial cancellation of the recoil momenta of the neutron-capture gamma rays. Thus even at infinite dilution some chromate could be produced.[12] In the case of different elements forming oxyanions, Green, Harbottle, and Maddock[9] postulated that the greater the oxidation potential of the oxyanion, the fewer oxide ions would have to be lost before one reached a species which would oxidize water. Consequently, the greater the oxidation potential of the oxyanion, the lower the retention. On this view, chromate takes its natural place in a series such as permanganate (typical retentions around 10 percent),[4,5a] chromate (60 percent), perrhenate[13] and vanadate[14] (both nearly 100 percent retention).

(B) The second hypothesis assumed that as a consequence of the recoil process, hexavalent chromium was reduced so that the radioactive chromium was distributed among the oxidation states VI, V, and/or IV and/or III. The retention was then determined by the relative proportions of Cr VI and III, and the tendencies of the intermediate oxidation states to disproportionate or exchange.

We now feel on the basis of the experimental results obtained to date that this hypothesis is untenable, since the *p*H and temperature of dissolution, the presence of reducing agents or Cr VI or III carriers (Table IV) would be expected to affect reactions involving Cr V or Cr IV.[12] It seems unlikely that recoil would produce only Cr VI and III; in any case the thermal recombination data are very difficult to explain if this is assumed.

We therefore accept, for the present, hypothesis (*A*). The mixed crystal results suggest that a larger proportion of recoils go to reducible chromium fragments (CrO^{4+} or Cr^{6+}) in a mixed crystal containing no oxygen (potassium fluoberyllate, K_2BeF_4) than in an oxyanion crystal (pure potassium chromate or chromate in potassium sulfate). It would thus appear that there are hot-atom reactions of the type

$$Cr^*O^{4+}+CrO_4^{=}\rightarrow Cr^*O_2^{++}+CrO_3 \qquad (1)$$

in oxyanion crystals (the asterisk indicates a radioactive chromium atom). On dissolution active chromate would be formed by the hydrolysis of chromyl ion

$$Cr^*O_2^{++}+2H_2O\rightarrow Cr^*O_4^{=}+4H^+ \qquad (2)$$

and the retention would be high. In fluoberyllate, either such transfer reactions do not take place, or if they do the fluoride-containing species formed are reduced by water.

The radiation and thermal recombination processes may well prove to be the same over-all reaction as (1) above or possibly a diffusion-controlled reaction of the type

$$Cr^*O^{4+}+O^{=}\rightarrow Cr^*O_2^{++}. \qquad (3)$$

It has not been possible to measure the activation energy of the thermal recombination reaction in potassium chromate because of the complexity of the kinetics. In only one system, cobaltic trisethylenediamine nitrate, has such an activation energy been determined.[7] In this connection it is interesting that the rate of the radiation-induced recombination reaction in potassium chromate shows a small dependence on the temperature and dose rate of the crystal and a large dependence on the quality of the radiation (when a tantalum-182 gamma source was substituted for a cobalt-60). These observations agree with other work in this field. For example, Boyd *et al.*[6] find a radiation back-reaction in irradiated potassium bromate whose magnitude is nearly independent of dose rate but depends on the temperature of the crystals.

In the case of recoil in ammonium chromate and dichromate, where very much lower retentions were observed, it is necessary to consider the possibility of hot-atom reactions in which the recoil fragment, instead of retaining or acquiring oxide groups, strikes and reacts with an ammonium ion. It is quite conceivable that such a reaction would result in reduction of the "hot" hexavalent chromium fragment and oxidation of the ammonium ion, a process which is not possible in the alkali salts. Whether the chromium is reduced to the V, IV, or III oxidation state (or several of these) must await further study.

The data in Table II indicate that neutron capture

[12] L. Fishman and G. Harbottle, J. Chem. Phys. **22**, 1088 (1954).
[13] W. Herr, Z. Naturforsch. **7b**, 55 (1952).
[14] P. Sue and T. Yuasa, J. chim. Phys. **41**, 160 (1944).

TABLE VII. Comparison of retention in iodate (see reference 8) and chromate crystals.

Cation	R(chromate) percent	R(iodate) percent
Li^+	66 ±0.5	66
Na^+	73.6±1.4	67
K^+	60.8±0.3	67
NH_4^+	17.5±1	22

in trivalent chromic ions in crystalline salts produces radioactive hexavalent chromium 5 to 10 percent of the time. These results may be compared with the 11 percent hexavalent found in irradiated trivalent chromium solutions which were 0.1 and 1.0 formal.[12] It seems likely that the increase in oxidation number occurring when trivalent ions recoil may result either from hot-atom reactions with water, or by internal conversion of neutron-capture gamma radiation. With the removal of a K electron, the Auger process could easily increase the charge of the recoil chromium by three or more.

It is interesting to compare the chromium system with other inorganic crystalline systems in which recoil phenomena have been studied. Burgus and Kennedy[15] observed the valence states of chromium-51 formed in the decay of manganese-51 through the emission of a positron. Such chromium-51 atoms certainly have a different electronic configuration, recoil energy, and crystalline environment from those formed by the n,γ process in chromium crystals. Nevertheless, certain similarities are found in the two cases. For example, the decay of manganous ion (in $MnCO_3$) gives mainly (70 percent) trivalent chromium, while the decay of permanganate (in $CsMnO_4$) gives entirely (99.6 percent) hexavalent chromium. In neutron-activated chromic and chromate crystals the same trends are observed.

The work of Cleary, Hamill, and Williams[8] on the crystalline iodates reveals a striking similarity to the chromate system. In Table VII values of the retention in the two systems are compared. The low results for ammonium salts in either case suggest that ammonium ion can act as a "hot atom reductant" in crystals containing oxyanions. On the other hand, the chromate results show no similarity to those on permanganate.[4,5a]

NOTE ON THE DOSIMETRIC PROPERTY OF NEUTRON-ACTIVATED POTASSIUM CHROMATE

The fact that recombination occurs under the influence of radiation makes neutron-activated potassium chromate in effect a chemical gamma-ray dosimeter. Its range of utility is high: from a few million to a few hundred million roentgens could be measured (see Fig. 2). Such a dosimeter would presumably integrate the dose and has the advantage of small size: only a few milligrams of potassium chromate crystals are required. It has the disadvantage that the response per roentgen depends strongly on the quality of the radiation and to a small extent on the dose rate and temperature.

ACKNOWLEDGMENT

The author wishes to express his thanks to Mrs. Marry Lykaas and Mr. L. Fishman for help in counting some of the samples, to Dr. R. Stoenner for chemical analyses, and to Dr. Ruth Drew, Mr. Otto Kuhl, and Mr. R. Oriez for assistance in the gamma irradiations.

[15] W. Burgus and J. Kennedy, J. Chem. Phys. **18**, 97 (1950).

THE JOURNAL OF CHEMICAL PHYSICS VOLUME 22, NUMBER 6 JUNE, 1954

The Szilard-Chalmers Reaction in Aqueous Solutions of Tri- and Hexavalent Chromium*

LAWRENCE M. FISHMAN† AND GARMAN HARBOTTLE
Chemistry Department, Brookhaven National Laboratory, Upton, Long Island, New York
(Received February 24, 1954)

Szilard-Chalmers (nuclear recoil) reactions have been observed in aqueous solutions of tri- and hexavalent chromium. The effects of pH, concentration, and a number of other variables have been examined, and the retention is found to depend on several of these factors. The results are interpreted in terms of thermal oxidation-reduction and exchange reactions of chromium V and/or IV.

INTRODUCTION

IN 1940 Libby[1] published an extensive series of experiments on the chemical consequences of the nuclear recoil process following neutron capture in crystals and in solutions containing permanganate ions. In particular, he determined the effect of the pH (a) of the permanganate solution during irradiation and (b) of the solution into which the irradiated permanganate crystals were dissolved. Since one of the authors has been engaged in the study of the Szilard-Chalmers effect in crystalline compounds of chromium,[2,3] it was felt that investigation of the same

* Research carried out under the auspices of the U. S. Atomic Energy Commission.
† Present address: Adams House, Harvard College, Cambridge, Massachusetts.
[1] W. F. Libby, J. Am. Chem. Soc. **62**, 1930 (1940).
[2] G. Harbottle, J. Chem. Phys. **22**, 1083 (1954).
[3] Green, Harbottle, and Maddock, Trans. Faraday Soc. (London) **49**, 1413 (1953).

process in aqueous solution might provide an interesting comparison and would, in addition, complete the chromium study parallel to that on manganese.

EXPERIMENTAL

A 1 formal chromic acid stock solution was prepared from Baker and Adamson Reagent Grade chromic anhydride crystals. Other 1 formal stock solutions were prepared from Mallinckrodt Reagent sodium chromate ($Na_2CrO_4 \cdot 4H_2O$) and ammonium chromate. Chromic acid or ammonium chromate solutions were adjusted to various *p*H values between 0.3 and 10.0 by the addition of nitric acid or ammonium hydroxide; these solutions constituted one set in which the only cations were hydrogen and ammonium. During the adjustment of *p*H the initially-formal solutions were necessarily slightly diluted but in no solution was the formal concentration of chromium less than 0.9.

In the more alkaline region (*p*H>10) it was impossible, because of the buffering action of ammonia, to prepare solutions with only ammonium ion as cation. Therefore, approximately 1 molar sodium chromate solutions, adjusted as to *p*H with sodium hydroxide (or nitric acid) were employed. These solutions covered a *p*H range from 6 to 15 (the latter denoting 10 formal sodium hydroxide), overlapping the *p*H range of the ammonium solutions. For most *p*H adjustments, a Beckman *p*H meter was used. In alkaline solutions special electrodes of "type E" glass, with low sodium ion correction, were employed, and the *p*H 14 and 15 solutions were prepared by addition of a calculated quantity of solid sodium hydroxide. Likewise, the *p*H 0.3 and 1.1 solutions were prepared by addition of a calculated quantity of nitric acid to the chromic acid stock.

All hexavalent chromium solutions (unless otherwise noted) contained trivalent chromium carrier to the extent of 1 percent of the concentration of hexavalent chromium. The converse was true of trivalent chromium solutions.

All bombardments were made with thermal neutrons in the thermal column of the Brookhaven reactor. The neutron flux was 6×10^{8}/cm² sec. The gamma-radiation flux was about 50 roentgens/hour and the temperature 20–25°C. Most bombardments were 16 to 24 hours, but a few (as noted) were longer. All solutions were bombarded in polyethylene vials closed with screw caps.

RADIOCHEMICAL ANALYSIS

Irradiated solutions were analyzed as soon as possible, in most cases within two days of irradiation. Solutions containing much sodium became very radioactive and consequently were stored for several days before analysis to permit the decay of 15-hour sodium-24.

Irradiated solutions were analyzed for tri- and hexavalent chromium as follows: If the solution contained a visible precipitate (chromic chromate or chromic hydroxide), the entire solution was made acid, the polyethylene irradiation vial was washed out with dilute acid, and the washings were added to the acidified solution. A portion of the resulting homogeneous solution containing roughly 50 mg of hexavalent chromium was diluted to about 100 ml. If the irradiated solution was homogeneous, the preliminary acidification was omitted but the same quantity of chromium was taken. Two aliquot portions of 25 ml each were pipetted: the *p*H of one was adjusted to 2.3±0.2, and hexavalent chromium precipitated as lead chromate. The filtrate, containing trivalent chromium, was collected in a 50 ml volumetric flask, and the precipitate, representing hexavalent chromium, was washed and then dissolved in concentrated nitric acid and transferred to a second volumetric flask. The second aliquot portion was made strongly basic with sodium hydroxide and oxidized with excess sodium peroxide. Peroxide was destroyed by boiling, the chromate solution adjusted to *p*H 2.3±0.2, and lead chromate precipitated, washed, and dissolved as before. This separation had been previously tested and found to be clean and relatively free of error due to coprecipitation or induced exchange.[3] Three solutions were then counted: these represented trivalent, hexavalent, and total chromium, respectively. All analyses were carried out at least in duplicate.

COUNTING

Chromium-51, formed by radiative neutron capture from chromium-50 in the irradiated solutions, emits soft x-rays and, in about 9 percent of the disintegrations, gamma rays of 325-kev energy. The half-life is 27 days.[4] Each of the three solutions mentioned above was counted in turn in glass cells positioned beneath a scintillation counter assembly, which has been described elsewhere.[3] A chromium-51 standard was counted before and after each sample count and the background determined daily and subtracted. Counting rates were typically a few hundred per minute above background. In general, the sum of the tri- and hexavalent activities equalled (within experimental error) the activity of the total chromium fraction, showing that there were no serious radioactive contaminants present.

DEFINITION OF RETENTION

In agreement with general usage, we define "retention" as the probability that a radioactive atom formed by radiative neutron capture is found in the same oxidation state in which it began, the so-called parent state. The retention was determined for these solutions as the ratio of radioactivity in the hexavalent chromium fraction to total activity. The determination of radioactivity in the trivalent fraction was not used to estimate retention, but only as a check on the absence of foreign activity.

[4] (a) Nuclear Data, Natl. Bur. Standards (U. S.) Circular No. 499 (1950); (b) A. Sunyar (private communication).

TABLE I. Effect of time of analysis on determination of retention in irradiated chromium solutions.

Solution	Time after irradiation, days	Retention, percent
CrVI 1 f, CrIII 0.01 f	5	19.0±0.4
*p*H 1.1	19	18.9±0.5
Same, *p*H 6.0	4	43.6±1
	10	42.7±1
Same, *p*H 9.0	4	30.4±0.5
	10	31.1±0.7

RESULTS

The Thermal Exchange Reaction of Tri- and Hexavalent Chromium

Burgus and Kennedy[5] and Menker and Garner[6] have studied the exchange reaction between the oxidation states of chromium in solution at various *p*H's, but in general they were only able to set lower limits for the half-time of the exchange reaction at room temperature. However, they worked with much more dilute solutions (0.01–0.03 f) than those employed in this research. If their minimum half-times are taken and the exchange reaction assumed to be bimolecular, then it could be calculated that thermal exchange in a day or two would introduce a serious error into our results.

To check this possibility, we analyzed one acidic, one nearly neutral, and one alkaline solution at various times after irradiation. Since trivalent chromium was present to the extent of only one percent of the total, any exchange would tend to increase the apparent retention. The results of these experiments, which are shown in Table I, indicate that thermal exchange at room temperature does not introduce serious error. The errors given in Table I are the spread in duplicate determinations.

Investigation of Possible Radiation-Induced Exchange between Tri- and Hexavalent Chromium

Although the results cited in Table I tended to show that thermal exchange following irradiation was not a serious factor, the possibility remained that under the influence of the relatively high radiation level existing at the thermal column irradiation site (~50 roentgens/hour), exchange might still take place. Such an exchange might be catalyzed, for example, by the free radicals formed in the irradiated aqueous solution. To test this possibility, a solution 0.05 f in both tri- and hexavalent chromium was prepared, and the trivalent chromium was labeled with so large an activity of chromium-51 that the additional activity generated during neutron irradiation was negligible by comparison. This solution was then irradiated in the thermal column and aliquot portions were withdrawn at intervals and analyzed. The results of this experiment are reported in Table II. The errors given are the spread in duplicate determinations. The reported "percent exchanged," $100X/X_\infty$, is the ratio of the specific activity in the initially-inactive fraction (hexavalent chromium) at a given time to the specific activity at infinite time. The results indicate that the presence of a radiation field does not seriously catalyze the exchange reaction.

Radiation Chemical Effects in Irradiated Chromium Solutions

Because of the formation of peroxide by the action of radiation on aqueous solutions, it was anticipated that some reduction of hexavalent chromium would occur in bombarded aqueous solutions. On the basis of published data,[7] it was felt that this effect could not be serious in a 1 formal solution; however, there seemed to be some danger that in the most dilute solutions investigated (0.001 f) radiation would reduce an appreciable fraction of the hexavalent chromium present. To determine the reduction of chromate solutions by radiation, portions of a solution 9.8×10^{-5} f in CrVI (*p*H 2.0) were irradiated for different periods of time and the decrease in concentration determined spectrophotometrically. A Beckman spectrophotometer was used and the solutions were examined at a wavelength of 366 mμ, the position of an absorption maximum. Beer's law was assumed to be obeyed and the extinction was calculated to be 1130 formal^{-1} cm^{-1}. The irradiations were made in the same polyethylene vials, and at the same position in the thermal column, as were the retention determinations. The results of these experiments indicated that the rate of reduction of dilute hexavalent chromium solutions irradiated in the thermal column was 11±1 μmoles/liter day. Thus, the effect of radiation in reducing hexavalent chromium is probably not serious even in 0.001 formal solution (1000 μmoles/liter) for one-day irradiations.

Effect of Irradiation Time and Presence of Trivalent Carrier on the Retention of Chromate in Solution

Although the experiments described above indicated that exchange reactions did not cause serious error, it was decided to make an over-all test by varying the time of irradiation to see if the measured retention was affected in any way. Solutions were irradiated with chromic ion carrier present to the extent of 1 percent of the hexavalent chromium and without any carrier.

TABLE II. Effect of radiation (50 roentgens/hr) on the exchange reaction of tri- and hexavalent chromium in solution.

Time irradiated hours	Total time elapsed hours	Percent exchanged $(X/X_\infty)\times100$
0	0	0.7±0.1
12.8	43	1.9±0.2
44.7	95	2.6±0.2

[5] W. Burgus and J. Kennedy, J. Chem. Phys. **18**, 97 (1950).
[6] H. Menker and C. Garner, J. Am. Chem. Soc. **71**, 371 (1949).
[7] T. J. Sworski, J. Chem. Phys. **21**, 375 (1953).

The results of these experiments, which are reported in Table III, indicate that for irradiation times normally employed (16 to 24 hours), the retention does not strongly depend on irradiation time or the presence of carrier. The latter conclusion is not surprising since even with initially carrier-free solutions a small amount of carrier chromic ion is generated through radiation decomposition. The attached errors indicate the spread in duplicate determinations.

Effect of *p*H of Solution on Retention

The principal effort expended in this work was to determine the relationship between the *p*H of irradiated CrVI solutions and the observed retention. One unavoidable complication arises from the fact that trivalent chromium added as carrier does not remain in solution over the entire *p*H range: in the solutions which were one formal in CrVI the nominal concentration of CrIII carrier was 0.01 f, but in the *p*H range 4 to 9 the brown compound chromic chromate precipitates, and in the *p*H range 9 or 10 to 13 green chromic hydroxide is present. However, it has been shown that in the precipitation of chromic chromate the tri- and hexavalent chromium atoms do not exchange[8]: likewise, the precipitation of chromic hydroxide does not induce exchange.[3] In solutions more alkaline than *p*H 12 or 13, chromic hydroxide begins to redissolve to form chromite (CrO_2^- or $Cr(OH)_4^-$) and the solution again becomes homogeneous.

As mentioned in the "Experimental" section, two types of CrVI solutions were investigated: (a) solutions with hydrogen and ammonium, and (b) solutions with hydrogen and sodium as cations. The observed retentions, each of which is an average of two or more determinations, are plotted in Fig. 1 *versus* *p*H of the irradiated solution. The errors are the spread in duplicate determinations, or root-mean-square deviations if three or more determinations were made. The bombardment conditions were 16–24 hours in the thermal column, neutron flux 6×10^{8}/cm² sec, gamma radiation flux 50 roentgens/hour, room temperature. All solutions were approximately 1 f in CrVI, 0.01 f (nominally) in CrIII.

Effect of Concentration of Solution

A series of solutions containing different concentrations of hexavalent chromium were bombarded.

TABLE III. Effect of irradiation time and presence of trivalent carrier on retention in chromate solutions (CrVI 0.1 f, *p*H 2).

Irradiation time hours	Trivalent carrier added (0.001 f)	Retention percent
16	no	18.2±0.4
16	yes	19.5±0.5
72	no	21.5±0.4
72	yes	22.2±0.4
184	yes	31.1±0.3

[8] A. G. Maddock, unpublished research.

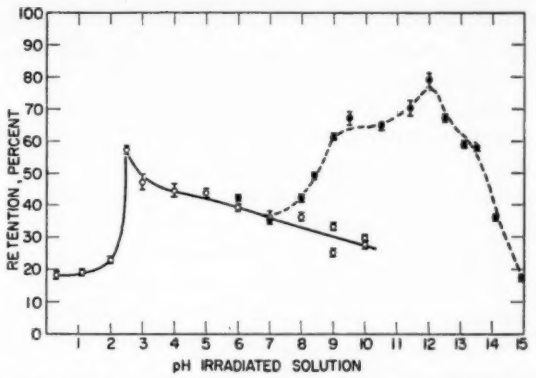

FIG. 1. Effect of *p*H of irradiated solution on retention. CrVI 1 formal CrIII 0.01 f. Open circles, ammonium solutions. Closed circles, sodium solutions.

Carrier trivalent chromium to the extent of one percent of the CrVI concentration was present. Acid (*p*H 2) and alkaline (*p*H 10.5) solutions were employed. The results of these experiments are presented in Table IV and plotted in Fig. 2. The errors are the spread in duplicate determinations.

Effect of Initial Oxidation State

All the experiments reported above have referred to solutions of hexavalent chromium. It was thought interesting to see whether solutions of trivalent chromium would produce hexavalent radioactive chromium as the result of recoil processes. Solutions one formal and one-tenth formal in chromic nitrate were adjusted to *p*H 2 and irradiated with thermal neutrons as before. All solutions contained one percent hexavalent carrier. The retention, or percent remaining as CrIII after activation, was 89.4±1.8 for the 1 formal and 88.8±1.9 for the 0.1 formal solution.

SUMMARY AND DISCUSSION

The following are the principle experimental observations emergent from this work:

(a) The retention in solution is strongly dependent on the *p*H of the solution, but nowhere goes to zero or to one hundred percent.
(b) The retention depends on the concentration of CrVI at both *p*H 2 and 10.5.
(c) In the alkaline region (*p*H 9 to 10) the retention in solutions containing ammonium ion is markedly lower than in solutions containing sodium ion.
(d) Irradiation of trivalent solutions produces about 10 percent hexavalent radioactive chromium.

TABLE IV. Effect of concentration of solution on retention.

*p*H	Concentration, formal	Retention percent
2	1.0	22.8±0.9
	0.1	19.5±0.5
	0.01	14.4±0.5
	0.001	11.5±0.6
10.5	1.0	64.7±1
	0.1	50.5±1

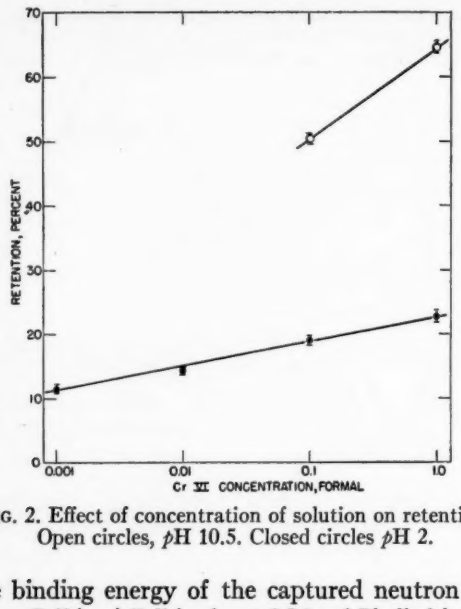

FIG. 2. Effect of concentration of solution on retention. Open circles, *p*H 10.5. Closed circles *p*H 2.

The binding energy of the captured neutron in the reaction $Cr^{50}(n,\gamma)Cr^{51}$ is about 9 Mev.[9] If all this energy were given up as a single gamma ray, the recoil energy of the Cr^{51} atom would be about 850 electron volts. If the molecular ion $CrO_4^{=}$ as a whole recoiled, then the energy available for bond breaking would be 64/115 of this value,[10] or 475 ev, more than adequate to break all chromium-oxygen bonds. However, it seems quite certain on the basis of experiments by Kinsey and Bartholomew that the binding energy of the extra neutron in Cr^{51} is not given up in one gamma ray, since they were unable to observe any ground-state transitions.[9] If several gamma rays are emitted following neutron capture, there is a possibility that the momenta imparted to the chromium atom would cancel vectorially, and the radioactive molecule would remain intact. The probability of such a process, termed "nuclear inefficiency" by McCallum and Maddock,[11] has been calculated for selected cases by Cobble and Boyd.[12] Since in the most dilute solutions studied in our work the retention was only about 11 percent (see Fig. 2) this is the upper limit of the nuclear inefficiency in chromium-51.

In any case, the net effect of the emission of several, rather than one, gamma rays is to lower the average recoil energy.[13] It seems quite possible that typical recoil energies could be sufficiently low that not all of the Cr−O bonds in chromate (or dichromate) would be broken, and the recoil fragment would contain oxygen. It does not seem profitable to speculate further concerning the nature of the initial "hot" fragment formed, or the processes by which its energy is reduced to that of thermal equilibrium, except to note that virtually all "cooling" of the recoil fragment must occur through collision with water molecules, since the mol fraction of chromium never exceeds about 0.02, even in the most concentrated solutions.[14]

The observed *p*H dependence (Fig. 1) must therefore refer to *p*H-dependent reactions of one or more radioactive chromium species formed by reaction of a recoil chromium fragment with water. Such species can hardly be tri- or hexavalent chromium, as these would show no *p*H-dependent thermal reactions with anything present in the solution. We therefore, by a process of elimination, are forced to consider such oxidation states as chromium V and/or IV as responsible for the observed *p*H-sensitivity. Divalent chromium and oxidation states higher than VI are not considered because of their extreme instability toward oxidation and reduction.

Although there are some kinetic data which demonstrate the existence of penta- and tetravalent chromium as intermediates in the reduction of chromic acid,[15] the information that is available is not of much help in interpreting our results. Both CrV and IV are powerful oxidizing agents, CrIV probably being the stronger. Both disproportionate, and dissolution of compounds of pentavalent chromium always produces the tri- and hexavalent states.[15] What is most needed is information on the exchange reactions of CrV and IV with CrVI and III, and this information does not exist in the literature. The results presented in Tables III and IV and Fig. 2, however, yield some information concerning the exchange reactions of the unknown thermalized active chromium species at *p*H 2. The data in Table III indicate that the active species does not exchange with trivalent chromium; on the other hand, the data in Table IV show that the retention is dependent on the concentration of hexavalent chromium at both *p*H 2 and 10.5. This dependence may be interpreted as evidence for an exchange reaction between the unknown active species and hexavalent chromium. The rate of such a reaction is probably greater at *p*H 10.5 than at *p*H 2.

An examination of the complex curve relating retention with *p*H for 1 formal solutions (Fig. 1) reveals several striking features. One of these is the abrupt rise between *p*H 2 and 2.5, and again between *p*H 8 and 9.5. It is perhaps significant that the latter rise occurs at approximately the point where hexavalent chromium in solution passes over entirely to chromate, $CrO_4^{=}$, and the trivalent shifts from solid chromic chromate to solid chromic hydroxide. The rise at *p*H 2.5 gives the appearance of a titration curve, and one infers that here a species of CrV or IV is perhaps hydrolyzed to one less capable of oxidizing water and/or more susceptible to exchange with CrVI. A second step of

[9] B. B. Kinsey and G. Bartholomew, Phys. Rev. **89**, 375 (1953).
[10] H. Suess, Z. physik. Chem. **B45**, 297, 312 (1940).
[11] K. J. McCallum and A. G. Maddock, Trans. Faraday Soc. (London) **49**, 1150 (1953).
[12] J. W. Cobble and G. E. Boyd, J. Chem. Soc. **74**, 1282 (1952).
[13] A. C. Wahl and N. Bonner, *Radioactivity Applied to Chemistry* (John Wiley and Sons, Inc., New York, 1951), p. 246.
[14] W. F. Libby, J. Am. Chem. Soc. **69**, 2523 (1947) gives an expression for the average number of elastic collisions necessary to reduce the energy of a recoil atom by a given amount.
[15] F. Westheimer, Chem. Revs. **45**, 429 (1949).

hydrolysis could account for the rise at *p*H 8–9.5, with exchange now taking place with chromate rather than dichromate or hydrochromate, $HCrO_4^-$. The final fall-off for *p*H>12 is surprising since for very alkaline solutions any mild oxidizing agent will oxidize trivalent chromium to chromate. If tetravalent chromium is present here as CrO_2, then a simple electron-transfer exchange could take place with trivalent species such as chromite CrO_2^- and this would lower the retention.

Neutron-irradiated solutions of trivalent chromium at *p*H 2 produce radioactive hexavalent chromium with a probability of nearly 11 percent. It is interesting that the retention observed when the most dilute solutions of hexavalent chromium are irradiated is also 11 percent (Table IV). It thus appears that the chemical consequences of nuclear recoil in both tri- and hexavalent chromium may be similar and independent of the initial oxidation state; that about 11 percent of the recoils in either case go to hexavalent chromium, and the remainder are divided between trivalent chromium (the proportion of which cannot exceed about 20 percent) and some unknown species, hypothetically chromium V or IV, which shows *p*H-dependent exchange reactions with hexavalent chromium and can be reduced by water. It has been observed that the neutron irradiation of various crystalline salts of trivalent chromium produces about 9 percent hexavalent chromium by recoil.[2]

The large difference observed between sodium and ammonium cation solutions at *p*H 9–10 is further evidence that some of the thermalized recoil fragments are neither tri- nor hexavalent chromium, for neither of these oxidation states react with ammonium ions. The observed difference is probably due to reactions in which ammonium ion acts as a reducing agent for the (hypothetical) quinque- or quadrivalent chromium. It is interesting that the same tendency is found in irradiated crystals of sodium and ammonium chromate when these are dissolved at *p*H 2 and analyzed.[2] In contrast with the solution *p*H-retention results (Fig. 1), the retention for irradiated solid potassium chromate dissolved in solutions of differing *p*H remains relatively constant.[3] One infers that the substitution of water for crystal as a slowing-down medium profoundly affects the oxidation-state assumed by the recoil fragment.

The chromate system in neither the solid nor dissolved state shows any resemblance to the analogous permanganate system. In particular, the *p*H dependence of retention in permanganate shows no peak but only a rise for high and low *p*H with a plateau region in between.[1,11]

ACKNOWLEDGMENT

The authors wish to thank Messrs. Joel Henkel, J. Floyd, and F. Reeves for assistance with the irradiations, and Dr. R. Stoenner for chemical analyses. One of the authors (L.M.F.) is grateful to Associated Universities, Inc. for the grant of a summer fellowship which permitted his participation in this work.

The Statistical-Mechanical Theory of Transport Processes. VIII. Quantum Theory of Transport in Gases

JOHN ROSS* AND JOHN G. KIRKWOOD
Sterling Chemistry Laboratory, Yale University, New Haven, Connecticut
(Received February 22, 1954)

The quantum-mechanical analog of the Maxwell-Boltzmann equation of transport in gases of low density is derived from the quantum-mechanical equation for the motion in phase space of the Wigner function. The derivation is based upon the theory of phase-space transformation functions which is developed in this article. Although the present treatment resembles the derivation of Mori and Ono, it is simpler and more general. Particularly, the assumption of random *a priori* phases, an integral part of Mori and Ono's work, need not be applied explicitly. The Uhling and Uhlenbeck equation is verified in the Born collision approximation.

THE fundamental equation of the kinetic theory of transport phenomena in dilute gases is the integro-differential Maxwell-Boltzmann equation. Kirkwood[1] obtained this equation from the principles of classical statistical mechanics in an analytic derivation which proceeded from the Liouville equation. The purpose of his analysis was: to establish a molecular theory of transport in gases based upon the statistical mechanical theory of transport processes presented in a previous paper[2]; to elucidate the usual physical arguments employed in deriving the Boltzmann equation; and to outline clearly the assumptions and approximations needed to arrive at this equation. Solutions of the Boltzmann equation, correct to various orders, have been obtained by Enskog, Chapman,[3] and Grad,[4] among others. These solutions have provided adequate theories of transport in dilute gases obeying classical mechanics by establishing relations between the macroscopic transport coefficients and molecular properties.

For quantum-mechanical systems composed of gases of low density the analog of the Maxwell-Boltzmann equation was formulated first by Nordheim[5] and Uhling and Uhlenbeck[6] in heuristic arguments proceeding from the classical equation. Essentially, these authors assumed the validity and sufficiency of the replacement of the classical collision cross section by its quantum-mechanical counterpart. All theories and computations[7–10] of transport phenomena in quantum mechanical systems have been based upon this equation. Mori and Ono[11] obtained the Uhling and Uhlenbeck equation in a development which generalized Kirkwood's analysis to the quantum-mechanical problem. Their derivation proceeded from the quantum-mechanical Liouville equation in terms of the Wigner distribution function, the Wigner equation, as established by Wigner[12] and Irving and Zwanzig.[13] Their work, in relation to this article, is discussed below.

We shall present a derivation of the quantum-mechanical Boltzmann equation for reasons similar to those which motivated the derivation of the classical Boltzmann equation. Although our development, like Mori and Ono's, employs the Wigner equation as a starting point and bears some resemblance to their work, the present analysis is more general and is believed to be simpler.

In a previous paper of this series[13] the equation of motion of a quantum-mechanical N-particle system was written as

$$\frac{\partial f^{(N)}}{\partial t}+\sum_{k=1}^{N}\frac{\mathbf{p}_k}{m_k}\cdot\nabla_{\mathbf{R}_k}f^{(N)}+\boldsymbol{\theta}\cdot f^{(N)}=0, \tag{1}$$

where $\mathbf{p}_k$ and $\mathbf{R}_k$ are the momenta and coordinates of the kth particle, and t is the time. The Wigner function,[12] $f^{(N)}$, can be considered as a quantum-mechanical phase space distribution function and it is defined as a Fourier transform of the density matrix:

$$f^{(N)}(\mathbf{R},\mathbf{p};t)=\left(\frac{1}{\pi\hbar}\right)^{3N}\int\cdots\int\exp\left(\frac{2i}{\hbar}\mathbf{p}\cdot\mathbf{Y}\right)\times\rho^{(N)}(\mathbf{R}-\mathbf{Y},\mathbf{R}+\mathbf{Y};t)d\mathbf{Y}, \tag{2}$$

where $\hbar$ is Planck's constant divided by 2π. The symbols $\mathbf{R}$, $\mathbf{Y}$, $\mathbf{p}$, etc. denote coordinates, etc., of the entire set of particles under consideration; integrations are understood to extend from $-\infty$ to $+\infty$ unless specified otherwise. The density matrix[14] is defined as

$$\rho^{(N)}(\mathbf{R}-\mathbf{Y},\mathbf{R}+\mathbf{Y};t)=\Psi^*(\mathbf{R}+\mathbf{Y};t)\Psi(\mathbf{R}-\mathbf{Y};t) \tag{3}$$

* National Science Foundation Post-Doctoral Fellow, 1952–1953. Present address: Department of Chemistry, Brown University, Providence, Rhode Island.

[1] J. G. Kirkwood, J. Chem. Phys. **15**, 72 (1947).
[2] J. G. Kirkwood, J. Chem. Phys. **14**, 180 (1946).
[3] S. Chapman and T. G. Cowling, *Mathematical Theory of Non-Uniform Gases* (Cambridge University Press, Cambridge, 1939).
[4] H. Grad, Comm. Pure Appl. Math. **2**, 331 (1949).
[5] L. Nordheim, Proc. Roy. Soc. (London) **A119**, 689 (1928).
[6] E. A. Uhling and G. E. Uhlenbeck, Phys. Rev. **43**, 552 (1933).
[7] E. A. Uhling, Phys. Rev. **46**, 917 (1934).
[8] E. J. Hellund and E. A. Uhling, Phys. Rev. **56**, 818 (1939).
[9] A. Isihara, J. Phys. Soc. (Japan) **5**, 213, 217 (1950).
[10] J. de Boer and R. B. Bird, University of Wisconsin Naval Research Laboratory Research Report CF 1509–13 (June, 1952).
[11] H. Mori and S. Ono, Progr. Theoret. Phys. (Japan) **8**, 327 (1952).
[12] E. P. Wigner, Phys. Rev. **40**, 749 (1932).
[13] J. M. Irving and R. W. Zwanzig, J. Chem. Phys. **19**, 1173 (1951).
[14] See J. von Neumann, *Mathematische Grundlage der Quantenmechanik* (Dover Publications, New York, 1943).

for a pure state, and as

$$\rho^{(N)}(\mathbf{R}-\mathbf{Y},\mathbf{R}+\mathbf{Y};t) = \sum_j w_j \Psi_j^*(\mathbf{R}+\mathbf{Y};t)\Psi_j(\mathbf{R}-\mathbf{Y};t) \quad (4)$$

for a mixed state (ensemble of systems), where Ψ_j is the wave function, and w_j the statistical weight of the jth state of the ensemble. The operator $\boldsymbol{\theta}$ can be written in various forms; an integral representation is

$$\boldsymbol{\theta}\cdot f^{(N)} = \frac{i}{h}\left(\frac{1}{\pi h}\right)^{3N}\int\cdots\int[V(\mathbf{R}-\mathbf{x})-V(\mathbf{R}+\mathbf{x})] \times\exp\left[\frac{2i}{h}(\mathbf{p}-\mathbf{p}')\cdot\mathbf{x}\right]f^{(N)}(\mathbf{R},\mathbf{p}';t)d\mathbf{p}'d\mathbf{x}, \quad (5)$$

where V is the potential derived from external and internal forces acting on the N-particle system. If the potential energy can be expanded in a Taylor series, then the $\boldsymbol{\theta}$ operator can also be written as a differential operator,

$$\boldsymbol{\theta}\cdot f^{(N)}(\mathbf{R},\mathbf{p};t) = -\frac{2}{h}\sin\left[\frac{h}{2}\nabla_{\mathbf{R}}\nabla_{\mathbf{p}}\right]V(\mathbf{R})f^{(N)}(\mathbf{R},\mathbf{p};t), \quad (6)$$

where $\nabla_{\mathbf{R}}$ operates on the potential only. From the above definitions it is clear that the Wigner equation, Eq. (1), is a Fourier transform of Schrödinger's time dependent equation expressed in terms of the density matrix. The introduction of the Wigner function is justified by the advantage that the formation of phase space averages requires only direct integration of the product of the distribution function and the quantity to be averaged, whereas the density matrix formalism requires operator techniques.

As in the classical derivation it is necessary here to use distribution functions "coarse-grained" in time. These functions are defined as averages over an interval τ subsequent to the time t,

$$\bar{f}^{(N)}(\mathbf{R},\mathbf{p};t) = \frac{1}{\tau}\int_0^\tau f^{(N)}(\mathbf{R},\mathbf{p};t+s)ds. \quad (7)$$

It will be found that it is the time-smoothed distribution function $\bar{f}^{(1)}$ which will satisfy the quantum-mechanical Boltzmann equation.

Reduced distribution functions and reduced equations of motion are established in an analogous manner to the classical ones. Thus $f_N^{(n)}$, the distribution function of the subset $\{n\}$ taken from the set $\{N\}$ is formally

$$f_N^{(n)}(\mathbf{r},\mathbf{p};t) = \int\cdots\int f^{(N)}(\mathbf{r},\mathbf{p},\mathbf{R},\mathbf{P};t)d\mathbf{R}d\mathbf{P}, \quad (8)$$

where $\mathbf{r}$ and $\mathbf{p}$ refer to the set $\{n\}$, and $\mathbf{R}$ and $\mathbf{P}$ to the set $\{N-n\}$. The subscript N on the reduced distribution function serves as a reminder that generally these functions depend on the statistics obeyed by the N-particle system. The reduced equation of motion will be formulated with the aid of two hypotheses. First, it is assumed that the total potential can be written as a sum of pair potentials and external potentials,

$$V(\mathbf{R}) = \sum_{i=1}^N \phi_i(\mathbf{R}_i) + \tfrac{1}{2}\sum_{\substack{i=1\\ i\neq j}}^N\sum_{j=1}^N U_{ij}(\mathbf{R}_i,\mathbf{R}_j). \quad (9)$$

The intermolecular potential U_{ij} is taken to be dependent upon the intermolecular distance $R_{ij}=|\mathbf{R}_j-\mathbf{R}_i|$ only, and thus is spherically symmetric; the range of the intermolecular potential is taken to be finite so that $U_{ij}=0$ if $R_{ij}>\rho^0$. These two restrictions are not necessary requirements for the formulation of the reduced equation of motion but the present analysis is confined to such types of potentials. Secondly, it is postulated that the system is sufficiently dilute to permit the omission of interactions due to the indistinguishability of identical particles for all but a pair of particles at a time. This interaction, which is an apparent attraction between particles in the case of Bose-Einstein statistics but an apparent repulsion in the case of Fermi-Dirac statistics, becomes of importance when the average de Broglie wavelength of the particles of the system approaches the average distance between them. Later we shall be required to adopt the binary collision assumption which permits the reduction of the complex N body problem to the soluble pair equation of motion. This hypothesis roughly implies a state of dilution in the gas such that the average distance between molecules is large compared to the range of the intermolecular potential. Thus the interactions due to the statistics between the subset of two particles and the subset of the remaining $N-2$ particles need to be considered only when the de Broglie wavelength is large compared to the range of the intermolecular potential; in helium for example, this situation arises at approximately 1°K. Furthermore, the approximate corrections for this density-dependent aspect of interactions due to quantum statistics introduce distribution functions, and thus density dependences, of a higher order than those remaining in the Boltzmann equation as a consequence of the binary collision assumption.

By means of the above two assumptions, Eq. (1) can be integrated over all coordinates and momenta, except those of the 1st particle, to yield, on construction of time averages,

$$\frac{\partial\bar{f}^{(1)}}{\partial t}+\frac{\mathbf{p}_1}{m_1}\cdot\nabla_{\mathbf{R}_1}\bar{f}^{(1)}+\boldsymbol{\theta}^{(e)}\cdot\bar{f}^{(1)} = -\frac{N_2}{\tau}\int\cdots\int_0^\tau \times\boldsymbol{\theta}^{(2)}\cdot f^{(2)}(\mathbf{R}_1\mathbf{R}_2\mathbf{p}_1\mathbf{p}_2;t+s)d\mathbf{R}_2d\mathbf{p}_2ds, \quad (10)$$

where $\boldsymbol{\theta}^{(e)}$, and $\boldsymbol{\theta}^{(2)}$ represent, respectively, the operators corresponding to external forces acting on the 1st particle and the intermolecular potential between the

1st and any other molecule of the remaining set of $(N-1)$ identical molecules, denoted here by N_2.

The pair distribution function $f^{(2)}$ can be expressed in terms of singlet distribution functions

$$f^{(2)}(\mathbf{R}_1\mathbf{R}_2\mathbf{p}_1\mathbf{p}_2;t+s)=[1+\vartheta(\mathbf{R}_1\mathbf{R}_2\mathbf{p}_1\mathbf{p}_2;t+s)]\times\{[\mathbf{O}_\pm]f^{(1)}(\mathbf{R}_1\mathbf{p}_1;t+s)f^{(1)}(\mathbf{R}_2\mathbf{p}_2;t+s)\},\quad(11)$$

where $[\mathbf{O}_\pm]$ is the symmetry operator for Wigner distribution functions describing systems of independent particles which obey Bose-Einstein, $[\mathbf{O}_+]$, or Fermi-Dirac statistics, $[\mathbf{O}_-]$. This symmetry operator, discussed in Appendix B, is obtained by symmetrizing the wave functions from which the Wigner distribution function is formulated. $[\mathbf{O}_\pm]$ is not a simple permutation operator but an integral operator. The correlation function $[1+\vartheta(\mathbf{R}_1\mathbf{R}_2\mathbf{p}_1\mathbf{p}_2;t+s)]$ is defined by Eq. (11). The analysis will be restricted here to conditions for which the correlation integral

$$-N_2\int\cdots\int_0^\tau\theta^{(2)}\cdot[\vartheta(\mathbf{R}_1\mathbf{R}_2\mathbf{p}_1\mathbf{p}_2;t+s)]\times\{[\mathbf{O}_\pm]f^{(1)}(\mathbf{R}_1\mathbf{p}_1;t+s)f^{(1)}(\mathbf{R}_2\mathbf{p}_2;t+s)\}d\mathbf{R}_2d\mathbf{p}_2ds$$

is bounded and of the order of a finite time interval τ_k; if this prevails, Eq. (10) reduces then to

$$\frac{\partial\bar{f}^{(1)}}{\partial t}+\frac{\mathbf{p}_1}{m_1}\cdot\nabla_{\mathbf{R}_1}\bar{f}^{(1)}+\theta^{(e)}\cdot\bar{f}^{(1)}=-\frac{N_2}{\tau}\int\cdots\int_0^\tau\theta^{(2)}\cdot\{[\mathbf{O}_\pm]f^{(1)}(\mathbf{R}_1\mathbf{p}_1;t+s)\times f^{(1)}(\mathbf{R}_2\mathbf{p}_2;t+s)\}d\mathbf{R}_2d\mathbf{p}_2ds+O\left(\frac{\tau_k}{\tau}\right).\quad(12)$$

The integral in Eq. (12) will be shown to be proportional to τ so that for sufficiently large values of τ the contributions of the deviation of the correlation function from unity to Eq. (12) can be made as small as desirable. This statement is similar to the assumption applied in the derivation of the classical Boltzmann equation, namely that the deviation of the correlation function from unity is a short-range function of the intermolecular forces and can be made negligibly small for sufficiently large values of τ. The requirement that the correlation integral be bounded is to be considered a part of the molecular chaos assumption, which is thus a necessary condition for this derivation.

At this point it is instructive to discuss the essential differences between the classical and quantum-mechanical derivation and the additional complications encountered in the latter case. The classical analysis proceeds from the equivalent of Eq. (10), where $\theta^{(e)}$ and $\theta^{(2)}$ in this case correspond to $-[\nabla_{\mathbf{R}_1}\phi(\mathbf{R}_1)]\cdot\nabla_{\mathbf{p}_1}$ and $-[\nabla_{\mathbf{R}_{12}}U(R_{12})]\cdot\nabla_{\mathbf{p}_1}$, by introducing phase-space transformation functions† which are found to satisfy the partial differential Liouville equation. The solutions of this equation are readily obtained and are Dirac δ functions which express the contact transformation of classical mechanics. They describe the path of motion of the system in phase space, a trajectory along which the distribution function remains invariant. Thus the time-smoothing process can be performed on the δ functions, which are the transformation functions of the distribution function, rather than on the distribution function itself. Subsequent integration over relative configuration space leads to the Maxwell-Boltzmann equation.

The quantum-mechanical analysis is more complex and the additional difficulties have their origin in the more intricate equation of motion. The Liouville equation for $f^{(2)}$ is a first-order, partial differential equation which is linear and homogeneous. It follows that $f^{(2)}$ is constant along the characteristics, which are the classical trajectories in phase space. Thus the only physically interesting solution of the Liouville equation is the one exhibiting invariance along the path of motion. The Wigner equation, however, is an integro-differential equation, and the distribution function $f^{(2)}$, which provides a complete description in the two body problem, is generally not invariant as the motion proceeds through phase space. The lack of invariance, which amounts to an apparent diffusion of the probability fluid in phase space, can be surmised from the formal analogy between the Schrödinger equation and the diffusion equation. It follows from this that the δ function is in general inadequate as a transformation function since it cannot account for the diffraction phenomena of quantum mechanical processes. Despite these additional difficulties, the theory of quantum-mechanical phase-space transformation functions seems a convenient as well as a very general formalism for the treatment of quantum dynamics.

In general, the temporal transformation function can be defined as the kernel of the following integral equation

$$f^{(N)}(\mathbf{R},\mathbf{p};t+s)=\int\cdots\int\times K^{(N)}(\mathbf{R},\mathbf{p}\,|\,\mathbf{R}',\mathbf{p}';s)f^{(N)}(\mathbf{R}',\mathbf{p}';t)d\mathbf{R}'d\mathbf{p}',\quad(13)$$

yielding the distribution function at a given instant and position in phase space in terms of the known distribution at a previous time. Moyal[15] formulated a statistical theory of quantum mechanics in which he presented some of the properties of $K^{(N)}$.[16] The transformation function is a conditional probability formally analogous to such functions encountered in other

† In Kirkwood's derivation this was accomplished in effect in his equivalent of Eq. (10) by introducing the Dirac δ functions and integrating over the phase-space of the 1st particle in the collision term.

[15] J. E. Moyal, Proc. Cambridge Phil. Soc. **45**, 99 (1949).

[16] See also H. Jeffreys, Phil. Mag. **33**, 815 (1942).

stochastic processes as Brownian motion. It is a product of δ functions, $K^{(N)}=\delta(\mathbf{R}-\mathbf{R}')\delta(\mathbf{p}-\mathbf{p}')$, at $s=0$ for all dynamical problems; this merely expresses the required initial condition. Furthermore, the transformation function is for all intervals a product of δ functions,

$$K^{(N)}=\delta[\mathbf{R}-\mathbf{R}(\mathbf{R}',\mathbf{p}';s)]\delta[\mathbf{p}-\mathbf{p}(\mathbf{R}',\mathbf{p}';s)],$$

expressing the contact transformation, for the deterministic problems of quantum mechanics: the free particle, the uniformly accelerated particle, and the harmonic oscillator. The dynamical properties of the quantum-mechanical system are contained implicitly in this function which thus expresses the probabilistic nature of the transitions characterizing the motion.

The formalism of the phase-space transformation function permits the reduction of the problem of the determination of the distribution function to the determination of the transformation function in terms of its parameters. Moyal obtained K as an infinite power series in s in which the coefficients are functions of the Hamiltonian of the system. This expansion is not convenient for an evaluation of K, not only because of possible convergence difficulties encountered at larger values of s, but also because the approximation of termination of the series does not seem to correspond to any useful perturbation treatment.

A more general method for the determination of the transformation function can be found by recourse to the theory of the analogous Markoffian transformation kernel which obeys the same differential equation as the distribution function itself. Substitution of Eq. (13) into Eq. (1) shows that $K^{(N)}$ is in fact the solution of the integro-differential equation

$$\frac{\partial K^{(N)}}{\partial s}+\sum_{k=1}^{N}\frac{\mathbf{p}_k}{m_k}\cdot\nabla_{\mathbf{R}_k}K^{(N)}+\theta\cdot K^{(N)}=0, \tag{14}$$

with initial condition

$$K^{(N)}(\mathbf{R},\mathbf{p}|\mathbf{R}',\mathbf{p}';0)=\delta(\mathbf{R}-\mathbf{R}')\delta(\mathbf{p}-\mathbf{p}'), \tag{15}$$

at $s=0$. Equation (14) reduces to the classical equation if the third and higher derivatives of the potential vanish. Under such conditions, $K^{(N)}$ reduces to a product of δ functions, as stated above.

Equation (14) must be considered a fundamental equation of quantum dynamics. The advantage of this equation over the corresponding one for the Wigner distribution function is established by the existence of known initial conditions which allow the construction of solutions. The importance of the transformation function, obtained as a solution of Eq. (14), for a rigorous treatment of scattering problems might be stressed here. The relations between the phase-space transformation function $K^{(N)}$, the wave transformation function, and the scattering cross section are given in Appendix A.

The analytic form of Eq. (14), as well as the initial condition, Eq. (15), for $K^{(N)}$ as defined by Eq. (13), is independent of the statistics obeyed by the particular system. It follows that this transformation function, which is completely determined by Eq. (14) and the given initial condition, does not depend on the statistics of the system. This fact facilitates greatly the solution of the equation for $K^{(N)}$.

The reduced transformation functions are formulated in a similar manner as the reduced distribution functions. In particular, the pair transformation function $K^{(2)}$ is given by

$$K^{(2)}(\mathbf{R}_1\mathbf{R}_2\mathbf{p}_1\mathbf{p}_2|\mathbf{R}_1'\mathbf{R}_2'\mathbf{p}_1'\mathbf{p}_2';s)=\int\cdots\int \times K^{(N)}(\mathbf{R}_1\cdots\mathbf{R}_N\mathbf{p}_1\cdots\mathbf{p}_N|\mathbf{R}_1'\cdots\mathbf{R}_N'\mathbf{p}_1'\cdots\mathbf{p}_N';s) \times d\mathbf{R}_3\cdots d\mathbf{R}_N d\mathbf{p}_3\cdots d\mathbf{p}_N. \tag{16}$$

Integration of Eq. (13) over the unprimed coordinates and momenta of all particles except 1 and 2 yields

$$f^{(2)}(\mathbf{R}_1\mathbf{R}_2\mathbf{p}_1\mathbf{p}_2;t+s) =\int\cdots\int K^{(2)}(\mathbf{R}_1\mathbf{R}_2\mathbf{p}_1\mathbf{p}_2|\mathbf{R}_1'\mathbf{R}_2'\mathbf{p}_1'\mathbf{p}_2';s) \times f^{(N)}(\mathbf{R}_1'\cdots\mathbf{R}_N'\mathbf{p}_1'\cdots\mathbf{p}_N';t) \times d\mathbf{R}_1'\cdots d\mathbf{R}_N' d\mathbf{p}_1'\cdots d\mathbf{p}_N', \tag{17}$$

$$f^{(2)}(\mathbf{R}_1\mathbf{R}_2\mathbf{p}_1\mathbf{p}_2;t+s) =\int\cdots\int K^{(2)}(\mathbf{R}_1\mathbf{R}_2\mathbf{p}_1\mathbf{p}_2|\mathbf{R}_1'\mathbf{R}_2'\mathbf{p}_1'\mathbf{p}_2';s) \times f^{(2)}(\mathbf{R}_1'\mathbf{R}_2'\mathbf{p}_1'\mathbf{p}_2';t)d\mathbf{R}_1'd\mathbf{R}_2'd\mathbf{p}_1'd\mathbf{p}_2',$$

where the integrations of the distribution functions are performed with the aid of the hypothesis discussed above, that interactions due to quantum statistics between particles 1 or 2 and the set of the remaining $(N-2)$ particles can be neglected.

The pair transformation function is determined as a solution of the integro-differential equation for $K^{(2)}$ obtained by integrating Eq. (14) over the coordinates and momenta of all particles except 1 and 2. If the density of the system under consideration is sufficiently small it becomes possible to apply the binary collision approximation, i.e., it is assumed that an adequate description of all encounters among the molecules of the system can be given in terms of collisions involving two molecules only. This implies that the probability of the simultaneous presence of three molecules in a volume of configuration space of approximate linear dimension L_τ is negligible compared to the probability of two molecules occupying this volume. (L_τ is the distance traversed by a *classical* particle with the same initial momentum as in the quantum-mechanical case in the time interval τ.) Then the triplet transformation function plays no role and the pair transformation function $K^{(2)}$ is determined as a solution of the pair transformation function equation at zero density, which

can be written in center-of-mass coordinates as

$$K^{(2)}(\mathbf{R}_1\mathbf{R}_2\mathbf{p}_1\mathbf{p}_2|\mathbf{R}_1'\mathbf{R}_2'\mathbf{p}_1'\mathbf{p}_2';s)$$
$$=\delta(\mathbf{R}_c-\mathbf{R}_c')\delta(\mathbf{p}_c-\mathbf{p}_c')K^{(2)}(\mathbf{R},\mathbf{p}|\mathbf{R}',\mathbf{p}';s) \quad (19)$$

$$\mathbf{R}_c=\tfrac{1}{2}(\mathbf{R}_2+\mathbf{R}_1) \quad \mathbf{R}=\mathbf{R}_2-\mathbf{R}_1$$
$$\mathbf{p}_c=\mathbf{p}_2+\mathbf{p}_1 \qquad \mathbf{p}=\tfrac{1}{2}(\mathbf{p}_2-\mathbf{p}_1), \quad (20)$$

$$\frac{\partial K^{(2)}}{\partial s}+\frac{\mathbf{p}}{m}\cdot\nabla_{\mathbf{R}}K^{(2)}+\boldsymbol{\theta}\cdot K^{(2)}(\mathbf{R},\mathbf{p}|\mathbf{R}',\mathbf{p}';s)=0$$
$$\frac{1}{m}=\frac{1}{m_1}+\frac{1}{m_2},$$

$$\boldsymbol{\theta}\cdot K^{(2)}(\mathbf{R},\mathbf{p}|\mathbf{R}',\mathbf{p}';s)$$
$$=\frac{i}{\hbar}\left(\frac{1}{\pi\hbar}\right)^3\int\cdots\int[U(\mathbf{R}-\mathbf{x})-U(\mathbf{R}+\mathbf{x})]$$
$$\times\exp\left[\frac{2i}{\hbar}(\mathbf{p}-\boldsymbol{\xi})\cdot\mathbf{x}\right]K^{(2)}(\mathbf{R},\boldsymbol{\xi}|\mathbf{R}',\mathbf{p}';s)d\mathbf{x}d\boldsymbol{\xi}, \quad (21)$$

with the initial condition

$$K^{(2)}(\mathbf{R},\mathbf{p}|\mathbf{R}',\mathbf{p}';0)=\delta(\mathbf{R}-\mathbf{R}')\delta(\mathbf{p}-\mathbf{p}').$$

External forces are assumed to have sufficiently slowly-varying spatial dependence so as not to affect the collision between two particles.

An explicit solution of Eq. (20) can be effected by successive approximations based upon an expansion of the transformation function in which the potential of intermolecular force is treated as a perturbation, as in the Born collision theory. Thus, $K^{(2)}$ can be written as

$$K^{(2)}=K_0^{(2)}+K_1^{(2)}+K_2^{(2)}\cdots, \quad (22)$$

where the representation of the transformation function by the first two terms only corresponds to the well-known Born approximation in the solution of scattering problems. This expansion is analogous to the one usually employed for the wave transformation function, as shown in Appendix B. Substitution of this series into Eq. (20) yields, on equating terms of the same order of approximation, the set of equations

$$\frac{\partial K_0^{(2)}}{\partial s}+\frac{\mathbf{p}}{m}\cdot\nabla_{\mathbf{R}}K_0^{(2)}(\mathbf{R},\mathbf{p}|\mathbf{R}',\mathbf{p}';s)=0$$
$$\frac{\partial K_1^{(2)}}{\partial s}+\frac{\mathbf{p}}{m}\cdot\nabla_{\mathbf{R}}K_1^{(2)}+\boldsymbol{\theta}\cdot K_0^{(2)}=0 \quad (23)$$
$$\frac{\partial K_2^{(2)}}{\partial s}+\frac{\mathbf{p}}{m}\cdot\nabla_{\mathbf{R}}K_2^{(2)}+\boldsymbol{\theta}\cdot K_1^{(2)}=0$$

etc. with solutions

$$K_0^{(2)}(\mathbf{R},\mathbf{p}|\mathbf{R}',\mathbf{p}';s)=\delta(\mathbf{p}-\mathbf{p}')\delta(\mathbf{R}-\mathbf{R}'-\Delta\mathbf{R})$$
$$\Delta\mathbf{R}=\mathbf{R}-\mathbf{R}'=\left(\frac{\mathbf{p}}{m}\right)s$$

$$K_1^{(2)}(\mathbf{R},\mathbf{p}|\mathbf{R}',\mathbf{p}';s)$$
$$=-\int_0^s\exp\left[(s'-s)\frac{\mathbf{p}}{m}\cdot\nabla_{\mathbf{R}}\right]\boldsymbol{\theta}\cdot K_0^{(2)}ds' \quad (24)$$
$$K_2^{(2)}(\mathbf{R},\mathbf{p}|\mathbf{R}',\mathbf{p}';s)$$
$$=-\int_0^s\exp\left[(s'-s)\frac{\mathbf{p}}{m}\cdot\nabla_{\mathbf{R}}\right]\boldsymbol{\theta}\cdot K_1^{(2)}ds'$$

etc. These Eqs. (24) represent the solution for $K^{(2)}$, when this function can be expanded as shown in Eq. (22).

The formal expression for the quantum-mechanical Boltzmann equation is obtained by the introduction of the transformation function into Eq. (12),

$$\frac{\partial\bar{f}^{(1)}}{\partial t}+\frac{\mathbf{p}_1}{m_1}\cdot\nabla_{\mathbf{R}_1}\bar{f}^{(1)}+\boldsymbol{\theta}^{(e)}\cdot\bar{f}^{(1)}$$
$$=-\frac{N_2}{\tau}\int\cdots\int_0^\tau\boldsymbol{\theta}^{(2)}\cdot K^{(2)}(\mathbf{R}_1\mathbf{R}_2\mathbf{p}_1\mathbf{p}_2|\mathbf{R}_1'\mathbf{R}_2'\mathbf{p}_1'\mathbf{p}_2';s)$$
$$\times\{[\mathbf{O}_\pm]f^{(1)}(\mathbf{R}_1'\mathbf{p}_1';t)f^{(1)}(\mathbf{R}_2'\mathbf{p}_2';t)\}$$
$$\times d\mathbf{R}_1'd\mathbf{R}_2'd\mathbf{R}_2d\mathbf{p}_1'd\mathbf{p}_2'd\mathbf{p}_2ds+O\left(\frac{\tau_k}{\tau}\right). \quad (25)$$

The pair transformation function $K^{(2)}$ is determined as indicated in the series of Eqs. (19)–(24), and Eq. (25) represents the quantum-mechanical Boltzmann equation of transport for dilute gases.

The particular case for which the series expansion of $K^{(2)}$ can be terminated after the second term will now be carried through explicitly. As stated this problem will be found equivalent to the Born approximation in the solution of scattering problems. Equation (25) can then be expressed by

$$\frac{\partial\bar{f}^{(1)}}{\partial t}+\frac{\mathbf{p}_1}{m_1}\cdot\nabla_{\mathbf{R}_1}\bar{f}^{(1)}+\boldsymbol{\theta}^{(e)}\cdot\bar{f}^{(1)}$$
$$=-\frac{N_2}{2\tau}\left(\frac{1}{2\pi\hbar}\right)^3\int\cdots\int_0^\tau\boldsymbol{\theta}^{(2)}\cdot[T_r]$$
$$\times\left\{\exp\left[\frac{i}{\hbar}(\mathbf{p}''-\mathbf{p}')\cdot\mathbf{R}'\right](K_0^{(2)}+K_1^{(2)})\right.$$
$$\times f^{(1)}\left[\left(\mathbf{R}_c-\frac{\mathbf{R}^0}{2}\right),\left(\frac{\mathbf{p}_c}{2}-\mathbf{p}^0\right);t\right]$$
$$\left.\times f^{(1)}\left[\left(\mathbf{R}_c+\frac{\mathbf{R}^0}{2}\right),\left(\frac{\mathbf{p}_c}{2}+\mathbf{p}^0\right);t\right]\right\}$$
$$\times d\mathbf{R}^0d\mathbf{R}'d\mathbf{R}_2d\mathbf{p}'d\mathbf{p}''d\mathbf{p}_2d\mathbf{p}^0ds, \quad (26)$$

$$K_0^{(2)}=K_0^{(2)}\left[\mathbf{R}',\left(\frac{\mathbf{p}'+\mathbf{p}''}{2}\right)\middle|\mathbf{R}^0,\mathbf{p}^0;s\right];$$
$$[T_r]=[T_r(\mathbf{p},\mathbf{p}',\mathbf{p}'',\mathbf{R})]$$
$$\mathbf{R}=\mathbf{R}_2-\mathbf{R}_1 \quad \mathbf{R}_c=\tfrac{1}{2}(\mathbf{R}_2+\mathbf{R}_1)$$
$$\mathbf{p}=\tfrac{1}{2}(\mathbf{p}_2-\mathbf{p}_1) \quad \mathbf{p}_c=\mathbf{p}_2+\mathbf{p}_1,$$

where the symmetrization operator is shown explicitly, and $[T_\tau]$ is given by Eq. (B10) of Appendix B. Quantities of the order of (τ_k/τ) have been omitted in Eq. (26). The terms containing $K_0^{(2)}$ can be shown to be zero with the aid of arguments analogous to those given below (see Appendix C).

The second term in the expansion of the transformation function, $K^{(2)}$, can be written from Eq. (24) as

$$K_1^{(2)}\left[\mathbf{R}',\left(\frac{\mathbf{p}'+\mathbf{p}''}{2}\right)\middle|\mathbf{R}^0,\mathbf{p}^0;s\right]$$
$$=-\frac{i}{\hbar}\left(\frac{1}{\pi\hbar}\right)^3\int_0^s\exp\left[(s'-s)\left(\frac{\mathbf{p}'+\mathbf{p}''}{2m}\right)\cdot\nabla_{\mathbf{R}'}\right]$$
$$\times U(R'')\delta(\xi-\mathbf{p}^0)\delta(\mathbf{R}'-\mathbf{R}^0-\Delta\mathbf{R})$$
$$\times\left[\exp\left\{\frac{2i}{\hbar}\left[\left(\frac{\mathbf{p}'+\mathbf{p}''}{2}\right)-\xi\right]\cdot(\mathbf{R}'-\mathbf{R}'')\right\}\right.$$
$$\left.-\exp\left\{-\frac{2i}{\hbar}\left[\left(\frac{\mathbf{p}'+\mathbf{p}''}{2}\right)-\xi\right]\cdot(\mathbf{R}'-\mathbf{R}'')\right\}\right]$$
$$\times d\mathbf{R}''d\xi ds' \quad (27)$$

on rearranging the θ operator. Integration over ξ and s' is straightforward and the resultant expression for $K_1^{(2)}$ is introduced into Eq. (26). Integration over $\mathbf{R}^0$ is performed with the assumption that the distribution functions have only macroscopic space dependence that variations in these functions occur only over distances L_1, such that $L_1 \gg L_\tau$, where L_τ has been defined above. Then, to terms of the order of L_τ/L_1, $\delta(\mathbf{R}'-\mathbf{R}^0-\Delta\mathbf{R})$ can be approximated by $\delta(\mathbf{R}'-\mathbf{R}^0)$. It should be noted that the range of integration over $\mathbf{R}^0$, and thus $\mathbf{R}'$, can be restricted to volumes in relative configuration space of linear extent L_τ, since the transformation function, i.e., the conditional probability of transition, is zero for R^0, $R' > L_\tau$. For this to hold true the range of the intermolecular forces, ρ^0, must be short such that $\rho^0 \ll L_\tau$. Thus, to these orders of approximation, the configurational arguments of the distribution functions, $(\mathbf{R}_c-\frac{1}{2}\mathbf{R}')$ and $(\mathbf{R}_c+\frac{1}{2}\mathbf{R}')$ can both be replaced by $\mathbf{R}_1$. It is this approximation which permits the integration of the remaining terms which depend upon $\mathbf{R}'$. Furthermore, it is this approximation which replaces the more restrictive assumption of random *a priori* phases which Mori and Ono found necessary to apply in their derivation.

With the aid of the preceding assumptions and the use of Eq. (27), Eq. (26) can be altered to read

$$\frac{\partial\tilde{f}^{(1)}}{\partial t}+\frac{\mathbf{p}_1}{m_1}\cdot\nabla_{\mathbf{R}_1}\tilde{f}^{(1)}+\theta^{(e)}\cdot\tilde{f}^{(1)}$$
$$=\frac{N_2}{2\tau}\frac{i}{\hbar}\left(\frac{1}{2\pi\hbar}\right)^3\left(\frac{1}{\pi\hbar}\right)^6\int\cdots\int_0^\tau\frac{U(R'')\exp\left[\frac{i}{\hbar}(\mathbf{p}''-\mathbf{p}')\cdot\mathbf{R}'\right]}{2\left[\left(\frac{\mathbf{p}'+\mathbf{p}''}{2}\right)-\mathbf{p}^0\right]\cdot\left(\frac{\mathbf{p}'+\mathbf{p}''}{2m}\right)}[\Lambda][B+B^*]f^{(1)}[\mathbf{R}_1,(\tfrac{1}{2}\mathbf{p}_c-\mathbf{p}^0);t]$$
$$\times f^{(1)}[\mathbf{R}_1,(\tfrac{1}{2}\mathbf{p}_c+\mathbf{p}^0);t]d\mathbf{R}'d\mathbf{R}''d\mathbf{R}_2d\mathbf{p}'d\mathbf{p}''d\mathbf{p}^0d\mathbf{p}_2ds \quad (28)$$

$$[\Lambda]=\Lambda_1+\Lambda_2+\Lambda_3+\Lambda_4$$

$$\Lambda_1=\exp\left[\frac{i}{\hbar}(\mathbf{p}'-\mathbf{p}'')\cdot\mathbf{R}\right](e^{\alpha_1}-e^{-\alpha_1}); \qquad \alpha_1=\frac{i}{\hbar}[2\mathbf{p}-(\mathbf{p}'+\mathbf{p}'')]\cdot(\mathbf{R}-\mathbf{R}'')$$

$$\Lambda_2=\exp\left[\frac{i}{\hbar}(-\mathbf{p}'+\mathbf{p}'')\cdot\mathbf{R}\right](e^{\alpha_2}-e^{-\alpha_2}); \qquad \alpha_2=\frac{i}{\hbar}[2\mathbf{p}-(-\mathbf{p}'-\mathbf{p}'')]\cdot(\mathbf{R}-\mathbf{R}'')$$

$$\Lambda_3=\pm\exp\left[\frac{i}{\hbar}(-\mathbf{p}'-\mathbf{p}'')\cdot\mathbf{R}\right](e^{\alpha_3}-e^{-\alpha_3}); \qquad \alpha_3=\frac{i}{\hbar}[2\mathbf{p}-(-\mathbf{p}'+\mathbf{p}'')]\cdot(\mathbf{R}-\mathbf{R}'')$$

$$\Lambda_4=\pm\exp\left[\frac{i}{\hbar}(\mathbf{p}'+\mathbf{p}'')\cdot\mathbf{R}\right](e^{\alpha_4}-e^{-\alpha_4}); \qquad \alpha_4=\frac{i}{\hbar}[2\mathbf{p}-(\mathbf{p}'-\mathbf{p}'')]\cdot(\mathbf{R}-\mathbf{R}'')$$

$$B=\left[1-\exp\left\{-\frac{2i}{\hbar}\left[\left(\frac{\mathbf{p}'+\mathbf{p}''}{2}\right)-\mathbf{p}^0\right]\cdot\left(\frac{\mathbf{p}'+\mathbf{p}''}{2m}\right)s\right\}\right]\exp\left\{\frac{i}{\hbar}\left[\left(\frac{\mathbf{p}'+\mathbf{p}''}{2}\right)-\mathbf{p}^0\right]\cdot\mathbf{R}'\right\}I(\mathbf{p}'+\mathbf{p}''-2\mathbf{p}^0)$$

$$I(\mathbf{p}'+\mathbf{p}''-2\mathbf{p}^0)=\int\exp\left[-\frac{i}{\hbar}(\mathbf{p}'+\mathbf{p}''-2\mathbf{p}^0)\cdot\mathbf{R}\right]U(R)d\mathbf{R},$$

where B^* is the complex conjugate of B, and I^* the complex conjugate of I. Since the derivation is restricted to spherically symmetric intermolecular potentials, I^* equals I. The differential $d\mathbf{R}_2$ can be replaced by $d\mathbf{R}$, and the integrations over $\mathbf{R}'$ and $\mathbf{R}$ yield Dirac δ functions. These steps lead to the following equation after some tedious algebraic manipulations:

$$\frac{\partial \bar{f}^{(1)}}{\partial t}+\frac{\mathbf{p}_1}{m_1}\cdot\nabla_{\mathbf{R}_1}\bar{f}^{(1)}+\boldsymbol{\theta}^{(e)}\cdot\bar{f}^{(1)}$$

$$=\frac{N_2}{2\tau}\frac{i}{\hbar}\left(\frac{1}{2\pi\hbar}\right)^3\int\cdots\int_0^\tau[I(\mathbf{p}-\mathbf{p}')\pm I(-\mathbf{p}-\mathbf{p}')]^2\left\{\frac{\exp\left[-\frac{i}{\hbar}\left(\frac{p^2-p'^2}{2m}\right)s\right]-\exp\left[\frac{i}{\hbar}\left(\frac{p^2-p'^2}{2m}\right)s\right]}{\left(\frac{p^2-p'^2}{2m}\right)}\right\}$$

$$\times\{f^{(1)}(\mathbf{R}_1\mathbf{p}_1';t)f^{(1)}(\mathbf{R}_1\mathbf{p}_2';t)-f^{(1)}(\mathbf{R}_1\mathbf{p}_1;t)f^{(1)}(\mathbf{R}_1\mathbf{p}_2;t)\}d\mathbf{p}'d\mathbf{p}_2ds. \quad (29)$$

The argument proceeds analogously to the solution of scattering problems by the method of variation of constants in the Schrödinger equation in the momentum representation. The remaining functions of s in Eq. (29) are easily reduced, and for sufficiently large values of τ this term

$$\frac{\sin^2\left[\left(\frac{p^2-p'^2}{4m\hbar}\right)\tau\right]}{\left(\frac{p^2-p'^2}{4m}\right)^2},$$

becomes a sharply-peaked function, similar to a δ function, at $p=p'$. This fact permits the evaluation of all other functions of $\mathbf{p}'$ at $p=p'$, which reduces the integration over $\mathbf{p}'$ to

$$\lim_{\tau\to\infty}\frac{1}{\tau}\int\frac{\sin^2\left[\left(\frac{p^2-p'^2}{4m\hbar}\right)\tau\right]}{\left(\frac{p^2-p'^2}{4m}\right)^2}p'^2dp'd\Omega=\frac{2}{\hbar}m\pi pd\Omega.$$

Equation (29) now becomes

$$\frac{\partial \bar{f}^{(1)}}{\partial t}+\frac{\mathbf{p}_1}{m_1}\cdot\nabla_{\mathbf{R}_1}\bar{f}^{(1)}+\boldsymbol{\theta}^{(e)}\cdot\bar{f}^{(1)}$$

$$=N_2\int\cdots\int\sigma(p,\Omega)\frac{p}{m}[f^{(1)}(\mathbf{R}_1\mathbf{p}_1';t)f^{(1)}(\mathbf{R}_1\mathbf{p}_2';t)$$

$$-f^{(1)}(\mathbf{R}_1\mathbf{p}_1;t)f^{(1)}(\mathbf{R}_1\mathbf{p}_2;t)]d\Omega d\mathbf{p}_2, \quad (30)$$

where $\sigma(p,\Omega)$ is the scattering cross section defined by

$$\sigma(p,\Omega)=\frac{1}{2}\left(\frac{m}{2\pi\hbar^2}\right)^2[I(\mathbf{p}-\mathbf{p}')\pm I(-\mathbf{p}-\mathbf{p}')]^2 \quad (31)$$

and

$$|\mathbf{p}-\mathbf{p}'|=2p\sin\left(\frac{\theta}{2}\right);$$

the polar axis is taken along $\mathbf{p}'$. Time averaging Eq. (30) over an interval τ, which leaves the left-hand side unaffected, yields

$$\frac{\partial \bar{f}^{(1)}}{\partial t}+\frac{\mathbf{p}_1}{m_1}\cdot\nabla_{\mathbf{R}_1}\bar{f}^{(1)}+\boldsymbol{\theta}^{(e)}\cdot\bar{f}^{(1)}$$

$$=N_2\int\cdots\int\sigma(p,\Omega)\frac{p}{m}[\bar{f}^{(1)}(\mathbf{R}_1\mathbf{p}_1';t)\bar{f}^{(1)}(\mathbf{R}_1\mathbf{p}_2';t)$$

$$-\bar{f}^{(1)}(\mathbf{R}_1\mathbf{p}_1;t)\bar{f}^{(1)}(\mathbf{R}_1\mathbf{p}_2;t)]d\Omega d\mathbf{p}_2. \quad (32)$$

To obtain the above equation it is necessary to apply the additional condition

$$\overline{f^{(1)}f^{(1)}}=\bar{f}^{(1)}\bar{f}^{(1)}. \quad (33)$$

This is true to terms of first order for distributions close to equilibrium.

Equation (32) reduces to the Uhling and Uhlenbeck equation, (aside from the density dependent factors due to quantum statistics, which we ignored), if the external forces are assumed to be sufficiently slowly varying to warrant simplification of the term $\boldsymbol{\theta}^{(e)}\cdot\bar{f}^{(1)}$ to $-\nabla_{\mathbf{R}_1}\phi_1(\mathbf{R}_1)\cdot\nabla_{\mathbf{p}_1}\bar{f}^{(1)}$.

Although the question of the applicability of the Uhling and Uhlenbeck equation as an explicit formulation of the general quantum-mechanical Boltzmann equation remains unanswered, an opinion of the unlikelihood of its validity beyond the restrictions of the Born approximation seems warranted. This follows from the belief that the usual formulation of the quantum-mechanical scattering cross sections may be inadequate to describe the transition probabilities due to scattering as determined rigorously in terms of solutions of the integro-differential equation for the transformation function K. Proof of these assertions is under consideration.

Two derivations of the Boltzmann equation in quantum mechanics have been published previously. Mori and Ono's[11] analysis, like the present one, is based upon the Wigner equation. They apply time dependent perturbation methods to the density matrix and retain

first order terms only. This is equivalent to the Born approximation in the solution of quantum-mechanical scattering problems; no formalism for a general solution is presented. To proceed, they find it necessary to simplify the density matrix by neglecting all non-diagonal terms of the matrix, which is equivalent to the hypothesis of random *a priori* phases and is an integral part of their treatment. It is this step which removes all configuration space dependence from the distribution functions and their derivation is limited to this extent. Use of the methods of second quantization yields the density dependent factors due to quantum statistics. Inclusion of these interactions seems superfluous since they become of importance under conditions where in general the Born approximation is inapplicable.

The other derivation, by H. S. Green,[17] also uses the Wigner equation as a starting point, but the concept of time-smoothed distribution functions is not introduced. The effect of quantum statistics is neglected entirely. Green attempts to obtain the Boltzmann equation by solving the Wigner equation for the pair distribution function directly, without any perturbation methods. Although he seems to effect such a solution, no final equation is given in a recognizable form of the Boltzmann equation. The quantum-mechanical cross section does not appear explicitly in his treatment, and no indications are apparent under what conditions his method leads to the Uhling and Uhlenbeck equation.

APPENDIX A

The wave transformation function $k(\mathbf{R}|\mathbf{R}';s)$ is defined by the equation

$$\psi(\mathbf{R};t+s)=\int k(\mathbf{R}|\mathbf{R}';s)\psi(\mathbf{R}';t)d\mathbf{R}', \qquad \text{(A1)}$$

where ψ denotes the Schrödinger wave function, $\mathbf{R}$ the coordinates, t the time, and s a time interval. From the definitions of the Wigner distribution function, Eq. (2), and the phase-space transformation function, Eq. (13), the relation of the latter to the wave transformation function is seen to be

$$K^{(N)}(\mathbf{R},\mathbf{p}|\mathbf{R}',\mathbf{p}';s)=\left(\frac{2}{\pi\hbar}\right)^{3N}\int\cdots\int \times\exp\left[\frac{2i}{\hbar}(\mathbf{p}\cdot\mathbf{Y}-\mathbf{p}'\cdot\mathbf{Y}')\right]k^{*(N)}(\mathbf{R}+\mathbf{Y}|\mathbf{R}'+\mathbf{Y}';s) \times k^{(N)}(\mathbf{R}-\mathbf{Y}|\mathbf{R}'-\mathbf{Y}';s)d\mathbf{Y}d\mathbf{Y}', \qquad \text{(A2)}$$

where N is the number of particles in the system.

The wave transformation function can be expanded in the form[18]

$$k=k_0+k_1+k_2\cdots, \qquad \text{(A3)}$$

where the potential of intermolecular force is treated as a perturbation. The physical significance of each term in this series is simply that the subscript of each term denotes the number of times the wave interacts with, or is scattered by, the potential field during the transition considered. The total conditional probability of transition of the wave function, $k^{(N)}(\mathbf{R}|\mathbf{R}';s)$, consists then of the sum of ways in which the wave function can proceed from $\mathbf{R}'$ to $\mathbf{R}$ in the interval s. The individual terms of the expansion for the phase space transformation function, Eq. (22), are composed of corresponding terms of the expansion (A3) according to the relation (A2).

It is convenient sometimes to introduce the wave transformation function in the momentum representation, $k^{(N)}(\mathbf{p}|\mathbf{p}';s)$. From the well-known Fourier transform relation between the wave functions in the coordinate and momentum representation, the equation for $k^{(N)}(\mathbf{p}|\mathbf{p}';s)$, is

$$k^{(N)}(\mathbf{p}|\mathbf{p}';s)=\left(\frac{1}{2\pi\hbar}\right)^{3N}\int\cdots\int \times\exp\left[-\frac{i}{\hbar}(\mathbf{p}\cdot\mathbf{R}-\mathbf{p}'\cdot\mathbf{R}')\right]k^{(N)}(\mathbf{R}|\mathbf{R}';s)d\mathbf{R}d\mathbf{R}'. \qquad \text{(A4)}$$

Integration of Eq. (A2) over $\mathbf{R}$ and $\mathbf{R}'$ yields, with the aid of Eq. (A4)

$$|k^{(N)}(\mathbf{p}|\mathbf{p}';s)|^2=\left(\frac{1}{2\pi\hbar}\right)^{3N}\int\cdots\int \times K^{(N)}(\mathbf{R},\mathbf{p}|\mathbf{R}',\mathbf{p}';s)d\mathbf{R}d\mathbf{R}'. \qquad \text{(A5)}$$

For the determination of the relation between the phase-space transformation function and the scattering cross section, we shall define the term

$$B'\equiv\int\cdots\int[K(\mathbf{R},\mathbf{p}|\mathbf{R}',\mathbf{p}';s) -K_0(\mathbf{R},\mathbf{p}|\mathbf{R}',\mathbf{p}';s)]d\mathbf{R}d\mathbf{R}', \qquad \text{(A6)}$$

where K_0 is the first term in the expansion of K, Eq. (22). B' is seen to be the particular kind of conditional probability that the system will have momentum space coordinates $\mathbf{p}$ after an interval s, given the initial coordinates $\mathbf{p}'$. The subtraction of the K_0 term excludes transitions not induced by the potential field; these free-particle transitions are of no physical interest in the scattering problem. The probability of a transition from $\mathbf{p}'$ at $s=0$ to the range of momenta $\mathbf{p}$, $\mathbf{p}+d\mathbf{p}$, after the interval s is $B'd\mathbf{p}$ or, in spherical coordinates, $B'p^2dpd\Omega$. Thus, the probability of a transition specified merely by the change of direction of the momentum vector, in the interval s, from the polar axis into the solid angle Ω, $\Omega+d\Omega$, is $[\int B'p^2dp]d\Omega$. But this probability per unit time, unit current, and unit solid angle

[17] H. S. Green, Proc. Phys. Soc. (London) **A66**, 325 (1953).
[18] R. P. Feynman, Revs. Modern Phys. **20**, 367 (1948).

is the definition of the scattering cross section, $\sigma(p,\Omega)$:

$$\sigma(p,\Omega)=\frac{\int B' p^2 dp}{s\left(\frac{p}{m}\right)}. \tag{A7}$$

APPENDIX B‡

Consider a system composed of two independent particles denoted by 1 and 2. At first, let the particles be distinguishable, i.e., assume they obey Boltzmann statistics. In this case we choose the orthonormal set of plane wave functions

$$\phi_1(\mathbf{p}_1)=\left(\frac{1}{2\pi\hbar}\right)^{\frac{3}{2}}\exp\left(\frac{i}{\hbar}\mathbf{p}_1\cdot\mathbf{R}_1\right), \tag{B1}$$

in terms of which the wave function can be written as

$$\psi_1(\mathbf{R}_1;t)=\left(\frac{1}{2\pi\hbar}\right)^{\frac{3}{2}}\int a_1(\mathbf{p}_1;t)\exp\left(\frac{i}{\hbar}\mathbf{p}_1\cdot\mathbf{R}_1\right)d\mathbf{p}_1, \tag{B2}$$

and similarly for particle 2. The Fourier transform of Eq. (B2) leads to an expression for $a_1(\mathbf{p}_1;t)$,

$$a_1(\mathbf{p}_1;t)=\left(\frac{1}{2\pi\hbar}\right)^{\frac{3}{2}}\int\psi_1(\mathbf{R}_1;t)\exp\left(-\frac{i}{\hbar}\mathbf{p}_1\cdot\mathbf{R}_1\right)d\mathbf{R}_1. \tag{B3}$$

The Wigner function for the two particle system is easily obtained from its definition Eq. (2). Since the density matrix of this system is

$$\psi_1^*(\mathbf{R}_1';t)\psi_2^*(\mathbf{R}_2';t)\psi_1(\mathbf{R}_1;t)\psi_2(\mathbf{R}_2;t),$$

it is seen that the pair Wigner function factors straightforwardly into the corresponding singlet Wigner functions,

$$f^{(2)}(\mathbf{R}_1\mathbf{R}_2\mathbf{p}_1\mathbf{p}_2;t)=f^{(1)}(\mathbf{R}_1\mathbf{p}_1;t)f^{(1)}(\mathbf{R}_2\mathbf{p}_2;t). \tag{B4}$$

For the case of indistinguishable particles, i.e., for systems obeying Bose-Einstein or Fermi-Dirac statistics, we choose the properly symmetrized plane wave function

$$\Phi(\mathbf{p}_1\mathbf{p}_2)=\frac{1}{\sqrt{2}}\left(\frac{1}{2\pi\hbar}\right)^3\left\{\exp\left[\frac{i}{\hbar}(\mathbf{p}_1\cdot\mathbf{R}_1+\mathbf{p}_2\cdot\mathbf{R}_2)\right]\pm\exp\left[\frac{i}{\hbar}(\mathbf{p}_1\cdot\mathbf{R}_2+\mathbf{p}_2\cdot\mathbf{R}_1)\right]\right\}, \tag{B5}$$

in terms of which the wave function for the two-particle system is written as

$$\psi(\mathbf{R}_1\mathbf{R}_2;t)=\int\int a_1(\mathbf{p}_1;t)a_2(\mathbf{p}_2;t)\Phi(\mathbf{p}_1\mathbf{p}_2)d\mathbf{p}_1d\mathbf{p}_2. \tag{B6}$$

Wherever a choice of sign ($\pm$) occurs it is understood that the positive sign is applicable to Bose-Einstein systems whereas the negative sign is applicable to Fermi-Dirac statistics. It should be noted here that the symmetrization of wave functions, and of the density matrix, is adequately described by a permutation operation. This simplicity does not prevail in the symmetrization of Wigner functions

The pair Wigner distribution function can be formulated with the aid of Eq. (B6) and becomes

$$f^{(2)}(\mathbf{R}_1\mathbf{R}_2\mathbf{p}_1\mathbf{p}_2;t)=\frac{1}{2}\left(\frac{1}{2\pi\hbar}\right)^6\int\cdots\int\times a_1^*(\mathbf{p}_1'';t)a_2^*(\mathbf{p}_2'';t)a_1(\mathbf{p}_1';t)a_2(\mathbf{p}_2';t)[T]\times d\mathbf{p}_1'd\mathbf{p}_2'd\mathbf{p}_1''d\mathbf{p}_2'', \tag{B7}$$

$$[T]=\chi_1+\chi_2\pm\chi_3\pm\chi_4$$

$$\chi_1=\delta\left(\mathbf{p}_1-\frac{\mathbf{p}_1'+\mathbf{p}_1''}{2}\right)\delta\left(\mathbf{p}_2-\frac{\mathbf{p}_2'+\mathbf{p}_2''}{2}\right)\times\exp\left\{\frac{i}{\hbar}[\mathbf{R}_1\cdot(\mathbf{p}_1'-\mathbf{p}_1'')+\mathbf{R}_2\cdot(\mathbf{p}_2'-\mathbf{p}_2'')]\right\},$$

$$\chi_2=\delta\left(\mathbf{p}_1-\frac{\mathbf{p}_2'+\mathbf{p}_2''}{2}\right)\delta\left(\mathbf{p}_2-\frac{\mathbf{p}_1'+\mathbf{p}_1''}{2}\right)\times\exp\left\{\frac{i}{\hbar}[\mathbf{R}_1\cdot(\mathbf{p}_2'-\mathbf{p}_2'')+\mathbf{R}_2\cdot(\mathbf{p}_1'-\mathbf{p}_1'')]\right\}, \tag{B8}$$

$$\chi_3=\delta\left(\mathbf{p}_1-\frac{\mathbf{p}_2'+\mathbf{p}_1''}{2}\right)\delta\left(\mathbf{p}_2-\frac{\mathbf{p}_1'+\mathbf{p}_2''}{2}\right)\times\exp\left\{\frac{i}{\hbar}[\mathbf{R}_1\cdot(\mathbf{p}_2'-\mathbf{p}_1'')+\mathbf{R}_2\cdot(\mathbf{p}_1'-\mathbf{p}_2'')]\right\},$$

$$\chi_4=\delta\left(\mathbf{p}_1-\frac{\mathbf{p}_1'+\mathbf{p}_2''}{2}\right)\delta\left(\mathbf{p}_2-\frac{\mathbf{p}_1''+\mathbf{p}_2'}{2}\right)\times\exp\left\{\frac{i}{\hbar}[\mathbf{R}_1\cdot(\mathbf{p}_1'-\mathbf{p}_2'')+\mathbf{R}_2\cdot(\mathbf{p}_2'-\mathbf{p}_1'')]\right\}.$$

Equation (B3) is now used to reexpress the various a's in terms of wave functions. This procedure leads to the following equation

$$f^{(2)}(\mathbf{R}_1\mathbf{R}_2\mathbf{p}_1\mathbf{p}_2;t)=\frac{1}{2}\left(\frac{1}{2\pi\hbar}\right)^6\int\cdots\int\times\exp\left\{\frac{i}{\hbar}[\mathbf{R}_1'\cdot(\mathbf{p}_1''-\mathbf{p}_1')+\mathbf{R}_2'\cdot(\mathbf{p}_2''-\mathbf{p}_2')]\right\}[T]\times f^{(1)}[\mathbf{R}_1',\tfrac{1}{2}(\mathbf{p}_1'+\mathbf{p}_1'');t]f^{(1)}[\mathbf{R}_2',\tfrac{1}{2}(\mathbf{p}_2'+\mathbf{p}_2'');t]\times d\mathbf{R}_1'd\mathbf{R}_2'd\mathbf{p}_1'd\mathbf{p}_2'd\mathbf{p}_1''d\mathbf{p}_2''. \tag{B9}$$

‡ *Note added in proof.*—The treatment is restricted here to systems of two independent particles for which the unsymmetrized phase-space distribution function, i.e., the distribution function of a quantum-mechanical system obeying Boltzmann statistics, can be expressed at any one instant of time as a product of two singlet distribution functions, $f^{(2)}(R_1R_2p_1p_2;t)=f^{(1)}(R_1p_1;t)f^{(1)}(R_2p_2;t)$.

The equivalent of Eq. (B9) written in relative coordinates can be shown to be

$$f^{(2)}(\mathbf{R}_1\mathbf{R}_2\mathbf{p}_1\mathbf{p}_2;t)=\frac{1}{2}\left(\frac{1}{2\pi\hbar}\right)^3\int\cdots\int \times\exp\left\{\frac{i}{\hbar}[\mathbf{R}'\cdot(\mathbf{p}''-\mathbf{p}')]\right\}[T_\tau] \times f^{(1)}[(\mathbf{R}_c-\tfrac{1}{2}\mathbf{R}'),\tfrac{1}{2}(\mathbf{p}_c-\mathbf{p}'-\mathbf{p}'');t] \times f^{(1)}[(\mathbf{R}_c+\tfrac{1}{2}\mathbf{R}'),\tfrac{1}{2}(\mathbf{p}_c+\mathbf{p}'+\mathbf{p}'');t]d\mathbf{R}'d\mathbf{p}'d\mathbf{p}''$$

$$[T_\tau]=\chi_1'+\chi_2'\pm\chi_3'\pm\chi_4'$$

$$\chi_1'=\delta[\mathbf{p}-\tfrac{1}{2}(\mathbf{p}'+\mathbf{p}'')]\exp\left[\frac{i}{\hbar}\mathbf{R}\cdot(\mathbf{p}'-\mathbf{p}'')\right] \tag{B10}$$

$$\chi_2'=\delta[\mathbf{p}-\tfrac{1}{2}(-\mathbf{p}'-\mathbf{p}'')]\exp\left[\frac{i}{\hbar}\mathbf{R}\cdot(-\mathbf{p}'+\mathbf{p}'')\right]$$

$$\chi_3'=\delta[\mathbf{p}-\tfrac{1}{2}(-\mathbf{p}'+\mathbf{p}'')]\exp\left[\frac{i}{\hbar}\mathbf{R}\cdot(-\mathbf{p}'-\mathbf{p}'')\right]$$

$$\chi_4'=\delta[\mathbf{p}-\tfrac{1}{2}(\mathbf{p}'-\mathbf{p}'')]\exp\left[\frac{i}{\hbar}\mathbf{R}\cdot(\mathbf{p}'+\mathbf{p}'')\right]$$

$$\mathbf{R}_c=\tfrac{1}{2}(\mathbf{R}_2+\mathbf{R}_1);\quad \mathbf{R}=\mathbf{R}_2-\mathbf{R}_1;$$

$$\mathbf{p}_c=\mathbf{p}_2+\mathbf{p}_1;\qquad \mathbf{p}=\tfrac{1}{2}(\mathbf{p}_2-\mathbf{p}_1).$$

Equation (B9) or (B10) shows clearly that the symmetrization operation on the Wigner distribution functions cannot be represented by a permutation operator but is in fact represented by an integral operator. This integral operator, defined by Eq. (B9), can be written formally as

$$f^{(2)}(\mathbf{R}_1\mathbf{R}_2\mathbf{p}_1\mathbf{p}_2;t)=[\mathbf{O}_\pm]f^{(1)}(\mathbf{R}_1\mathbf{p}_1;t)f^{(1)}(\mathbf{R}_2\mathbf{p}_2;t). \tag{B11}$$

APPENDIX C

It is desired to show that the expression

$$A\equiv-\frac{N_2}{2\tau}\left(\frac{1}{2\pi\hbar}\right)^3\int\cdots\int_0^\tau\theta^{(2)}\cdot\left\{\exp\left[\frac{i}{\hbar}\mathbf{R}'\cdot(\mathbf{p}''-\mathbf{p}')\right][T_\tau]\right\}K_0^{(2)} \times f^{(1)}[(\mathbf{R}_c-\tfrac{1}{2}\mathbf{R}^0)(\tfrac{1}{2}\mathbf{p}_c-\mathbf{p}^0);t]f^{(1)}[(\mathbf{R}_c+\tfrac{1}{2}\mathbf{R}^0)(\tfrac{1}{2}\mathbf{p}_c+\mathbf{p}^0);t]d\mathbf{R}'d\mathbf{R}^0d\mathbf{R}_2d\mathbf{p}'d\mathbf{p}''d\mathbf{p}^0d\mathbf{p}_2ds \tag{C1}$$

$$K_0^{(2)}[\mathbf{R}',\tfrac{1}{2}(\mathbf{p}'+\mathbf{p}'')\,|\,\mathbf{R}^0,\mathbf{p}^0;s]=\delta[\mathbf{R}'-\mathbf{R}^0-\Delta\mathbf{R}]\delta[\tfrac{1}{2}(\mathbf{p}'+\mathbf{p}'')-\mathbf{p}^0]$$

where $[T_\tau]$ is given by Eq. (B10) of Appendix B. The argument is analogous to the one presented above. It is assumed that the distribution functions have only macroscopic configuration space dependence such that variations of these functions occur only over distances L_1, where $L_1\gg L_\tau$. L_τ is the distance traversed by a classical particle with the same initial momentum as in the quantum-mechanical problem in the time interval τ. Since the range of integration over $\mathbf{R}^0$ can be restricted to volumes of linear extent L_τ, it is seen that, to terms of the order of L_τ/L_1 $\delta(\mathbf{R}'-\mathbf{R}^0-\Delta\mathbf{R})$ can be approximated by $\delta(\mathbf{R}'-\mathbf{R}^0)$, and the distribution functions can be written as $f^{(1)}[\mathbf{R}_1,(\tfrac{1}{2}\mathbf{p}_c-\mathbf{p}^0);t]$ and $f^{(1)}[\mathbf{R}_1,(\tfrac{1}{2}\mathbf{p}_c+\mathbf{p}^0);t]$. The integrations over $\mathbf{R}^0$, $\mathbf{R}'$, and $\mathbf{R}$, where $d\mathbf{R}_2$ is replaced by $d\mathbf{R}$, can be carried out simply to yield

$$A=-\frac{i}{\hbar}\frac{N_2}{2\tau}\int\cdots\int_0^\tau f^{(1)}[\mathbf{R}_1,(\tfrac{1}{2}\mathbf{p}_c-\mathbf{p}');t]f^{(1)}[\mathbf{R}_1,(\tfrac{1}{2}\mathbf{p}_c+\mathbf{p}');t][\Lambda']U(R')d\mathbf{R}'d\mathbf{p}'d\mathbf{p}_2ds$$

$$[\Lambda']=\Lambda_1'+\Lambda_2'\pm\Lambda_3'\pm\Lambda_4'$$

$$\Lambda_1'=\delta(\mathbf{p}-\mathbf{p}')\left\{\exp\left[-\frac{2i}{\hbar}\mathbf{R}'\cdot(\mathbf{p}-\mathbf{p}')\right]-\exp\left[\frac{2i}{\hbar}\mathbf{R}'\cdot(\mathbf{p}-\mathbf{p}')\right]\right\}$$

$$\Lambda_2'=\delta(\mathbf{p}+\mathbf{p}')\left\{\exp\left[-\frac{2i}{\hbar}\mathbf{R}'\cdot(\mathbf{p}+\mathbf{p}')\right]-\exp\left[\frac{2i}{\hbar}\mathbf{R}'\cdot(\mathbf{p}+\mathbf{p}')\right]\right\} \tag{C2}$$

$$\Lambda_3'=\delta(\mathbf{p}-\mathbf{p}')\exp\left(-\frac{2i}{\hbar}\mathbf{p}\cdot\mathbf{R}'\right)-\delta(\mathbf{p}+\mathbf{p}')\exp\left(\frac{2i}{\hbar}\mathbf{p}\cdot\mathbf{R}'\right)$$

$$\Lambda_4'=\delta(\mathbf{p}+\mathbf{p}')\exp\left(-\frac{2i}{\hbar}\mathbf{p}\cdot\mathbf{R}'\right)-\delta(\mathbf{p}-\mathbf{p}')\exp\left(\frac{2i}{\hbar}\mathbf{p}\cdot\mathbf{R}'\right),$$

which, upon integration over $\mathbf{p}'$, reduces to zero.

Infrared Spectrum of Hydrogen Sulfide. II. The 5100 cm^{-1} Region*

HARRY C. ALLEN, JR.,† *Mallinckrodt Chemical Laboratory, Harvard University, Cambridge, Massachusetts*

AND

EARLE K. PLYLER, *National Bureau of Standards, Washington D. C.*

(Received January 28, 1954)

The absorption of hydrogen sulfide in the region near 2μ has been measured under high resolution. The rotational fine structure has been analyzed with the use of published energy tables for the rigid rotor. A classical centrifugal distortion correction was applied to the rigid rotor energy levels. The absorption can be accounted for by three bands plus overlapping water-vapor absorption. The three bands are the (n_1,n_2,n_3) = (1,0,1) at 5147.36 cm^{-1}, the (0,2,1) at 4939.23 cm^{-1}, and the lower component of the resonating pair (2,0,0) and (0,0,2) at 5145.12 cm^{-1}. The excited-state inertial parameters in cm^{-1} giving the best fits are

	A^*	B^*	C^*
(1,0,1)	10.076	8.709	4.608
(2,0,0)	10.059	8.719	4.612
(0,2,1)	10.871	9.332	4.562.

With the location of the (0,2,1) band it is possible to place the (0,0,1) band at 2628 cm^{-1}.

IN the study of the (1,1,1) band of hydrogen sulfide it was shown that a weak band (2,1,0) appeared in the spectrum, overlapping the (1,1,1) band.[1] In the present work of the 2μ region, which is the second region being studied in great detail, another weak band (0,2,1) has been found.

The absorption in the region around 5100 cm^{-1} has been observed under low resolution by several workers.[2–5] Recently[5] the band envelope has been analyzed and shown to arise from two superimposed bands. In this work, three of the six excited-state constants were not precisely obtained because of insufficient resolution. This region has been re-investigated under high resolution (~0.1 cm^{-1}) in order to enable a better analysis of the rotational fine structure. The main conclusions of the previous analysis have been confirmed. A third band, the (n_1,n_2,n_3) = (0,2,1), has been located on the low-frequency end of the region of absorption at 4939 cm^{-1}, and values obtained for the inertial parameters of the excited state.

EXPERIMENTAL PROCEDURE

The absorption spectrum of hydrogen sulfide was observed in the region of 2μ with a grating spectrometer. The grating has 15 000 lines/in. and has a ruled surface of about 8 inches in width. Other details of the instrument have been previously described and will not be repeated here.[6]

The hydrogen sulfide was obtained from The Matheson Company and was specified as having a purity of 99.9 percent. The gas was placed in a multiple-reflection cell of 6 m path. Different pressures were used so that various parts of the band could be observed in greatest detail. Figure 1 shows the results obtained with 10 cm pressure. This figure is a reproduction of the recorder trace made on white paper. In the region of wavelengths shorter than 1.96μ many lines arising from atmospheric water vapor are observed and most of these have been labelled *w* on the figure. In some instances the water lines overlap the hydrogen sulfide lines as can be seen by their change in relative intensity. The positions of the lines were determined by superimposing many lines of an iron arc on the absorption spectra. The fourth order of the iron lines was used, and because they are known to a high accuracy, our scale was known to a few hundredths of a wave number. Because some lines of the spectrum are overlapped, the position of lines may be in error by ±0.1 cm^{-1}. Two sets of measurements were made of the observations and the final values obtained by taking the average of the determinations.

When the analysis of the 2μ region was made, it was found that several strong lines were observed which could not be assigned to the (1,0,1) or (2,0,0) bands and must be, therefore, a part of another band. On measuring with 76 cm pressure of H_2S in the cell it was found that another band was present and lines extended to about 4800 cm^{-1}. This band is shown in Fig. 2 and is classified as the (0,2,1) band.

On each figure the calculated positions, intensities, and the assignments have been placed on the spectra. In Table I are listed the calculated and observed fre-

* The work reported herein was supported in part by the U. S. Office of Naval Research under ONR Contract N5ori76, Task Order V.

† U. S. Atomic Energy Commission Postdoctoral Fellow. Present address, Department of Physics, Michigan State College, East Lansing, Michigan.

[1] H. C. Allen and E. K. Plyler, J. Research Natl. Bur. Standards **52**, 205 (1954).

[2] A. D. Sprague and H. H. Nielsen, J. Chem. Phys. **5**, 85 (1937).

[3] Bailey, Thompson, and Hale, J. Chem. Phys. **4**, 625 (1936).

[4] R. H. Noble, thesis, Ohio State University (1946).

[5] Allen, Cross, and Wilson, J. Chem. Phys. **20**, 1709 (1953).

[6] E. K. Plyler and N. Gailar, J. Research Natl. Bur. Standards **47**, 248 (1951).

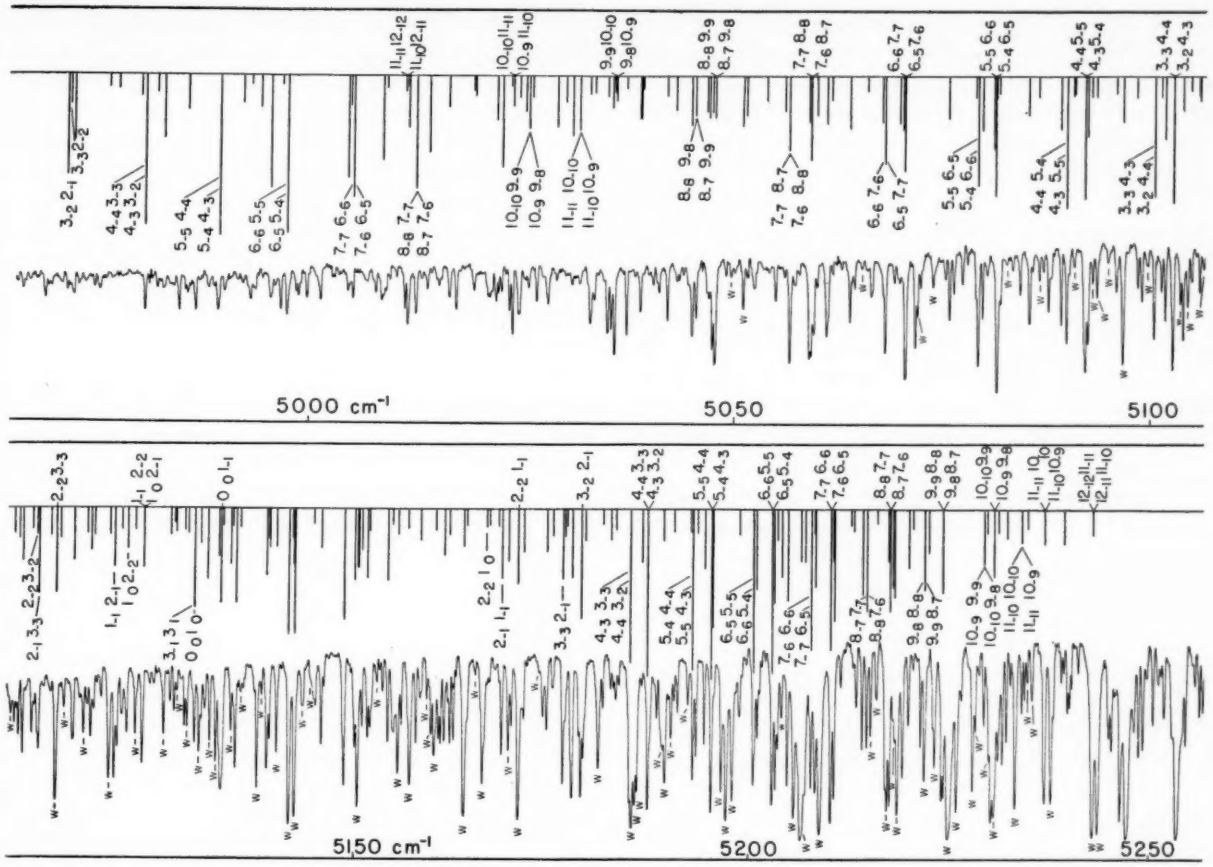

FIG. 1. The infrared absorption spectrum of hydrogen sulfide in the region of from 4950 to 5250 cm^{-1}. The pressure was 10 cm of Hg. The calculated wave numbers and the relative intensities are marked above the absorption spectra.

TABLE I. Calculated and observed frequencies for main wings of (1,0,1), (2,0,0), and (0,2,1) bands.

Transition	Observed frequency	Calculated (1,0,1)	Calculated (2,0,0)	Calculated (0,2,1)
$8_{-8} - 9_{-9}$	4841.70			4841.79
$7_{-6} - 8_{-7}$	4853.24			4853.32
$6_{-6} - 7_{-7}$	4864.61			4864.55
$5_{-4} - 6_{-5}$	4875.34			4875.43
$4_{-4} - 5_{-5}$	4885.96			4885.96
$3_{-2} - 4_{-3}$	4896.10			4896.22
$2_{-2} - 3_{-3}$	4905.90			4905.75
$1_0 - 2_{-1}$	4916.27			4916.37
$0_0 - 1_{-1}$	4925.61			4925.51
$2_{-2} - 1_{-1}$	4963.70			4963.65
$3_{-2} - 2_{-1}$	4972.18			4972.11
$4_{-4} - 3_{-3}$	4980.89			4980.93
$5_{-4} - 4_{-3}$	4989.24			4989.24
$6_{-6} - 5_{-5}$	4997.18			4997.22
$7_{-6} - 6_{-5}$	5004.77			5004.86
$11_{-10} - 12_{-11}$	5011.12	5011.13		
$8_{-8} - 7_{-7}$	5012.12			5012.17
$10_{-9} - 11_{-11}$	5021.49		5021.55	
$10_{-11} - 11_{-11}$	5023.47	5023.40		
$9_{-9} - 10_{-9}$	5033.22		5033.13	
$9_{-8} - 10_{-9}$	5035.46	5035.49		
$8_{-7} - 9_{-7}$	5044.63		5044.66	
$8_{-8} - 9_{-9}$	5047.34	5047.30		
$7_{-7} - 8_{-7}$	5056.35		5056.28	
$7_{-6} - 8_{-7}$	5058.76	5058.81		
$6_{-5} - 7_{-7}$	5067.71		5067.69	
$6_{-6} - 7_{-7}$	5070.06	5070.11		
$5_{-5} - 6_{-5}$	5078.91		5078.84	
$5_{-4} - 6_{-5}$	5081.18	5081.21		

Transition	Observed frequency	Calculated (1,0,1)	Calculated (2,0,0)	Calculated (0,2,1)
$4_{-3} - 5_{-5}$	5089.77		5089.72	
$4_{-4} - 5_{-5}$	5092.03	5092.04		
$3_{-3} - 4_{-3}$	5100.41		5100.36	
$3_{-2} - 4_{-3}$	5102.64	5102.66		
$2_{-1} - 3_{-3}$	5110.83		5110.92	
$2_{-2} - 3_{-3}$	5112.96	5112.87		
$1_{-1} - 2_{-1}$	5120.23		5120.18	
$1_0 - 2_{-1}$	5123.74	5123.76		
$0_0 - 1_0$	5130.06		5130.04	
$3_{-1} - 3_1$	5130.06		5130.08	
$2_{-1} - 1_{-1}$	5168.52		5168.62	
$2_{-2} - 1_{-1}$	5170.48	5170.58		
$3_{-3} - 2_{-1}$	5176.33		5176.25	
$3_{-2} - 2_{-1}$	5178.62	5178.55		
$4_{-3} - 3_{-3}$	5184.76		5184.65	
$4_{-4} - 3_{-3}$	5187.05	5186.98		
$5_{-5} - 4_{-3}$	5192.61		5192.65	
$5_{-4} - 4_{-3}$	5195.02	5195.02		
$6_{-5} - 5_{-5}$	5200.44		5200.36	
$6_{-6} - 5_{-5}$	5202.78	5202.80		
$7_{-7} - 6_{-5}$	5207.78		5207.82	
$7_{-6} - 6_{-5}$	5210.29	5210.35		
$8_{-7} - 7_{-7}$	5215.00		5215.01	
$8_{-8} - 7_{-7}$	5217.60	5217.62		
$9_{-9} - 8_{-7}$	5221.85		5221.81	
$9_{-8} - 8_{-7}$	5224.60	5224.63		
$10_{-10} - 9_{-9}$	5231.28	5231.32		
$11_{-10} - 10_{-9}$	5237.73	5237.79		

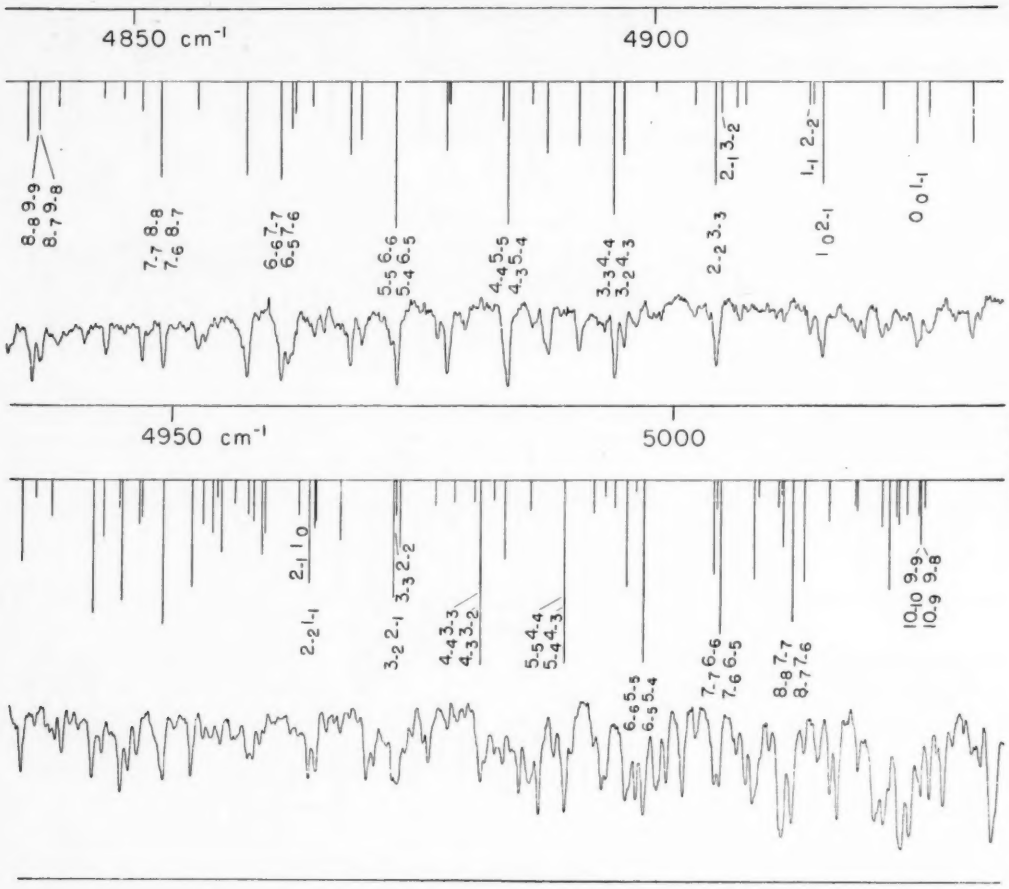

FIG. 2. The infrared absorption spectrum of hydrogen sulfide in the region from 4850 to 5025 cm^{-1}. The pressure was 76 cm of Hg.

quencies for the main wings of the (1,0,1), (2,0,0), and (0,2,1) bands.

ANALYSIS

The previous analysis of this region was compared to the new data and the calculated spectra brought into correspondence with the observed absorption. It was found that the observed absorption could be adequately accounted for in the higher frequency portion by two bands, an A-type band, the (1,0,1) at 5147.36 cm^{-1}, and a B-type band, the lower component of the resonating pair (2,0,0) and (0,0,2) at 5145.12 cm^{-1}. This latter band will henceforth be called the (2,0,0) for convenience. The analysis of the absorption in this region was complicated by the overlapping of the water band at 5332 cm^{-1}. However, sufficient hydrogen sulfide transitions could be assigned to insure a reliable analysis. The absorption extended below 4800 cm^{-1} on the low-frequency end of this region. This seemed to be too low to be attributed to these two bands. A closer inspection revealed a third band centered at about 4940 cm^{-1}. Through the use of known ground-state energy levels[7] it was possible to make assignments and deduce inertial parameters for the excited state of this band. It was necessary to use A-type selection rules to fit this band. This means that n_3 must be odd, hence the vibrational assignment for this band must be (0,2,1). The band center for this band calculated from the quadratic expression for the energy levels,[8] predicts a band center of 4942 cm^{-1} compared to the 4939.23 cm^{-1} which is observed. The quadratic expression also predicts the (1,2,0) band at 4927 cm^{-1}. No evidence for absorption of a band with this excited state was found. It is surprising that no evidence of the (1,2,0) band was found for in most other regions in which an A-type (0,2,1) and a B-type (1,2,0) band are predicted, the B-type band has been found, although in general it has been weaker than the A-type band. Since the (0,2,1) band is already less than $\frac{1}{3}$ as strong as the (1,0,1) and (2,0,0) bands, it is probable that the (1,2,0) band is just too weak to be observed.

The other half of the resonating pair (2,0,0), (0,0,2) is predicted to appear at 5240 cm^{-1}. This also would be a B-type band. No evidence was found for this band either. However, the absorption is so complicated in this region with the R branches of the two strong bands and with strong overlapping H_2O absorption that there would not be much hope of finding it, if it did absorb fairly strongly.

In the (0,2,1) and (1,1,0) bands the mean deviation

[7] P. C. Cross, Phys. Rev. **47**, 7 (1935).

[8] H. C. Allen, Jr., thesis, University of Washington (1951).

of the 100 strongest transitions below $J=8$ is about 0.09 cm^{-1}. The mean deviation for the 100 strongest transitions in the (2,0,0) band is slightly less. These facts offer convincing proof of the essential correctness of the analysis. That some of the individual deviations are greater than the mean must be ascribed to several reasons. First, the effect of a finite slit in integrating the intensities of the numerous close lying transitions giving a resultant peak which does not correspond uniquely to any single transition. Second, a classical centrifugal distortion correction[7] has been used. It is quite possible that this could introduce errors as large as 0.2 cm^{-1} in transitions between levels of intermediate and high τ. Lastly, the (1,0,1) and (2,0,0) as well as the (0,2,1) and (1,2,0), both fit the criteria for Coriolis interaction although no consistent perturbation could be found on any of the individual levels of these bands.

The constants in cm^{-1} giving the fit shown in Figs. 1 and 2 are

	A^*	B^*	C^*	ν_0
(1,0,1)	10.076	8.709	4.608	5147.36
(2,0,0)	10.059	8.719	4.612	5145.12
(0,2,1)	10.871	9.332	4.562	4939.23.

DISCUSSION

In plotting the calculated spectra in Fig. 1, only the strongest transitions have been plotted, i.e., those greater than 1 in an arbitrary relative intensity scale in which the most intense transition is 7.5. The intensities shown are only relative within a given band. No attempt has been made to adjust for the relative magnitude of the dipole moment change among the various bands. It is felt that including the many weaker transitions would only obscure the picture.

The vibrational assignment given the previously unreported band (0,2,1) at 4939 cm^{-1} is further supported by the value of $\Delta=I_C-I_A-I_C=0.56$ gm-cm^2. This is to be compared to the value calculated from the theory of $\Delta=0.56$. Since the observed value is so near that predicted from theory, it is probable the Coriolis interaction between the (0,2,1) and (1,2,0) bands is indeed small. The large value of Δ indicates that n_2 is greater than 1.

The effect of Coriolis interaction between the (1,0,1) and (2,0,0) bands on the inertial constants is apparently combined into the effective moments of inertia. The constants for the two excited states are nearly the same; hence the unperturbed levels will be nearly the same. Since both the energy and the Coriolis perturbation vary very nearly as K^2, such a situation is possible. The intensity of the (2,0,0) band is surprising in view of the fact no evidence was found for the (0,0,2) band. This lends support to the arguments that intensity must be borrowed by the (2,0,0) band from the (1,0,1) band through the Coriolis interaction.

The location of the (0,2,1) band, together with the already known band centers for the (0,2,0)[8] at 2355 cm^{-1}, (0,1,0)[9] at 1183 cm^{-1} and the (1,1,0)[10] at 3789 cm^{-1}, allows the evaluation of the approximate band center of the antisymmetric fundamental (0,0,1) as 2628 cm^{-1}. This is in close agreement with that proposed by Hainer and King[11] and some 50 cm^{-1} lower than the generally accepted value.[10]

The authors wish to thank Professor E. Bright Wilson, Jr., in whose laboratory the analysis was carried out.

[9] H. C. Allen, Jr. and P. C. Cross, J. Chem. Phys. **19**, 140 (1951).

[10] G. Herzberg, *Infrared and Raman Spectra of Polyatomic Molecules* (D. Van Nostrand Company, Inc., New York, 1945), p. 283.

[11] R. M. Hainer and G. W. King, J. Chem. Phys. **15**, 89 (1947).

Frequency Spectrum and Specific Heat of a Face-Centered Cubic Lattice. I

CARL W. GARLAND AND GEORGE JURA
The Department of Chemistry and Chemical Engineering, University of California, Berkeley, California
(Received June 18, 1953)

A Born-von Karman treatment is carried out for a face-centered cubic lattice using the techniques developed by Montroll. The frequency spectrum of the normal modes of vibration has been calculated. From this distribution function C_v is obtained. A power series in $1/T$ has been developed for C_v at high temperatures. An asymptotic approximation is discussed for C_v at very low temperatures. Numerical results are presented for silver; these results are compared with those obtained by Leighton and with experimental data.

I. INTRODUCTION

BORN and von Karman[1] have proposed a method for finding the frequency spectrum and heat capacity of a solid in terms of the dynamics of the crystal lattice. Blackman[2] and Fine[3] have carried out numerical calculations for a simple cubic and body-centered cubic lattice, respectively. Leighton[4] has presented a treatment of silver, a face-centered cubic lattice. He obtained the vibrational distribution function by modeling the constant-frequency surfaces of the secular determinant in plaster and measuring the volume enclosed between successive surfaces. This method obviously is not as general as desired. Recently, Montroll[5,6] has developed a different technique for obtaining the distribution function for simple cubic and body-centered cubic lattices. This method is general in its application, and is applied in this paper to the face-centered lattice. The resulting specific heats are computed for silver. A comparison is made between these values, and those obtained by Leighton,[4] and the experimental results of Keesom and Clark[7] and Meads, Forsythe, and Giauque.[8]

The heat capacity at constant volume is given by the familiar expression

$$C_v=k\int_0^{\nu_L} g(\nu)(h\nu/kT)^2e^{h\nu/kT}d\nu/(e^{h\nu/kT}-1)^2, \quad (1)$$

where ν_L is the maximum vibrational frequency. The distribution function, $g(\nu)$, is defined such that $g(\nu)d\nu$ is the number of normal modes in the interval, ν, $\nu+d\nu$. The problem of calculating C_v lies in formulating an appropriate expression for $g(\nu)$. We shall approximate $g(\nu)$ by a power series in ν. The coefficients of this series will be expressed in terms of the moments of the frequency spectrum as defined by Montroll.[5] These moments will be obtained from the secular equation arising from a Born-von Karman treatment of the dynamics of the lattice.

II. DYNAMICS OF A FACE-CENTERED CUBIC LATTICE

A face-centered cubic lattice with N atoms along each principal axis contains $4N^3$ atoms. One can think of this lattice as four interpenetrating simple cubic lattices of equally spaced atoms with a distance a between nearest neighbors of the same simple cubic lattice, and a distance $a/\sqrt{2}$ between an atom of one simple cubic lattice and the nearest neighbors on the others. The mass of each atom is designated as M. This model is shown in Fig. 1, where the atoms are distinguished by the subscripts l, m, n. Displacements of an atom from its equilibrium position are designated by a vector with components $\mathbf{u}$, $\mathbf{v}$, $\mathbf{w}$ which are defined to be positive in the directions shown in the figure.

The kinetic energy of the system is

$$T=\frac{M}{2}\sum(\dot{\mathbf{u}}^2_{l,m,n}+\dot{\mathbf{v}}^2_{l,m,n}+\dot{\mathbf{w}}^2_{l,m,n}), \quad (2)$$

where the summation is over all the atoms of the crystal. In deriving the potential energy, we make the usual assumptions: (1) only central forces, (2) harmonic displacements, and (3) only the interactions of an atom with its nearest and next nearest neighbors need be considered. The total potential energy is then given by

$$\begin{aligned}V=&\frac{\delta}{2}\sum_{l,m,n}[(\mathbf{u}_{l,m,n}-\mathbf{u}_{l+2,m,n})^2+(\mathbf{v}_{l,m,n}-\mathbf{v}_{l,m+2,n})^2\\&+(\mathbf{w}_{l,m,n}-\mathbf{w}_{l,m,n+2})^2]+\frac{\beta}{2}\sum_{l,m,n}\sum_{a=\pm1}\\&\times\{[(\mathbf{u}_{l,m,n}-\mathbf{u}_{l+1,m,n+a})+a(\mathbf{w}_{l,m,n}-\mathbf{w}_{l+1,m,n+a})]^2\\&+[a(\mathbf{u}_{l,m,n}-\mathbf{u}_{l+a,m+1,n})+(\mathbf{v}_{l,m,n}-\mathbf{v}_{l+a,m+1,n})]^2\\&+[a(\mathbf{v}_{l,m,n}-\mathbf{v}_{l,m+a,n+1})+(\mathbf{w}_{l,m,n}-\mathbf{w}_{l,m+a,n+1})]^2\}.\end{aligned} \quad (3)$$

In the above,

$$2\beta=V''(a_{ij}) \quad \delta=V''(a_{ik}), \quad (4)$$

where V'' is the second derivative of the potential func-

[1] M. Born and T. von Karman, Physik. Z. **13**, 297 (1912); **14**, 15 (1913).
[2] M. Blackman, Proc. Roy. Soc. (London) **148**, 365, 384 (1935); **159**, 416 (1937); Proc. Cambridge Phil. Soc. **33**, 94 (1937).
[3] P. C. Fine, Phys. Rev. **55**, 355 (1939).
[4] R. B. Leighton, Revs. Modern Phys. **20**, 165 (1948).
[5] E. Montroll, J. Chem. Phys. **11**, 481 (1943).
[6] E. Montroll and D. C. Peaslee, J. Chem. Phys. **12**, 98 (1944).
[7] W. H. Keesom and C. W. Clark, Physica **2**, 698 (1935).
[8] Meads, Forsythe, and Giauque, J. Am. Chem. Soc. **63**, 1902 (1941).

tion evaluated at equilibrium, a_{ij} is the distance between nearest neighbors, and a_{ik} is the distance between next nearest neighbors. These expressions for the kinetic and potential energy are now substituted into the Lagrange equations for the crystal. This procedure yields three differential equations describing the motion of the (l,m,n)th atom. The equation describing the motion in the u direction is given below.

$$0=M\ddot{u}_{l,m,n}+\delta(2u_{l,m,n}-u_{l+2,m,n}-u_{l-2,m,n})$$
$$+\beta[8u_{l,m,n}-\sum_{a,b=\pm1}\{(u_{l+b,m,n+a}+u_{l+a,m+b,n})$$
$$+ab(v_{l+a,m+b,n}+w_{l+b,m,n+a})\}]. \quad (5)$$

Next, the boundary conditions are applied and the periodic solutions of these Lagrange differential equations determined. Two procedures are possible. One can make a simple periodic assumption for all the atoms in the lattice; that is, express the displacement coordinates u, v, w of every atom in terms of the same constants u_0, v_0, w_0. If this is done, there are $24N^3$ roots to the secular determinant, whereas a $N\times N\times N$ face-centered cubic lattice has only $12N^3$ degree of freedom, and therefore $12N^3$ normal modes of vibration. To obtain the correct number of normal modes, alternate roots are discarded. In this paper a different assumption is made which will yield just $12N^3$ roots. We assume separate periodic solutions for the atoms in each of the four interlocking simple cubic lattices which make up the face-centered lattice. These solutions are

$$\begin{Bmatrix} u_{l+a,m+b,n+c} \\ v_{l+a,m+b,n+c} \\ w_{l+a,m+b,n+c} \end{Bmatrix} = \begin{Bmatrix} u_0 \\ v_0 \\ w_0 \end{Bmatrix}$$
$$\times\exp[i(2\pi\nu t+(l+a)\phi_1+(m+b)\phi_2+(n+c)\phi_3)], \quad (6)$$

for a, b, $c=0$ or ±2. Nine other equations are written by changing u_0, v_0, w_0, to u_0', v_0', w_0' for $a=0$ or ±2 and b, $c=\pm1$; to u_0'', v_0'', w_0'' for $b=0$ or ±2 and a, $c=\pm1$; to u_0''', v_0''', w_0''' for $c=0$ or ±2 and a, $b=\pm1$. In the equations above, the ϕ_i's are the phase differences of successive atoms in the three directions of the crystal axes of each simple cubic lattice and can be written as

$$\phi_i=2\pi a_i/N \quad i=1,2,3, \quad (7)$$

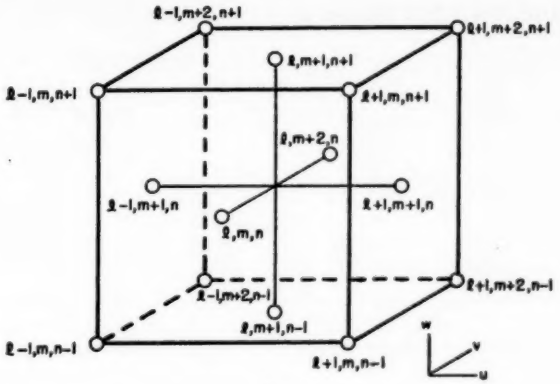

FIG. 1.

where a_i's are integers such that $-N/2\leq a_i\leq N/2$. In this way we achieve an independent solution for each degree of freedom of the system.

Substituting these solutions (6) into the differential equations of motion one obtains twelve equations of the following form

$$(8\beta+4\delta\sin^2\phi_1-4\pi^2\nu^2M)u_0-4\beta u_0''\cos\phi_1\cos\phi_3$$
$$-4\beta u_0'''\cos\phi_1\cos\phi_2+4\beta v_0'''\sin\phi_1\sin\phi_2$$
$$+4\beta w_0''\sin\phi_1\sin\phi_3=0.$$

The above can be simplified by letting

$$\alpha=\beta/4\pi^2M, \quad \gamma=\delta/4\pi^2M, \quad (8)$$

and

$$b_i=8\alpha+4\gamma\sin^2\phi_i,$$
$$a_{ij}=4\alpha\sin\phi_i\sin\phi_j, \quad (9)$$
$$b_{ij}=4\alpha\cos\phi_i\cos\phi_j.$$

One now has

$$(b_1-\nu^2)u_0-b_{13}u_0''-b_{12}u_0'''+a_{12}v_0'''+a_{13}w_0''=0,$$

and eleven similar equations in the twelve variables $u_0,\ldots,w_0'''$.

For this set of simultaneous equations to yield solutions different from zero, the determinant of the coefficients of the variables must equal zero. By successive subtraction and addition of rows and columns, this 12 by 12 determinant can be factored into the four 3 by 3 determinants given below. The notation used is such that the upper *subscript* on $|U^2|$ is associated with the upper sign in the expressions $\pm$ and $\mp$.

$$|U_1^2|=\begin{vmatrix} b_1\mp b_{12}\mp b_{13}-\nu^2 & \pm a_{12} & \pm a_{13} \\ \pm a_{12} & b_2\mp b_{12}-b_{23}-\nu^2 & a_{23} \\ \pm a_{13} & a_{23} & b_3\mp b_{13}-b_{23}-\nu^2 \end{vmatrix}=0$$
$$|U_3^2|=\begin{vmatrix} b_1\pm b_{12}\mp b_{13}-\nu^2 & \mp a_{12} & \pm a_{13} \\ \mp a_{12} & b_2\pm b_{12}+b_{23}-\nu^2 & -a_{23} \\ \pm a_{13} & -a_{23} & b_3\mp b_{13}+b_{23}-\nu^2 \end{vmatrix}=0. \quad (10)$$

Equations (10) yield 12 of the $12N^3$ normal modes. The characteristic determinant is a function of ϕ_i's, and therefore of a_i's. Since the a_i's have N integral values from $-N/2$ to $N/2$, the secular determinant for the

entire $N\times N\times N$ lattice is

$$|U^2_{\text{total}}| = \begin{vmatrix} U_1^2(-N/2,-N/2,-N/2) & & & & \\ \cdots & & & & \\ & U_1^2(N/2,N/2,N/2) & & 0 & \\ & & U_2^2(-N/2,-N/2,-N/2) & & \\ & & \cdots & & \\ & & & U_2^2(N/2,N/2,N/2) & \\ & & & & U_3^2(-N/2,-N/2,-N/2) \\ & & & & \cdots \\ & & & & U_3^2(N/2,N/2,N/2) \\ & 0 & & & U_4^2(-N/2,-N/2,-N/2) \\ & & & & \cdots \\ & & & & U_4^2(N/2,N/2,N/2) \end{vmatrix} = 0. \tag{11}$$

III. USE OF THE MOMENTS OF THE FREQUENCY SPECTRUM TO DETERMINE THE DISTRIBUTION FUNCTION AND THE HEAT CAPACITY

Since the distribution function is an even function, the odd moments of $g(\nu)$ vanish. The even moments μ_{2n} are given by

$$\mu_{2n}=\int_0^\infty \nu^{2n}g(\nu)d\nu/12N^3, \tag{12}$$

where the upper limit of integration may be replaced by ν_L, since $g(\nu)$ is zero for $\nu>\nu_L$. Montroll[5] has shown that these moments can be obtained from the traces of the powers of the matrix U^2_{total}. For the face-centered case,

$$\mu_{2n}=(1/12N^3)\ \text{Trace}\ U_i^{2n}. \tag{13}$$

Using these definitions of μ_{2n}, one can write a high-temperature series expression for C_v and a least squares approximation of the distribution function.

At high temperatures one can express the heat capacity as a power series in $1/T$. Montroll[5] has shown that

$$C_v/12N^3k=1-\sum_{n=1}^{\infty}(-1)^n(1-2n)B_n(h/kT)^{2n}\mu_{2n}/(2n)!. \tag{14}$$

These series converge for $T>h\nu_L/2\pi k$, and the first few Bernoulli numbers are $B_1=1/6$, $B_2=1/30$, $B_3=1/42$. If the moments of the distribution function are known, then the specific heat can be calculated at high temperatures from (14).

The next problem is to develop a polynomial approximation to $g(\nu)$ in terms of the moments. The approximating function chosen is

$$g(\nu)=\sum_{n=0}^{k-1}a_{2n}(\nu/\nu_L)^{2n}, \tag{15}$$

where the odd coefficients a_{2n+1} in the power series have been set equal to zero since $g(\nu)=g(-\nu)$. Montroll[5] has applied the calculus of variations to find the coefficients a_{2n} which give the best fit of this polynomial to $g(\nu)$ in the least squares sense. After considerable manipulation it is possible to write an expression in terms of the moments for $a_i(k)=a_{2n}$, (where $i=n+1$ and $k-1=$ largest value of n)

$$a_i(k)=\frac{(2i+2k-3)!}{2^{4k-4}(2i-2)!(i+k-2)!(k-i)!}\sum_{j=1}^{k}\times\frac{(-1)^{i+j}(2j+2k-3)!\mu_j(k)}{(2j-2)!(j+k-2)!(k-j)![2(i+j)-3]}, \tag{16}$$

where

$$\mu_j(k)=(12N^3/\nu_L)\mu_{2(j-1)}/\nu_L^{2(j-1)}. \tag{17}$$

The equation in Montroll's[5] paper from which the above (16–17) is taken contains several typographical errors which have been eliminated from the above. Thus, if the moments of the distribution function are known, it is possible to calculate the coefficients a_{2n} of the polynomial approximation to $g(\nu)$ defined in Eq. (15).

IV. COMPUTATION OF THE MOMENTS

We have seen from Eq. (13) that the moments may be obtained directly from the trace of the matrix $U_{\text{total}}{}^{2n}$. Two methods will be used to compute these traces thus providing a check on the moments calculated.

If we write

$$\Sigma=\sum_{a_1,a_2,a_3=-N/2}^{N/2}\sum\sum\sum,$$

we see from Eqs. (11) and (13) that

$$\mu_{2n}=(1/12N^3)\Sigma\sum_{i=1}^{4}\text{Trace}\ U_i^{2n}. \tag{18}$$

Since we now have the moments as functions of the traces of powers of 3×3 symmetrical matrices, it is convenient to use formulas given by Montroll[5] for the traces of powers of a general symmetric matrix. Also useful are expressions for the sums over a_i's of the powers of sines and cosines.[6] The above is the necessary machinery for the calculation of the moments.

Moments have been calculated up to μ_{12}. These can

TABLE I. Coefficients b_{nm} of $\mu_{2n}/\nu_L^{2n}=\sum_{m=0}^{n} b_{nm}\tau^m$.

n \ m	0	1	2	3	4	5	6
0	1						
1	1/2	1/4					
2	5/16	1/4	3/32				
3	57/256	15/64	9/64	5/128			
4	703/4096	115/512	179/1024	5/64	35/2048		
5	4549/32768	3585/16384	3415/16384	1975/16384	175/4096	63/8192	
6	30353/262144	3513/16384	63669/262144	2803/16384	1287/16384	189/8192	231/65536

be written in the form

$$\mu_{2n}/(8\alpha)^n=\sum_{m=0}^{n} c_{nm}(\gamma/2\alpha)^m. \tag{19}$$

The matrices of the secular Eqs. (10) can be written in the form

$$U_i^2=4\gamma A+8\alpha B_i, \tag{20}$$

where A is a diagonal matrix, and B_i a symmetrical matrix, and neither A nor B contain α or γ. Then,

$$U_i^{2n}=(4\gamma)^n[A+(2\alpha/\gamma)B_i]^n.$$

This can be expanded and rearranged to give

$$U_i^{2n}=(8\alpha)^n\left\{\left(\frac{\gamma}{2\alpha}\right)^n A^n+\left(\frac{\gamma}{2\alpha}\right)^{n-1}\times\sum_{n_1=1}^{n} A^{n-n_1}B_iA^{n_1-1}+\left(\frac{\gamma}{2\alpha}\right)^{n-2}\sum_{n_1=2}^{n}\sum_{n_2=2}^{n_1}\times A^{n-n_1}B_iA^{n_1-n_2}B_iA^{n_2-2}+\cdots\right\}. \tag{21}$$

Substituting (21) into Eq. (18), and comparing the result with (19) we see that

$$(1/12N^3)\Sigma\sum_{i=1}^{4}\text{Trace}\,A^n=c_{nn} \tag{22}$$

$$(1/12N^3)\Sigma\sum_{i=1}^{4}\text{Trace}\sum_{n_1=1}^{n}A^{n-n_1}B_iA^{n_1-1}=c_{n,n-1},$$

and similarly for the other coefficients down to c_{n0}. The first few coefficients are $c_{nn}=(2n)!/4^n n!n!$ and

$$c_{n,n-1}=n(2n-2)!/4^{n-1}(n-1)!(n-1)!.$$

All coefficients, c_{nm}, have been computed by both methods.

The largest frequency ν_L corresponds to the largest root of (11). Blackman[2] has shown that maxima should occur in an equation of this type when ϕ_1, ϕ_2, and ϕ_3 have any of the values $0, \pi/2$, and π; with $0,0,0$ excluded. Remembering that for a face-centered cubic crystal γ is negative, trial solutions give $\nu_L^2=16\alpha$. This is in agreement with the expression used by Leighton.[4] If we now define a new parameter $\tau=\gamma/2\alpha$ and use $\nu_L^2=16\alpha$, Eq. (19) can be written

$$\mu_{2n}/\nu_L^{2n}=\sum_{m=0}^{n} b_{nm}\tau^m;\quad b_{nm}=c_{nm}/2^n. \tag{23}$$

The coefficients b_{nm} have been listed in Table I.

V. FREQUENCY SPECTRUM

Substituting the moments given in Table I into Eqs. (16)–(17), one can calculate the coefficients a_{2n} of the polynomial approximation

$$g(\nu)=\sum_{n=0}^{6} a_{2n}(\nu/\nu_L)^{2n}.$$

It is now possible to rewrite this expression in a more convenient form:

$$\nu_L g(\nu)/12N^3=\sum_{m=0}^{6}[\sum_{s=0}^{6} d_{ms}(\nu/\nu_L)^{2s}]\tau^m. \tag{24}$$

The coefficients d_{ms} are tabulated in Table II. To facilitate numerical calculation of $g(\nu)$, $\sum_s d_{ms}(\nu/\nu_L)^{2s}$ has been computed for various values of ν/ν_L from zero to one, and these sums are given in Table III. This table is sufficient for the calculation of $g(\nu)$ for the small values of τ which occur in face-centered cubic crystals.

TABLE II. Coefficients d_{ms} of Eq. (24) coefficients of τ^m.

Coefficients of x^{2s} \ m	0	1	2	3	4	5	6
0	+0.041215	−0.24238	+0.41416	+11.7450	+33.5243	−3.4360	+13.1237
1	−0.052815	+29.0011	−17.0387	−1246.5354	−2495.3828	+103.0806	−1023.6476
2	+13.6611	−700.3752	+949.1704	+18 032.4355	+30 627.9148	+223.3413	+12 795.5952
3	+177.5527	+3926.0500	−7976.1978	−89 595.4258	−138 164.8761	−6253.5563	−58 006.6980
4	−813.9070	−8625.9516	+23 206.7703	+194 796.0307	+281 671.1286	+21 153.6113	+118 085.0639
5	+1106.3295	+8183.9217	−27 546.0702	−191 284.3088	−264 068.5871	−26 107.5341	−110 212.7263
6	−484.4041	−2804.9644	+11 447.1168	+69 447.3700	+92 559.6056	+10 930.1877	+38 407.4652

TABLE III. Coefficients p_m of $\nu_L g(\nu)/12N^3=\Sigma p_m \tau^m$.

ν/ν_L	p_0	p_1	p_2	p_3	p_4	p_5	p_6
0.10	0.04222	−0.01857	0.33094	0.9951	11.4979	−2.3890	4.1100
0.20	0.07036	0.02708	0.79744	−14.5192	−25.4344	0.6958	−10.7704
0.25	0.12324	−0.33113	1.43815	−14.8041	−32.4768	2.6508	−13.3343
0.30	0.22943	−0.96234	2.12033	−8.0076	−26.7260	4.3311	−10.5300
0.35	0.41174	−1.70882	2.41273	3.7670	−10.0766	5.0674	−3.2101
0.40	0.68423	−2.29272	1.82865	15.7157	10.8737	4.4688	5.7879
0.45	1.03979	−2.39980	0.08544	21.9919	26.9552	2.1021	12.5422
0.50	1.43892	−1.80884	−2.60476	18.2857	30.0930	−1.6146	13.5988
0.55	1.80605	−0.53090	−5.35373	4.4916	17.4154	−5.5461	7.7223
0.60	2.04119	1.09956	−6.70281	−13.7943	−5.9026	−7.9182	−2.8747
0.65	2.05255	2.44948	−5.17050	−26.3212	−27.0457	−6.9120	−12.6588
0.70	1.81044	2.78620	−0.27202	−22.7455	−30.7704	−1.7486	−14.9302
0.75	1.40909	1.66539	6.24579	−0.3707	−9.4063	5.9859	−6.0354
0.80	1.09967	−0.57323	9.73028	27.8860	25.6527	11.5127	9.6829
0.85	1.22167	−2.44989	4.12431	32.7001	39.9659	8.0821	17.8625
0.90	1.90320	−1.64079	−11.47827	−10.9725	−2.5124	−6.9932	2.3706
0.925	2.26816	0.32579	−18.19860	−42.7722	−39.4663	−15.1451	−12.8495
0.950	2.32332	3.17154	−16.53553	−57.3207	−61.5301	−17.0014	−23.4044
0.975	1.57460	6.11411	4.84571	−13.2402	−21.8338	−2.3030	−10.8502

In Fig. 2 we have plotted $\nu_L g(\nu)/12N^3$ as a function of (ν/ν_L) for τ equal to -0.08 and -0.15 using Table III. It can be noticed that the distribution function is not highly sensitive to changes in the ratio of the force constants τ. As in the case of simple cubic and body-centered cubic lattices calculated by Montroll,[5-6] there are two peaks in the distribution function. These peaks occur at approximately the same frequencies as those in the frequency spectrum given by Leighton[4] for a face-centered cubic lattice. Van Hove[9] has made a general prediction on topological grounds concerning the distribution function for any three-dimensional crystal. He states that (1) $g(\nu)$ is continuous, and (2) $dg(\nu)/d\nu$ has at least two infinite discontinuities and takes the value $-\infty$ at the upper end of the spectrum. The distribution function given here satisfies these predictions except that the small number of moments used to fit the polynomial approximation to $g(\nu)$ in a least squares sense does not permit location of any discontinuities in slope.

Also because of this roughness in the curve fitting, the polynomial approximation is poor at very small ν/ν_L and does not go to zero at $\nu/\nu_L=0$ as it should. In this low-frequency range we shall discuss an asymptotic approximation.

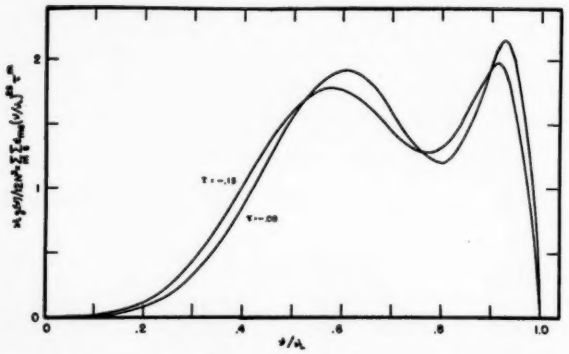

FIG. 2. Frequency spectrum of a face-centered cubic lattice. $\nu_L g(\nu)/12N^3$ is plotted *versus* (ν/ν_L) for $\tau=-0.08$ and -0.15.

[9] L. Van Hove, Phys. Rev. **89**, 1189 (1953).

VI. LOW-FREQUENCY APPROXIMATION

An attempt to find an asymptotic approximation valid at low frequencies has been made by following the development suggested by Montroll[5-6] for simple and body-centered cubic lattices. A drastic simplification is achieved in this procedure by neglecting the off diagonal elements of the secular determinants U_i^2. It is then possible to solve Eq. (10) analytically for ν in terms of α and γ. From these solutions one obtains at very small ν,

$$g(\nu)/12N^3=\frac{16}{\pi^2(1+2\tau)^{\frac{1}{2}}}(\nu/\nu_L)^2. \tag{25}$$

From the above it follows that C_v at low temperatures is given by

$$C_v/3R=\frac{64\pi^2}{15(1+2\tau)^{\frac{1}{2}}}\left(\frac{kT}{h\nu_L}\right)^3. \tag{26}$$

Rough numerical calculations indicate that inclusion of the off diagonal terms will increase $g(\nu)$ considerably from the value given by (25). Therefore, Eqs. (25) and (26) are not good approximations even at the lowest temperatures, and the results presented here in the low-temperature region represent merely a lower limit for C_v. A detailed study of the distribution function at low frequencies is reported in the following paper.

VII. SPECIFIC HEAT OF SILVER

Leighton[4] has given a value for the ratio of the force constant between next nearest neighbors to the force constant between nearest neighbors, and a value for the nearest neighbor force constant at absolute zero for silver. Using Eqs. (4), (8), and the definitions of τ and

ν_L given in Sec. IV, we find

$$\tau=-0.08 \quad \nu_L=4.90\times10^{12}. \tag{27}$$

With these values we are now able to calculate C_v for silver from 0°K to 200°K, and compare the results with the experimental data of Keesom and Clark[7] and Mead, Forsythe, and Giauque.[8]

Using the moments exhibited in Table I, one can calculate the first seven terms of the power series for C_v given in Eq. (14). The first few terms of this series are shown below.

$$C_v/3R=1-(x^2/24)(1+\tfrac{1}{2}\tau) +(x^4/960)(10/8+\tau+3\tau^2/8)-\cdots, \tag{28}$$

where x equals $(h\nu_L/kT)$. In the case of silver, $x=235/T$ and the series converges for $T>37$°K. The heat capacity can be computed down to 50°K with a maximum error of a few percent using the seven terms available here. Values of C_v from 50°K to 200°K were obtained using (28).

Fourteen values of C_v from 5°K to 137°K were obtained by graphical integration of (1) using the appropriate distribution function shown in Fig. 2. In the overlap region from 50°K to 137°K the heat capacities calculated from the two methods above are in excellent agreement.

At temperatures below 5°K, C_v was obtained by substituting the values of τ and ν_L in Eq. (26). For silver, $C_v/3R=3.54\times10^{-6}T^3$. This is a T^3 dependence as is the expression from the Debye theory. This constant can be attained using the Debye expression for C_v if θ_D is set equal to 280. This value is higher than the empirical value determined by experiment. Thus, our formula (26) predicts heat capacities at low temperatures which are lower than the experimental values. It was pointed out in Sec. VI that the low temperature approximation is inadequate as a result of neglecting the off diagonal terms in the secular determinant. The rough correction factor discussed there will correct C_v in the right direction and, it is hoped, by about the proper amount to make the theory agree with experiment. At this time, our low temperature results only give a lower limit on C_v (or upper limit on θ_D).

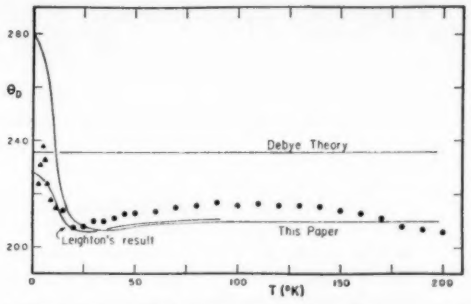

FIG. 3. Heat capacity of silver: equivalent Debye θ *vs* temperature. The experimental data of Mead, Forsythe, and Giauque are represented by circles, that of Keesom and Clark by triangles. The latter data are in agreement with the data of the more recent investigation of Keesom and Pearlman.

A comparison of our results with the experimental data, the result from the Debye theory, and the result obtained by Leighton[4] is presented in Fig. 3. This comparison is given in terms of the equivalent Debye temperature (the value of θ_D at a given temperature which when used in the Debye theory will give the desired C_v) which is a very sensitive parameter at low T. Our result is much better than that from the Debye treatment. Except at the lowest temperatures, where the treatment is known to be inadequate, it agrees well with experiment as does Leighton's result. Our calculation has the advantage of greater generality than Leighton's since it gives expressions for $g(\nu)$ in terms of any arbitrary value of the interatomic force constants.

Frequency Spectrum and Specific Heat of a Face-Centered Cubic Lattice. II. Low Temperature Region

CARL W. GARLAND AND GEORGE JURA
The Department of Chemistry and Chemical Engineering, University of California, Berkeley, California

(Received June 18, 1953)

From the Born-von Kármán treatment of a face-centered cubic lattice a simplified secular equation valid for low frequencies has been obtained. The frequency spectrum of low frequency normal modes of vibration has been calculated using the root sampling technique of Blackman. From this distribution function a T^3 law is obtained for C_v at low temperatures. The effect on the low temperature specific heat of including interactions with neighbors more remote than the next nearest neighbors is discussed. Numerical results are presented for silver.

IN the preceding paper[1] the heat capacity of a face-centered cubic lattice was computed using Montroll's development of the treatment suggested by Born and von Kármán. The computations were made for a single value of the ratio of the force constants of the nearest and next nearest neighbors, -0.08. This permitted the evaluation of the heat capacity of silver from 0°K to high temperatures. The agreement between observed and computed results was as good as could be expected for temperatures above 10°K. Below this temperature, this treatment gave poor results in that the computed heat capacity was about one-half that observed. The asymptotic approximation used for C_v at low temperatures was felt to be inadequate due to the drastic assumption of neglecting the off-diagonal elements of the secular determinant. From the work which was done, it was apparent that the amount of arithmetical labor involved in extending the method of moments to obtain more reliable specific heat computations at the lowest temperatures would be prohibitive. Therefore, for better results, it was necessary to use another technique. The root sampling technique suggested by Blackman[2] was found to be more satisfactory. The final results for silver, which gave a T^3 law for C_v, are in fair agreement with the experimental values at very low temperatures. We feel, however, that the results are not final. The work involved in getting better results would be prohibitive without the use of an electronic computing machine.

The specific heat is given by the usual expression

$$C_v = k\int_0^{\nu_L} g(\nu)(h\nu/kT)^2 e^{h\nu/kT}d\nu/(e^{h\nu/kT}-1)^2, \quad (1)$$

where all of the symbols have their usual significance. We wish to evaluate $g(\nu)$ for low frequencies in order to obtain the specific heat as the temperature approaches zero. The secular equations of motion for a face-centered lattice are given in Eq. (10) of Paper I. These are derived with the aid of the usual assumptions: (1) central forces, (2) harmonic displacements, (3) only nearest and next nearest neighbors need be considered, and (4) the Born-von Kármán periodic boundary conditions.

In order to find a solution valid at low temperatures we must find values for the a_i's (or ϕ_i's) which give roots of Eqs. (10) of Paper I close to zero since only the low frequency modes of vibration are important at low temperatures. To make the roots approach zero in U_1^2 we let ϕ_1, ϕ_2, ϕ_3 approach (0,0,0) or $(\pm\pi,\pm\pi,\pm\pi)$; in U_2^2, $(0,\pm\pi,\pm\pi)$ or $(\pm\pi,0,0)$; in U_3^2, $(0,\pm\pi,0)$ or $(\pm\pi,0,\pm\pi)$; in U_4^2, $(0,0,\pm\pi)$ or $(\pm\pi,\pm\pi,0)$. Making the trigonometric substitutions $\sin\phi=\phi$ and $\cos\phi=1-\phi^2/2$ in the first case above, and other appropriate substitutions in the other cases, each characteristic determinant, U_i^2, reduces to

$$\begin{vmatrix} \left(1+\frac{\gamma}{\alpha}\right)\frac{a_1^2}{N^2}+\frac{1}{2}\left(\frac{a_2^2}{N^2}+\frac{a_3^2}{N^2}\right)-(1/\pi^2)(\nu/\nu_L)^2 & \frac{a_1a_2}{N^2} & \frac{a_1a_3}{N^2} \\ \frac{a_1a_2}{N^2} & \left(1+\frac{\gamma}{\alpha}\right)\frac{a_2^2}{N^2}+\frac{1}{2}\left(\frac{a_1^2}{N^2}+\frac{a_3^2}{N^2}\right)-(1/\pi^2)(\nu/\nu_L)^2 & \frac{a_2a_3}{N^2} \\ \frac{a_1a_3}{N^2} & \frac{a_2a_3}{N^2} & \left(1+\frac{\gamma}{\alpha}\right)\frac{a_3^2}{N^2}+\frac{1}{2}\left(\frac{a_1^2}{N^2}+\frac{a_2^2}{N^2}\right)-(1/\pi^2)(\nu/\nu_L)^2 \end{vmatrix} = 0, \quad (2)$$

[1] Hereafter referred to as Paper I.
[2] M. Blackman, Proc. Roy. Soc. (London) **159A**, 416 (1937).

where $a_i=N\phi_i/2\pi$ (as defined by Eq. (7) of Paper I), ν_L is the maximum vibrational frequency, and $\gamma/2\alpha$ is the ratio of the next-nearest neighbor force constant to the nearest-neighbor force constant. The trigonometric approximations are good within one percent for $|a_i|<N/20$. Since there are seven other regions in a_i (or ϕ_i) space which give the same expression as Eq. (2) for points near (0,0,0), we can deal only with this region and multiply the result by eight. Also the roots of Eq. (1) are unaltered by changes in sign of the a_i's; thus we need consider only the positive octant of a_i space about (0,0,0).

If we let

$$b_i=ya_i/N \quad \text{and} \quad x=(y^2/\pi^2)(\nu/\nu_L)^2, \tag{3}$$

Eq. (2) can be written as

$$\begin{vmatrix} \left(1+\frac{\gamma}{\alpha}\right)b_1^2+\tfrac{1}{2}(b_2^2+b_3^2)-x & b_1b_2 & b_1b_3 \\ b_1b_2 & \left(1+\frac{\gamma}{\alpha}\right)b_2^2+\tfrac{1}{2}(b_1^2+b_3^2)-x & b_2b_3 \\ b_1b_3 & b_2b_3 & \left(1+\frac{\gamma}{\alpha}\right)b_3^2+\tfrac{1}{2}(b_1^2+b_2^2)-x \end{vmatrix}=0. \tag{4}$$

The advantage of this change from (2) to (4) is as follows. It is desired to calculate roots of Eq. (4) for 1000 uniformly distributed points in the positive octant of a_i space about (0,0,0). These are points for which $b_i=1, 2, \cdots, 10$. Substitution of all possible combinations b_1, b_2, b_3 into (4) would yield 1000 cubic equations to be solved, of which only 220 are distinct. Before solving these 220 equations, a value must be chosen for $(1+\gamma/\alpha)$. In this work we have set the ratio of force constants, $\gamma/2\alpha$, equal to -0.08, the value given by Leighton[3] for silver. The cubic equations were solved by using Graeffe's root-squaring method. The 3000 roots are found only for this value of the force constant ratio. The roots will give the frequencies, ν/ν_L, which correspond to any arbitrary sized cell in a_i space. One merely chooses a cell such that the largest value of a_i is $10N/y$. Having thus fixed the value of y, the values of ν/ν_L for this cell are calculated directly from the roots using Eq. (3).

The quantity which we wish to compute from these roots is the vibrational distribution function $g(\nu)$ which depends on $N(\nu)$, the number of normal modes of vibration less than a given frequency ν. This $N(\nu)$ is equal to the fraction of the 3000 calculated frequencies which are less than a given ν *times* the total number of frequencies which are present in the cell for which these frequencies were calculated, *times* 64. The factor 64 accounts for the fact that we are considering only one octant of one out of eight equivalent regions in a_i space. For a cell in a_i space for which the maximum a_i equals $10N/y$,

$$N(\nu)=(64N^3/y^3)N_{<\nu}, \tag{5}$$

where $N_{<\nu}$ is the number of calculated frequencies less than a given ν and is directly obtained from the frequencies which are determined from the roots of Eq. (4). The procedure is to fix a value of y, find $N_{<\nu}$ by counting the number of roots which correspond to frequencies less than a given ν/ν_L, and then compute $N(\nu)$ for that ν/ν_L using Eq. (5). Decreasing the cell size in a_i space (by increasing y), one can obtain better values of $N(\nu)$ at lower frequencies. This is true since for a smaller cell one has a denser distribution of calculated roots in the lower frequency region and therefore a better approximation. Values of y were varied from 200 (the largest cell for which the trigonometric approximations hold) to 3000; values of $N(\nu)$ were obtained from $\nu/\nu_L=0.005$ to 0.125. A plot of $N(\nu)/N^3$ *versus* $(\nu/\nu_L)^3$ gave an excellent straight line (see Fig. 1) which is given by

$$N(\nu)/N^3=10.9(\nu/\nu_L)^3. \tag{6}$$

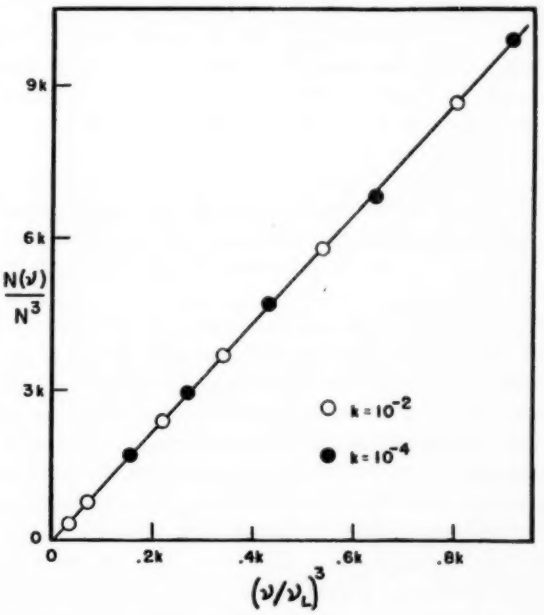

FIG. 1. Plot of $N(\nu)/N^3$ *versus* $(\nu/\nu_L)^3$. The points for very low frequencies have been plotted as solid circles on the expanded scale, with $k=10^{-4}$, to show that the linearity holds well over the entire range. The highest frequency for which this line is valid is $\nu/\nu_L=0.125$.

[3] R. B. Leighton, Revs. Modern Phys. **20**, 165 (1948).

Equation (6) is in agreement with a dimensional analysis of (4).

Since the vibrational distribution function $g(\nu)=\partial N(\nu)/\partial\nu$,

$$g(\nu)=32.7(N^3/\nu_L^3)\nu^2. \tag{7}$$

Substituting this $g(\nu)$ into Eq. (1) we find

$$Cv/3R=\frac{32.7}{12}\left(\frac{kT}{h\nu_L}\right)^3\int_0^{h\nu_L/kT}\frac{x^4e^x dx}{(e^x-1)^2}. \tag{8}$$

As $T\to 0$, the upper limit of this integral approaches infinity. Since

$$\int_0^\infty \frac{x^4e^x dx}{(e^x-1)^2}=\frac{4\pi^4}{15},$$

one obtains for C_v at very low temperatures

$$Cv/3R=\frac{32.7}{12}\left(\frac{4\pi^4}{15}\right)\left(\frac{kT}{h\nu_L}\right)^3=70.35\left(\frac{kT}{h\nu_L}\right)^3. \tag{9}$$

Substituting into (9) $\nu_L=4.90\times10^{12}$, the value for silver given in Paper I, one computes a specific heat which corresponds to an equivalent Debye θ of 243. The approximation used here is valid up to about 2.5°K. The experimental value of θ_D is 230 and the value from the Debye theory using the same elastic constants is 233.[4] Therefore the present calculated C_v is about 15 percent below the experimental values in contrast to 100 percent low from the approximation made in Paper I.

The secular equation was also derived including the interactions of the next-next-nearest neighbors to see what effect this has on the calculated specific heats. When these new terms are included, one finds a characteristic determinant very similar to Eq. (2) for low frequencies, but involving three force constants rather than the two previously used. Both Eq. (2) and this new secular equation can be transformed into equations in reciprocal space and identified with the Born "dynamical matrix" of the lattice.[5] It is then possible in each case to correlate combinations of the force constants with the elastic constants. When this is done, both the low frequency secular Eq. (2) and the equation involving all neighbors up to the next-next nearest reduce to the same equation in terms of the elastic constants,

$$\begin{vmatrix}
\left(1+\frac{c_{11}-c_{12}}{c_{44}}\right)\frac{a_1^2}{N^2}+\frac{a_2^2}{N^2}+\frac{a_3^2}{N^2}-Mv^2/dc_{44} & \frac{2a_1a_2}{N^2} & \frac{2a_1a_3}{N^2} \\
\frac{2a_1a_2}{N^2} & \left(1+\frac{c_{11}-c_{12}}{c_{44}}\right)\frac{a_2^2}{N^2}+\frac{a_1^2}{N^2}+\frac{a_3^2}{N^2}-Mv^2/dc_{44} & \frac{2a_2a_3}{N^2} \\
\frac{2a_1a_3}{N^2} & \frac{2a_2a_3}{N^2} & \left(1+\frac{c_{11}-c_{12}}{c_{44}}\right)\frac{a_3^2}{N^2}+\frac{a_1^2}{N^2}+\frac{a_2^2}{N^2}-Mv^2/dc_{44}
\end{vmatrix}=0, \tag{10}$$

where d is the lattice cell constant. In obtaining (10) use was made of the fact that only the elastic constants c_{44} and $c_{11}-c_{12}$ are independent of the Fermi electron gas pressure.[3]

The fact that both secular equations reduced to the same equation in the elastic constants means that inclusion of next-next-nearest neighbors will not alter the low frequency distribution function or the heat capacity at low temperatures calculated from it. It should be emphasized, though, that no conclusions can be drawn concerning the effect of considering the next-next-nearest neighbors at high temperatures. For $(c_{11}-c_{12})/c_{44}=0.68$ (the value used in solving the representative sample of roots of Eq. (4)), the specific heat at low temperatures is given in terms of the elastic constant c_{44} by

$$C_v/3R=70.35(M/2dc_{44})^{\frac{3}{2}}(\pi kT/h)^3, \tag{11}$$

where M is the atomic mass. Heat capacities calculated from Eq. (11) give the same results as Eq. (9) for silver, but the assumption of only nearest and next-nearest neighbor interactions has been removed.

Disagreement between the calculated and experimental specific heats is most probably due to (1) possible errors in the values of the elastic constants used at low temperatures, (2) the assumption of central forces, and (3) inadequate sampling of roots. The distribution function is not highly sensitive to changes in $(c_{11}-c_{12})/c_{44}$, but a change in c_{44} from 4.4×10^{11} to 4.0×10^{11} would bring the calculated C_v into agreement with experiment. Both the abandonment of central forces and the calculation of a significantly greater number of roots of Eq. (4) would entail considerably more mathematical labor. The effect of the central force

[4] P. H. Keesom and N. Pearlman, Phys. Rev. **88**, 140 (1952).
[5] H. M. J. Smith, Phil. Trans. Roy. Soc. (London) **A241**, 105 (1948).

approximation cannot be readily predicted. We believe that the present result may be low owing to inadequate root sampling. When the calculation was made by dividing a cell into 216 instead of 1000 parts, the computed value of the effective Debye temperature was 270. Also, this computation did not give a T^3 dependence over any finite range of temperature and the internal agreement between values of $N(\nu)$ calculated in different cells was not good. The present work indicates that any changes in $g(\nu)$ resulting from a more extensive root sampling can only increase the calculated specific heats.

THE JOURNAL OF CHEMICAL PHYSICS VOLUME 22, NUMBER 6 JUNE, 1954

Equilibrium Constant, Infrared Spectrum, and Thermodynamic Properties of Bromine Chloride

H. C. MATTRAW, C. F. PACHUCKI AND N. J. HAWKINS
Knolls Atomic Power Laboratory, General Electric Company, Schenectady, New York*
(Received January 25, 1954)

The equilibrium constant of 0.15 for the gaseous system $2BrCl = Br_2 + Cl_2$ has been determined by means of a mass spectrometer. The fundamental vibration frequency of BrCl was observed at 439.5 cm^{-1} wave numbers in the infrared spectrum. The thermodynamic properties $-(F-E_0^0)$, S, and Cp were calculated for one mole of gas at atmospheric pressure from 100–1000°K. From the thermodynamic properties, equilibrium constant and known standard state properties of Br_2 and Cl_2, the standard state properties of BrCl were computed. There was no evidence for the existence of $BrCl_3$.

1. INTRODUCTION

THE ability to modify or increase the reactivity of the halogens by using the interhalogens, such as ICl, BrF_3, ClF_3, and BrCl, has led many investigators to study the properties of these compounds. However, the properties of one of the main members of this group of compounds BrCl have not been fully established. In particular, the problems of the existence, the fundamental vibration frequency and the equilibrium constant of formation have been extant since the compound was thought to have been discovered.[1] Recent reviews of the interhalogen field and BrCl are given by Greenwood[2] and Beeson and Yost,[3] respectively.

The equilibrium $2BrCl = Br_2 + Cl_2$ has been studied by the following methods: absorption in the ultraviolet in various solvents,[4] emf measurements in HCl solutions,[5] equilibria in complex systems involving salt halides[6] and nitrogen oxide and oxyhalides.[3] Most of these experiments have given values for the equilibrium constant from 0.11 to 0.34 at room temperature. It is noteworthy that no direct measurement of the equilibrium constant of the two component gaseous equilibrium has been reported. Such a direct method is available with the mass spectrometer. By this means a value of 0.15 has been obtained in this study.

In addition to the solution studies by ultraviolet absorption, there have been a variety of other spectroscopic measurements to obtain the constants required for the calculation of the thermodynamic properties of BrCl. Cordes and Sponer[7] determined the fundamental vibration frequency as 430 cm^{-1} from measurements on the edges of the absorption bands in the vacuum ultraviolet. Recently Stammreich and Forneris[8] obtained a value of 428 ± 2 cm^{-1} from the Raman spectrum. However, in their study of the mixture of Br_2, Cl_2, and BrCl in CCl_4 solution, they found the Cl_2 fundamental at 551 cm^{-1}, which is lower than the accepted value.[9] In this study the BrCl fundamental was observed at 439.5 ± 0.5 cm^{-1} by means of infrared spectroscopy.

The microwave spectrum of BrCl, studied by Smith, Tidwell, and Williams[10] provides very accurate data on the rotation spectrum and, parenthetically, the most convincing evidence for the existence of the compound.

Coles and Elverum[11] have computed the thermodynamic properties of all the diatomic interhalogens from spectral data using mass interpolation for the quantities not yet observed. Unfortunately, in the

* The Knolls Atomic Power Laboratory is operated by the General Electric Company for the U. S. Atomic Energy Commission. The work reported here was carried out under contract No. W-31-109 Eng-52.

[1] A. J. Balard, Ann. chim. et phys. **32**, 371 (1826).
[2] N. N. Greenwood, Revs. Pure Appl. Chem. **1**, 84 (1951).
[3] C. M. Beeson and D. M. Yost, J. Am. Chem. Soc. **61**, 1432 (1939).
[4] H. G. Vesper and G. K. Rollefson, J. Am. Chem. Soc. **56**, 620 (1934).
[5] G. S. Forbes and R. M. Fuoss, J. Am. Chem. Soc. **49**, 142 (1927).
[6] K. Jellinek and H. Schutza, Z. anorg. Chem. **227**, 52 (1936).
[7] von H. Cordes and H. Sponer, Z. Physik **63**, 334 (1930); **79**, 170 (1932).
[8] H. Stammreich and R. Forneris, J. Chem. Phys. **21**, 944 (1953).
[9] G. Herzberg, *Spectra of Diatomic Molecules* (McGraw-Hill Book Company, Inc., New York, 1950), second edition.
[10] Smith, Tidwell, and Williams, Phys. Rev. **79**, 1007 (1950).
[11] L. G. Cole and G. W. Elverum, J. Chem. Phys. **20**, 1543 (1953).

case of BrCl, the microwave data was not available and their calculated properties are too low. They used the value of Sponer, 430 cm^{-1}, as the fundamental vibration frequency of BrCl.

2. EXPERIMENTAL

For the determination of the equilibrium constant, samples were prepared by condensing known quantities of Br_2 and Cl_2 in a quartz bulb in a vacuum system containing a Bourdon gauge with all stopcocks lubricated with fluorothene grease. Care was taken to maintain the Br_2 pressure less than 200 mm; i.e., below the condensation pressure, because preliminary experiments showed that Cl_2 was soluble in liquid Br_2 resulting in gas composition variation with changes in pressure. The mixture, allowed to warm to room temperature, was irradiated with a mercury lamp (G.E., AU-3) for one-half hour. The distance from the lamp was five inches, and the temperature was 40°±5°C.

Mass spectrometer gas sensitivities (mv/mm) were determined for Br_2 and for Cl_2. Within the limit of experimental error, ±1 percent, the sensitivities were equal. Analyses of the mixtures indicated the sensitivity of BrCl to be equal to that of Br_2 and Cl_2. A G.E. Analytical Mass Spectrometer was used for all the work reported here.

Mixtures of Br_2 and Cl_2 were prepared covering the range from roughly 90 percent Br_2−10 percent Cl_2 to 80 percent Cl_2−20 percent Br_2. The data for some of these analyses are presented in Table I.

The Ke value approached a lower limit of approximately 0.148 in a matter of a few hours and held constant until the sample was pumped out. Because this lower limit is usually 0.15− and the average of samples indicated is usually 0.15+ a Ke value of 0.15 best represents the over-all data.

The analysis is of utmost importance since, in the expression for the equilibrium constant, the percent Cl_2 and percent Br_2 are multiplied, and the percent BrCl is squared. The mixture shown in sample number 1 was made up to be a 50–50 mixture of Br_2 and Cl_2 which is fairly close as can be seen from the data. A 2 percent variation in analysis results in an 8 percent change in the calculated Ke.

Fractionation of the components of the mass spectrometer leak is important, but is partially compensated by the fact that the Cl_2, which will diffuse faster than BrCl, is multiplied by the Br_2, which diffuses slower than BrCl. As anticipated the mass spectrometer had to be conditioned repeatedly for the studies. Samples allowed to pass continuously through the spectrometer for 24 hours, with periodic analyses being made, showed a gradual drop in percent Cl_2 and a corresponding increase in percent Br_2.

TABLE I. Mass spectrometer analyses of Br_2–Cl_2 mixtures.

Sample No.	Br_2,%	Cl_2,%	BrCl,%	$Ke=\frac{(Br_2)(Cl_2)}{(BrCl)^2}$
1	22.1	21.9	56.0	0.154
2	31.5	14.7	53.8	0.160
3	14.6	31.5	53.9	0.158
4	12.0	36.6	52.4	0.160
5	5.9	50.6	43.5	0.158
6	71.0	1.6	27.4	0.151

The mass spectrum of BrCl consists of three masses, 114, 116, and 118. Mass 114 is due to $Br^{79}Cl^{35}$, mass 118 is due to $Br^{81}Cl^{37}$, and mass 116 is due to $Br^{79}Cl^{37}$ and $Br^{81}Cl^{35}$. Isotope analyses agree with the established values of Cl^{35}/Cl^{37} and Br^{79}/Br^{81}.

The very fact that these masses are present along with the correct relative intensity of the peaks provide additional extremely convincing evidence for the existence of BrCl.

The band associated with the fundamental vibration frequency of bromine chloride was observed in the KBr region of the infrared spectrum. A Baird double-beam infrared spectrophotometer was used. The gas cell was of the standard 10 cm length, constructed of double-tough Pyrex with silver chloride windows. In order to obtain a good seal, a Teflon gasket, coated with a thin film of fluorothene grease, was placed between the glass cell-flanges and the silver chloride windows. Aluminum end-plates and Teflon gaskets were then applied over the silver chloride windows. The end-plates were bolted together. As an additional precaution, a ring of Apiezon W was applied over the silver chloride-Teflon-glass joint. Gas pressures slightly in excess of one atmosphere could be studied with this cell.

TABLE II. Spectroscopic constants of BrCl.

Constant	Value
ω observed	439.5±0.5 cm^{-1}
ω_e	443.1 cm^{-1}
$X_e\omega_e$	1.8 cm^{-1}
B_e	0.150 909 cm^{-1}
α_e	7.595×10^{-4}
D_e	6.8×10^{-8}
Molecular weight	115.373

The line shape was that of two close maxima with the longer wavelength P branch less intense than the R branch, typical of the Bjerrum double-band shape for a diatomic molecule. The observed frequency at the minimum between the maxima was 439.5±0.5 cm^{-1}. The separation between the maxima was 15 cm^{-1}±1, in agreement with the theoretical prediction of 16 cm^{-1}. The spectrophotometer trace was calibrated with 1,2,4-trichlorobenzene which has "lines" at 439.4 and 458.7 cm^{-1}.

3. RESULTS

The spectroscopic constants for BrCl are listed in Table II. The values of B_e and α_e were obtained from

Smith *et al.*[10] by averaging the normal isotope distribution. The value of $X_e\omega_e$ was determined from Morse's equation.[9] The centrifugal distortion constant D_e was calculated from $4B_e^3/\omega^2$.

From the spectroscopic constants, the values of the thermodynamic properties $-(F-E_0^0)$, S, and C_p were calculated for one mole of gas at atmospheric pressure, by the method of Gordon and Barnes.[12] Nuclear spin and mixing contributions to the functions have not been included. The results of these calculations are tabulated (Table III); they are given to three decimal places in view of uncertainty in the calculation of anharmonicity and centrifugal effects. Values of fundamental constants were taken from Bearden and Watts.[13] The gas constant was taken to be 1.98719 cal/deg mole.[14]

From the observed value of 0.15 for the equilibrium constant of $2BrCl(g)=Br_2(g)+Cl_2(g)$, and from the thermodynamic properties of $BrCl(g)$ in Table III and from known standard state values of $Br_2(l)$, $Br_2(g)$ and $Cl_2(g)$,[14] the standard state thermodynamic properties of $BrCl(g)$ at 298°K were computed, compared with the Bureau of Standards[14] and summarized in Table IV for the reaction $\frac{1}{2}Cl_2(g)+\frac{1}{2}Br_2(l)=BrCl(g)$. The equilibrium constant for $BrCl(g)=Br(g)+Cl(g)$ for the atoms in their ground states is computed to be 4.9×10^{-34}.

Two points of interest were noted in these studies. First of all, the value of the fundamental vibration frequency is very close to the value of 439.7 cm^{-1} predicted from the equations of Guggenheimer.[15] The second point is that there was no observable evidence either in the infrared or on the mass spectrometer for any higher chloride of bromine such as $BrCl_3$.

TABLE III. Thermodynamic properties of BrCl.

Temperature °K	$-(F-E_0^0)$ kcal/mole	S Entropy units	C_p Calories
100	4.194	48.919	7.101
150	6.721	51.869	7.499
200	9.369	54.081	7.884
250	12.119	55.874	8.169
298	14.837	57.325	8.362
300	14.952	57.381	8.369
350	17.854	58.684	8.510
400	20.817	59.825	8.611
500	26.900	61.763	8.745
600	33.159	63.366	8.827
700	39.566	64.732	8.885
800	46.092	65.920	8.926
900	52.746	66.974	8.959
1000	59.492	67.921	9.007

TABLE IV. Standard state thermodynamic properties of $BrCl(g)$ at 298.1°K.

Quantity	$\frac{1}{2}Cl_2(g)+\frac{1}{2}Br_2(l)=BrCl(g)$ This study	NBS circular No. 500
$\log K_f$	0.137	0.1539
F_f^0	−0.187	−0.210 kcal/mole
H_f^0	3.53	3.51 kcal/mole
S^0	57.325	57.34 cal/deg mole
C_p^0	8.362	cal/deg mole

[12] A. R. Gordon and C. Barnes, J. Chem. Phys. **1**, 297 (1933).
[13] J. A. Bearden and H. M. Watts, Phys. Rev. **81**, 73 (1951).
[14] Selected Values of Chemical Thermodynamic Properties Circular No. 500, National Bureau of Standards.
[15] K. M. Guggenheimer, Proc. Phys. Soc. (London) **58**, 456 (1946).

The Vapor Pressure of Zinc between 150° and 350°C*

JOHN D. MCKINLEY, JR. † AND JOHN E. VANCE
Chemical Laboratories of New York University, New York, New York

(Received January 4, 1954)

The vapor pressure of zinc has been measured by the Knudsen effusion method using the radioisotope Zn^{65}. Measurements have been made from 150° to 350°C, and the temperature-vapor pressure relation over this range was found to be $\log_{10}P_{mm}=-7198/T+9.664$. The heat of vaporization was calculated to be 31.35 kcal per mole at 0°K. A test has been made of the Clausing probability factor regarding the dependence of the effusion rate on the dimensions of the effusion orifice.

MEASUREMENTS of the vapor pressure of zinc between 300° and 360°C have been reported recently by Vance and Whitman.[1] The present paper describes an extension of the measurements to lower temperatures by a modification of the Knudsen effusion method.[2] This method was chosen in preference to the Langmuir evaporation rate method[3] in order to obviate the necessity of measuring accurately the surface area of the evaporating sample, and to make negligible errors arising from an uncertainty in the value of the condensation coefficient. The relative merits of these two techniques have been discussed by Speiser and Johnston.[4] While these experiments were in progress, effusion measurements of the vapor pressures of gold,[5] germanium,[6] and copper,[7] have been described.

The Knudsen method consists of a determination of the rate at which vapor effuses through an orifice from a container in which the vapor is in contact with the condensed phase. The form of Knudsen's equation used in this work is

$$P=(g/1333WatB)(2\pi RT/M)^{\frac{1}{2}}, \qquad (1)$$

in which P is the equilibrium vapor pressure in mm Hg, g is the grams of vapor of molecular weight M effusing in t seconds through an orifice of cross-sectional area, a cm², T is the absolute temperature, and R is the molar gas constant in ergs per mole degree. W represents the fraction of atoms which pass through the orifice without being returned to the effusion chamber as a result of diffuse scattering at the orifice walls. Clausing[8] has evaluated this quantity for gases streaming through cylindrical tubes at low pressures, the situation which pertains to effusion experiments of the present design. A discussion of this factor as it applies to vapor pressure determinations has been given by Whitman.[9] The requirement that the orifice be at the same temperature as the evaporating sample can be met most easily (when resistance heating is used) by cutting the orifice in a plate thick enough to provide adequate heat conduction. The present research includes experiments, described in the following, which verify some of the theoretical values of W calculated by Clausing for orifices of various dimensions.

The inclusion of the term B in Eq. (1) has been suggested in recent years[4,9,10] to take into account the fact that the process of effusion causes the steady state pressure P' in the chamber to assume a value slightly lower than the equilibrium vapor pressure P. The extent of the difference is determined by the relative areas of the orifice a and of the effusion chamber cross section A. An equation has been given relating these quantities and the condensation coefficient α as follows,

$$B=P'/P=1/(1+a/A\alpha). \qquad (2)$$

In the present experiments, the calculated values of B ranged from 0.910 to 0.998. Whitman[11] has pointed out that the assumption of a steady-state pressure, on which this equation is based, is valid only when the surface of the evaporating solid is close to the effusion orifice.

Because of the low vapor pressures measured in this work, it was desirable to use large effusion orifices in order that the effusion would proceed at a conveniently measurable rate.

There are two limitations to this practice. First the free molecule flow, on which the validity of Eq. (1) depends, can be expected to occur only if the mean free path of the effusing atoms is at least ten times greater than the diameter of the orifice[12].

In the low-pressure range, where the larger orifices are useful, the mean free path is large and this is not a serious restriction. Secondly, it is apparent from Eq. (2) that the effect of increasing the ratio a/A is to make the correction for the unsaturation of the vapor pressure relatively more important. In the limit $a=A$ the method

* This paper is an abstract of a thesis presented by J. D. McKinley in partial fulfillment of the requirements for the degree of Doctor of Philosophy at New York University.

† Present address, Department of Chemistry, Princeton University, Princeton, New Jersey.

[1] John E. Vance and C. I. Whitman, J. Chem. Phys. **19**, 744 (1951).

[2] M. Knudsen, Ann. Physik **29**, 179 (1909).

[3] I. Langmuir, Phys. Rev. **2**, 329 (1913).

[4] R. Speiser and H. L. Johnston, Trans Am. Soc. Metals **42**, 283 (1950).

[5] L. D. Hall, J. Am. Chem. Soc. **73**, 757 (1951).

[6] A. W. Searcy, J. Am. Chem. Soc. **74**, 4789 (1952).

[7] N. H. Hersh, J. Am. Chem. Soc. **75**, 1529 (1953).

[8] P. Clausing, Ann. Physik **12**, 961 (1932).

[9] C. I. Whitman, J. Chem. Phys. **20**, 161 (1952).

[10] M. G. Rossman, and J. Yarwood, J. Chem. Phys. **21**, 1406 (1953).

[11] C. I. Whitman, J. Chem. Phys. **21**, 1407 (1953).

[12] M. Knudsen, Ann. Physik, **28**, 999 (1909).

becomes effectively that of Langmuir; the effusion rate is then actually the evaporation rate and is directly proportional to the condensation coefficient. Consequently, to retain the desirable features of the Knudsen method, the ratio $a/A = A$ must be kept small enough that an uncertainty in α does not cause a significant uncertainty in B. In this work the largest value of a/A used was 1/10 and α was assumed to be equal to unity. A value as low as 0.7 would produce a 3 percent error in B under these conditions. There are no values available for the condensation coefficient of zinc vapor on solid zinc; however, recent measurements of this quantity for other metals[13] indicate that it is equal to unity for a scrupulously clean surface.

An increase in the sensitivity of the method was achieved by using zinc containing the radioisotope Zn^{65}; in this way the usual gravimetric determination of effused material could be replaced by a more sensitive radiochemical analysis. Since Zn^{65} does not have the same atomic weight as stable zinc, corrections for isotope fractionation have been considered. Those related to the effusion itself are less than 0.3 percent and are negligible compared to other uncertainties. Isotope fractionation between solid and vapor has been neglected.

In using Eq. (1) it has been assumed that the zinc vapor is monatomic. Winan[14] has obtained spectral evidence for an unstable Zn_2 molecule and Gaydon[15] gives a value of 6 kcal per mole for its dissociation energy. Using this value, Brewer[16] has calculated the heat of vaporization of Zn_2 to be 55 kcal per mole which would make it a minor constituent of the zinc vapor.

APPARATUS AND PROCEDURE

The apparatus used by Vance and Whitman[1] was modified by a redesign of the effusion furnace to increase the reliability of the temperature measurement and to permit the orifice to be changed easily. The furnace, Fig. 1, was machined from a pure copper rod. The cylindrical cavity was 1 inch deep and 1 inch in diameter. Three long thermocouple wells were drilled into the base of the furnace so that temperature measurements could be made at the base and top of the cavity and in the center of the vaporizing sample. A ledge at the top of the cavity served as a seat for the aluminum cover into which the orifice was cut. The cover was fastened in place with a clamp ring and six machine screws as shown, to facilitate inspection and filling and to make possible the use of a variety of orifices without disturbing the rest of the apparatus. A tight seal was provided by placing an aluminum foil gasket between the aluminum cover and the copper ledge. Differential thermal expansion of the steel, aluminum, and copper forced the cover against the chamber. A hole of the proper cylindrical shape for the application of the Clausing factor was drilled into a cover while it was tightly clamped between two heavy aluminum plates.

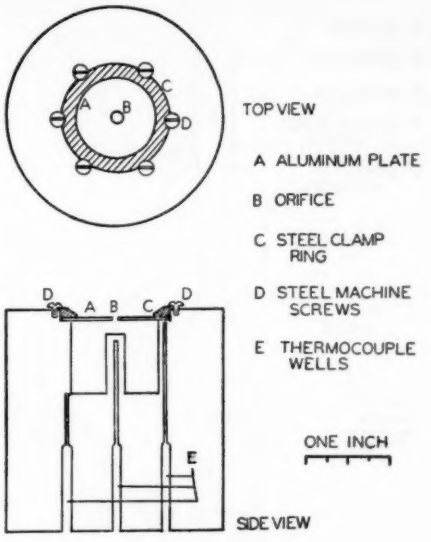

FIG. 1. Copper effusion furnace.

Four different orifices were used in these experiments; all had diameters such that the ratio of mean free path of the zinc atoms to the orifice diameter was always larger than 10. In each case the appropriate value of Clausing's factor was obtained from a plot of the values covering the orifice radius—depth ratio in question. The orifice depth was measured with a micrometer; areas were determined by measuring the diameters with a comparator and also with a microscope containing a calibrated eyepiece micrometer.

A 200-ohm coil of Nichrome resistance wire wound around the outside of the furnace and insulated by a layer of Sauereisen cement served as a heater. Heating current was supplied from a constant voltage transformer and was controlled with a variable resistor in series with the windings. Two concentric shields of aluminum foil around the winding and an additional piece of foil under the furnace provided adequate thermal shielding. Temperatures were measured with copper-constantan thermocouples calibrated against a platinum resistance thermometer having a Bureau of Standards certificate. The potentials were measured with a Leeds and Northrup type K-2 potentiometer and a Leeds and Northrup HS galvanometer. Silver powder was tamped around the insulated leads in the thermocouple wells; the leads were wrapped twice around the furnace to reduce heat losses by conduction.

The furnace was supported by three Pyrex legs on the floor of a modified 5-liter flask, Fig. 2, attached to a conventional vacuum system with which a vacuum of 10^{-6} mm could be attained as measured with a McLeod

[13] G. Wessel, Z. Physik **130**, 539 (1951).
[14] J. G. Winan, Phil. Mag. **7**, 555 (1929).
[15] A. G. Gaydon, *Dissociation Energies and Spectra of Diatomic Molecules* (Chapman and Hall, Ltd., London 1943).
[16] L. Brewer, *Chemistry and Metallurgy of Miscellaneous Materials* (McGraw-Hill Book Company, Inc., New York, 1950) edited by L. L. Quill.

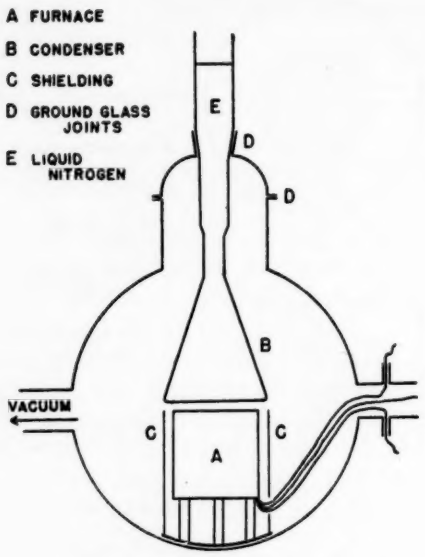

FIG. 2. Effusion apparatus.

gauge. Short Pyrex capillaries were fused onto a side arm of the large flask through which the thermocouple and heater leads were passed. Apiezon *W* wax was used to close each outlet.

A conical condenser for collecting the effused zinc was sealed into the cover of the five-liter flask. Its flat base was parallel to the top of the furnace, and positioned so as to intercept directly 98 percent of the effusing beam, assuming that the spatial distribution of the effusing atoms followed the cosine law. It is believed that the remainder of the zinc was caught on the upper surfaces of the condenser as was found to be the case in similar experiments reported by Vance and Whitman.[1]

The zinc charge for the effusion furnace was prepared as follows. Ten grams of stable zinc (reported purity, 99.98 percent) and five grams of radioactive zinc dust obtained from the Oak Ridge National Laboratories were dissolved in 1*N* sulfuric acid; after removal of the acid hydrogen sulfide group the solution was buffered and electrolyzed. The cathode, an 85-cm length of B&S No. 18 copper wire, was plated with a firmly adhering layer of zinc, 1 mm thick. Since the electrolysis was continued until the solution was virtually freed of zinc the correction for isotope fractionation between the plating bath and the plated zinc has been neglected. Short lengths of the cathode were used to fill the effusion chamber to within three mm of the top. The total charge contained about 10 mc of the Zn^{65} isotope, a beta and gamma emitter with a half-life of 250 days. Several experiments above 300°C using a stable zinc sample in the form of small lumps gave close agreement with radioactive determinations at the same temperatures, indicating that the plated zinc was a satisfactory form to use. Experiments were also performed with stable zinc plated in the manner described above to check the procedure; again satisfactory agreement was obtained.

Before each vapor pressure determination the apparatus was evacuated and the furnace was outgassed. The apparatus was then cooled, and while it was being flushed with nitrogen, the condenser was removed, cleaned thoroughly, and replaced. The system was re-evacuated, and the condenser was filled with liquid nitrogen. The furnace was quickly brought to the experimental temperature and the heating current adjusted to maintain this temperature. Depending on the effusion rate, the experiments lasted from 25 minutes to six hours during which time the temperature was read at ten- or fifteen-minute intervals. An experiment was stopped by filling the apparatus with nitrogen, cutting off the heating current and removing the condenser. The layer of effused zinc was dissolved from the condenser, converted to the sulfate by evaporation in a sulfuric acid solution, and transferred to a calibrated volumetric flask. 25-ml aliquots were counted in a *Q* gas flow counter. A stock solution containing a known amount of zinc with the same specific activity as the effused samples was prepared by diluting a portion of the plating solution. The relationship between counting rate and milligrams of zinc was found to be linear in both counting assemblies; thus the amount of zinc in an effused sample could be determined by comparing its activity with that of a stock solution sample counted in an identical manner. At least 10^4 counts were recorded in each activity determination; the sample sizes were such that the counting rate was at least 3 times and was usually 10 or 20 times background.

The small amount of zinc which effused while the furnace was being brought to temperature was determined in separate experiments at each temperature. It was possible to reproduce the heating rate almost exactly and the zinc collected in each of these experiments was subtracted from the total amount found in the corresponding vapor pressure measurement. At the highest temperature (353°C) this correction was 0.21 mg and became negligible below 180°C.

Some brass formation was noted on the walls of the effusion chamber; however, the outgassing and cooling procedure left the walls covered with condensed zinc so that the zinc vapor was not in contact with the copper. The agreement between the results of experiments above 300°C reported here and those of Vance and Whitman, which were obtained with an aluminum furnace, indicates that the presence of copper had no effect on the vapor pressure measurements.

ERRORS

The greatest uncertainty in these experiments is the determination of the temperature of the evaporating solid. The differences between the three thermocouple readings were not greater than 0.5°C at any one time, and the temperature at each thermocouple junction varied by 0.5°C at most during an experiment. The uncertainty arising from these two sources and from possible errors in the thermocouple calibration and

potentiometer readings has been estimated to be not greater than ±1°C. This corresponds to an error of ±5 percent in the pressure as determined by Eq. (3).

Replicate determinations of the activity of the stock solution which included the manipulations involved in the determination of an effused sample showed occasional deviations as large as 5 percent from the average. This has been chosen as the maximum uncertainty in the value of g.

Clausing places an uncertainty of ±2 percent on the calculated values of W. The orifice diameters were measured with a precision of 0.5 percent and a corresponding uncertainty of ±1 percent in the areas.

The maximum error in the vapor pressure which can be expected from the above sources is about ±15 percent.

RESULTS AND CONCLUSIONS

Effusion data from thirty determinations between 150° and 350°C are shown in Table I with the corresponding vapor pressures calculated by means of Eq. (1). The temperatures at the three thermocouple junctions differed by about 0.5° and the temperatures indicated in Table I are the mean of these three values averaged for time fluctuations. Effusion times and weights of effused zinc have been corrected for the initial heating period. The Clausing factors used for orifices a, b, c, and d were 0.833, 0.848, 0.847, and 0.941, respectively.

The individual values of log P and $1/T$ have been plotted in Fig. 3 together with the values reported by Vance and Whitman[1] and some earlier effusion method

TABLE I. Vapor pressure of zinc

Expt. No.	Temp. °K	Effusion time Seconds	Orifice	Wt. zinc Mg	Vapor pressure, mm Hg ×10³ Observed	Calculated
60	626.2	1500	a	3.83	13.7	14.8
59	611.6	1680	a	3.00	9.49	7.85
14	583.1	10620	a	4.86	2.38	2.09
58	580.6	1860	a	0.616	1.72	1.85
34	573.2	5760	b	1.00	0.906	1.28
15	573.1	9000	a	2.65	1.52	1.27
20	568.6	7200	c	2.61	1.02	1.01
30	568.6	6660	b	1.12	0.867	1.01
17	562.9	12240	a	2.33	0.974	0.753
27	561.9	6600	c	1.56	0.665	0.707
45	560.5	2280	d	0.623	0.646	0.649
21	555.9	7200	c	1.45	0.560	0.520
18	554.6	13800	a	1.50	0.551	0.485
31	550.6	7800	b	0.531	0.348	0.390
28	545.0	7380	c	0.730	0.273	0.286
19	544.7	14700	a	1.06	0.363	0.281
22	538.4	6600	c	0.633	0.264	0.197
32	536.0	7500	b	0.254	0.171	0.172
29	531.2	7140	c	0.277	0.106	0.130
23	523.9	7800	c	0.268	0.0936	0.0841
33	519.1	7560	b	0.577	0.0378	0.0490
24	507.3	8760	c	0.0703	0.0225	0.0299
36	497.6	12480	c	0.0861	0.0183	0.0158
37	483.7	14520	c	0.0278	0.00501	0.00607
38	474.4	16200	c	0.0202	0.00323	0.00310
54	466.1	9000	d	0.119	0.00140	0.00166
56	456.1	8100	d	0.0452	0.000589	0.000763
57	442.6	15300	d	0.0483	0.000330	0.000251
55	433.9	10200	d	0.0115	0.000116	0.000119
47	421.9	19560	d	0.00985	0.0000513	0.0000401
		Orifice	Area, cm²	B	W	
		a	0.01129	0.998	0.833	
		b	0.01137	0.997	0.848	
		c	0.02084	0.996	0.847	
		d	0.4890	0.910	0.941	

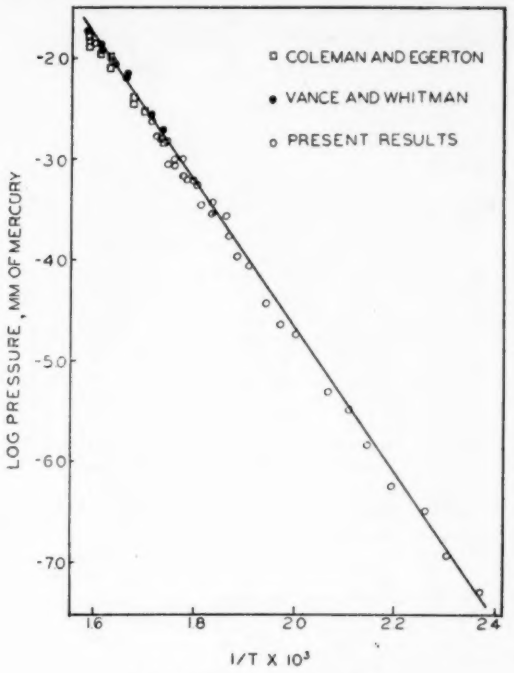

FIG. 3. Plot of log$P$ *vs* $1/T$.

data of Coleman and Egerton.[17] An equation representing the best line through the points obtained in this research was calculated by the method of least squares. An equation of the form, $\log P = a/T + b \log T + c$ (the $\log T$ term to account for the change in the heat of vaporization over the 200° temperature range), did not fit the data more closely than the simple linear form of the integrated Clapeyron Clausius equation. Consequently, a linear equation was chosen to represent the data as follows,

$$\log_{10} P_{\text{mm}} = -7198/T + 9.664. \quad (3)$$

In calculating ΔH_0^0, the heat of vaporization at 0°K, use was made of the following equation which can be derived from the second and third laws of thermodynamics,

$$R \ln P = \left(1/T \int_0^T C p_s dT - \int_0^T C p_s d \ln T\right) - (R \ln Q - R) - \frac{\Delta H_0^0}{T} \quad (4)$$

where Cp_s is the molar heat capacity of the solid and Q is the partition function of the vapor. The terms in the first and second parentheses are the free energy functions of the solid and vapor, respectively, and Eq. (4) is usually written in the more concise form,

$$R \ln P = \left(\frac{F^0 - H_0^0}{T}\right)_s - \left(\frac{F^0 - H_0^0}{T}\right)_v - \frac{\Delta H_0^0}{T}. \quad (5)$$

[17] F. F. Coleman, and A. C. Egerton, Trans. Roy. Soc. (London) **A234**, 177 (1935).

TABLE II. Heat of vaporization of zinc.

Expt. No.	Temp. °K	$-R\ln P$ cal mole^{-1} deg.$^{-1}$	$-\left(\frac{F^0-H_0^0}{T}\right)_s$ cal mole^{-1} deg.$^{-1}$	$-\left(\frac{F^0-H_0^0}{T}\right)_a$ cal mole^{-1} deg.$^{-1}$	ΔH_0^0 kcal mole^{-1}
60	626.2	21.707	37.170	9.188	31.12
59	611.6	22.440	37.053	9.057	30.85
14	583.1	25.189	36.816	8.795	31.03
58	580.6	25.236	36.795	8.772	31.27
34	573.2	26.109	36.731	8.702	31.60
15	573.1	26.083	36.730	8.701	31.01
20	568.6	26.873	36.691	8.658	31.22
30	568.6	27.196	36.891	8.658	31.40
17	562.9	26.966	36.641	8.604	30.96
27	561.9	27.725	36.632	8.593	31.33
43	560.5	27.782	36.620	8.580	31.29
21	555.9	28.086	36.579	8.536	31.19
18	554.6	28.100	36.567	8.523	31.14
31	550.6	29.010	36.531	8.484	31.42
28	545.0	29.482	36.480	8.429	31.36
19	544.7	28.926	36.478	8.426	31.04
22	538.4	29.563	36.420	8.364	31.02
32	536.0	30.421	36.397	8.340	31.34
29	531.2	31.377	36.353	8.292	31.57
23	523.9	31.627	36.284	8.218	31.27
33	519.1	33.422	36.200	8.129	31.87
24	507.3	34.438	36.124	8.047	31.72
36	497.6	34.867	36.028	7.946	31.32
37	483.7	37.442	35.888	7.799	31.70
38	474.4	38.388	35.719	7.697	31.50
54	466.1	39.969	35.705	7.608	31.73
56	456.1	41.696	35.596	7.493	31.83
57	442.6	42.846	35.447	7.342	31.40
55	433.9	44.925	35.348	7.241	31.68
47	421.9	46.348	35.209	7.099	31.50
					Av=31.35±0.24

Using Kelley's data[18] for the heat capacity of zinc, and the partition function for zinc vapor, which in this temperature range includes only translational terms, values of ΔH_0^0 have been calculated for each vapor pressure determination. These values and the corresponding free energy functions are shown in Table II. The mean value of ΔH_0^0 is 31.35±0.24 kcal per mole.

The value of ΔH_0^0 reported by Vance and Whitman is 30.93 kcal per mole and is within two standard deviations of Fig. (3). The value in this report is believed to be more reliable as it is based on experimental values covering a considerably wider temperature range. Brewer[16] gives a value of 31.19 kcal per mole for the heat of vaporization of zinc at 25°C which corresponds to a value of 31.06 kcal per mole at 0°K, midway between the above values.

[18] K. K. Kelley, Bur. Mines Bull. **383** (1935).

EXPERIMENTAL TEST OF THE CLAUSING FACTOR

A test of Clausing's values of the factor W in Eq. (1) has been made using the effusion furnace and experimental procedure already described. A set of four aluminum covers with equal cross-sectional areas was made from aluminum disks of different thicknesses. Stable zinc (reported purity 99.98 percent) was used to fill the effusion chamber. The effused samples were determined by a phosphate procedure.[19]

The dried zinc pyrophosphate precipitates weighing 6 to 10 mg were weighed in 1-ml Selas crucibles on a micro balance.

Effusion rate measurements were made at about 311°C and three or four determinations were made with each orifice. Each effusion rate was then corrected to a common temperature by means of Eq. (3). This correction was necessary since it was not possible to obtain exactly the same temperature in each experiment. The largest correction was for a temperature difference of 0.5° and amounted to 2 percent in the effusion rate. An average rate for each orifice was calculated and is shown with the corresponding data in Table III.

TABLE III. Experimental test of Clausing factor.

Depth of orifice L mm	Radius of orifice R mm	Clausing factor W	Effusion rate E micrograms per second	E/W
0.128	1.410	0.9575	1.869	1.952
0.496	1.412	0.8500	1.738	2.045
2.275	1.400	0.5625	1.115	1.982
3.170	1.409	0.4865	1.015	2.086

The averaged effusion rates divided by the appropriate Clausing factors should be constant for this series of experiments if Clausing's predictions are correct. The figures in the last column of Table III differ from the mean by about 5 percent which is well within the experimental uncertainty. This agreement supports the validity of Clausing's values.

[19] John E. Vance and R. E. Bomp, Anal. Chem. **25**, 610 (1953).

Note on the Theory of Directed Valence

TA-YOU WU
Division of Physics, National Research Council, Ottawa, Canada
(Received January 14, 1954)

The recent observation of Zimmerman and Rysselberghe, and Linnett and Pöe that the wave functions ψ of free atoms, when put in the form of determinants, exhibit the directional property of valence of these atoms, has been examined. It is pointed out that a consistent theory of directed valence cannot be based on these determinantal wave functions of one single state of the free atom alone.

THE theory of directed valence of Slater and Pauling based on the approximation of electron pair bond and the assumption of hybridized wave functions is well known. Recently there have appeared papers by Zimmerman and Rysselberghe[1] and by Linnett and Pöe[2] which show that the squares of the wave functions of the electrons of the free atoms, when put in the determinant form, are maximum when one electron is along one of the directions of the valence of the atoms, and that when the idea of maximum overlap (exchange integral) is used, these wave functions will give the correct directed valence in the formation of molecules. The implication is that one can account for the directional property of valence without having to introduce the concept of hybridization or its equivalents. The purpose of the present note is to examine these new suggestions for the understanding of directed valence.

To facilitate the discussion let us summarize briefly the essential features of the Slater-Pauling theory.[3] The starting point is the Heitler-London approximation. The formation of a molecule is brought about by the formation of electron pair bonds. The criterion for the greatest stability of the molecule is that of the maximum numerical value of the exchange integrals for the two electrons in each bond. To account for the directional property of valence (such as the regular tetrahedron structure of CH_4), hybridized wave functions are introduced in place of the atomic orbitals. These hybridized wave functions accomplish two purposes, namely, (1) they add a flexibility to the electron wave functions to be directed in different directions thereby allowing the system to seek the configuration of lowest energy and the directed valence associated with it, and (2) they give rise to a greater bond strength, or lower energy, by increasing the overlap and hence the numerical value of the exchange integral for the two electrons in a bond.

Let us now consider the suggestions of Zimmerman and Rysselberghe, and of Linnett and Pöe. While certain determinantal wave functions, such as

$$\Psi=\begin{vmatrix} s(1)p_x(1)p_y(1)p_z(1) \\ s(2)p_x(2)p_y(2)p_z(2) \\ s(3)p_x(3)p_y(3)p_z(3) \\ s(4)p_x(4)p_y(4)p_z(4) \end{vmatrix}$$

for the $2s2p^3\ {}^5S$ of the carbon atom, do possess a maximum in the configuration space when one electron is found along each of certain directions (the corner of a regular tetrahedron for the Ψ above), the connection with the question of directed valence is not obvious. The reasons for this statement are the following.

(1) The whole idea of using antisymmetric wave functions is to conform to the Pauli principle for indistinguishable particles. For this reason one must include the electrons of the attached atoms in the antisymmetric wave function. Thus for the case of CH_4, if one ignores the two $1s$ electrons of the C atom, one must still start with wave functions constructed of 8×8 determinants instead of the 4×4 determinant above. It must be remembered that all the exchange integrals that play such an important part in the Heitler-London theory come from the use of antisymmetrized wave functions for the electrons of the central and the attached atoms. To antisymmetrize the wave function for the electrons of the central atom alone but to think in terms of the exchange of these electrons with those of the attached atoms is not only an inconsistent procedure, but is one which will not give rise to any exchange integrals between the electrons of the central and the attached atom. As long as the idea of maximum overlap is still retained as the criterion for maximum stability, one must work with wave functions antisymmetrized with respect to all the electrons taking part in the formation of the bonds.

(2) Another objection may be raised against the attempt to obtain the valence property of an atom from one atomic state alone. Consider again the tetravalent carbon atom. When one works in the theory of electron pair bonds, the most stable state is one in which the wave function is antisymmetric in the spins of the two electrons in each bond. Such a state for the molecule, say CH_4, does not correspond to the C atom being in the $2s2p^3\ {}^5S$ state, but to a combination of many states. Thus Voge[4] has shown that the following states

[1] H. K. Zimmerman and P. Rysselberghe, J. Chem. Phys. **17**, 598 (1949).
[2] J. W. Linnett and J. Pöe, Trans. Faraday Soc. **47**, 1033 (1951).
[3] See the excellent article by J. H. Van Vleck and A. Sherman, Revs. Modern Phys. **7**, 167 (1935).
[4] H. H. Voge, J. Chem. Phys. **4**, 581 (1936).

of the C atom contribute significantly to the tetravalent state of C: $2s^22p^2\ ^3P$, ^1D; $2s2p^3\ ^5S$, ^3D, ^1D; $2p^4\ ^3P$, ^1D. If one regards the CH_4 system as an 8 electron problem and expands the antisymmetrized wave function in a series of terms corresponding to 4 electrons in various L, S states of various configurations of a free C atom and 4 electrons in hydrogenic states centered on four hydrogen nuclei, it is then understandable that even other states of the C atom than the above contribute to the molecular state. Thus, in general, it is an oversimplification to explain a molecular state, and the valence properties, in terms of one single atomic state.

(3) It may perhaps be emphasized that as long as one works on the theory of electron pair bonds, the use of atomic orbitals alone is not sufficient to obtain the directional properties of valence. Orbitals with parameters adjustable in the sense of the variational principle will furnish the flexibility for the electrons to seek the configuration of the lowest energy for the system thereby accounting for the directed valence. A convenient and simple form of such orbitals is the usual hybridized wave functions introduced by Slater and Pauling. It does not seem possible to dispense with this refinement—the use of some forms of "hybridized" wave functions in place of atomic orbitals—to account for the directed valence of C if one starts with the Heitler-London approximation.

In view of these considerations, especially (1), it is seen that the observations of Zimmerman *et al.*,[1,2] can be regarded as interesting and suggestive, but will not form a theory of directed valence.

THE JOURNAL OF CHEMICAL PHYSICS VOLUME 22, NUMBER 6 JUNE, 1954

Inter- and Intramolecular Energy Transfer Processes. 4. Hydrogen-Hydrocarbon Systems

MARGARET M. MOODIE AND C. REID
Department of Chemistry, University of British Columbia, Vancouver, British Columbia, Canada
(Received November 30, 1953)

Extensive experiments have confirmed our earlier conclusion that long-range energy transfer does not occur between pairs of molecules in solution. Evidence is brought forward to show that the transfer of excitation energy from terphenyl to diphenyl hexatriene under x-ray bombardment in liquid scintillators must be due to a short-range process which occurs after the formation of a molecular complex between diphenyl hexatriene and either a positive terphenyl ion or a very highly excited terphenyl molecule.

Results of experiments in heterogeneous systems, in which transfer of excitation energy from adsorbed component to host crystal, and vice versa sometimes occurs, are summarized.

INTRODUCTION

IN a previous publication[1] on inter- and intramolecular energy transfer processes it was shown that energy transfer from one aromatic hydrocarbon species to another occurs only between the components of a surface complex formed by the adsorption of one hydrocarbon onto microcrystals of the second. No evidence was found for energy transfer between molecules of different hydrocarbons in true solution. However, indirect evidence for transfer between pairs of identical molecules was obtained.

This work has been extended in an attempt to find general conditions governing the phenomena.

EXPERIMENTAL METHOD

Purified aromatic hydrocarbons were dissolved or suspended in solvents of varying polarity which formed clear glasses when cooled in liquid nitrogen contained in an unsilvered Dewar vessel.[1] These samples were irradiated with monochromatic light from a General Electric AH6 mercury arc with suitable filters. The fluorescence from the system was analyzed using an E2 Hilger quartz prism spectrograph, sometimes photographically and sometimes using the Hilger scanning unit. Complete details of the solvents used and of the methods of making suspensions are given in our earlier paper.

RESULTS

A. Systems with Two Different Hydrocarbons in Solution

Extensive work has confirmed our earlier conclusion that under the conditions of limited solubility at 78°K, there is no observable interaction between molecules of two different aromatic hydrocarbons when both are in solution. Trials were made at various concentrations and in different solvents with combinations of more than fifty compounds, including benzene, naphthalene, anthracene and its 9,10-derivatives, napthacene, pentacene, 1,2-benzanthracene and its mono-methyl derivatives, benzo(c)phenanthrene and its mono-methyl derivatives, chrysene, coronene, 1,2,5,6-dibenzanthracene, diphenylhexatriene, phenathrene, and terphenyl.

[1] M. M. Moodie and C. Reid, J. Chem. Phys. **20**, 1510 (1952).

These systems were also examined at 293°K, but again no interaction was found.

Kallmann and Furst[2,3] have reported that on irradiation with x-rays, the system containing both terphenyl and diphenylhexatriene at 293°K shows only a fluorescence which is characteristic of diphenylhexatriene and which is of greater intensity than that from a system containing only diphenylhexatriene.

In view of this clear evidence of energy transfer in solution it was hoped that this system might also show transfer of uv excitation energy. Accordingly a xylene solution containing diphenyl hexatriene and terphenyl at concentrations of 4.31×10^{-5} and 1.3×10^{-2} mole/liter, respectively, was irradiated at 293°K. In separate experiments the Hg 2537 and 3130 lines were used as exciting sources. In both cases, however, the spectrum of the combined system was simply that to be expected if the two substances absorbed and emitted independently of each other, showing a marked contrast with Kallmann and Furst's results.

B. Systems with One Hydrocarbon in Solution and the Other in Suspension, the Latter Absorbing Radiation of Lower Energy than the Former

Previously it was reported[1] that the addition of a solution of anthracene, chrysene, or 1,2,5,6-dibenzanthracene to a naphthacene suspension at 78°K produced a shift and an intensity increase in the emission bands of the latter substance. Similar experiments have been carried out with more than forty hydrocarbons, but only a few effected any change in the naphthacene emission.

The positions of the shifted bands are recorded in Table I. Energy transfer from naphthalene, 2-naphthol, and terphenyl in solution to anthracene microcrystals was also observed. The dependence of this phenomenon on solvent polarity and position of absorption and emission bands has already been discussed.

C. Systems with One Hydrocarbon in Solution and the Other as a Suspension, the Former Absorbing Radiation of Lower Energy than the Latter

We have already indicated that on the addition of naphthacene solution to a suspension of anthracene at 78°K to give a naphthacene/anthracene ratio of 10^{-8}, the naphthacene is readily detectable because of its enhanced fluorescence.[1] Dry crystals of anthracene contaminated with naphthacene show similar emission bands. However, the amount of "impurity" detectable is much less than in our "suspension" systems.[4]

In most cases the addition to a hydrocarbon suspension of a solution of a second hydrocarbon with lower energy levels produces an intensity increase and a shift in position in the latter's emission bands. A comprehensive summary of these shifts is given in Table II.

TABLE I. Position in A of the new emission band arising from the transfer of energy at 78°K in systems which contain one hydrocarbon component in solution and the other as a suspension. The latter absorbs radiation of lower energy than the former.

Hydrocarbon in suspension	Hydrocarbon in solution	Wavelength of new emission band in A	Solvents in which "transfers" occur
Anthracene	Naphthalene	4140	EPA, ether-isopentane, isopentane-methyl cyclohexane.
Anthracene	2-Naphthol	4140	EPA, isopentane-ether, isopentane-methyl cyclohexane.
Anthracene	Terphenyl	4140	EPA, isopentane-ether, isopentane-methyl cyclohexane.
Naphthacene	Anthracene	5330	EPA, isopentane-ether, isopentane-methyl cyclohexane.
Naphthacene	2-methyl anthracene	5320	EPA, isopentane-ether, isopentane-methyl cyclohexane.
Naphthacene	Chrysene	5440	Isopentane-ether, isopentane-methyl cyclohexane.
Naphthacene	1,2,5,6-dibenzanthracene	5500	Isopentane-ether, isopentane-methyl cyclohexane.
Naphthacene	Phenanthrene	5380	EPA, isopentane-ether, isopentane-methyl cyclohexane.

D. Systems Containing Only One Hydrocarbon Component

Our previous paper[1] contains traces showing the emission of anthracene and chrysene suspensions in solvents of varying polarity. In more polar solvents (e.g., those containing ethanol) the bands characteristic of the hydrocarbon solution mask the weaker emission of the suspended solid. As the solvent polarity decreases, these bands are replaced by a new type of emission system which lies in the same region as the emission of dry solid but is devoid of structure. Solutions of these compounds have the same fluorescence in both polar and nonpolar solvents. This phenomenon has been interpreted as providing evidence for a resonance transfer of energy between identical molecules in solution followed by short-range transfer to the microcrystals.

The results of a similar study with other hydrocarbons are collected together in Table III. The compounds studied are divided into two classes according to whether or not energy transfer, indicated by increased intensity of emission from the crystalline phase, was found in our experiments. The first class is further divided into hydrocarbons whose suspension emission differs from

[2] M. Furst and H. Kallmann, Phys. Rev., **85**, 816 (1952).
[3] H. Kallmann and M. Furst, Phys. Rev., **79**, 857 (1950); **81**, 853 (1951); Nucleonics **8**, 42 (1951).
[4] F. R. Lipsett and A. J. Dekker, Can. J. Phys. **30**, 165 (1952).

TABLE II. Position, energy, and shift of the center of the highest energy emission band of the component in solution in energy transfer systems, where the hydrocarbon in solution absorbs radiation of lower energy than does the component in suspension. These values were obtained in methyl cyclohexane-isopentane solvent at 78°K.

Component in solution	Component as suspension	Highest energy emission band of solution component		
		Position in A	Energy in cm^{-1}	Shift in cm^{-1}
Anthracene	...	3790	26 358	...
Anthracene	Acenaphthene	3845	26 041	317
Anthracene	Benzene	3853	25 951	407
Anthracene	Fluorene	3925	25 478	880
Anthracene	Naphthalene	3900	25 641	717
Anthracene	2-Naphthol	3880	25 773	585
Anthracene	Terphenyl	4010	24 938	1420
Anthracene	Toluene	3830	26 109	249
2-methyl anthracene	...	3860	25 907	...
2-methyl anthracene	Naphthalene	4000	25 000	907
1,2-benzanthracene	...	3875	25 806	...
1,2-benzanthracene	Naphthalene	3918	25 523	283
1,2-benzanthracene	Terphenyl	3990	25 063	743
1′-methyl-1,2-benzanthracene	...	3892	25 694	...
1′-methyl-1,2-benzanthracene	Naphthalene	3960	25 252	441
1′-methyl-1,2-benzanthracene	Terphenyl	4040	24 752	942
2′-methyl-1,2-benzanthracene	...	3880	25 773	...
2′-methyl-1,2-benzanthracene	Naphthalene	3940	25 380	393
2′-methyl-1,2-benzanthracene	Terphenyl	4100	24 390	1383
3′-methyl-1,2-benzanthracene	...	3860	25 907	...
3′-methyl-1,2-benzanthracene	Naphthalene	3905	25 608	299
3′-methyl-1,2-benzanthracene	Terphenyl	3980	25 126	781
4′-methyl-1,2-benzanthracene	...	3880	25 773	...
4′-methyl-1,2-benzanthracene	Naphthalene	3920	25 510	263
4′-methyl-1,2-benzanthracene	Terphenyl	4020	24 876	897
3-methyl-1,2-benzanthracene	...	3890	25 707	...
3-methyl-1,2-benzanthracene	Naphthalene	3918	25 523	184
3-methyl-1,2-benzanthracene	Terphenyl	3990	25 063	644
4-methyl-1,2-benzanthracene	...	3860	25 907	...
4-methyl-1,2-benzanthracene	Naphthalene	3900	25 641	366
4-methyl-1,2-benzanthracene	Terphenyl	3985	25 094	813
5-methyl-1,2-benzanthracene	...	3860	25 907	...
5-methyl-1,2-benzanthracene	Naphthalene	3900	25 641	266
5-methyl-1,2-benzanthracene	Terphenyl	4010	24 938	969
6-methyl-1,2-benzanthracene	...	3860	25 907	...
6-methyl-1,2-benzanthracene	Naphthalene	3955	25 284	623
6-methyl-1,2-benzanthracene	Terphenyl	3965	25 220	687
7-methyl-1,2-benzanthracene	...	3890	25 707	...
7-methyl-1,2-benzanthracene	Naphthalene	3955	25 284	423
7-methyl-1,2-benzanthracene	Terphenyl	4020	24 876	831
8-methyl-1,2-benzanthracene	...	3875	25 806	...
8-methyl-1,2-benzanthracene	Naphthalene	3925	25 478	328
8-methyl-1,2-benzanthracene	Terphenyl	4000	25 000	806
9-methyl-1,2-benzanthracene	...	3950	25 316	...
9-methyl-1,2-benzanthracene	Naphthalene	4020	24 876	440
9-methyl-1,2-benzanthracene	Terphenyl	4080	24 510	806
10-methyl-1,2-benzanthracene	...	3900	25 641	...
10-methyl-1,2-benzanthracene	Naphthalene	3955	25 284	357
10-methyl-1,2-benzanthracene	Terphenyl	4025	24 844	797
10-ethyl-1,2-benzanthracene	...	3900	25 641	...
10-ethyl-1,2-benzanthracene	Naphthalene	3945	25 348	293
10-ethyl-1,2-benzanthracene	Terphenyl	3995	25 031	610
9,10-dimethyl-1,2-benzanthracene	...	4030	24 814	...
9,10-dimethyl-1,2-benzanthracene	Naphthalene	4090	24 450	364
9,10-dimethyl-1,2-benzanthracene	Terphenyl	4120	24 272	542
9,10-dimethyl-1,2-benzanthracene	2-naphthol	No transfer of energy		
Benzo(c)phenanthrene	...	3750	26 667	...
Benzo(c)phenanthrene	Naphthalene	3795	26 350	317
Benzo(c)phenanthrene	Terphenyl	3785	26 420	247

TABLE II—*Continued.*

Component in solution	Component as suspension	Highest energy emission band of solution component: Position in A	Energy in cm^{-1}	Shift in cm^{-1}
1-methyl-benzo(c)phenanthrene	...	3935	25 413	...
1-methyl-benzo(c)phenanthrene	Naphthalene	3975	25 168	245
2-methyl-benzo(c)phenanthrene	...	3780	26 455	...
2-methyl-benzo(c)phenanthrene	Naphthalene	3820	26 178	277
2-methyl-benzo(c)phenanthrene	Terphenyl	3790	26 385	70
3-methyl-benzo(c)phenanthrene	...	3770	26 525	...
3-methyl-benzo(c)phenanthrene	Naphthalene	3890	25 707	818
3-methyl-benzo(c)phenanthrene	Terphenyl	3800	26 316	209
4-methyl-benzo(c)phenanthrene	...	3800	26 316	...
4-methyl-benzo(c)phenanthrene	Naphthalene	3920	25 510	806
4-methyl-benzo(c)phenanthrene	Terphenyl	3820	26 178	138
5-methyl-benzo(c)phenanthrene	...	3780	26 455	...
5-methyl-benzo(c)phenanthrene	Naphthalene	3810	26 247	208
5-methyl-benzo(c)phenanthrene	Terphenyl	3815	26 212	243
6-methyl-benzo(c)phenanthrene	...	3800	26 316	...
6-methyl-benzo(c)phenanthrene	Naphthalene	3835	26 075	241
6-methyl-benzo(c)phenanthrene	Terphenyl	3820	26 178	138
Diphenylhexatriene	...	4010	24 938	...
Diphenylhexatriene	Naphthalene	4128	24 255	713
Diphenylhexatriene	2-naphthol	No transfer of energy		
Diphenylhexatriene	Terphenyl	4040	24 752	186
Naphthacene	...	4750	21 053	...
Naphthacene	Acenaphthene	4822	20 735	318
Naphthacene	Anthracene	4970	20 121	932
Naphthacene	2-methyl-anthracene	4960	20 161	892
Naphthacene	9,10-dichloro-anthracene	4840	20 661	392
Naphthacene	1,2-benzanthracene	4890	20 450	603
Naphthacene	9,10-dimethyl-1,2-benzanthracene	4820	20 747	306
Naphthacene	10-ethyl-1,2-benzanthracene	4840	20 661	392
Naphthacene	1′-methyl-1,2-benzanthracene	4880	20 492	561
Naphthacene	2′-methyl-1,2-benzanthracene	4900	20 408	645
Naphthacene	3′-methyl-1,2-benzanthracene	4897	20 419	634
Naphthacene	4′-methyl-1,2-benzanthracene	4865	20 555	498
Naphthacene	3-methyl-1,2-benzanthracene	4895	20 429	624
Naphthacene	4-methyl-1,2-benzanthracene	4840	20 661	392
Naphthacene	5-methyl-1,2-benzanthracene	4840	20 661	392
Naphthacene	6-methyl-1,2-benzanthracene	4900	20 408	645
Naphthacene	7-methyl-1,2-benzanthracene	4910	20 367	686
Naphthacene	8-methyl-1,2-benzanthracene	4865	20 555	498
Naphthacene	9-methyl-1,2-benzanthracene	4840	20 492	561
Naphthacene	10-methyl-1,2-benzanthracene	4850	20 619	434
Naphthacene	Benzene	4830	20 704	349
Naphthacene	Benzo(c)phenanthrene	4830	20 704	349
Naphthacene	1-methyl-benzo(c)phenanthrene	4822	20 735	318
Naphthacene	2-methyl-benzo(c)phenanthrene	4822	20 735	318
Naphthacene	3-methyl-benzo(c)phenanthrene	4835	20 682	371
Naphthacene	4-methyl-benzo(c)phenanthrene	4810	20 790	263
Naphthacene	5-methyl-benzo(c)phenanthrene	4830	20 704	349
Naphthacene	6-methyl-benzo(c)phenanthrene	4840	20 661	392
Naphthacene	Methyl cholanthrene	4840	20 661	392
Naphthacene	Chrysene	4860	20 576	477
Naphthacene	Coronene	No transfer of energy		
Naphthacene	1,2,5,6-dibenzanthracene	4900	20 408	645
Naphthacene	Diphenylhexatriene	5040	19 841	1212
Naphthacene	Fluorene	No transfer of energy		
Naphthacene	Naphthalene	4970	20 121	932
Naphthacene	2-naphthol	4830	20 704	349
Naphthacene	Pyrene	No transfer of energy		
Naphthacene	Terphenyl	4950	20 202	851
Naphthacene	Toluene	4818	20 757	296
Naphthacene	Trans-stilbene	4870	20 534	519
Phenanthrene	...	3460	28 902	...
Phenanthrene	Naphthalene	3520	28 410	492
Trans-stilbene	...	3510	28 490	...
Trans-stilbene	Naphthalene	3640	27 472	1018
Trans-stilbene	Terphenyl	3650	27 397	1093

TABLE III. Properties of the emission of suspensions of a single aromatic hydrocarbon in methyl cyclohexane-isopentane solvent at 78°K. Systems marked with an asterisk are those whose solution, suspension, and dry crystal spectra have indistinguishable band envelopes.

Hydrocarbons in whose suspensions energy transfer is found		
Suspension emission differs from that of the crystals	Suspension emission is similar to that of the crystals	Hydrocarbons in whose suspensions no energy transfer is found
Anthracene	2-methyl anthracene	*9,10-di-β-naphthyl anthracene
9,10-dibromo-anthracene	1,2-benzanthracene	9,10-diphenyl anthracene
9,10-dichloro-anthracene	3′-methyl-1,2-benzanthracene	*6-methyl-1,2-benzanthracene
9,10-dimethyl-anthracene	4′-methyl-1,2-benzanthracene	8-methyl-1,2-benzanthracene
1′-methyl-1,2-benzanthracene	7-methyl-1,2-benzanthracene	*1-methyl-benzo(c)phenanthrene
2′-methyl-1,2-benzanthracene	3-methyl-benzo(c)phenanthrene	Coronene
3-methyl-1,2-benzanthracene	Naphthacene	*Fluoranthene
4-methyl-1,2-benzanthracene		Pyrene
5-methyl-1,2-benzanthracene		
9-methyl-1,2-benzanthracene		
10-methyl-1,2-benzanthracene		
10-ethyl-1,2-benzanthracene		
9,10-dimethyl-1,2-benzanthracene		
Benzo(c)phenanthrene		
2-methyl-benzo(c)phenanthrene		
4-methyl-benzo(c)phenanthrene		
5-methyl-benzo(c)phenanthrene		
6-methyl-benzo(c)phenanthrene		
Chrysene		
1,2,5,6-dibenzanthracene		
Diphenylhexatriene		
Trans-stilbene		

that of the dry crystals and those whose suspension emission is similar to that from the dry solid.

DISCUSSION

Transfer in Solution

Our terphenyl-diphenyl hexatriene experiment suggests that no energy transfer occurs even at the comparatively high concentrations used (corresponding to average terphenyl-diphenyl hexatriene distances of *ca* 30K), in spite of the fact that the absorption and emission bands of these molecules are favorably placed for energy transfer by the Forster mechanism.[5] We conclude that Forster's experiment with molecules (trypaflavin and Rhodamine B) of similar size but with considerable permanent dipole moment may have depended for its success on the fact that complex formation between the two components had occurred. If so, it is a short-range rather than a long-range phenomenon, and the Forster mechanism need not be invoked.

Our negative results with the terphenyl-diphenyl hexatriene system, when compared with Kallman and Furst's x-ray result, raise the question of what special excited-state conditions may result in energy transfer.[6]

In the liquid solutions now being considered, if a reactive enough species of the excited molecule is produced it may be able to form an excited state complex with the second component during the 10^4–10^5 collisions which may occur between excitation and re-emission. Such complex formation between *ions* of the excited species and the receiver molecule seems very probable, since a very considerable induced dipole will appear on these very polarizable molecules in the field of the positive ion. In fact, if the conjugated system of one molecule loses an electron, we are left with something quite similar to the "electron deficient" compounds trinitrobenzene or picric acid, which are well known to form π complexes with hydrocarbons. Once such a complex is formed, energy transfer to the component with lowest-lying absorption bands is to be expected, and probably accounts for the x-ray results.

To summarize, we feel that there is little evidence for long-range transfer of energy in solution. Even our own experiments, suggesting "self-transfer" between dissolved molecules of the same species, give this result only for substances such as anthracene, well known to dimerize, and must therefore be regarded with some suspicion.*

Transfer in Type B Heterogeneous Systems

We have already satisfied ourselves[1] that the energy transfer which we have observed in heterogeneous systems is a short-range phenomenon depending on surface-complex formation and that the presence or absence of the latter depends on the relative size of the dipoles (permanent and induced) of the solvent and the second component. It should therefore be possible to arrange the aromatic hydrocarbons in order of increas-

[5] Th. Förster, Ann. Physik **2**, 55 (1948); Z. Naturforsch. **4a**, 321 (1949); Z. Elektrochem. **53**, 93 (1949).

[6] C. Reid, Phys. Rev. **88**, 422 (1952).

* Since the completion of this paper Bowen [E. J. Bowen and B. Brocklehurst, Trans. Faraday Soc. **49**, 1131 (1953)] has reported "long-range" (50A) energy transfer in concentrated liquid solutions at room temperature and has interpreted this result as evidence for the Forster mechanism. However, since in both cases reported one component is a relatively polar halogenated hydrocarbon it seems that the possibility of complex formation, or at least of sufficient interaction between the components to cause "sticky collisions" of duration long enough for short-range energy transfer, has not been ruled out.

ing polarizability on the basis of their transfer efficiency as the dissolved component of such systems. In such an arrangement, however, we would expect deviations due to differences in the relative absorption and emission regions of the crystal and the dissolved component.

However, it has not been possible to make convincing correlations of this kind. Nor is there any correlation between energy transfer and the presence of exceptional "bond orders" or "free valences" as calculated by the various theoretical approaches.

Transfer in Type C Heterogeneous Systems

Only one correlation has been found in this group of phenomena. The observations of interest (Table IV) are the shifts in position (from the value in solution) of the emission bands of naphthacene adsorbed on various host crystals. There is some correlation with the self-polarizabilities calculated by Greenwood[7] for the set of substituted 1,2-benzanthracenes.

This fact is of considerable interest since the self-polarizabilities show a better correlation with carcinogenic activity than do any other physical constants. Our new correlation suggests that perhaps more attention should be paid to this quantity as an index of chemical behavior, and less to bond orders and other local effects.

The actual observation is that the higher the self-polarizability of the crystalline component, the smaller the shift of the naphthacene bands. Presumably this means that the more polarizable the host crystal, the more the distortion of its orbitals, during complex formation, and the less the distortion of the naphthacene orbitals.

For molecules other than the 1,2-benzanthracenes, self-polarizabilities were not available to us, but the correlations with biological activity were less convincing.

To summarize the results of our four energy transfer papers, almost all of the new phenomena observed come from systems in which one partner of a closely associated pair of molecules is excited. The association may be of the strong "molecular complex" kind found for hydrocarbons and polynitro compounds, in which case true solutions may be employed, or may be an adsorption phenomenon in a heterogeneous system. The spectral shifts and changes in character of the band envelopes as well as the energy transfer phenomenon may prove useful in the characterization of electronic transitions. The perturbations resulting from complex formation are in general considerably greater than those resulting from interaction with the solvent which have already proved useful in suggesting spectral assignments.[8,9]

[7] H. H. Greenwood, Brit. J. Cancer **5**, 441 (1951).

TABLE IV. The shift of the highest-energy naphthacene solution band at 78°K in suspensions of various hydrocarbons compared with the carcinogenic activity[a] and self-polarizability values,[b] at the particular substituent position.

Component in suspension	Naphthacene solution band shift	Carcinogenic activity	Self-polariz-ability
1,2-benzanthracene	603 cm^{-1}	0	
9,10-dimethyl-1,2-benzanthracene	306 cm^{-1}	++++	
10-ethyl-1,2-benzanthracene	392 cm^{-1}	+++	
1′-methyl-1,2-benzanthracene	561 cm^{-1}	0	0.439
2′-methyl-1,2-benzanthracene	645 cm^{-1}	0	0.410
3′-methyl-1,2-benzanthracene	634 cm^{-1}	0	0.404
4′-methyl-1,2-benzanthracene	498 cm^{-1}	0	0.439
3-methyl-1,2-benzanthracene	624 cm^{-1}	+	0.448
4-methyl-1,2-benzanthracene	392 cm^{-1}	+	0.447
5-methyl-1,2-benzanthracene	392 cm^{-1}	++	0.452
6-methyl-1,2-benzanthracene	645 cm^{-1}	+	0.409
7-methyl-1,2-benzanthracene	686 cm^{-1}	+	0.410
8-methyl-1,2-benzanthracene	498 cm^{-1}	+	0.449
9-methyl-1,2-benzanthracene	561 cm^{-1}	++	0.496
10-methyl-1,2-benzanthracene	434 cm^{-1}	+++	0.514
Benzo(c)phenanthrene	349 cm^{-1}	+	
1-methyl-benzo(c)phenanthrene	318 cm^{-1}	...	
2-methyl-benzo(c)phenanthrene	318 cm^{-1}	++	
3-methyl-benzo(c)phenanthrene	371 cm^{-1}	++	
4-methyl-benzo(c)phenanthrene	263 cm^{-1}	++	
5-methyl-benzo(c)phenanthrene	349 cm^{-1}	+++	
6-methyl-benzo(c)phenanthrene	392 cm^{-1}	+++	
20-methyl cholanthrene	392 cm^{-1}	++++	
1,2,5,6-dibenzanthracene	645 cm^{-1}	++++	
Acenaphthene	318 cm^{-1}	0	
Benzene	349 cm^{-1}	0	
Chrysene	477 cm^{-1}	0	
Terphenyl	851 cm^{-1}	0	
Toluene	296 cm^{-1}	0	

[a] A. Pullman, Compt. rend. Soc. de biol. **139**, 1056 (1945); Compt. rend. **224**, 120 (1947); Ann. chim. **2**, 5 (1947).
[b] See reference 7.

ACKNOWLEDGMENTS

We wish to express our thanks to the National Research Council of Canada for a studentship to one of us (M.M.M.) and for a grant-in-aid of research, and to the National Cancer Institute of Canada for a grant-in-aid of research. Dr. M. S. Newman kindly provided samples of the methyl derivatives of 1,2-benzanthracene and of benzo(c)phenanthrene. Samples of other hydrocarbons were sent to us by Dr. A. W. Johnson, Dr. R. N. Jones, and Dr. R. B. Sandin.

[8] Harden McConnell, J. Chem. Phys. **20**, 700 (1952).
[9] J. R. Platt, J. Opt. Soc. Amer. **43**, 252 (1953).

Letters to the Editor

THIS section will accept reports of new work, provided these are terse and contain few figures, and especially few half-tone cuts. The Editorial Board will not hold itself responsible for opinions expressed by the correspondents. Contributions to this section should not exceed 600 words in length and must reach the office of the Editor not later than the 15th of the second month preceding that of the issue in which the Letter is to appear. No proof will be sent to the authors. A publication charge of $10.00 per Letter is made which, when honored, will entitle the Institution to 100 free reprints.

On the Kinetics of the Exchange Processes in Ion Exchangers*†

LENNART W. HOLM
Nobel Institute of Physics, Stockholm 50, Sweden
(Received January 4, 1953)

IT has been postulated[1] that for the exchange reaction between an ion A originally in solution (1) and an ion B in an ion exchange resin (s):

$$z_B A(1)+z_A B(s)\rightleftharpoons z_A B(1)+z_B A(s)$$

(z_A and z_B are the ionic charges) one or more of the following processes may be rate determining, namely, the diffusion of ion A or B in the solution, the diffusion of A or B in the resin, and/or the exchange reaction between A and B. The exchange reaction as rate determining may be ruled out just by considering that an ion exchange resin saturated with an ion is in many respects equivalent to a concentrated salt solution,[2] that is, the ions are not fixed to certain positions, but are free to diffuse around *inside* the resin. Some experimental evidence supporting this conclusion has been given.[1,3,4]

The most interesting mechanism is the diffusion inside the resin. Quite generally we have for the concentration $c_A{}^s$ of ion A at a point inside the resin at the time t, according to the second law of

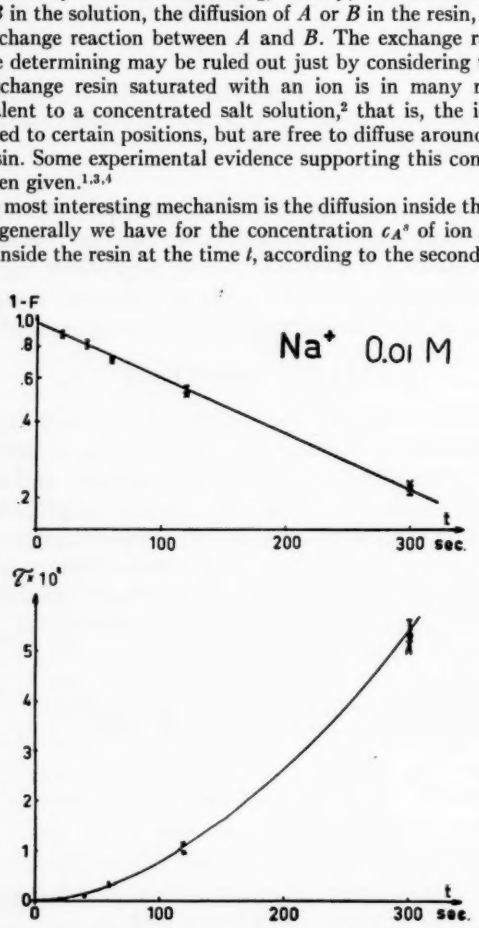

FIG. 1. Diffusion in the liquid film rate determining. Exchange of Na^+ ions between Na^+ saturated Dowex 50 and 0.01-M NaCl solution at 25°C. I = solution initially radioactive; X = exchanger initially radioactive. (Na^{22} as tracer.)

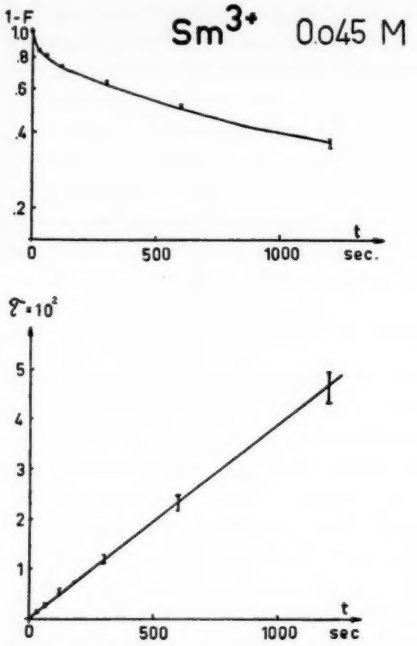

FIG. 2. Diffusion in the resin phase rate determining. Exchange of Sm^{3+} ions between Sm^{3+} saturated Dowex 50 and 0.045-M $Sm(NO_3)_3$ solution at 25°C. (Sm^{153} as tracer.)

Fick, $\partial c_A{}^s/\partial t=\mathrm{div}(D_A{}^s\,\mathrm{grad}c_A{}^s)$ and for the ion B $\partial c_B{}^s/\partial t=\mathrm{div}(D_B{}^s\,\mathrm{grad}c_B{}^s)$ where $D_A{}^s$ and $D_B{}^s$ are the nonconstant ion diffusion coefficients in the solid phase. The amount of free electrolyte in the resin is very small owing to Donnan effects and may be neglected in solutions of moderate concentrations, which also may be seen from the results of Gregor.[5] The requirement of electroneutrality thus gives $z_A c_A{}^s+z_B c_B{}^s=\text{const}$ which, on differentiation, becomes $dc_B{}^s=-(z_A/z_B)dc_A{}^s$ and, combined with the diffusion equations, gives $D_A{}^s=D_B{}^s$. The physical meaning of this result is that only one diffusion coefficient D^s can be obtained from an exchange experiment and that this coefficient cannot be assigned to one ion or the other. Inherent in the formulation is that D^s is not a constant. Among factors which affect the value of D^s may be mentioned the ion saturation, i.e., the relative amounts of the two exchanging ions in the exchanger. Different ion saturations result in different degrees of swelling, which, in turn, will cause more or less electrical and mechanical hindrance to the diffusion, giving a varying diffusion coefficient. When ions of unequal charges are exchanged the degree of swelling will also change owing to variations in the ionic strength of the solution surrounding the exchanger. Moreover, the change in degree of swelling will cause a variation in the boundary conditions of the diffusion equations. To take into account these factors theoretically is as yet almost impossible. However, by studying isotopic exchange[6] there is *a priori* only one diffusion coefficient, and this will not vary, as the bulk concentration is constant, and there will be no change in size of the resin during the exchange process. The diffusion coefficient so obtained will be characteristic of a single ion.

An exchange with isotopic ions can conveniently be carried out in a system containing a solution of the ion A, to be investigated, in dynamic equilibrium with an exchange resin saturated with the same ion,[6] using a radioactive tracer nuclide isotopic to A to follow the process. If the resin consists of spherical particles of equal diameters and diffusion inside the resin is considered as the only rate determining process, the problem is quite analogous to the heat transfer case, treated generally by Paterson.[7] By means of his solution a value of the parameter τ is obtained for each value of the fractional attainment of equilibrium F. $\tau=D^s t/a^2$, where t is the time corresponding to F, and a, the radius of the resin

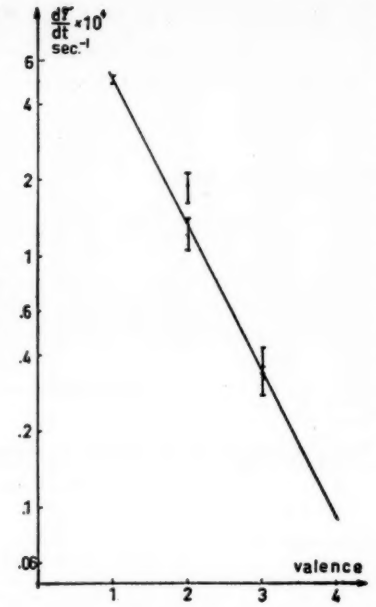

FIG. 3. Dependence of diffusion coefficient D^s ($d\tau/dt = D^s/a^2$) on the valence of the exchanging ion. (Na^+, Ca^{2+}, Sm^{3+}.)

spheres. Experimentally one gets $F=f(t)$. When the τ values corresponding to these F values are plotted against t a straight line should result if diffusion in the resin phase is rate determining. When the diffusion in the solution (by stirring reduced to a liquid film adhering to the resin) is rate determining, the first law of Fick gives $\ln(1-F)=kt$, where k is a constant proportional to the diffusion coefficient solution, and thus a plot of $\ln(1-F)$ *versus* t will give a straight line in this case. An example of the latter case is obvious from the curves, $\log(1-F)=g_1(t)$ a straight line and $\tau=g_2(t)$ curved, in Fig. 1. Figure 2 shows an equally striking example of the opposite case, a result which could be anticipated for this rather high concentration of a three-valent ion. The approximately straight line in Fig. 3 indicates a decrease by a factor of about four in the diffusion coefficient, for an increase of one unit in the charge of the ion. These low diffusion coefficients—for a four-valent ion more than a factor of 100 (extrapolated value) less than in solution—may be of interest in connection with studies on the behavior of so-called radiocolloids, which are most frequently observed with highly charged ions. The radiocolloids may consist of insoluble matter, which have sorbed the radioactive ions.[8] From the present results it seems plausible that the sorption may be reversible, the low rate being the reason that it often has appeared as irreversible.[6]

A detailed account of this work will be published elsewhere.

* This letter is a part of a paper presented orally at the XIIIth International Congress of Pure and Applied Chemistry, Stockholm, 1953.

† Note: After this paper was sent for publication a paper by Boyd *et al.* of similar content in some aspects appeared in the J. Am. Chem. Soc. **75**, 6091 (1953).

[1] Boyd, Adamson, and Myers, J. Am. Chem. Soc. **69**, 2836 (1947).
[2] G. E. Boyd, Ann. Rev. Phys. Chem. **2**, 309 (1951).
[3] J. J. Grossman and A. W. Adamson, J. Phys. Chem. **56**, 97 (1952).
[4] D. K. Hale and D. Reichenberg, Discussions Faraday Soc. No. 7, 79 (1949).
[5] H. P. Gregor, J. Am. Chem. Soc. **73**, 642 (1951).
[6] L. W. Holm and T. Westermark, Acta Chem. Scand. **4**, 968 (1950).
[7] S. Paterson, Proc. Phys. Soc. (London) **59**, 50 (1947).
[8] O. Hahn, *Applied Radiochemistry* (Cornell University Press, Ithaca, 1936).

Elastic Constants of Gels

M. KRISHNAMURTHI AND G. SIVARAMA SASTRY
Physical Laboratories, Osmania University, Hyderabad, India
(Received February 22, 1954)

ELASTIC constants of gels were determined in the past by Sheppard and Sweet,[1] Prasad,[2] and Poole,[3] using static methods and more recently by Srivastava[4] using an ultrasonic method. The difficulty of the static method is that gels are usually very delicate and fragile and it is not easy to apply any but the smallest stress, especially of the torsional type, without breaking up the gel itself. In the present work, a dynamic ultrasonic method described by Krishnamurthi and Balakrishna[5] is employed to determine the elastic constants of silica and alumina silica gels. These gels are prepared by mixing an aqueous solution of sodium silicate with that of hydrochloric acid or sodium aluminate, respectively, as described by Merrill and Spencer.[6] A metallic frame with windows for transmitting the ultrasonic beam is immersed in the solutions prior to the formation of the gel. After the gel is set, the frame is removed carefully by cutting off the superfluous mass of gel by a fine blade. This frame is attached to the axis of a screw motion drive having a graduated screw with a least count of 0.072°. The frame, so mounted, is interposed in the path of the ultrasonic beam and rotated. The two critical angles for total internal reflection of the longitudinal and torsional waves are determined and the velocities obtained therefrom. To overcome any discrepancies due to thickness effect, a sample of about 7-mm thickness is used in these experiments.

TABLE I. Velocity in carbon tetrachloride = 926m/sec.

Substance	i_L	i_T	V_L	V_T	ρ	Y	n	σ
Silica gel								
Authors	28.8	47.9	1909	1242	1.13	0.395	0.174	+0.135
Srivastava	...	...	1850	1570	1.14	0.201	0.284	−0.63
Static method	...	...	...	...	...	...	...	+0.13
Silica alumina gel								
Authors	31.9	49.6	1744	1211	1.11	0.337	0.163	+0.034
Static method	...	...	...	...	...	...	...	+

The results obtained for the two gels are given in Table I. i_L and i_T are the longitudinal and torsional angles in degrees, and V_L and V_T the corresponding velocities in meters/second while ρ is density in g/cc. Y and n are given in units of 10^{11} dynes per sq cm and σ is Poisson's ratio. The result of striking importance is the positive sign of σ. This is in complete disagreement with Srivastava's results. He reported a very high negative Poisson's ratio for silica gel. His results are also given in Table I for comparison. It is seen that while V_L is in good agreement in the two cases, the values for V_T show a lot of divergence. An examination of Srivastava's ultrasonic transmission curve for silica gel shows that at his torsional critical angle there is only a dip in the intensity of transmission of the ultrasonic beam and that after this position the ultrasonic beam is still being transmitted with full intensity. It is therefore thought necessary that a search for the position of complete extinction must be made with a liquid of much lower velocity than water. Hence carbon tetrachloride is used. Another point of great interest is that after the longitudinal component is totally reflected, the intensity of transmitted ultrasonic beam is extremely small showing that a gel simulates very closely a liquid in its inability to propagate torsional waves.

Confirmation of results obtained by us in the ultrasonic method is obtained by conducting a static experiment on silica gel to determine the sign and magnitude of σ. A small block of the gel of rectangular section is compressed to a known extent between the jaws of a vernier calipers. The resulting change in the other dimension is observed by an optical lever method. The result of this experiment is also given in Table I and shows that σ is positive and its magnitude is also in agreement with that obtained by the ultrasonic method. A similar experiment on the other gel was not possible as even the slightest pressure broke it up. The sign of σ was, however, confirmed to be positive.

In conclusion, the authors wish to express their grateful thanks to Professor S. Bhagavantam for his guidance and keen interest throughout this work.

[1] S. E. Sheppard and S. S. Sweet, J. Am. Chem. Soc. **33**, 539 (1921).
[2] Prasad, Kolloid Z. **33**, 279 (1923).
[3] H. J. Poole, J. Faraday Soc. **21**, 114 (1925); **22**, 81 (1926).
[4] A. M. Srivastava, Proc. Nat. Acad. Sci. India **18A**, 51 (1949).
[5] M. Krishnamurthi and S. Balakrishna, Proc. Indian Acad. Sci. **38**, 495 (1953).
[6] R. C. Merrill and R. W. Spencer, J. Phys. Colloid Chem. **54**, 806 (1950).

Mean Dimensions of Rubber-Like Molecules

T. B. GRIMLEY
Department of Physical Chemistry, University of Liverpool, Liverpool, England
(Received February 24, 1954)

IN a recent paper, Wall[1] has derived an expression for the average square end-to-end distance of a chain molecule using an approximate method intended to take into account the excluded volume effect. It is the main purpose of this note to point out that Wall's result applies, not to a chain molecule, but to a "chain" in which the probability distribution of any element is uniquely determined by that of the preceding elements. The conversion from a chain molecule to a "chain" with the above properties is effectively made by the assumption[1] $P+Q+R+S+T+U=1$ which Wall actually recognizes as introducing an error.

Let the elements of a chain with N links be numbered 0, 1, 2, ..., N and let element number O be fixed at the origin of a coordinate system. The transition probability $\psi_{mN}(\mathbf{r},\mathbf{s})d\mathbf{s}$ is defined as the probability that the link connecting elements $m-1$ and m is given by $\mathbf{s}$ to within $d\mathbf{s}$ if the vector joining elements O and $m-1$ is given by $\mathbf{r}$. Evidently $\int\psi_{mN}(\mathbf{r},\mathbf{s})d\mathbf{s}=1$. For a chain with links of length l, the end point of $\mathbf{s}$ moves on the surface of a sphere of radius l and center $\mathbf{r}$. If $f_N(\mathbf{r};m-1)$ is the distribution function for element number $m-1$ with respect to element number O, then $\langle r_m^2\rangle_N$, the average square distance of element number m from the origin, is given by

$$\langle r_m^2\rangle_N-\langle r_{m-1}^2\rangle_N=l^2+2\int\int(\mathbf{r}\cdot\mathbf{s})f_N(\mathbf{r};m-1)\psi_{mN}(\mathbf{r},\mathbf{s})d\mathbf{r}d\mathbf{s}. \quad (1)$$

Now if the probability distribution of element number m depends only on that of the preceding elements 0, 1, ..., $m-1$, then $f_N(\mathbf{r};m-1)=f_{m-1}(\mathbf{r};m-1)$. Moreover, ψ_{mN} is independent of N and is accurately expressed by[2]

$$\psi_{mN}(\mathbf{r},\mathbf{s})=\lambda_m(\mathbf{r})\{1+[\beta_1/f_{m-1}(\mathbf{r};m-1)]\sum_{j=1}^{m-1}\times f_{m-1}(\mathbf{r},\mathbf{r}+\mathbf{s};m-1,j)\} \quad (2)$$

if ternary and higher-order complexes of chain elements can be ignored. In (2), β_1 is the excluded volume integral for free chain elements, $f_{m-1}(\mathbf{r},\mathbf{r}';m-1,j)$ is the distribution function for elements $m-1$ and j in a chain of $m-1$ links, and $\lambda_m(\mathbf{r})$ is a normalizing factor, determined by $\int\psi_{mN}(\mathbf{r},\mathbf{s})d\mathbf{s}=1$. Using (2) in (1) and applying a perturbation method based on the use of the random flight functions in the second term on the right in (1), we obtain

$$\langle r_N^2\rangle_N=l^2[N-2(3/2\pi)^{\frac{1}{2}}(\beta_1/l^3)\sum_{j=1}^{N-1}(N-j)j^{-\frac{1}{2}}]. \quad (3)$$

For large N therefore $\langle r_N^2\rangle_N\sim Nl^2[1-1.724(\beta_1/l^3)]$. For a chain on a square lattice, $-\beta_1=l^3$ and (3) is Wall's result. It does not however apply to a chain molecule. In a chain molecule the probability distribution of any element is determined by that of *all* the other elements in the chain, and classical statistical mechanics may be used to show that, in this case,

$$\psi_{mN}(\mathbf{r},\mathbf{s})=\lambda_{mN}(\mathbf{r})\{1+[\beta_1/f_{m-1}(\mathbf{r};m-1)]\sum_{j=0}^{m-2}\sum_{k=0}^{N-m}\times\int f_{m-1}(\mathbf{r},\mathbf{r}';m-1,j)f_{N-m}(\mathbf{r}'-\mathbf{r}-\mathbf{s};k)d\mathbf{r}'\} \quad (4)$$

if ternary and higher-order complexes of chain elements can be ignored. In (4) $\lambda_{mN}(\mathbf{r})$ is a normalizing factor determined by $\int\psi_{mN}(\mathbf{r},\mathbf{s})d\mathbf{s}=1$. Using (4) in (1) and applying the perturbation method, we find

$$\langle r_m^2\rangle_N-\langle r_{m-1}^2\rangle_N=l^2[1-2(3/2\pi)^{\frac{1}{2}}(\beta_1/l^3)\sum_{k=m}^{N}\sum_{n=1}^{m-1}\times(m-n)(k-n)^{-5/2}], \quad (5)$$

so that

$$\langle r_N^2\rangle_N=l^2\{N-(3/2\pi)^{\frac{1}{2}}(\beta_1/l^3)\sum_{k=1}^{N}\sum_{n=1}^{k-1}[(k-n)^{-\frac{1}{2}}+(k-n)^{-1}]\}.$$

For large N, therefore, we have the familiar result[2-4]

$$\langle r_N^2\rangle_N\sim Nl^2[1-(4/3)(3/2\pi)^{\frac{1}{2}}(\beta_1/l^3)N^{\frac{1}{2}}].$$

Equation (5) also leads to a value for

$$\sum_{m=1}^{N}\langle r_m^2\rangle_N.$$

For large N the result is

$$\sum_{m=1}^{N}\langle r_m^2\rangle_N\sim\tfrac{1}{2}N^2l^2[1-(56/45)(3/2\pi)^{\frac{1}{2}}(\beta_1/l^3)N^{\frac{1}{2}}].$$

[1] F. T. Wall, J. Chem. Phys. **21**, 1914 (1953).
[2] T. B. Grimley, J. Chem. Phys. **21**, 185 (1953).
[3] H. M. James, J. Chem. Phys. **21**, 1628 (1953).
[4] Zimm, Stockmayer, and Fixman, J. Chem. Phys. **21**, 1716 (1953).

Dependence of Surface Tension on Temperature

SHASHANKA SHEKHAR MITRA,
Physics Department, Allahabad University, Allahabad, India
AND
SURENDRA NATH SRIVASTAVA,
Indian Lac Research Institute, Namkum, Ranchi, India
(Received February 25, 1954)

THE surface tension of liquids decreases linearly with temperature over small temperature ranges. However, until now several formulas have been put forward for the exact dependence of the quantity on temperature. The generally accepted one is due to Ferguson[1]

$$S=A\left(1-\frac{T}{T_c}\right)^n;$$

symbols have their usual meaning. The formula fails when applied to associated liquids like water and alcohols and is to be supplemented by a number of power terms in $(1-T/T_c)$ reducing it to

$$S=A\left(1-\frac{T}{T_c}\right)^n-B\left(1-\frac{T}{T_c}\right)^2+C\left(1-\frac{T}{T_c}\right)^3.$$

Two empirical formulas are presented here, which are applicable both to associated and nonassociated liquids. The formulas are

$$\log S=\log S_0-kT^n\left(1-\frac{T_0}{T}\right) \quad (1)$$

and

$$\log S=\log S_0-L(\log T)^m\left(1-\frac{T_0}{T}\right), \quad (2)$$

where K, n, L, and m are constants and S_0 is the surface tension at any temperature T_0.

TABLE I.

T°K	S_{calc} (1)	S_{calc} (2)	S_{obs}
273	...	...	75.64
283	74.22	74.22	74.22
293	72.74	72.74	72.75
303	71.18	71.19	71.18
313	69.57	69.57	69.56
323	67.90	67.89	67.91
333	66.19	66.19	66.18
343	64.44	64.42	64.42
353	62.59	62.59	62.61
363	60.76	60.76	60.75
373	58.89	58.89	58.85

Table I records the calculated values of the surface tension from (1) and (2) at different temperatures along with the observed[2] one in the case of water. The maximum error is 0.067 percent.

The values of the constants for some twenty liquids are given in Table II.

TABLE II.

Liquids	n	$K\times10^5$	m	$L\times10^5$	T_0°K
Water	2.028	0.2464	11.80	0.5815	273
Ethyl alcohol	1.126	82.12	7.112	78.89	273
Benzene	1.532	9.44	8.861	19.01	273
Carbon disulfide	1.734	2.941	10.03	6.463	273
Phenol	1.656	2.638	9.891	4.192	273
Bromobenzene	1.631	4.519	9.601	6.823	283
Iodobenzene	1.699	2.242	10.02	4.178	293
n-Hexane	2.010	0.7980	11.47	2.168	273
n-Octane	1.648	4.786	9.432	11.19	273
2,5-Dimethyl hexane	1.821	2.163	10.72	3.681	273
Ethyl formate	2.267	0.2360	13.28	0.3846	273
Methyl propionate	2.041	0.7015	12.34	0.8511	283
Propyl formate	1.833	2.065	10.61	3.899	273
Ethyl propionate	1.734	2.056	10.03	6.839	278
n-Propyl acetate	1.685	3.648	9.750	8.570	273
Chloroform	1.916	1.167	11.04	2.917	283
Acetone	1.972	0.7447	11.28	2.430	273
Ethyl ether	2.926	0.00309	17.22	0.0138	293
Isoamyl alcohol	1.653	0.4395	9.568	6.879	273
Ammonia	2.215	0.4603	12.73	1.371	284.1

The authors wish to thank Dr. K. Majumdar and Mr. Y. P. Varshni for their interest in the investigation.

[1] Ferguson, Trans. Faraday Soc. **19**, 408 (1923).
[2] *International Critical Tables* (McGraw-Hill Book Company, Inc., New York).

Polarized Infrared Spectrum of $KAu(CN)_2$: Revision and Refinement*

LLEWELLYN H. JONES
Los Alamos Scientific Laboratory, University of California, Los Alamos, New Mexico
(Received March 1, 1954)

A RECENT letter[1] stated that the polarization of the infrared absorption bands of $KAu(CN)_2$ shows that the linear N−C−Au−C−N groups lie along the C axis. In that experimental work there was some absorption of light polarized perpendicular to the C axis. It was thought that this observed "perpendicular absorption" arose from incomplete polarization of the incident light and imperfections in the crystal. However, Professor Linus Pauling of the California Institute of Technology pointed out that the linear N−C−Au−C−N groups may make a small angle with the C axis, since in potassium silver dicyanide[2] the linear N−C−Ag−C−N groups are inclined at an angle of 27° with the C axis in trigonal symmetry about this axis. Cromer[3] has compared the x-ray diffraction patterns of $KAu(CN)_2$ and $KAg(CN)_2$ and has concluded that, though they are not isomorphous, the arrangement of linear groups is probably similar in the two substances.

More quantitative polarization studies have now been made on two single crystals of $KAu(CN)_2$ mounted with the C axis perpendicular to the direction of propagation of light. Instead of the fundamental absorption band at 2140 cm^{-1}, a combination band at 2586 cm^{-1} was studied, as this permitted the use of a thicker crystal. The band at 2586 cm^{-1} has been assigned[4] as a summation band of the asymmetric C−N stretching vibration (2140 cm^{-1}) and the symmetric gold-carbon stretching vibration (*ca* 446 cm^{-1}). This band at 2585 cm^{-1} is polarized in the same direction as the band at 2140 cm^{-1}, as required by its symmetry class.

The crystal was assumed to have linear N−C−Au−C−N groups arranged in trigonal symmetry about the C axis and inclined to the C axis at an angle α, similar to the arrangement in $KAg(CN)_2$ for which $\alpha=27°$. For this system, since the extinction coefficient is proportional to the square of the transition moment (which is along the linear N−C−Au−C−N axis), the geometry requires that for a given crystal

$$\frac{OD_{90°}}{OD_{0°}}=(1/2)\tan^2\alpha$$

$OD_{90°}$ = optical density of light polarized perpendicular to C axis
$OD_{0°}$ = optical density of light polarized parallel to C axis
α = angle of inclination of N−C−Au−C−N groups with the C axis.

The above expression assumes Beer's law holds at the slit widths used. Beer's law was obeyed by known path lengths of powdered $KAu(CN)_2$ (intimately ground with potassium iodide and pressed into plates) at any given slit width—from 0.200 to 2.000 mm.

The results for measurements on two different crystals are given in Table I. Two different experiments were made on each crystal—one with the C axis parallel to the spectrograph slit, and one with the C axis perpendicular to the slit ($\gamma=0$ and 90, respectively).

TABLE I. Polarization of 2586 cm^{-1} peak of $KAu(CN)_2$.

Crystal No.	Slit width	γ[a]	OD_0[b]	OD_{90}[b]	α
1	2.00 mm	0°	0.491	0.076	29.0°
1	2.00 mm	90°	0.542	0.079	28.35°
2	0.70 mm	0°	1.328	0.191	28.2°
2	0.70 mm	90°	1.467	0.183	26.5°

[a] γ = angle C axis makes with slit.
[b] OD_β = optical density at 2586 cm^{-1} corrected for inefficiency of polarizer and for apparatus polarization. β = angle which plane of polarization of light makes with C axis.

Applying the statistics of small numbers[5] to the four determinations of α, we find that

$$\alpha=28.0\pm1.8° \text{ at the 95 percent confidence level.}[6]$$

Thus, the linear N−C−Au−C−N groups of $KAu(CN)_2$ make an angle of about 28° with the C axis. This value is the same as that for $KAg(CN)_2$ (27°) within experimental error.

* This work was sponsored by the U. S. Atomic Energy Commission.
[1] Llewellyn H. Jones, J. Chem. Phys. **21**, 1891 (1953).
[2] J. L. Hoard, Z. Krist. **84**, 231 (1933).
[3] Unpublished work by D. Cromer of this laboratory.
[4] Unpublished work by the author.
[5] R. B. Dean and W. J. Dixon, Anal. Chem. **23**, 636 (1951).
[6] In reporting this value, it has been assumed that there are no appreciable systematic errors. A similar study of $KAg(CN)_2$ (now in progress) should provide a check of this assumption.

Paramagnetic Resonance Spectra of Wurster's Free Radical Ions*

S. I. WEISSMAN
Washington University, St. Louis, Missouri
(Received March 22, 1954)

THE complex hyperfine structure in the paramagnetic resonance spectrum of Wurster's blue free radical ion has been described in an earlier communication[1] from this laboratory. The spectra of a series of related free radicals have since been observed. Further, the spectrum of Wurster's blue ion, re-examined under higher sensitivity, has been found to contain thirty-nine lines disposed in thirteen triplets rather than thirty-three lines in eleven triplets as previously reported.

A description of the spectra of the free radicals (listed according to the names of the parent paraphenylenediamines) is given in Table I. The spectra of all the free radicals except the positive ion of NN dimethyl N′N′ dideutero-*p*-phenylenediamine were observed from dilute solutions in ordinary water; the latter was dissolved in heavy water.

Unambiguous assignment of the origin of most of the splittings cannot yet be made. Comparison of the spectra of the NN dimethyl and NN dimethyl N′N′ dideutero derivatives leads, however, to assignment of the 2.8-oersted interval in the former to interaction of the unpaired electron with the two amino protons. This splitting corresponds to a value of $|\psi|^2$, the square of the wave function of the unpaired electron, at each of these positions of 11.2×10^{22} cm^{-3} as compared with 2660×10^{22} cm^{-3} at the position of the proton in a 1*s* hydrogen atom. The 8.5-oersted interval in the dideutero compound may arise from interaction with the methyl protons. This assignment leads to a value 33×10^{22} cm^{-3}

TABLE I. Spectra of positive ions of *p*-phenylenediaminal derivatives.

Derivative	Nature of spectrum
NNN'N' tetramethyl (Wurster's blue)	Thirteen triplets 7.4 oersteds between centers of triplets; 2.1 oersted between members of each triplet.
NN dimethyl (Wurster's red)	Twenty-seven almost equally spaced components. Interval 2.8 oersteds.
NN dimethyl-N'N' dideutero	Seven groups. Interval between groups 8.5 oersteds. Each group contains at least three components. Two more weaker groups may be present.
NN' dimethyl	Nine groups. Interval between groups 9.5 oersteds. Each group is complex, containing at least three components.
N methyl[a]	Twenty-four almost equally spaced lines. Interval about 2 oersteds.
Unsubstituted[a]	Fifteen lines; interval about 2 oersteds.

[a] Because of the instability of these free radicals their spectra were taken at sweep rates too rapid for trustworthy recording.

for $|\psi|^2$ at each of these positions. Summed over the six equivalent methyl protons, $|\psi|^2$ is about ten percent of the hydrogen 1*s* value. For the other compounds no assignments completely consistent with the observations have yet been devised. It is hoped that the investigations now being carried out in this laboratory of various isotopically substituted derivatives of these free radicals will lead to detailed interpretations of the splittings.

* Assisted by the joint program of the U. S. Office of Naval Research and U. S. Atomic Energy Commission.

[1] Weissman, Townsend, Paul, and Pake, J. Chem. Phys. **21**, 2227 (1953).

The Lattice Energies of Copper Subgroup and Thallous Halides

AUBREY P. ALTSHULLER
1911 Clover Street, Cleveland 9, Ohio
(Received March 22, 1954)

THE more accurate determinations of the heats of sublimation, ΔH_{subl}, at 0°K of copper,[1,2] silver,[2,3] gold,[2,4] and thallium[2,5] now available together with better values for the electron affinities of the halogen atoms[6] makes a recalculation of the experimental lattice energies of the copper subgroup halides and the thallous halides of interest. The experimental lattice energies are compared with Mayer's theoretical lattice energies.[7]

The heat of sublimation of Cu determined recently by Hersh[1] of 81.1 kcal/mole is in excellent agreement with the value of 81.2 kcal/mole in the National Bureau of Standards compilation.[2] The average value of 70.9 kcal/mole for Ag given recently by McCabe and Birchenall[5] will be employed rather than the somewhat lower value given by the NBS.[2] The recent determination of the heat of sublimation of Au by Hall[4] of 84.6 kcal/mole will be used rather than the value given by the NBS which is based on previous values which are rather widely scattered. The NBS value for the heat of sublimation of Tl of 43.3 kcal/mole is used.

The experimental lattice energies for Cu, Ag, Au, and Tl halides are given in Table I. The electron affinities E of the halogen atoms at 0°K are the most probable values[6] rounded off to the nearest kcal. The heats of formation of the metal halides ΔH_f at 298°K are taken from the NBS tables,[2] except for the value for TlF.[8] The ionization potentials I of the metals at 0°K are taken from Landolt-Börnstein.[9] The dissociation energies D of Cl_2, Br_2, and I_2 at 298°K are also taken from the NBS tables.[2] Most of the recently proposed values of $D(F_2)$ are in the range from 35–40 kcal.[10,11] Employing an electron affinity of 83 kcal for F in the Born-Haber cycle for the alkali metal fluorides, a dissociation energy of 38 kcal for F_2 may be calculated. In Table I one-half of the dissociation energy of F_2 is taken as 19 kcal. The energy involved in heating or cooling the metal, halogen gas, and metal halide between 0° and 298°K is also included in the calculation of the lattice energy although not given explicitly in the table.

TABLE I. Lattice energies of Cu subgroup and Tl halides (kcal/mole).

Salt	$-\Delta H_f$	$\frac{1}{2}D$	$-E$	$\Delta H_{\text{subl.}}$	I	U_{exp}	U_{theor}	ΔU
CuCl	32.2	29.0	−88	81.1	178.0	232	216	16
CuBr	25.1	23.0	−82	81.1	178.0	226	208	18
CuI	16.2	18.0	−75	81.1	178.0	219	199	20
AgF	48.5	19	−83	70.9	174.7	229	219	10
AgCl	30.4	29.0	−88	70.9	174.7	217	203	14
AgBr	23.8	23.0	−82	70.9	174.7	211	197	14
AgI	14.9	18.0	−75	70.9	174.7	204	190	14
AuCl	8.4	29.0	−88	84.6	212.8	247	...	...
AuBr	4.4	23.0	−82	84.6	212.8	243	...	...
AuI	−0.2	18.0	−75	84.6	212.8	241	...	...
TlF	76.8	19	−83	43.3	141.1	196	...	...
TlCl	49.0	29.0	−88	43.3	141.1	174	167	7
TlBr	41.2	23.0	−82	43.3	141.1	167	164	3
TlI	29.7	18.0	−75	43.3	141.1	158	159	−1

Mayer[7] concluded on the basis of the information available at the time for the computation of the experimental lattice energies that AgF, AgCl, and AgBr were ionic while AgI and the Cu halides are somewhat covalent. It is evident from Table I that there are appreciable homopolar contributions to the lattice energies of the Cu and Ag halides listed from the positive differences between the experimental and theoretical values. Although the lattice constants and compressibilities apparently are not available for the aurous halides so that a theoretical calculation of the lattice energies may be made, it is quite probable that there is also a homopolar contribution to the lattice energies of the aurous halides.

The variation in ΔU for the Tl halides in passing from the chloride to the iodide is rather peculiar in that it apparently indicates a small increase in ionic character in going from TlCl to TlI. Since such an increase in ionic character is not very reasonable, the differences are probably due to errors in the theoretical lattice energies (±3–4 kcal) and/or in the experimental lattice energies (±2–3 kcal). Actually the thallous halides in the solid state are probably almost if not entirely ionic. In the gaseous state TlCl has a 15–20 percent contribution from sp hybridization[12] to the binding energy, but microwave data[12] indicates that the ionic character of compounds appears to increase in passing from the gaseous to the solid state. The TlF lattice has a distorted structure (rhombic face-centered) owing to the polarization of Tl^+ by the F^-.

[1] H. N. Hersh, J. Am. Chem. Soc. **75**, 1529 (1953).
[2] F. D. Rossini *et al.*, Selected Values of Chemical Thermodynamic Properties, NBS Circular 500, 1952.
[3] C. L. McCabe and C. E. Birchenall, J. Metals, **5**, 707 (1953).
[4] L. D. Hall, J. Am. Chem. Soc. **73**, 757 (1951).
[5] F. F. Coleman and A. Egerton, Trans. Roy. Soc. (London) **A234**, 177 (1935).
[6] H. O. Pritchard, Chem. Revs. **52**, 529 (1953).
[7] J. E. Mayer, J. Chem. Phys. **1**, 327 (1933).
[8] A. D. Caunt and R. F. Barrow, Trans. Faraday Soc. **46**, 154 (1950).
[9] Landolt-Börnstein, "Numerical Values and Functions from Physics, Chemistry, Astronomy, Geophysics and Technology," *Atoms and Ions* (Springer-Verlag, Berlin, 1950).
[10] R. N. Doescher, J. Chem. Phys. **20**, 330 (1952).
[11] H. Wise, J. Chem. Phys. **20**, 927 (1952).
[12] B. P. Dailey, J. Phys. Chem. **57**, 490 (1953).

Paramagnetic Resonance in Phthalocyanine, Chlorophyll, and Haemoglobin Derivatives

D. J. E. INGRAM AND J. E. BENNETT
University of Southampton, Southampton, England
(Received March 23, 1954)

SEVERAL important organic compounds have a structure which contains one metallic atom at its center, this being surrounded by four coplanar nitrogens. Thus haemoglobin has a central iron atom, chlorophyll a central magnesium atom, and the metallic phthalocyanine derivatives[1] have an identical central structure, it being possible to substitute several different metal

atoms into the center of the four nitrogens. Although considerable work[2,3] has been done to elucidate this metal-nitrogen combination, very little detailed data is actually available on what is one of the most important of biophysical structures. Since the method of paramagnetic resonance absorption can give a very detailed picture of the electron orbitals involved in the binding of the paramagnetic atom, it was thought that it might be able to throw considerable light on this problem. This hope seems to be confirmed by the preliminary results reported below, which give a lot of new data and indicate that it should be possible to construct a detailed theoretical picture when measurements on the single crystals are completed.

The phthalocyanine crystals are the easiest to grow, and their detailed x-ray analysis is available.[4] The measurements on the crystals were made at 1.25 cm wavelength at temperatures ranging from 270° to 20°K, the "g" values were checked in the powders at 3.2 cm. The results obtained so far can be summarized as follows.

Copper phthalocyanine.—The absorption in this is large enough for measurements to be made on a single crystal. Each of the two copper atoms per unit cell produces an anisotropic absorption line which has a width varying from 20 to 100 gauss as its "g" value varies from 2.04 to 2.10, the minimum values being parallel to the nitrogen-metal plane.

Cobalt phthalocyanine.—This has two absorption lines, one remaining nearly isotropic with a "g" value of 2.9, while the other has a large anisotropy, its "g" value varying from 2.4 to 1.98 for rotation in the "ab" plane. The width of these lines is about 800 gauss and does not seem to vary much between 270° and 20°K.

Iron phthalocyanine gives a broad absorption at "g" values corresponding to 3.8 and 2.0, with weaker side lines, no measurements on a single crystal of this, or the following compounds, have yet been made.

Manganese and vanadium phthalocyanines both show an absorption line at $g=2.0$ with a width of 500 gauss.

Nickel phthalocyanine gives a broad absorption line of 800 gauss width at a "g" value of 2.20, a similar line also being obtained from metal-free phthalocyanine.

Aluminium, lead, zinc, and magnesium phthalocyanines give no absorption from crystals, but the powders, before crystallization, all show a narrow absorption line at $g=2.0$ of 10 gauss width. A similar but wider line (30 gauss) is obtained from the impure nickel salt, and the source of these is still being investigated.

Coppered chlorophylls.—Four different derivatives all gave an absorption line 100 gauss wide with a "g" value of 2.05 ± 0.01 at 1.25 and 3.2 cm, and 90° and 270°K.

Haemoglobin.—Small crystals of human haemoglobin supplied by Dr. Perutz showed only a very faint signal.

Further measurements are in progress on single crystals of the above compounds, and it is hoped that increased sensitivity and dilution will resolve the hyperfine structure due to both the metal and nitrogen atoms, which should give very detailed information on the nitrogen-metal bond.

We would like to thank Dr. K. W. H. Stevens for much help in the theoretical discussion of the subject.

[1] R. P. Linstead, J. Chem. Soc. **1934**, II, 1016.
[2] C. C. Steele, Chem. Revs. **20**, 1 (1937).
[3] L. Pauling and C. D. Coryell, Proc. Nat. Acad. Sci. U. S. **22**, 159, 210 (1936).
[4] J. M. Robertson, J. Chem. Soc. **1935**, I, 615.

Calculation of the Fraction of Effusing Molecules which Strike a Collector Plate above a Channel Hole*

ROBERT D. FREEMAN AND ALAN W. SEARCY
Department of Chemistry, Purdue University, West Lafayette, Indiana
(Received March 23, 1954)

IN determinations of vapor pressures by the Knudsen method[1] the weight of vapor escaping through the effusion hole is often calculated from the weight of material deposited on a collector plate above the hole. If the length of the hole is infinitesimal compared to its radius, the fraction of effusing molecules that strike the collector plate can be calculated from the cosine distribution law. If the length of the hole is appreciable, however, the cosine law is not obeyed. The precise relationship between the number of molecules striking a collector above such holes and the number of molecules which would escape from the effusion cell if the length of the hole were negligible has not been known.[2] We shall show how the desired relationship can be obtained from equations derived by Clausing[3] for the angular distribution of effusing molecules.

Clausing applied his equations for the angular distribution to calculation of the fraction of molecules which, having entered one end of a channel hole, escape from the opposite end. Values calculated[4] are in excellent agreement with values calculated by a different method.[5] Of the molecules entering the hole, the fraction n which escape at the other end into a cone whose sides are at angle θ with the normal to the hole is given by [Eq. (11), reference 3],

$$n=\int_0^\theta T\sin 2\theta d\theta \qquad (1)$$

where T is a complicated function of the length L and the radius r of the hole, and of the angle θ. If a collector forms the base of the cone whose sides are at the angle θ measured from the normal to the hole, the fraction n is also the ratio of the number of molecules striking the collector plate to the total number of molecules that would escape from the hole if its length were infinitesimal.

Equation (1) cannot, in general, be integrated analytically. However, it can be evaluated by Simpson's method if T is known for the required values of θ. Values of T which we have calculated for various values of L/r and θ are given in Table I. Intermediate values of T may be obtained by graphical interpolation in plots of T *vs* L/r for the various values of θ, or of T *vs* θ for the various values of L/r.

TABLE I. Values of T for various values of L/r and θ.[a]

L/r \ θ	15°	30°	45°	60°	75°	90°
0.0	1.0000	1.0000	1.0000	1.0000	1.0000	1.0000
0.2	0.9830	0.9632	0.9365	0.8903	0.7678	0.4536
0.4	0.9659	0.9266	0.8735	0.7836	0.5693	0.4139
0.6	0.9489	0.8903	0.8116	0.6829	0.4710	0.3800
0.8	0.9319	0.8541	0.7512	0.5915	0.4358	0.3511
1.0	0.9147	0.8183	0.6930	0.5141	0.4053	0.3263
1.2	0.8936	0.7832	0.6375	0.4642	0.3789	0.3049
1.4	0.8811	0.7484	0.5853	0.4358	0.3555	0.2860
1.6	0.8643	0.7143	0.5375	0.4108	0.3352	0.2697
1.8	0.8477	0.6810	0.4950	0.3887	0.3174	0.2557
2.0	0.8309	0.6484	0.4612	0.3688	0.3013	0.2428

[a] For all values of L/r, $T=1.0000$ when $\theta=0°$.

It is uncommon, however, to use collection systems for which θ is greater than 20°. Between $\theta=0°$ and $\theta=20°$, T is a nearly linear function of θ for a given value of L/r. Thus, expressing θ in radians, $T=1.0000-a\theta$, for $0\leq\theta\leq0.35$. Furthermore, the constant a is, to a good approximation, linearly related to L/r, so that

$$T=1.0000-b(L/r)\theta \qquad (2)$$

with b equal to 0.3260.

Substitution of Eq. (2) in Eq. (1) and subsequent integration gives

$$n=\sin^2\theta-0.0815(L/r)(\sin 2\theta-2\theta\cos 2\theta). \qquad (3)$$

Estimated accuracy of Eq. (3) is ±1 percent for $0\leq L/r\leq2.0$ and $0\leq\theta\leq0.35$, ±2 percent for $0\leq L/r\leq2.0$ and $0.35\leq\theta\leq0.53$, ±5 percent for $2.0\leq L/r\leq8.0$ and $0\leq\theta\leq0.18$.

An example of measurements in which the cosine law value for n has been tacitly assumed is the work of Rudberg[6] on the vapor pressure of calcium. For his system the collection angle θ was about 7°; L/r varied with the quantity of metal in the effusion cylinder, its maximum value being as high as 8.5. Assuming $L/r=8.0$, the fraction n for Rudberg's collection system calculated with Eq. (3) is 0.0117. The cosine law value is 0.01485. Hence, Rudberg's

calculated pressures for calcium are in error by as much as 25 percent.

* This work was supported by the U. S. Office of Naval Research.
[1] M. Knudsen, Ann. Physik (4) **28**, 999 (1909).
[2] C. I. Whitman, J. Chem. Phys. **20**, 161 (1952).
[3] P. Clausing, Z. Physik **66**, 471 (1930).
[4] R. D. Freeman and A. W. Searcy, J. Chem. Phys. **22**, 762 (1954).
[5] P. Clausing, Ann. Physik. (5) **12**, 961 (1932).
[6] E. Rudberg, Phys. Rev. **46**, 763 (1934).

Modification of the Naive MO Method*

LIONEL GOODMAN† AND HARRISON SHULL
Department of Chemistry and Institute for Atomic Research, Iowa State College, Ames, Iowa
(Received March 15, 1954)

THE usual empirical MO procedure suffers from (among others) the following well-known disadvantages: (1) No distinction is made between states of different multiplicity. (2) Electron repulsion splitting of zeroth order excited states is not accounted for. (3) Configuration interaction cannot be taken into account.

Because of the ease of application, the method has become popular for application to complex molecules despite these disadvantages. On the other hand, the purely theoretical ASMO method has none of these restrictions, but it requires a large expenditure of labor, and in addition suffers from the core potential problem in the usual π-electron approximation.

A procedure is outlined here for combining the advantages of each method while avoiding their respective disadvantages. In the naive LCAO MO method, the π orbital energies of a conjugated hydrocarbon are obtained by solution of an appropriate secular equation: $|H_{ij}-S_{ij}\epsilon|$, where H_{ij} is taken as an empirical parameter, α, and H_{ij} as a parameter, β, for nearest neighbors, zero otherwise. S_{ij} is the overlap integral between nearest neighbors. The solutions of this secular equation are of the form $\epsilon_j=\alpha+\eta_j\beta$, where η_j is determined by the form of the secular equation, and hence by the molecular geometry. One is able to determine β empirically from observed spectra by assuming that the excitation energy is given by $\epsilon_b-\epsilon_a$ for the transition $a\rightarrow b$:

$$\beta=\langle\Delta E\rangle_{Av}/(\eta_b-\eta_a) \tag{1}$$

where $\langle\Delta E\rangle_{Av}$ represents the observed center of gravity of the excitation processes, both singlet and triplet, involved in the transition $a\rightarrow b$. The Coulomb integral α may be determined from this value of β together with an observed ionization potential.

One obtains by the ASMO method a transition energy for the process $a\rightarrow b$,

$$^{1,3}\Delta E=\epsilon_b-\epsilon_a-(J_{ab}-K_{ab})\pm K_{ab} \tag{2}$$

utilizing the ground state Hamiltonian for the excited state as well as the closed-shell ground state.[1] In this procedure, ϵ_b, the orbital energy, is the negative of the ionization potential, and may logically be equated to the corresponding solution of the secular equation of the naive empirical procedure given above. If one makes this empirical substitution, one obtains

$$^{1,3}\Delta E=(\eta_b-\eta_a)\beta^*-(J_{ab}-K_{ab})\pm K_{ab}. \tag{3}$$

This equation now enables one to determine an empirical β^* from the observed singlet (or triplet) absorption band, or from the center of gravity by computing the electron repulsion integrals, J_{ab} and K_{ab}, using the wave functions obtained from the naive treatment. From this single transition energy, one can compute transition energies to other states, and configuration interaction can be taken into account in the usual manner.

This basic procedure of complementing the naive semi-empirical approach with theoretically computed repulsion integrals may be conveniently and successfully applied to substituted hydrocarbons. It is assumed that the carbon-carbon exchange integral is unchanged from that of the parent hydrocarbon, and that the Coulomb integral of the substituent π orbital is $\alpha+\delta\beta$, δ being a new empirical parameter. By analogy with the above treatment the *shift* in the lowest excitation energy upon substitution is given by

$$^{1,3}\Delta^2E=(\epsilon_b'-\epsilon_b)-(\epsilon_a'-\epsilon_a)-(J_{ab}'-K_{ab}')\pm K_{ab}'+(J_{ab}-K_{ab})\mp K_{ab}. \tag{4}$$

The primed quantities are obtained from the eigenvalues and eigenfunctions of the secular equation for the substituted hydrocarbon, the unprimed from those for the parent hydrocarbon. One can thus compute shifts of levels from parameters determined from independent transitions, thus avoiding the disadvantage, for example, of the too-large singlet-triplet separation and the core problem of the theoretical procedure.

The formulas given above assume no degeneracy for the ϵ_j. Analogous formulas can be derived for the case of degeneracies or near degeneracies (as in benzene), and these have been treated in detail in a forthcoming publication.

* Work supported in part by the Ames Laboratory of the U. S. Atomic Energy Commission.
† Now at Department of Chemistry, Florida State University, Tallahassee, Florida.
[1] C. C. J. Roothaan, Revs. Modern Phys. **23**, 69 (1951).

A Semiempirical Treatment of $n-\pi$ Transitions†

LIONEL GOODMAN* AND HARRISON SHULL
Department of Chemistry and Institute for Atomic Research, Iowa State College, Ames, Iowa
(Received March 15, 1954)

BY using the fundamental approach we have outlined in the preceding letter we have treated the special case of a transition from a nonbonding (n) orbital to an antibonding π_z orbital, b. The energy of such a transition is given by

$$^{1,3}\Delta E=\epsilon_b-\epsilon_n-(J_{nb}'-K_{nb}')\pm K_{nb}', \tag{1}$$

the + sign holding for the singlet state, and the primes indicating that the electron repulsion integrals are to be taken over the hydrocarbon MO's as perturbed by the substituent. The term ϵ_b may be evaluated via the methods of the previous letter from $\pi-\pi$ spectra with the use of empirically determined resonance and inductive parameters, δ and δ_s.[1] The approximation of ϵ_n by the $\alpha+\delta\beta$ derived from $\pi-\pi$ spectra may be justified by straightforward methods. Furthermore one can expand the integrals over MO's in Eq. (1) into integrals over AO's, leaving as leading terms electron repulsion integrals involving only the nonbonding AO, n, and the substituent π AO, ϕ_x:

$$^{1,3}\Delta E=\epsilon_b-(\alpha+\delta\beta)-a_{bx}^2(J_{nx}-K_{nx}\mp K_{nx}) \tag{2}$$

in which a_{bx} is the coefficient of ϕ_x in the π MO ψ_b. Expansion of the MO integrals in the usual oscillator strength formula into AO integrals gives as the leading term the transition moment integral involving n and the substituted carbon π AO, ϕ_s, since $\int\phi_n z\phi_z d\tau$ vanishes on symmetry grounds:

$$f_{n-b}=2.170\times10^{11}\nu\Big(\int\phi_n z\phi_s d\tau\sum_{i=1}^{N}a_{bi}c_{is}\Big)^2. \tag{3}$$

From Eqs. (2) and (3) one can compute $n-\pi$ transition energies, and oscillator strengths from data obtained completely independently from $\pi-\pi$ spectra.

Several important conclusions can be drawn from these computations.

1. For a series of substituents in which δ decreases (the smaller δ, the more resonance), the $n-\pi$ transition energy decreases much faster than the $\pi-\pi$ transition energy. This makes $n-\pi$ transitions a better potential source of empirical δ values than $\pi-\pi$ spectra and provides a potentially valuable means of identifying the nature of a given experimental transition.

2. The magnitude of singlet-triplet splitting in an $n-\pi$ transition is largely determined by the magnitude of $2a_{bz}^2K_{nz}$.[2] As a_{bz} may vary very widely, and K_{nz} is large,[3] one predicts that the singlet-triplet splitting of $n-\pi$ states will show considerably

greater variation than that for $\pi-\pi$ states. Examination of these factors shows:

(a) For conjugated heterocyclics in which the heteroatom is not very electronegative compared to carbon (N,S), the $S-T$ splitting is predicted to be large (up to 10 000 wave numbers)[4] since $|a_{bz}|\sim 1$.

(b) For all but very large interactions between hydrocarbons and an *external* substituent, $a_{bz}^2 \ll 1$, hence the singlet-triplet splitting is expected to be considerably smaller than for $\pi-\pi$ states. For weak resonance interaction the singlet and triplet will be nearly degenerate.

(c) If in two center π electron systems (e.g., saturated aldehydes and ketones) the bond is strongly polar (towards the atom containing the n orbital), the $a_{bz}^2 \ll 1$, giving small $S-T$ separation.

(d) $n-\pi$ transitions to π states having a node through the atom containing the n orbital will have very nearly degenerate singlet and triplet states.

3. There is no configuration interaction between n and π states because of difference of symmetry with respect to the molecular plane.

4. Upon additional substitution (in say, different positions of a benzene ring), the theory predicts a blue shift and decreasing singlet-triplet separation for an $n-\pi$ transition for substituents with resonance interaction only whereas $\pi-\pi$ transitions must show a red shift. In general, inductive effects will exert much stronger influences on $n-\pi$, than on $\pi-\pi$ transition energies.

5. In general both n_x[5] and n_y transitions are formally allowed. The $n_y-\pi$ oscillator strength is smaller than $n_x-\pi$, since unlike the n_x-b transitions, the leading terms in the n_y-b transition involve transition moments between non-nearest neighbors, which are smaller than the moment between n_x and s.

With respect to n_x-b transitions: (a) For conjugated parent hydrocarbons $(\Sigma a_{bi}c_{is})^2 \sim 1/N$. Hence the $n-\pi$ oscillator strength should decrease as the size of the parent hydrocarbon increases. In general the $n-\pi$ oscillator strength will be rather small: $f \lesssim 0.05$. (b) Additional substituents will change the $n-\pi$ oscillator strength but slightly. However upon "loading" of the parent hydrocarbon with identical n centers, the intensity is expected to increase relative to that of the $\pi-\pi$ transition.

† Work supported in part by the Ames Laboratory of the U. S. Atomic Energy Commission.

* Present address: Department of Chemistry, Florida State University, Tallahassee, Florida.

[1] See Matsen *et al.*, J. Am. Chem. Soc. **72**, 5243, 5252 (1950); Matsen's δ_i is our δ_s.

[2] For light atoms, where $j-j$ coupling effects are small.

[3] Although the integral K_{nz} is proportional to Z, any conclusions drawn from the variation of Z must include spin-orbit coupling.

[4] An opposite conclusion was drawn by C. Reid, J. Chem. Phys. **21**, 1906 (1953), on the basis of less detailed considerations.

[5] We take x parallel to, y perpendicular to a C–X bond.

The Exchange Reaction between Iodine and Methyl Iodide

H. Behrens and Alfred G. Maddock
Department of Chemistry, Pembroke Street, Cambridge, England
(Received March 25, 1954)

If the over-all rate of an exchange reaction depends on the mth and nth powers of the concentrations of the two reacting species, a and b, then $k(a^{n-1}b^m+a^nb^{m-1}) = -\log\frac{1}{2}/t_{\frac{1}{2}}$ where $t_{\frac{1}{2}}$ is the time for half-exchange. An interesting case is found when m or n is less than one, and experiments are carried out at constant concentration of the other species; the value of $t_{\frac{1}{2}}$ will then decrease with the concentration of the first species, provided it is below some critical value. Few exchange reactions illustrating these features have been described, although ionization or dissociation mechanisms should often satisfy the necessary conditions.

It has long been known that traces of dissolved halogen influence the retention of the radioactive halogen in organic molecules following the slow neutron irradiation of the alkyl halides.[1,2] For the last three years we have been exploring the nature of these effects. Evidence of an exchange reaction was obtained when radioactive iodine I_2^{131} was dissolved in methyl iodide. For reproducible results it was necessary to use mixtures of pure dry methyl iodide and radioactive iodine sealed *in vacuo*. Each mixture was prepared, distributed between a series of ampoules and sealed *in vacuo*. The macroscopic concentration of the iodine was determined spectrophotometrically. The ampoules were stored at 0°C, 20°C, and 35°C in the absence of light and opened at various intervals. The macroscopic concentration of iodine at the time of analysis was checked spectrophotometrically using one aliquot. Another was extracted with sulfurous acid solution containing potassium iodide. The activities of the aqueous and organic phases were measured and compared with the total activity found in a third aliquot, to which iodine was added to avoid adsorption δ in the annular liquid Geiger counter. After correction for differing electron densities of the liquids, and the solubility of the methyl iodide in the aqueous reagent, excellent material balance was obtained.

The identity of the exchange reaction was demonstrated conclusively in a few experiments in which a mixture of iodine, methylene iodide, and hydrogen iodide was added to the methyl iodide-iodine mixture and the components of the mixture separated by vacuum distillation and condensation at temperatures at or below 20°C. When the exchange had reached completion at 15 mg/L of iodine the latter separation showed 92 percent of the activity in the methyl iodide fraction, less than 1 percent in the hydrogen iodide, about 1 percent in the iodine, and 6 percent in the methylene iodide. The methylene iodide activity was confirmed by further experiments in which the methyl-methylene iodide separation was repeated after the addition of more inactive methyl iodide.

The half-life for the exchange reaction was found to fall from 45 days at 300 mg/L of iodine to a few hours at 4 mg/L. The detailed kinetics of the exchange will shortly be published. It belongs to the class previously described. A similar exchange between ethyl iodide and iodine has been noticed by Shaw and Collie, although their interpretation of their results is different.[3]

These exchange processes must be responsible, at least in part, for the effect of the free iodine concentration on the retention in the alkyl iodides.[4] It might also explain the sensitivity of the retention in pure methyl iodide to the concomitant dose of ionizing radiation, and to other factors influencing the formation of traces of free halogen. This aspect of the exchange will be discussed in a future publication.

Since radio-iodine is readily available at very high specific activities the exchange reaction described and others of the same character, should have some value for synthetic purposes.

[1] J. W. J. Fay and F. A. Paneth, J. Chem. Soc. **1936**, 384.
[2] A. S. Lu and S. Sugden, J. Chem. Soc. **1939**, 1273.
[3] P. F. D. Shaw and C. H. Collie, J. Chem. Soc. **1949**, 1217.
[4] S. Goldhaber and J. E. Willard, J. Am. Chem. Soc. **74**, 318 (1952).

Oxidation and Reduction of Aqueous Ferrous-Ferric Sulfate Induced by Visible Light Absorption of Mercuric Sulfide

Leonard I. Grossweiner and Sheffield Gordon
Chemistry Division, Argonne National Laboratory, Lemont, Illinois
(Received March 25, 1954)

It has been found that light absorbed by a suspension of red mercuric sulfide in ferrous and ferric sulfate ($0.8N$ H_2SO_4) will induce oxidation and reduction. Some features of these conversions are sufficiently different from γ-ray induced effects to warrant description. It is believed that the systems described may be useful actinometers for visible light.[1]

The irradiations were performed by illuminating a stirred suspension of HgS powder at 18°C with an AH-6 mercury lamp.

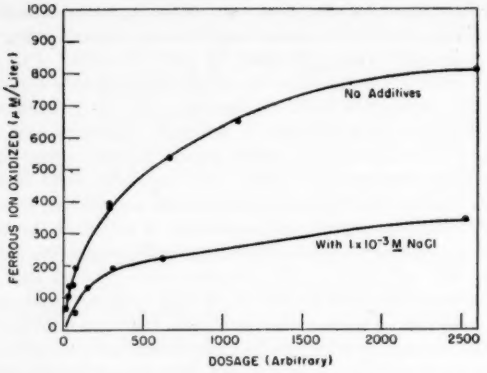

FIG. 1. Oxidation of air-saturated ferrous sulfate by light absorbed by mercuric sulfide (1000 μM/liter in 0.8*N* H_2SO_4; 18°C; No. 3385 filter).

A Corning No. 3385 filter was used to eliminate ultraviolet light. Blank experiments with various concentrations of ferrous and ferric sulfate showed that neither contact between the HgS and solutions nor irradiation of the separate materials, followed by mixing, will cause appreciable conversion.

Dose curves for air-saturated solutions are shown in Figs. 1 and 2. A comparison of the yields with various additives and gases bubbling through the solutions is shown in Table I. It is concluded

TABLE I. Effect of additives on conversion of ferrous-ferric sulfate induced by light absorption by mercuric sulfide.

Oxidation of ferrous sulfate (1.0 mM/liter in 0.8*N* H_2SO_4)

	Oxidation (μM/liter)				
	No additive Dosage		NaCl (1.0 mM/liter) Dosage		HCOOH (1.0 mM/liter) Dosage
Gas	78	156	78	156	78
Helium	<10	...	<10	...	...
Air	150	250	50	145	170
Oxygen	225	425	160	235	...

Reduction of ferric sulfate (0.4 mM/liter in 0.8*N* H_2SO_4)

	Reduction (μM/liter)				
	No additive Dosage		NaCl (1.0 mM/liter) Dosage		HCOOH (1.0 mM/liter) Dosage
Gas	78	156	78	156	78
Helium	115	120	165	180	...
Air	100	115	135	160	70
Oxygen	25	57	70	85	...

that sodium chloride inhibits oxidation of ferrous ion and enhances reduction of ferric ion and that oxygen is required for oxidation and strongly inhibits reduction. Further, the yields for

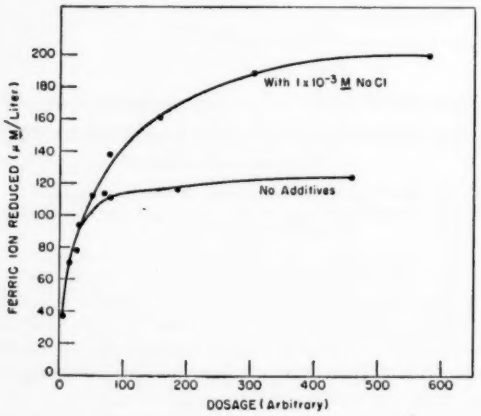

FIG. 2. Reduction of air-saturated ferric sulfate by light absorbed by mercuric sulfide (400 μM/liter in 0.8*N* H_2SO_4; 18°C; No. 3385 filter).

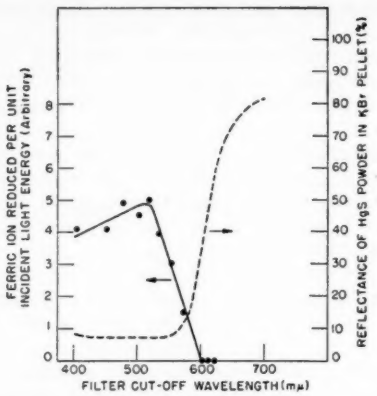
FERRIC ION REDUCED PER UNIT INCIDENT LIGHT ENERGY (Arbitrary)
REFLECTANCE OF HgS POWDER IN KBr PELLET(%)
FILTER CUT-OFF WAVELENGTH(mμ)

FIG. 3. Effect of filter cutoff on the yield of ferric ion reduction (400 μM/liter $Fe_2(SO_4)_3$ in 0.8*N* H_2SO_4, air-saturated; 18°C; dosage: 30).

air-saturated solutions are not appreciably affected by the addition of formic acid which indicates that easily oxidizable organic materials are not important in these results. Experiments at low dosage with air-saturated solutions of various concentrations showed that the initial conversions are neither a function of the initial concentrations of ferrous or ferric ion over a range of at least 0.2 to 5 mM/liter nor the HgS concentration, when it exceeds 50 g per liter, an opaque suspension.

No free sulfur was found in irradiated solutions. In addition, air-free ferric sulfate, containing NaCl, was irradiated in vacuum and analyzed for gaseous products. Only hydrogen and acidic gas, probably SO_2, were found.

The effect of the spectral distribution of incident light on the reduction of air-saturated ferric sulfate was measured with a series of Corning filters. The light flux transmitted by each filter was determined with an Eppley thermopile. The quantity of ferric ion reduced per unit incident light energy is plotted against the filter cutoff in Fig. 3. The sharp decrease at 600 mμ is close to the photoconductive cutoff of HgS crystal at 630 mμ[2] and to the wavelength where the reflectance of the powder shows an abrupt increase.[3]

A tentative scheme for the conversions may be suggested. A reasonable primary reaction is the emission: $HgS + light = Hg^{++} + S^{-} + e$, occurring at the crystal surface. Possible successive reactions are: (a) internal conversion of Hg^{++} to Hg^{+} and S^0, which remain insoluble in the crystal, or; (b) formation of HS at the surface which reduces H_2SO_4 to SO_2 gas.

A reaction not significant in γ-ray induced reactions at this *p*H is the reduction of ferric ion. A possible mechanism is the capture of photoelectrons by hydrogen ions at the HgS surface to form hydrogen atoms. The reduction of ferric ion, which does not require oxygen, may be due to the oxidation of the hydrogen atom to hydrogen ion. The oxidation of ferrous ion, which requires oxygen, is similar to that induced by γ-rays, with HO_2 as a possible oxidant.[4]

The conversion efficiencies were estimated from the thermopile measurements using the inverse square law to calculate the incident light energy. The average efficiency for reduction of air-saturated ferric sulfate is 630±95 incident photons per ferric ion reduced, based on the light from the No. 3385 filter cutoff to 600 mμ. The highest efficiency found was that for oxygen-saturated ferrous sulfate, 280±40 incident photons per ferrous ion oxidized.

The authors are indebted to E. J. Hart, M. S. Matheson, and O. C. Simpson for valuable discussions and suggestions and to J. L. Weeks for collaboration in the thermopile measurements.

[1] Similar effects in other systems have been found by irradiation of ZnO with ultraviolet light. Rubin, Calvert, Rankin, and MacNevin, J. Am. Chem. Soc. **75**, 2850 (1953).

[2] B. Gudden and R. W. Pohl, Z. Physik **2**, 361 (1920).

[3] The reflectance of HgS powder was measured by mixing about 1 percent in a KBr pellet, pressed at 200,000 psi, and measuring the pellet reflectance.

[4] M. Burton, *Annual Review of Physical Chemistry* (Annual Reviews, Inc., Stanford, California, 1950), Vol. I, p. 125.

Theory of Absorption Spectra of Unsymmetrical Cyanines

GENTARO ARAKI AND SIGERU HUZINAGA
Faculty of Engineering, Kyoto University, Yosida, Kyoto, Japan
(Received March 16, 1954)

NONCONVERGENT vinylene shifts in the absorption spectra of symmetrical cyanine series have successfully been interpreted by assuming a molecular model in which one-electron levels in a deep square-well potential are occupied by π electrons belonging to the conjugated double bonds.[1] Further, it was shown that the convergence of the shift is due to interactions between π electrons.[2]

Brooker[3] showed that the absorption maximum of an unsymmetrical cyanine with two different nuclei is generally of the shorter wavelength than a mean value of absorption maxima of two symmetrical cyanines with the respective nuclei. It was further shown that the deviation from the mean value varies according as the basicity of nuclei. The free-electron model in a square well cannot explain the deviation because it includes only one parameter giving a measure of the molecular length. In order to account for this phenomenon, we should modify the square-well potential so as to include the effect of end nuclei. The effect may be represented in various ways.

A convenient way may be to make use of the Pöschl-Teller[4] potential (see Fig. 1) which is given by (in atomic units)

$$V(x)=\frac{\pi^2}{8b^2}\left\{\frac{\delta_1(\delta_1+1)}{\sin^2\frac{\pi}{2b}x}+\frac{\delta_2(\delta_2+1)}{\cos^2\frac{\pi}{2b}x}\right\},\quad 0<x<b,\quad \delta_1,\delta_2>0. \tag{1}$$

When δ_1 and δ_2 are the same, the potential is symmetrical, and, when they become smaller and smaller, the potential approaches to a square well with a breadth of b. Therefore δ_1 and δ_2 give a measure of deviation from a square well (see Fig. 1). We assume that, in the ground state of a cyanine molecule, lower one-electron levels up to the n_0th in this potential are occupied by π electrons and further assume that $b=(m+\gamma_1+\gamma_2)l$ where m is the number of carbon atoms in conjugated double bonds between two nitrogen atoms, $l=1.4$A is the bond length between two carbon atoms, and

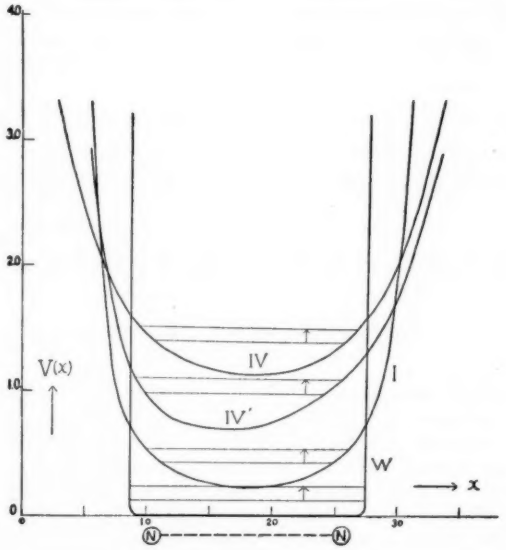

FIG. 1. Pöschl-Teller potential.

W:	$\gamma=1.0$	$\delta\gg 1$
I:	$\gamma=3.266$	$\delta=6.082$
IV:	$\gamma=7.333$	$\delta=24.590$
IV′:	a combination of I and IV	

Energy levels giving absorption maxima are indicated. All quantities are measured in atomic units.

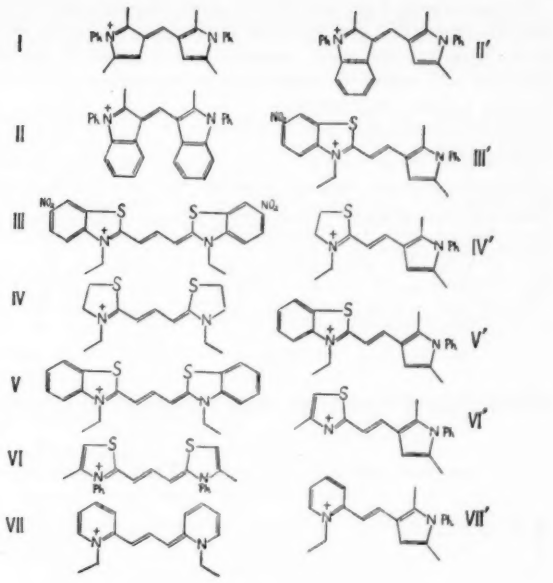

FIG. 2.

γ_1 and γ_2 are parameters, respectively, belonging to each of the end nuclei (see Fig. 1 and Fig. 2). We have then the first excitation energy as follows (in atomic units):

$$\Delta E=2^{-1}(\pi/l)^2(2n_0+\delta_1+\delta_2+1)/(m+\gamma_1+\gamma_2)^2. \tag{2}$$

We can adjust the values of the parameters γ and δ for each of various nuclei discussed by Brooker so that calculated wavelengths of absorption maxima agree with observed values for both symmetrical and unsymmetrical cyanines in which one definite nucleus is combined with different nuclei (Fig. 2). Some examples of parameter values are shown in Table I. Comparing the result

TABLE I. Symmetrical cyanines.

	Absorp. max. in mμ	γ	δ
I	448.5	3.266	6.082
II	490	5.139	11.893
III	583.5	6.500	13.444
IV	445	7.333	24.590
V	557.5	9.258	27.556
VI	561	14.017	59.36
VII	562	16.853	82.64

with Brooker's experiment we see that a set of γ and δ can give a measure of the basicity of nuclei. In fact, the larger the value of $\gamma\delta^2$ the stronger the basicity (see Table II). We have thus a modified free-electron model which enables us to account for the basicity of nuclei in absorption spectra of cyanine dyes. It should here be noted that b itself does not mean the molecular length. Particularly these two are quite different in case of large γ. Nevertheless the region in which the wave function differs distinctly from zero is located within the real molecule even if the values of γ_1 and γ_2 are very large. This is due to large values of δ_1 and δ_2 (see Fig. 1).

TABLE II. Unsymmetrical cyanines.

	Absorp. max. in mμ	Deviation $\lambda_{mean}-\lambda$	$\gamma\delta^2$
II′	465	4.5	73×10
III′	495	22	12×10^2
IV′	417.5	29.5	44×10^2
V′	465.5	37.5	70×10^2
VI′	443	62	49×10^3
VII′	426	79.5	12×10^4

In case of large δ the potential is quite different from the square well. In this case π electrons are always acted on by a restoring force. Therefore our result means that π electrons in the shorter cyanines with nuclei of strong basicity cannot move so freely as those in a square-well model.

The full account will later be published in *Progress of Theoretical Physics (Japan)*.

[1] S. Baylis, J. Chem. Phys. **16**, 287 (1948); H. Kuhn, J. Chem. Phys. **16**, 840 (1948); W. T. Simpson, J. Chem. Phys. **16**, 1124 (1948).
[2] G. Araki and T. Murai, J. Chem. Phys. **20**, 1661 (1952); **21**, 381 (1953); Progr. Theoret. Phys. Japan **8**, 639 (1952); G. Araki and H. Araki, Progr. Theoret. Phys. Japan **11**, 20 (1954).
[3] L. G. S. Brooker, Revs. Modern Phys. **14**, 275 (1942); L. G. S. Brooker and co-workers, J. Am. Chem. Soc. **62**, 1116 (1940); **67**, 1871 (1945); **73**, 1087 (1951).
[4] G. Pöschl and E. Teller, Z. Physik **83**, 143 (1933).

The Infrared Spectrum and Structure of Collagen*†

RICHARD M. BADGER AND A. D. E. PULLIN
Gates and Crellin Laboratories of Chemistry, California Institute of Technology, Pasadena, California
(Received March 25, 1954)

IN view of the present interest in the structure of collagen it may be useful to point out that spectroscopic observations may greatly assist one in discarding preliminary structural models, though they do not, by themselves, lead to a solution of the problem. For example, the question has arisen as to whether the collagen structure may be entirely, or even in considerable part, based on peptide links with the *cis*-configuration.[1,2] From existing spectroscopic evidence this seems very unlikely. It is even more improbable that the structure contains a significant fraction of such groups hydrogen bonded to each other so as to form the eight-membered rings required by the Crick model.[2] The first conclusion is based on the intensity of absorption in the amide II,[3] or 1540 cm^{-1} band, which appears to be quite normal in collagen and gelatin. This fundamental, characteristic of *trans* amide groups, appears to correspond to the higher frequency member of a pair of modes resulting primarily from the interaction of a symmetrical vibration of the O=C−N group and a N−H bend.[4] In the *cis*-configuration this interaction becomes negligible for geometrical reasons, and the amide II frequency should consequently decrease considerably, probably with the loss of considerable intensity. The plausibility of this conclusion is attested by the fact that normal amide II absorption is quite absent in the spectra of cyclic amides, which offer the only certain examples of the *cis*-configuration.[5]

We have previously pointed out that the eight-membered ring configuration is characterized by an abnormally low N−H valence frequency.[6] This fundamental in collagen, however, appears to be quite normal.

In regard to positive requirements for a collagen model, we present polarization data (Fig. 1) recently obtained by us which are considerably superior to results previously reported on collagen,[7] though they are similar to observations on stretched gelatin.[8] They were obtained on 2-micron sections of kangaroo tail dried under tension.[9] Exploration of the sample with a polarizing optical microscope indicated a root mean square disorientation of about 9°, though this is certainly not conclusive. This degree of disorder would not materially affect the polarization spectra, but some allowance must be made for other factors which minimize the dichroism. These include the presence of some amide absorption other than that of the peptide links, which very probably makes a significant unpolarized contribution in the regions of interest.

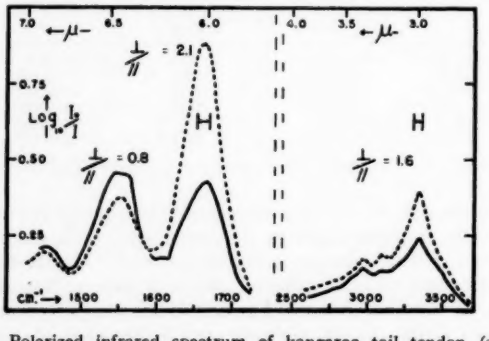

FIG. 1. Polarized infrared spectrum of kangaroo tail tendon (section approximately 2μ thick). Dichroic ratios at band maxima are indicated.

Even a qualitative use of the polarization data, particularly of the positive dichroism of amide II, excludes the possibility of some types of model. Their quantitative application requires a knowledge of the direction of the change in dipole in the various fundamental vibrations. Information on this point is at present inadequate and is difficult to obtain, but from available evidence and from plausible considerations we have been led to the following conclusions. In the N−H valence vibration the direction of change of moment is not quite parallel to the N−H bond, but is inclined by a maximum of 8° toward the projection of the C−N peptide bond. In the amide I vibration the direction is not parallel to the C=O bond, but is even more nearly parallel to the O−N direction than is suggested by Price and Fraser.[4]

There is considerable evidence which suggests that the amide II vibration owes its activity largely to the contribution of the N−H bend, though its frequency is primarily determined by the O=C−N group. If this is the case one should expect the fundamental to be polarized nearly perpendicular to the N−H bond, and the first overtone nearly parallel to this bond. This interpretation is supported by the observed polarization of the band near 3080 cm^{-1}, generally found in peptides and N-substituted amides, which is plausibly assigned to the overtone of amide II.

In any quantitative application of the polarization data it must be remembered that for peptide links involving proline nitrogen, absorption will be absent not only in the N−H valence region but presumably also in the amide II region. The latter statement is supported by the absence of such absorption in N,N-disubstituted amides, especially in N-acetyl piperidine.[3]

* Contribution No. 1890 from the Gates and Crellin Laboratories.
† Based on investigations supported by the U. S. Office of Naval Research, Contract N6-ori-102, VI.
[1] Pauling, Corey, and Branson, Proc. Natl. Acad. Sci. U. S. **37**, 272 (1951).
[2] F. H. C. Crick, J. Chem. Phys. **22**, 347 (1954).
[3] We follow the nomenclature of Randall, Fowler, Fuson, and Dangl, *Infrared Determination of Organic Structures* (D. Van Nostrand Company, Inc., New York, 1949).
[4] This interpretation was suggested by W. C. Price and R. D. B. Fraser, Nature **170**, 490 (1952); Proc. Roy. Soc. (London) **B141**, 66 (1953); and has been confirmed and elaborated by us by the use of a mechanical vibrating model.
[5] H. Lenormant, Bull. Soc. Chim. **15**, 33 (1948).
[6] R. M. Badger and H. Rubalcava, Proc. Natl. Acad. Sci. U. S. **40**, 12 (1954).
[7] Martin Goldstein, Ph.D. thesis, Columbia University (1950).
[8] E. J. Ambrose and A. Elliott, Proc. Roy. Soc. (London) **206**, 206 (1951).
[9] We are greatly indebted to Dr. R. F. Baker for the preparation of these specimens.

The Activation Energy of the $H+H_2$ Reaction

VIRGINIA GRIFFING AND JOSEPH T. VANDERSLICE
Chemistry Department, The Catholic University of America, Washington 17, D. C.
(Received March 31, 1954)

THERE have been a number of attempts at calculating the activation energy of the $H+H_2$ process by *a priori* theoretical methods. However, when these values are compared with the experimental values of the activation energy, the theoretical values are in error by a factor of 10.[1] This is not surprising since these calculations yield the total energy of the complex with reference to three separated hydrogen nuclei and electrons and thus the binding energy is given as a small difference between two large numbers. Furthermore, one knows that the MO method does not yield wave functions which converge to the correct atomic states as the internuclear distances go to infinity. Thus, it is to be expected that the activation energies calculated in this way will be in error. However, since the activation energy is the difference in

energy between the energy of a stable H_2 molecule plus that of a hydrogen atom and the energy of the linear symmetrical complex, and since the MO method does give good values for energy differences, it would seem that this approach can be made to give good values for activation energies. One can use the same method of calculation for obtaining the energy of the complex and the energy of the hydrogen molecule plus the hydrogen atom and then take the difference of the two values. Thus, if one takes the MO-configuration-interaction calculation for the energy of the H_3 complex as -43.539 ev, as reported by Walsh and Matsen[2] and subtracts from that the MO-configuration-interaction calculated value for the hydrogen molecule[3] -30.317 ev, plus the energy of a hydrogen atom -13.602 ev, one obtains for the activation energy of the reaction $H+H_2$ a value of 0.380 ev, or 8.76 kcal. This may be compared with the estimated experimental value of from 5–10 kcal[4] and also with the value of 8.50 kcal estimated from spectroscopic data by Eyring and co-workers.[5]

The molecular orbital method applied in this way has been used in our laboratories in considering several simple systems and the details will soon be published elsewhere.

[1] Glasstone, Laidler, and Eyring, *The Theory of Rate Processes* (McGraw-Hill Book Company, Inc., New York, 1941).
[2] J. M. Walsh and F. A. Matsen, J. Chem. Phys. **19**, 526 (1951).
[3] J. C. Slater, Electronic Structure of Atoms and Molecules, Technical Report No. 3 of the Solid State and Molecular Theory Group, M.I.T.
[4] A. Farkas and L. Farkas, Proc. Roy. Soc. (London) **A152**, 124 (1935).
[5] See reference 1, p. 206.

Configuration Coordinate Model for Luminescence in KCl:Tl

PETER D. JOHNSON
General Electric Research Laboratory, Schenectady, New York
(Received April 2, 1954)

IN KCl:Tl, the potential energy of the activator system in the $^1S_0$ or $^3P_1^0$ state of Tl^+ is determined to a good approximation by the symmetrical radial displacement of the nearest-neighbor Cl^- ions from the Tl^+. Experimental confirmations of the predictions of the theory are in accord with this conclusion.[1–4] It has been suggested that the energies of other states of the activator may also be defined by this single configuration coordinate.[4] Recent improvements in the calculation for $^3P_1^0Tl^+$ in KCl make it possible to test the validity of this suggestion.

The potential energy in electron volts of the $^3P_1^0$ state is:

$$E_1=4.417(\Delta a+0.1759)^2+4.850, \qquad (1)$$

where Δa is the radial displacement in angstroms of the six nearest-neighbor Cl^- ions from their equilibrium positions in the pure KCl lattice. In Eq. (1), the force constant and equilibrium position are those calculated by Williams.[5] A small adjustment in the constant term has been made so that this equation, in conjunction with the theoretically determined energy of the unexcited $^1S_0$ state,

$$E_0=8.425(\Delta a-0.095)^2+0.1600, \qquad (2)$$

yields precisely both the observed absorption and emission spectra.

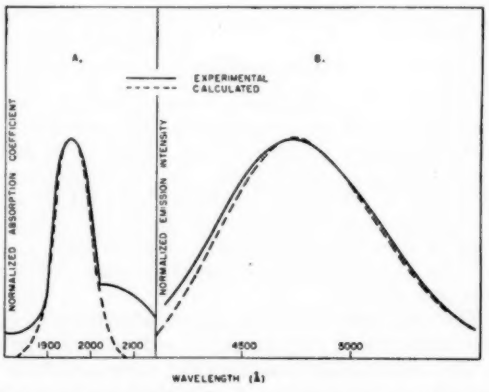

FIG. 1. Calculated and experimental spectra of absorption (A) and emission (B) for the $^1S_0\leftrightarrow{}^1P_1^0$ transitions in KCl:Tl at 80°K.

The energy of the $^1P_1^0$ state can be calculated from the energies at the peaks of absorption and emission for the optical transitions $^1S_0\leftrightarrow{}^1P_1^0$ and from the energy difference between the minima of the $^3P_1^0$ and $^1P_1^0$ states,[4] and is given by:

$$E_2=6.50(\Delta a+0.404)^2+4.825. \qquad (3)$$

From Eqs. (2) and (3), the complete absorption and emission spectra for the transitions $^1S_0\leftrightarrow{}^1P_1^0$ can be calculated[1] and are compared with experiment in Fig. 1. The agreement between calculated and experimental spectra strongly supports the idea that the energy of the $^1P_1^0$ state depends principally on the configuration coordinate Δa.

From Eqs. (1) and (3), and from a consideration of the rate processes involving the two emitting states,[4] the frequency factors for the thermal transitions $^3P_1^0\leftrightarrow{}^1P_1^0$ are found to be of the order of 10^{10} sec^{-1}. Since the frequency factor for the radiationless process $^3P_1^0\rightarrow{}^1S_0$ is about 10^{12} sec^{-1}, radiationless de-excitation of $^3P_1^0$ does not occur predominantly by way of the $^1P_1^0$ state. The fact that the experimental activation energy for radiationless de-excitation of $^3P_1^0$ is somewhat less than that calculated from Eqs. (1) and (2) is not surprising in view of the approximations involved in extrapolating the energy calculations to large displacements.

[1] F. E. Williams, J. Chem. Phys. **19**, 457 (1951); Phys. Rev. **82**, 281 (1951).
[2] P. D. Johnson and F. E. Williams, Phys. Rev. (to be published).
[3] P. D. Johnson and F. J. Studer, Phys. Rev. **82**, 976 (1951).
[4] P. D. Johnson and F. E. Williams, J. Chem. Phys. **20**, 124 (1952).
[5] F. E. Williams, J. Phys. Chem. **57**, 780 (1953).

Nuclear Relaxation and Quasi-Crystalline Structure of Liquids

L. GIULOTTO, G. CHIAROTTI, AND G. CRISTIANI
Istituto di Fisica dell'Università di Pavia, Pavia, Italy
(Received March 30, 1954)

INFORMATION about the molecular motion in liquids can be obtained from the anomalous dispersion at radiofrequencies for polar molecules and from the Raman wings for optically anisotropic molecules.

Measurements of nuclear thermal relaxation times in liquids can give another method to obtain some information about the rotation spectrum for frequencies in the range of the Larmor frequency. In some cases the experimental results agree well with the theory of relaxation of Purcell *et al.*,[1,2] which assumes for a molecule of a liquid Debye's simple model of a rigid sphere subject to Brownian motion in a viscous medium. The agreement seems remarkably good in the case of protons in water.[3]

Measurements performed by us with a method previously described[3] yielded in other cases somewhat longer times than Purcell's theory would predict. Usually oxygen in solution has a strong influence on the relaxation time in liquids and it is therefore necessary to eliminate it completely. For instance the thermal relaxation time of protons in benzene in presence of air is 2.7 sec, whilst in the case of benzene free of oxygen this time is 18 sec. An exact calculation of the relaxation time of protons in benzene following Purcell's theory would be very difficult. An approximate evaluation shows that the contribution of the rotations is predominant with respect to that of the translations; the thermal relaxation time results about 8 sec. We found differences in the same sense between experimental and theoretical values, e.g., for C_6H_5Cl and $C_6H_5NO_2$. We think therefore that for these liquids the rotation spectrum at a frequency of the order of the Larmor frequency (in our case 7 mc) is less intense than we could expect from Debye's picture. This might be caused by a quasi-crystalline

structure of the liquid and the following hindering of the rotations. Owing to the orienting field, the molecules execute angular oscillations about the direction of the field at a frequency much greater than the Larmor frequency. At Larmor frequency the rotation spectrum must therefore result less intense than Debye's theory would predict. We must think that in a liquid in which the hindrance potential is somewhat greater than kT the intensity of the rotation spectrum at Larmor frequency is determined by fluctuations in direction of the orienting field.

A description of the apparatus used and other results on nuclear relaxation in liquids will soon appear in *Il Nuovo Cimento*.

[1] Bloembergen, Purcell, and Pound, Phys. Rev. **73**, 679 (1948).
[2] N. Bloembergen, *Nuclear Magnetic Relaxation* (The Hague, 1948).
[3] G. Chiarotti and L. Giulotto, Phys. Rev. **93**, 1241 (1954).

The Microwave Spectrum of Fluorobenzene*

K. E. McCulloh and Gilbert F. Pollnow
Department of Chemistry, State University of Iowa, Iowa City, Iowa
(Received April 2, 1954)

INVESTIGATION of the microwave spectrum of fluorobenzene was in progress at this laboratory when Erlandsson's report[1] of observation and interpretation of this spectrum became available to the authors. Frequency measurements in the present study were carried out to an accuracy of ±0.1 mc, the results in most cases falling within Erlandsson's stated limits of error, ±5 mc. This investigation confirms Erlandsson's assignment of frequencies and his proposed values for the rotational constants b and c, but a significantly different value is obtained for the parameter a.

Assignable absorption frequencies of fluorobenzene in the region 22.1–27.3 kmc were measured to ±0.1 mc with the recording spectrometer[2] in use at the State University of Iowa. Of the 148 observed absorption lines, only those which have been assigned to specific rotational transitions are herein reported (see Table I).

Table I. Microwave frequencies of fluorobenzene.

Transition	Observed frequency	Calculated frequency
$4_{21}-5_{32}$	22322.2 mc	22322.0 mc
$5_{15}-6_{16}$	22863.5	22863.3
$4_{13}-5_{14}$	22940.9	22940.8
$5_{05}-6_{06}$	23134.7	23134.7
$4_{23}-5_{23}$	23393.8	23393.6
$5_{24}-6_{25}$	25427.4	25427.6
$5_{51}-6_{52}$	26378.8[a]	26378.3
$5_{50}-6_{51}$	26378.8[a]	26379.4
$5_{33}-6_{34}$	26445.2	26445.3
$6_{16}-7_{17}$	26460.7	26460.9
$5_{42}-6_{43}$	26483.2	26483.1
$5_{41}-6_{42}$	26528.9[b]	26529.5
$6_{06}-7_{07}$	26605.3	26605.5
$5_{14}-6_{15}$	26960.2	26960.4
$5_{32}-6_{33}$	27163.3	27163.5

[a] Unresolved because of low intensities.
[b] Value uncertain because of broad line peak.

Observed intensities are consistent with the nuclear spin statistical weights of 10 for even K_{-1} and 6 for odd K_{-1}. In the computation of molecular constants (listed in Table II), reduced energies obtained by the continued-fraction method[3] were employed throughout. No attempt was made to account for the effects of centrifugal distortion.

Table II. Molecular constants of fluorobenzene.

$\kappa =$	-0.58790 ± 0.00002
$(a-c)/2 =$	1947.91 mc
$(a+c)/2 =$	3715.85 mc
$I_a =$	89.248 amu A²
$I_b =$	196.63 amu A²
$I_c =$	285.92 amu A²
$I_c - I_a - I_b =$	0.04 amu A²

The experimentally determined moments of inertia and the observed dependence of line intensities upon the parity of K_{-1} lead to the conclusion that the molecule has a planar C_{2v} configuration. In order to examine the structure in more detail, the simplifying assumptions were made that the aromatic ring is a regular hexagon and that the HCC angles are 120°. An estimated value of 1.08A was assigned to the C−H distance. The interatomic distances obtained on this basis from the observed moments I_a and I_b are 1.40A for C−C (0.01A greater than Erlandsson's value) and 1.29A for C−F (Erlandsson gives 1.348A). Although it is difficult to appraise the reliability of the above-stated assumptions, it is interesting to note that Stoicheff's recent investigation[4] of the rotational Raman spectrum of benzene has yielded a value for I_a which is only 0.3 amu A² lower than the corresponding moment of fluorobenzene as found in the present study.

* Work supported by the U. S. Office of Naval Research.
[1] G. Erlandsson, Arkiv Fysik **6**, 477 (1953).
[2] G. W. Robinson, J. Chem. Phys. **21**, 1741 (1953).
[3] King, Hainer, and Cross, J. Chem. Phys. **11**, 27 (1943).
[4] B. Stoicheff, J. Chem. Phys. **21**, 1410 (1953).

Errata and Addenda: Theory of Dielectric Relaxation for a Single-Axis Rotator in a Crystalline Field

[J. Chem. Phys. **22**, 132–141 (1954)]

John D. Hoffman
National Bureau of Standards, Washington, D. C.
(Received April 5, 1954)

IN a recent issue[1] of this Journal a theory was given which described the distribution of dielectric relaxation times associated with a single-axis polar rotator in a crystalline field. This work included a calculation of the polarizability associated with each relaxation time. Although the polarizabilities quoted in the paper were correct, the description of the calculations was overly brief. Therefore, some relevant details are given in the following. This opportunity is also taken to correct some minor misprints, and to mention work now in progress.

The general method by which the polarizability value associated with a given relaxation time was obtained for a model with a given number of sites is illustrated for mode 2, i.e., we calculate the α_2 which appears with τ_2.

(1) First, the polarization associated with each site [the coefficients of ψ_2 in Eqs. (18) and (25) or Tables I and II[2]] was resolved into its components in the x, y, and z directions. These resolved polarizations were denoted P_x, P_y, and P_z; in the models considered P_z was always zero. In the paper, the factors $\sin\theta \sin\xi$ and $\cos\theta \sin\xi$ in the expressions for P_x and P_y preceding Eqs. (26) and (35) should be omitted.

(2) Next, the average values of P_x and P_y were obtained for all possible orientations of the applied field. These averaged polarizations were denoted by $\bar{P}_x$ and $\bar{P}_y$ and are given by

$$\bar{P}_x = \langle P_x \cos\theta \sin\xi \rangle_{Av}$$

and

$$\bar{P}_y = \langle P_y \sin\theta \sin\xi \rangle_{Av}.$$

The averaging of P_x and P_y over all orientations of the field implies that the sample is polycrystalline. It should be noted that the field F used in the paper was $F = F_0 \sin\xi$, i.e., F is the component of the field in the $x-y$ plane. This introduces a factor of $\sin\xi$ in P_x and P_y. The latter quantities always involve a term in $\sin\theta$ or $\cos\theta$, so one encounters the quantities $\langle \sin^2\theta \sin^2\xi \rangle_{Av}$ or $\langle \cos^2\theta \sin^2\xi \rangle_{Av}$ in calculating $\bar{P}_x$ and $\bar{P}_y$. Both averages are readily shown to be $\frac{1}{3}$. The $\sin^2\xi$ term in these averages was misprinted $\sin\xi$ just after Eq. (26).

(3) The total polarization associated with mode 2 was then obtained using $P_2 = \bar{P}_x + \bar{P}_y$. Either $\bar{P}_x$ or $\bar{P}_y$ was zero for a given mode. The polarizability was obtained using $\alpha_2 = P_2/NF_0$. The polarizability for the other modes was calculated by an analogous procedure.

Calculations on several three-dimensional models with symmetrical spatial arrangement of the possible sites have been completed, and the results are qualitatively similar to those for a single-axis rotator. A distribution of dielectric relaxation times and a low polarizability appear when one site is more stable than the others, but only a single relaxation time with a polarizability of $\mu_0^2/3kT$ is found when the sites are equivalent. Work has also been completed on a single-axis rotator with four rate constants.

[1] J. D. Hoffman and H. G. Pfeiffer, J. Chem. Phys. **22**, 132 (1954).
[2] It should be noted that Table II is for the $C_{i\beta}$ for $k' \gg k$ and not $k' = k$.

Rare Gas Permeation through Polymers

FRANCIS J. NORTON
General Electric Research Laboratory, Schenectady, New York
(Received April 12, 1954)

IN a study of gas permeation through solids, an unexpected result was obtained. It was found that the heavier rare gases may have a faster steady-state rate of permeation through some polymers than does helium.

The procedure for measuring rates of permeation was similar to that employed in the determination of helium diffusion through a variety of glasses.[1] The mass spectrometer was used to positively identify the gas and to measure its permeation rate through a 50-mil polymer sheet.

The permeation rate is given in units employed by Dushman[2] and Barrer,[3] that is, in cubic centimeters of gas at normal temperature and pressure (760 mm Hg, 0°C) per second per cm² area per millimeter thickness per cm Hg gas differential, partial pressure.

At 25°C, the following rates of permeation were found.

	Xenon	Helium
Perbunan	8×10^{-10}	38×10^{-10}
Butyl rubber	11×10^{-10}	40×10^{-10}
Neoprene	100×10^{-10}	45×10^{-10}
Natural rubber	430×10^{-10}	230×10^{-10}.

The explanation probably lies in the balance between the two factors for permeation: solubility and internal diffusion. One would expect the diffusion to be faster for the smaller atom. However, in some cases, as for water, xenon solubility is higher than helium solubility.[4] High solubility is also often accompanied by high permeability. So here, the high permeability for natural rubber would probably be accompanied by high solubility for xenon. This is related to the fact that long times, often several days, were required to establish steady-state flow rates for xenon at 25°C, and long periods were subsequently needed to degas the 50-mil membrane free of xenon. Where the permeation rate is low, as xenon through perbunan, the diffusion factor predominates over the solubility factor.

[1] F. J. Norton, J. Am. Ceramic Soc. **36**, 90–96 (1953).
[2] S. Dushman, *Scientific Foundations of Vacuum Technique* (John Wiley and Sons, Inc., New York, 1949).
[3] R. M. Barrer, *Diffusion In and Through Solids* (Macmillan Company, New York, 1941).
[4] E. Lange and R. Watzel, Z. physik. Chem. (A) **181**, 1 (1938).

Erratum: Flame Zone Studies by the Particle Track Technique. I. Apparatus and Technique

[J. Chem. Phys. **22**, 106 (1954)]

R. M. FRISTROM, W. H. AVERY, R. PRESCOTT, AND A. MATTUCK
Applied Physics Laboratory, The Johns Hopkins University, Silver Spring, Maryland

THE last term in Eq. (2), page 107, was inverted. The equation should read

$$T_1 = T_0[v_i/v_0][r_i/r_0][M_i/M_0]. \quad (2)$$

The authors are indebted to Mr. E. E. Frost for bringing this error to our attention.

The Anomalous Magnetic Behavior of UI_3 from 1–4.2°K

L. D. ROBERTS AND D. E. LAVALLE,
Oak Ridge National Laboratory, Oak Ridge, Tennessee
AND
R. A. ERICKSON, *University of Tennessee, Knoxville, Tennessee*
(Received April 12, 1954)

MEASUREMENTS[1] by J. K. Dawson have shown that the magnetic susceptibility of UI_3 follows a Curie-Weiss law in the temperature region 200°K–394°K with a Weiss constant of 5°K. The small value of the Weiss constant suggested the possibility of a magnetic transition in the liquid helium temperature region. We have measured the differential magnetic susceptibility at 500 cycles on two 10-gram powder UI_3 samples using a cryostat and mutual inductance bridge described elsewhere.[2] Figures 1 and 2 give plots of the reactive component χ''

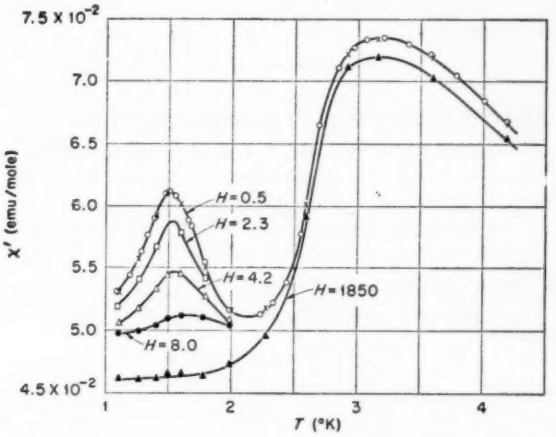

FIG. 1. Reactive component of the magnetic susceptibility of UI_3 as a function of temperature and magnetic field—H is in gauss.

and the resistive component χ'' of the susceptibility as a function of temperature and magnetic field. The maximum in χ' at 3.20°K is interpreted to be an antiferromagnetic transition. In this temperature region χ'' remains very small, and both components of the susceptibility are found to be insensitive to the magnetic field up to 500 gauss. The peak at 1.50°K in χ' is quite different from that at the Néel temperature. In this region the loss component χ'' rises sharply to a maximum at 1.38°K and both components are remarkably sensitive to a static magnetic field which is applied with a solenoid magnet mounted coaxially with the susceptibility measuring coils.[2] Both χ' and χ'' are found to decrease almost linearly with increasing field up to about 5 oersted and this decrease appears to saturate at 300 to 500 gauss. These phenomena were observed to be virtually independent of frequency and amplitude of the oscillating field up to 1000 cycles and 3 oersted.

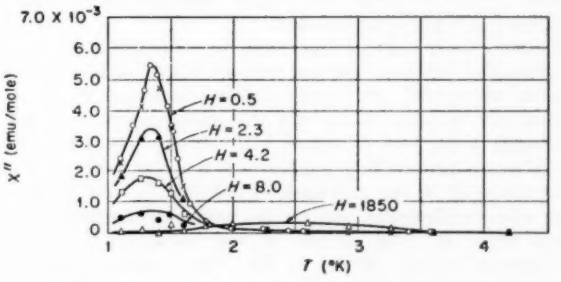

FIG. 2. Resistive component of the magnetic susceptibility of UI_3 as a function of temperature and magnetic field—H is in gauss.

The foregoing behavior was duplicated in two samples of UI_3 prepared by different chemical procedures: one by direct combination of the elements and the other by the action of methyl iodide on UH_3.[3] This fact suggests that these are intrinsic properties of this compound. To prevent chemical decomposition of the sample by oxygen or water, the samples were handled only in a dry box and were sealed under a helium atmosphere in a glass vial. It is noted that the anomalous behavior of χ' and χ'' in the lower temperature region is in some respects similar to the ferromagnetic effects found by Kurti and Simon in manganous ammonium sulfate near 0.1°K and more recently investigated by Hudson and McLane[4] and by Steenland[5] for chromium methylamine sulfate at even lower temperatures. Further susceptibility measurements and a specific heat measurement are in progress.

[1] J. K. Dawson, AERE C/R 578, September, 1950.
[2] Erickson, Roberts, and Dabbs, Rev. Sci. Instr. (in press).
[3] National Nuclear Energy Series VIII-5, "The Chemistry of Uranium," pp. 533–536.
[4] R. P. Hudson and C. K. McLane, International Conference on Low Temperature Physics, Houston (1953).
[5] M. J. Steenland, International Conference on Low Temperature Physics, Houston (1953).

Altered Proportions of Isotopes of Molecular Nitrogen as Evidence for a Monomolecular Reaction

M. Walser, J. George, and L. J. Bodenlos
Naval Medical Research Institute, Bethesda, Maryland
(Received April 8, 1954)

When nitrogen gas is prepared by adding hypobromite to an amine or ammonium salt, the gas satisfies the following equilibrium

$$N^{14}N^{14}+N^{15}N^{15}\rightleftharpoons 2N^{14}N^{15}.$$

Similarly, in compounds of the form $H_2N-X-NH_2$ the proportions of the forms $H_2N^{14}-X-N^{14}H_2$, $H_2N^{15}-X-N^{15}H_2$, and $H_2N^{14}-X-N^{15}H_2$ are described by the same equilibrium constant

$$K=\frac{[N^{14}N^{15}]^2}{[N^{14}N^{14}][N^{15}N^{15}]}=\frac{[H_2N^{14}-X-N^{15}H_2]^2}{[H_2N^{14}-X-N^{14}H_2][H_2N^{15}-X-N^{15}H_2]}=4.$$

However, when N^{15}-enriched nitrogen gas is mixed with normal nitrogen the equilibrium is not attained under ordinary conditions, and a calculated $K\neq 4$. Similarly, when a portion of a compound containing two nitrogen atoms synthesized from N^{15}-enriched nitrogen is combined with an unenriched portion of the same compound, $K_{calc}\neq 4$.

It occurred to us that nitrogen evolved from such a mixture should produce gas in which $K_{calc}\neq 4$, provided that the reaction is monomolecular. In other words, provided that both of the nitrogen atoms in each nitrogen molecule are derived from the same $H_2N-X-NH_2$ molecule, the distribution of the three isotopes of molecular nitrogen will be identical to the distribution of the three isotopic forms of the compound. If the three isotopic forms are not present in proportions which fulfill the statistical equilibrium shown above, the evolved nitrogen gas will not exhibit statistical equilibrium either.

We have confirmed this hypothesis by examination of the proportions of nitrogen gas isotopes evolved in the reaction of hypobromite with urea. N^{15}-enriched urea containing 61.8 atoms percent N^{15} was synthesized by the ammonolysis of diphenyl carbonate. 1 mg was combined with 99 mg of ordinary urea (0.3676 atoms percent N^{15}) and dissolved in water. Portions of this mixture and of the two urea samples individually were allowed to react with hypobromite, and the intensities of the peaks at apparent mass (M/e) 28, 29, and 30 were measured in the mass spectrometer (C.E.C. Model 21-201). The results are shown in Table I. Calculated values were obtained by computing the weights of the three molecular species, $H_2N^{14}CON^{14}H_2$, $H_2N^{15}CON^{15}H_2$, and $H_2N^{14}CON^{15}H_2$ in the individual samples and in the mixture. Assuming that the reaction is monomolecular, the proportions of the three species should give the relative intensities of the three peaks. The close agreement between observed and calculated values confirms that the reaction is monomolecular.

Table I. Proportions of isotopes of molecular nitrogen evolved from normal urea, enriched urea, and a mixture of the two.

Sample		N_2^{29}/N_2^{28}	×	N_2^{29}/N_2^{30}	=	K_{calc}
Ordinary urea		0.007381		—[a]		3.992[b]
Enriched urea		3.23		1.20		3.88
99:1 Mixture	obs	0.01232		3.20		0.0394
	calc	0.01216		3.13		0.0381

[a] The peak at M/e 30 in normal nitrogen is too small to be measured accurately.
[b] Theoretical value, see H. C. Urey, J. Chem. Soc. **1947**; 562.

It is interesting to note that calculation of the atoms percent N^{15} in the mixture from the ratio of M/e 29 to M/e 28 in the usual fashion yields a value of 0.6122 atoms percent, whereas the true value is 0.9819 atoms percent. This latter value was obtained when the urea mixture was converted to ammonium sulfate before addition of hypobromite.

It appears that this principle might be useful in distinguishing whether other gas-evolving reactions are monomolecular. Any N_2-evolving reaction in which both nitrogen atoms are released from the same molecule might be employed.

W. J. McCarville kindly synthesized the urea from N^{15} which was generously provided by Dr. J. Sendroy. Dr. S. L. Friess gave much helpful criticism.

Electrically and Elastically Active Relaxation Modes

Y. Haven and J. H. van Santen
Phillips Research Laboratories, N. V. Philips' Gloeilampenfabrieken, Eindhoven, Netherlands
(Received April 12, 1954)

In a recent paper[1] Hoffman and Pfeiffer discuss the dielectric relaxation of a single-axis rotator in a crystalline field. Closely related to their problem is the behavior of an ion that can occupy a number of potential wells, separated from one another by energy barriers.

Examples: (A) cations in inorganic glasses,[2] and (B) cation vacancies in alkali halides each captured either by a divalent impurity cation (e.g., in NaCl containing a small amount of Cd^{2+}) or by an anion vacancy.[3,4]

The number of electrically active polarization modes may be found by group-theoretical methods: the representation induced by the wells of the wells-and-barriers systems is written as a sum of irreducible representations of the corresponding symmetry group and the number of electrically active modes is equal to the number of those irreducible representations in the sum, to which polar vectors (e.g., the coordinates x,y,z) belong.

Consider as an example an octahedral system of equivalent wells and barriers with wells 1, 2 at $(x,y,z)=(\pm l,0,0)$; 3, 4 at $(0,\pm l,0)$; and 5, 6 at $(0,0,\pm l)$. The system induces the representations $A_{1g}+E_g+T_{1u}$ of symmetry group O_h.[5] The identity representation A_{1g} corresponds to the equilibrium distribution. T_{1u} is a triply degenerate electrically active representation. It corresponds to particle jumps from well 1 either directly or via wells 3, 4, 5, 6, to well 2 and vice versa, to particle transfer from 3 to 4 and from 5 to 6.

The doubly degenerate representation E_g corresponds to particle jumps from wells 1 and 2 to wells 3, 4, 5, 6, and vice versa, and to transfer from wells 3 and 4 to wells 5 and 6 and vice versa. Such a transfer does not correspond to a change of polarization and is therefore electrically inactive. It may, however, be caused by suitable elastic stresses and will therefore be called elastically

active. In the case considered a hydrostatic pressure is ineffective (the representation A_{1g} to which $x^2+y^2+z^2$ belongs is not available since it is "used" for the equilibrium-distribution mode), normal stresses that are different along the cubic axes will be active (E_{1g} to which belong $x^2+y^2-2z^2$ and x^2-y^2, occurs), and shearing stresses should have no effect (T_{2g} to which belong xy, yz, zx does not occur).

According to Fast and Dijkstra[6] this type of elastic relaxation occurs in α iron, containing small amounts of manganese and interstitially dissolved nitrogen.

The N atoms are captured by the Mn atoms and occupy 6 surrounding interstitial positions. In the presence of elastic stresses the N atoms are redistributed over these positions.

Returning to the octahedral system, denoting the transition probabilities for jumps to nearest neighbors by k and neglecting other jumps, the relaxation times τ are found to be $\tau=\infty$ for A_{1g}, $\tau=1/6k$ for E_g, and $\tau=1/4k$ for T_{1u}.

In the NaCl·Cd system we have a cubic close-packed system of equivalent wells. It induces the representations $A_{1g}+E_g+T_{1u}+T_{2g}+T_{2u}$ of symmetry group O_h, the relaxation times being $\infty, 1/6k, 1/2k, 1/4k, 1/6k$, respectively. Electrically, therefore, the system is characterized by a single relaxation time $1/2k$.

Another system, which may be important for glasses, is a linear array of n equivalent wells separated by $n-1$ barriers. For $n=2r$ or $2r+1$ there are r electrically active modes. Denoting all nearest-neighbor transition probabilities by k and neglecting others, the relaxation times of electrically active and inactive modes are given by

$$1/\tau=2k+2k\cos\frac{s\pi}{n}, \quad s=1, 2, \cdots, n.$$

[1] J. D. Hoffman and H. G. Pfeiffer, J. Chem. Phys. **22**, 132 (1954).
[2] Volger, Stevels, and van Amerongen, Philips Research Repts. **8**, 452 (1953).
[3] R. G. Breckenridge, J. Chem. Phys. **16**, 959 (1948); **18**, 913 (1950).
[4] Y. Haven, J. Chem. Phys. **21**, 171 (1952).
[5] Eyring, Walter, and Kimball, *Quantum Chemistry* (John Wiley and Sons, Inc., New York, 1944).
[6] J. D. Fast and L. J. Dijkstra, Philips Tech. Rev. **13**, 172 (1951/52).

An Emission Spectrum Attributed to Acetaldehyde*

G. Wilse Robinson†
Department of Chemistry, University of Rochester, Rochester, New York
(Received April 12, 1954)

A COMPLEX emission spectrum (Fig. 1) attributed to acetaldehyde, extending from 3500A into the red with a maximum intensity at about 4200A, has been obtained with a high frequency electrodeless discharge. A rather simple technique, the details of which will be described in another paper,[1] employs a relatively high-pressure discharge coupled with an extremely rapid pumping rate. The addition of benzene to the discharge[1] increased the emission intensity and at the same time retarded dissociation. A Bausch and Lomb large Littrow-type quartz spectrograph employing Eastman-type 103a-G plates was used for the study.

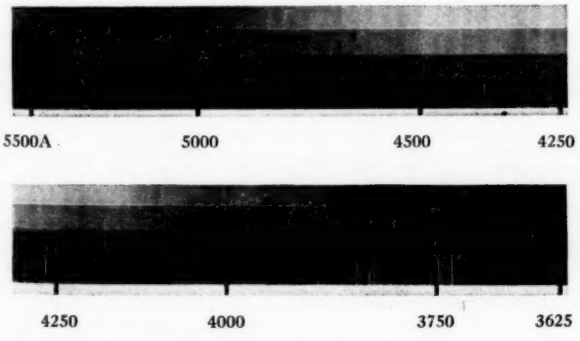

FIG. 1. Emission spectrum of acetaldehyde at three different intensities. An iron arc spectrum is included for wavelength reference. The apparent minimum around 5000A is due to the type G sensitizer.

That all or part of the spectrum is not due to an emitter other than acetaldehyde is evidenced by a number of observations. First of all the benzene used was found to have no emission of its own in the region of interest.‡ Secondly, to study the possibility of spectral impurities arising from a discharge reaction between acetaldehyde and benzene, the emission was produced with very pure acetaldehyde alone and with toluene substituted for benzene. In these instances the spectra were found to be identical in every respect to that observed for the acetaldehyde-benzene mixture. Some early plates showed weak benzaldehyde emission but this was eliminated by increasing the pumping rate. Thirdly, a search was made for the well-known spectra of possible diatomic emitters but these were completely absent except on prolonged exposure when CO bands weakly appear. Likewise, the known spectrum of biacetyl[2] was absent, as were the so-called ethylene flame bands (CHO)[3] which extend to a shorter wavelength than any of the bands observed here. Finally, the spectra obtained for acetone, acetic acid, and propionaldehyde, molecules which might be expected to yield the same dissociation fragments, were found to contain no identical features with the spectrum of acetaldehyde.

This emission spectrum of acetaldehyde is not unexpected in view of the fact that both formaldehyde[4] and acetone[5] as well as other aldehydes and ketones are known to exhibit emission in this spectral region. Interestingly enough, the longwave portion of the spectrum (see Fig. 1) closely resembles the fluorescence of flowing acetone vapor[5] where a long series of bands 120 cm^{-1} apart was observed. The separation in the present instance is about 150 cm^{-1}. A vibrational analysis of the bands is now being attempted along with a similar study of other simple aldehydes and ketones, and a complete report of this work will appear in a future paper.

* This work was supported in part by the Office of Ordnance Research under contract with the University of Rochester.
† Post-Doctoral Fellow, 1952–1954. Present address: Department of Chemistry, The Johns Hopkins University, Baltimore, Maryland.
[1] G. W. Robinson, J. Chem. Phys. (to be published).
‡ The triplet-singlet emission in the neighborhood of 3400A was not observed even on long exposures.
[2] Almy, Fuller, and Kinzer, J. Chem. Phys. **8**, 37 (1940).
[3] W. M. Vaidya, Proc. Roy. Soc. (London) **A147**, 513 (1934).
[4] P. J. Dyne, J. Chem. Phys. **20**, 811 (1952).
[5] Luckey, Duncan, and Noyes, J. Chem. Phys. **16**, 407 (1948).

s-Triazine. I. The Unit Cell

L. A. Siegel and E. F. Williams
Stamford Research Laboratories, American Cyanamid Company, Stamford, Connecticut
(Received April 14, 1954)

THE existence of *s*-triazine (1,3,5-triazine) has been demonstrated recently by Grundmann and Kreutzberger,[1] Fig. 1. Dr. I. Hechenbleikner of these laboratories has prepared this material[2] for a study of its various physical properties.

The material is volatile and large single crystals are readily grown by sublimation. Optical examination shows these crystals to be uniaxial negative and probably in the ditrigonal-scalenohedral crystal class of the trigonal system (point group $\bar{3}m$). An x-ray investigation has been made using a crystal sealed in a glass capillary, and rotation and Weissenberg patterns indicate

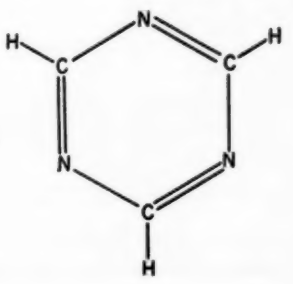

FIG. 1. *s*-triazine.

that the unit cell is rhombohedral. The measured constants of the triply primitive hexagonal cell are $a=9.70$A and $c=7.38$A, while the rhombohedral constants derived from them are $a=6.11$A, $\alpha=104.8°$. A rough density determination (1.38 g/cm³) corresponds to two molecules in the rhombohedral cell.

The combination of the rhombohedral lattice and the probable point group $\bar{3}m$ suggests $R\bar{3}m$ and $R\bar{3}c$ as probable space groups. The extinction condition, $hkil$ only for l even (hexagonal indices), is observed to hold for the layer line $l=1$, thus favoring $R\bar{3}c$. A more general establishment of this condition has not been possible since the odd layer lines of the c-axis rotation pattern are very weak. For either space group the condition of two molecules per unit cell makes the threefold axis of the cell a molecular symmetry axis as well, and this is in agreement with the chemical structure proposed by Grundmann and Kreutzberger. Space group $R\bar{3}c$ would in addition require the molecule to be planar.

Planarity of the triazine ring has been observed in the crystal structures of melamine[3] and cyanuric acid,[4] which also show that the ring deviates only slightly from a regular hexagon. This is true in terms of scattering power as well as geometry, since the carbon and nitrogen scattering factors do not differ greatly. Using the hexagonal approximation for the ring, intensity calculations for the $hk0$ reflections (hexagonal indices) of s-triazine favor space group $R\bar{3}c$. The separation of the two molecules, in this space group, by $c/2$ would lead to the vanishing of the odd layer lines of the c-axis rotation pattern for molecules of sixfold symmetry. The observed weakness of the odd layer lines is therefore in agreement with the arrangement of two nearly sixfold molecules in $R\bar{3}c$. A more detailed investigation of the structure is in progress.

[1] C. Grundmann and A. Kreutzberger, J. Am. Chem. Soc. **76**, 632 (1954).
[2] L. E. Hinkel and R. T. Dunn, J. Chem. Soc. (London) **1930**, 1834.
[3] E. W. Hughes, J. Am. Chem. Soc. **63**, 1737 (1941).
[4] E. H. Wiebenga, J. Am. Chem. Soc. **74**, 6156 (1952).

s-Triazine. II. The Near Ultraviolet Absorption Spectrum

R. C. Hirt, F. Halverson, and R. G. Schmitt
Stamford Research Laboratories, American Cyanamid Company, Stamford, Connecticut
(Received April 14, 1954)

THE near ultraviolet spectrum of s-triazine (analog of benzene in which alternate C−H groups are replaced by nitrogen atoms) is of considerable interest in connection with the appearance of nonbonding electron transitions. An empirical estimate of its spectrum was made from observations on related compounds,[1,2] but certain features have awaited direct measurements on the compound itself. As a result of the identification of s-triazine, recently published by Grundmann and Kreutzberger,[3] these data have now been obtained.

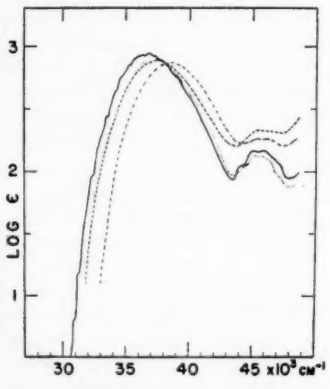

FIG. 1. s-Triazine in cyclohexane ————, in acetonitrile . . . . . , in methanol - - - - - - -, and in water ---------- (ϵ is the molar absorptivity or molar extinction; data are from a Cary spectrophotometer).

The solution spectrum in various solvents is shown in Fig. 1, and the vapor spectrum is shown in Fig. 2. In general appearance the observed spectrum agrees with the predictions. The band centered at 45 350 cm^{-1} in solution shows virtually no solvent shift and must be the lowest singlet $\pi-\pi$ transition ($^1A_1'-{}^1A_2'$) for consistency with the spectra of benzene and of other nitrogen heterocyclics.[1] Use of this transition to evaluate the C−N resonance integral in Pariser and Parr's semi-empirical molecular orbital treatment[4] yields the value $\beta_{CN}=-2.74$ ev. This revision does not disturb the relative positions of computed transitions in the various heterocyclics. Any attempt to assign a band near 36 780 cm^{-1} to the lowest singlet $\pi-\pi$ transition, however, introduces major discrepancies.

The band (or bands) near 36 780 cm^{-1} shows the distinct solvent shift characteristic of transitions involving nonbonding electrons, and in the vapor at least a portion of it has the sharp line character observed for the $n-\pi$ transitions in the diazines.[1] This positive evidence coupled with the improbability of a $\pi-\pi$

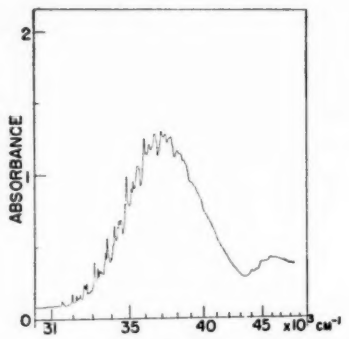

FIG. 2. Cary trace of vapor spectrum of s-triazine. (50-mm cell, at vapor pressure at room temperature.)

transition in this range forces assignment of the band (or bands) to an $n-\pi$ transition. Intensity considerations[5] then indicate at least one allowed transition must be involved. The appearance of the vapor spectrum indicates the presence of two-band systems, however, a sharp one overlapping a diffuse one. These will be described in detail in a future publication.

An examination of the region from 13 000 to 31 000 cm^{-1} with concentrated solutions and 100-mm cells has shown the lack of any bands with ϵ greater than 0.02. This is consistent with the prediction that the triplet transition ($^1A_1'-{}^3A_1'$) would fall near 37 030 cm^{-1}, obtained using $\beta_{CN}=-2.74$ ev in Pariser and Parr's treatment,[4] and thus would be obscured by the $n-\pi$ transitions.

The spectrum of s-triazine resembles that of 2,4,6-trimethyl-s-triazine, as Grundmann and Kruetzberger[3] pointed out, as shown in Table I. This resemblance is expected, since the two

TABLE I. Ultraviolet spectral data on s-triazine and trimethyl-s-triazine.

Band type	$n-\pi$				$\pi-\pi$			
Compound	s-Triazine		Trimethyl-s-triazine		s-Triazine		Trimethyl-s-triazine	
	cm^{-1}	ϵ	cm^{-1}	ϵ	cm^{-1}	ϵ	cm^{-1}	ϵ
In cyclohexane	36 780	881	37 880[a]	701	45 050	146	43 960[a]	289
In acetonitrile	37 300	791	. . .	. . .	45 100	137	. . .	. . .
In methanol	37 450	768	39 000[b]	795	45 250	213	44 000[c]	475
In water	38 450	747	40 320[a]	692	45 250	183	43 960[a]	554

[a] L. Paoloni, Rome, Italy (private communication); to be published in Gazz. Chim. Ital.
[b] Cairns, Larchar, and McKusick, J. Am. Chem. Soc. **74**, 5633 (1952).
[c] B. C. McKusick, Chemical Department, E. I. du Pont de Nemours and Company (private communication).

molecules have essentially the same symmetry and the methyl groups have little effect on the spectrum. Since s-triazine decom-

poses at an appreciable rate in water, the data for the water solutions (*p*H 6) were obtained by extrapolation to zero time.

[1] F. Halverson and R. C. Hirt, J. Chem. Phys. **19**, 711 (1951).
[2] R. C. Hirt and D. J. Salley, J. Chem. Phys. **21**, 1181 (1953).
[3] C. Grundmann and A. Kreutzberger, J. Am. Chem. Soc. **76**, 632 (1954).
[4] R. Pariser and R. G. Parr, J. Chem. Phys. **21**, 466, 767 (1953).
[5] J. R. Platt, J. Opt. Soc. Am. **43**, 252 (1953).

s-Triazine. III. The Infrared Spectrum

JOHN E. LANCASTER AND NORMAN B. COLTHUP
Stamford Research Laboratories, American Cyanamid Company, Stamford, Connecticut
(Received April 14, 1954)

GRUNDMANN and Kreutzberger[1] have stated in thir recent note that the infrared absorption spectrum of *s*-triazine is closely related to other simple 1,3,5 triazine derivatives. We have observed the infrared spectrum of *s*-triazine in greater detail in the vapor, liquid, and solid states, using model 21 and model 12C Perkin-Elmer spectrometers with LiF, NaCl, and KBr optics.

Table I describes the fundamentals of *s*-triazine and gives the

TABLE I. Expected values for the vibrational frequencies of *s*-triazine, by analogy with related molecules. A_1', A_2', E' are planar vibrations; A_2'', E'' are nonplanar. The numbering follows the Herzberg scheme.

		Expected frequencies (cm^{-1})	Observed frequencies (cm^{-1})
Raman	ν_2 ring breathing (C and N atoms out	3000	
A_1'	ν_1 symmetric CH stretching		
(pol.)	of phase)	1000	
	ν_3 ring breathing (all atoms in phase)	1000	
A_2'	ν_4 C atoms twisting against the N		
Inactive	atoms	1650	
	ν_5 H atoms twisting against the ring	1200	
E'	ν_6 CH stretching	3000	3056
Infrared,	ν_7 ring stretching	1550	1556
Raman	ν_8 ring stretching	1450	1410
(depol.)	ν_9 CH rocking	1100	?
	ν_{10} ring angle bending	600	?
A_2''	ν_{11} CH wagging (H atoms in phase)	800	735
Infrared	ν_{12} out-of-plane ring mode (C and N atoms out of phase)	680	675
E''	ν_{13} CH wagging	900	
Raman	ν_{14} out-of-plane ring mode	400	
(depol.)			

symmetry classifications based on D_{3h} symmetry. (The spectrum appears to be in agreement with the D_{3A} model.) The vapor spectrum shows two types of band contours: one type shows well-defined *PQR* branches and must be associated with the parallel (out-of-plane) vibrations (A_2''); the other type shows a poorly defined and variable structure, and no doubt belongs to the perpendicular (planar, doubly degenerate) modes (E'). The strongest bands are the perpendicular bands at 1556 and 1410 cm^{-1}, which are clearly ν_7 and ν_8. A medium-intensity perpendicular band at 3056 cm^{-1} is readily identified as ν_6. The remaining E' vibrations, ν_9 and ν_{10}, are not so apparent. Several weak bands between 800 and 1200 cm^{-1} could qualify for the CH rocking mode, ν_9. No bands have as yet been found in the KBr region, where ν_{10} is expected to appear. The two infrared-active, nonplanar (A_2'') modes are doubtless the two strong bands with well-defined *PQR* branches seen at 675 and 735 cm^{-1}. The upper one is most probably ν_{11}; the lower one, ν_{12}. Both have *Q* branches that are split; this may be caused by the close superposition of a difference band of the type $\nu_i+\nu_{14}-\nu_{14}$.

Many overtones and combinations are seen above 1600 cm^{-1}, but none yield indisputable evidence for the location of the inactive modes.

A study of the Raman spectrum is under way. This should confirm ν_9, locate ν_{10}, and yield the remaining active frequencies. We are also undertaking the preparation of *s*-triazine-d_3 and will report on the complete spectra of both molecules in a later paper. It is to be noted that these two isotopic molecules will yield sufficient vibrational data to solve for the complete nonplanar F (symmetrized) matrix.

[1] C. Grundmann and A. Kreutzberger, J. Am. Chem. Soc. **76**, 632 (1954).

Anomalous Faraday Effect in Aqueous Solutions of Inorganic Salts

D. D. RANDALL AND A. M. TAYLOR
Physical Laboratory, The University of Southampton, England
(Received April 12, 1954)

MEASUREMENTS have been made in this laboratory of the magneto-optical Faraday effect in aqueous solutions of inorganic salts, by means of a photoelectric polarimeter developed from the apparatus described by Archard *et al.*[1] The sensitivity of the polarimeter is a few seconds of arc and the rotations measured have been of the order of several minutes. To produce such rotations fields of about 30 oersted over a 10-cm path have been employed. The wavelength range covered is 3600–6000A, with solutions of concentration varying between zero and half molar. According to Schönrock's mixture rule[2] the magneto-optical rotation of dilute solutions should be an approximately linear function of concentration. However, when the Verdet constant is plotted against concentration (Fig. 1 shows typical results) an anomaly is found which is most marked in the blue-violet region of the spectrum. The concentration at which the anomaly is greatest is independent of wavelength, but differs from salt to salt, and with divalent or trivalent positive ions appears to be independent of the negative ion. For monovalent positive ions the anomaly is less marked and the nature of the negative ion seems to have a perceptible effect.

It is suggested that the anomaly is brought about by a change in the structure of water caused by the introduction of dissolved ions.[3] It may be surmised that the larger the energy of the ion the more effective it is in promoting the structural change and hence the lower the concentration at which the maximum anomaly occurs. Figure 2, where the ionization energy has been plotted against the molar concentration at which the anomaly is greatest, shows that this surmise is apparently true. The experimental points lie on a smooth curve, two ions excepted, *viz.*, Be^{++} and Hg^{++}. These exceptions are not unexpected[4] since Be^{++} is unique among divalent ions in having a coordination number of four, all others having one of six, while mercuric salts are probably incompletely dissociated in solution so that the concentration of Hg^{++} ions is less than that of the salt.

Okazaki[5] has measured the magneto-optical rotation of strong electrolytes, in aqueous solutions of higher concentration than

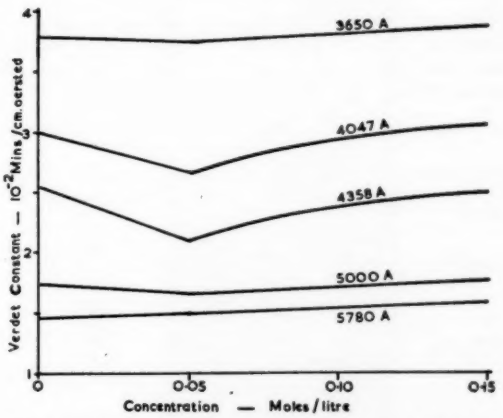

FIG. 1. Verdet constants of dilute aqueous solutions of $CuCl_2$.

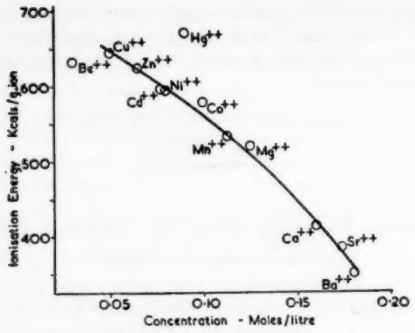

FIG. 2. Ionization energy of divalent ions plotted against concentration at which the anomaly is greatest.

ours, throughout a wavelength range 3400–5900A, with magnetic fields of the order of 10 000 oersted. His diagrams of the specific rotation of the solutes as functions of wavelength show smooth curves drawn through the experimental points; in all cases, however, the points in the blue-violet region lie consistently above the curves, although this deviation passed unnoticed in his papers. His treatment of the data rests on his assumption of constancy of the specific rotation of the water component of the solutions, and systematic deviation of the experimental points from the smooth curves suggests that the assumption is not fully justified and indicates anomalous behavior of the water in solution.

Magneto-optical rotation and refractive index are intimately connected, and it may be expected that a corresponding anomaly should be found in the variation of the refractive index with concentration. Preliminary measurements of the refractive index of various solutions of $CuSO_4$ have been made, and while the Pulfrich refractometer used did not give sufficient accuracy for definite confirmation, the expected anomaly appears to be present.

Further measurements are in progress.

[1] Archard, Clegg, and Taylor, Proc. Phys. Soc. (London) **B65**, 758 (1952).
[2] O. Schönrock, Z. Physik **46**, 314 (1928).
[3] G. W. Stewart, J. Chem. Phys. **7**, 869 (1939).
[4] J. D. Bernal and R. H. Fowler, J. Chem. Phys. **1**, 515 (1933).
[5] A. Okazaki, Mem. Ryojun Coll. Eng. **8**, 1 (1935).

Radiation Chemistry of Luminescent Solutions*

MILTON BURTON AND W. N. PATRICK
Department of Chemistry, University of Notre Dame, Notre Dame, Indiana
(Received April 15, 1954)

WHEN benzene containing 4.5 g *p*-terphenyl per liter or 1g anthracene per liter is exposed to gamma radiation the induced fluorescence from such solutions is greater by a factor of ~28 or ~6, respectively, than it would be from pure benzene.[1] This increase of fluorescence is attributed to particularly favorable conditions for transfer of energy from benzene to the solute.[1–3] Criteria which affect such transfer have been examined and considered by Förster[4] as well as by Kallman and Furst.[1–3] Transfer of excitation energy must compete with self-fluorescence of the benzene, collisional deactivation (i.e., "self-protection" in the sense of possible radiation chemical effects), and chemical decomposition. Self-fluorescence is small and unimportant.

TABLE I. 100 ev yields of H_2, $G(H_2)$, in irradiation of benzene containing various solutes by 1.5-Mev electrons.

Substance	Electron %	Current μamp	Energy input 10^{22} ev	$G(H_2)$
	0	0.75	1.44	0.0363
p-terphenyl	0.141	0.75	1.88	0.0370
	0.281	0.75	1.59	0.0372
	0.562	0.75	1.41	0.0358
	0.844	0.75	1.48	0.0365
	1.125	1.0	2.09	0.038
m-terphenyl	7.32	1.0	2.01	0.027
anthracene	1.26	1.0	2.19	0.035
	pure[a] powder	1.15	2.30	0.0053

[a] In this case $G(C_2$ gases$) = 0.0098$.

It has been suggested by Maddock[5] that, if the competition is between fluorescence and chemical decomposition, compounds like terphenyl may show an extraordinarily high protective effect (compare the action of benzene-d_6[6]) in inhibition of decomposition of benzene.[7] We have examined this possibility using techniques already described[7] for solutions of *p*-terphenyl, *m*-terphenyl, and anthracene with the results shown in Table I, which also includes some results for pure anthracene powder. In this work only materials of very high purity were used.[8]

Table I shows that neither *p*-terphenyl nor anthracene confers any perceptible protection on benzene in the range of their solubility. The explanation may be of at least two kinds: (a) the fraction of energy tapped off for induced fluorescence is far less than even the relatively small amount of energy which goes into decomposition processes; (b) the energy tapped off for induced fluorescence comes from states which would not lead to decomposition in any event. Using the value for the radiation yield, $G(H_2) \sim 0.036$, and assuming ~5 ev necessary for a bond rupture or other primary decomposition process, we find $\gtrsim 0.2$ percent of the energy absorbed causes decomposition, so that either or both of the suggested explanations may apply.

The protective effect of *m*-terphenyl at the relatively high electron percent of 7.32 (it has much higher solubility than the other two solutes) is real. The smallness of the effect suggests that it follows a conventional mechanism in which benzene molecules, excited with enough energy to decompose, transfer a portion of that energy to a molecule with smaller excitation energy with resultant protection and energy degradation without decomposition.[7]

* Contribution from the Radiation Project of the University of Notre Dame, supported in part under U. S. Atomic Energy Commission contract AT(11-1)-38 and Navy equipment loan contract Nonr-06900.
[1] H. Kallman and M. Furst, Phys. Rev. **79**, 857 (1950).
[2] H. Kallman and M. Furst, Phys. Rev. **81**, 853 (1951).
[3] M. Furst and H. Kallman, Phys. Rev. **85**, 816 (1952).
[4] C. Förster, Naturwiss. **33**, 166 (1946); Ann. Physik **2**, 56 (1948).
[5] A. G. Maddock, Discussions Faraday Soc. No. 12, 124 (1952).
[6] S. Gordon and M. Burton, Discussions Faraday Soc. No. 12, 88 (1952).
[7] Evidence for protection *by* benzene in mixtures with other liquids has been given by J. P. Manion and M. Burton, J. Phys. Chem. **56**, 560 (1952) and by M. Burton and W. N. Patrick, ibid. **58** (to be published).
[8] Samples were purified as follows: *p*-terphenyl and *m*-terphenyl by recrystallization from benzene; anthracene by methods involving four successive co-distillations with ethylene glycol and subsequent washing and drying (see L. S. Fieser, *Experiments in Organic Chemistry* (D. C. Heath and Company, Boston, 1941), p. 345, footnote 13); benzene as described by W. N. Patrick and M. Burton, J. Phys. Chem. **58** (to be published).

Precombustion Reactions in Hydrocarbon Diffusion Flames: The Paraffin Candle Flame

S. RUVEN SMITH AND ALVIN S. GORDON
Research Department, U. S. Naval Ordnance Test Station, China Lake, Inyokern, California
(Received April 14, 1954)

USING a technique similar to that recently reported by Prescott, Hudson, Foner, and Avery,[1] we have probed a paraffin candle burning in air at one atmosphere pressure. Various regions inside the glowing mantle, on the glowing mantle, and outside the glowing mantle were sampled with a fine quartz probe. The end of the probe was constricted so that the sample pressure dropped from one atmosphere to between a few millimeters and a few centimeters as it passed through the constriction. At the same time the flame temperature was measured with a one-mil Pt-Pt-10 percent Rh thermocouple covered with Pyrex glass and placed so that it did not see the mouth of the probe.

The sample gases spend about one millisecond in the hot part of the probe. The residence time in the probe was varied about tenfold without appreciable effect on the composition, showing that catalysis in the probe was not very important.

The samples were collected in flasks and analyzed with a Consolidated 21–103 mass spectrometer. In addition to the gross analysis, the sample was fractionated into five cuts at temperatures between liquid nitrogen and 60°C as an aid in identifying the products.

TABLE I. Approximate composition of samples probed from paraffin candle (In order of decreasing abundance).

	Center of glowing mantle	Inside edge of glowing mantle
>60%	Nitrogen	Nitrogen
>10%	Carbon dioxide Water	Carbon dioxide Water
> 2%	Carbon monoxide Ethylene	Carbon monoxide
> 0.5%	Hydrogen Acetylene Methane Propylene Argon	Oxygen Argon
> 0.2%	Butene Butadiene Methyl acetylene Ethane	Hydrogen
< 0.2%	Pentene Benzene Hexene Cyclopentadiene Cyclohexadiene Heptene Vinyl acetylene Diacetylene Toluene Oxygen (Propane)	Acetylene Ethylene Methane Propylene

The results are shown in Table I for a sample in approximately the center of the glowing mantle and fairly close to the wick, and for a second sample near the inside edge of the glowing mantle at the same height above the wick. It should be noted that these analyses are on a percentage basis of the products collected; all the very high boiling hydrocarbons condense and are lost.

It may be noted from the results in Table I that, except for methane, ethene, and possibly an extremely small percentage of propane, all the hydrocarbons are unsaturated. If the saturated hydrocarbons were the precursors of the unsaturates, they would in general be identifiable with our technique.

From the center of the glowing mantle to the inside edge of the glowing mantle, the temperature rises from 700°C to 900°C. While a number of hydrocarbons are present in concentrations of one percent or greater in the center of the mantle, all the hydrocarbons except acetylene have decreased to less than 0.1 percent in the inside edge of the glowing mantle. The absence of oxygenated hydrocarbons is especially noteworthy. In experiments with slow oxidation of hydrocarbons in vessels, alcohol and aldehydes, especially formaldehyde, are quite prominent products. In our experiments there was slight mass spectrometric evidence for the presence of formaldehyde from the fraction not volatile at −100°C. To confirm this, especially large samples were treated with Schiff's base. These tests showed total aldehyde concentration of one part in 10^5 to 10^6. There appears to be a higher concentration of the formaldehyde in the center of the glowing mantle sample, although this is deceptive, since there is also a much larger wax concentration here which concentrates the gaseous sample when it condenses.

The mechanism of precombustion reactions appears to involve mainly the cracking of hydrocarbons predominantly to unsaturates. Formaldehyde is present in very low concentrations, but it may still play a role in the combustion, its low concentration resulting from extremely rapid consumption. To check this point, formaldehyde vapor has been added to a methane diffusion flame, which is a considerably hotter flame than the paraffin candle flame. Upon sampling this flame, appreciable quantities of formaldehyde (about 0.1 percent) were found even in regions in which there were a couple tenths percentage of oxygen. Without added formaldehyde there is about 1 part in 10^5 to 10^6 formaldehyde present in these regions. More work has to be done before the point can be completely established but present indications are that formaldehyde does not play an important role in the mechanism of the combustion of saturated hydrocarbons in diffusion flames.

Water is very hard to identify since it is so easily absorbed on many surfaces. By conditioning the mass spectrometer, it has been possible to get concentrations of water which are reasonably close to the expected concentrations.

[1] Prescott, Hudson, Foner, and Avery, J. Chem. Phys. 22, 145 (1954).

Solid Ozone

CALLAWAY BROWN, ABRAHAM W. BERGER, AND CHARLES K. HERSH
Armour Research Foundation, Illinois Institute of Technology, Chicago 16, Illinois
(Received April 12, 1954)

THE only report of solid ozone in the literature is that of Schwab[1] who determined a number of the physical constants of ozone including the melting point. He observed that blue-black crystals of ozone formed on cooling liquid ozone in boiling liquid hydrogen. The temperature-time curve on warming from liquid hydrogen temperature showed a pronounced halt at −251.4°C which was interpreted as the melting point.

Workers with liquid ozone are familiar with its fluidity at the temperature of boiling liquid nitrogen. Brown and Franson[2] determined the density of liquid ozone at −195°C by a manometric method which involved measurement of the hydrostatic head of liquid produced by a known pressure difference across the manometer. Liquid ozone was distilled in vacuum into the U-tube manometer cooled in liquid nitrogen.

Usually this step proceeded without incident but occasionally it was observed that some kind of transition in the liquid ozone occurred abruptly in the course of the distillation. Smooth flow of the liquid ozone down the walls of the receiver halted, and additional ozone distilled into the receiver adhered to the walls and hung in a sizeable lump of irregular shape. On one occasion when this occurred, some liquid had already been collected in the U tube. Application of helium pressure to one arm of the U tube, with a vacuum on the other arm, produced no movement of the ozone in the U tube even when the pressure differential reached one atmosphere. The ozone in the U tube was effectively "frozen"

FIG. 1.

and served as a vacuum seal against helium on one side of the manometer.

In subsequent work it has been found that the solidified ozone may be formed invariably by distillation of liquid ozone into a container cooled to the triple point of nitrogen (−210°C). Once formed the material does not become fluid in a liquid nitrogen bath but two observations with a nitrogen bath warmed slowly by the addition of oxygen showed a transition to the fluid form at −193±0.5°C.

In one experiment the liquid nitrogen bath was warmed by the addition of oxygen at a rate of 0.06°/min. Melting of solidified ozone was observed to begin at 79.7°K (−193.4°C) and melting was complete at 80.6K (−192.5°C). Bath temperature was read on an oxygen vapor pressure thermometer from various pressure data of Henning and Otto.[3] Details of the apparatus and procedure are given in a series of papers on the physical properties of liquid ozone-oxygen mixtures which will be published shortly.

The obvious interpretation of these observations is that liquid ozone supercools readily and is normally fluid at −195° but that the true melting point is −193°±0.5°C. A photograph of a solidified sample of ozone in an 8×8-mm square glass cuvette is shown in Fig. 1. Color photographs and visual observation strongly suggest a crystalline material.

A low-temperature x-ray camera has been built in the hope of establishing the crystal structure. This work has been temporarily delayed so the present note is released in order to present the evidence now available for solid ozone, melting at −193°C.

[1] G. M. Schwab, Z. physik. Chem. **110**, 599 (1924).
[2] C. Brown and K. D. Franson, J. Chem. Phys. **21**, 917 (1953).
[3] F. Henning and J. Otto, Physik. Z. **37**, 633 (1936).

Fermi Level, Chemical Potential, and Gibbs Free Energy

MALCOLM K. BRACHMAN
Texas Instruments Incorporated, Dallas, Texas
(Received April 14, 1954)

REISS[1] has drawn attention to the fact that although the Fermi level $\zeta=\eta kT$ "always represents the chemical potential of a weakly coupled electron assembly, it is hardly ever the Gibbs free energy per electron." We wish to remark on the relationship between these quantities for a specific case, the generalized Fermi-Thomas model of an atom,[2] where the relevant thermodynamic functions[3] are known.

Introduce the Gibbs free energy G by the equation $G=F+pv$. The chemical potential may be defined by the equivalent relations

$$\mu=\left(\frac{\partial F}{\partial Z}\right)_{T,v}=\left(\frac{\partial G}{\partial Z}\right)_{T,p}. \tag{1}$$

It may be demonstrated by direct differentiation[4] that

$$\mu=\zeta. \tag{2}$$

Thus the chemical potential and the Fermi level are equal for this case, where there is strong electron-electron coupling. Equation (7b) of reference 3 may be rearranged to give

$$Z\zeta=G+\tfrac{1}{3}(2E_{e,e}-E_{e,N}), \tag{3}$$

which clearly exhibits the difference between ζ and G/Z. Since $E_{e,e}$ is positive (electron-electron interaction) and $E_{e,N}$ is negative (electron-nucleus interaction), this difference is positive. In agreement with Reiss, it is evident that it is not always legitimate to equate μ and G/Z. It may be noted that setting e equal to zero gives $\zeta=G/Z$.

An explicit calculation of the thermodynamic functions requires a knowledge of V, the potential, as a function of r. This may be obtained by solving the generalized Fermi-Thomas differential equation, and this is treated in reference 2.

[1] H. Reiss, J. Chem. Phys. **21**, 1209 (1953).
[2] Feynman, Metropolis, and Teller, Phys. Rev. **75**, 1561 (1949).
[3] M. K. Brachman, Phys. Rev. **84**, 1263 (1951).
[4] The formulas of reference 3 contain Z's that arise from the facts that the nuclear charge is Ze and that the total number of electrons is Z. Care must be taken to differentiate only with respect to the latter, although the Z's are equal.

Microwave Spectrum of Benzonitrile

GUNNAR ERLANDSSON
Laboratory of Physics, The University of Stockholm, Stockholm, Sweden
(Received April 8, 1954)

THE transitions $J=7$–8 and $J=8$–9 in the pure rotational spectrum of benzonitrile have been measured in the k-band microwave region. The transition frequencies found are as follows (in Mc/sec):

$7_{0.7}-8_{0.8}$	20826	$8_{0.8}-9_{0.9}$	23226
$7_{1.7}-8_{1.8}$	20449	$8_{1.8}-9_{1.9}$	22936
$7_{1.6}-8_{1.7}$	22936	$8_{1.7}-9_{1.8}$	25628
$7_{2.6}-8_{2.7}$	21857	$8_{2.7}-9_{2.8}$	24507
$7_{2.5}-8_{2.6}$	23110	$8_{2.6}-9_{2.7}$	—
$7_{3.5}-8_{3.6}$	22239	$8_{3.6}-9_{3.7}$	25030
$7_{3.4}-8_{3.5}$	22406	$8_{3.5}-9_{3.6}$	25328
$7_{4.4}-8_{4.5}$	22220	$8_{4.5}-9_{4.6}$	25030
$7_{4.3}-8_{4.4}$	22231	$8_{4.4}-9_{4.5}$	25044
$7_{5.3}-8_{5.4}$, $7_{5.2}-8_{5.3}$	22177	$8_{5.4}-9_{5.5}$, $8_{5.3}-9_{5.4}$	24972
$7_{6.2}-8_{6.3}$, $7_{6.1}-8_{6.2}$	22157	$8_{6.3}-9_{6.4}$, $8_{6.2}-9_{6.3}$	24938
$7_{7.1}-8_{7.2}$, $7_{7.0}-8_{7.1}$	22144	$8_{7.2}-9_{7.3}$, $8_{7.1}-9_{7.2}$	24924
		$8_{8.1}-9_{8.2}$, $8_{8.0}-9_{8.1}$	24912
		$9_{0.9}-10_{0.10}$	25625.

The rotational constants are found to be (in kMc/sec)

$$A=5.654 \quad B=1.546 \quad C=1.2145,$$

the asymmetry parameter $\kappa=-0.8505$, and the moments of inertia (in atomic units×Angström²)

$$I_A=89.39 \quad I_B=326.9 \quad I_C=416.2.$$

Frequency values calculated from these constants agree within the limits of error (±5 Mc/sec) with observed values given in the foregoing.

The value of I_A may be compared to the corresponding value found for monofluorobenzene[1] $I_A=89.230$ AA². The present value is less accurate and the difference is not outside the limits of error.

[1] G. Erlandsson, Arkiv Fysik **7**, 189 (1953).

Letters to the Editor:

Conductivities of the Exchange Resins in the Hydrogen Form . . . Leonard W. Holm 1132

Elastic Constants of Gels . . . M. Bhagavantam and G. Suryanarayana Sastry 1133

Stress-Relaxations of Rubber-Like Materials . . . E. R. Gumbley 1134

Determination of Surface Tension on Thin Films . . . Bhupendra Shekhar Mitra 1134

Polarized Infrared Spectrum of Ethylene Oxide and Ethylene-d4 Oxide . Llewellyn H. Jones 1135

Paramagnetic Resonance Spectra of Some Organic Free Radical Ions . . . S. I. Weissman 1135

Lattice Energies of Copper Subgroup Monovalent Halides . . . Aubrey P. Altshuller 1136

Paramagnetic Resonance in Phthalocyanine, Chlorophyll, and Hemoglobin Derivatives . . . D. J. E. Ingram and J. E. Bennett 1136

Calculation of the Fraction of Effusing Molecules which Strike a Collector Plate above a Channel Hole . . . Robert D. Present and Alan W. Searcy 1137

Modification of the Naïve MO Method . . . Lionel Goodman and Harrison Shull 1138

Semiempirical Treatment of π-σ Transitions . . . Lionel Goodman and Harrison Shull 1138

Exchange Reaction between Iodine and Mercuric Iodide . H. Behrens and Alfred G. Maddock 1139

Oxidation and Reduction of Aqueous Ferrous-Ferric Sulfate Induced by Visible Light Absorption of Mercuric Sulfide . . . Edward I. Greenwald and Sheffield Gordon 1139

Theory of Absorption Spectra of Unsymmetrical Cyanines . . . Gentaro Araki and Sigeru Huzinaga 1141

Infrared Spectrum and Structure of Collagen . . . Richard M. Badger and A. D. E. Pullin 1142

Activation Energy of the H+H2 Reaction . . . Virginia Griffing and Joseph T. Vanderslice 1142

Configuration Coordinate Model for Luminescence in KCl:Tl . . . Peter D. Johnson 1143

Nuclear Relaxation and Quasi-Crystalline Structure of Liquids . . . L. Giulotto, G. Chiarotti, and G. Cristiani 1143

Microwave Spectrum of Fluorobenzene . . . K. E. McCulloh and Gilbert F. Polanow 1144

Errata and Addenda: Theory of Dielectric Relaxation for a Single-Axis Rotator in a Crystalline Field . . . John D. Hoffman 1144

Rare Gas Permeation through Polymers . . . Francis J. Norton 1145

Erratum: Flame Zone Studies by the Particle Track Technique. I. Apparatus and Technique . . . R. M. Fristrom, W. H. Avery, R. Prescott, and A. Mattuck 1145

Anomalous Magnetic Behavior of UH_{3-x} below 4.2°K . . . L. D. Roberts, D. E. Lavalle, and E. A. Erickson 1145

Altered Proportions of Isotopes of Molecular Nitrogen as Evidence for a Monomolecular Reaction . . . M. Walser, J. George, and L. J. Bodenlos 1146

Electrically and Elastically Active Relaxation Modes . . . Y. Haven and J. H. van Santen 1146

Emission Spectrum Attributed to Acetaldehyde . . . G. W. Robinson 1147

s-Triazine. I. The Unit Cell . . . L. A. Siegel and R. F. Williams 1147

s-Triazine. II. The Near Ultraviolet Absorption Spectrum . . . R. C. Hirt, F. Halverson, and R. G. Schmitt 1148

s-Triazine. III. The Infrared Spectrum . . . John E. Lancaster and Norman B. Colthup 1149

Anomalous Faraday Effect in Aqueous Solutions of Inorganic Salts . . . D. D. Randall and A. M. Taylor 1149

Radiation Chemistry of Luminescent Solutions . . . Milton Burton and W. N. Patrick 1150

Precombustion Reactions in Hydrocarbon-Nitrogen Flames: The Paraffin Candle Flame . . . S. Ruven Smith and Alvin S. Gordon 1150

Solid Ozone . . . Calloway Bibler, Abraham W. Berger, and Charles K. Hersh 1151

Fermi Level, Chemical Potential, and Surface Free Energy . . . Malcolm K. Brachman 1152

Microwave Spectrum of Benzaldehyde . . . Gunnar Erlandsson 1152